Loughborough University

Crossflow Microfiltration of Oil from Synthetic Produced Water

By

Yousef H .Dh. Alanezi

A Doctoral Thesis Submitted In Partial Fulfilment of the Requirement for the Award of the Doctor of Philosophy of Loughborough University

April 2009

Abstract

Produced water is formed in underground formations and brought up to the surface along with crude oil during production. It is by far the largest volume by-product or waste stream. The most popular preference to deal with produced water is to re-inject it back into the formation. Produced water re-injection (PWRI) needs a treatment before injection to prevent formation blockage. Due to the increase of produced water during oil production in the west of Kuwait, an effluent treatment and water injection plants were established and commissioned in 2004 so that produced water could be used for re-injection purposes. It is estimated that oil wells in the west of Kuwait produce 15 to 40 % of produced water. The main aim of this treatment train is to reduce not only the oil-in-water amount to less than 10 ppm, but also total suspended solids to 5 ppm which is the maximum allowable concentration for re-injection and disposal. Furthermore, with respect to the upper limit for injection, the maximum number of particles between 5 and 8 microns is 200 in 0.1 ml. In practice the number is found to exceed this limit by 10 times.

Hence, crossflow microfiltration of oil from synthetic produced water was studied experimentally under various operating conditions using a tubular multi-channel ceramic membrane. Crossflow velocities, transmebrane pressures, oil concentrations, ionic strength, ion valency, pH variation effects on critical flux and equilibrium permeate flux were investigated. An increase in crossflow velocity for oil emulsions from 1.14 to 2.28 m/s caused an increase in the critical flux. In contrast, as feed oil concentrations increased from 300 to 2400 ppm, critical fluxes were decreased. Likewise, when the ionic strength for the feed emulsions was increased by addition NaCl salt, the critical flux declined. While, as the ionic strength increased by addition of $CaCl_2$ and $FeCl_3$, the critical flux increased. These different observations are discussed in term of the hydrodynamics and particle interactions in relation to the filtration process.

For the modelling of experimental results in this research work, the unique applications of the back transport models (such as torque balance, inertial lift, and shear-induced models) and deposition rate models such as SEM model in the area of liquid-liquid separations could be claimed a contribution to new knowledge. For the experimental critical flux results, shear-induced model showed a better prediction in comparison with the other back transport models. Particle size was used as a parameter to fit the shear-induced diffusion model to the experimental results. From the particle size distribution analysis, the number frequency of these fine droplets was less than 5 % in the poly disperse emulsions. Hence, the smaller particles are causing fouling, which in agreement with the findings of pervious studies. For equilibrium fluxes at cake formation region (i.e. after reaching the critical flux), the modified SEM model by introducing effective diffusion term(the sum of Brownian and shear-induced diffusion) demonstrated a better forecasting of the experimental data compared to the original SEM model. New development of critical parameters such as $J_{crit} /(\tau_w * a_{crit})$ and $J_{crit} /(\tau_w * a_{crit}^{4/3})$ by incorporating the critical particle radius showed linear relationship for oil-in-water emulsions.

KEYWORDS

Ceramic Membrane, Crossflow Microfiltration, Oil Filtration, Effluent, Emulsion

Acknowledgements

This thesis could not have been accomplished without the help of Almighty God. I am really grateful to your bounties which bestowed on me. Also, the support of many people whom I would hereby like to acknowledge.

First and foremost, I would like to express my sincere appreciation and deepest gratitude to Professor R.J. Wakeman for his dedicated and excellent supervision which includes the invaluable advice, discussions, co-operation, and guidance. Also, my deepest thanks goes to Professor R.G. Holdich for his support and assistance.

I would like to take this opportunity to show my appreciation and deep thanks to Chris Manning who has been supportive and helpful. And also would like to extend my thanks to Dave, Sean, Kim and Graham from the department laboratory for their assistance and support.

I also wish to extend my gratitude to my sponsor Public Authority for Applied Education and Training (Kuwait), for granting me the scholarship to pursue my PhD.

I would also like to thank my beloved parent whom their kind prayers were appreciated and last but not least, like to deepest gratitude and indebted to my wife and my children (Hajer, Sarah, Maryam, Othman, Deema, and little Mohammad) who gave me the love, encouragement and support throughout the years of my study in Loughborough.

TABLE OF CONTENTS

LIST OF FIGURES

List of Tables

Nomenclature

A_s	Correction function for Stokes' law based on Happel's cell model
a	Particle radius (m)
C	Excess particle number concentration
C_o	Bulk (feed) particle number concentration
C_w	Wall particle number concentration (at y = 0)
c	Solute concentration in the feed (mgL^{-1})
c_b	Solute concentration in the bulk suspension ($mg\ L^{-1}$)
c_m	Solute concentration at the membrane ($mg\ L^{-1}$)
c_p	Solute concentration in the permeate ($mg\ L^{-1}$)
d_p	Particle radius (m)
D	Diffusivity (m^2 s)
Dp	Particle diffusivity (m^2 s)
D_{eff}	Effective diffusion coefficient (m^2 s)
D_{BW}	Brownian diffusion coefficient (m^2 s)
D_m	Molecular diffusion coefficient (m^2 s)
D_s	Shear induced diffusion coefficient (m^2 s)
f	Fanning friction factor (-)
Fi	Flow indicator
g	Gravitational acceleration (ms^{-2})
J	Permeate flux ($L\ m^{-2}\ h^{-1}$)
J_{crit}	Critical permeation flux ($L\ m^{-2}\ h^{-1}$)
J_w	Clean water permeation flux ($L\ m^{-2}\ h^{-1}$)
k	Mass transfer coefficient ($m\ s^{-1}$)
k_B	Boltzmann constant ($kg.\ m^2\ s^{-2}\ K^{-1}$)
L	Channel length (m)
N_c	Cake thickness factor
N_F	Ratio of the energy needed to bring a particle from membrane surface to bulk suspension to the thermal (dissipative) energy of the particle
N_{Fc}	Critical filtration number for cake forming

Pe	Peclet number (-)
Pi	Pressure indicator
Re	Reynolds number (-)
TMP	Transmembrane pressure (kPa)
t	Time (min)
T	Absolute temperature (Kº)
U_E	Electrophoretic mobility
V	Average permeate velocity (flux)
V_A	Attractive potential energy (J)
V_R	Repulsive potential energy (J)
V_T	Total potential energy of interaction (J)
V_t	Terminal velocity (ms^{-1})
X	Membrane length (m)
x	Distance from membrane entrance (m)
x_{crit}	Critical distance from membrane entrance (m)

Greek Letter

δ	Boundary layer thickness (m)
μ_p	Dynamic viscosity of permeate (Pa s)
ρ_r	Density of the retentate (kg m^{-3})
ρ_o	Density of oil (kg m^{-3})
ρ_w	Density of water (kg m^{-3})
τ_w	Shear stress at the membrane wall (Pa)
ϕ_b	Volume fraction of particles in the bulk
θ	Angle of repose (-)
θ_{max}	θ value corresponding to maximum packing of the retained particles
θ_w	Value of θ at the membrane surface
θ^*	Value of θ between zero and θ_w
γ	Fluid shear rate
ε	Cake or particle porosit

CHAPTER 1

INTRODUCTION

1.1 Background

Produced water is formed in underground formations and brought up to the surface along with crude oil during production. It is considered by far the largest volume by-product or waste stream. The most popular preference to deal with produced water is to re-inject it back into the formation. Produced water re-injection (PWRI) needs treatment before injection to prevent formation damage. The common objectives for produced water treatment are de-oiling, suspended solids removal, and softening i.e. removal of excess water hardness.

Due to the increase of produced water during oil production in Kuwait oil wells, an effluent treatment plant has been established and commissioned in 2004 so that produced water could be used for re-injection purposes. Usually it is estimated that oil wells in Kuwait produce 15 to 40 % of produced water. The main aim of this treatment train is reduce the oil in water to less than 10 ppm and the total suspended solids to 5 ppm, which is the maximum allowable concentration for re-injection and disposal. Furthermore, with respect to the upper limit for injection, the number of particles between 5 and 8 microns is 200 in 0.1 ml. In practice the number is found to exceed this limit by 10 times.

Cross-flow micro-filtration (CFMF) is a promising membrane technology to deal with this problem. The technique gives a filtrate with an oil concentration of less than 5 mg/l and also eliminates any solids in suspension. The main drawback relates to fouling, i.e. the membrane pores become clogged, which results in a need for frequent flushing and chemical cleaning, and the fitting of pre-treatment units

upstream, thus increasing the complication and the expenditure of such solutions.

Microfiltration has been used for removal of suspended particles and emulsified oil droplets in the size range of 0.1-20 µm from feed suspensions (Zaidi et al., 1992). In order to control membrane fouling in filtration, a cross flow configuration is applied to the membrane where tangential wall shear forces are exerted on its surface. However, the use of crossflow microfiltration has been restricted due to permeate flux decline caused by two main factors, concentration polarization and fouling. Hence, identification of the critical flux value, below which there is no significant fouling, becomes crucial. Therefore, filtration experiments have been conducted with emulsions of various properties (such as oil concentration) and hydrodynamic operating conditions (such as crossflow velocity) to identify the effects of these factors on critical permeate flux values.

1.2 Objective

The objective of this study on crossflow microfiltration of oil from synthetic produced water using a tubular ceramic membrane of 0.2 µm pore size is the evaluation of effects for varying suspension properties and hydrodynamic variables on the filtration performance. Furthermore, the coupling effects of altering the hydrodynamic parameters and suspension properties on filterability during the microfiltration of oil-in-water emulsions are investigated.

1.3 Structure of the Thesis

Chapter 2 Literature Review

In this chapter a literature survey is presented with regards to the following topics relevant to this study: produced water characteristics, produced water treatment, colloid science fundamentals, critical flux determination, and factors influencing the critical permeate flux. The survey includes previous studies concerning the

conventional treatment methods for de-oiling of produced water such as gravity separation, gas flotation, and filtration. Furthermore, it addresses advanced techniques such as membrane separation for produced water treatment and its challenges. A number of numerical models for crossflow microfiltration are described here to support the modelling work later in this thesis.

Chapter 3: Case Study

The chapter describes produced water treatment in the crude oil industry. A case study of Agash wastewater treatment and produced water re-injection plants is presented. An overview of both plants is discussed based on valuable data collected from Kuwait through long communications (2005) and through an industrial visit conducted in January 2006 as part of this research project.

Chapter 4: Experimental Procedures and Materials

This chapter presents details of the experimental procedure used for the filtration experiments. Sample preparation procedures for the oil-in-water emulsions using an homogenizer are illustrated, along with the chemical cleaning procedure for the membrane element used for the filtration. In addition, the experimental set up for crossflow filtration, the apparatuses for particle size distribution and zeta potential are described, together with the materials that have been used in the experiments.

Chapter 5: Characterization of Oil in Water Emulsions

This chapter presents both fundamental and experimental data for characterization of oil in water emulsions. The concept of emulsion formation is described in detail to cover other emulsion features such as the strength and the stability of emulsions. The role of the surfactant in stabilizing the oil-in-water emulsions is demonstrated experimentally in this chapter.

Chapter 6: Experimental Results

In this chapter a comparison between the methods used for estimation of the critical flux values was provided to illustrate their relative features. Particle size analyses of permeate samples were reported to show their compliance with the required product quality specifications. The results obtained from the experimental studies of the effect of suspension properties and hydrodynamics on the crossflow microfiltration of oil-in-water emulsions were presented.

Chapter 7: Modelling and Discussion

This chapter discusses the effects of oil-in-water emulsion properties and the hydrodynamics on the critical flux. A comparison between obtained results and several models is offered to support some of the interpretations and discussions of the experimental results.

Chapter 8: Practical Implications

Practical implications of this research project are discussed in this chapter.

Chapter 9: Conclusions

In this chapter, general conclusions are presented for the findings of this research in relation to the case study data, the experimental results, and the interpretation of predicted models.

Chapter 10: Future work & Recommendations

In this chapter, recommendations for future work are discussed in order to put forward a number of research proposal ideas for later workers in this research field.

CHAPTER 2

LITERATURE REVIEW

2.1 Introduction

Produced water is water trapped in underground formations and is brought to the surface during oil or gas production. Produced water constitutes the largest volume by-product and the most important waste stream. In the USA, 14 -18 billion barrels of produced water are generated annually (Veil et al., 2004). For each barrel of crude oil produced, there are 3 barrels of produced water in most of the world locations including the USA and South Oman in the Gulf region. Thus, more than 75% of oil and gas production is produced water. According to the energy report on UK oil and gas resources (1997), the quantity of produced water has surpassed crude oil quantity in the UK sector of the North Sea since 1988.

2.2 Composition

Produced water contains mainly water, and small quantities of inorganic and organic constituents. The substances normally found are clay or sand, scale crystallites, corrosion product, bacteria, and oil from incomplete separation or emulsification of produced fluids. Produced water may contain small amounts of chemicals that have been added to the treatment of produced water which are listed in Table 2.1. Usually the quantity of suspended matter must be decreased to some suitable level before the produced water can be re-injected or disposed of. This decrease is achieved with specialized chemicals and equipment.

2.3 Treatment Chemicals

Treatment chemicals are used as a direct solution to existing problems or to reduce their anticipated risks as precautionary measures. The most likely problems could be met in oil and gas production operation and the chemicals added for treatment are shown in Table 2.1.

Table 2.1: Problems associated with produced water and their treatment chemicals.

Problem	**Treatment Chemical**
Water Vapour	Dehydrator
Mineral Deposits	Scale Inhibitor
Chemical Corrosion	Corrosion Inhibitor
Dissolved Oxygen Removal	Oxygen Scavenger
Bacterial Corrosion	Bactericide
Emulsions	Emulsion Breakers, Coagulants, Flocculants
Foaming	Antifoam

Use of corrosion inhibitors, bactericides, and oxygen scavengers is required during oil and gas production operations. Also, dehydrators such as tri-ethylene glycol , (TEG) are widely used as a hygroscopic chemical to remove water vapour from the gas stream. Emulsion breakers are dosed in the desalter header to enhance the separation of dispersed or emulsified water droplets in the crude oil. Demulsifiers are added in the gas flotation header to improve the coalescence of oil droplets dispersed in the produced water to increase the efficiency of separation.

Coagulation involves neutralization of the surface charge (zeta potential) on suspended particles to overcome the repulsion forces, thereby destabilizing the suspension. Coagulation and flocculation are pre-treatment processes that alter the effective particle size and size distribution of the solids, to enhance separation by chemical addition to aggregate the particles.

Coagulant is therefore discussed as a preliminary step in this report, which requires consideration of basics of colloidal particle interactions in aqueous solution.

2.4 The DLVO Theory

The DLVO (Derjaguin-Landau-Verwey-Overbeek) theory describes the potential energy of interaction between a pair of particles and consists of two components:

a) A repulsive component V_R arising from the overlap of the electric double layers.

b) A component V_A due to van der Waals attraction arising from electromagnetic effects.

Thus, the total potential energy of interaction (Wakeman and Tarleton, 1999), V_T is

$$V_T = V_R + V_A \tag{2.1}$$

$$V_R = \frac{\pi \varepsilon_p a_1 a_2 (\psi_1^2 + \psi_2^2)}{a_1 + a_2} \left(\frac{2\psi_1 \psi_2}{\psi_1^2 + \psi_2^2} \ln \frac{1 + \exp(-\kappa H)}{1 - \exp(\kappa H)} + \ln(1 - \exp(-2\kappa H)) \right) \tag{2.2}$$

$$V_A = -\frac{A}{12} \left(\frac{y}{x^2 + xy + x} + \frac{y}{x^2 + xy + x + y} + 2 \ln \left(\frac{x^2 + xy + x}{x^2 + xy + x + y} \right) \right) \tag{2.3}$$

where a_1 and a_2 are particle radius, ψ_1 and ψ_2 are the measured potential at the outer boundary of the Stern layer, κ is the reciprocal electrical double layer thickness, H is the interparticle distance, and A is the Hamakar constant.

The double layer interaction (V_R) originates from the interaction between charged molecules, and its strength and range is strongly affected by the presence of surrounding ions. Independent of charging mechanism of any surface, the surface charge is balanced (electro-neutrality) by an equal but oppositely charged region

of counter-ions. Some of these counter-ions are, usually transiently, bound to the surface and build up the so called Stern layer. Outside this region, interactions of the not fully neutralized surface and the ions in the solution result in an 'atmosphere' of accumulated counter-ions and depleted co-ions, which with increasing distance from the surface asymptotically reaches the ion concentration. Schematic diagram of the potential energy variation with particle separation according to the DLVO theory is demonstrated in Figure 2.1.

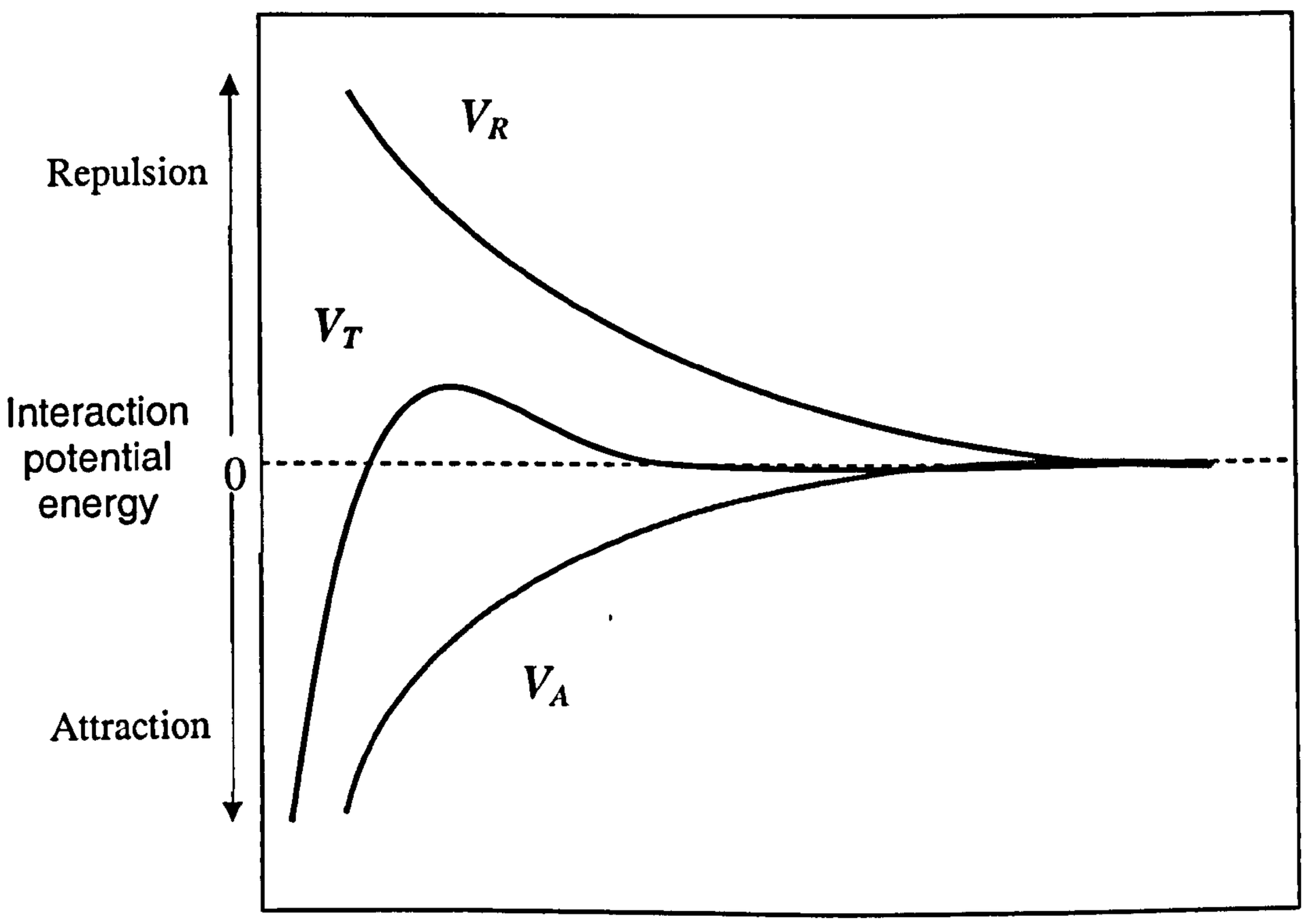

Figure 2.1: Schematic diagram of the potential energy variation with particle separation according to the DLVO theory

2.4.1 Electrical Double Layer Repulsion (EDL)

Most particles acquire a surface electric charge when in contact with a polar medium. Ions of opposite charge in the medium are attracted towards the surface and ions of similar charge are repelled This process, as well as the mixing

tendency due to thermal motion, results in formation of an electrical double-layer that includes the charged surface and the neutralising excess of counter-ions over co-ions distributed in a diffuse manner in the polar medium. The electric double layer is presented in term of Stern's model wherein the double layer is divided into two parts separated by a plane (Stern plane or layer) located at a distance of about one hydrated-ion radius from the surface. Within the stern layer partly de-solvated ions adsorbed by electrostatic attraction or specifically adsorbed ions may be present. Figure 2.2 is a systematic representation of double layer for a particle.

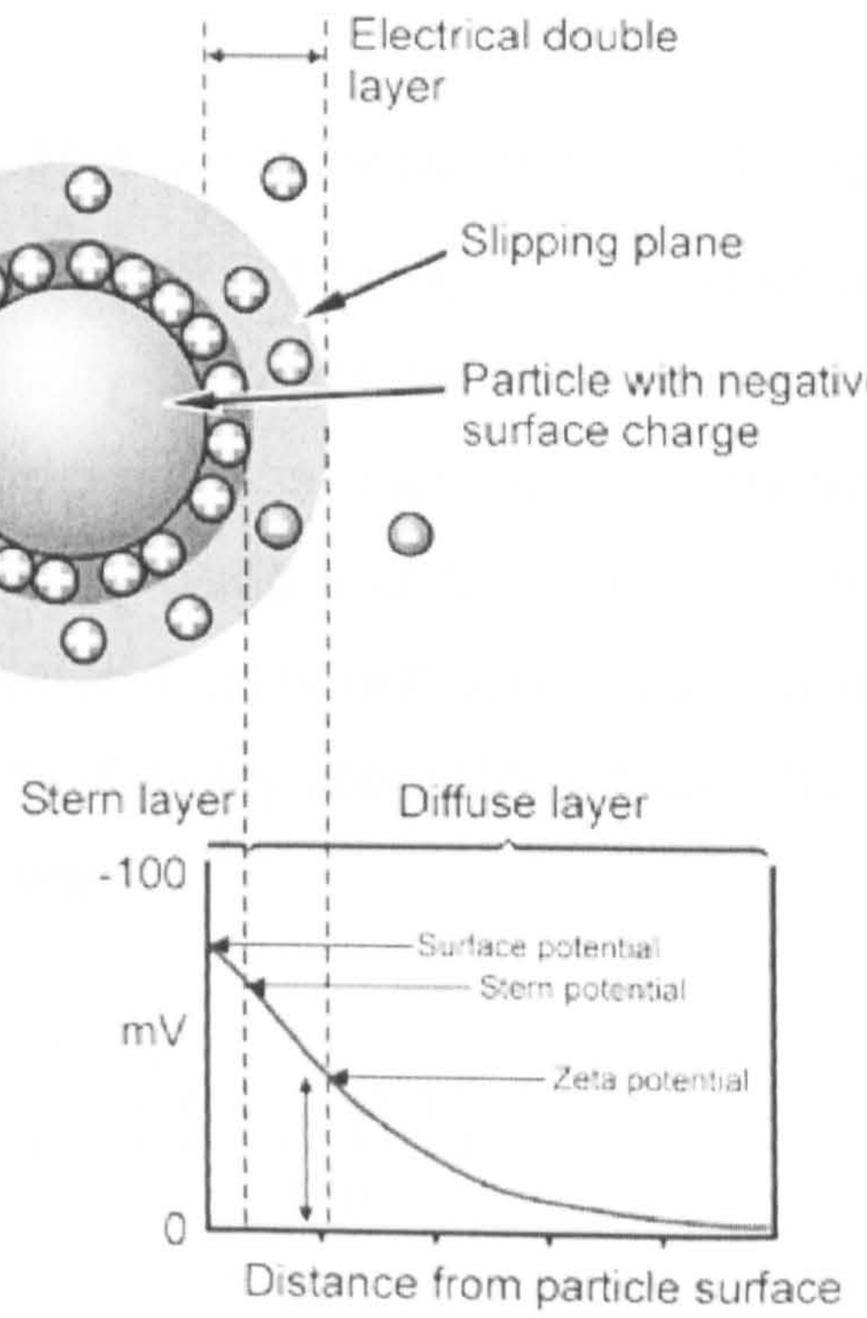

Figure 2.2: Double layer of a particle with negative charge suspended in water

2.5 Conventional Produced Water Treatment

A de-oiling system in produced water treatment plant normally consists of an American Petroleum Institute (API) gravity or corrugated plate separator and gas flotation unit. API separator performance depends on retention time, tank design,

oil specifications and the outcomes of flocculants or coagulants addition. However, gravity separation is unsuccessful with small droplets of emulsified oil. As the oil droplet size reduces, the essential retention time considerably increases in order to get better efficiency. Consequently, higher capital, maintenance and cleaning are required for gravity separation for removal of fine oil droplets. The needs of produced water treatment are dependent on its source, its state, and the used technique for its discharge. Due to stringent discharge regulations and reduction of fouling risks, further polishing treatments used are skimmer tanks, plate interceptors, gas flotation, and hydrocyclones.

2.5.1 Gravity Separators

The gravity separator is capable of removing free oil with particle size diameter > 150 μm, however, it is incapable of removing of emulsified and dissolved oil from water. The droplet rise velocity is correlated to several parameters and hence acceleration of the separation process, can be done by various techniques; an increase in the rate of gravity by using a centrifuge, a decrease in water viscosity by heating, an increase in water density with salinity, and a reduction of oil density by air or gas flotation process. Gravity separators' separation mechanisms can be interpreted by using Stokes law.

$$V_t = \left(\frac{g(\rho_w - \rho_o) d_p^2}{18\mu} \right) \tag{2.4}$$

To improve the efficiency of gravity separation tanks, corrugated plates that are made of a hydrophobic material are packed inside them. The oil droplets tend to stick on the corrugated plate surface and coalesce, and then move to the top of the tank. In effect, the depth of each separator path is subdivided by insertion of a pack of closely spaced plates. Oil droplets coalesce on the underside of each plate and the overall surface area is increased by the sum of the areas of the individual plates. The distance through which an oil droplet will have to rise is also reduced, enabling separation of smaller droplets for a similar residence time.

Table 2.2: Technical summary of corrugated plate separator.

Description	Separation of free oil from water under gravity effects enhanced by flocculation on the surface of corrugated plates.
Advantages	No energy required, cheaper, effective for bulk oil & suspended solid removal, no moving parts, robust technology.
Disadvantage	Inefficient for fine oil particles, requirement of high retention time, maintenance.
Waste Stream	Suspended particles slurry at the bottom of the separator.
Produced Water Application	Oil recovery from emulsions or water with high oil content prior to discharge. Produced water from water-drive reservoirs and water flood production are most likely feed stocks. Water may contain oil & grease in excess of 1000 mg/l.

2.5.2 Gas Flotation

A gas flotation unit utilizes gas or air to float oil out of the produced water on the surface where it is skimmed off. The speed of oil flotation improves significantly due to the reduction of oil droplet density when they are attached to gas bubbles. The process of gas flotation includes four fundamental stages; production of small gas bubbles in the oily water, contact between the bubbles and the suspended oil droplets, attachment of the oil droplets to the gas bubbles, and flow of bubble/oil drop mixture to the surface for removal by skimming.

The technique of bubble generation is critical. It determines the size and concentration of gas bubbles for a given influent flow which in turn influences the collision rate between the oil drops and gas bubbles and therefore enhances oil removal efficiency. In order for the oil droplet to stick to a bubble on contact, the hydrodynamics and the surface chemistry of both the drop and the bubble should be favourable. When the drop and bubble approach, the thin 'disjoining' film between them has to come apart. Behaviour of the water film is controlled by viscosity, interfacial tension, surface electrical charge, and pH.

Dissolved air flotation (DAF) operates on pressurizing the dissolving gas in water

upstream of the flotation unit. When the saturated water enters the flotation vessel, the pressure decrease results in the discharge of a large number of gas bubbles. Induced gas flotation (IGF) is the method in which gas is introduced to the polluted water stream. IGF engages the use of gas at effectively ambient pressure, drawn from the surface of the flotation.

Table 2.3: Technical summary of gas flotation separator

Treatment	Gas floatation
Description	Oil particles attached to induced gas bubbles and float to the surface.
Advantages	No moving parts, higher efficiency due to coalescence, easy operation ,robust.
Dis-advant.	Generation of large amount of air, retention time for separation, skim volume.
Waste Stream	Skim off volume lumps of oil.
Produced Water Applications	Oil recovery from emulsions or water with high oil content prior to discharge of produced water from water-drive reservoirs and water flood production are most likely feed- stocks. Water may contain oil & grease in excess of 1000 mg/l.

2.5.2.1 Gas Flotation Principle

In gas flotation fine bubbles are introduced into a water system that has dispersed liquid droplets (oil) or oily solid particles in order to affix the gas bubbles to the oil droplets. As a result of such an attachment the density difference between the oil cluster and the water is enlarged and thus the oil ascends quicker facilitating a faster and efficient separation from the aqueous phase. The oil droplets and oil-covered solids go up to the surface where they are trapped in the resulting foam and then skimmed off form the flotation unit.

With respect to the efficiency of gas flotation of oily wastewater, various dominant parameters which have not been investigated in detail are gas bubble size and its size distribution, degree of dispersion and oil concentration in the feed and its variability, chemical composition of the wastewater and the oil, pH and viscosity of

the aqueous phase, and interfacial properties between the oil, gas, and brine such as interfacial tension, wettability, and spreading coefficient.

REAY and Ratcliff (1973) pointed out that gas flotation is most useful when oil droplets have a diameter between 3 and 100 μm. Also, the flotation efficiency is not significantly influenced by gas bubble size but is considerably influenced by bubble number density. Table 2.4 compares induced and dissolved gas flotation processes.

Table 2.4: Comparison between induced and dissolved gas flotation.

Flotation method	Induced Gas Flotation (IGF)	Dissolved Gas flotation (DGF)
Description	Gas is drawn into the flotation chamber through dispersers such as impellers or ejectors.	Water is saturated with gas under the pressure and then passed to the flotation chamber. The pressure is reduced at the unit inlet, which leads to the release of gas bubbles.
Gas bubble size	In the range of 1000 μm.	with diameter in the range of 40-100 μm.
Retention time	Can be as low as 4 minutes.	15-30 minutes.

Floatability is defined as the ability of bubble-particle attachment and followed by floating to the surface of liquid. It can be measured indirectly in terms of the surface properties of particles, including hydrophobicity and zeta potential. The most important interfacial properties in the study of fine particle flotation comprise contact angle of solid, zeta potential of fine particles, and surface tension of liquid (Olivier *et al.*, 1999).

2.5.2.2 Flotation Efficiency

Flotation efficiency is improved by promoting attachment between the oil droplets and gas bubbles so that the effective or apparent density of the droplet becomes less, which leads to their quick floatation to the surface. Flotation mechanisms depend on hydrodynamic and thermodynamic forces, and physiochemical properties. Separation efficiency improves by coalescence of oil drops, aided by

surfactants and/or chemical demulsifier. The attachment of the oil drops to gas bubble and the formation of a stable bubble drop aggregate are rate controlling steps. The fine dispersed oil droplets generally have big negative surface charges in water and therefore remain separately due to the mutual repulsive forces.

A flow chart of flotation recovery steps is outlined in Figure 2.3 , where the most significant and the rate controlling stage is considered the attachment of bubble to particle step.

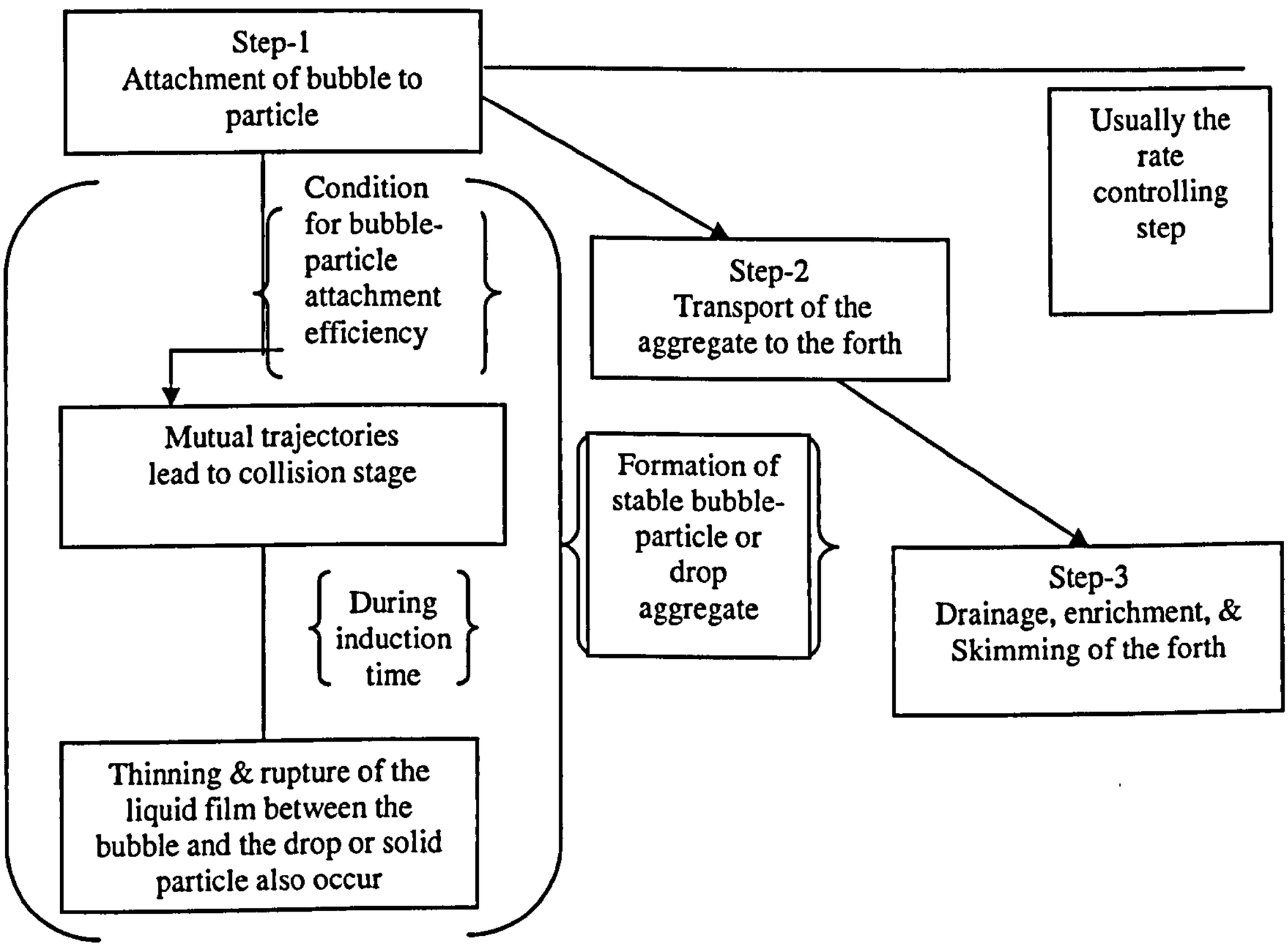

Figure 2.3: A flow chart of flotation recovery stages.

Hence to enhance separation by coalescing of oil droplets, addition of chemicals to counteract these charge forces becomes essential. Oil in wastewater is normally in dispersed form with mainly droplets diameter of less than 20 μm. Hence by using the gravity separator, the required retention time for these fine oil droplets to float to the surface will not be practical. Therefore, flotation can be effective industrially

when coupled with coagulation and demulsification as a pre-treatment stage.

2.5.3 Hydrocyclone

A hydrocyclone uses a swirling (rotating) flow to give a radial acceleration the emulsion. The natural gravitational separation of the oil and water phases is significantly increased, reducing the residence time essential for full separation to happen. Due to the density difference between the water and oil, a high rotating speed becomes essential for separation, while maintaining low turbulence and hence shear to avoid further emulsification. A hydrocyclone requires the installation of a surge tank upstream to intercept gross oil, and also to give a degree of residence time and controllability to the system. Such a tank will clearly reduce the size and the weight advantage offered by hydrocyclone operation and may cause the system to be unsuitable for particular applications. Hydrocyclones also need high pumping power to supply the adequately high flow rates for separation and also to overcome the pressure drop normally (1 to 5 bars) required to drive a cyclone.

Table 2.5: Technical summary of hydrocyclone separator.

Treatment	Hydrocyclone
Description	Free oil separation under centrifugal force generated by pressurized tangential input of influent stream.
Advantages	Compact modules, higher efficiency and throughput for smaller oil particles.
Dis-advantages	Energy requirement to pressurize inlet, no solid separation, fouling, higher maintenance cost.
Waste Stream	Suspended particle slurry as pre-treatment waste.
Produced Water Application	Oil recovery from emulsions or water with high oil content prior to discharge .Produced water from water-drive reservoirs and water flood production are most likely feed- stocks. Water may contain oil & grease in excess of 1000 mg/l.

A produced water treatment comparisons summary was provided by the Norwegian oil industry association (1991) for USA, UK, Norway, and Canada. As shown in Table.2.6. The best available technology mostly employed for treatment of produced water was gas flotation.

Table 2.6 Produced water treatment comparisons, OLF, the Norwegian Oil industry Association (1991).

Country	Best Available Technology	Effluent Limits	Monitoring Requirements	Exception Thresholds	Routine Reporting
USA	Gas Flotation	29mg/L monthly avg. 42 mg/L daily max.	Total O & G Gravimetric	Any exception	Annual
UK	Gas Flotation Hydrocyclones	40 ppm monthly avg. 30 ppm annual avg.	Dispersed O& G 1/day composite O&G 1/yr comprehensive	> 100 ppm	Monthly O&G Annual Comprehensive
Norway	Gas Flotation	40 ppm monthly avg.	Dispersed O& G 1/day composite O&G 1/yr comprehensive	> 40 ppm Monthly avg.	Monthly O&G Annual Comprehensive
Canada	Not stated	40 ppm 30 day avg. 80 ppm 2 day avg.	Dispersed O& G 2x/day	Any exception	Monthly

Ciarapica and Giacchetta (2003) conducted a technical and economical comparison study, between various types of conventional and innovative separation plants at offshore rigs, as a function of the treated flow rates up to 1000 m^3/h. By comparing the separating efficiency with respect to the average size of the oily particles they claimed that all conventional treatment systems were inefficient for oily particles below 20 μm, although the separating efficiency of hydrocylcone and flotation units were more than 90 % for the average size of oily particles above 20-30 μm. With respect to the size of the separation units for the flow rate of 1000 m^3/h. The hydrocylone was estimated to be 20 m^2 (smallest); the filter was 40 m^2; the flotation was 60 m^2; the corrugated plate interceptor was 70 m^2; and the skimmer was 90 m^2 (largest). Also, in term of the equipment mass for a flow rate of 1000 m^3/h, the hydrocyclone was claimed to be the lowest (25 ton), while the traditional filter was considered the heaviest (160 ton).

2.6 Advanced Produced Water Treatment

2.6.1 Membrane Separation of Produced Water

Choices for oil removal processes include microfiltration (MF) and ultrafiltration (UF). Membrane systems have the prospects to produce effluent water with the highest quality and at the lowest cost. Ciarapica and Giacchetta (2003) found that polymeric UF membrane systems were be cost-effective and attractive for treatment of produced water with high oil concentration and small particle sizes in offshore rigs. MF and UF have been anticipated as efficient and economical alternatives to conventional oil removal technology which normally consists of some grouping of gravity separation, plate interceptors, gas flotation units, and granular media filtration in offshore treatment. A tubular ceramic MF system that makes use of back flushing and chemical pre-treatment is considered the most widely established membrane technology for oilfield brine handling in North America (Zaidi et al., 1992).

Flux decline, low average permeate fluxes, and uncertain membrane life are regarded as the main technical difficulties associated with application of membranes. Membrane sensitivity to deviations in flow and oilfield brine characteristics have raised a few concerns about incorporation of membrane techniques at produced water treatment units. Flux decline is usually linked with fouling owing to adsorption or deposition onto the membrane surface or internal structure.

Concerning crossflow microfiltration of oily wastewater, most of the investigations have been conducted to study the effects of operating parameters such as crossflow velocity, transmembrane pressure, and feed concentration on oil rejection and permeate flux behaviour. The selection of an appropriate crossflow velocity involves finding the middle ground between membrane performance (flux) and energy utilization. With time, particles in the feed foul and block the membrane surface and the permeate flux declines. In a crossflow membrane system, the feed runs in parallel to the membrane surface which results in increasing the shear rate and delaying the fouling deposition rate. When the flux declines severely due to the formation of an irreversible fouling layer, it becomes essential to clean the

membrane chemically. (Bilstad et al.,1996).

Promising membrane technology for the future depends on membrane is based on tangential (crossflow) MF and UF. Crossflow filtration is able to reduce the oil feed concentration to less than 5 mg/l and also eliminate any solids in suspension (Zaidi et al., 1992). Other advantages, practically for offshore installation, lie in the compatibility of the system and their smaller dimensions. However, its main drawback is fouling, i.e. the membrane pores become clogged, which results in the need for frequent flushing and chemical cleaning, and the fitting of pre-treatment units upstream, increasing complication and expenditure (Ciarapica and Giacchetta, 2003).

Table 2.7: Comparisons between membrane systems
(Ciarapica and Giacchetta, 2003)

Type	Membralox	PCI	X-Flow	Metallic
Application	Microfiltration	Ultrafiltration	Microfiltration	Microfiltration
Pore size	0.2-0.8 µm	-	0.1-0.2 µm	3.5- 8 µm
Material	Ceramic [αAl_2O_3]	Polymeric[PVDF]	Polymeric[PES]	Nickel
Module	Tubular	Tubular	Capillary tube	Tubular
Pre-treatment	Yes	No	No	No
Pre-filtration	No	No	80-150 µm	No
Removal of solids	Yes	Yes	Yes	Yes

Furthermore, they compared between the four types of membrane as presented in the Table 2.7. The size and weight of the ceramic and metal membrane systems were much higher than those of the polymer membrane systems. Generally, the ceramic and metal membranes were less favourable than the polymer types.

However, for the commercial X-Flow system there is a need for a pre-filtration unit, which adds extra weight. From a cost comparison between the X-Flow and PCI membrane systems, they suggested that the PCI membrane system was the best available technology becuase its performance was partially independent of the treated produced water characteristics. Hence, this type of membrane was

compared with the conventional technologies for produced water treatment.

The comparison between the capital costs of conventional units and membrane treatment units demonstrated that the conventional ones, such as corrugated plate interceptor and gas flotation, were cheaper for flow rate up to 130 m^3/h. But, the cost of installation for corrugated plate interceptor (CPI) was 10 times lower than that for the membrane system. However, such an interceptor cannot be used to treat water with a high content of suspended solids. Similarly, the comparisons between the running costs demonstrated that the conventional technologies were less expensive than the membrane systems. Also with respect to the total unit cost, the conventional technologies (CPI) remained the cheaper option for treating water containing particles with mean diameters bigger than 50 μm. However, with smaller particle sizes and higher flow rates some of these conventional units became less cost effective options.

The most favourable technology for treatment of large flow rates of produced water offshore was the hydrocyclone, due to its smaller dimensions were smaller than flotation units and plate interceptors. Nonetheless, its efficiency declines when separating particles with sizes below 20 μm, and thus the provision of further downstream treatment became necessary using filters or flotation units. Ciarapica and Giacchetta (2003) compared the specifications of these facilities, and their results are presented in Table 2.8.

Table 2.8 Specifications of facilities (Ciarapica and Giacchetta, 2003).

Facility	Maximum inlet oil concentration	Medium (Minimum) Size of particle	Removal of suspended solids
Hydrocyclones 60 mm	120 mg/l 330 mg/l	14.5 μm (10μm) 30 μm (20μm)	No
Hydrocyclones 35 mm	160 mg/l 500 mg/l 2000 mg/l	15μm (10μm) 31 μm (20μm) 45 μm (30μm)	No
Hydrocyclones 35 mm + filter	400 mg/l 1250 mg/l	14.5 μm (20μm) 30μm (20μm)	Yes, efficiency 98%
Hydrocyclones 35 mm + flotation	> 2000 mg/l	< 10 μm	Yes, efficiency 90%
2Hdyroc. In serious 35 mm with screw pump	520 mg/l 2000 mg/l	11.5 μm (10μm) 23μm (20μm)	No
Membrane PCI	> 2000 mg/l	< 5 μm	Yes, efficiency 99%

Ciarapica and Giacchetta (2003) stated that "membranes prove more cost-effective than hydrocyclone + flotation solution for flow rates below around 650 m^3/h and better than the hydrocyclone + filter solution for flow rates up to about 300 m^3/h".

2.6.2 Crossflow Microfiltration

More recently, membrane separations have been considered more attractive methods and as economical concentration techniques. They have become significant tools for separation of a variety of suspensions ranging from oil/water emulsions to waste sludge. Microfiltration has been used for removal of suspended particles and emulsified oil droplets in the size range of 0.1-20 μm from their feed suspensions. Zhu et al. (2000) found that the oil rejection was greater than 99% for a membrane with pore size of 0.46 μm under the operating parameters where the crossflow velocity was 2.1 m/s and the transmembrane pressure was 0.10 MPa. Mueller et al. (1997) noticed that as the oil concentration was increased in the feed stock, a decline in the final flux was observed, while the variation in the crossflow rate, transmembrane pressure, and temperature seemed to have little impact on the final flux. Fan and Wang (2000) observed that the oil removal efficiency was higher than 95 % after conducting filtration tests for oily water at various operating conditions.

The use of crossflow microfiltration has been restricted as a result of permeation flux decline due to two main factors, namely, concentration polarization and fouling. Concentration polarization is a normal outcome of the membrane selectivity, which results in accumulation of solutes in a mass boundary film at the membrane surface that can lead to flux decline.

Fouling involves the material build up that may be due to one or more of the following mechanisms; adsorption, pore blocking, deposition, and cake formation. Concentration polarization can lead to cake formation as the concentration at the membrane wall builds up to the solubility limits of the solute. The major distinction between cake structure and membrane fouling is that the cake film is created at

the membrane surface, while the fouling layer is produced by particle-membrane interaction and is more directly attached to the membrane surface. Fouling is an irreversible adsorption of macromolecules while cake formation is reversible due to the low interactive forces in the solute and the membrane..

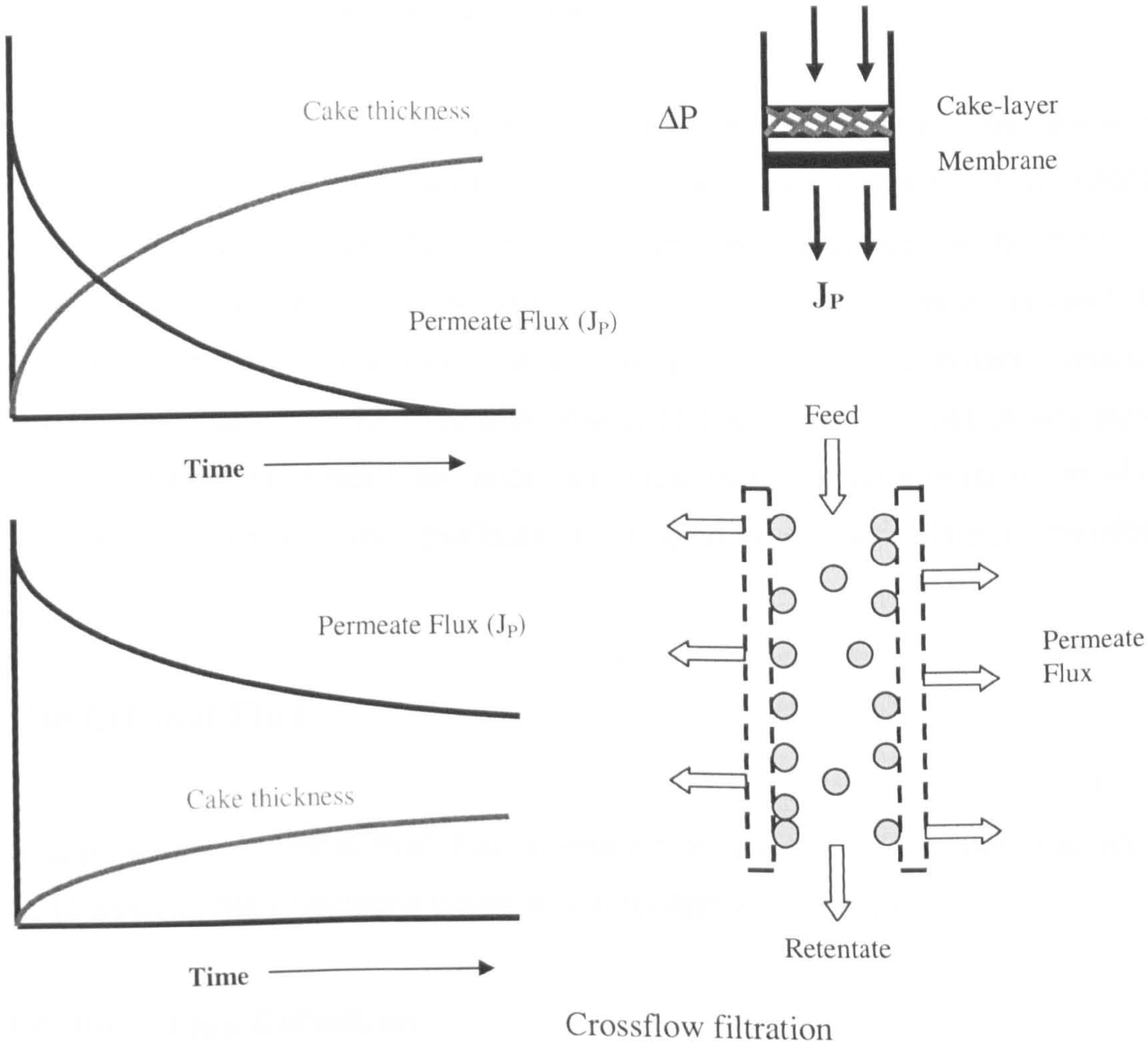

Figure 2.4: Diagram of deadend and crossflow filtration showing the variations of cake-layer thickness and permeate flux with filtration time.

Among the advantages of crossflow operation is that the filterability is not strongly a function of particle size due to an existence of a sieving barrier, which retains the particles by surface filtration. Also, particle accumulation is minimized. Thus, a higher filtration rate is obtained compared with conventional cake filtration processes. Furthermore, chemical additives such as flocculents or coagulants are not required. Hence, the filtered products are not contaminated with such chemicals. On the other hand, one of the disadvantages of crossflow filtration is that it cannot categorize or separate different sized particles from suspensions. In addition, the filter can be reversibly fouled when gel-forming components are present. Also, just only a thin cake layer can be formed as a concentrated feed suspension will plug the flow channels of the microfilter.

The existence of a critical flux below which the phenomenon of flux decline with time is absent is one of the features of crossflow filtration (Field *et al*, 1995). Moreover, a selective deposition of finer particles in crossflow filtration of polydisperse suspensions is considered one of the features. With respect to filtration performance above the critical flux point, in the constant-pressure situation the permeate flux declines with time until it reaches its quasi-steady state value. Crossflow filtration has been applied to wastewater treatment for removal of solids and oil droplets, and purification of potable water without chemical conditioning.

2.7 The Critical Flux

In the last decade, "critical flux" has appeared frequently in the literature as a means of shaping the conditions under which fouling will happen.

2.7.1 Critical Flux Definition

Howell (1995) described the critical flux as "a flux below which there is no fouling by colloidal particles" and also stated that it could be estimated as a function of particle size, hydrodynamics and membrane–colloid interactions. The critical flux has been defined physically as the first permeate flux where irreversible fouling

appears that could lead to coagulation and then deposition upon the membrane. Field et al. (1995) proposed that the critical flux is a flux above which fouling is observed on the membrane. Conversely, no fouling on the membrane would occur below the critical flux. It is identified experimentally as the flux leading to the first deviation from a linear variation of flux with transmembrane pressure (TMP). Critical flux could be a good indicator for operating a membrane filtration system with not only constant productivity but also with little or no fouling when operated at sub-critical flux condition. Field et al. (1995) clarified more the critical flux definition by the following statement; "The critical hypothesis for MF is that on start-up there exists a flux below which a decline of flux with time does not occur; above it fouling is observed. This flux is the critical flux and its value depends on the hydrodynamics and probably other variables".

Wu et al. (1999) discussed the vagueness regarding the precise definition of the critical flux with respect to the resistance variation when the flux increased. They queried whether the critical flux is the one at which irreversible fouling was generated (despite of slight increase in resistance at lower fluxes), or whether it is the flux which produces the initial increase in the hydrodynamic resistance. After the initial sighting of the critical flux, Li et al (1998) demonstrated that the driving force decrease or the crossflow velocity increase had caused the system to go back to the sub-critical condition (constant TMP for constant flux). Hence, this suggested that the fouling process was initially reversible. While, in earlier literature reviewing the critical flux concept, the critical flux was described as the flux that was reached when the resistance will started to increase. Thus, the critical flux might be the start of irreversible fouling (detachable) or the previous point in which fouling layer (detachable) becomes noticeable. Eventually, it has became obvious that there was some uncertainty in the literature regarding the critical flux definitions and applications.

Bacchin (2004) suggested that there is a possible theoretical link between the critical and limiting fluxes for colloidal systems. However, critical and limiting fluxes differ in their important roles and definitions. After the start of filtration, for certain period limiting flux is normally reached when the flux becomes independent of the

driving force (TMP). The limiting flux is considered the outcome of the concentration polarisation and membrane fouling, while the critical flux is the point where the fouling starts to deposit onto the membrane. With specific assumptions, Bacchin (2004) demonstrated that the critical flux is 2/3 of the limiting flux as presented in Figure 2.5.

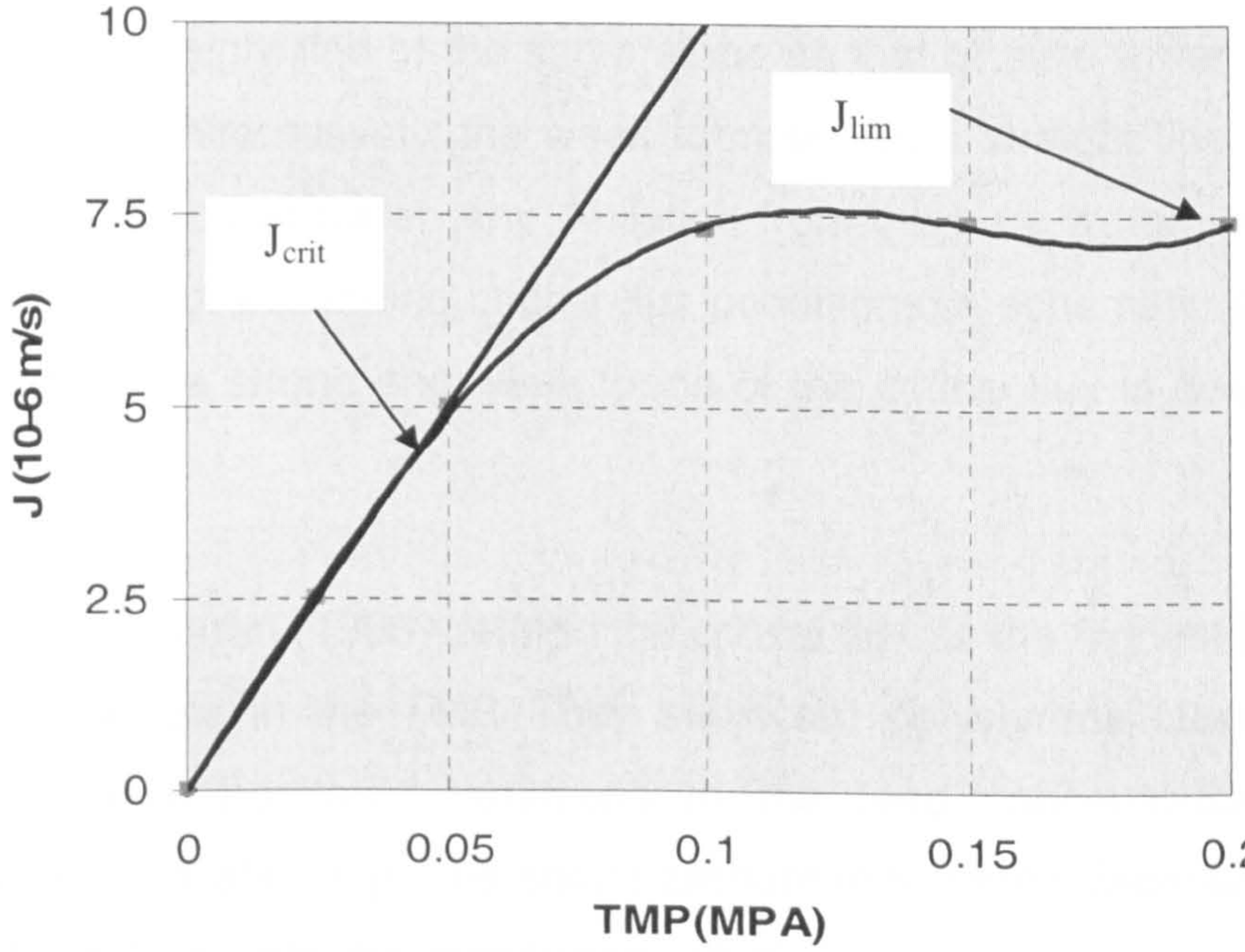

Figure 2.5: The relationship between critical flux and limiting flux (Redrawn from Bacchin, 2004).

The flux is correlated linearly with the TMP until it reaches the critical flux point, where deposition starts to form a cake layer which causes the resistance increase and thus results in a non-linear relationship between the flux and the TMP. By further increasing the TMP the flux approaches the limiting flux condition, where it becomes fully independent of the applied pressure (driving force). Limiting flux is also defined as the condition of dynamic equilibrium in which the net rate of cake formation is zero. Conversely, Bacchin (2004) offered an explanation for the limiting flux condition as the state of having a critical flux existing over the whole membrane surface.

2.7.2 Critical Flux Measurement

The critical flux can be determined experimentally by several methods. For example, Wu et al (1999) determined the critical flux by monitoring for TMP increase while increasing the flux in "steps" of constant flux. When the flux was plotted against TMP, strong and weak forms of the critical flux have been identified. The strong type states that the sub-critical flux-TMP relationship demonstrates a straight line of the same slope as that of pure water for the same working pressure. Alternatively, the weak form shows a straight line whose slope varies from that of clean water. Any deviation from the pure water straight line for any type is a sign of exceeding critical flux conditions. A schematic illustration for determination of the strong and weak forms of the critical flux is demonstrated in Figure 2.6.

Kwon and Vigneswaran (1998) defined the critical flux as the highest flux for which there is no increase in the TMP. They subjected polystyrene latex particles to microfiltration and monitored variations in the feed concentration with TMP increase during flux stepping. The solute amount in the feed declines significantly due to its deposition onto the membrane, which results in increasing TMP rapidly due to formed cake resistance.

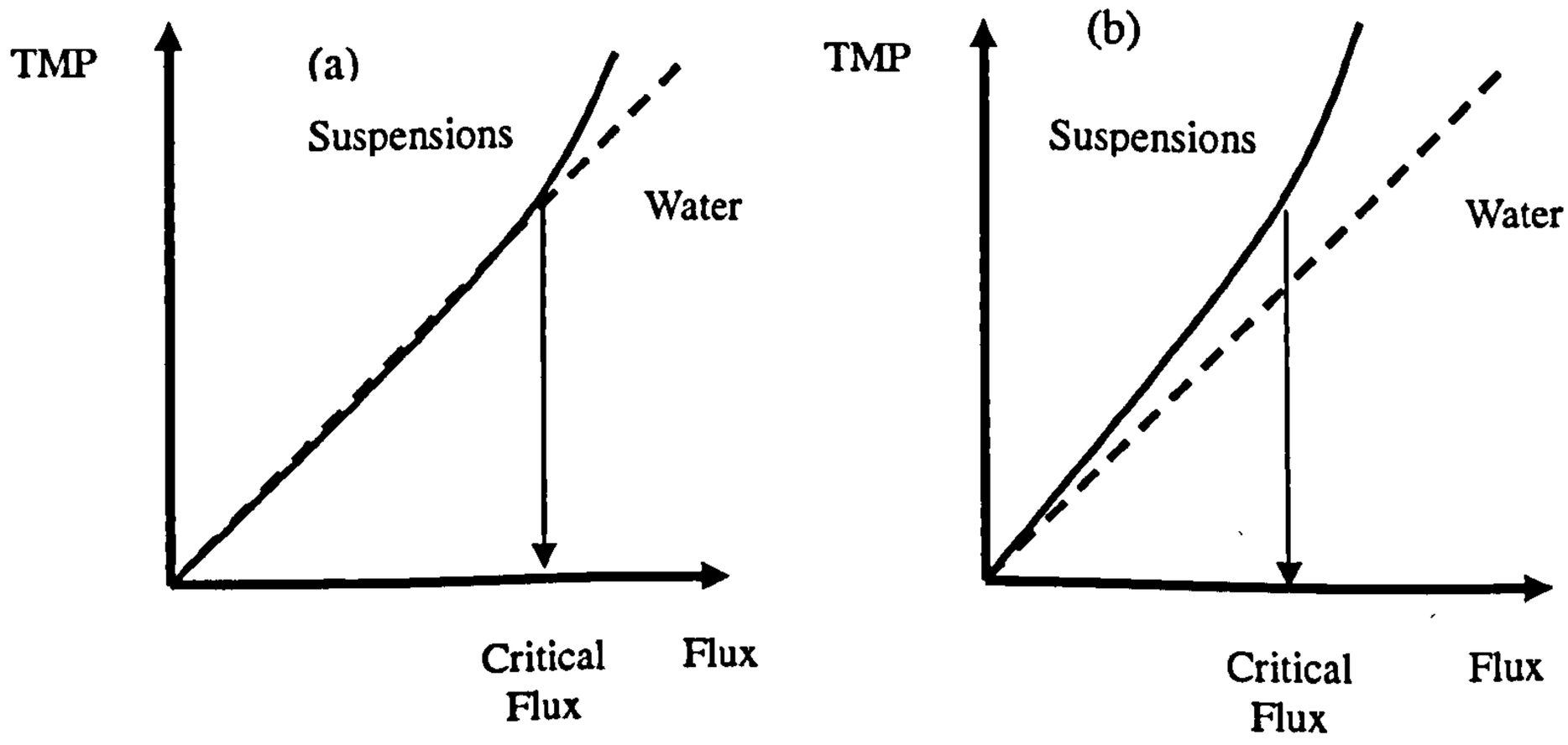

Figure 2.6: Schematic illustration of the determination of: (a) the strong form of the critical flux, and (b) the weak form of the critical flux (Fradin and Field, 1999).

Kwon et al (2000) carried out a comparison study of both measuring techniques for critical flux of latex particle suspensions, based on particle mass balance (i.e. feed concentration variation) and TMP rise. Critical flux values between both techniques varied significantly with larger particle sizes which indicated that membrane fouling was more susceptible to smaller particles. Also, different behaviours of critical fluxes of both methods was noticed in the presence of salts.

Li et al (1998) applied a direct observation technique through the membrane (DOTM) to monitor visually the crossflow microfiltration of yeast and latex particles in separate experiments. The critical flux was determined as the flux under which particles were observed to start depositing in an enormous amount . Below the critical flux, insignificant deposition was observed whereas substantial deposition was viewed at or above the critical flux..

2.8 Methods for Critical Flux Determination

The critical flux has been largely inferred from flux-TMP measurements by pressure or flux stepping. In addition, other techniques used have been direct observation through membrane (DOTM), particle mass balance, and fouling rate analysis. Inferences from flux-pressure experiments are obtained by applying pressure and measuring flux or by applying flux and measuring pressure. A comparison between constant pressure experiments and constant flux experiments is presented in Table 2.9.

Table 2.9: Comparison between constant pressure & constant flux experiments.

Constant Pressure Experiment	Constant Flux Experiment
Allows determination of a steady state flux, where filtration system turn into self regulated.	As a result of a constant fouling rate, pressure continuously increased with running time.
Steady state data is given to be used in scaling up filtration processes.	The dynamic data gives idea about the sustainability of the process.
Recommended for application when suspension constituents have little tendency for adsorption on the membrane, as steady state fluxes attained	Recommended for application to complex suspensions as steady state fluxes may not be attainable.

2.8.1 Extrapolations from Flux-Pressure Observation

Both constant flux and constant pressure experiments have been employed to measure the critical flux. The most popular technique used for critical flux determination was the constant flux operation (Field *et al.* 1995, Chen *et al.* 1997, Wu *et al.* 1999, Li *et al.* 1998, Madaeni *et al.* 1999, Kwon *et al.* 2000, Le Clech *et al.*, 2003). Field *et al.* (1995) found that filtration at constant flux had a preference to filtration at constant pressure because of its prevention of over fouling in the first flitration steps. This was confirmed by the results obtained from the research work conducted by Defrance and Jaffrin (1998). Also, a comparative study between filtrations at fixed pressure and fixed flux under same conditions, demonstrated that the critical flux is nearly the same as the limiting or pressure independent flux.

During constant flux operation, flux is regulated by the pumping system in the feed stream while monitoring the TMP. Any increase in TMP is considered as a sign for approaching critical flux at a particular flux step. For constant pressure steps, flux decline is an indicator of fouling. Alternatively, despite being less popular, preference for constant flux tests constant pressure experiments have been conducted to measure the critical flux by several researchers (Gesan-Guiziou *et al.*, 2001, Chiu and James, 2005).

Bacchin *et al.* (2006) discussed the importance of time scale. They stated that "a flux might be steady over a short time scale but in reality over a few days or weeks it is not. Indeed, all of the methods of measuring critical flux only detect that the fouling rate is below a threshold of sensitivity for the method and the time scale used". Le Clech *et al.* (2003) noticed that *dP/dt* values were much lower for long-term (days) experiments compared to those obtained for the short-term test, where each flux step was sustained for a maximum duration of 120 minutes. They found that flux-step determination of the critical flux cannot be used to predict the total fouling rate for longer-term period of operation with a real sewage feed. They recommended that a small step height coupled with a reasonable step length (15-30 min) seemed to be the best choice for the start-up operation for imposing of flux steps. There were uncertainty regarding the precise rate at which the flux should

be enforced, and for what, and for how long despite its dependence on the feed matrix.

2.8.1.1 Flux or TMP stepping technique

The flux or TMP stepping methods were applied to several crossflow filtration studies of colloidal particles such as titanium dioxide (Chiu and James, 2005), macromolecular solution such as emulsions (Field *et al.*, 1995), and complex fluids such as skimmed milk (Gesan-Guiziou *et al.*, 2000).

The implementation of the step by step technique is considered comparatively simpler than the other methods for critical flux measurement. However, for constant flux operation, there are limitations due to the sensitivity of pressure transducers, and the local resistance of the formed cake layer. The flux-step technique was more favourable than TMP-step technique due to its better control over the fouling rate by maintaining particle convective transport to the membrane constant (Defrance and Jaffrin, 1999).

However despite broad applications of the flux-step method, Le Clech *et al.* (2003) developed a standard flux-step method for fouling assessment in membrane bioreactors operating under constant flux. They stated that "no single and precise agreed protocol exists for critical flux measurement, making comparison of reported data difficult. Variables include step duration, step height, initial state of the membrane (new/backwashed), feed characteristics and system hydraulics".

Therefore, Le Clech and co-authors conducted an experimental investigation to obtain better knowledge about the influence of these variables in the determination method on the results. Furthermore, they derived three central TMP-based variables to portray the fouling manner and detect the start of fouling at the critical flux. The initial TMP (TMP_i) and the final TMP (TMP_f) values are recorded for every flux-step.

The TMP_i is the *TMP* attained subsequent to the initial abrupt boost in filtration resistance succeeding the step rise in flux, while TMP_f represents the TMP value reported at the end of the step and the step duration ($\Delta=t_f^n-t_i^n$). From these two TMP values, variables in relation to fouling can then be defined as follows;

- Initial TMP increase(ΔP_0), from $\Delta P_0=TMP_i^n-TMP_f^{n-1}$
- TMP increase rate (dP/dt), from $dP/dt=(TMP_f^n-TMP_i^n)/(t_f^n-t_i^n)$
- TMP average (P_{ave}), from ($P_{ave}=(TMP_f^n+TMP_i^n)/2$)

These derived parameters were used to characterise the impact of alterations in the main variables on critical flux determination.

By ascending and then descending the flux repeatedly, Le Clech *et al.* (2003) found the limit of reversible fouling. Also, the membrane age had no effect on the average pressure of the lowest and highest flux steps. Nevertheless, above the critical flux it was noticed that the rate of rise in TMP rate for the used membranes was approximately 10 times higher than for the new membranes. Such a rate increase was discovered to be correlated exponentially to the flux and highlighted the advantages of working at low flux operation. Additionally, the ΔP_{ave} was noticed to stay constant for low fluxes and later start to rise with flux, hence illustrating that the weak form of critical flux was surpassed.

Also, among their interesting findings was that detectability of critical flux was oppositely interrelated to step length, where as step length increased the average TMP started to increase at lower fluxes. Similarly, the TMP rise rate increased more rapidly for longer flux steps. Le Clech et al. deduced that the flux-step method cannot be employed to forecast long-term TMP conduct in real MBR systems, yet gives helpful information on relative fouling tendency.

2.8.1.2 Flux cycling

For every pressure or flux step, analysis of fouling reversibility could provide a more precise critical flux measurement. The transformation to irreversible fouling happens either at a similar point of divergence from linearity or it happens at upper fluxes. Assessment of reversibility is conducted by using a flux stepping where the flux increased by two steps and then reduced by one and TMP is determined at every step. If the TMP, as the flux is reduced, is not equal to the previous one measured at the same step height, irreversible fouling has happened and the critical flux for irreversibility has been surpassed. Wu *et al.* (1998) were the first to apply this technique where pressure steps compiled of alternate ascending and descending steps.

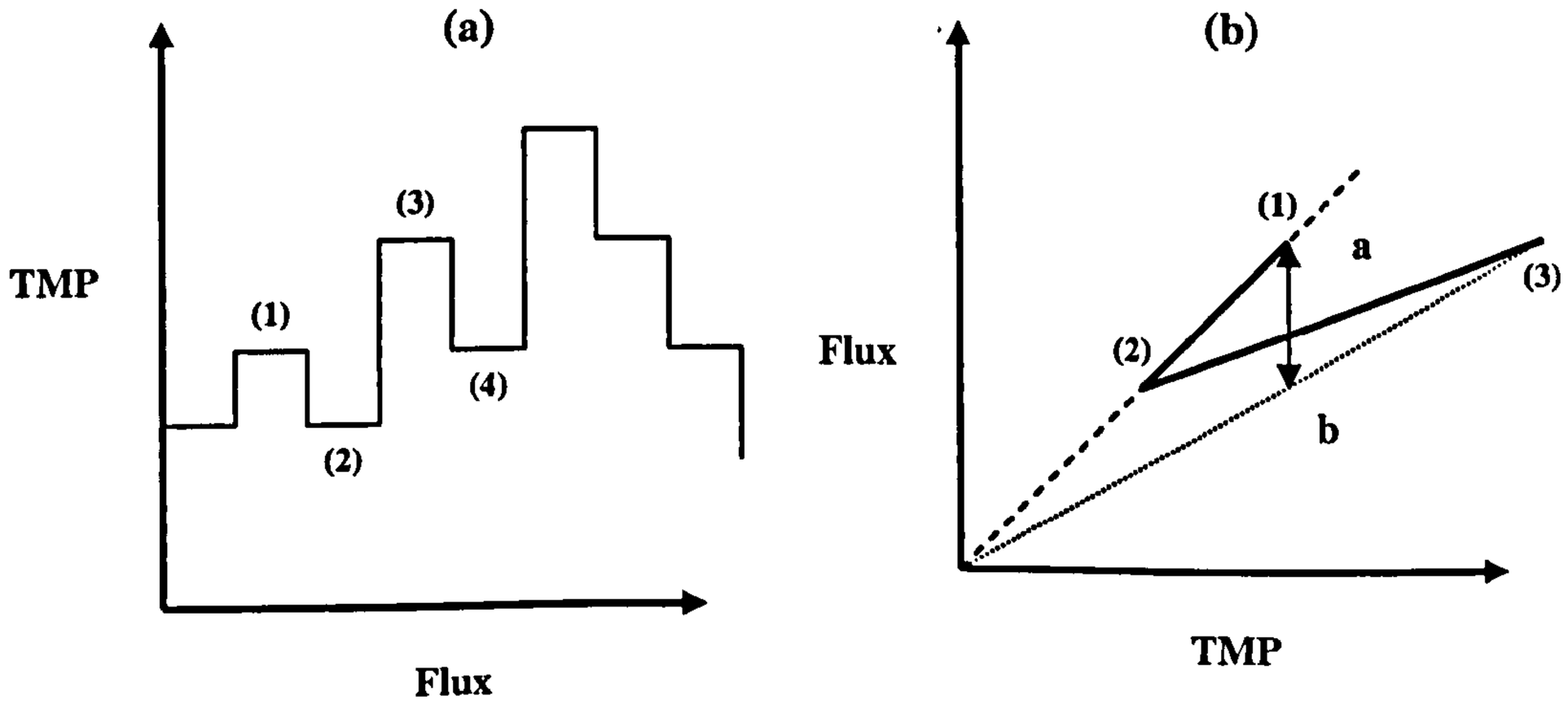

Figure 2.7: Pressure step used for an accurate determination of critical flux. Comparison of permeate flux/pressure obtained in steps 4 and 1 permits as to an assessment of the degree of fouling irreversibility (Espinasse *et al.*, 2002).

Espinasse *et al.* (2002) improved further this experimental technique for critical flux measurement by using a pressure stepping method as illustrated in the Figure 2.7(a). First, flux is raised up to a set point from an original point (1), keeping it up there for the length of the step and followed by decreasing the pressure to the original point (2). The pressure is then increased to a point above the prior set point (3), and then returned to the earlier step (4). Thus, by evaluation of the steady fluxes measured for steps 1 to 4 it could be seen whether the flux decline is caused by reversible or irreversible fouling. As presented in Figure 2.7(b), if the flux data for step 4 lies at point a, hence it will be reversible, and if it lies at point b it will be irreversible.

2.8.2 DOTM Method

In DOTM, a microscope is utilized to look through an Anopore membrane, that is transparent when wet due to its high porosity and low tortuosity. Critical flux is measured by the similar manner as the previous technique, but rather than using an increase in TMP with time, the membrane surface is examined by utilizing a microscope to find out if particle deposition has started. Li *et al.* (1998, 2000) employed this method and revealed that differences in pressure produced by deposition can be incredibly tiny.

DOTM is considered to be a sensitive technique of noticing particle deposition, apart from that it is limited to transparent membranes only. However, this method is the one that can be employed for direct examination of the initial cake formation on the membrane (Bacchin *et al.*, 2006). In addition, this method is restricted to the size of particles to be investigated due the magnification limit of the microscope. The huge benefit of the technique is that it has assisted in understanding how the cake formed and how easily the cake is removed. Electron micrographs have provided evidence for non-presence of deposit on the membrane following operating below critical flux. While as critical flux was surpassed, electron micrographs have provided a proof for the cake formation (Chen *et al.*, 1996).

2.8.3 Particle mass balance

Based on a particle mass balance Kwon et al. (2000) estimated the critical flux by observing the particle concentration in the retentate stream. Initially with no flux, particle adsorption was determined. Afterwards, any further decrease in particle concentration in the outlet stream was credited to deposition. Then a graph of flux against deposition rate was drawn after determination of the rate at a number of fluxes. The critical flux was extrapolated from this graph where it was regarded as the flux at which the rate of deposition is zero. Nevertheless, the critical fluxes were also determined by constant flux technique and they were two times higher than those obtained from the mass balance method.

In order to explain this discrepancy, Bacchin *et al.* (2006) stated that "the point of first deposition is not the point of large change in the resistance". This method does not differentiate between strong and weak types of critical flux. Although Gesan-Guiziou *et al.* (2002) point out that their critical flux was obtained from a mass balance and TMP stepping methods, they did not reveal whether there was an agreement between these fluxes. The mass balance method is considered to be more sensitive to critical flux than the TMP technique, particularly for bigger sized particles (Kwon and Vigneswaran, 1998). This is due to the fine particles impact on the hydrodynamic resistance being greater than that for large particles. The TMP technique depends on the increase in the fouling resistance which relies on particle size, cake compressibility and cake porosity. On the other hand, the sensitivity of critical flux measured by the mass balance method is independent of particle size.

2.8.4 Fouling rate analysis

Le Clech *et al.* (2003) observed that a zero rate of TMP increase might never be achieved during experiments with synthetic and real sewage. Therefore, by applying any other technique to measure the critical flux would generate a result that might not be present. Other valuable outcomes of the constant flux trials linked to the rate of fouling, was identification of the importance of *dP/dt*. Although for subcritical operation, the TMP rise rate (d*P*/d*t*) ought to be zero, it was found

not to be the case. The reasons for such behaviour could be related to the effect of an excess quantity of extremely fine particles present in the feed stock. The key factor impacting on d*P*/d*t* was noticed to be the flux-step height. This observable fact could be explained by the character of the fouling matter, differing with the manner the flux is increased.

2.8.5 A comparison of methods of critical flux determination

Although critical flux is a useful expression for the characterization of membrane operation, its definition is still under dispute among researchers in the field. In addition, a variety of methods for critical flux determination was not supportive for those engaged in such research. For example, the strong and the weak form of critical flux can be described by a divergence from the water flux line. The irreversible form of critical flux can be measured by pressure stepping up and down or flux cycling.

The mass balance technique could be implied as a supplement for these techniques in measuring the mass of deposited material. While for suspensions with complex components, the fouling rate analysis method has proved to be more appropriate (Jefferson *et al.*, 2004). Field *et al.* (2006) argued that the fouling rate, especially for multi-component systems, is of a key importance in industry since the membrane normally operates at an acceptable rate between cleans.

Although most investigations for critical flux measurements were conducted by using constant flux or TMP method, the DOTM, mass balance, and fouling rate techniques were used occasionally due to their insensitivity under particular circumstances and their own limitations. A comparison summary between the determination methods for critical flux has been presented in Table 2.10 showing their various advantages and disadvantages (Bacchin et al., 2006).

Table 2.10: Methods of measurement for critical flux: a comparison (Bacchin *et al.2006*).

Method	Advantages	Disadvantages	Form Measured	Suitability
Flux-pressure profile: deviation from linearity	Simplicity.	Can be subjective. No link with reversibility.	Strong and weak form J_{cs} , J_{cw}.	Feeds with low osmotic pressure.
Flux or pressure vs. time: flux stepping	With up and down steps, fouling hysteresis found. Resistance should be determined for each step.	Unlike flux cycling, points of transition to irreversibility can be missed.	Strong and weak form J_{cs} , J_{cw}.	Feeds with low osmotic pressure; if correction is to be made for osmotic pressure flux cycling is to be preferred.
Flux or pressure vs. time: flux cycling	Rigorous when allowance made for osmotic pressure.	Time consuming and complex.	All forms strong and weak form J_{cs} , J_{cw} and J_{ci}.	All kinds of feed.
Direct observation through the membrane	Direct observation of flux giving deposition. Potential for measuring J_{ci} yet to be exploited.	Limited to particulate feeds and membranes that are transparent when wet.	Linkage to J_{cs} , J_{cw} or J_{ci} not obvious, but value measured is significant.	Particulate feeds.
Mass balance	Linked to a complementary parameter, the deposited mass	Need to be used in conjunction with another method.	Linkage to J_{cs} , J_{cw} or J_{ci} not obvious, but value measured is significant.	Particulate feeds.
Determination by fouling rate analysis	If a flux for "low. fouling" is not found then determination of *dp/dt* (under fixed fluxes) may identify a point of sustainable flux. Absolute "nofouling" corresponds to a critical flux.	Can be subjective. No link with reversibility.	Strong and weak form J_{cs} , J_{cw} , also J_{sus} .	All feeds.

2.9 Factors Influencing the Critical Flux

The critical flux has been measured for several feed suspensions ranging from sub-micron size particles (Kwon and Vigneswaran, 1998; Wu *et al.*, 1999) and colloidal particles (Chen *et al.*, 1997) to emulsions (Field *et al.*, 1995). Also, critical flux was determined for magnesium hydroxide suspensions (Fradin and Field, 1999) and yeast particles (Li *et al.*, 1998; Metsamuuronen *et al.*, 2002) where their particle sizes were significantly bigger than 1 micron. Furthermore, the critical flux measurement was conducted for complex fluids such as a bioreactor sludge (Defrance and Jaffrin, 1999; Gander *et al.*, 2000) and fermentation broth (Persson et al., 2000; Milcent and Carrre *et al.*, 2001). In general, the factors affecting the critical flux are similar to those elements that cause membrane fouling, and can be summarized as crossflow velocity, particle size, feed concentration, pH and ionic strength, and membrane properties.

2.9.1 Crossflow Velocity

An increase in the critical flux is expected as the crossflow velocity is raised. This results in an increase in the shear forces along membrane surface and causes higher back diffusion rates of solutes, thereby decreasing concentration polarization and/or fouling. For example, in a crossflow microfiltration of colloidal silica suspensions, Chen et al (1997) noticed experimentally as the crossflow velocity was raised from 0.2 to 1 m/s, the critical flux increased from 30-160 l/m^2h to 220-285 l/m^2h. Madaeni (1997) observed that the critical flux increased linearly with crossflow velocity using a similar membrane for suspensions of latex particles with diameter of 0.1 and 1 μm.

Also, by using the DOTM method, *Li et al.* (1998) observed a similar linear relationship between critical flux and crossflow velocity for latex particles with various sizes 3, 6.4, and 11.9 μm. In a number of microfiltration experiments, such as those carried out by Fradin (1999) and Madaeni et al. (1999), it was observed that a linear proportional relationship between critical flux and crossflow velocity existed.

Furthermore, the same relationship of increasing critical flux with increasing crossflow velocity was noticed during filtration of a bioreactor sludge (Gander *et al.*, 2000) and of a fermentation broth (Persson *et al.*, 2000; Milcent and Carrre *et al.*, 2001).

2.9.2 Particle Size

According to a number of research studies in crossflow microfiltration (Madaeni, 1997; Li *et al.*, 1998; Kwon *et al.*, 1998, 2000), the critical flux increases as the particle size increases. This direct proportionality relationship could be explained for bigger particles where they do not foul inside membrane pores and are probably swept away from the membrane surface by axial forces and lateral migration. Kwon *et al.* (2000) studied the effect of particle size on critical flux experimentally by conducting a series of filtration tests with various particle sizes (ranging from 0.1 to 12 μm). The critical flux measurement was carried out based on the TMP increase for constant flux and mass balance methods for comparison purposes. For particle sizes ranging from 0.32 to 11.9 μm, it was found (for both techniques) that critical fluxes increased with increase in particle size.

2.9.3 Feed Concentration

An increase in feed concentration will result in a decrease in the critical flux (Madaeni, 1997; Chen, 1998; Fradin and Field, 1999; *Kwon et al.*, 2000). A consequence of the feed concentration increase is a rise in the solute mass transfer rate and then accumulation in the boundary film near the membrane surface. Accordingly, a rise in hydraulic resistance is observed due to the polarization and the higher probability of fouling. Chen (1998) suggested that local concentration was the main influential parameter in determining the critical flux through carrying experimentally two different BSA concentrations (at 0.1 and 1.0 wt %). The critical flux for lower concentration was measured to be approximately 66 l/m^2h while the higher concentration was 200 l/m^2h.

Kwon *et al.* (2000) observed that both critical fluxes (based on mass balance and increase in TMP) decreased as the feed concentration increased. They suggested that this behaviour was due to the higher accumulation of particles onto the membrane surface. Furthermore, the specific deposition rates (0.0023, 0.0042 and 0.0098 g/cm for 50, 100 and 200 mg/l, respectively) were estimated from the deposited amount at each flux step and they increased as the feed concentration increased. Hence, at higher feed concentration more particles tend to accumulate onto the membrane surface for the similar flux step.

However, the membrane fouling rate was found higher at lower feed concentration, where comparatively high rate of TMP increase was noticed (Wakeman and Tarleton, 1993). The accumulated particles tend to plug the membrane pores (optimal position) at low feed concentration, since the competition for such position is not high (Figure 2.8). In contrast, the lower rate of TMP increase at high feed concentration might be caused by the particle bridging onto the pores of membrane to compete for the optimal position which lead to cake layer formation (Kwon *et al.*, 2000).

(a) Low concentration

(a) High concentration

Figure 2.8: Diagram of different mechanisms of particle deposition at low and high feed concentration (Wakeman and Tarleton, 1993)

2.9.4 Ionic strength and pH

Adjustment of the suspension pH and ionic strength is a process whereby particle-particle and particle-membrane electrostatic forces can be manipulated. Generally, at pH values for suspended particles below or above the isolectric point (IEP), the particles acquire net negative or positive charges. The magnitude of these charges increases as the divergence away from the IEP point increases. As a result of electrostatic charge repulsion between the particles, which deviated further away from the IEP point, their apparent particle sizes would be bigger closer to the IEP. Consequently, when these particles deposit onto the membrane surface, they would form a relatively permeable cake layer as shown on Figure 2.9. When the charge sign of suspended particles is similar to that of the membrane surface, the electrostatic repulsion would prevail and hence cause a decrease in the deposited material on the membrane surface. Conversely, when they hold opposite charges, hence causing electrostatic attraction, the deposition of particles encouraged.

The electrostatic influences of pH can be counterbalanced by the addition of electrolytes to the feed suspension. Electrolyte ions attach to ionised parts of the particles and generate a charge shielding effect, and thus diminishing any electrostatic repulsive or attractive forces and compressing the double layer. Hence, a decrease in the scale of electrostatic repulsive or attractive forces would take place as the ionic strength increases. The Debye length is a physical measure of such scale for these repulsive electrostatic forces between charged colloidal particles. When the electrolyte concentration (for a 1:1 electrolyte) increases, the Debye length decreases which could lead to compression of the electric double-layer. In SI units, the Debye length for a 1:1 electrolyte is given by:

$$\kappa^{-1} = \left(\frac{2 \times 10^3 e^2 N_A I}{\varepsilon_r \varepsilon_0 kT} \right) \qquad (2.5)$$

where e = elementary charge (1.6×10^{-19} C)

N_A = Avogadro's number (6.02 x 10^{23} mol^{-1})

I = ionic strength (mol/m^3)

ε_r = dielectric permittivity of water

ε_0 = permittivity of free space (8.85 x 10^{-23} $C^2J^{-1}m^{-1}$)

k = Boltzmann constant (1.38 x 10^{-23} J/K)

T = absolute temperature (K)

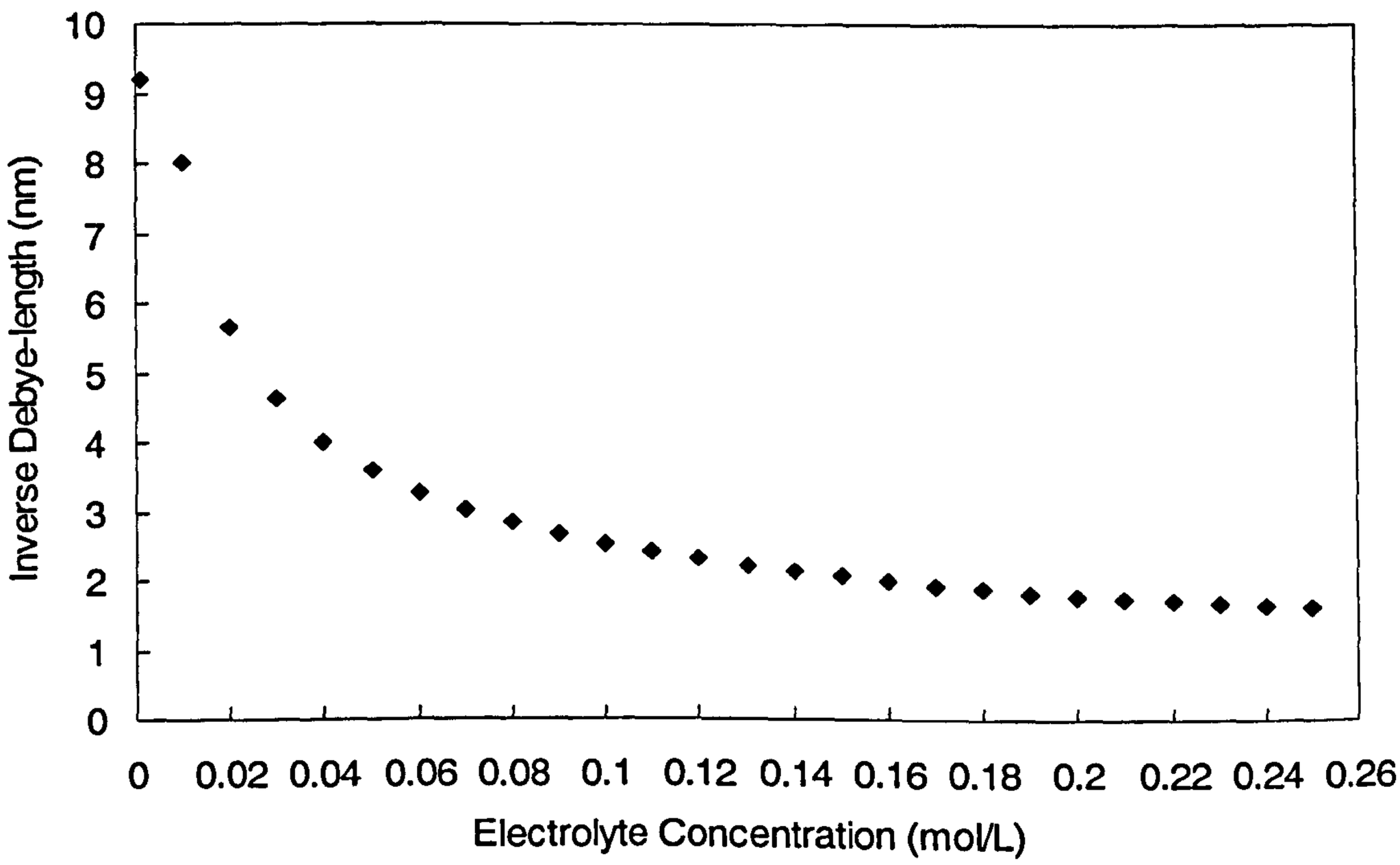

Figure 2.9: Inverse Debye-length variation with electrolyte concentration (mol/L).

The impact of pH on the critical flux is not only that it increases with pH deviation on either side of the IEP, but also it turns out to be lowest at the IEP of the solute. For example, Chen *et al.* (1997) noticed the critical flux to rise together with pH higher than the IEP (pH 1.6) during the microfiltration of colloidal silica. Hence, as a consequence of pH deviation from IEP, the negative charge of colloidal silica particles had increased. Furthermore, when pH was increased from 3 to 5 the critical flux increased 145 to 195 L/m^2h.

Chen *et al.* (1998) observed that the lowest critical flux of BSA dilute solutions was at pH 3, where the electrostatic attraction linking positively charged protein and negatively charged membrane occurred. Moreover, Metsamuuronen *et al.* (2002) demonstrated during hydrophilic membrane filtration of myoglobin solutions that the lowest critical flux was reached at a pH equivalent to the IEP of the protein. Also, during yeast solution filtration by hydrophilic and hydrophobic membranes, they observed at the IEP of the solute (pH 4) the critical flux was at a minimum. Universally, an increase in pH higher than the isoelectric point (IEP) yields an increase in the critical flux. Metsamuuronen *et al.* also found that the critical flux increased from 60 to 105 L/m^2h when the pH increased from 7 to 8.

According to the majority of cases, it appears that the critical flux is controlled by the particle-particle interaction rather than particle-membrane interaction. Such particle-particle interaction is ruled by electrostatic forces. Marshall *et al.* (1993) proposed that the determination of fouling amount is directly related to charge on the protein molecules rather than dissimilarity in charge between proteins and membrane. Particle-particle and particle-membrane interactions are influenced by the physicochemical and hydrodynamic conditions. Therefore, any modification within these conditions would result in apparent changes in behaviour of the flux decline. For instance, in stable colloidal suspensions, as a consequence of the increase in ionic strength, the diffuse double layer around the charged particles would be compressed. Therefore, particles would be densely packed in the cake, hence leading to quick decrease in the permeate flux.

Suki *et al.* (1984) conducted an investigation into the crossflow ultrafiltration of BSA suspensions (0.1 wt %) and found the maximum deposition amount on the membrane was at the IEP. Furthermore, the deposition quantity has increased considerably with the addition of 0.2 M NaCl and at lower crossflow velocities. As a result of the salt addition, the tendency of accumulation increased due to the ion bridging between BSA protein and the membrane surface. Palecek and Zydney (1994) investigated the hydraulic permeability of protein deposits formed during microfiltration at different pH and ionic strength. They revealed that variation in salt concentration generated the charge-shielding effect and the build up of electro-

osmotic counterflow (EOF). An electro-osmotic counterflow (EOF) includes pulling out the bulk solution on the opposite direction of the convective flow as shown in Figure 2.10.

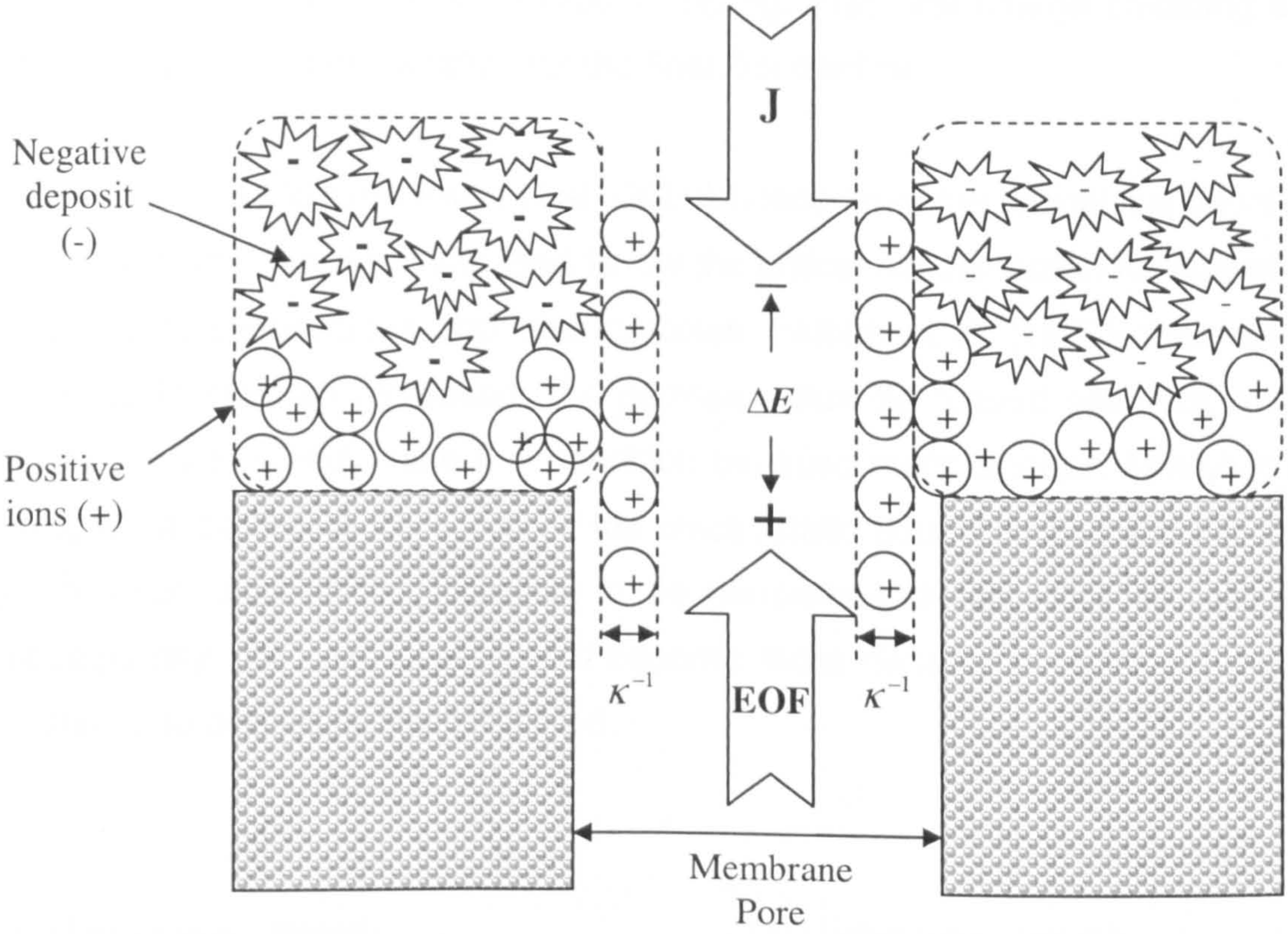

Figure 2.10: Systematic diagram of the electro osmotic counterflow (EOF) of bulk solvent.

Palecek and Zdney (1994) stated that an uneven division of positive and negative ions in a cake layer of charged protein molecules has produced an EOF. When the fouling material is negatively charged, the solvent bulk flow generates a bigger convective transport of positive ions because of their higher concentration in the foulant. The outcome is a streaming potential (ΔE) through the fouling layer that produces an electrophoretic flux of positive ions in the opposite way to that of the bulk solution stream. This counter stream of ions produces a Maxwell (electrical)

stress in the liquid ensuing in a total decrease in the solvent flow, or a flux decline, which is directly proportional to the produced streaming potential. Nonetheless, as the electrolyte concentration increases, the thickness of the diffuse double layer decreases and the streaming potential decreases, thus causing the increase in the flux. Palecek and Zydney (1994) made use of the EOF phenomenon to describe the transient increase in flux as the outcome of the increase in electrolyte concentration during filtration of protein fouling. Also, the charge shielding effect was used to give an explanation for the final flux decline.

Bacchin et al. (1995) and Kwon et al. (2000) noticed that the critical flux decreased as the ionic strength was increased below the critical concentration for coagulation for both clay suspensions and latex particles. Faibish et al. (1998) observed that as the ionic strength increased, the permeate flux decreased severely, and the period to reach steady state flux condition because much shorter. At higher ionic strengths, a decline in the range of the electrostatic double layer repulsive forces would occur, resulting in a decrease in the interparticle distances in the cake layer. Subsequently, the cake layer would become more densely packed and thus the resistance to permeate flux increased.

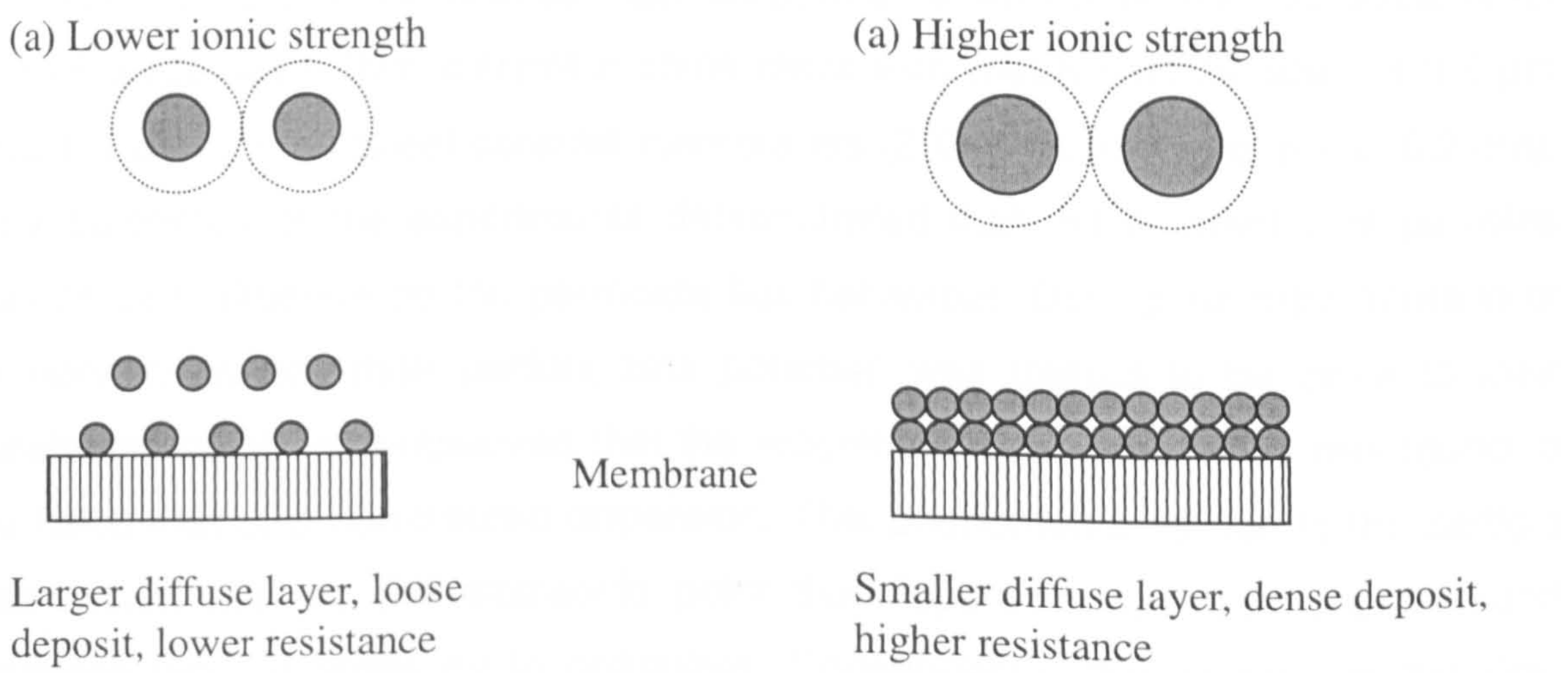

Figure 2.11: Diagram of layers formed by particle at lower and higher ionic strength (Kwon *et al.*, 2000).

Elzo et al (1998) reported similar results, high permeate fluxes were observed at low salt concentration. Kwon *et al.* (2000) studied the effect of ionic strength on critical flux based on the TMP increase. They found that the critical flux decreased as the ionic strength increased from 10^{-5} to 10^{-2} M. While as the ionic strength increased above 10^{-2} M the critical flux increased. A possible explanation for the critical flux decrease at ionic strength 10^{-2} M was related to high hydraulic resistance caused by the dense fouled layer of particles (with reduced diffusive layer).

During the microfiltration tests of oily water, Hua *et al.* (2007) noticed that at higher salt concentration a lower steady flux was given. At a lower salt concentration (0.001M) the measured flux was more than double that at higher salt concentration (0.05M). However, the effect of salt concentration on permeate flux is still debated among researchers in the field. According to Tambe and Sharma (1992), high ionic strength lessens the film thickness around the oil droplets, thus reducing the electrostatic repulsion, thereby encouraging coalescence leading to higher permeate flux. In addition, Zhao et al. (2005) found that when the ionic strength increased, the steady permeate flux became higher.

Šmídová *et al.* (2004) investigated the effect of particle shape, ζ-potential and size with variation of pH and ionic strength on permeate flux during the microfiltration of model dispersions (two dissimilar china clays with mean particle sizes of 3.5 μm and 1.5 μm) on flat sheet ceramic membranes (ZrO_2, mean size of pores 0.2 μm). The outcomes of the experiments demonstrated that the ζ-potential of particles has crucial influence on the permeate flux behaviour. During the microfiltration of dispersions where their particle zeta potential was treated to be close to their isoelectric point, they observed that the magnitude of permeate flux was found to be twice that of a non-treated dispersion. This phenomenon is due to the particle interaction; near to the isoelectric point the dispersion was less unstable and particles have a tendency to coagulate. Consequently, the porosity of the filter cake becomes higher and so the permeate flux is higher, whereas the filter cake resistance approaches a lower value.

2.9.5 Membrane Properties

The effects of membrane properties, such as pore size, porosity, morphology, surface charge, and hydrophilic/hydrophobic effect, on the critical flux have been investigated (Chen, 1998, Huisman *et al.*, 1999, Madaeni *et al.*, 1999, Wu *et al.*, 1999, Kwon *et al.*, 2000, Bromley *et al.*, 2002).

The geometric configuration of the membrane, such as the pore shape, porosity, and cut-off, has been shown to be significant for critical flux. Bromley *et al.* (2002) compared experimentally the effects of different membrane pore shapes on the critical flux using surface microfilters with circular and slotted pores. They found that the critical flux values for those filters with circular pores were five times lower than those with slotted pores. By using identical track-etched membranes at different pore sizes (0.1, 0.2, and 0.4 μm), Chen (1998) observed that the measured critical flux increased as the pore size of the membrane increased. Also, it was noticed that the critical flux increased slightly as the porosity increased four times (from 2% to 8%) for the 0.2 μm membranes used for filtration tests.

In addition, a comparison study of membrane morphology between 0.22 μm PVDF membranes with isotropic nature (hydrophilic and hydrophobic types) and 0.2 μm track-etched membranes (capillary-pore) was conducted. It was observed that higher critical fluxes were reached as a result of the isotropic nature of PVDF membranes, hence lower resistances, compared to the track-etched membranes (with capillary-pore). However, the critical flux values remained the same at different hydrophobic values of PVDF membranes. Madaeni (1999) observed that the critical flux values became insignificantly lower for hydrophobic membranes, indicating slight hydrophobic interactions between particle and membrane.

For the ultrafiltration of BSA, Silica X30, and yeast suspensions using PES membranes, *Wu et al.* (1999) noticed that the critical flux decreased as the membrane cut-off increased from 50 to 100 kDa. However, Madaeni (1999) observed that the critical flux was the same for different pore size membrane during the microfiltration of activated sludge. Similarly, *Kwon et al.* (2000) noticed that the critical flux values were the same for the different membrane sizes (0.1, 0.2, 0.45, and 0.65 μm) during the microfiltration of 0.816 μm latex particles.

Hence, they claimed that as a result of operating all filtration tests in the controlled flux mode, the net convective drag force remained similar for all tests despite the pore size.

With respect to the influence of the membrane surface (hydrophilic or hydrophobic) and membrane cleaning on critical flux, Manttari and Nystrom (2000) demonstrated that no effects were observed on the measurement of critical flux. During ultrafiltration of baker's yeast, Metsamuuronen *et al.* (2002) observed that critical flux values were greatly lower for a polysulfone membrane (hydrophobic) compared to a cellulose membrane (hydrophilic). They linked this difference in the critical fluxes to the hydrophobic interactions at different pH values 3, 4 and 6. The measured zeta potential for polysulfone membrane (hydrophobic) is found to be highly positive at pH 3, and diminishes to zero at pH 6. Whereas over this pH range, the measured zeta potential for cellulose membrane (hydrophilic) remained constant at a value near to zero. For both membranes, the measured critical flux values were lowest at pH 4 and also the IEP of baker's yeast was at pH 4. Hence, this confirmed that the critical flux is controlled by the particle-particle interaction (electrostatic) rather than the particle-membrane interaction, especially when the measured zeta potential of both membranes was zero at pH 6.

On the other hand, Huisman *et al.* (1999) conducted an experimental investigation on the influences of both the membrane zeta potential and the particle zeta potential on the measured critical flux during crossflow microfiltration of silica suspension. Despite using three different membrane materials (titania, zirconia, and α-alumina) having the same cut-off, they observed that the critical flux values were influenced only by varying the hydrodynamic parameters and feed suspension's concentration. No effect on the critical flux was noticed by changing either the zeta potential of the membrane or the zeta potential of the silica particles. Likewise, Persson *et al.* (2001) demonstrated that the zeta potential of the ceramic membrane had no influence on the critical flux values during microfiltration of bacteria from fermentation forth.

2.10 Crossflow Microfiltration Theory

Microfiltration is a pressure driven process where the filter acts as a barrier for size-exclusion. Due to the pressure gradient across the membrane, the particles are transported convectively towards and accumulate on the membrane surface. Eventually a condition occurs that the retained particles form a distinct cake layer that produces considerable resistance to the permeate flux. As the resistance to filtration increases, and the filtration rate decreases. As result of back transport mechanisms, particles may move back diffuse into the bulk solution. The permeate flux reaches its steady state condition when the rate of particles being deposited at the membrane is balanced by the rate of back diffusion, as illustrated in Figure 2.6.

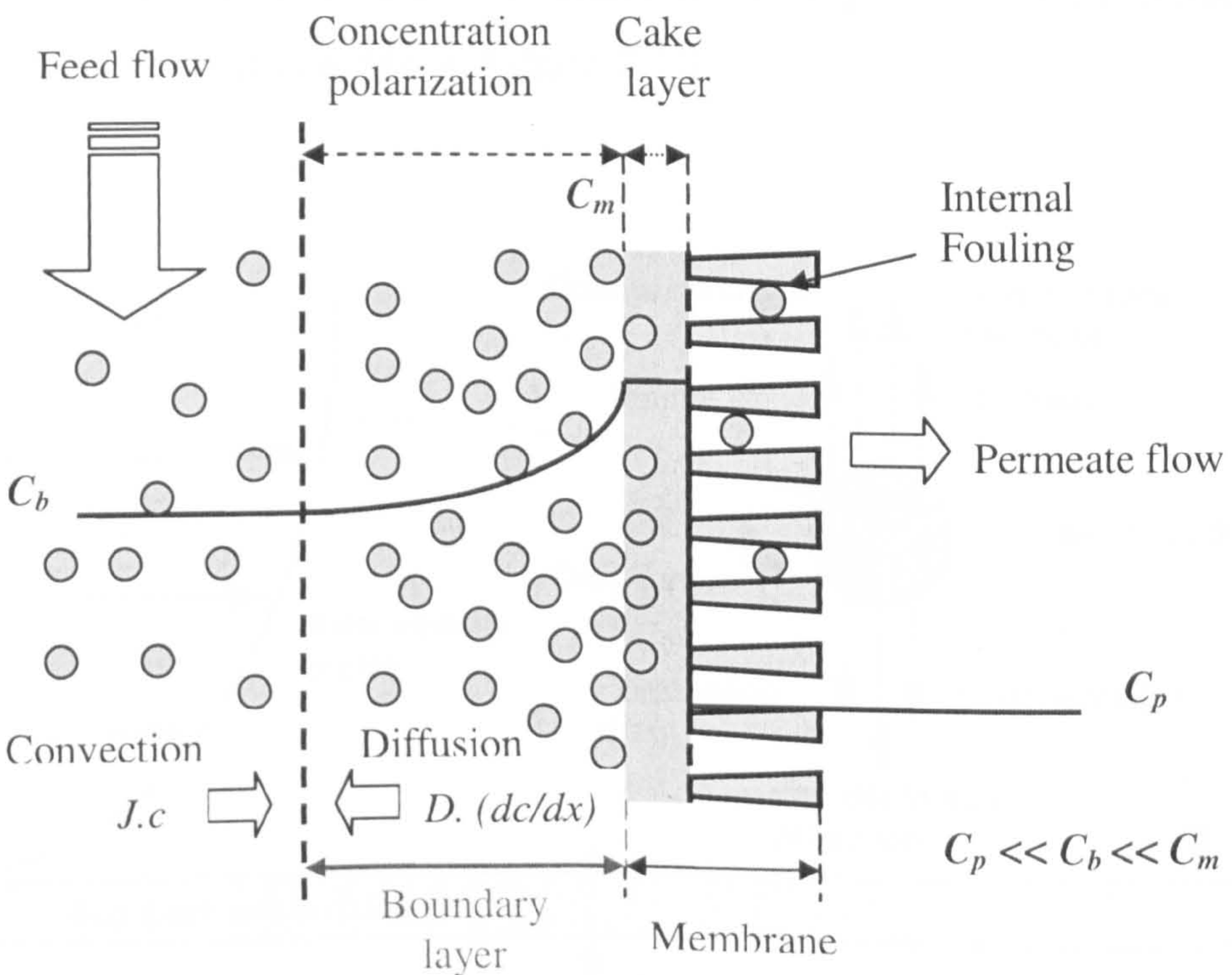

Figure 2.12 Concentration polarization and cake formation during crossflow filtration.

2.11 Modelling of Permeate Flux Behaviour

In crossflow filtration, the bulk suspension flows tangentially to the membrane surface, applying high shear at the surface that hinders the accumulation of a cake layer. Consequently, the cake film stays thin, assuring higher permeate fluxes over extensive periods. Formation of a cake layer on the membrane surface is considered a major limiting element for the broader application of microfiltration (Belfort *et al.*, 1994).

Modelling research has focused on a variety of mechanisms by which the tangential shear prevents cake layer expansion, leading to different models for predicting the permeate flux. Several mechanisms such as Brownian diffusion, shear induced diffusion, inertial lift forces, and torque-balance models have been proposed to account for such back transport. A review is presented here of the models that predict steady-state permeate flux during crossflow microfiltration. A summary diagram of all forces that could be acting on spherical particle during crossflow filtration is presented in Figure 2.13.

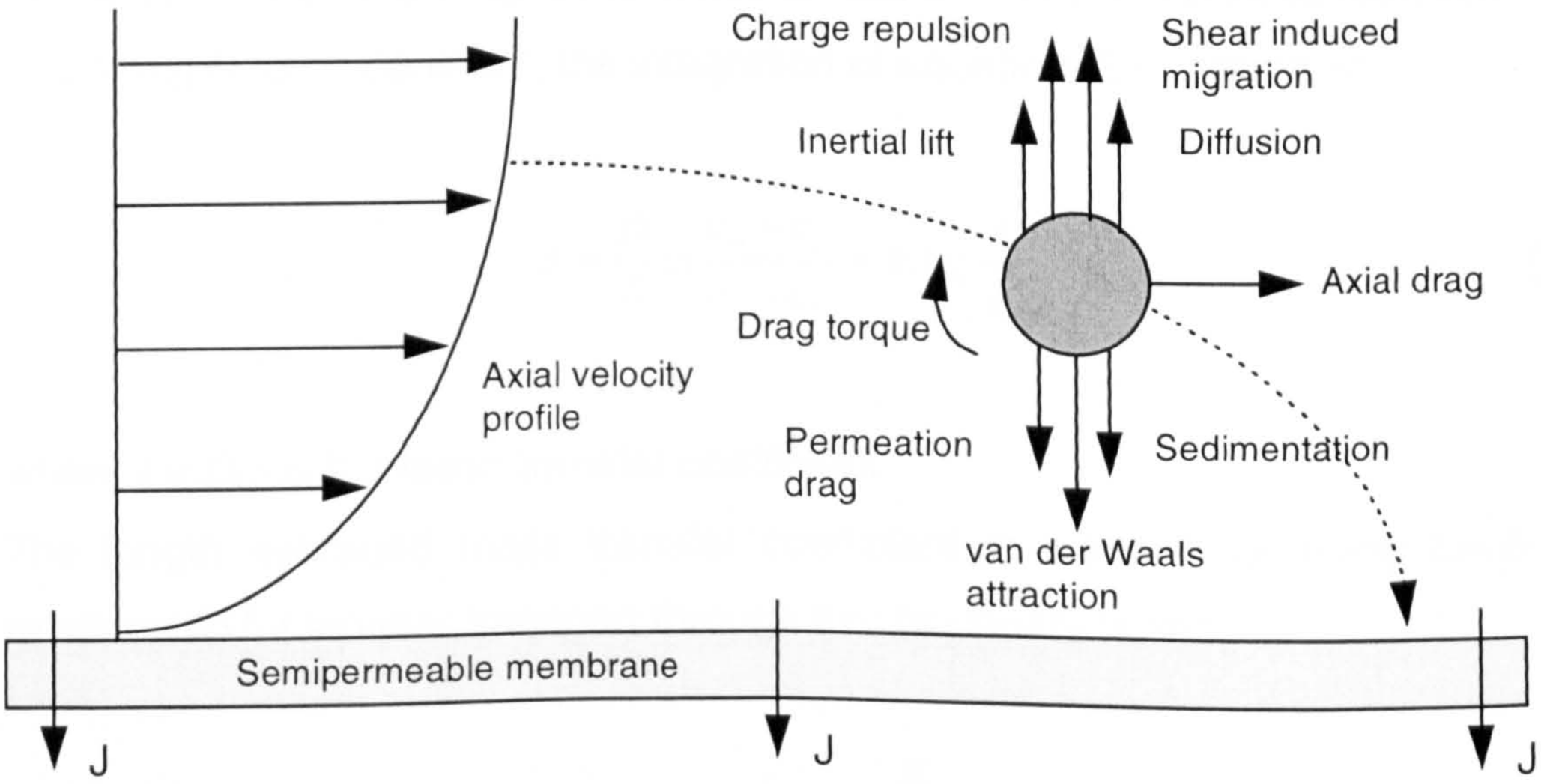

Figure 2.13: Forces and torques acting on a charged, spherical particle suspended in a viscous fluid undergoing laminar flow in the proximity of a flat porous surface.

2.10.1 Film Theory Model

The film theory model is the simplest and most broadly employed model for predicting permeate flux. The concept behind this model is that a thin film will be formed as a result of the retained solute build up at the membrane surface. When the permeate flux reaches the steady state condition, an equilibrium has been established between the convective suspension flow through the membrane and the diffusive flow back to the bulk feed due to the concentration differential (Mulder 1991).

The equation demonstrating film theory is:

$$J.c + D.\frac{dc}{dx} = J.c_p \qquad (2.6)$$

where c and c_p is the solute concentration in feed and permeate, and D is diffusivity. The boundary conditions are

$$x = 0,\ c = c_m \text{ and } x = \delta,\ c = c_b$$

where δ is the boundary film thickness, c_m is the solute concentration at the membrane surface, and c_b is the solute concentration in the bulk suspension.
Assuming D to be constant, the integration of equation (2.6) results in

$$J = \frac{D}{\delta}\ln\frac{c_m - c_p}{c_b - c_p} = k.\ln\left(\frac{\phi_c}{\phi_b}\right) \qquad (2.7)$$

where $k = D/\delta$ is the mass transfer coefficient.
The length averaged mass transfer coefficient is worked out using Lévêques' relationship for laminar transport through thin boundary layers:

$$\langle k \rangle = 0.807\left(\frac{\gamma D_P^{\ 2}}{L}\right)^{1/3} \qquad (2.8)$$

where <*k*> is the averaged mass transfer coefficient, L is the channel length, D_P is particle diffusivity, and γ the shear rate in the boundary layer. Combining Equations (2.7) and (2.8) leads to

$$\langle J \rangle = 0.807 \left(\frac{\gamma D_P{}^2}{L} \right)^{1/3} \ln \frac{\phi_c}{\phi_b} \tag{2.9}$$

where $\langle J \rangle$ is the length-averaged permeate flux.

The diffusion coefficient has been generally approximated by the Stokes-Einstein equation presented in equation (2.10) that relates particle transfer from high to low concentration (away from the membrane) due to kinetic interactions between the colloidal particles and molecules of the solvent.

$$D_{BD} = \frac{k_B T}{6\pi\mu a} \tag{2. 10}$$

where D_{BD} is the Brownian diffusivity, k_B is the Boltzmann constant, T is the absolute temperature, and a is the particle radius. Hence, the film model will be expressed in terms of fluid properties as shown below;

$$\langle J \rangle = 0.807 \left(\frac{\gamma D_{BD}{}^2}{L} \right)^{1/3} \ln \frac{\phi_c}{\phi_b} \tag{2.11}$$

The Peclet number has been used to describe the balance of convection to back diffusion for the film model.

$$Pe = \frac{J\delta}{D} = \frac{J}{k} \tag{2.12}$$

Despite the fact that the prediction of the permeate flux by using the film model gives good results with sub-micron sized particles, it underestimates the flux when larger (micron sized) particles are considered. This discrepancy was described by Green and Belfort (1980) as the "flux paradox" and credited to several further mechanisms. Some of the mechanisms that have been proposed to provide an explanation of such dissimilarity will be discussed here.

2.10.2 Resistance Model

According to Darcy's relationship, the permeate flux is directly proportional to the transmembrane pressure and inversely proportional to the solution viscosity and the filtration resistances due to the clean membrane (R_m), cake formation (R_c), concentration polarization (R_{cp}), and internal fouling (R_{if}) as shown in Figure 2.12.

$$J = \frac{\Delta P}{\mu(R_t)} = \frac{\Delta P}{\mu(R_m + R_c + R_{cp} + R_{if})} \tag{2.13}$$

The resistance due to a cake formed on the membrane surface can be determined for a model incompressible cake using the Carman-Kozeny equation

$$R_c = \frac{45\,(1-\varepsilon_c)^2\,\delta_c}{\varepsilon_c^3\,a^2} \tag{2.14}$$

where ε_c is cake porosity, δ_c is the cake thickness, a is the particle radius. The cake porosity can be computed empirically or estimated geometrically from sphere packing models.

2.10.3 Inertial Lift Model

In order to explain the observed the "flux paradox", Green and Belfort (1994) put forward a model that considered a lateral migration of particles away from the membrane wall due to inertial lift enhancing the back diffusion. This model is based on particle migration across the fluid streamlines as they interact with the surrounding laminar velocity distribution. The significant velocity variation across the particle induces rotary motion and causes it to move away from the membrane by the Magnus effect. The inertial lift input to the relocation of particles can be estimated using

$$J_{IL} = 0.036\frac{\rho_0 a^3 \gamma_m{}^2}{\mu} \tag{2.15}$$

This mechanism demonstrated the sensitive relationship between flux, the particle size (a^3) and the shear rate ($\gamma_m{}^2$).

2.10.4 Shear-induced diffusion Model

Zydney and Colton (1986) have used the shear induced diffusion as the main mechanism responsible for particle back transport instead of Brownian diffusion. As a result of the concentration of particles near the membrane surface, numerous collisions will be occurring between the particles, but fewer collisions will occur at greater distances away from the membrane. Hence, as a result of their net momentum being directed away from membrane the particles move away to the bulk stream as the shear rate increases. Such particle back transport could be accounted for by including the shear induced coefficient. Davis and Sherwood (1990) had conducted numerical calculations of shear-induced diffusion for low particle concentrations and ϕ_{max}= 0.58, resulting the expression

$$J = 0.060 \frac{\tau_w}{\mu_0} \left(\frac{a^4}{\phi_b L} \right)^{1/3} \tag{2.16}$$

Romero and Davis (1988) evaluated analytically the limiting flux by using the shear induced diffusion coefficient, which is valid for ϕ_b < 0.2 , as given by the following equation:

$$J = 0.060 \frac{\tau_w}{\mu_0} \left(\frac{a^4 (1 - 3.8\phi_b)}{\phi_b L} \right)^{1/3} \tag{2.17}$$

2.10.5 Critical Flux Estimation by Shear Induced Diffusion Model

Davis and Leighton (1987) employed a similar process to the gel layer model for concentration polarization to hypothesize that permanent particle deposition on the membrane surface will take place beyond a certain distance from the feed entry point of the module, x_{cr}. As long as the effective viscosity of the suspension in the concentration polarised layer is low enough so that the existing shear flow is able to sweep the particles downstream, the membrane surface remains clean. The local concentration, and hence the local viscosity, increases along the length of the membrane until a critical distance x_{crit} from the membrane entrance. At this distance the shear flow is no longer able to sweep downstream all of the deposited particles, and permanent particle deposition on the membrane surface occurs at

$x \geq x_{crit}$. The model uses a shear induced hydrodynamic diffusivity rather than the Stokes-Einstein diffusivity.

If the main particle back transport mechanism is shear-induced diffusion, then x_{cr} is given by:

$$x_{cr} = 1.0 \times 10^{-4} \frac{\tau_w^3 a^4}{\phi_b \mu_p^3 J_w^3} \tag{2.18}$$

where ϕ_b is the volume fraction of particles in the bulk and a the particle radius. At the critical flux, x_{cr} will be equal to the membrane length. This hypothesis means that at J_{crit}, $x_{crit} = X$, where X is the length of the membrane. Substituting for x_{crit} and solving for J_{crit} gives:

$$J_{crit} = \frac{\tau_w}{\mu_p}\left(\frac{1 \times 10^{-4} a^4}{\phi_b X}\right)^{1/3} \tag{2.19}$$

2.10.6 Surface Transport Model

The previous models discussed were based on the assumption that the cake layer being stagnant. Nevertheless, a number of studies have proposed that particles roll or slip alongside the membrane surface (Green and Belfort ,1994, Lojkine *et al.*, 1992). The fundamental idea of the surface transport model is to take into account the force balance for a globular particle and find out whether it will attach or detach and move along the membrane surface (Belfort et al 1994). The steady state flux of this mechanism could be determined using

$$J_{STM} = 2.4 a \gamma_m (a^2 \hat{R}_c)^{2/5} \cot\theta \tag{2.20}$$

where θ is the angle of repose that depends on the membrane surface morphology.

2.10.7 Bacchin Model for Colloidal Deposition Rate

A deposition rate model was established by Bacchin *et al.* (1995) based on the net continuity of mass flux (convective, diffusive, and interactive) and using a boundary condition of an ideal sink at the film surface. The principal hypothesis is that all particles coming to rest on the surface are rapidly grabbed and vanished from the system. These models describe the change of the mass transfer (fouling rate) with operating conditions.

Bacchin et al. (1995) developed this model to describe the deposition on a membrane surface responsible for surface interactions. The model is a mass transfer equation that relates the fouling rate to hydrodynamic conditions (permeate flux and crossflow velocity across the boundary layer thickness) and suspension surface properties. Operating conditions are explained through a Peclet number uniting in one term both the influence of permeation and tangential flow, and in a second term suspension stability. A critical Peclet number (Pe) is then described to be bounded by the fouling and no fouling regions (Bacchin et al., 2006):

$$Pe_{crit} = \frac{J_{crit}\delta}{D_0}\ln\left(\frac{V_B}{\delta}\right) \tag{2.21}$$

where D_0 is the diffusivity at infinite dilution, V_B is the potential barrier due to the repulsive interaction between particles (DLVO theory), δ is the boundary layer thickness for mass transport generated by the tangential flow. For microfiltration and ultrafiltration of colloidal particles, the critical flux could be predicted using this model:

$$J_{crit} = \frac{D}{\delta}\ln\left(\frac{V_B}{\delta}\right) \tag{2.22}$$

During this model evolution, Bacchin et al. (1995) represented the Sherwood number as a function of the potential barrier and Peclet number

$$Sh = \frac{1}{\left(\frac{V_B}{\delta}\right)e^{-Pe} + \frac{1}{Pe}(1+e^{-Pe})} \tag{2.23}$$

Also, the stability of a single particle (W_d) was defined in relation to deposition onto the membrane surface by:

$$W_d = 1+\left(\frac{V_B}{\delta}\right) \tag{2.24}$$

This eqaution decribes a standard for the effectiveness of both the potential barrier(V_B) and the hydrodynamics (δ) in stopping particle deposition over the membrane surface.

Connecting the previous two eqaution gives:

$$Sh = \frac{1}{(W_d - 1)e^{-Pe} + \frac{1}{Pe}(1+e^{-Pe})} \tag{2.25}$$

By using this equation, Bacchin *et al.*(1995) outlined zones in which particle deposition would be favourable or unfavourable. Three regions were classified as follows: adsorption, dead end filtration, and no fouling conditions with a transition region between them. These regions show the comparative significance of convection and particle-particle interaction in relation to the particle deposition and fouling. For example, at high diffusivity (small Pe) and small potential barrier (low W_d) the predominant mechanism would be adsorption. In addition, they provided a correlation for the stability ratio for coagulation:

$$W_c = 1+\left(\frac{V_B}{2a}\right) \tag{2.26}$$

where a is the radius of the particle, and W_c is a measure of the probability of the potential barrier to prevent coagulation. As stated by Bacchin et al. (1995), a system becomes stable (slight coagulation) if W_c > 10,000. While the system becomes unstable (quick coagulation) if W_c = 1.

2.10.8 Song and Elimelech Model (SEM)

Song and Elimelech (Song, 1995) developed a novel theory for concentration polarization of non-interacting particles in crossflow filtration systems. This hypothesis showed a dimensionless number (N_F) that can characterize the extent of concentration polarization and the behaviour of the permeate flux. The definition of N_F is given by:

$$N_F = \frac{4\pi a_p^3}{3kT}\Delta P_P \qquad (2.27)$$

N_F is the ratio of the energy needed to bring a particle from the membrane surface to the bulk suspension to the thermal (dissipative) energy of the particle. A larger value of N_F indicates that more energy is needed to bring a particle from the membrane surface to the bulk suspension.

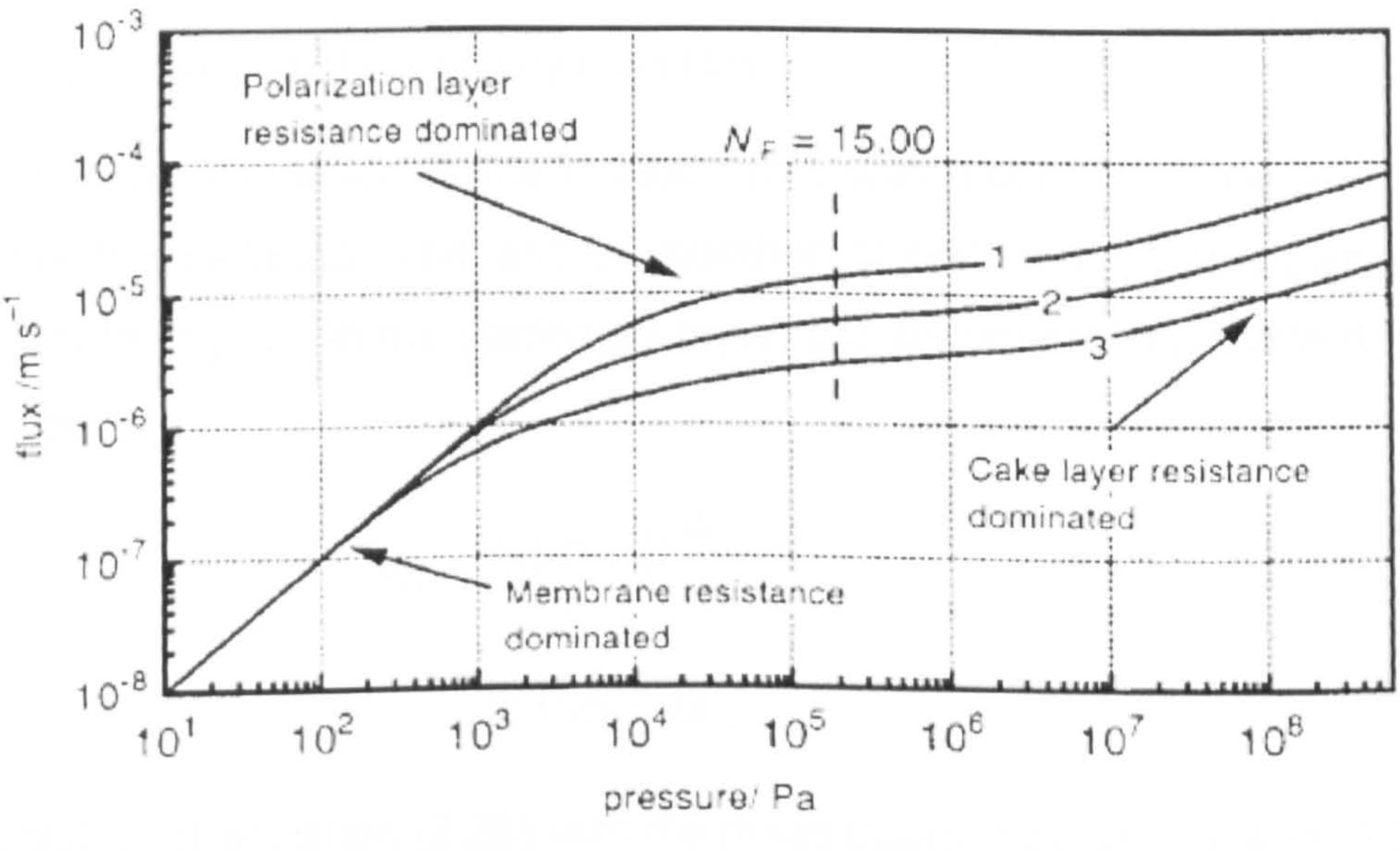

Figure 2.14: 'The complete filtration curve': permeate flux as a function of applied pressure for (bulk) concentration (Song, 1995).

For a particular suspension at specified operational conditions, there would be a critical value of the filtration number. Once the filtration number is below the critical

value, a polarization layer is present directly above the membrane surface and the wall particle concentration is governed by the pressure and temperature. At higher filtration numbers i.e. when $N_F > N_{CF}$ (=15.00), a cake layer forms between the polarization layer and the membrane surface. Thus, the complete filtration curve could be divide in three regions as shown in Figure 2.14.

A numerical model was constructed by Song and Elimelech (1995) for predicting permeate flux in both the concentration polarization and the cake formation regions, and analytical solutions for the permeate flux were derived. A development of this novel theory was described comprehensively including the mathematical derivations of the SEM model from various fundamental principles (Song, 1995). These principles, involved in the crossflow filtration, are hydrodynamic, which explain the flow field and drag force, and thermodynamic, that governed bulk properties of particle suspension. Hence, a summary of SEM model development from basic theory is revealed here with specified assumptions to construct this novel model.

(a) Particle concentration polarization film

An additional resistance to the filtration rate was assumed to be only due to the accumulated particles. The excess number of particles in the polarization layer was denoted by C. In the stationary layer, the accumulated particle distribution is governed by;

$$v(x)\,C + D\frac{dc}{dy} = 0 \tag{2.28}$$

$$\int_0^{\infty} C\,dy = M_p \tag{2.29}$$

The solution of equation (2.28) with the mass balance condition (eqn.(2.29)) is

$$C = \frac{M_p v(x)}{D}\exp[-v(x)\,y/D] \tag{2.30}$$

where $v(x)$ is the permeate velocity, D is the diffusion coefficient, and M_p is the total number of excess particles accumulated over a unit membrane surface area

and is determined as follows.

(b) Particle-flux conservation

At steady state, the particle flux along the channel is constant, where the flux conservation relationship is described by:

$$\int_0^\infty uCdy + \overline{u}C_0B = \overline{u}_0C_0B \tag{2.31}$$

where u is the axial fluid velocity in the polarization layer, $\overline{u}$ is the average crossflow velocity, $\overline{u}_0$ is the average inlet velocity of fluid (at $x = 0$), and B is the channel height.

Substituting equation (2.30) into equation (2.31) and solving the resulting equation for M_p at position x, yields

$$M_p = \frac{C_0}{D\gamma} v(x) \int_0^x v(x')\, dx' \tag{2.32}$$

To reach the above solution, γ is the shear rate of the axial flow and is determined by:

$$u = \gamma y \tag{2.33}$$

By using it in solving for equation (2.32), the mass balance of the fluid is:

$$(\overline{u}_0 - \overline{u})\, B = \int_0^x v(x')\, dx' \tag{2.34}$$

Inserting equation (2.32) into equation (2.30) gives the particle concentration distribution in the channel:

$$C = \frac{C_0}{D\gamma}\left[v(x)^2 \int_0^x v(x')\, dx'\right] \exp[-v(x)\, y / D] \tag{2.35}$$

It appears from equation (2.35) that the wall concentration (i.e. at $y = 0$) is strongly

dependent on the permeate velocity. Nevertheless, it is primarily dependent on thermodynamic variables which will be discussed later. With the assumption that the filter is under ideal filter condition, the expression in first square bracket in equation (2.35) will become constant (Song and Elimelech, 1995). This implies that the wall concentration is not influenced by the permeate velocity.

(c) Crossflow filtration equation

The pressure drop across the accumulated particle layer, ΔP_p, is estimated from

$$\Delta P_p = \int_0^{\delta} F\, C\, dy \qquad (2.36)$$

where F is the drag force exerted by an immobile retained particle on the permeate flow and δ is the thickness of the accumulated particle layer. The product of the membrane resistance and the permeate velocity represents basically the pressure drop across the membrane. Thus, the overall applied pressure would be the sum of both resistances as shown in the relationship:

$$\Delta P = \lambda\, v(x) + \int_0^{\infty} \left[\frac{kT}{D} A_s\, v(x) \right] C\, dy \qquad (2.37)$$

where ΔP is the transmembrane pressure, λ is the membrane resistance, k is the Bolzmann constant, T is the absolute temperature and A_s is the correction factor for Stokes' law. The expression in square brackets of equation (2.37) stands for the drag force applied by a stationary held particles on the permeate flow. It was derived from Einstein-Stokes' law, and combined with Happel's cell model to account for the influence of neighbouring particles held at the membrane surface.

Within the concentration polarization layer of crossflow filtration, where particle concentration is high, the drag force applied by a particle on the fluid diverges considerably from Stokes' law. Thus a new correlation for a correcting function (A_s), was introduced into Stokes' law. Happel's cell model is used to find A_s;

$$A_s = \frac{1+\frac{2}{3}\theta^5}{1-\frac{3}{2}\theta+\frac{3}{2}\theta^5-\theta^6} \tag{2.38}$$

where $\theta=(1-\varepsilon)^{1/3}$ is a porosity(ε) dependent parameter and is correlated to the number particle concentration:

$$\theta = \left(\frac{4}{3}\pi a_P^3 C\right)^{1/3} \tag{2.39}$$

Rearranging equation (2.39) to $C = \frac{3\theta^3}{4\pi a_p^3}$, and inserting it in equation (2.28) to get

$$v(x)C\,dy = -\frac{9D}{4\pi a_p^3}\theta^2\,d\theta \tag{2.40}$$

Then by replacing equation (2.40) in equation (2.37) and altering the corresponding integration limits, one obtains the following governing equation for the permeate velocity in crossflow filtrations systems:

$$\Delta P = \lambda v(x) + \frac{kT}{D}\frac{3D}{4\pi a_p^3}\int_0^{\theta w} A_s(\theta)3\theta^2\,d\theta \tag{2.41}$$

where θ_w is the value of θ at the membrane surface and is estimated by substituting equation (2.40) into (2.37) and allowing $y = 0$ which give:

$$\theta_w = \left[\frac{4\pi C_0 a_p^3}{3D^2\gamma}v(x)^2\int_0^x v(x')\,dx'\right]^{1/3} \tag{2.42}$$

(d) Solution of the crossflow-filtration eqaution

To solve the crossflow filtration equation, the mean volume theorem is applied to equation (2.41) and inserted onto equation (2.42) to the form:

$$\Delta P = \lambda v(x) + \frac{kTC_0}{D^2\gamma}A_S(\theta^*)\,v(x)^2\int_0^x v(x')\,dx' \tag{2.43}$$

where $0<\theta^*<\theta_w$. Defining new term $\beta = \frac{kTC_0A_S(\theta^*)}{D^2\gamma}$, then rewriting equation (2.43) to get:

$$\Delta P = \lambda v(x) + \beta v(x)^2 \int_0^x v(x')\,dx' \tag{2.44}$$

By additional derivation steps and setting boundary conditions, the permeate velocity in crossflow filtration can be expressed generally as

$$v(x) = \frac{\Delta P}{(\lambda^3 + 6\beta\Delta P^2 x)^{1/3}} \times \left\langle \left\{ \left[\lambda^3 / (\lambda^3 + 6\beta\Delta P^2 x) + 4 \right]^{1/2} + 2 \right\}^{1/3} - \left\{ \left[\lambda^3 / (\lambda^3 + 6\beta\Delta P^2 x) + 4 \right]^{1/2} - 2 \right\}^{1/3} \right\rangle \tag{2.45}$$

The average permeate flux, V, is a significant variable which is used to illustrate the behaviour of crossflow filtration systems. The average flux can be evaluated from

$$V = \frac{1}{L} \int_0^L v(x)\,dx \tag{2.46}$$

where L is the channel length.

The integral term can be determined from equation (2.45), and so the expression of average permeate flux becomes

$$V = \frac{\Delta P}{L\beta v(x)^2} \left[1 - \frac{\lambda}{\Delta P} v(L) \right] \tag{2.47}$$

With assumption of an ideal filter case, the concentration polarization is fully developed and the filter resistance is caused predominantly by the retained particle layer. For the case where the membrane resistance is negligible (*i.e.* $\lambda \to 0$), equation (2.45) and (2.46) can be reduced to

$$V = \left(\frac{3}{2}\right)^{2/3} \left[D^{2/3} \gamma^{2/3} L^{-1/3} \right] \left(\frac{\Delta P_p}{A_S(\theta^*_{\max}) kTC_0} \right)^{1/3} \tag{2.48}$$

Accordingly, the equation for determination of average permeate flux which was developed for the case of cake formation ,i.e. $N_F > N_{CF}$(=15.00), is

$$V = (\frac{3}{2})^{2/3}\left[D^{2/3}\gamma^{2/3}(1+N_c)^{1/3}L^{-1/3}\right]\left(\frac{\Delta P_p}{A_S(\theta^*_{\max})kTC_0}\right)^{2/3} \quad (2.49)$$

Most parameters introduced in the previous equations need more explanation and clarification of the terminology used. Hence, a comprehensive description will be provided for the Song and Elimelech model at the determination steps section in Chapter 6.

CHAPTER 3

CASE STUDY: AGISH WASTEWATER TREATMENT AND PRODUCED WATER RE-INJECTION

Confidentiality Statement

The case study was chosen to represent an existing industrial plants used for treatment and injection of produced water. Data is a real analysis data collected from an industrial company for one year operation. For data confidentiality and protection, the names of the company and the treatment plants were kept secret and instead arbitrary names were given. This has been done with agreement with the industrial company body.

3.1 Wastewater Treatment Plant

The crude oil which is generated from the Agish reservoir has an amount of produced water, which is removed from the crude oil by various methods of separation at the gathering centres (GC-1, GC-2 and GC-3) and then gathered in a balance tank at each GC. A pumping system transports the effluent (or "produced") water through a pipeline system to a balance tank at the Agish water injection plant (AWIP). Due to the increase of produced water during oil production in Kuwait, a waste water plant had been established at Agish and commissioned in 2004 so that it could be used for produced water re-injection purposes. It estimated that oil wells in Kuwait produce 15 to 40 % of produced water.

The waste water treatment unit in Kuwait consists of a waste water surge tank, oily water treatment, and an oil drum. The oily water treatment comprises of a parallel/corrugated plate separator and an induced gas flotation. An overview of the plant is demonstrated in Figure 3.1. The flow rate of water to be treated per train is 50,000 BPD (Barrels/day) with a temperature range from 25 to 65 °C and it's expected characteristics are shown in Table 3.1. The main objective of this treatment train is to reduce the oil in water parameter to 10 ppm, which is the maximum allowable concentration for re-injection and disposal.

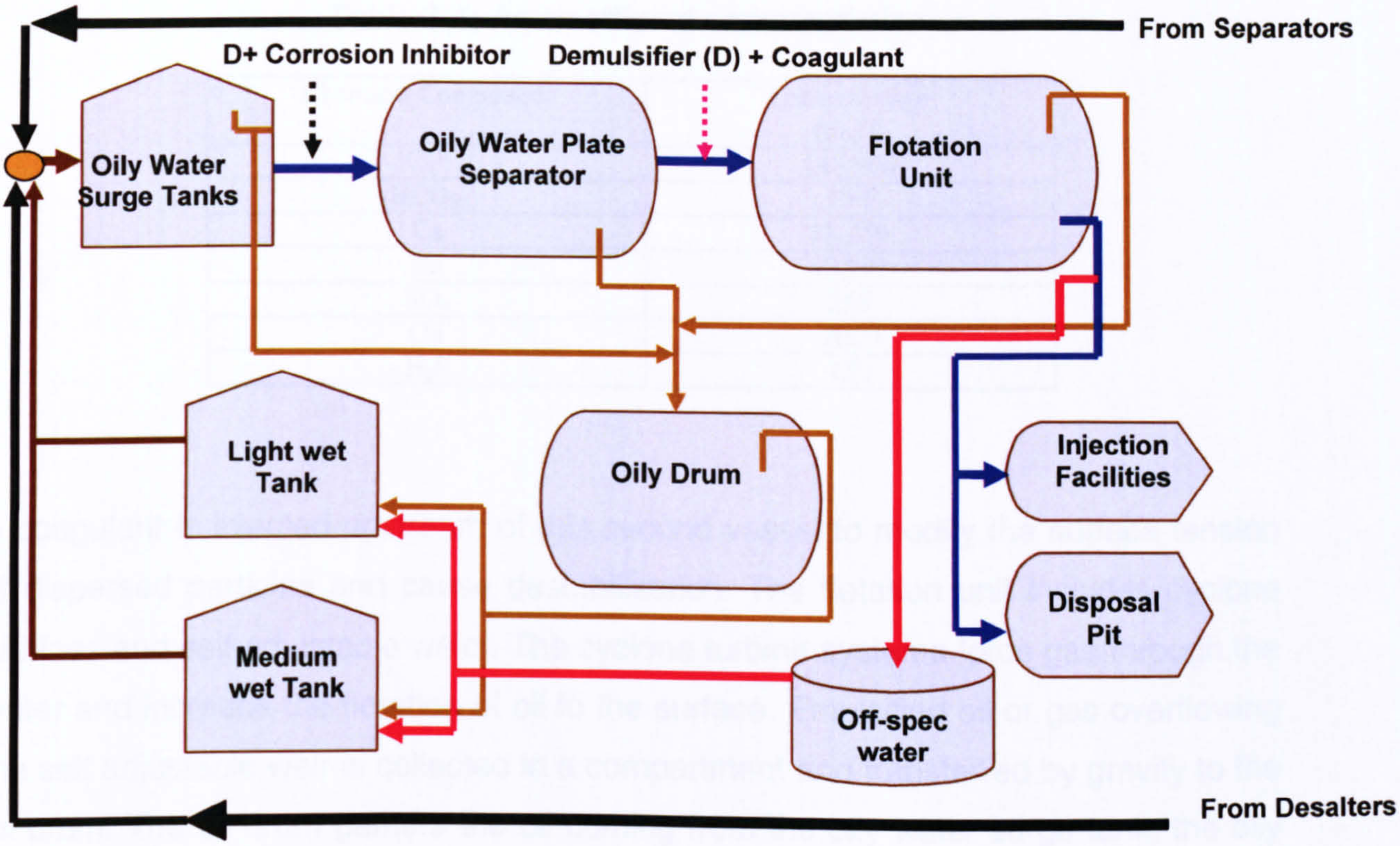

Figure 3.1: Waste water treatment plant overview.

Waste water to be treated is distributed from an oily water surge tank installed downstream of desalters and oil separators. This tank's residence time is about 2 hours. A demulsifier as well as a corrosion inhibitor is injected upstream of the oily water plate separator. The major part of the oil and suspended solids will be removed in the parallel/corrugated plate separator. The oily water will be separated according to the densities of its components. The oil droplets float on the surface and suspended solids settle. The vessel is equipped with an isophthalic plate helping the oil droplets to coalesce and float. A retention time of about 7 minutes eliminates droplets having a diameter more than 60 µm. Sludge settles to the bottom of the unit. Hydrocarbons accumulated on the surface are recovered automatically by a rotating oil drum skimmer or other automatic system. The oil is discharged by gravity to an oil drum. The oil-water separation is achieved in the flotation unit.

Table 3.1: Agish effluent characteristics.

Chemical Component	Concentration (mg/l)
Cl^-	145,900
HCO_3^-	196
Ca	23,250
Na	42,191
SO_4	256
Oil	2000
H_2S	150

A coagulant is injected upstream of this second vessel to modify the surface tension of dispersed particles and cause destabilization. The flotation unit includes cyclone turbines and self adjustable weirs. The cyclone turbine systems force gas through the water and increase the flotation of oil to the surface. Emulsified oil or gas overflowing the self adjustable weir is collected in a compartment and transferred by gravity to the oil drum. The oil drum gathers the oil coming from the oily water surge tank, the oily plate separator and from the flotation unit. The flotation unit is a six compartment vessel including 4 flotation cells, inlet and outlet compartments, and two scum collecting pits. A summary of the Agish crude oil properties for GC-1and GC-2 during summer and winter seasons is presented in Table 3.2. It is noted that MCO stands for Medium Crude Oil while LCO stands for Light Crude Oil.

Table 3.2: Agish crude oil properties.

Gathering Centers	Parameters	Summer		Winter	
		LCO	MCO	LCO	MCO
GC-1	Temperature	58°C (136.4°F)	52°C (125.6°F)	29°C (84.2°F)	28°C (82.4°F)
	Spec. Gravity	0.836 (38° API)	0.897 (26° API)	0.8518 (35° API)	0.911 (24° API)
	Viscosity	3.8 cP	33.2 cP	7.82 cP	108 cP
GC-2	Temperature	62°C (143.6°F)	53°C (127.4°F)	32°C (89.6°F)	27°C (80.6°F)
	Spec. Gravity	0.814 (42°API)	0.873 (31°API)	0.830 (39°API)	0.888 (28°API)
	Viscosity	2.4 cP	17.46 cP	4.6 cP	53.3 cP

Produced water at Agish has an extremely high TDS value, 240,000 mg/L, which can form potentially large concentrations of scale products. These can block the pipe systems that transfer the effluent water. Therefore chemical dosing equipment has been designed to inject different chemicals to reduce these risks. The chemical injection facilities are identified at each gathering centre and are summarized in Table 3.3. Gathering centres effluents are chemically treated in order to control scale formation, corrosion, and bacteria growth on the pipeline system.

Table 3.3: Chemical injection systems of gathering centre effluents.

Chemical	Required Dosage (ppm)			Effluent Flow rate m^3/h (MBWPD) GC- 1	Effluent Flow rate m^3/h (MBWPD) GC- 2	Effluent Flow rate m^3/h (MBWPD) GC- 3
	MIN.	NORM.	MAX.			
Scale Inhibitor	15	15	30	662 (100)	1126 (170)	464(70)
Corrosion Inhibitor	25	25	30	662 (100)	1126 (170)	464(70)
Biocide A and B	200	200	500	662 (100)	1126 (170)	464(70)

3.2 Agish Water Injection Plant

The purpose of the plant is to receive effluent water from three gathering centres and inject it into the oil bearing reservoir in order to maintain the pressure in the reservoir and push the oil towards the producing wells. The amount of water required for injection is currently more than the amount of effluent available, so the difference is made up using aquifer water derived from local source wells. The effluent water and the aquifer are not chemically compatible, so the plant has been designed to inject them separately into dedicated wells.

The total injection capacity of the plant is 330,000 barrel water per day (bwpd) and allowance has been made in the plant design to expand the capacity by 30% in the future up to 429,000 bwpd. The average wellhead pressure is 2,500 psig. The bottom hole (or reservoir) pressure will be much greater than this because of the hydraulic pressure of the water in the well (Figure 3.2).

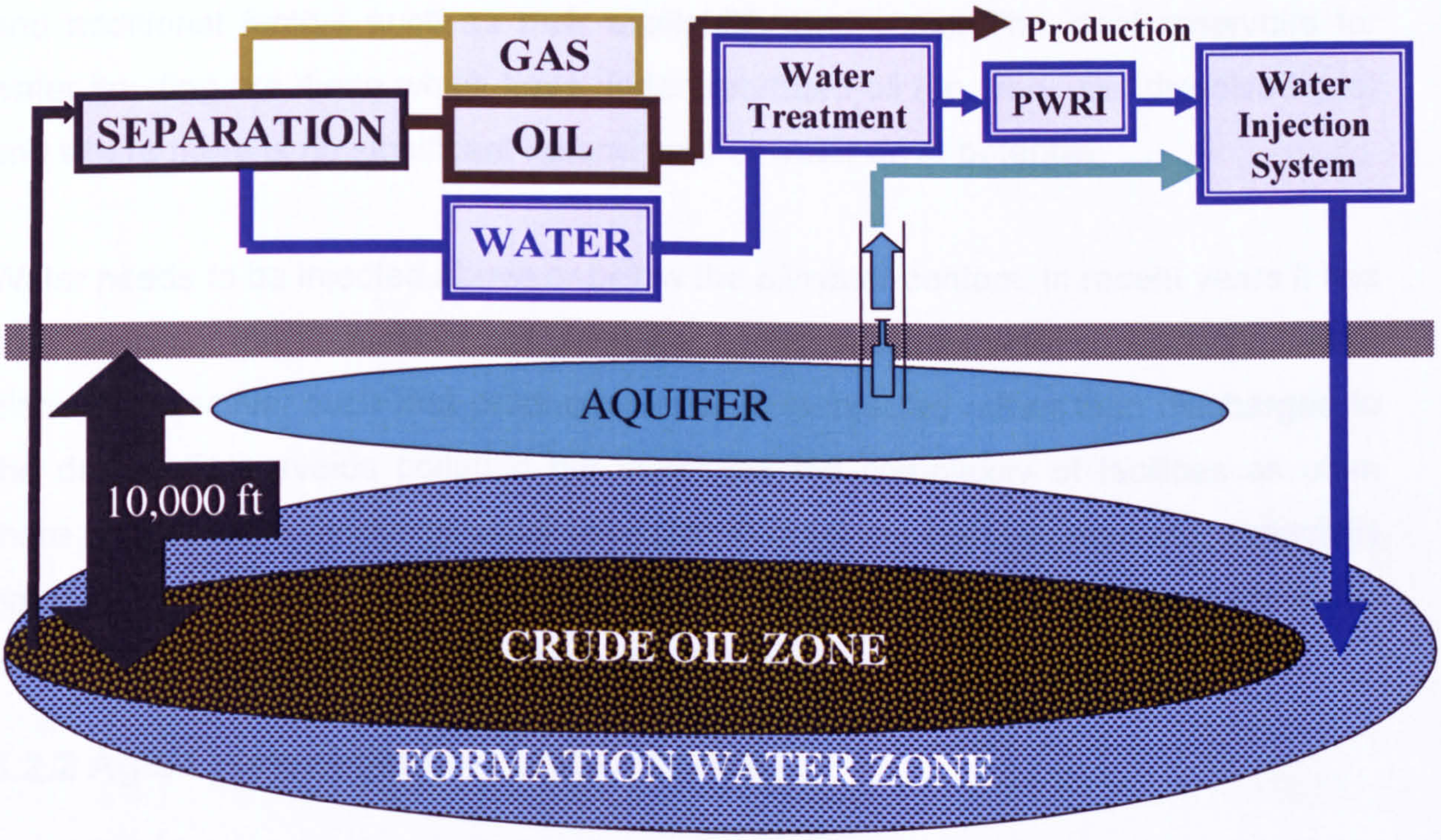

Figure 3.2: Systematic diagram of water cycle.

3.2.1 Water Injection Objective

The main objective of water injection or water flooding is to increase the efficiency of oil recovery from an oilfield or reservoir. Many oil reservoirs produce oil through wells due to natural forces driving oil into those wells and up to the surface production facilities, which is referred to as primary recovery. The three main driving forces are expansion of gas within a 'cap' above the oil layer, pressures of dissolved gas, and pressure and flow of water into the oil zone from aquifer under the oil layer.

These forces cannot sustain oil recovery for an indefinite period. Eventually the reservoir pressure will decrease to the "bubble point" when dissolved gas will come out of solution and start to hinder the passage of oil through the reservoir and into the production wells. The declining pressure then needs to be supplemented by imposing extra force, by means of gas or water injection. The choice of water or gas is also

dependent on factors such as reservoir geometry, permeability and fluid properties, and additional factors such as their availability and costs. The ideal reservoirs for water flooding are those which have under-saturated oil (i.e. very little dissolved gas) and where there is no significant natural aquifer water drive potential.

Water needs to be injected above or below the oil/water contact. In recent years it has also become more common to combine water injection with a produced water disposal objective, such that produced water is re-injected rather than discharged to the desert. This avoids pollution but increases the complexity of facilities as often there is insufficient produced water available to meet the injection demand, especially early in the field development. A dual system using both aquifer water and produced water is therefore required, as is the case at Agish.

3.2.2 Agish Water Injection Unit Overview

The major components of MWIP are effluent (D1) and aquifer (D2) waters balance tanks, and process pumps such as feed and injection pumps as shown in Figure 3.3.

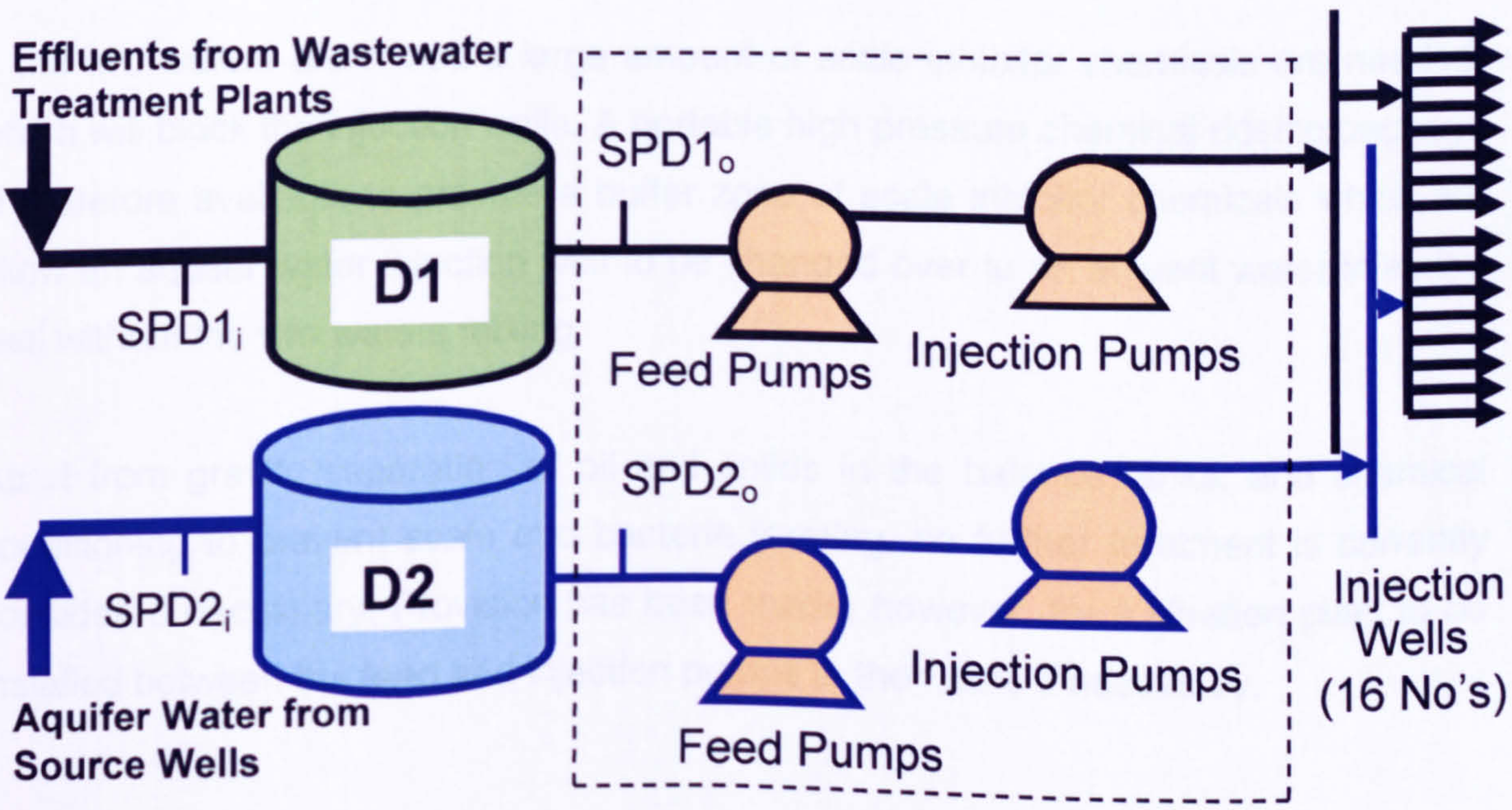

Figure 3.3 Systematic diagram of Agish water injection plant.

Both storage tanks are equipped with a floating oil skimmer that separates and drains off most of the floated oil, which then is transported to a recovered oil tank by gravity. Feed pumps provide the suction pressure (10 bar) to the water injection pumps, to increase the pressure further to reach the required injection pressure of 190 bar at each injection wellhead.

Effluent water from the gathering centres is collected in a balance tank which is supplied with a floating skimmer to remove any accumulated oil that may separate out by gravity. The water from the effluent water balance tank is piped to a number of booster pumps which supply high pressure injection pumps. These in turn pump the water through a series of pipelines to the effluent water injection wells.

Aquifer water (also known as "source") is pumped out of a number of source water wells connected to the Bair aquifer using electro-submersible down hole pumps (ESP's). The booster and injection pump manifolds have therefore been designed to allow more pumps to be changed over to injecting effluent water as the volume of effluent water supplied to AWIP increases with time.

If the two waters are mixed a large amount of scale inhibitor chemicals are needed, which will block the injection wells. A portable high pressure chemical dosing package is therefore available to provide a buffer zone of scale inhibitor chemicals which will allow an aquifer water injection well to be changed over to an effluent water injection well without the two waters mixing.

Apart from gravity separation of oil and solids in the balance tanks, and chemical conditioning to prevent scale and bacteria forming, no further treatment is currently considered necessary. Provision has been made, however, for a filtration plant to be installed between the feed and injection pumps in the future if necessary.

3.2.3 Agish Water Injection Specification

The following guidelines for injection water quality have been developed from a reservoir formation study, so that when the water is monitored and measured parameters lay outside the range specified, the control can be applied quickly. The effluent and aquifer water analyses are reported on Table 3.4 with respect to their desired and upper limit specifications for injection.

Table 3.4: Aquifer and oil field effluent water injection specification.

Parameter	Bair Aquifer water	Oil field Effluent Water	Desired Specifications for injection	Upper Limit For Injection
Particle Size Distribution (number of particles in 0.1 ml)				
1.5 Microns	7,566	3,519	-	-
2 Microns	3,298	1,400	-	-
3 Microns	745	576	-	-
5 Microns	117	175	120	200
8 Microns	22	50	25	75
10 Microns	5	4	10	25
12 Microns	1	16	1	20
15 Microns	0	7	0	10
20 Microns	0	0	0	0
Total	11,754	5,767	156	330
Total Dissolved solids (mg/l)	239,101	247,481	250,000	250,000
Turbidity (NTU)	ND	2.93	ND	ND
Total suspended Solids (mg/l)	0.49	3.99	0.50	5.00
Oil Free suspended Solids (mg/l)	NA	2.89	ND	ND
Total Oil –in-water (ppm)	Nil	7.4	5	10
Soluble Oil (ppm)	Nil	5.4	ND	ND
Oxygen (ppb)	Nil	Nil	0	5
Iron (ppm)	24.7	0.2	25	30

Notes: NA= Not Applicable, ND= No Data

3.2.4 Water Quality Monitoring

Water quality monitoring is required for optimizing chemical consumption rates and maintaining controlled dosing during plant commissioning and operation. Furthermore, water quality monitoring is essential not only to ensure no off-specification water is injected but also to aid trouble shooting throughout the operating life of the plant. Avoiding the injection of off-specification water is of prime importance. Relatively small quantities of sub-standard injection water can result in a general loss of injectivity and loss of recoverable oil by blocking the tighter zones, with preferential flow through other zones.

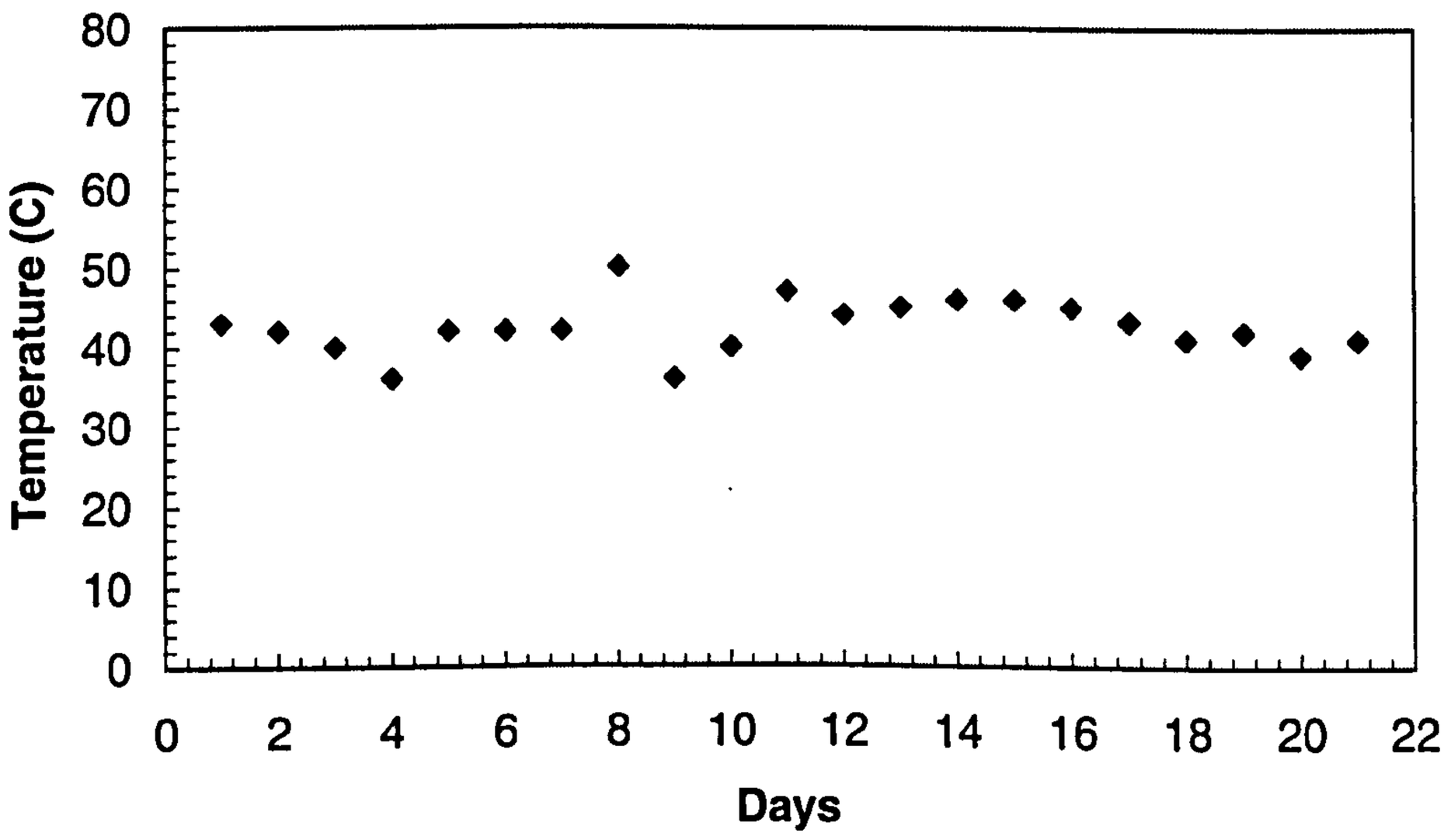

Figure 3.4: Temperature measurement variations over a number of consecutive days.

The following major variables are monitored in the Agish Water Injection system; pH, temperature, conductivity, turbidity, total suspended solids, total dissolved solids, oil-in-water, total iron, dissolved hydrogen sulphide, and dissolved oxygen. Furthermore, over a consecutive number of days, the measurements of parameters such pH, TDS, and conductivity remain almost the same (Figure 3.5-3.7), while the others such as temperature showed some fluctuations such as temperature (Figure 3.4).

The measurement of dissolved inorganic constituents (Table 3.1) is mainly significant at the design phase of a system in order to evaluate scaling tendency. It can also be useful as an indicator of injection water penetration in the last phases of a producing well's operational life.

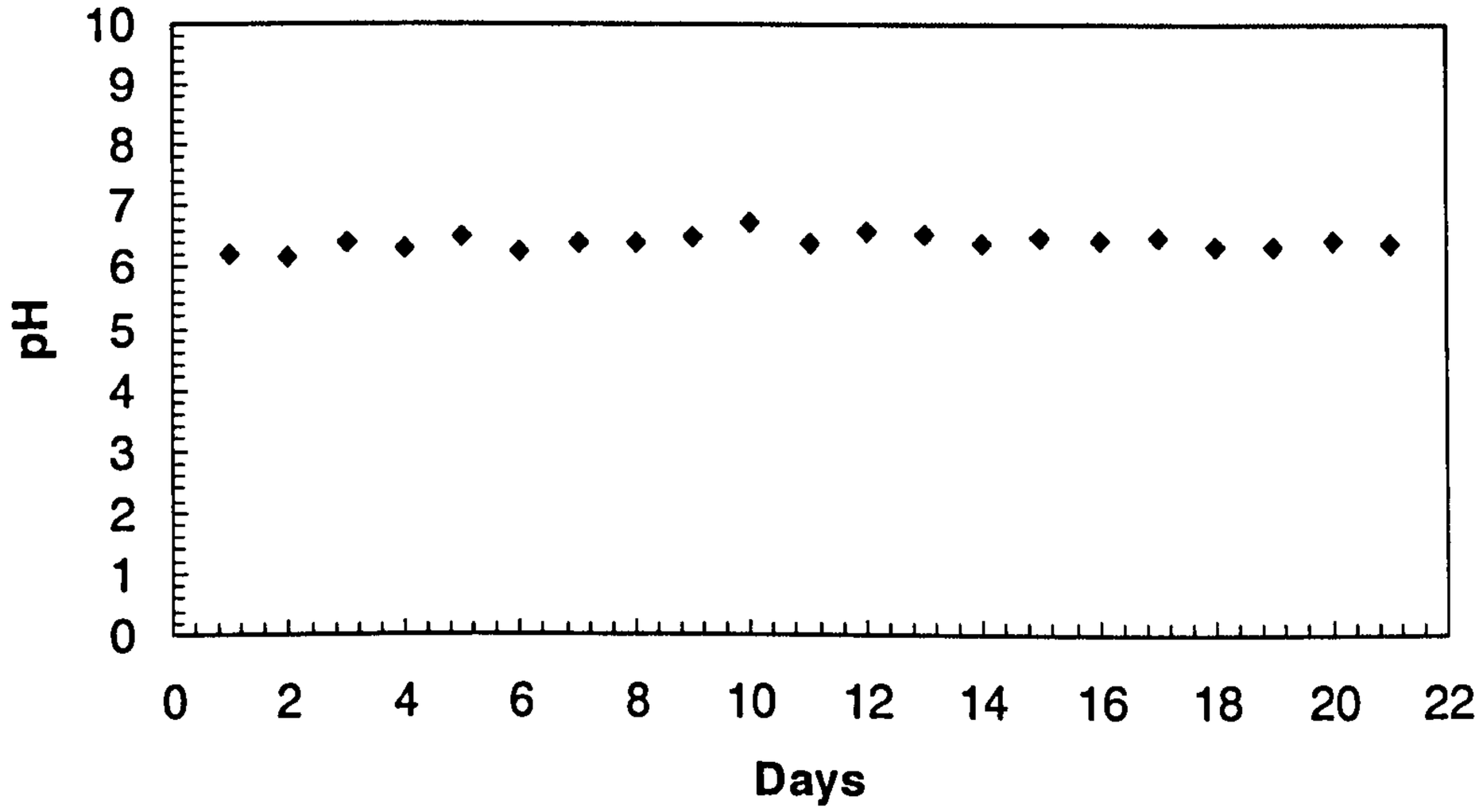

Figure 3.5: pH measurement variations over a number of consecutive days.

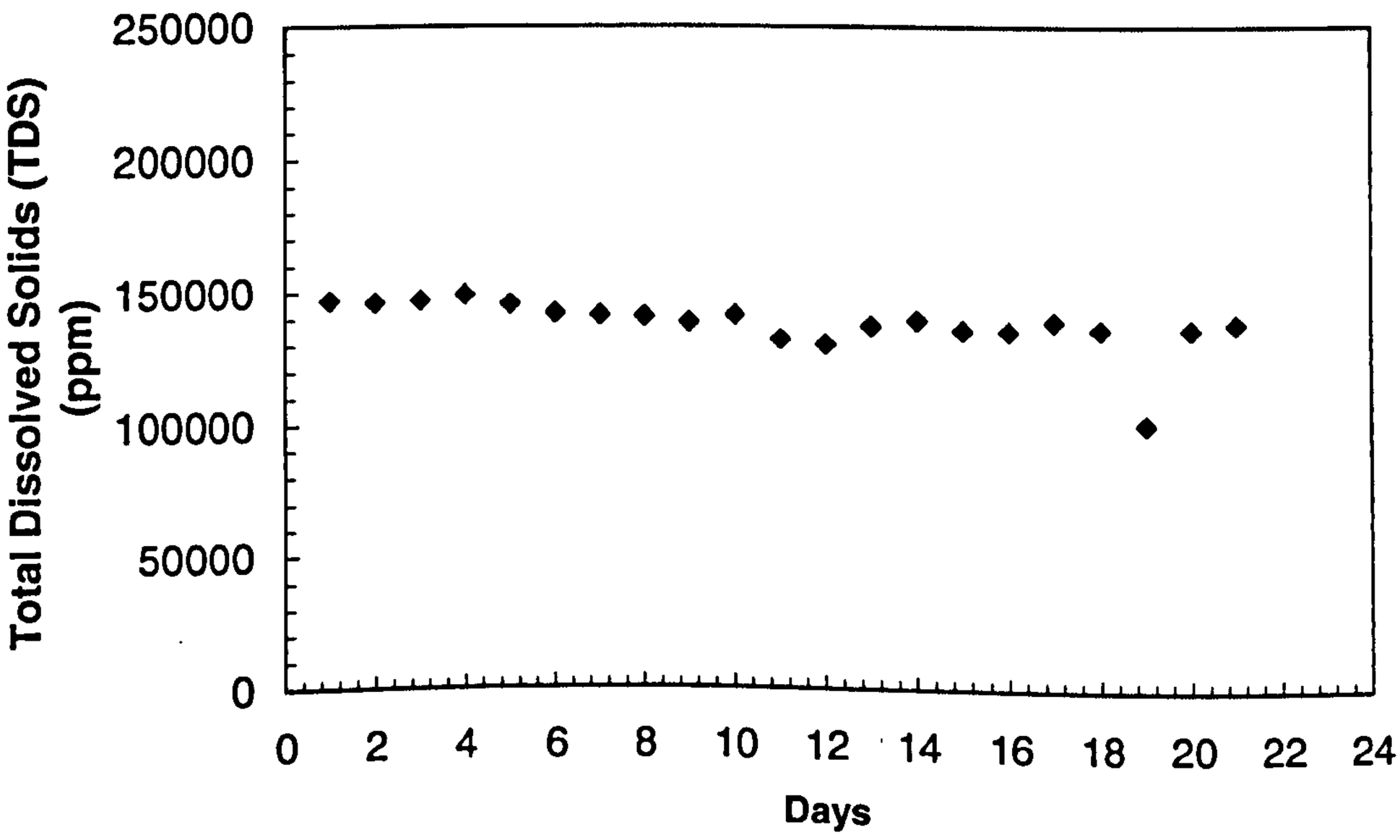

Figure 3.6: TDS measurement variations over a number of consecutive days.

In addition to scaling studies, the following factors have other implications. For example, temperature has an influence on chemical performance, emulsion stability, gas solubility, treatment plant performance, microbiological growth and corrosivity. Also, pH has an effect on corrosivity, chemical performance and microbiological growth. Sulphate influences the growth of sulphate-reducing bacteria. Furthermore, dissolved gases can significantly influence corrosivity.

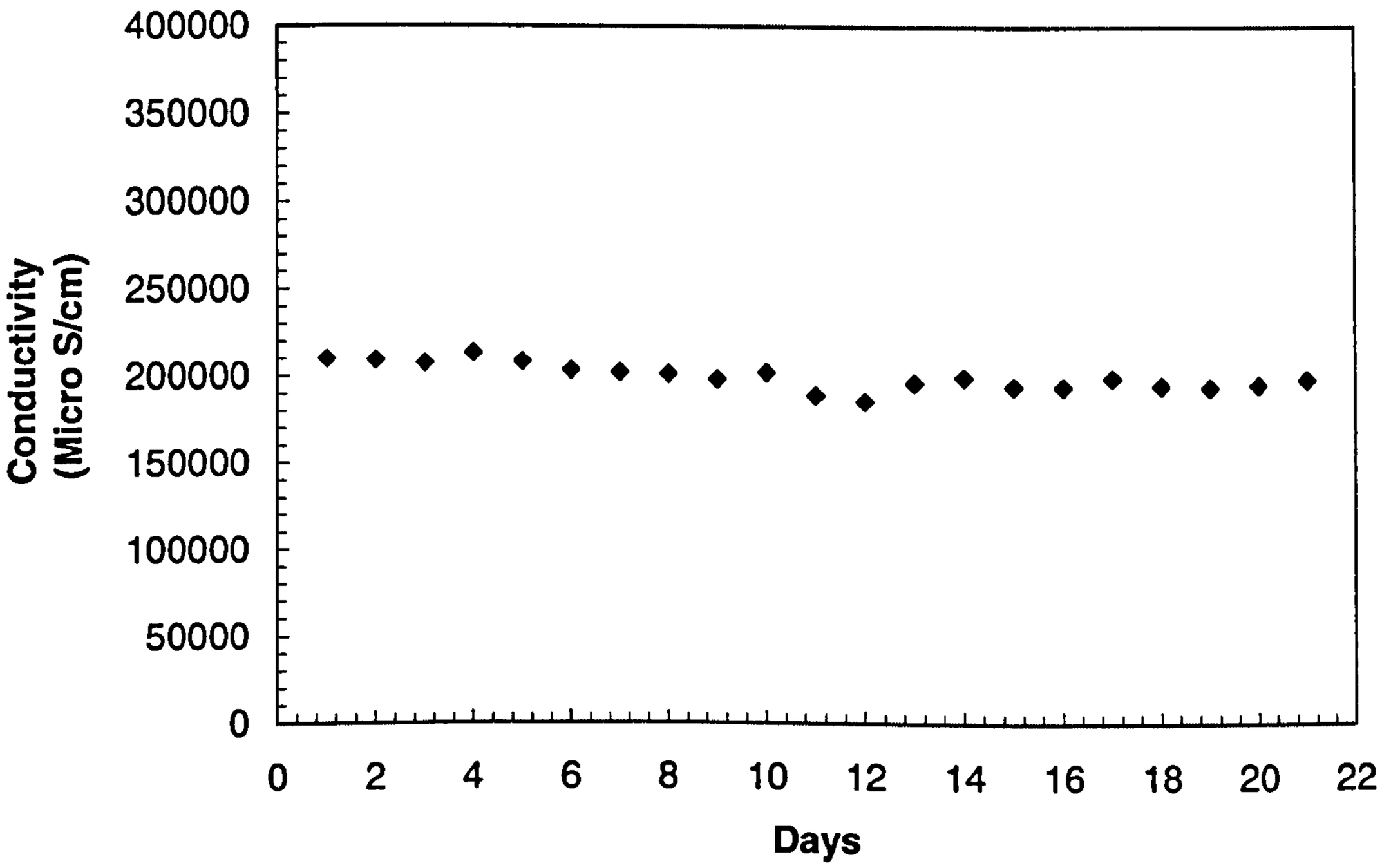

Figure 3.7: Conductivity measurement variations over a number of consecutive days.

Suspended particles or emulsified oil droplets present in the injection water can cause reservoir plugging. The particle may be previously present in the both aquifer and effluent water prior to treatment, e.g. formation grains, bacteria, scale, or corrosion products. Occasionally, incompatibility between chemicals or between chemicals and water cause particle creation. Compatibility problems between waters either on the surface, or down hole, when water injection water and formation water mix, may also produce particles in the form of insoluble scales.

Thus, there is a need to be able to characterize the waters with respect particle content during the plant operation in order to evaluate the performance of solids removal equipment. Three techniques are commonly used to determine the particulate content in water; particle size and distribution, membrane filter (slope) tests and suspended solids, and turbidity measurement. Particle counts are the most relevant parameter in determining injection water quality. Although suspended solids levels are high, if the particle counts are satisfactory then there is unlikely to be any loss of injectivity. For this reason, a Coulter particle counter is used to monitor water quality.

3.2.4.1 Particle counts

The Coulter Counter works on the principle that if a suspension of particles in a conducting fluid is passed through a small orifice, across which an electric current is flowing, the impedance will increase briefly as each particle traverses the aperture. The resulting voltage pulse is amplified and applied to a counter. It is essential that the fluid is conductive. The instrument can analyse a range of particle sizes from 0.4 up to about 100 μm, but for Agish, the significant sizes generally tend to be in the 1 to 20 micron range.

One minor limitation is that the instrument determines the volume of each particle which is then related to the diameter of a sphere having the same volume. Hence, a particle several microns in length but only a fraction of a micron in width may, for example, be detected as a 2 micron spherical particle. Despite this limitation, particle counts remain the most significant parameter for injection water quality particle content monitoring. Because the count is a size parameter, it is often compared immediately to reservoir pore throat tolerances, unlike suspended solids concentration. In the case of turbidity readings can be misleading and what seems a high value may have an insignificant effect on the formation with respect to plugging. A final point is that with all particle sizing and turbidity measurement, it should be noted that oil droplets and gas bubbles are detected as a particles.

3.2.4.2 Total Suspended Solids (TSS)

Total suspended solids is defined as "the weight of solids retained by a 0.45 micron Millipore membrane filter after the filtration of a known volume of water with a constant pressure differential of 20 psi across the membrane throughout the test". The method used is a gravimetric, determining a strict weight parameter only and is limited by the fact that large, dense particles may significantly influence the result. However, as a general rule, the higher the suspended solids concentration is measured, the worse the water quality becomes. TSS measurement is not a sensitive indicator for absolute water quality measurement. The parameter is weight specific and may be greatly influenced by particles of different density. Particle size analysis, being a size specific parameter, remains the key test for particle content evaluation for water injection purposes. Most TSS measurements exceeded the upper limit for reinjection (5 ppm) which illustrates the inability of separation units in suspended solids removal to yield an acceptable level, as shown in Figure 3.8.

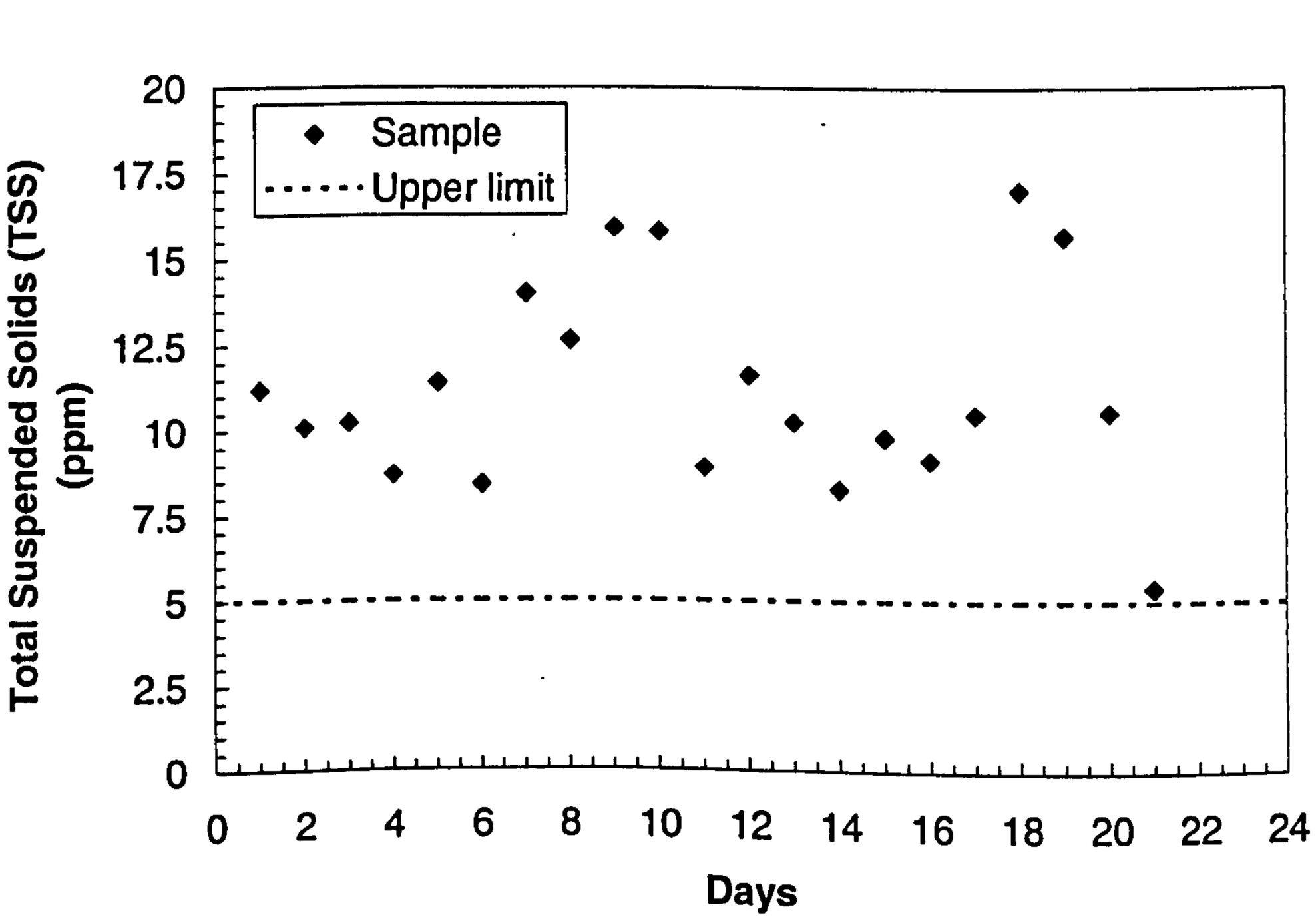

Figure 3.8: TSS measurement variations over a number of consecutive days.

3.2.4.3 Turbidity

Turbidity is used as a back up to particle counts and suspended solids. Nephelometric turbidity is defined as an empirical measure of turbidity based on measurement of light scattering characteristics (Tyndall effect) of the particulate matter in the sample. The instrument used for the measurement of turbidity at AWIP is the nephelometer. The measurement of nephelpmetric turbidity is accomplished by measuring the intensity of scattered light at 90°C to the incident beam. Numerical values (Nephelometric Turbidity Units, NTU) are obtained by comparison with light scattering characteristics of a known material in an equivalent optical system. The method is qualitative only and less sensitive than particle counters. Oil in the effluent water generates a haze which gives incorrectly high readings.

Figure 3.9 is an illustration of the change in measured turbidity over successive days. Although the upper limit is not specified for turbidity, it is preferable to maintain lower turbidity values .

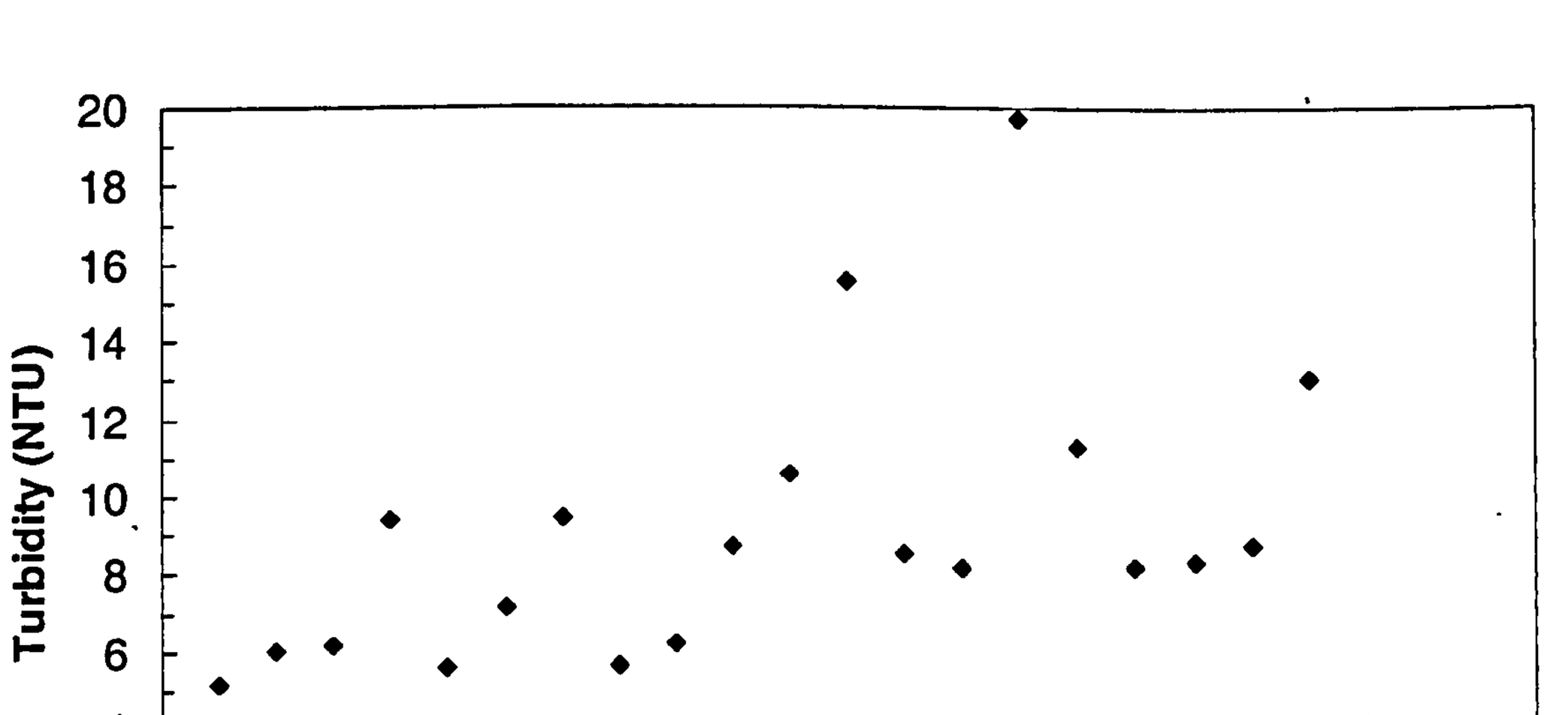

Figure 3.9: Turbidity measurement variations over a number of consecutive days.

3.2.4.4 Oil-in-Water

Measurement of the oil-in-water concentration both upstream and downstream of the effluent water balance tank at AWIP must be undertaken on a regular basis in order to prevent excessively high concentrations of oil being fed into the injection wells where it could cause loss of injectivity in the injection well.

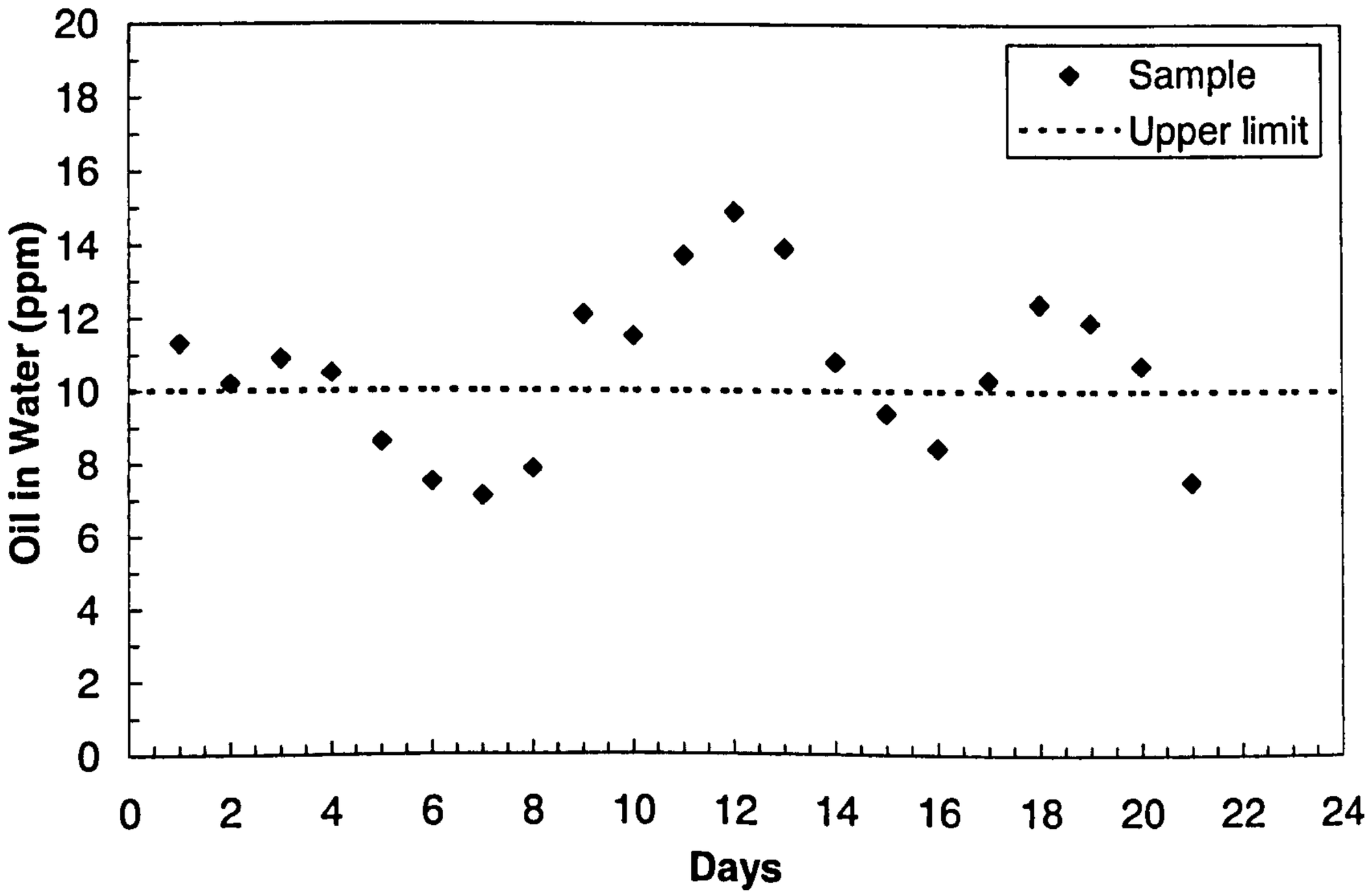

Figure 3.10: Oil in Water measurement variations over a number of consecutive days.

More than half of the oil in water measurements were above the upper limit specified for water injection as shown in Figure 3.10. Hence, this demonstrates the necessity for installation of a new separation system or modifying the current system to address this problem. Bearing in mind that as the age of oil wells increases, the production of water increases compared to the crude oil. Thus, the increase in quantity of oil in water will be more likely to happen in older wells, when the upper limit of inject for oil in water might exceeded by large amounts.

3.2.4.5 Dissolved Oxygen

Monitoring of dissolved oxygen levels is essential to determine the effectiveness of the gas blanketing systems, and will give a good indication of the corrosivity of the water. Dissolved oxygen concentration can be measured using a "Chemets" test kit of a suitable range, which also should be used during visits to wellhead sites. For dissolved oxygen parameter, the upper limit for injection is specified to be 5 ppb. Over a consecutive number of day, its measurement was found to be zero.

3.2.4.6 Dissolved Hydrogen Sulphide (H_2S)

Although the effluent and aquifer waters are not considered sour at present, they may sour over a period of time. It is therefore recommended that periodic monitoring for the presence of H_2S should be carried out at aquifer injection wellheads, using a Chemets. Although the H_2S upper limit for injection was not specified, it could noticed from Figure 3.11 that its concentration was above 10 ppm.

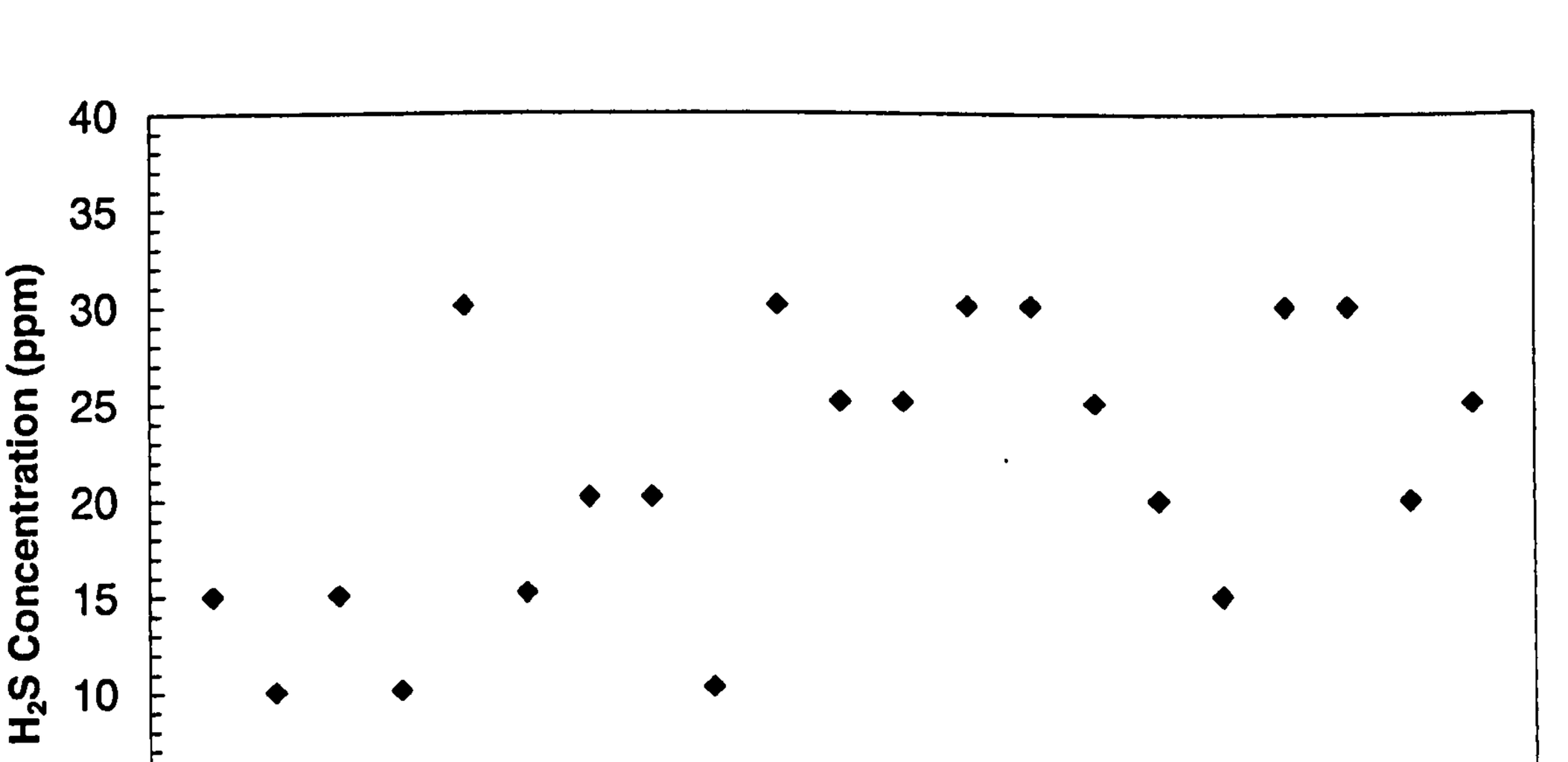

Figure 3.11: H_2S concentration variations over a number of consecutive days.

3.2.4.7 Particle Size Distribution

Particle size distribution is considered by far the most significant parameter whose upper limit needs be met before the injection of the effluent water. Therefore, as shown in Table 3.4, for each measured particle size, the maximum allowable number of particles for injection has been specified. For a number of consecutive days, measurements of the particle size distribution were taken for water injection monitoring as shown in Figure 3.12 to 3.16. Furthermore, these measurements were compared graphically not only to themselves but also to the upper limit for injection to asses their compliance with it. For example, Figure 3.12 demonstrated the incompliance of all measurements with the upper limit for injection, which was set for particle size above 5 microns. Also, most of the measurements exceeded the upper limit for particle sizes above 8 microns (Figure 3.13) and for particle sizes above 10 microns (Figure 3.14). For particle sizes above 12 microns, most of the measurements were below the upper limit for injection (Figure 3.15), as were all the measurements of particle size above 15 microns (Figure 3.16).

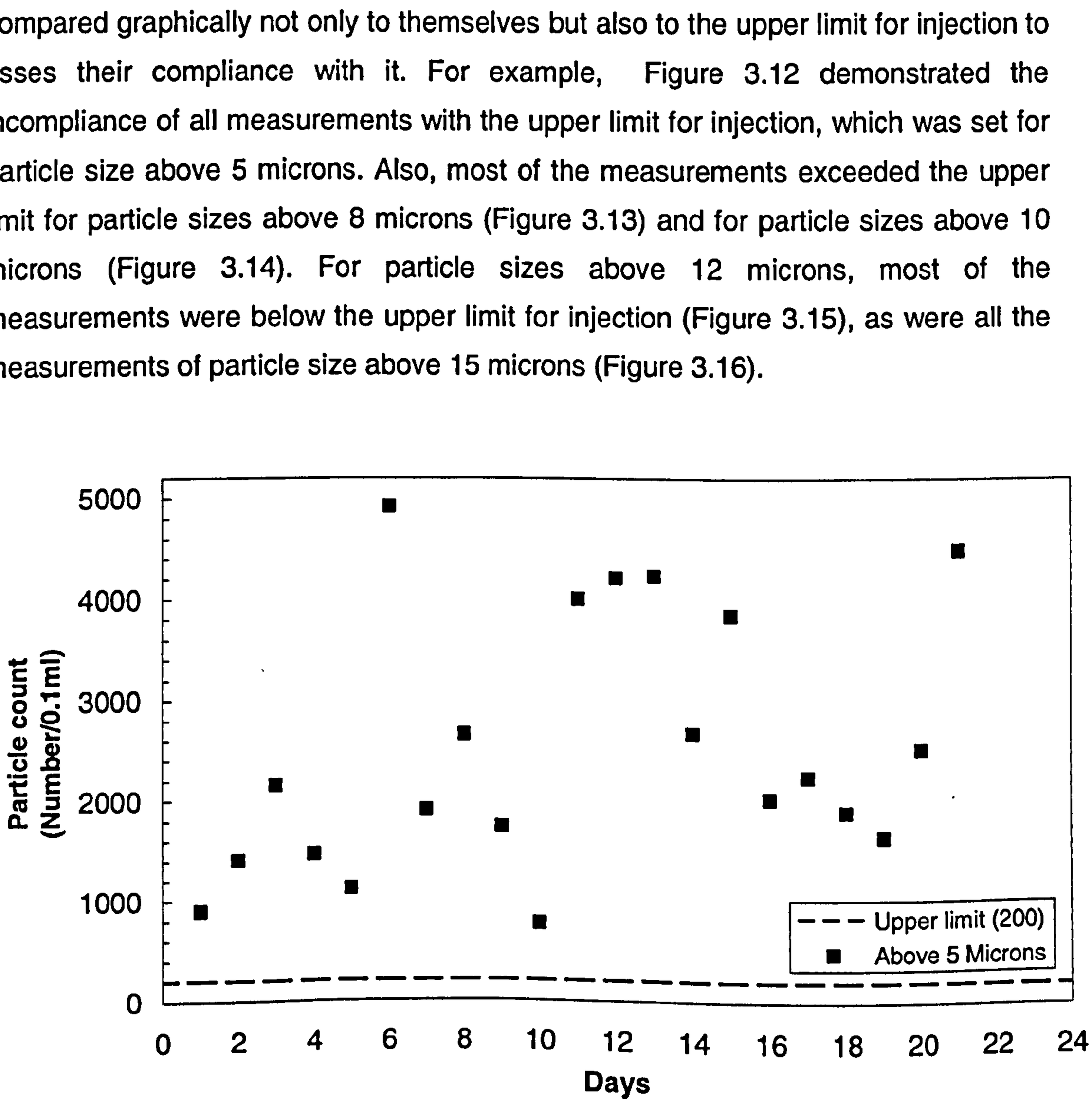

Figure 3.12: Particle count variations (above 5 Microns) over consecutive days.

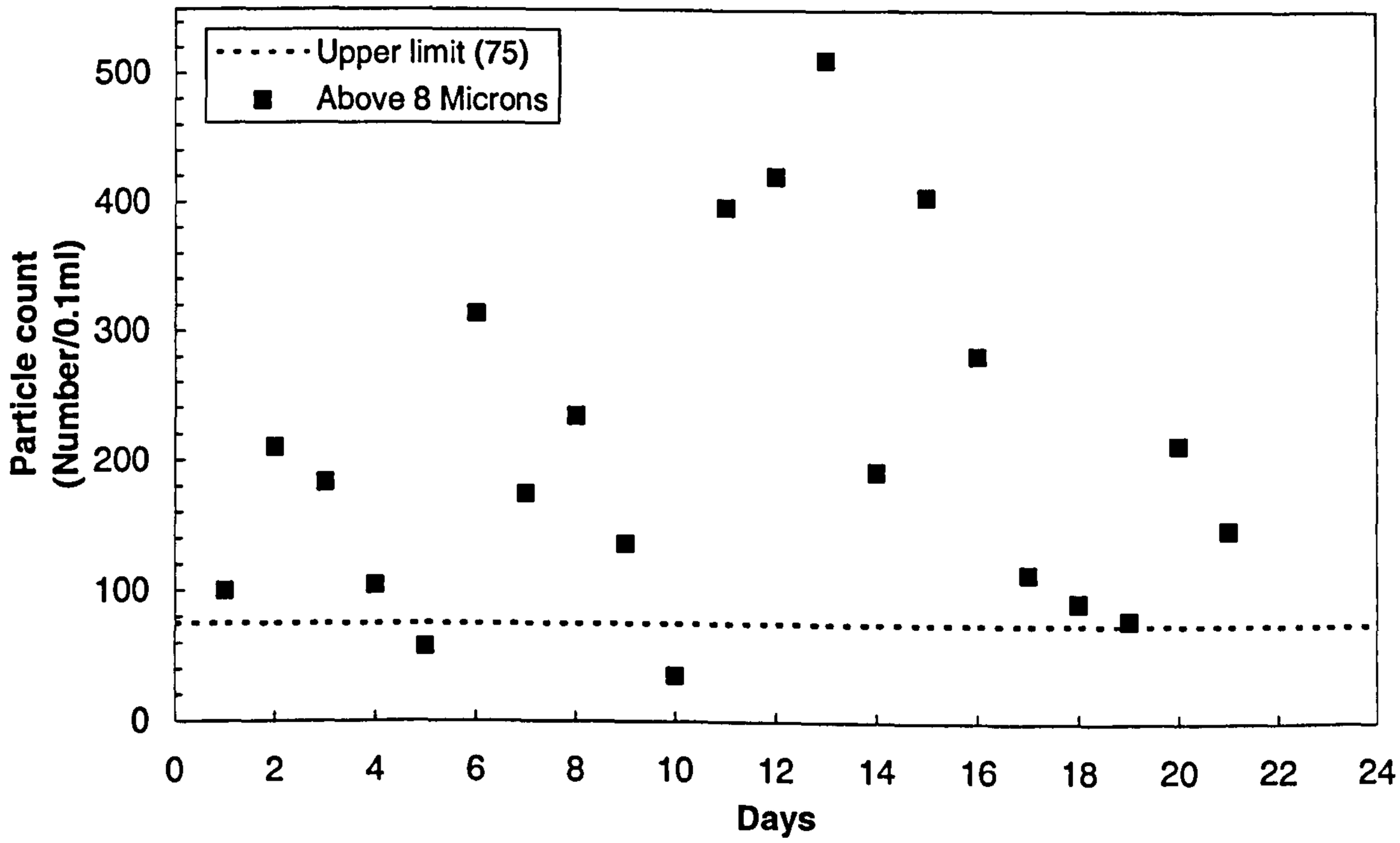

Figure 3.13: Particle count variations (above 8 Microns) over consecutive days.

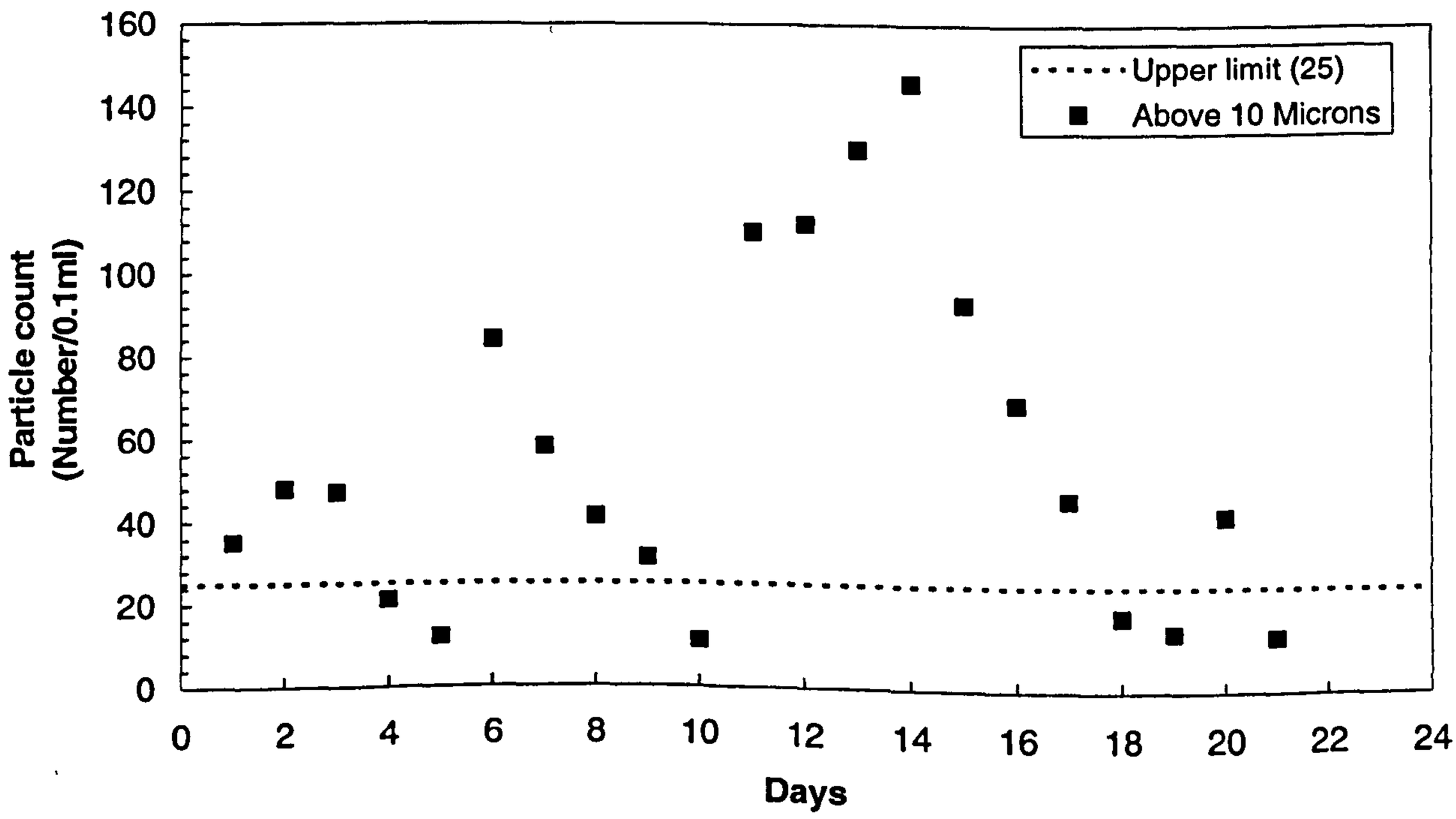

Figure 3.14: Particle count variations (above 10 Microns) over consecutive days.

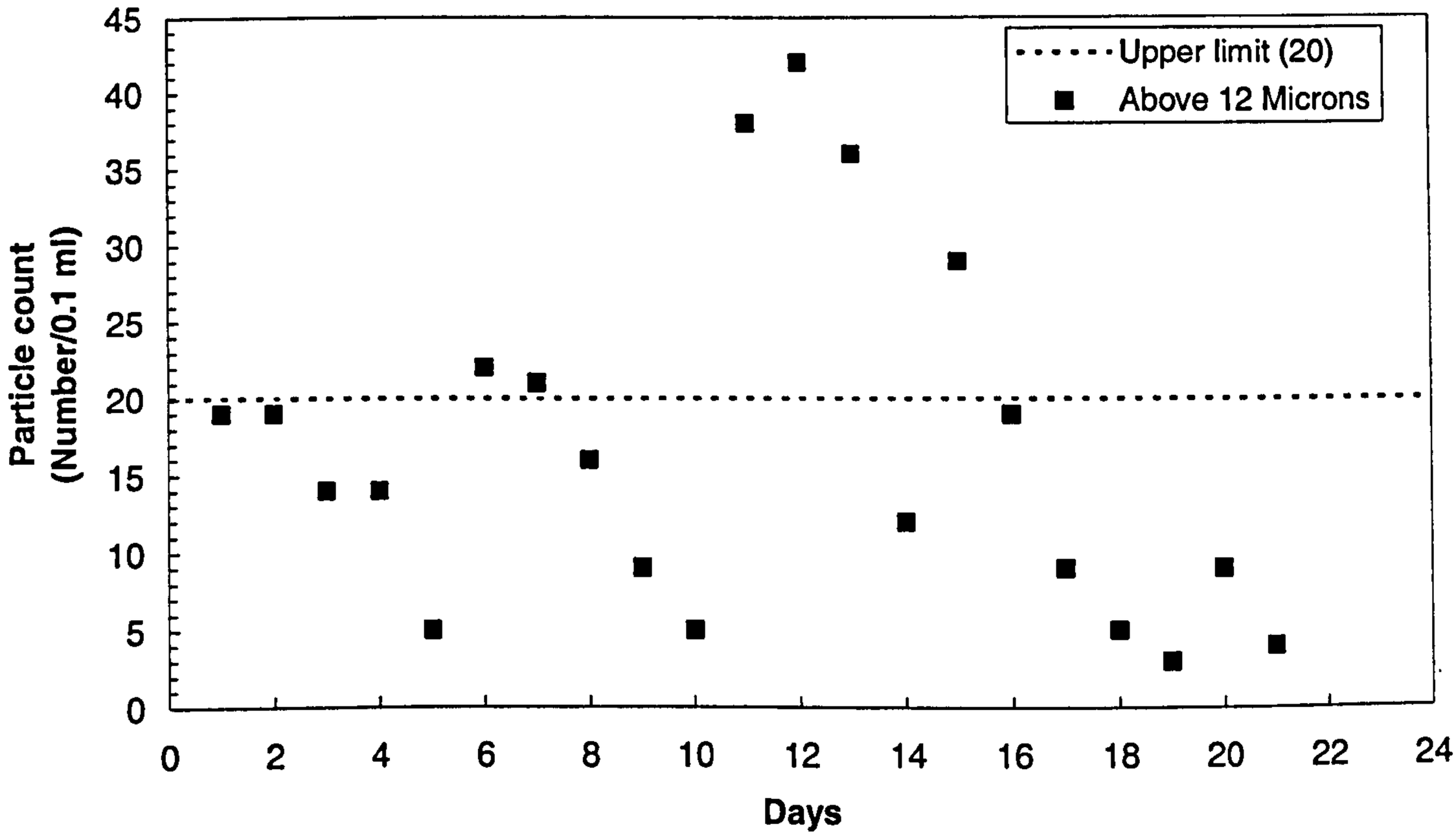

Figure 3.15: Particle count variations (above 12 Microns) over consecutive days.

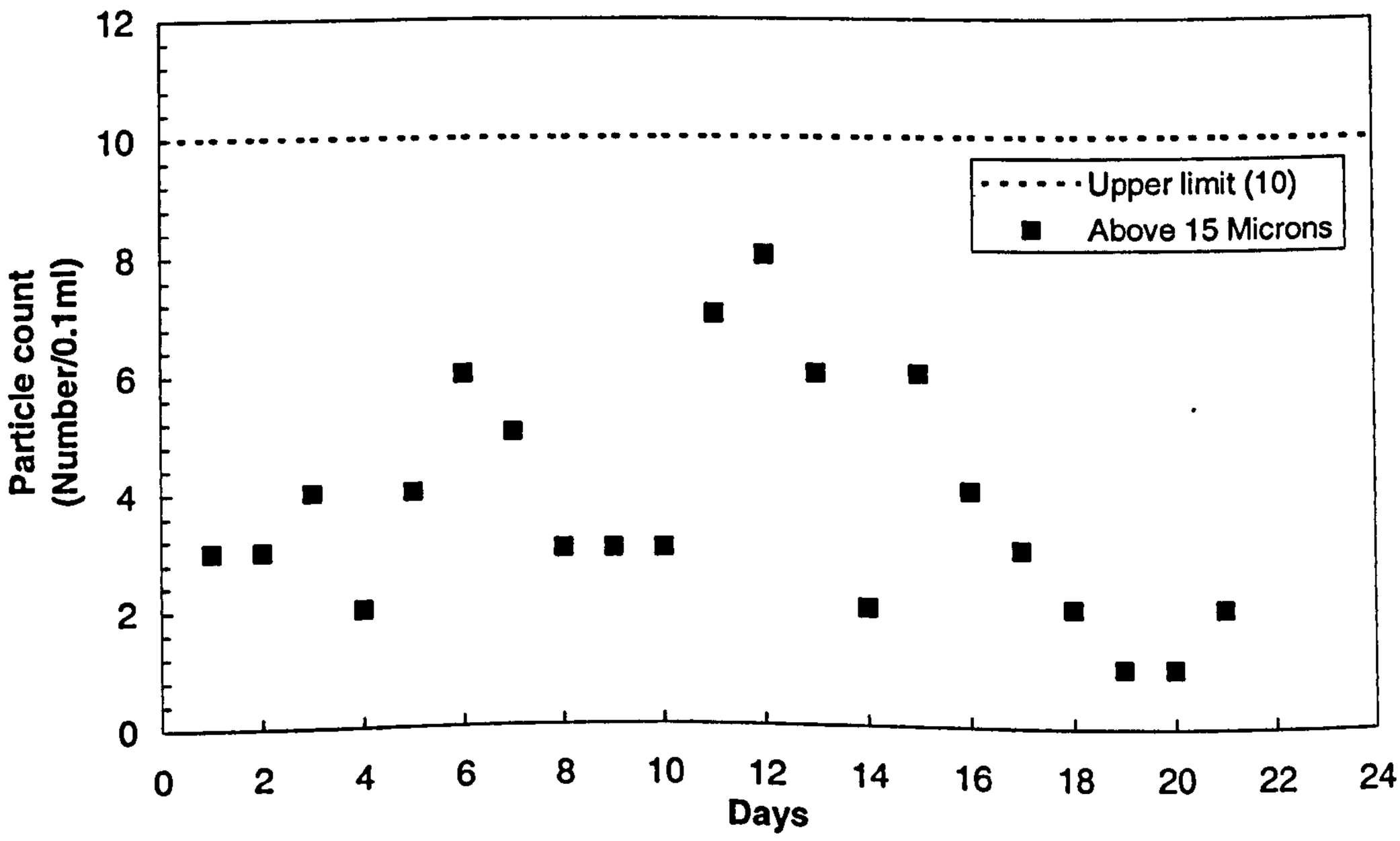

Figure 3.16: Particle count variations (above 15 Microns) over consecutive days.

3.2.5 Instruments and Measurement

The pH of effluent water is measured using a Hydrus 400 bench mounted meter. The pH range of this instrument is 0-14 with accuracy of ∓0.01. Conductivity is the measurement of the dissolved ion concentrations in an aqueous medium. Water conductivity is analyzed by using a model HI9033 conductivity meter. However, as the relationship between total dissolved solids and conductivity is dependent on the actual solids concentration, the data obtained should be viewed as qualitative rather than quantitative. This instrument has automatic temperature compensation which allows use of various temperatures. The range of HI9033 conductivity meter is 0-200 mS with accuracy of ∓1%. By multiplying the conductivity value by the factor 0.7, a reasonable approximation of the total dissolved solids can be obtained. The Nephelometric turbidity was measured by using the Hach 2100p turbidity meter. The range of this instrument is 0-100 NTU (Nephelomteric Turbidity Units) with accuracy of ∓2 %. This is a qualitative rather than quantitative measurement of the particulate/droplet concentration in a liquid phase.

The particle and size analysis are conducted using the Coulter Z series instrument (Z1 Dual-Threshold model). This instrument measures the number of individual particles of a pre-determined size that pass through an orifice of known diameter in a specific sample volume. The oil-in-water analysis is carried out using the model Horiba OCMA-310. Its measurement range is 0-200 ppm with the accuracy of ∓2%. Total Suspended Solids (TSS) is estimated using the following equation:

$$TSS(at\ 60°C\ mg/l = \frac{(B-A)\times 1000}{V} \tag{3.1}$$

where A is the weight of the plain filter paper in grams, B is the weight of the filter paper after filtration in grams, and V is the volume of the sample in litres.

A summary of the instruments and kits which have been used to measure monitoring parameters is presented in Table 3.5.

Table 3.5: Instruments and Kits.

S. No.	Instrument Name	Analysis to be done	Range
1	Hydrus 400 Fisher Brand	pH	0 -14
2	Hanna Conductivity Meter HI-9033	Conductivity	0-199.9 mS/cm
3	Hach-2100P Turbidity Meter	Turbidity	0-1000 NTU
4	Millipore for TSS	TSS	For lab.
5	Portable Millipore for TSS	TSS	For on line
6	Beckhman Coulter for particle count	Particle count	0-100000 Particles
7	Horiba OCMA-310 Oil Analyzer	Oil content	0-200 mg/L
8	Chemets kit for Dissolved Oxygen (DO)	DO	0-1 ppm
9	Chemets kit for (DO)	DO	0-100 ppb
10	Portable Orbisphere for DO	DO	1ppb-20 ppm
11	Hach Hydrogen Sulphide test kit	H_2S	0.1-5 ppm
12	Chemets Iron test kit	Total Iron and soluble Iron	1-10 ppm
13	Chemets Iron test kit	Total Iron and Soluble Iron	0.1-1 ppm

3.2.6 Results Analysis & Reporting

Data logging is carried out on a daily basis, with the parameters listed in Table 3.6 being monitored.

Table 3.6: Effluent water daily report (1/10/2004).

Parameter	Units	Upper limit for injection	Feed point	Storage tank inlet ($D1_{in}$)	Storage tank outlet ($D1_{out}$)
pH	at 25 C	NOT SPECIFIED	6.01	6.02	6
Temperature	Deg C	NOT SPECIFIED	31	34	30
Conductivity	Micro Siemens/Cm	NOT SPECIFIED	208000	209000	209000
Turbidity	NTU	NOT SPECIFIED	10.11	7.2	8.8
Total Suspended Solids	ppm	5	6.2	8.3	5.4
Total Dissolved Solids	ppm	250000	145600	146300	146300
Oil in Water	ppm	10	10	12.1	10.5
Total iron	ppm	30	0	0	0
H2S	ppm	NOT SPECIFIED	20	20	25
Dissolved Oxygen	ppb	5	0	0	0
Particle Size Distribution (Number in 0.1 ml)					
Above 2 Microns	Nos.,	NOT SPECIFIED	80412	43516	46352
Above 3 Microns	Nos.,	NOT SPECIFIED	26316	21681	23841
Above 5 Microns	Nos.,	200	1985	2102	2219
Above 8 Microns	Nos.,	75	200	720	320
Above 10 Microns	Nos.,	25	30	301	150
Above 12 Microns	Nos.,	20	11	140	71
Above 15 Microns	Nos.,	10	3	70	22
Above 20 Microns	Nos.,	0	1	20	4

3.2.7 Analysis Results and Calculations

For the particle size distribution analysis section, the measured number of particles for each particle size represents the total number of solid particles and oil droplets in 0.1 ml. Hence, suspended solids and oil concentration estimations based on particle size distribution analysis should be equivalent to the sum of the oil-in-water and total suspended solids measured concentrations. Mass balance calculations have been carried out (Table 3.7) using the following equation for effluent water analysis sample reported on 1.12.2004.

$$Total\ concentration\ (mg/l) = \sum\left[\frac{(\pi/6)\times\rho\times D^3\times N}{100000}\right] \qquad (3.2)$$

where ρ is the average density (g/ml), D is the mean diameter (m), and N is particle number.

Table 3.7: Mass balance calculation for effluent water sample analysis (1/12/2004).

(1) Input variables					
Density oil:		0.9	g/ml	π/6	0.5233
Density solids:		2.5	g/ml		
Ratio solids:		0.3396			
Ratio oil:		0.6604			
Concentration solids:		0.0022	ml/L	0.15622	v/v
Concentration oil:		0.0117	ml/L	0.84378	v/v
		0.0138			
Average density(ρ)		1.1499	g/ml	(NB Assumption)	
(2) Total concentration estimation based on particle size analysis					
Number of partides in 0.1 ml	Produced water	Mean diameter(D)	Particle Number(N)	D^3	N *ρ *D3
2 Microns	46,352	2.5	22,511	15.625	211676.6
3 Microns	23841	4	21622	64	832786.9
5 Microns	2219	6.5	1899	274.625	313850.7
8 Microns	320	9	170	729	74582.08
10 Microns	150	11	79	1331	63279.52
12 Microns	71	13.5	49	2460.375	72553.01
15 Microns	22	17.5	18	5359.375	58055.68
20 Microns	4	20	4	8000	0
Total	5,767		46,352	Σ	1626784
Thus, total concentration is estimated approximately is 16.3 mg/l				Σ/100000	16.2678

By comparing the total estimated concentration (16.3) with the directly measured concentration (15.9) from (Table 3.6), it is seen that they are similar and the small difference (0.3) is due to assumptions made during the calculation.

Table 3.8: Measured total suspended solids and oil concentration.

Measured effluent water analysis	Date	1.12.2004
Parameter	Unit	
Total Suspended Solids (TSS)	ppm (mg/l)	5.4
Oil-in-Water Concentration	ppm (mg/l)	10.5
Total Measured Concentration	ppm (mg/l)	15.9

The purpose of carrying out the previous calculations is to check the reliability of the collected data by evaluating the concentration based on particle size distribution and comparing it with the measured value.

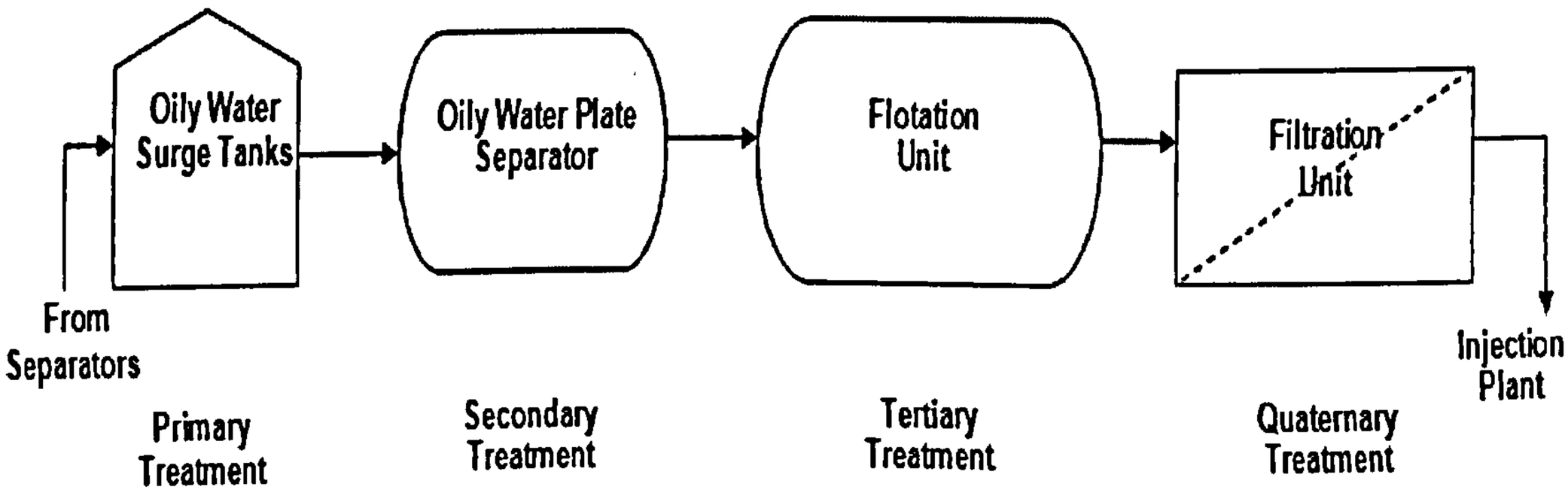

Figure 3.17 Diagram of waste water treatment plant with added filtration unit.

3.3 Filtration Unit

According to effluent water daily reports, particularly with respect to the upper limit for injection, the number of particles between 5 to 8 microns is 200 in 0.1 ml. In practice the number is found to exceed this limit by 10 times as shown in Table 3.6. Therefore, a filtration unit needed to be installed after the induced gas flotation unit as a polishing stage to remove these particles with this size ranges, as shown in Figure 3.17.

The proposed filtration unit will consist of tubular ceramic membranes with 0.2 μm pore size, will be fitted as quaternary treatment in the wastewater treatment plant as shown in Figure 3.17. The flow rate of water to be treated per train is 50,000 BPD (Barrels/day) with a temperature range from 25 to 65 °C. The characteristics of the feed-stock for the filtration unit is summarized in Table 3.9. The main objective of this filtration unit is to reduce the number of particles to acceptable levels according to the upper limits for re-injection for effluent water injection specification (Table 3.4).

Table 3.9: Specification of anticipated feed-stock of effluent water to filtration unit.

Parameter	Range
Design Flow Rate	50,000 BPD (Barrels/day)
Temperature	25-65 °C
Oxygen Design Spec	0 %
Oil-in-Water (OIW)	5-200 ppm
Total Suspended Solids	4-40 mg/l
Particle Size Distribution	(Number in 0.1 ml)
Above 2 Microns	30000-90000
Above 3 Microns	10000-30000
Above 5 Microns	300-3000
Above 8 Microns	100-1000
Above 10 Microns	50-500
Above 12 Microns	20-200
Above 15 Microns	10-100

3.5 Conclusion

As part of this research project, communication with the industry (2005) was a vital source to acquire knowledge and build solid background about produced water treatment and associated problems in the real world. Therefore, a field visit to Kuwait water injection plant took place in January 2006. A number of interviews with the operation staff were conducted to gain a valuable information by sharing their experience after the commissioning produced water plant for nearly two years.

From the daily effluent water reports collected for one year, the effluent treatment unit failed to meet the upper injection limit with respect to the particle size distribution in the range 5-15 μm. For example for particle in the size range 5-8 μm, the number of particles measured were almost 2000, while the upper limit for injection was 200. Keeping in mind that this limit was set based on physico-geological field tests of reservoir formation, where the rock porosity is typically 20 %, the quality of the injection water was very poor and was unsuitable for re-injection.

Therefore, an experimental investigation to deal with the excessive particle size and concentration problems is needed; crossflow microfiltration is a possible technology for alleviation of the problems. This case study has contributed not only in building a solid background behind of this research work, but also has helped to specify the objectives of this work. Also, from the case study data, the characteristics of the feed-stock to the future filtration unit which might be installed for treating effluent with higher number of particle with respect to the upper limit for injection has been established.

CHAPTER 4

EXPERIMENTAL PROCEDURES AND MATERIALS

4.1 Introduction

This section describes the equipments, experimental procedures and materials that have been used to carry out filtration tests of n-dodecane in deionised water emulsions. An experimental investigation has been carried out to study not only the effects of changing feed solution characteristics such as oil and surfactant concentration but also the effects of altering hydrodynamic conditions in the filtration operation. The optimum conditions for filtration performance are investigated by studying the critical flux, which was determined by using the step by step method at different feed solution characteristics and hydrodynamics.

4.2 EXPERIMENTAL SETUP

4.2.1 Crossflow Microfiltration rig

The experiment setup for the crossflow filtration is shown in figure below

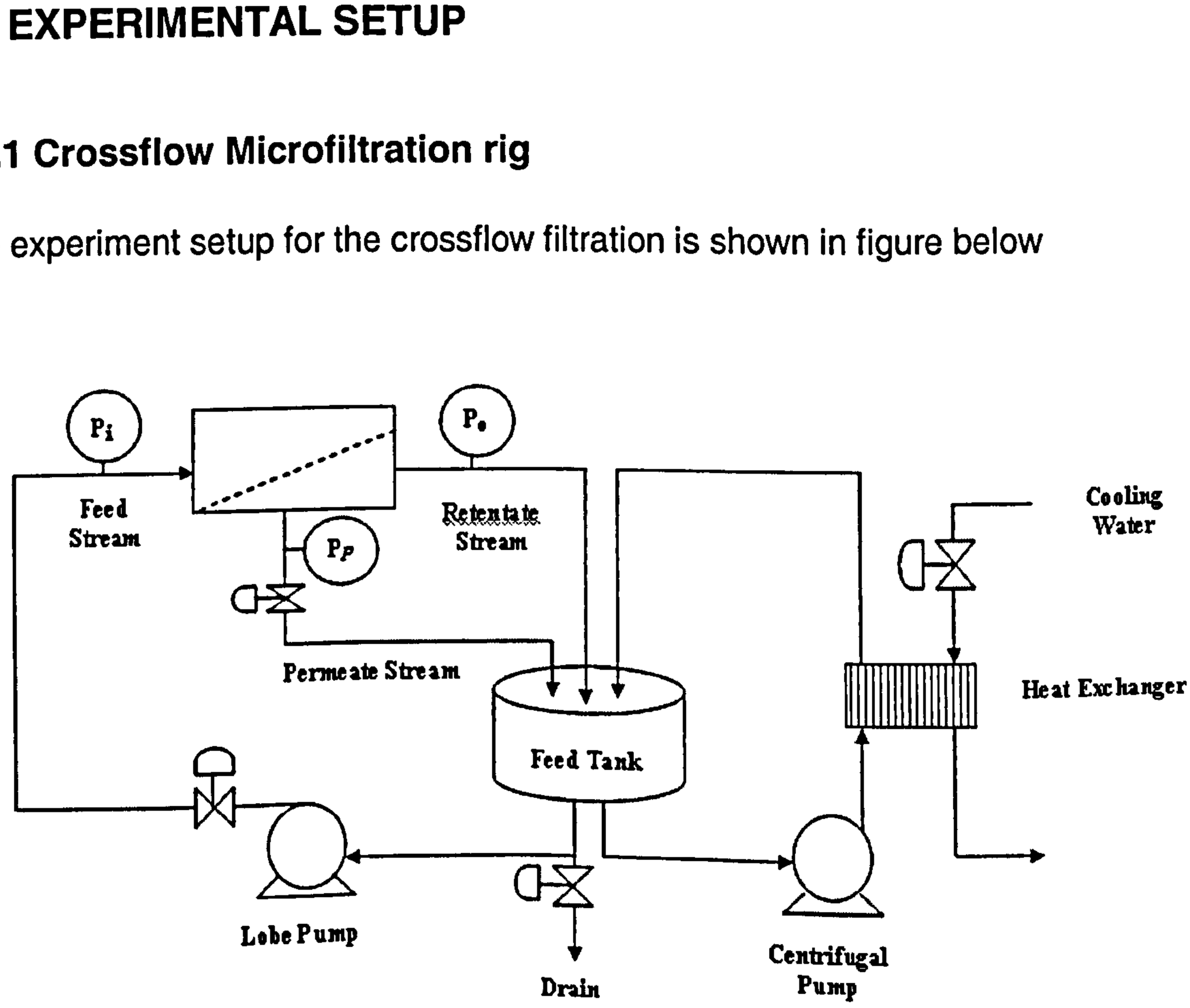

Figure 4.1: Experimental setup for crossflow filtration.

The crossflow filtration rig consists of a feed tank, pump, water cooler, pressure gauges, and a 0.2 μm tubular ceramic membrane. An image of the filtration rig is shown in the Figure 4.2. A flow circuit in which feeds of known, essentially constant, compositions were pumped continuously through the crossflow microfiltration module at specified crossflow velocities and transmembrane pressures.

The desired filtration conditions were maintained by using the valves shown in Figure 4.1. From Figure 4.2, it can be seen that the feed pressure is given by the gauge pressure indicator in the feed stream, the retentate pressure is given by the gauge pressure indicator in the retentate stream, and the permeate pressure is given by the gauge pressure indicator in the permeate stream. If these pressures are P_f, P_r and P_p respectively, then, the transmembrane pressure, ΔP, is given by:

$$\Delta P = \frac{P_f + P_r}{2} - P_p \tag{4.1}$$

The ΔP for a given crossflow velocity was therefore controlled by manipulating the permeate pressure, P_p, using the valve in the permeate stream.

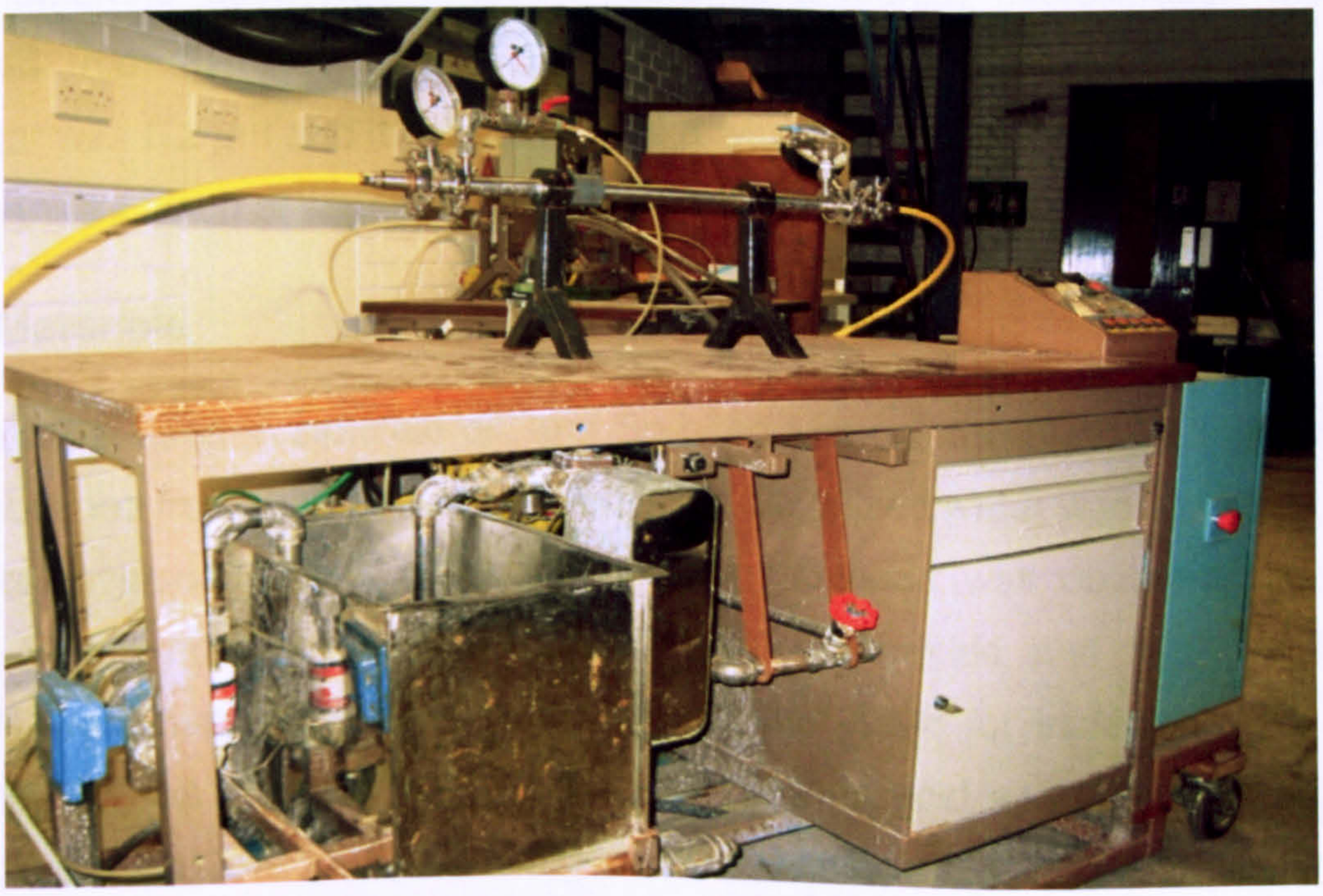

Figure 4.2: The microfiltration rig.

4.2.2 Operating conditions

The temperature of the feed stream was regulated using a secondary circuit in which a plate type heat exchanger working counter-currently to the feed kept the feed temperature essentially constant at 25 ± 2 °C. This was necessary as the lobe pump heats the feed and temperatures may rise to undesirable values. This secondary circuit also provides most of the mixing effects, to help keep particles in the suspension and well dispersed in the feed vessel.

The primary circuit also contributes to the mixing. The valves in the setup were calibrated to give a suitable range in which measurements could be made with accuracy. The range chosen was crossflow velocities from 1.14 to 2.28 m/s (± 0.01 m/s) and transmembrane pressures from 0 to 95 kPa gauge (±1 kPa).

4.3 Membrane and Material

4.3.1 Membrane

The membrane used was a tubular ceramic (zirconia) microfiltration module obtained from Fairey Industrial Ceramics Ltd. The membrane average pore diameter was 0.2 μm and its effective length was 0.55 m. The membrane consists of 7 channels, each of an inner diameter of 4.7 mm.

4.3.2 Materials

n-Dodecane, used to simulate oil, and Sorbitan Monooleate Span 80 (surfactant) were obtained from Ciba Specialty Chemicals. Deionised water was produced by a Millipore reverse osmosis unit. Ultra sodium chloride was obtained from the Sigma-Aldrich company, while hydrated calcium chloride and hydrated ferric chloride were supplied from Fisher Scientific and used for increasing the ionic strength. For the pH adjustments, both hydrochloric acid and sodium hydroxide were used. Also, Decon 90 (Fisher Scientific) was used for chemical cleaning of fouled membrane element.

4.4 Experimental Procedure

Prior to the start of a filtration experiment, the oil-in-water emulsion was prepared by mixing n-dodecane and sorbiton monooleate with deionised water for half an hour by using high shear laboratory mixer at its maximum speed, about 4000 rpm.

The emulsions were then run through the rig with the permeate valve closed for 10 mins before the start of an experiment to stabilize the crossflow velocity and to allow equilibrium to be achieved between the suspension and the surfaces in the rig (including the heat exchanger circuit).

The clean water flux and total membrane resistance was determined before and after each experiment to ensure that the permeability of the membrane was about the same at the start of each experiment, to analyse the extent of irreversible fouling and the effectiveness of the cleaning method

J_{crit}, the critical flux, was determined by successive variations of transmembrane pressure (using a step by step technique). The technique used consisted of systematic increases of ΔP, each step had a minimum duration of 15 minutes and a maximum till the equilibrium flux was reached. The first unstable permeation flux was determined when the flux decreased over the course of time at a given ΔP step. After stepping up the pressure to a point beyond the critical ΔP, the pressure is then stepped down again. The flux points corresponding to the upwards and downwards steps are plotted against ΔP, and the point of deviation from the clean water flux or first step extrapolation line is obtained.

The chemical cleaning procedure was implemented after the J_{crit}, determinations, and cleaning continued until the membrane resistance was within ±25 % the average resistance (5.811E+11 m^{-1}) at the start of experiment. These procedures will be elaborated in the following sections.

4.5 Homogenization Methods and Apparatus

Deionised water produced using Millipore RO membrane was used for each experiment. Then, a certain amount of n-dodecane and sorbitan monoleate surfactant was added to the pure water. After that, homogenization was carried out for 30 to 45 minutes using a high shear laboratory mixer (RBXL ABRAMIX) at its maximum speed of 4000 rpm to create an oil-in-water emulsion. The blending head used for creating the oil-in-water emulsions was the general purpose disintegration head; the homogenizer motor power is 185 W (0.25 hp). A picture of high shear laboratory mixer (RBMXL ABRAMIX) is displayed in Figure 4.3.

Figure 4.3: A picture of high shear laboratory mixer (RBMXL ABRAMIX).

4.11 Permeate Flux Measurement Method

1- Soon after the operating conditions have been set up for the filtration of the oil in water emulsion, open and adjust manually the permeate valve until the display on the permeate pressure gauge reaches the desired value of the first TMP step. Then the permeate will begin to enter the feed tank through the module outlet pipe (plastic) on the top side of the module. Wait for approximately for one minute for the system to stabilize .

2- Hold the measuring cylinder beneath the permeate outlet pipe and at the same time start the stopwatch. A number of measuring cylinders with different volume sizes (100, 250, 1000, 2000 ml) were used appropriately in measuring the permeate volume. The permeate volume is collected in the measuring cylinder for the specified time intervals (2-5 minutes) for each transmembrane pressure step. Usually the measuring cylinder with relatively smaller sizes (100 and 250 ml) were used in the first few TMP steps (smaller flow rate). The larger measuring cylinders (1000 and 2000 ml) were used at the final TMP steps (higher flow rate).

3- The flux (l/m^2h) is estimated by dividing the measured permeate volume over time (h) and the membrane area (m^2) for each of the volume measurements at the specified time intervals for such TMP step.

4- Then the permeate pressure was slowly adjusted to the next TMP step by manipulating the permeate valve until the desired pressure was reached. Wait for approximately 1 minute for the new process conditions to stabilize. Take a reading of flow rate using the same method as before and log it. Again, determine the flux of the permeate. Repeat this exercise (1-3) for the ascending and descending TMP steps.

4.6 Chemical Cleaning Procedure

At the end of the filtration experiment, the membrane is fouled and chemical cleaning was used to recoup the membrane properties. After each experiment, the following cleaning procedure was used.

1. Drain the rig using a valve at the bottom of the feed tank and by pressing the drain button in the panel control. The membrane was removed from the rig and washed thoroughly with deionised water, then left to soak in a 2-4 % (v/v) Decon 90 detergent solution overnight. The detergent solution was replaced periodically to increase its cleaning effect.

2. The filtration system was flushed with tap water for 10 minutes and drained. This step was repeated three times.

3. The whole rig was washed with a Decon 90 detergent solution 1 (v/v) % for approximately 30 minutes by running it through the entire rig: the feed tank, pumps and housing system were left full of the solution overnight.

4. On the next day the system was thoroughly flushed with deionised water for 10 minutes to remove any debris or remains. This step was repeated three times.

5. A clean water flux test was performed to verify the cleanliness of the membrane by estimating the membrane resistance using Darcy's law. The permeate flux was measured using deionized water after every cleaning operation.

6. If the membrane resistance value was within ±25 % of the mean resistance (5.811E+11 1/m), the chemical cleaning was regarded as completed.

7. If the membrane resistance value was not within the above range, then steps 1-3 were repeated.

4.7 Particle size measurements

For all filtration experiments, samples were taken from the retentate streams at specific time intervals during the filtration for particle size measurements using a Malvern Mastersizer. These measurements were carried out immediately after the filtration experiments to minimise any possible coalescence effects. For oil in water characterization tests, both Malvern Mastersizer and Coulter Multisizer were used at the preliminary stages of experimental work.

The main advantage of using the Coulter over the Malvern Mastersizer is that it provided the number of particles in a size range, from which the volume of each particle. From this, concentration of the sample could be determined. Hence, an estimation of the oil concentration for a number of prepared emulsions of oil-in-water was based on collected data from the Coulter Multisizer. However, the coulter has a measuring limitation in that it can only detect 1.4-28 μm particles, since a 70 μm aperture tube was used which is appropriate to oil droplet sizes. Bearing mind that a significant number of the emulsified oil droplet sizes were smaller than 1.4 μm, the Malvern Mastersizer was preferred for particle size distribution analysis for all filtration tests.

4.7.1 Malvern Mastersizer

The Malvern Mastersizer measures the particle size distribution based on a laser diffraction technique, where particles in a laser beam scatter light at angles that are inversely proportional to the size of the particles. Small particles scatter light at broad angles, whereas larger particles scatter light at smaller angles. The scatterings are copied to arrays of detectors at the central plane of the optics. A direct correlation exists between the scattered light energy distribution on these detectors and the particle size distribution.

The software in the Mastersizer analyses of this light energy distribution in order to predict the size distribution of the particles by using Mie theory as the measuring principle. Mie theory provides good solution for all transport media of particles, such as emulsions, and generally it is the best solution for particles smaller than

50 µm. A sample mixer speed of 1,750 rev/min^{-1} and a poly disperse model were employed for the particle size analysis under evaluation. At the start of experimental work, the particle size distribution type was in volume % for the characterisation of emulsions. However, for crossflow microfiltration tests, the particle size distribution type was in number % to investigate the filtration of the finer oil drops. An image of Malvern Mastersizer is shown Figure 4.4.

Figure 4.4: A picture of Malvern Mastersizer.

4.7.2 Coulter Multisizer

The COULTER® Multisizer II (COULTER COUNTER®, Coulter Electronics Ltd.) is an analytical apparatus employed to measure the number and size of suspended particles in an electrolyte solution. An electric current is applied between two electrodes submerged in a conductive fluid on each side of a small aperture, in

which the suspended particles are agitated and flowed through small aperture by a vacuum pump, is observed. Once a particle travels through the aperture, it displaces a volume of electrolyte and this modifies the impedance between the electrodes and generates a sequence of voltage pulses where the height of each pulse is proportional to the volume of particle. The pulses are counted and gathered in a number of size connected channels. The photograph of the Coulter Multisizer is presented in Figure 4.5.

Figure 4.5: Picture of a Coulter Counter Multisizer II.

A vacuum is produced by a vacuum pump and this yields an imbalance in a mercury siphon. After the valve is closed, the mercury column goes back to equilibrium and the sample suspension is drawn through the orifice tube permitting a replicable volume to be analyzed with a precision of ± 0.5 % on a 0.5 ml volume. The particle size range of 0.4 to 800 µm can be scrutinized by the Coulter, irrespective of particle type. The electrolyte is selected on the basis of the particle composition. The aperture tubes exist in a range of sizes in proportion to practical particle sizes and orifice tube data. The main feature of this apparatus over other size measuring equipment is that it supplies a number of particles of particular size

ranging in samples that are further analysed, such as for estimation of suspension concentration. Figure 4.6 demonstrates a schematic diagram of COULTER® Multisizer II.

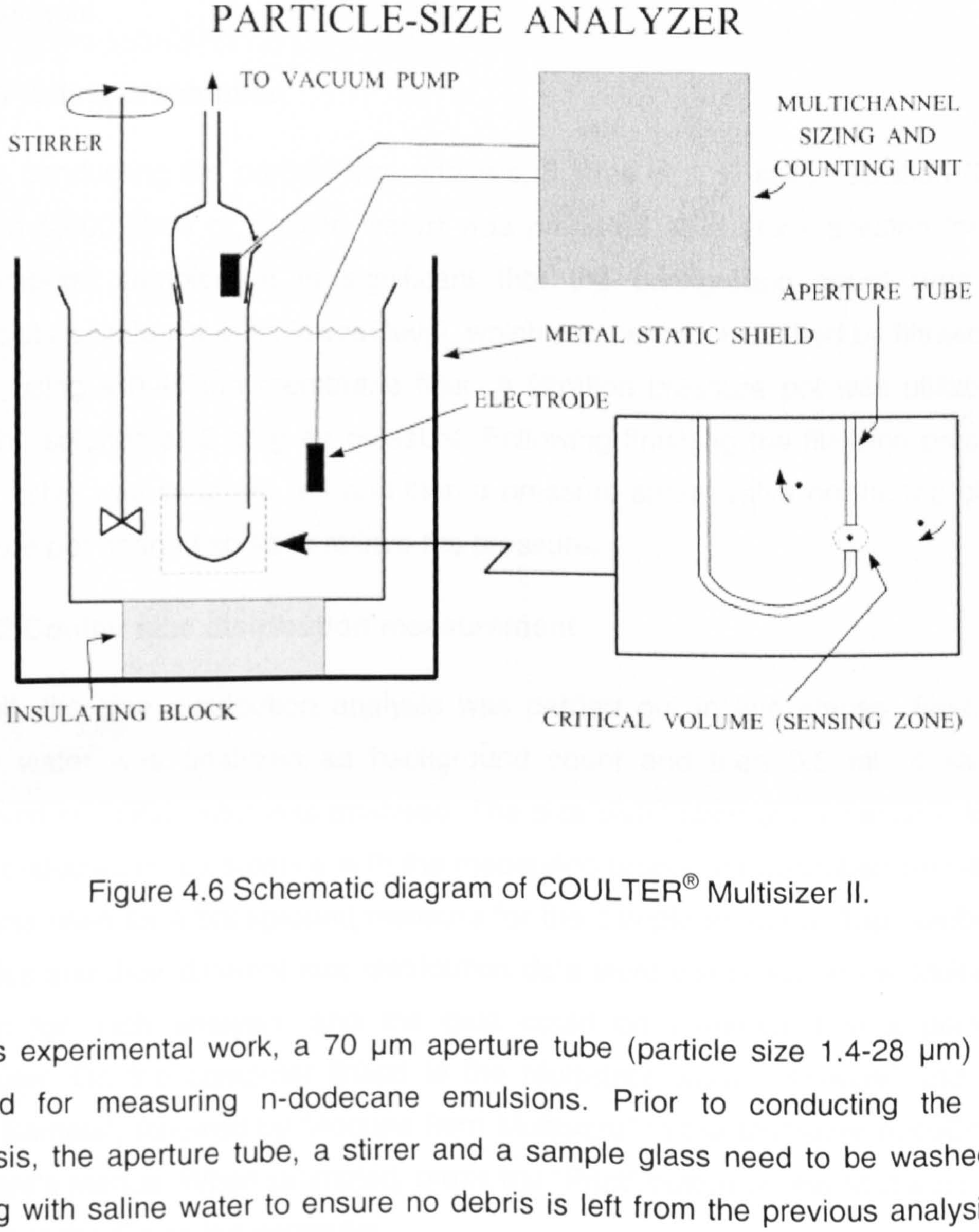

Figure 4.6 Schematic diagram of COULTER® Multisizer II.

In this experimental work, a 70 μm aperture tube (particle size 1.4-28 μm) was utilized for measuring n-dodecane emulsions. Prior to conducting the size analysis, the aperture tube, a stirrer and a sample glass need to be washed by rinsing with saline water to ensure no debris is left from the previous analysis. A sample was prepared in the sample beaker. Subsequent to turning on the multisizer, the unit's program is switched to automatic sort in the system menu, where the siphon mode is employed for the operation. The stirrer was turned on at this point to make sure that particles were well dispersed in the sample beaker.

Merely mild mixing was employed since high mixing rate might produce breakage of suspended particles, especially those like oil droplets or flocculated particles. To begin the particle size analysis, push the "Full" button and place the knob to the "Reset" spot. After waiting for few moments, place the knob to the "Count" spot so as to suck solution into the tube and wait until the reading is complete. The results are revealed on the Multisizer screen. Push the "Reset" button before acquiring a new analysis.

4.7.2.1 Saline preparation

Before conducting the particle size analysis, 5 litres of 1 % saline solution (50 g NaCl in 5,000 litres of distilled water) was prepared as a stock solution for the experimental samples. It is significant that the background count from the electrolyte solution is at its lowest level, which can be accomplished by filtration of saline using a 0.45 µm membrane filter. A filtration pressure pot was utilized to filter the solution at 2 barg air pressure. Following finishing the filtration process, an air valve was switched off and then a pressure safety valve on the top of the pressure pot opened so as to relieve the pressure.

4.7.2.2 Coulter size distribution measurement

Overall, the size distribution analysis was carried out in two stages. First, the saline water was analyzed as background count and then 0.5 ml of sample dissolved in saline water was analysed. The size distribution of the saline solution was conducted in accordance with the measuring procedure described previously and was used as a background measure for the sample analysis. The number of particles and their different size distribution data were displayed on the Multisizer screen for each analysis, and the data could be transmitted to a personal computer. On the computer linked to the Multisizer, select "Acquire" and then "New Sample", followed by "Acquire from Multisizer" in the Multisizer AccuComp® software's menus. When prompted, press the "Print" button on the Multisizer, and then save the file on the computer.

To commence a sample's size distribution analysis, put the sample into the saline solution (sample beaker) until a bar on the left hand side reads approximately 5 % or particle number is in the appropriate range according to the orifice tube data (

which is 58,300 particles (maximum) in 0.5 ml of solution for the aperture tube size of 70). Take the size distribution for sample in saline solution. Sample and saline weights are measured in order to get true concentrations. Repeat gaining the particle size analysis data, as described in the preceding stage for saline water, and next select "Analyze", "Subtract from background" and open background file which is the saline data file, followed by saving the file.

4.7.2.3 Trouble shooting

For a number of sample analyses, the Multisizer failed to complete the measurements. The majority of these problems were associated with the current being unavailable. First, blockage of the Coulter tube is frequently caused by an excessive number of particles being counted and a longer a counting time. The problem was resolved by cleaning of the tube's aperture using a saline wash bottle or a brush.

Secondly, pressure loss in the system or not building up was another problem, in which no fluid was present in the aperture tube and air bubbles were monitored in the tube. In such cases, the mercury level in the glass tube inside the multisizer was not be at a normal level, i.e. at the bottom of the sight glass. In order to get the pressure, the button on the lid of waste storage vessel was pressed for a short time or a heavy material placed on it to create a vacuum and set the knob to the "Reset" position, and then set it to the "Fill" location for a short period. After liquid has filled the Coulter tube, the switches were set to "Close" position. Thirdly, sometimes the door of sampling stand was not closed. Hence, by closing the door properly reconnected the current circuit in the system.

Finally, in relation to the saline water level, the low saline level in a flush beaker affects the analytical measurements since the saline is destined to clean or replace the previous sample liquid in the aperture tube. The typical saline level needed be at three quarters of the maximum level. On the other hand, an excessively high level of water accumulated in the waste beaker was generated a problem. It was emptied when the liquid level in the beaker was about at three quarters of the maximum level.

4.8 Zeta Potential

The zeta potential can provide an indication of the stability of oil-in-water emulsions; where when all the oil droplets have a high negative or positive zeta potential then they will tend to repel each other. Oil droplets with zeta potential smaller than -30 mV or larger than +30 mV are typically considered stable (Malvern training manual, 1998). The emulsion is not stable at the isoelectric point, where the zeta potential is zero (unless other stabilizing forces are induced within the dispersion).

When an electric field is applied across the electrolyte solution, the negatively charged dispersed oil droplets are attracted towards the positively charged electrode. The velocity at which they travel is dependent on many factors such as the electric field strength, the dielectric constant, the viscosity and the zeta potential. The velocity at which a particle travels in the electric field is identified as the electrophoretic mobility.

Figure 4.7: An image of Malvern Zetasizer 3000HS.

A Malvern Zetasizer 3000HS (Figure 4.7) was used for zeta potential measurements, where its image is displayed in Figure 4.7. Its measuring technique was based on Laser Droppler Velocimetry (LDV), which is used to measure the particle velocity through the fluid due to electrophoresis. Using a 20 ml syringe, about 20 ml of the sample was injected into the Zetasizer. Normal practice was to inject a 20 ml sample of deionised water before injection of the emulsion sample in order to ensure the displacement of the previous sample. Also, with respect to the injected samples, it was important to ensure that no air bubbles were in the samples or the sampling volume.

The electrophoretic mobility was estimated using a voltage of 150 mV and an electrode spacing of 50 mm. The measured electrophoretic mobility was then employed by the Zetasizer to calculate the zeta potential values of the particles. The zeta potential values are obtained from the electrophoretic mobility measurements via Henry's formula, which is:

$$U_E = \left[\frac{2\varepsilon\zeta}{3\eta}\right] f(\kappa a) \tag{4.2}$$

where U_E is the electrophoretic mobility , ε is the dielectric constant, ζ is the zeta potential, η is the viscosity, and $f(\kappa a)$is a changing monotonic function that increases from 1.0 at $\kappa a = 0$ up to 1.5 at $\kappa a = \infty$. The Debye-Huckel parameter (κ) has the dimensions of $(Length)^{-1}$, and is the reciprocal thickness of the electrical double layer. Since a refers to the radius of the particle, κa quantifies the ratio of the particle size to the electrical double layer thickness.

In the experimental work here, keeping in mind the relatively large colloidal oil droplets in the aqueous phase, this ratio can be taken to be infinity as the thickness of the double layer is negligible in comparison to the particle size. While working with particles in the micron or sub-micron size range, the dominant force on the particle is primarily the electrophoretic retardation whereby the ions in the double layer drag the solution with them and the particle travels in the opposite

direction. Thus, the Smoluchowski boundary was employed, where $f(\kappa a)$ is considered to be 1.5.

Consequently, by substituting the $f(\kappa a)$= 1.5 and rearranging Henry's formula to determine the zeta potential, the following equation is obtained;

$$\zeta = \left[\frac{U_E \eta}{\varepsilon}\right] \tag{4.3}$$

from which ζ can be calculated since U_E is measured by the instrument, and η and ε are known constants of the fluid system.

4.9 Determination of shear stress at the membrane wall

The wall shear stress, τ_w is the force applied by the fluid flowing tangentially to the membrane on an element of its surface area. The relation between τ_w and the Fanning friction factor, f, and the approximation of Blasius in turbulent flow, assuming the membrane to be a smooth tubular element (equation (4.5)), enable τ_w to be calculated from the Reynolds number, Re, in the manner used by Gésan-Guiziou *et al* (2002).

$$\tau_w = \frac{1}{2} f \rho_r v^2 \tag{4.4}$$

$$f = 0.08\,\mathrm{Re}^{-0.25} \tag{4.5}$$

$$\mathrm{Re} = \frac{\rho_r v d_e}{\mu_r} \tag{4.6}$$

where v, ρ_r, d_e and μ_r are the crossflow velocity, retentate density, effective channel diameter of the feed flow section, and retentate viscosity respectively.

When particle deposition begins, the flow section effective diameter can be less than the initial diameter. Some workers in the past have taken the diameter to be constant throughout. The effective diameter has been taken to be constant in this work due to the fact that in all the experiments the majority of time is spent below the critical flux.

4.10 Determination of membrane resistance

For deionised water, the water flux, J_w, is proportional to the transmembrane pressure according to Darcy's law:

$$J_w = \frac{\Delta P}{\mu_w R_T} \tag{4.7}$$

where ΔP is the transmembrane pressure, μ_w is the dynamic viscosity of water and R_T is the membrane total resistance, inclusive of membrane resistance and any fouling effects. The total resistance will therefore be:

$$R_T = \left(\frac{1}{J_w/\Delta P}\right)\frac{1}{\mu_w} \tag{4.8}$$

The dynamic viscosity of water at 25 °C is $\mu_w = 8.89\times10^{-4}$ Pa s

The clean water flux and total membrane resistance were determined before and after each experiment to ensure that the permeability of the membrane was approximately the same at the start of each experiment, to analyse the extent of irreversible fouling, and assess the effectiveness of the cleaning method.

4.11 Determination of critical flux (J_{crit})

J_{crit} is defined as the critical flux above which particles start to deposit significantly onto the membrane surface. J_{crit} was measured by consecutive increments of transmembrane pressure (the step by step technique), akin to the technique summarized by Gésan-Guiziou *et al.* (2002) but incorporating some modifications

that were presented in the previous section, such as the size for the early steps being shorter than later steps. The technique consists of regular increases of transmembrane pressure, where each ΔP step had a duration 10-30 minute with a reading of permeate flux taken every 2-5 minutes. The first unstable permeation flux was determined when the permeation flux decreased a given *TMP* step. After stepping up the pressure to a point beyond the critical *TMP*, the pressure was then stepped down again. An example output from the step by step technique is illustrated in Figure 4.8.

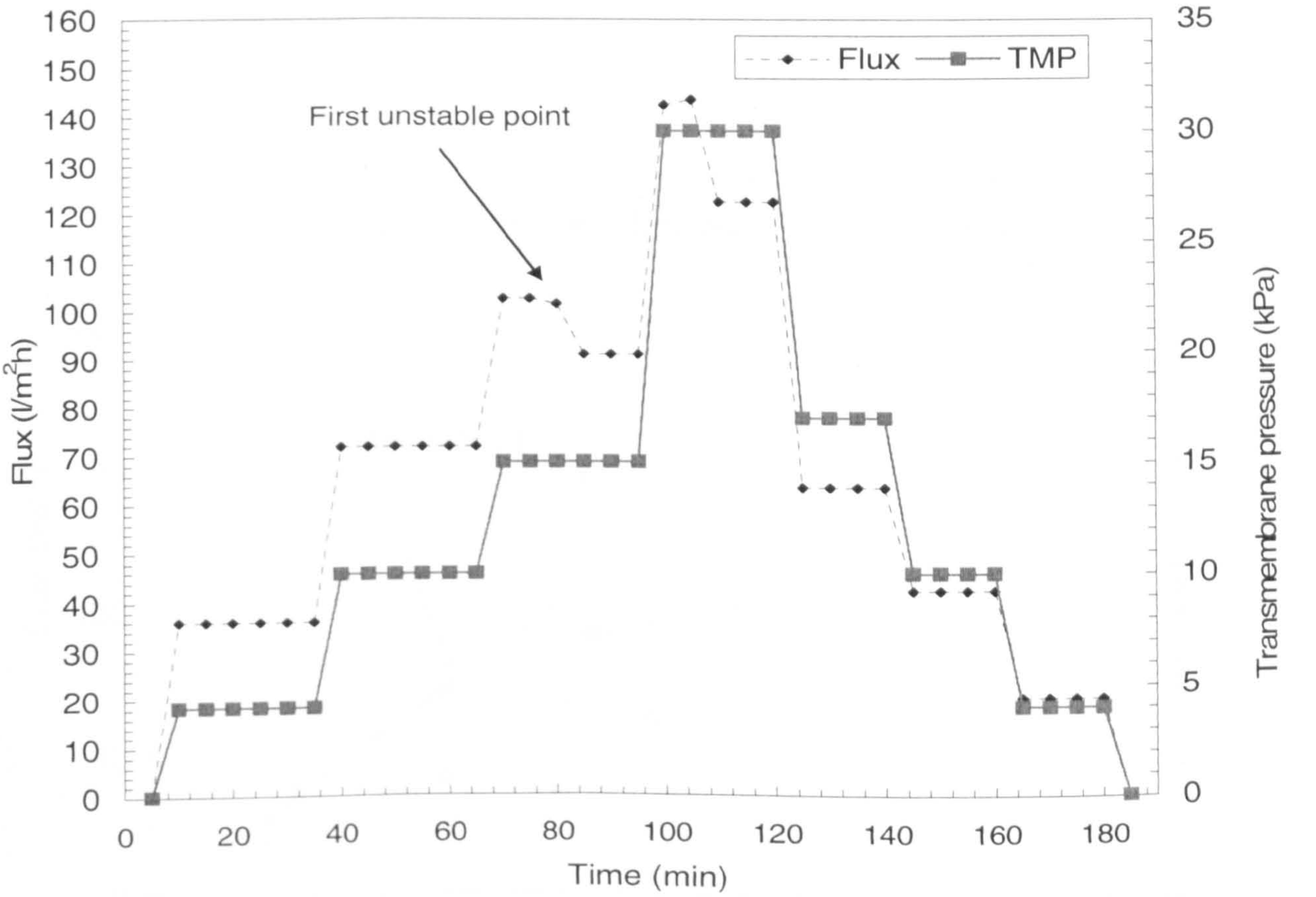

Figure 4.8: Determination of critical permeation flux by the step by step method at a crossflow velocity of 1.14 m s^{-1} for 1000 mg L^{-1} of n-dodecane emulsion with added sorbitan monoleate concentration of 100 mg L^{-1}.

For all experiments where the strong form of critical flux has been observed, the critical flux was taken to be the point at which the $J = f(\Delta P)$ curve first deviates by 1% from the linear relationship of $J = f(\Delta P)$ obtain earlier by clean water. An illustration of critical flux determination of the strong form using permeation flux versus transmembrane pressure plot is demonstrated in Figures 4.9. The critical flux measured by this technique provided critical flux values equal to the flux value at the first time dependent step or a flux value somewhere in between the final time independent step and the first time dependent step. The flux data equivalent to the upwards and downwards steps were plotted against *TMP* along with the clean water flux points acquired before conducting filtration tests for n-dodecane emulsions. An accuracy of ± 5 % was obtained for the J_{crit} values.

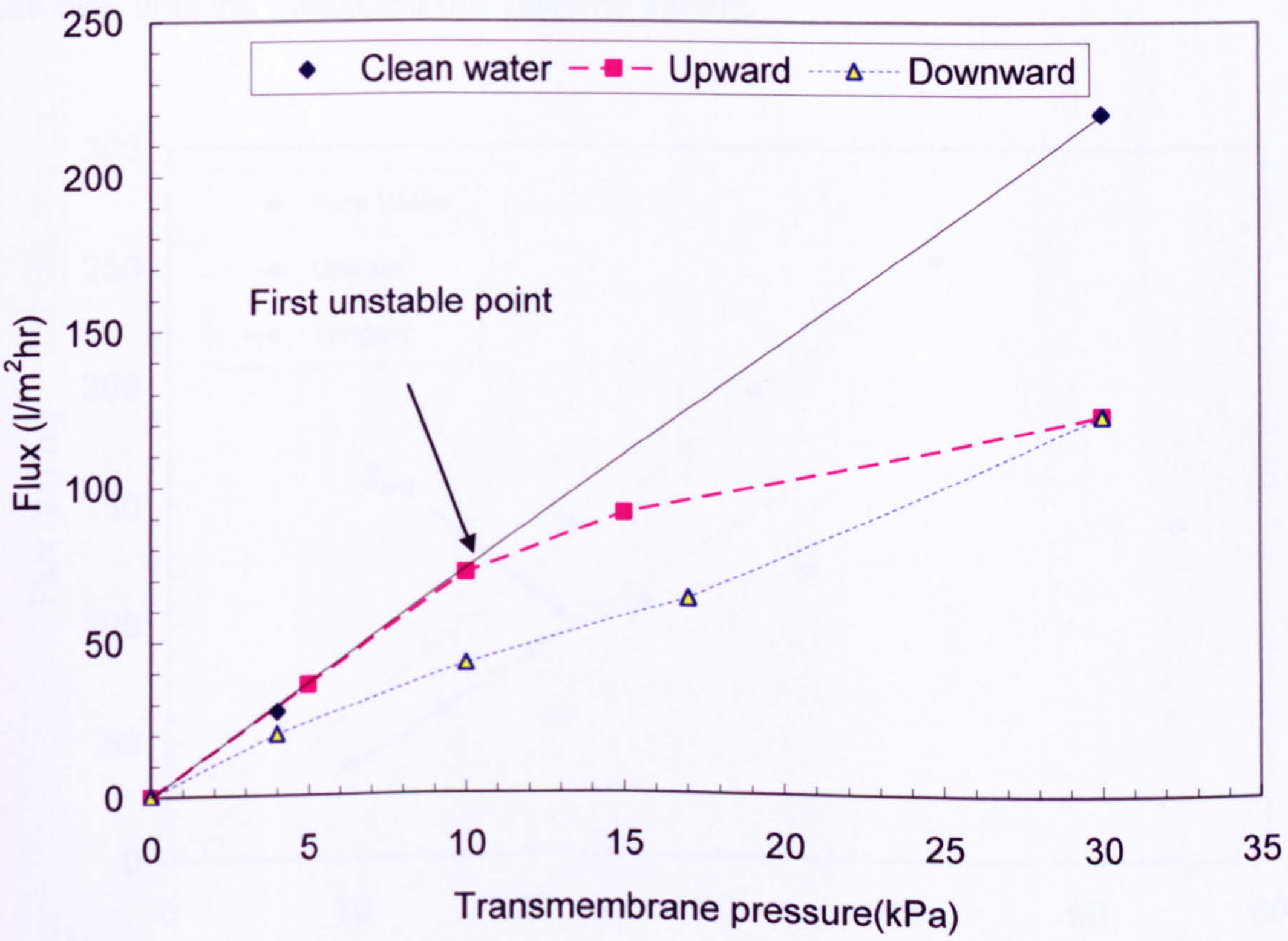

Figure 4.9: Determination of permeation critical flux from flux versus transmembrane pressure at a crossflow velocity of 1.14 m s^{-1} for 1000 mg L^{-1}. Data are shown for both the clean water, upwards and downwards.

For experiments where the weak form of critical flux was observed, the critical flux was taken to be the point at which the $J = f(\Delta P)$ curve first deviated by 1 % from the tangent line. The tangent line is drawn based on the first stable steps where there is a linear trend as shown in Figure 4.10. Similarly to the strong form, the critical flux measured by this method provided critical flux values equal to the flux value at the first time dependent step or a flux value somewhere in between the final time independent step and the first time dependent step.

For most experiments, the number of TMP steps upwards was up to 7, and up to 3 pressure step downs were made, with up to 5 readings of permeate flux taken at each pressure step. For most experiments, between 2 to 3 pressure step ups were made below the critical flux and 2 steps were made above the critical flux. For TMP steps above the critical, the number of readings of permeate flux was greater than five, until the measured flux became steady.

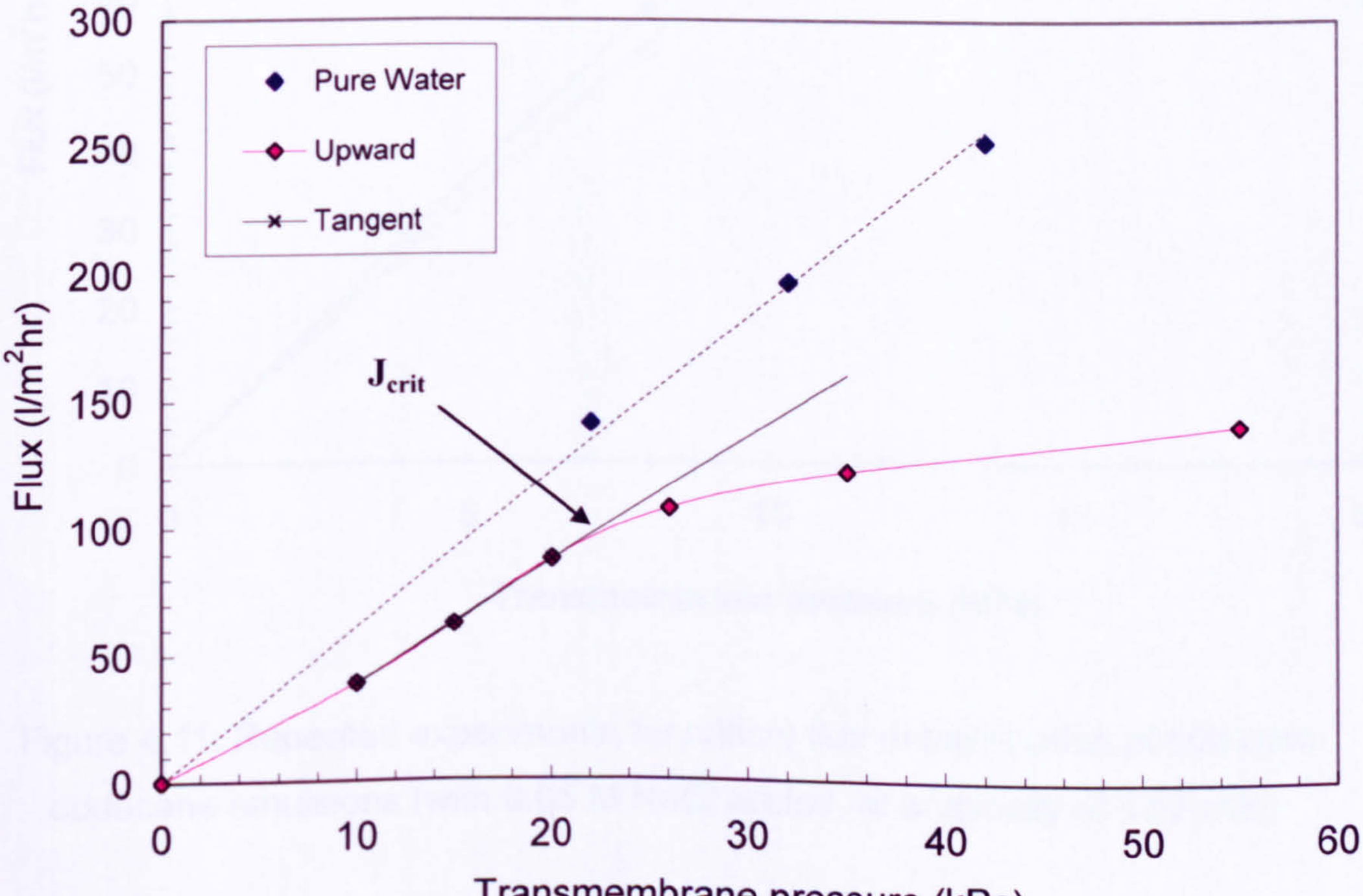

Figure 4.10: Determination of permeation critical flux from Flux versus transmembrane pressure at a crossflow velocity of 1.52 m s^{-1} for 1200 mg L^{-1}. Data are shown for both the clean water, upwards and tangent line.

The technique of measuring the critical flux used by Neal *et al.*(2003) was to take the critical flux as being the average of the last time independent flux step and the first time dependent step. However, as result of the irregularity of steps in term of their height and width in this work, this method has not been used. Also, the step height should be kept smaller, however, due to the experimental rig limitation that required the transmembrane pressure to be set by manipulating the permeate valve manually, the step heights were considered moderate to high.

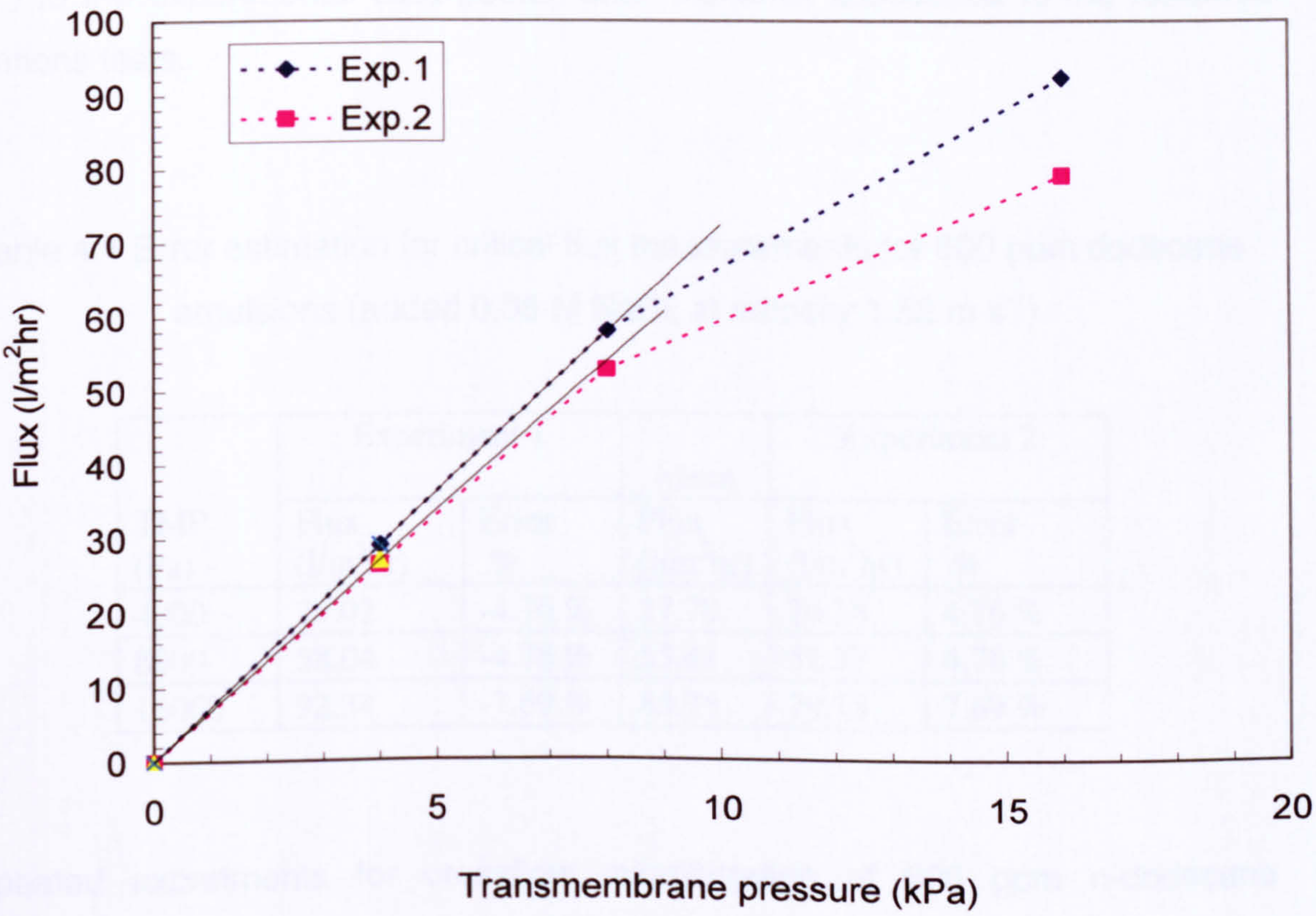

Figure 4.11: Repeated experiments for critical flux determination of 600 ppm dodecane emulsions (with 0.05 M NaCl added, at a velocity of 1.52 m/s).

4.12 Error Analysis and Reproducibility of Experimental data

A number of filtration tests were done again to the point at which the pressure step gave the first time dependent (unstable) permeation flux. These repeated filtration tests demonstrated a reasonable reproducibility of experimental data for oil in water emulsions (Figure 4.11 and Figure 4.12). The experimental error on critical flux is calculated to be up to ± 10 %. This error is the sum of some estimated errors such as the error related to the pressure step height and width in the upwards steps. Also, the error in the clean water flux is approximated to be the most dominant one. In addition, the error generated by the curve fitting of the $J = f(\Delta P)$ to the experimental data points, and the error associated to the repeated filtrations tests.

Table 4.1 Error estimation for critical flux measurements for 600 ppm dodecane emulsions (added 0.05 M NaCl, at velocity 1.52 m s^{-1}).

TMP (Pa)	Experiment 1		Mean	Experiment 2	
	Flux (l/m^2hr)	Error %	Flux (l/m^2hr)	Flux (l/m^2hr)	Error %
4000	29.02	-4.76 %	27.70	26.38	4.76 %
8000	58.04	-4.76 %	55.41	52.77	4.76 %
16000	92.34	-7.69 %	85.75	79.15	7.69 %

Repeated experiments for crossflow microfiltration of 600 ppm n-dodecane emulsions demonstrated that the reproducibility of experimental data at crossflow velocity 1.52 m/s and with addition of 0.05 M NaCl as presented in Figure 4.11. Furthermore, the maximum error related to the critical flux measurement was estimated to ±7.69 %, as shown in Table 4.1.

Similarly, repeat filtration tests for 1200 ppm n-dodecane emulsions demonstrated that the reproducibility of experimental data at crossflow velocity 1.52 m s^{-1}, despite of the irregularity in the size of TMP steps as illustrated in Figure 4.12.

For experiment 1 for filtration of 1200 ppm n-dodecane emulsion, the maximum error was calculated to be roughly 7.4 % (for the second TMP step) before reaching the critical flux point during filtration of 1200 ppm n-dodecane emulsions at crossflow velocity 1.52 m s^{-1}. Error estimation for the experimental data of each TMP step is summarized on Table 4.2.

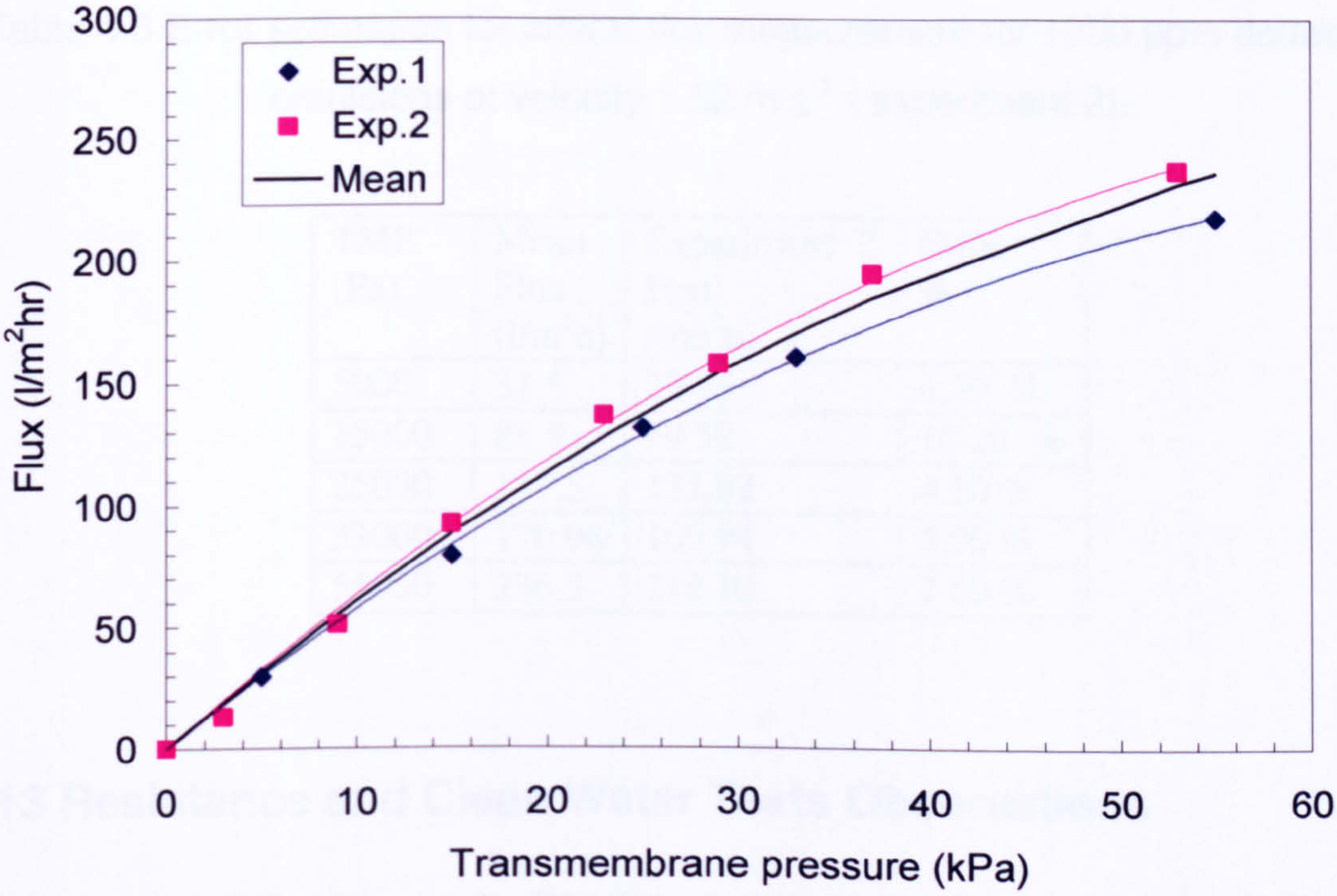

Figure 4.12: Repeated experiments for critical flux determination of 1200 ppm dodecane emulsions (with 120 ppm surfactant, at velocity 1.52 m/s).

Table 4.2 Error estimation for critical flux measurement for 1200 ppm dodecane emulsions at velocity 1.52 m s^{-1} (experiment 1).

TMP (Pa)	Mean Flux (l/m^2h)	Experiment 1 Flux (l/m^2h)	Error %
3000	19.14	13.19	6.50 %
9000	55.26	51.18	7.40 %
15000	88.5	92.34	-4.30 %
23000	128.34	137.19	-6.90 %
29000	154.86	158.30	-2.20 %
37000	185.74	195.24	-5.10 %
53000	232.14	237.45	-2.30 %

For experiment 2 at the same emulsion properties and operating conditions, the maximum error was calculated to be approximately 10.2 % (for the second TMP step) as outlined in Table 4.3. Hence the error for measurement of critical flux for 1200 ppm n-dodecane emulsions was estimated roughly to be ± 10 %.

Table 4.3 Error estimation for critical flux measurement for 1200 ppm dodecane emulsions at velocity 1.52 m s^{-1} (experiment 2).

TMP (Pa)	Mean Flux (l/m^2h)	Experiment 2 Flux (l/m^2h)	Error %
5000	31.5	29.55	6.20 %
15000	88.5	79.50	10.20 %
25000	137.5	131.92	4.10 %
33000	170.94	160.94	5.90 %
55000	236.5	218.10	7.80 %

4.13 Resistance and Clean Water Tests Observations

Prior to and following each filtration experiment, the clean water flux was determined as a function of pressure drop by running deionised water through the rig. The fouling type formed after each experiment appeared to be mainly irreversible. Therefore, the chemical cleaning procedure that has been developed and used here appeared to be effective for removing oil deposits from the membrane, as indicated in Figure 4.13 and Table 4.4. The commercial detergent (Decon 90) was effective for cleaning n-dodecane (oil) and sorbiton monoleate (surfactant) from the fouled membrane.

The cleaning procedure has been improved through several filtration experiments, since this is the only way to make sure that the suggested cleaning method is effective. For example, at the start of conducting oil filtration tests, deionised water was circulating through the rig for 3-6 hours at the maximum pressure and the membrane element was soaked in 2-2.5 (v/v) %. Although, it seemed to be working fine for filtration of low oil concentration (300 -400 ppm), it failed to clean

the fouled membrane after filtration of higher oil concentrations. Also, after a few experiments, the clean membrane resistance fluctuated to an unacceptable level which suggested that the cleaning procedure needed to be modified. Also, the period of cleaning was for 6 hours, where both circulated and mixing pumps were running, hence energy consumption was very high.

From Table 4.4, it can be seen that the there is a fluctuation of membrane resistance values after each chemical cleaning of the membrane. Therefore, after chemical cleaning following 20 filtration experiments, the mean membrane resistance is estimated to be 5.8E+11 m^{-1}, which was taken to be an acceptable value at which to start the next filtration experiment.

Table 4.4: Membrane resistance values after each chemical cleaning.

Exp. Number	Resistance (m^{-1})	R_{av}-R_m (m^{-1})	[(R_{av}-R_m)/R_{av}] %
1	6.00E+11	19140045400	3.29%
2	5.82E+11	1033679638	0.18%
3	5.48E+11	-3.29E+10	-5.67%
4	5.07E+11	-7.43E+10	-12.80%
5	5.35E+11	-4.57E+10	-7.87%
6	4.54E+11	-1.27E+11	-21.93%
7	5.35E+11	-4.56E+10	-7.86%
8	5.78E+11	-2727793090	-0.47%
9	5.49E+11	-3.18E+10	-5.47%
10	5.75E+11	-5887861253	-1.01%
11	5.82E+11	1304721041	0.22%
12	5.93E+11	11766593819	2.02%
13	5.54E+11	-2.72E+10	-4.69%
14	5.81E+11	18684829.8	0.00%
15	5.86E+11	4492117934	0.77%
16	6.54E+11	73392214235	12.63%
17	4.69E+11	-1.11E+11	-19.21%
18	5.19E+11	-6.21E+10	-10.69%
19	6.53E+11	72042808282	12.40%
20	6.06E+11	24626059349	4.24%
21	6.10E+11	29208248257	5.03%
R_{av}	5.81E+11		

Typically, after chemical cleaning the membrane following a full day experiment, three clean water tests were carried out and their mean total resistance (r_t) values were as follows; 5.6E+11, 4.64E+11, and 4.73 E+11 m^{-1}. On the following day, water tests were carried out again and the mean membrane resistance value was 5.81E+11 m^{-1}.

This observation raised a question about the acceptable level of fluctuations for total resistance. Therefore, the clean water tests were carried out just before the start of the oil emulsion filtration experiment. Due to the variations of membrane resistance during clean water tests before filtration experiments, it was found that membrane resistance for the first steps in the filtration tests, i.e. before reaching the critical flux, is almost the same as those of the clean water test. This could be due to low transmembrane pressure compared at the first steps, when negligible fouling will deposited on the membrane and thus the only membrane resistance would be dominant.

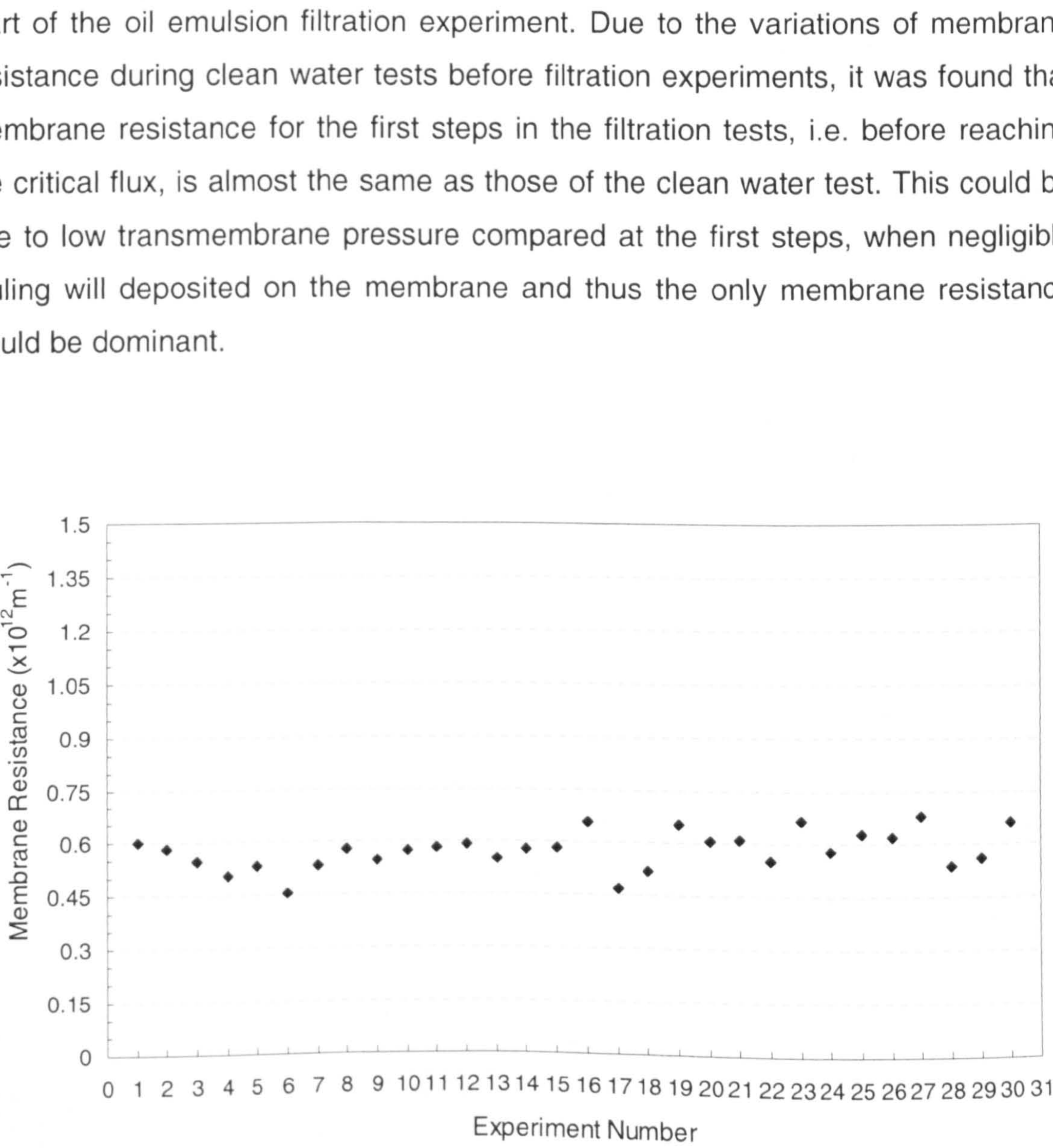

Figure 4.13: Membrane resistance after each filtration experiment.

As a result of the inevitable fluctuations of membrane resistances after chemical cleaning following each experiment, the comparisons between results might be become inappropriate. Thus to reduce the effect of this a normalization factor is introduced, defined by the ratio of membrane resistance after cleaning to the mean membrane resistance (5.8E+11m^{-1}). Hence, the resulting data for any filtration test conducted above or below 25 % of the mean membrane resistance was ruled out.

CHAPTER 5

Characterisation of Oil-in-Water Emulsions

5.1 Introduction

This chapter will discuss some aspects of emulsion science in relation to the analytical results for characterisation purposes. Measurements of the particle size distributions for the oil-in-water emulsions have been determined at different emulsion properties and operational conditions. The mean particle size and particle size distribution of oil emulsions was obtained at various time intervals during the crossflow experiments. Also, the purpose of particle size distribution characterisation is to compare with the pore size distribution of the membrane module used for microfiltration, in order to obtain separation by size exclusion.

5.2 Emulsion Formation

Emulsions are dispersions of one liquid (oil) in another immiscible liquid (water). Emulsion formation involves not only energy input but also surface active agents to provide stability. Therefore, mechanical energy has to be applied to the system to break large droplets into smaller ones. The final size distribution of the oil droplets in the emulsion depends on the power density of the homogenization technique. Typical oil droplets sizes are in the range from 0.1 to 10 μm. Given that the typical size of the emulsified oil droplets are similar in size to, or bigger than, the wavelength of visible light, emulsions appear milky white. Emulsions need to be stabilized with emulsifiers since oil-in-water mixtures are unstable thermodynamically. In addition, as of a result of being at their lowest free energy state, total separation would occur as the oil droplets coalesce and form an oil layer. Therefore, addition of surfactants is required to ensure the stability of oil-in-water emulsions and avoid the oil coalescence process. Emulsifiers concentrate at the oil-water interface and prevent oil droplet coalescence as shown systematically in Figure 5.1.

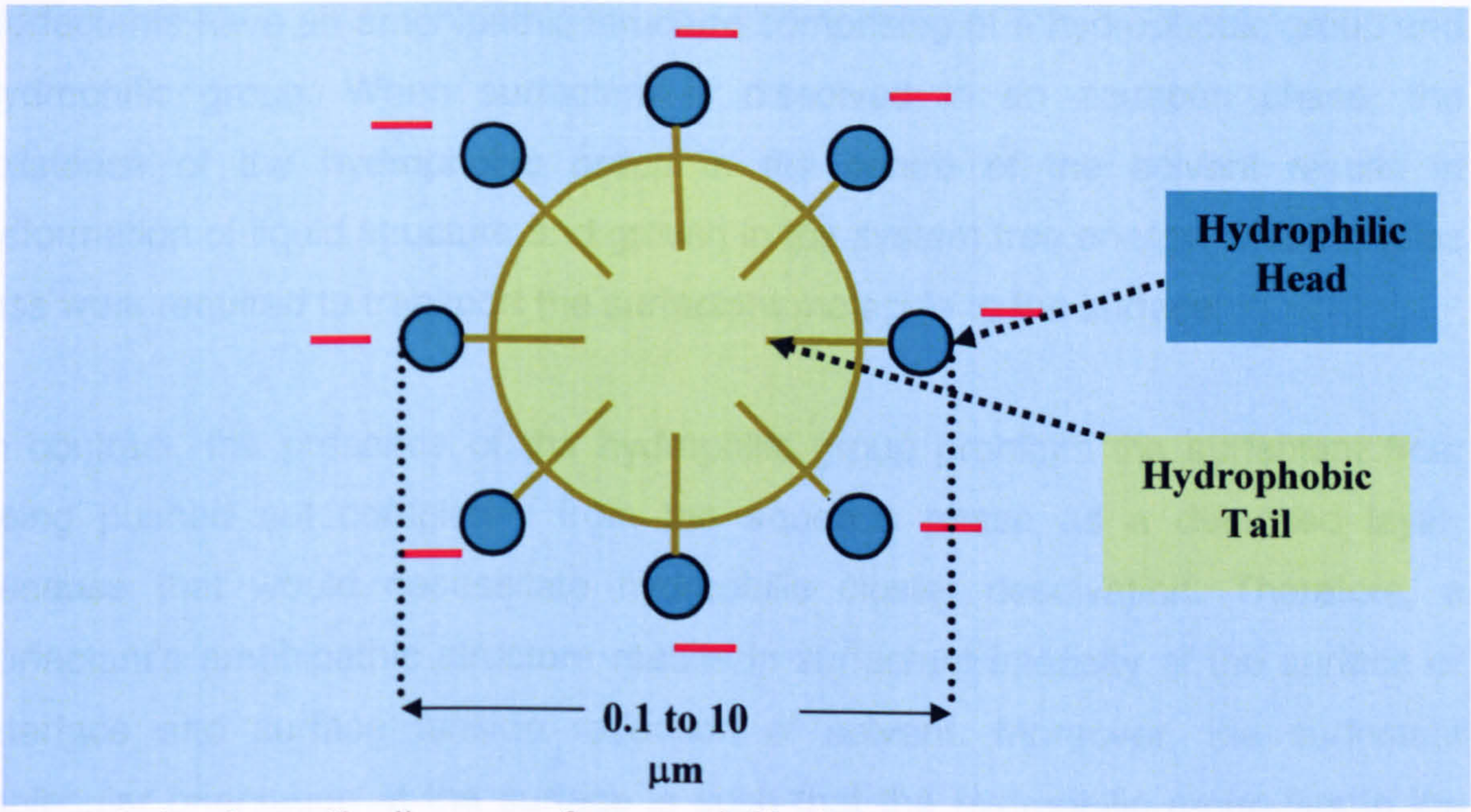

5.1: A schematic diagram of an emulsified oil droplets (anionic surfactant).

Emulsion stability variations depend on the chemical properties of the oil and its concentration, and on the emulsifier type such as cationic and anionic or non-ionic properties. For instance, when the hydrophilic head of an oil-in-water emulsion is negatively charged, the net surface charge of the emulsified oil droplet is negative. The emulsified oil droplets tend to stay dispersed due to electrostatic repulsion between them. The emulsion is thought then to be kinetically stable. The presence of a surfactant assists in speeding up the formation rate of the small drops, since it reduces the interfacial tension between the two phases. The solubility of the surfactant, its concentration, and the viscosity of the continuous phase influence the process of emulsification and the nature of the emulsion formed.

5.3 Surfactant

A surface-active agent is a chemical substance which, when present in low concentration, has the characteristic of adsorbing onto the system surfaces or interfaces and modifying their surface or interfacial free energies. The interfacial free energy could be defined as the least amount of work necessary to form such an interface. Surfactants normally operate to decrease interfacial free energy, even though in some circumstances they are applied to increase the interfacial free energy.

Surfactants have an amphipathic structure comprising of a hydrophobic group and hydrophilic group. When surfactant is dissolved in an aqueous phase, the existence of the hydrophobic group in the centre of the solvent results in deformation of liquid structure and growth in the system free energy, which implies less work required to transport the surfactant molecule to the surface.

In contrast, the presence of the hydrophilic group prohibits the surfactant from being pushed out completely from the aqueous phase as a detached layer, because that would necessitate hydrophilic cluster desolvation. Therefore, a surfactant's amphipathic structure results in surfactant intensity at the surface or interface and surface tension reduction of solvent. Moreover, the surfactant molecular orientation at the surface is such that the hydrophilic group lies in the aqueous phase and hydrophobic group is orientated away from the aqueous phase, as indicated in Figure 5.1.

Hydrophilic groups may be cationic (organic amines), anionic (fatty acids), and non-ionic (organic compounds with oxygen holding groups such as alcohols or esters). Lipophobic groups might be long, straight or branched chain hydrocarbons, aromatic hydrocarbons, cyclic hydrocarbons and or a mixture of them.

Surfactants are categorized in accordance with the balance between the hydrophilic and lipophilic parts of their molecules. The hydrophilic-lipophilic balance (HLB) number specifies randomly the molecule polarity in a range of 1-40, with the most frequently employed emulsifiers obtaining a value between 1 and 20. The HLB value increases with rising hydrophilicity. Surfactants with HLB numbers in the range of 3-6 promote W/O emulsions, whilst values in the range 8-18 promotes O/W emulsions.

Although the primary emulsion in this research is an O/W emulsion, a surfactant with an HLB in the range of 3-6 has been selected due to its presence in an effluent or produced water stream. Also, Riegelman *et al* (1962) found that O/W emulsions could be prepared with emulsifiers over the whole HLB range of 2-17. Therefore, span 80, Sorbitan monooleate, a non-ionic surfactant with HLB value

of 4.3 and molecular weight of 428 and molecular formula $C_{24}H_{44}O_6$, is used in this work as an emulsifier in an O/W system. Figure 5.2 represents the formula structure of sorbitan monooleate.

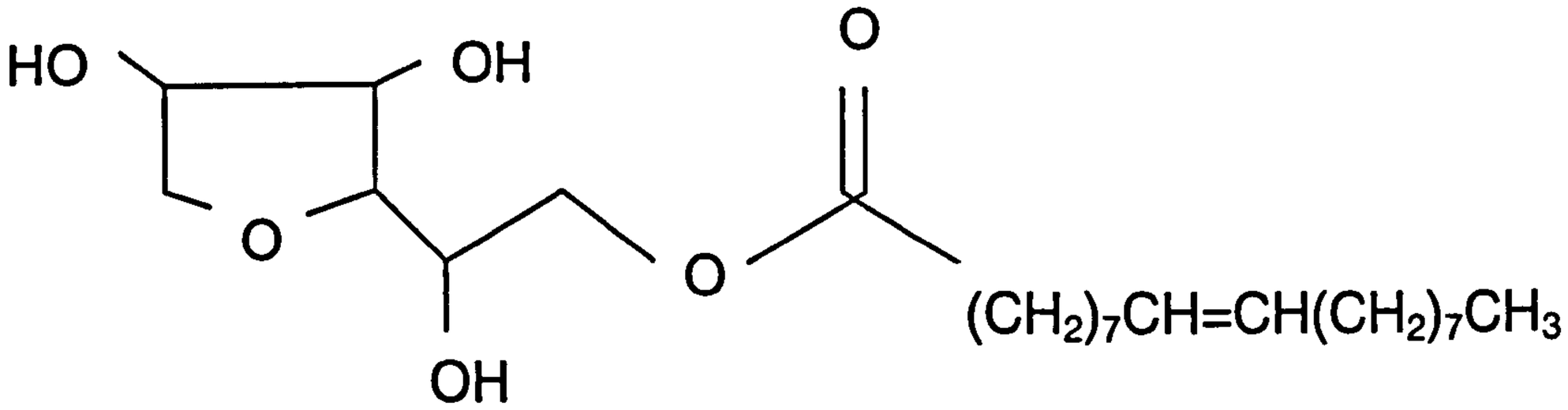

Figure 5.2: The structure of sorbitan monooleate (Span 80).

5.4 Oil-in-Water Emulsions Preparation

Oil-in-water emulsions were prepared at various oil and surfactant concentrations in order to prepare a dispersion for feeding to the crossflow filtration rig. In addition, a number of preliminary experiments were conducted to ensure the stability of oil-in-water emulsions at different operating conditions. To do this, emulsions were circulated through the rig in crossflow mode without any filtration for several hours and samples were taken for chemical analysis. The oil droplet size distributions and the oil-in-water concentration of the feed have been measured and their variations with time were investigated for characterization purposes. Oil-in-water samples were prepared at different oil and surfactant concentrations, and with the addition of different salts as shown in Table 5.1.

Table 5.1: Summary of prepared oil-in-water emulsion samples.

Sample	Deionised H_2O (Continues Phase)	n-Dodecane (oil model) Concentration (mg/L)	Sorbiton Monooleate Concentration (mg/L)	NaCl (M)	$CaCl_2$ (M)	$FeCl_3$ (M)
1	10 litre	300	0	-	-	-
2	10 litre	300	30	-	-	-
3	10 litre	300	60	-	-	-
4	10 litre	300	100	-	-	-
5	10 litre	400	40	-	-	-
6	10 litre	600	60	-	-	-
7	10 litre	600	160	-	-	-
8	10 litre	1000	0	-	-	-
9	10 litre	1000	100	-	-	-
10	10 litre	1200	0	-	-	-
11	10 litre	1200	120	-	-	-
12	10 litre	1200	240	-	-	-
13	10 litre	2400	240	-	-	-
14	10 litre	600	60	0.05	-	-
15	10 litre	600	60	0.1	-	-
16	10 litre	600	60	-	0.1	-
17	10 litre	1200	240	-	0.1	-
18	10 litre	2400	240	0.1	-	-
19	10 litre	2400	240	-	0.1	-
20	10 litre	2400	240	-	-	0.1

5.5 Analytical Results and Discussions

5.5.1 Oil droplet size distribution

Figures 5.3 and 5.4 represent the oil droplet size distributions of sample 2 at various time intervals during crossflow operation while both the circulating and mixing pumps were running, hence to make sure that during normal operation the emulsion neither broke nor coalesced. The particle size distributions for both experiments 1 and 2 remained quite constant, which demonstrated adequate emulsion stability.

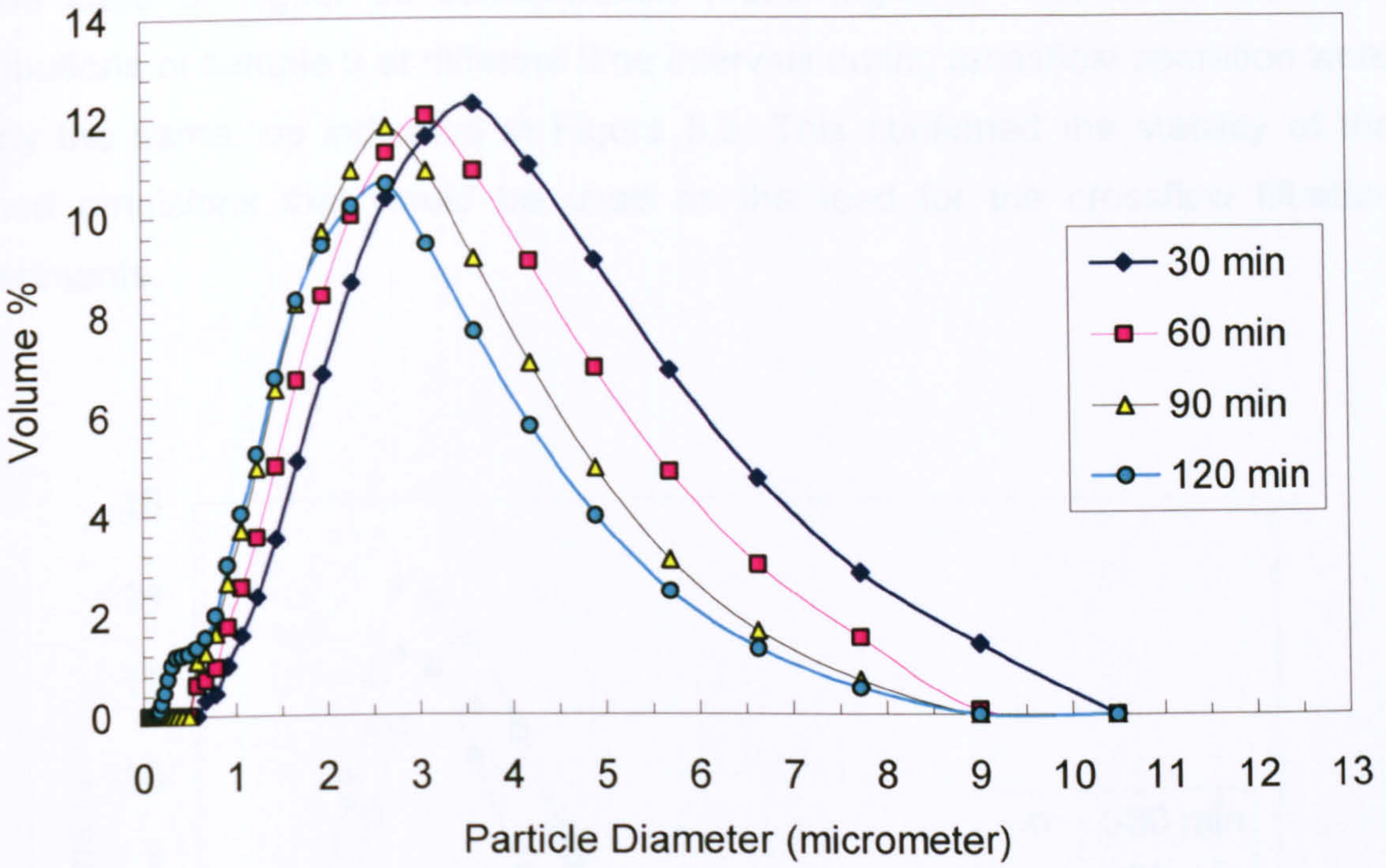

Figure 5.3: Oil droplets size distribution at various time intervals for test-1 300 mg L^{-1} n-dodecane emulsion with surfactant 30 mg L^{-1}.

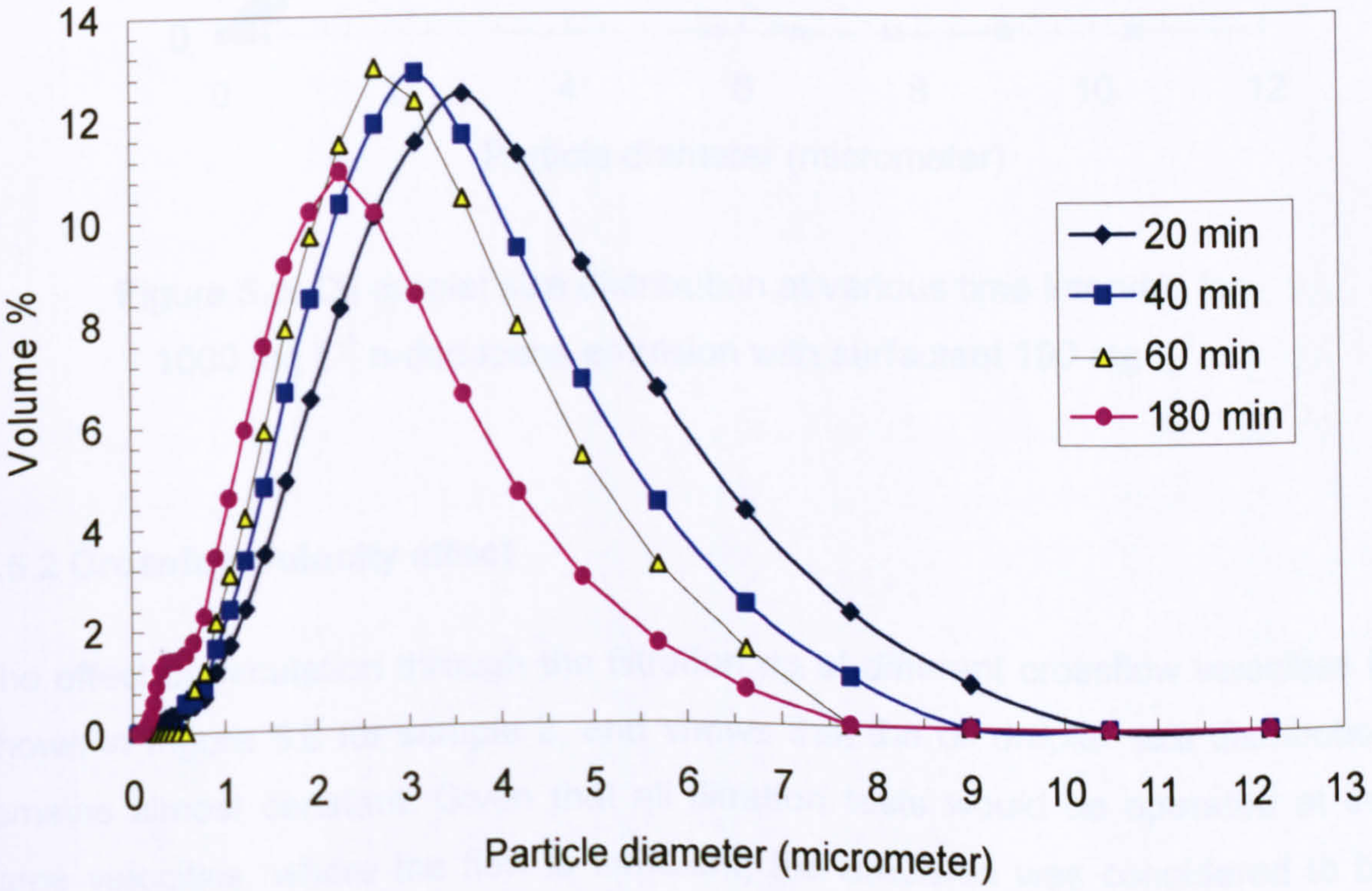

Figure 5.4: Oil droplets size distribution at various time intervals for test-2 300 mg L^{-1} n-dodecane emulsion with surfactant 30 mg L^{-1}.

In the case of higher oil concentration (1000 mg L^{-1}), the oil droplet size distributions of sample 9 at different time intervals during crossflow operation were nearly the same, as indicated in Figure 5.5. This confirmed the stability of the formed emulsions that would be used as the feed for the crossflow filtration experiments.

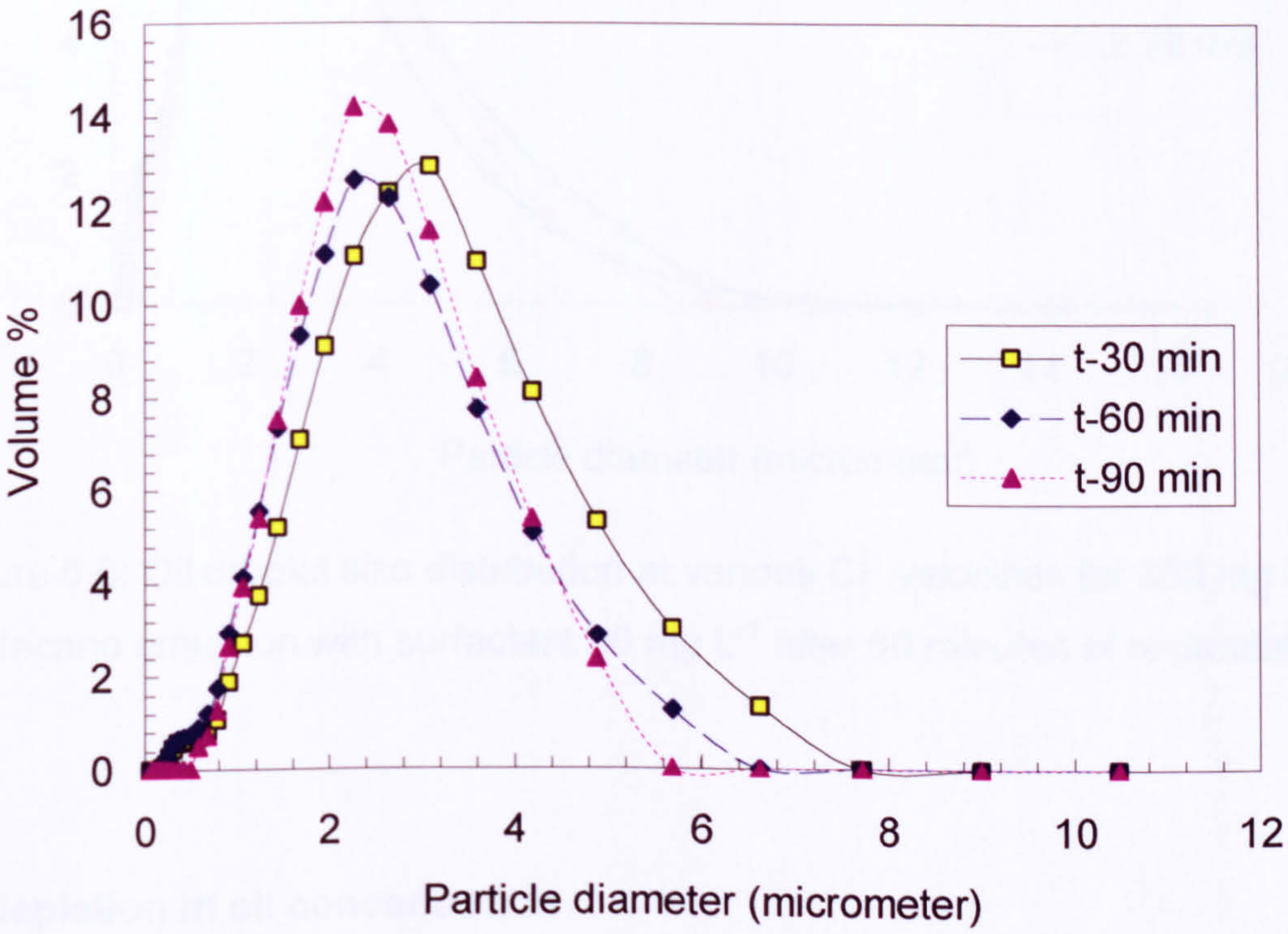

Figure 5.5: Oil droplet size distribution at various time intervals for 1000 mg L^{-1} n-dodecane emulsion with surfactant 100 mg L^{-1}.

5.5.2 Crossfow velocity effect

The effect of circulation through the filtration rig at different crossflow velocities is shown in Figure 5.6 for sample 2, and shows that the oil droplet size distribution remains almost constant. Given that all filtration tests would be operated at the same velocities, where the flow is turbulent, the emulsion was considered to be stable at all shear rates used in the experiments. Thus, for the increase in crossflow velocity from 1.14 to 2.28 m/s, negligible variations of the oil droplet size distributions were observed.

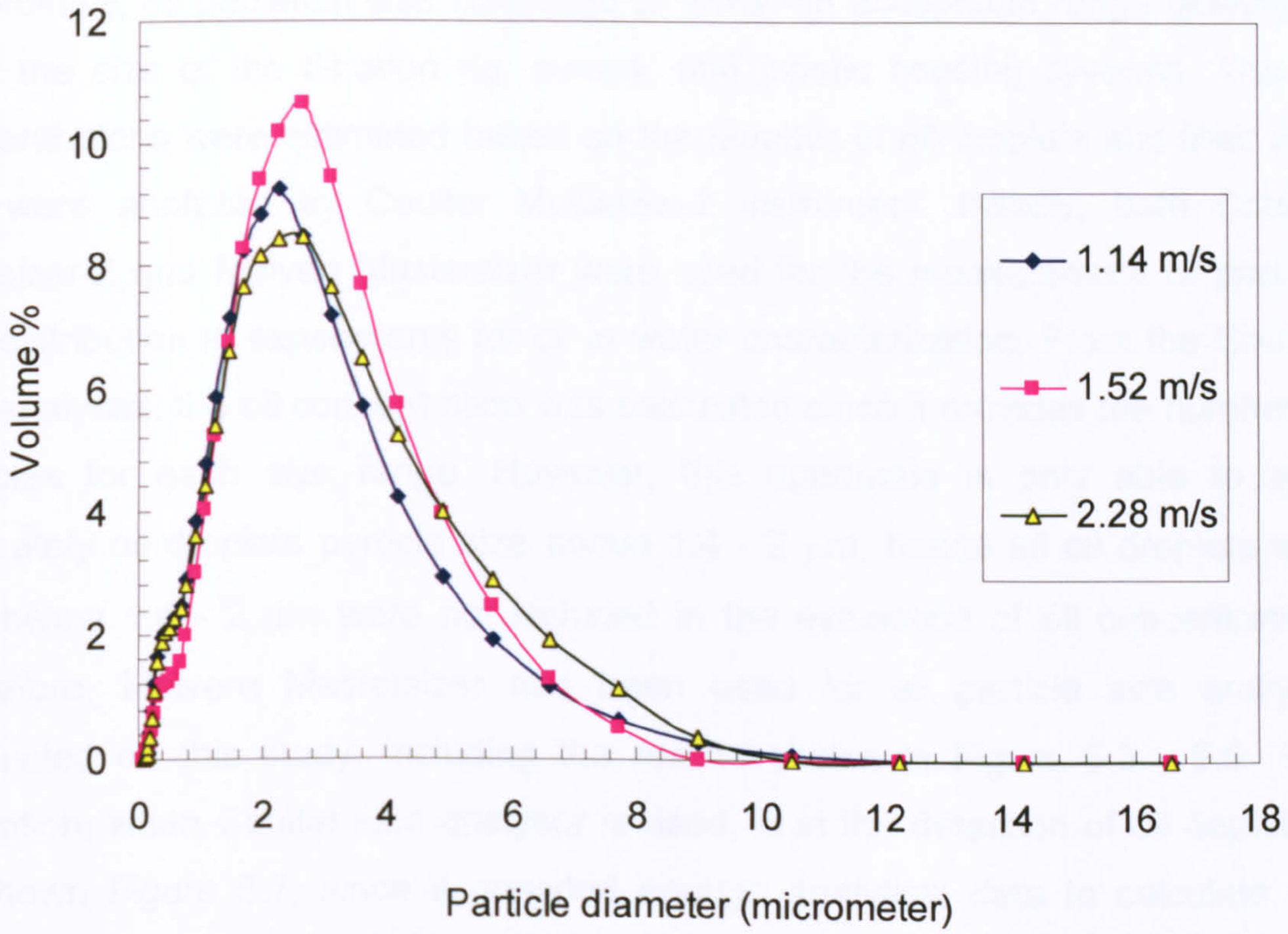

Figure 5.6: Oil droplet size distribution at various CF velocities for 300 mg L^{-1} n-dodecane emulsion with surfactant 30 mg L^{-1} after 60 minutes of recirculation.

5.5.3 Depletion in oil concentration

Among the issues that needed to be investigated is whether the oil concentration depletes with time during the crossflow operation. Therefore, as presented in Figure 5.7, a comparison has been performed between sample 1 and sample 2 regarding oil concentrations at different times at similar operating conditions. The outcome of such assessment was in favour of sample 2 (containing surfactant), where oil depletion was much less than from sample 1. Moreover, in sample 2 , an emulsifier has been mixed with oil-in-water emulsion, where the mass ratio of oil to surfactant was 10:1. Although the surfactant was selected because of its presence in effluents in the case study, the use of the surfactant for emulsion stability showed good improvement when it was introduced. Several emulsions prepared without using surfactant were unstable and the rate of oil depletion was very high.

Accordingly, oil depletion was controlled to within an acceptable range bearing in mind the size of the filtration rig, pumps, and plastic housing systems. The oil concentrations were estimated based on the number of oil droplets and their size that were analyzed by Coulter Multisizer-2 instrument. Initially, both Coulter Multisizer-2 and Malven Mastersizer were used for the measurement of particle size distribution in experiments for oil in water characterization. From the Coulter size analyses, the oil concentration was calculated since it provides the number of particles for each size range. However, this apparatus is only able to spot accurately oil droplets particle size above 1.4 - 2 μm, hence all oil droplets with size below 1.4 - 2 μm were not included in the evaluation of oil concentration. Therefore, Malvern Mastersizer has been used for all particle size analysis conducted on this study, including the results shown in Figure 5.3 - 5.6. The exception, when Coulter size analyser is used, is in the detection of oil depletion as shown Figure 5.7, since it provided enough analytical data to calculate the concentration.

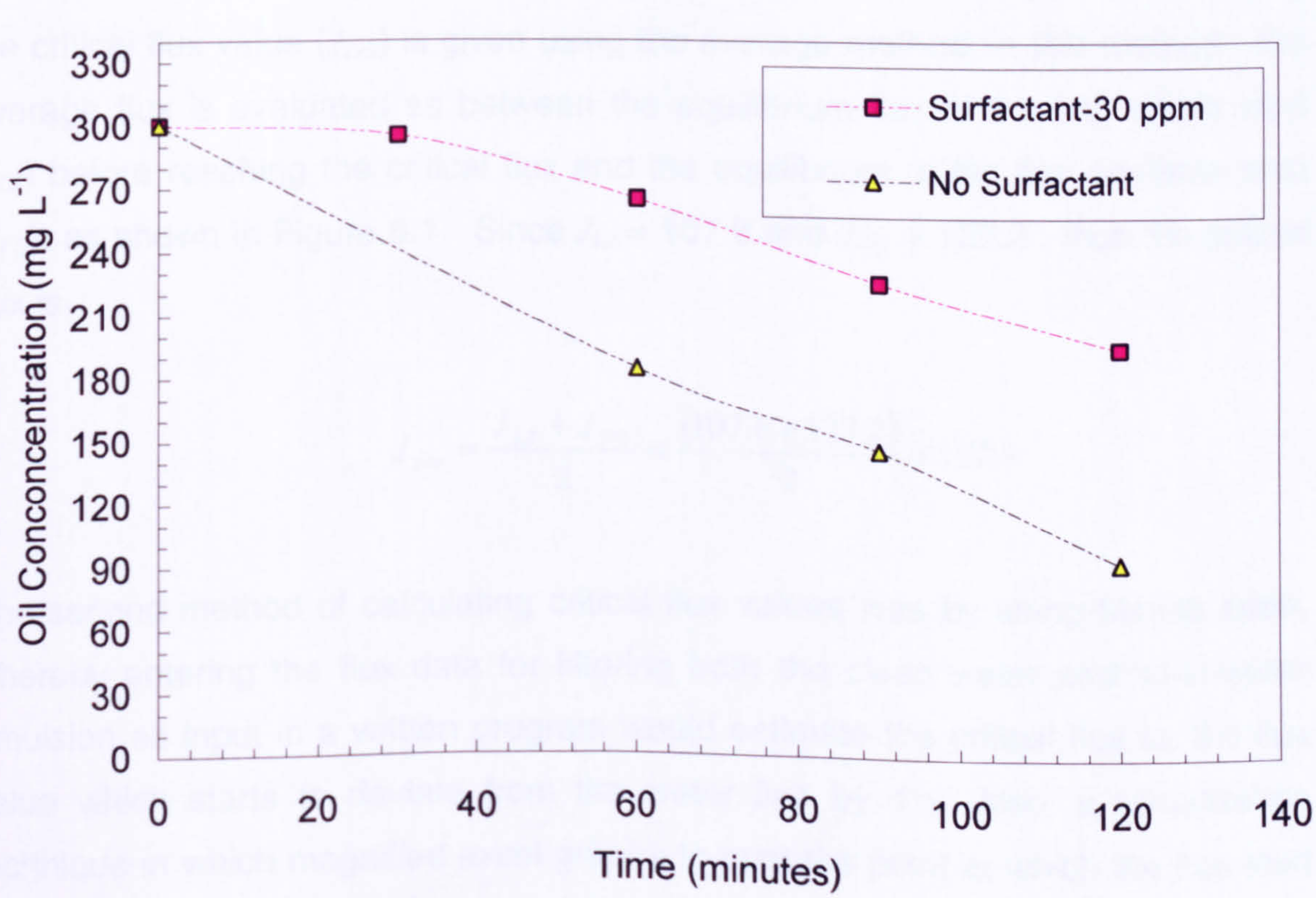

Figure 5.7: Estimated oil concentration depletion with time for 300 ppm n-dodecane emulsions.

CHAPTER 6

EXPERIMENTAL RESULTS

In this chapter a comparison between the methods used for estimation of the critical flux values is provided to illustrate their relative features. Particle size analyses of permeate samples are reported to show their compliance with the required product quality specifications. The results obtained from the experimental studies of the effect of suspension properties and hydrodynamics on the crossflow microfiltration of oil-in-water emulsions are also presented.

6.1 Critical Flux Estimation Methods

As mentioned in chapter 4, there two ways have been used to evaluate the critical flux values from the step by step technique plots. First, an example for estimating the critical flux value (J_{crit}) is given using the average method; in this method the average flux is evaluated as between the equilibrium flux of the last stable step (J_{LS}) before reaching the critical flux and the equilibrium of the first unstable step (J_{FU}), as shown in Figure 6.1. Since J_{LS} = 107.6 and J_{FU} = 137.2 , thus the critical flux is

$$J_{crit} = \frac{J_{LS} + J_{FU}}{2} = \frac{(107.6 + 137.2)}{2} = 122.4$$

The second method of calculating critical flux values was by using Matlab code, whereby entering the flux data for filtering both the clean water and oil-in-water emulsion as input in a written program would estimate the critical flux as the flux value which starts to deviate from the water line by 1%. Also, a visualization technique in which magnified excel graphs to spot the point at which the flux start to deviate from the water line was used. For the first 20 filtration tests, estimated critical fluxes by the different tools are presented in Table 6.1 and Figure 6.2.

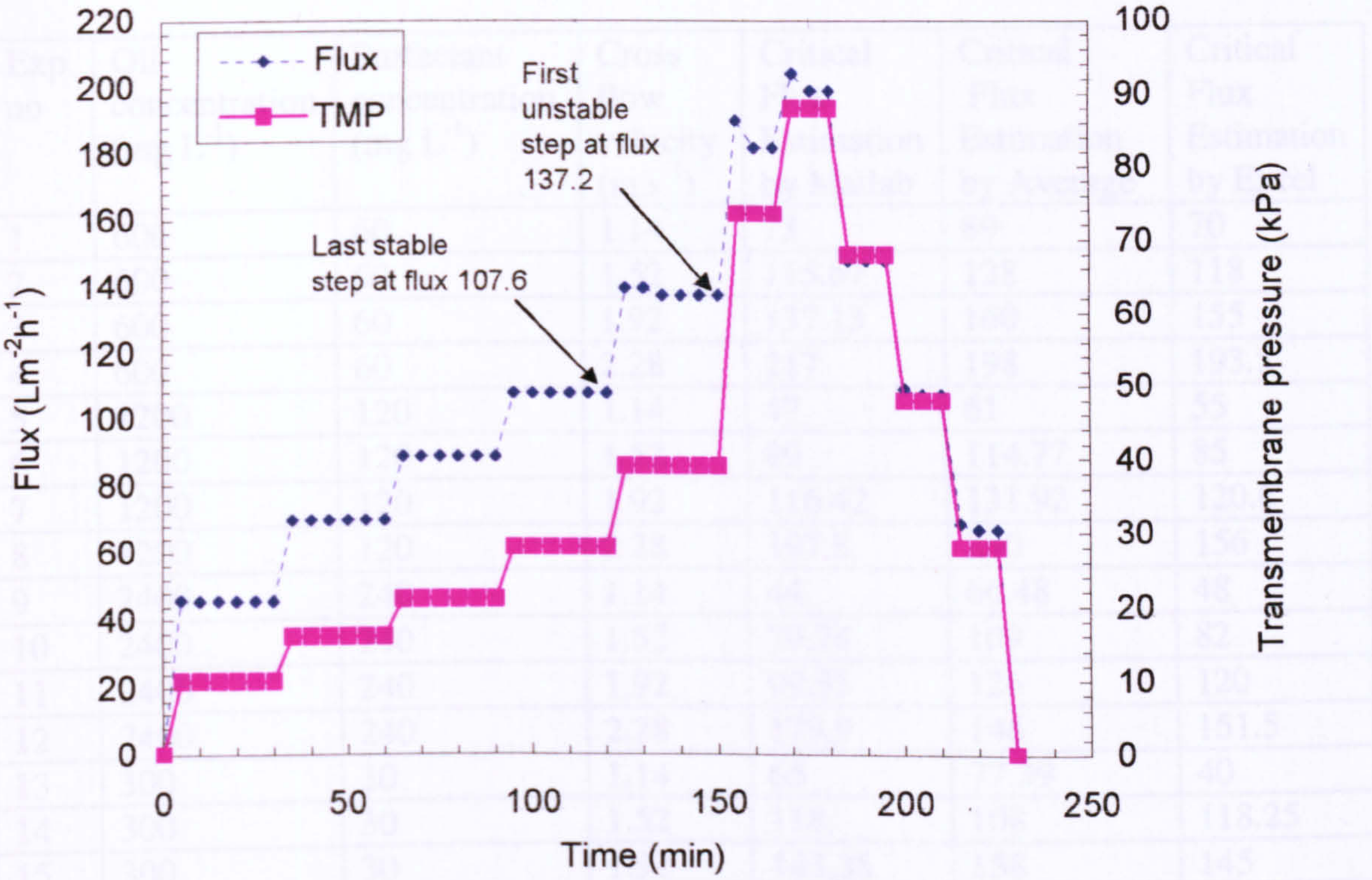

Figure 6.1: Determination of critical permeation flux by the step by step method at a crossflow velocity of 1.92 m s^{-1} for 1000 mg L^{-1} of n-dodecane emulsion with added sorbitan monoleate concentration of 100 mg L^{-1} (Experiment 20).

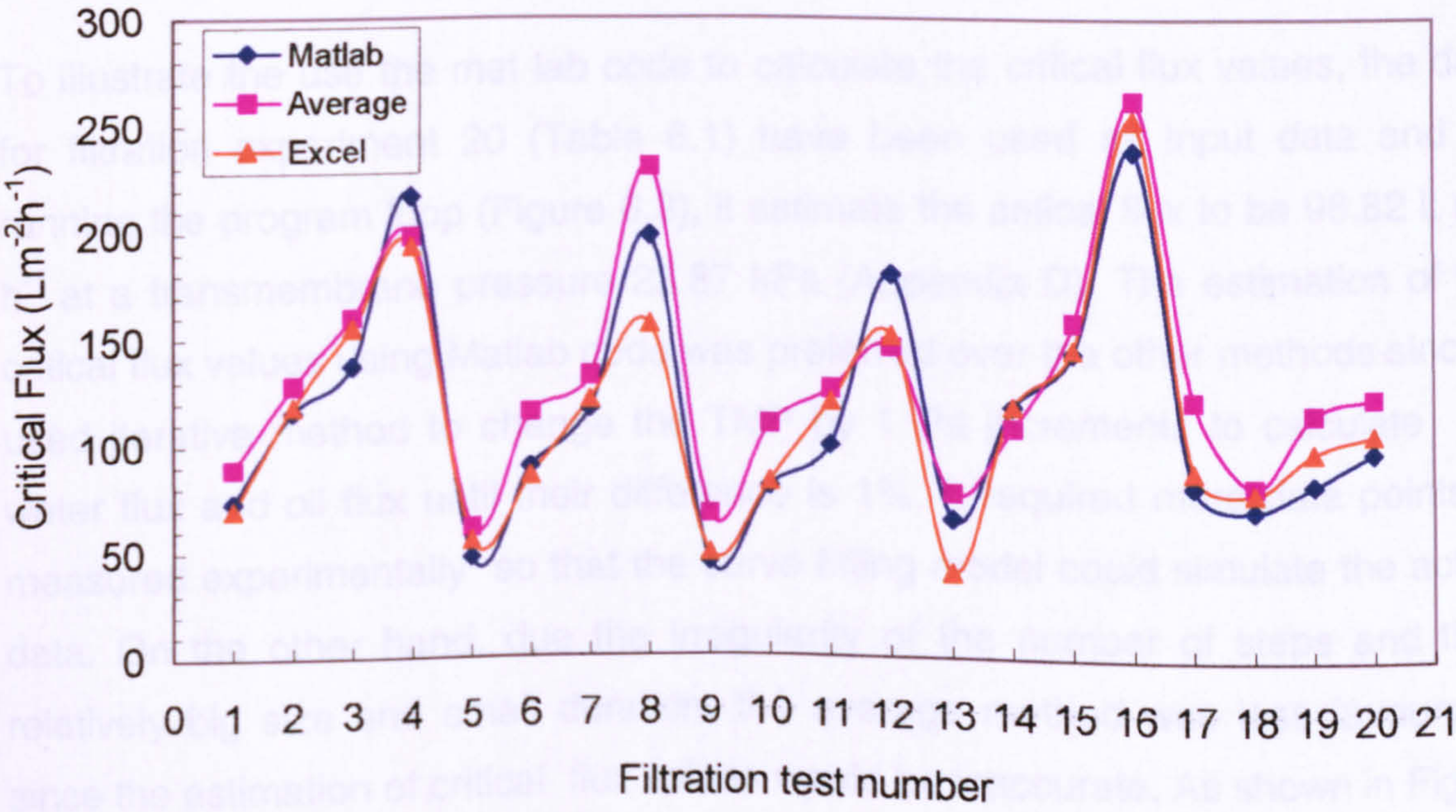

Figure 6.2: Critical flux values estimated by different methods.

Table 6.1: Measuring critical flux ($Lm^{-2}h^{-1}$) using different calculation tools.

Exp. no	Oil concentration ($mg\ L^{-1}$)	Surfactant concentration ($mg\ L^{-1}$)	Cross flow velocity ($m\ s^{-1}$)	Critical Flux Estimation by Matlab	Critical Flux Estimation by Average	Critical Flux Estimation by Excel
1	600	60	1.14	73	89	70
2	600	60	1.52	115.67	128	118
3	600	60	1.92	137.13	160	155
4	600	60	2.28	217	198	193.5
5	1200	120	1.14	47	61	55
6	1200	120	1.52	89	114.77	85
7	1200	120	1.92	116.42	131.92	120.6
8	1200	120	2.28	197.8	230	156
9	2400	240	1.14	44	66.48	48
10	2400	240	1.52	79.74	109	82
11	2400	240	1.92	99.33	126	120
12	2400	240	2.28	179.9	146	151.5
13	300	30	1.14	65	77.39	40
14	300	30	1.52	118	108	118.25
15	300	30	1.92	143.36	158	145
16	300	30	2.28	238	262.08	253
17	400	40	1.52	81.08	121.35	88
18	1000	100	1.14	69.9	81.26	78
19	1000	100	1.52	82	115	97
20	1000	100	1.92	96.82	122.42	105

To illustrate the use the mat lab code to calculate the critical flux values, the data for filtration experiment 20 (Table 6.1) have been used as input data and by running the program loop (Figure 6.3), it estimate the critical flux to be 96.82 L m^{-2} h^{-1} at a transmembrane pressure 23.87 kPa (Appendix D). The estimation of the critical flux values using Matlab code was preferred over the other methods since it used iterative method to change the TMP by 1 Pa increments to calculate the water flux and oil flux until their difference is 1%. It required more data points to measured experimentally so that the curve fitting model could simulate the actual data. On the other hand, due the irregularity of the number of steps and their relatively big size and small duration, the average method was less favourable since the estimation of critical flux values would be inaccurate. As shown in Figure 6.2 and Table 6.1, the overall variation of calculated critical flux values for the 20 filtration tests conducted demonstrated some discrepancies.

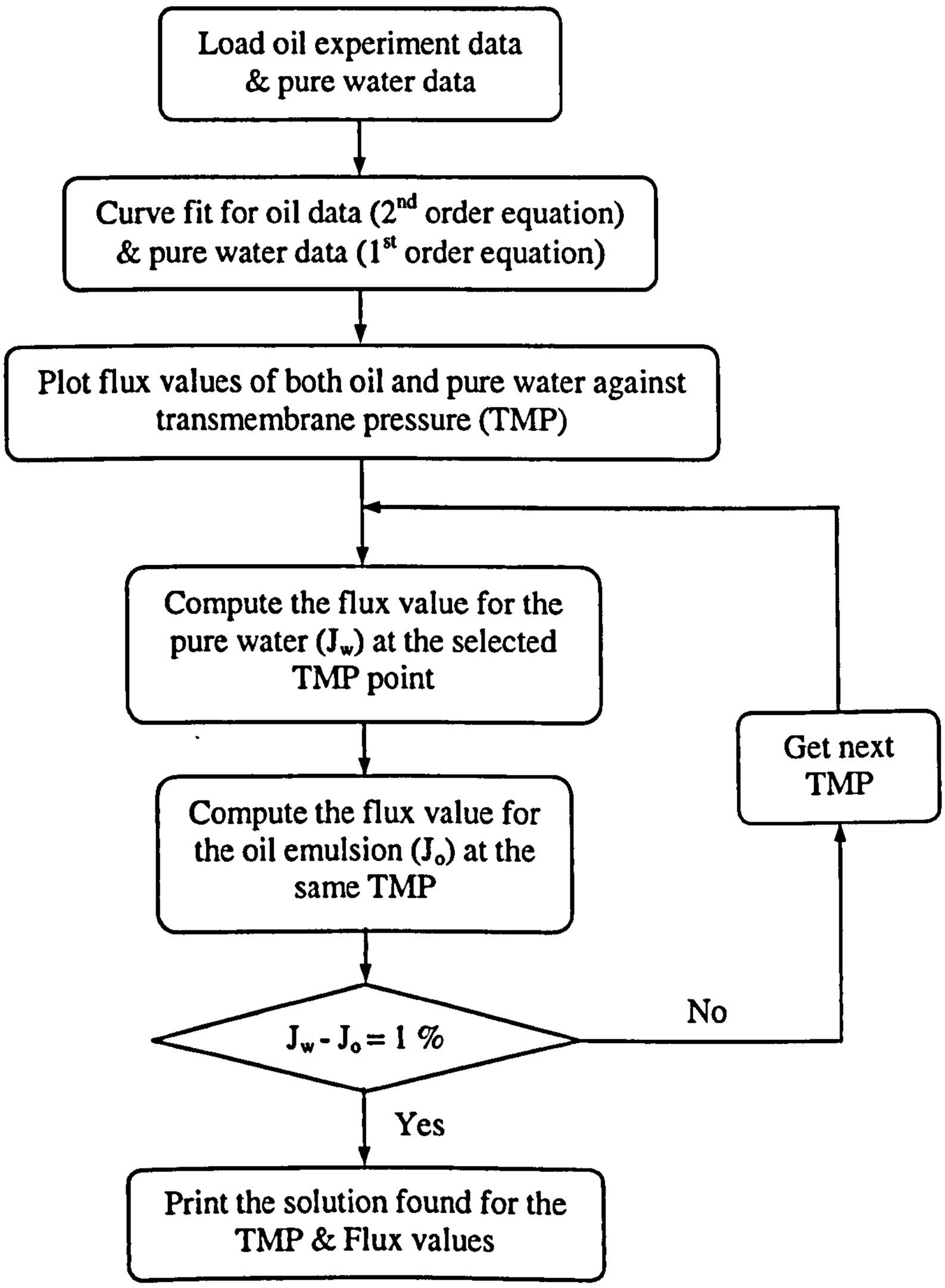

Figure 6.3 Flow chart for estimation of critical flux values using Matlab code.

An illustration of the two methods of determination of critical flux values from step by step tests is demonstrated in Figures 6.4 and 6.5 in order to compare further their merits. It can be seen on Figure 6.4 that the first time dependent flux (first unstable step) from incrementing pressure steps is at approximately flux 120 L m^{-2} h^{-1} (step 3), the previous time independent is roughly at a flux 80 L m^{-2} h^{-1}(step 2). Therefore, the critical flux is expected to lie between 80 -120 L m^{-2} h^{-1}. This type of plot showed the increase of flux decline rate with time (*dJ/dt*) particularly after reaching the critical flux point, which becomes quicker at the final two upward steps (step 6 and 7) as shown in Figure 6.5. Similarly, the behaviour of flux rate of change with time when stepping downward, where it could be that a cake layer had formed at previous upward steps is irreversible, despite operating at sub-critical flux. From examples at the same TMP, the measured flux at the second pressure step was 80 L m^{-2} h^{-1}, while after stepping down (at step 10) it was found to be 40 L m^{-2} h^{-1}. This suggests that the total membrane resistance, which is the sum of the membrane and cake layer resistances, has doubled. Bearing in mind that the measured flux at the first pressure step is identical to the pure water test, the total resistance represents only the membrane resistance. Thus, when the total resistance is doubled at the final pressure step (10), the cake layer resistance is equal to the membrane resistance.

On other hand, in the step by step method as demonstrated in Figure 6.5, the critical flux is measured as the point of deviation from clean water flux. This method would illustrate whether the strong or the weak form of critical flux has been encountered. Thus, the flux values for the clean water tests needed to measured carefully and accurately. However, from an experimental point of view, as discussed in chapter four, the pure water tests before conducting the filtration test showed small fluctuations which could affect the critical flux value measured by this technique or identifying the form of the critical flux. Nonetheless, comparing several filtration test results using the Flux-TMP plots seemed to be more appropriate at different operating conditions. Also, the existence of hysteresis between the flux values for pressure ascending and descending steps is displayed clearly by this method.

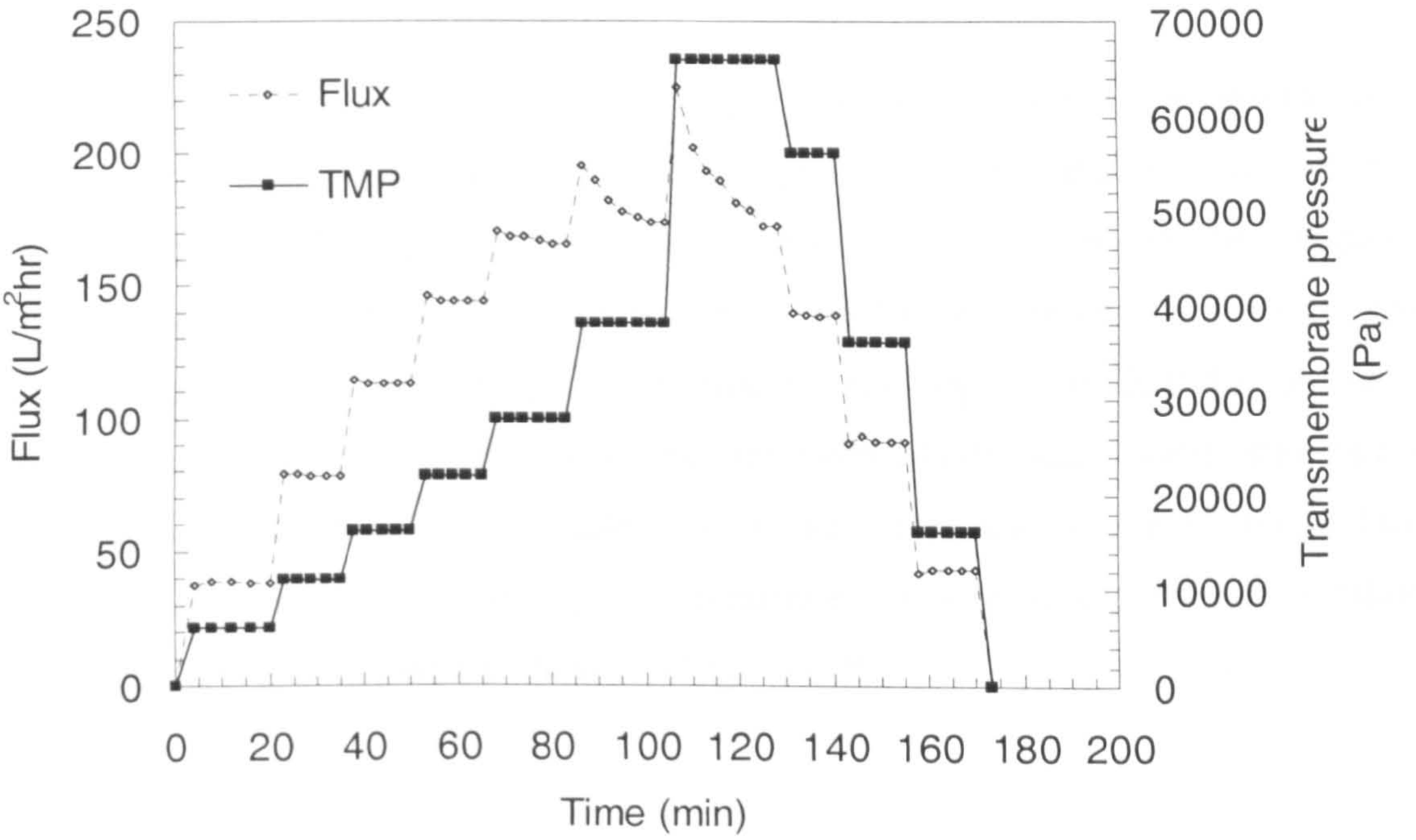

Figure 6.4: Step by step results for the filtration of 600 mg L^{-1} n-dodecane emulsions, surfactant concentration 60 mg L^{-1} crossflow velocity 1.52 m s^{-1}.

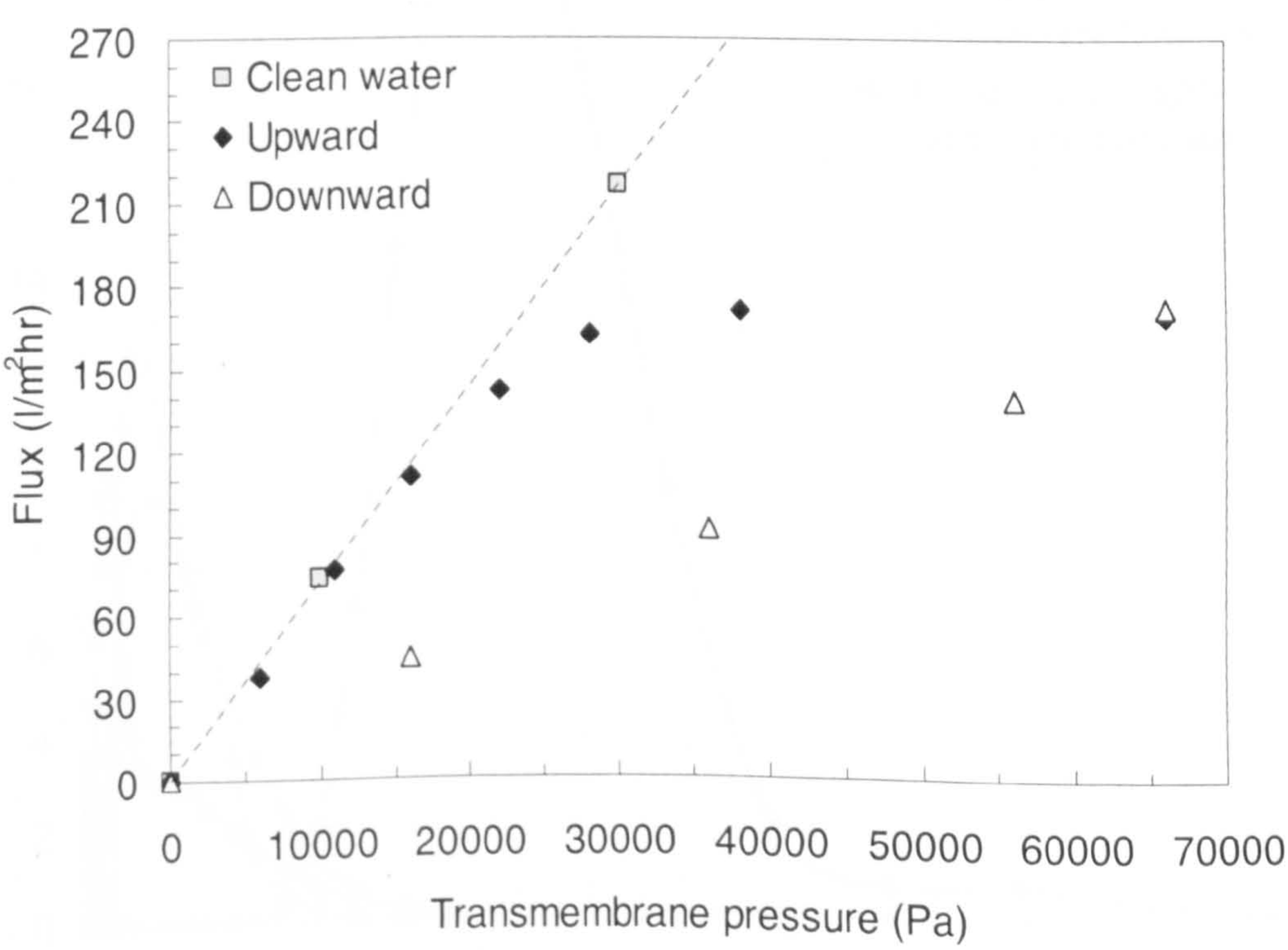

Figure 6.5: Flux versus transmembrane pressure for 600 mg L^{-1} n-dodecane emulsions, surfactant concentration 60 mg L^{-1}, crossflow velocity 1.52 m s^{-1}.

6.2 Permeate Particle Size Analysis

For all the filtration experiments, permeate samples were collected for particle size analysis before and after reaching the critical flux values, particularly at the maximum transmembrane pressure step, where the chance of oil droplets penetration to the permeate side is high. For all the filtration tests, the particle size analysis for collected permeate samples before reaching the critical flux showed that no particles were detected using the Malvern Mastersizer. Also, the same results were observed for all samples collected after reaching the critical flux values with the exception of 2400 ppm dodecane emulsions where a small number of oil droplets were detected as shown in Figure 6.6.

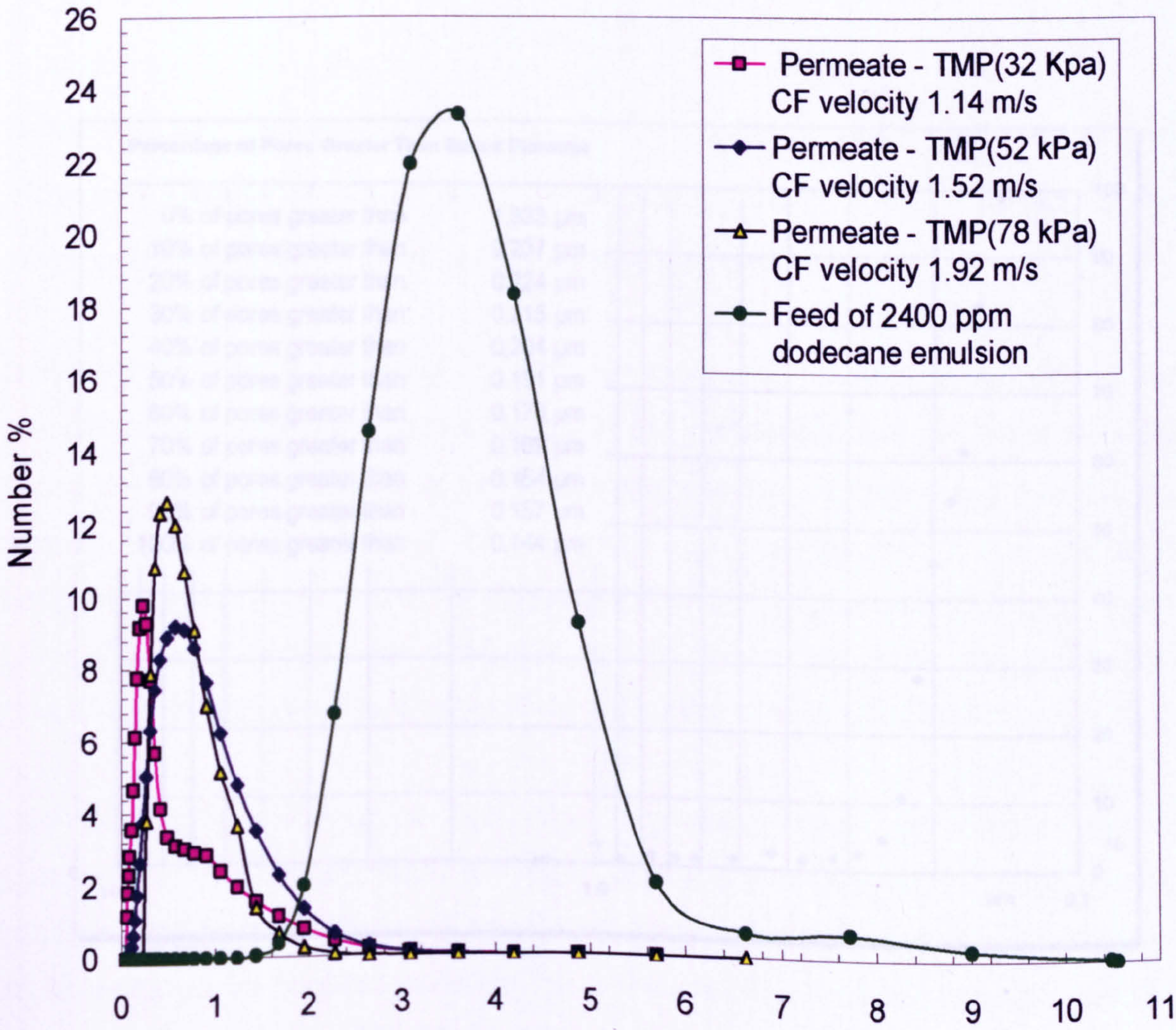

Figure 6.6 Particle size distributions for the permeate and feed samples.

In order to discuss these observations, a description of the obscuration term from Malvern analysis table is required. The obscuration is a measure of the quantity of laser light lost as a result of the induction of the sample and assists in adjusting the concentration of the sample as it is added to the dispersant (deionised water). An acceptable range is between 10 and 30 %. For all feed samples, the addition of 5 -10 ml of the sample to the dispersant gave an obscuration in the ideal range. For the permeate samples of 2400 ppm dodecane emulsion, the added amounts were approximately 80 -100 ml to get an obscuration of 10-15 %. Although the Mastersizer is a particle size distribution analyzer rather than a particle counter, it could be used as a qualitative indicator of the presence of an oil concentration. Hence, the concentration of oil droplets for the analysed permeate samples is much less than that measured feed sample (Figure 6.6).

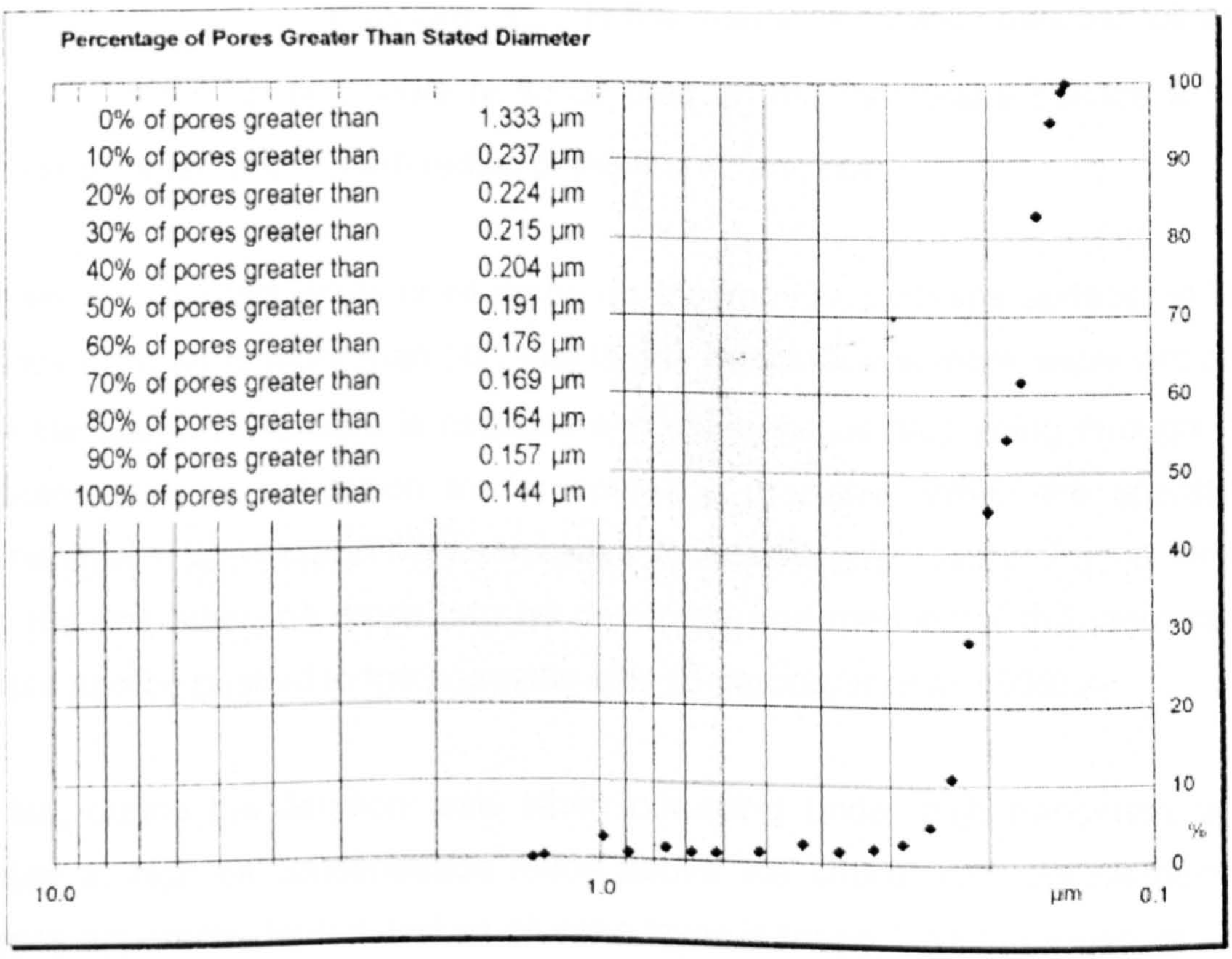

Figure 6.7: The pore size distribution of 0.2 µm tubular ceramic membrane (Fairey Industrial Ceramics Limited).

Furthermore, Lee *et al* (1984) stated that the emulsified drop rejection characteristics of a membrane are dependent mainly on the pore size distribution, the membrane nature, and the capillary pressure of oil drops in the membrane pores. The pore configuration of the membrane primarily influences the permeability of particles on the basis of size segregation. The pore size distribution of 0.2 μm ceramic membrane was obtained form Fairey Industrial Ceramics (Figure 6.8). It can be seen from Figure 6.8 that approximately 3 % of the membrane pores sizes are larger than 1 μm and 40 % of the pores are greater than 0.204 μm (all pores are smaller than 1.33 μm). The capillary pressure of an emulsified drop in the pore of a membrane could contirbute an significantly to the rejection and could be expressed as follows:

$$P_c = \frac{2 \times \gamma_{o/w} \times \cos\theta_{o/w}}{r} \qquad (6.1)$$

where P_c is the capillary pressure, $\gamma_{o/w}$ is the interfacial tension between oil and water, $\theta_{o/w}$ is the contact angle of an oil drop on the membrane surface in the presence of water, and r is the radius of the membrane pore.

Generally, the contact angle of oil drops on a ceramic membrane surface in the presence of water is more than 90°, that is, the membrane is more water wet and hence the capillary pressure is negative and stops the oil drop going through the membrane pore in opposition to the operating pressure. When the operating transmembrane pressure (TMP) surpasses the capillary pressure, P_c , at larger pores the emulsified oil drops can be deformed and then enter the membrane structure and be pushed to the permeate side (Srijaroonrat *et al*, 1999).

Likewise, during the filtration tests when operating under high transmembrane pressure at high oil concentration feeds above the critical flux, the membrane becomes apparently fouled and an oil cake layer is formed. As the pressure step incremented to the highest pressure the critical surface tension is altered , as the contact angle and pore size of the membrane. And so the capillary pressure of the oil droplets is overcome and droplets penetrate through the membrane pores to the permeate side.

According to all particles size analyses of permeate samples, which were collected while operating at sub-critical flux conditions, the obscuration to conduct the analysis could never be reached despite the large amount added. Hence, this confirms that the oil droplet rejection was very efficient. For a number of filtration experiments with high fouling tendency, such high oil feed concentration or at high ionic strength of monovalent salt (NaCl), a small quantity of emulsified droplets penetrated through the membrane pores with mean particle size less than 1 μm while operating at higher than the critical flux. These observations suggest that by operating below the critical flux the operating transmembrane pressure would be less than the capillary pressure, otherwise the oil droplets would pass through a small pore and contaminate the permeate.

6.3 Effect of Oil Concentration

It has been reported previously that an increase in feed concentration will result in a decrease in the critical flux (Madaeni, 1997; Chen, 1998; Fradin and Field, 1999; Kwon *et al*, 2000). As a consequence of a feed concentration increase, an increase in the solute mass transfer rate and consequent accumulation in the boundary film near the membrane surface is expected. Accordingly, an increase in hydraulic resistance is observed due to the enrichment of concentration polarization and probability of fouling. The influence of increasing oil concentration in the feed on the permeate flux behaviour is clearly shown in Figures 6.8 to 6.11, where it can be observed that as the oil concentration increased from 600 to 2400 mg L^{-1} the equilibrium flux declined. Furthermore, the influence of increasing oil feed concentration on flux-pressure curve behaviour is most profound in Figure 6.11 where the oil emulsions were filtered at the crossflow velocity of 2.28 m s^{-1}. However, for oil emulsions filtration at velocities of 1.52 and 1.92 m s^{-1}, two different behaviours of flux-pressure curves were observed before reaching the critical flux points. For oil feed concentration of 600 mg L^{-1}, it demonstrated a strong form of critical flux behaviour, whereas for feed with oil concentration of 1200 and 2400 mg L^{-1} the weak form of critical flux behaviour was observed. These observations are shown in Figure 6.9 and Figure 6.10.

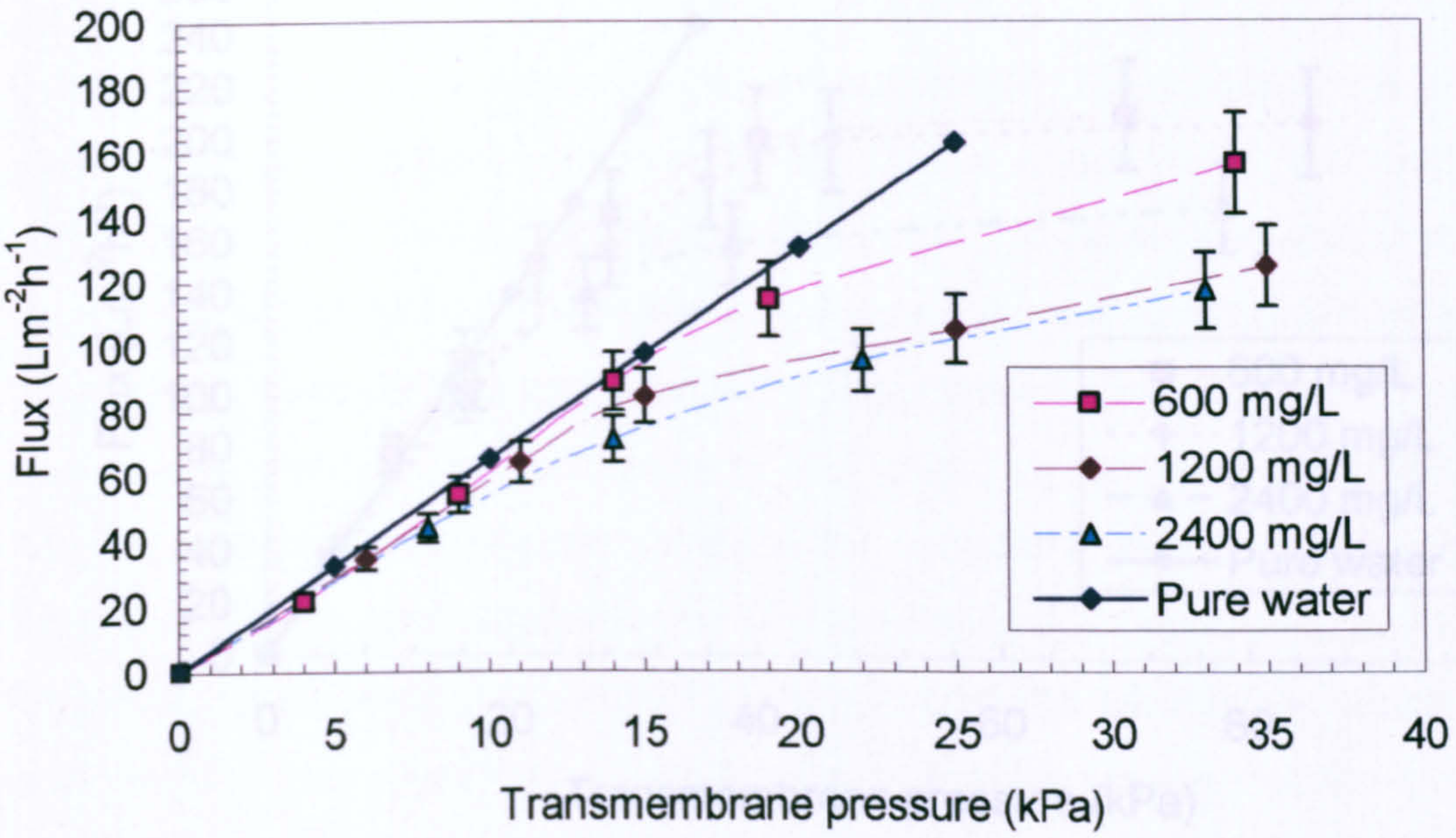

Figure 6.8: Flux performance at different oil feed concentrations for a cross-flow velocity 1.14 m s^{-1}.

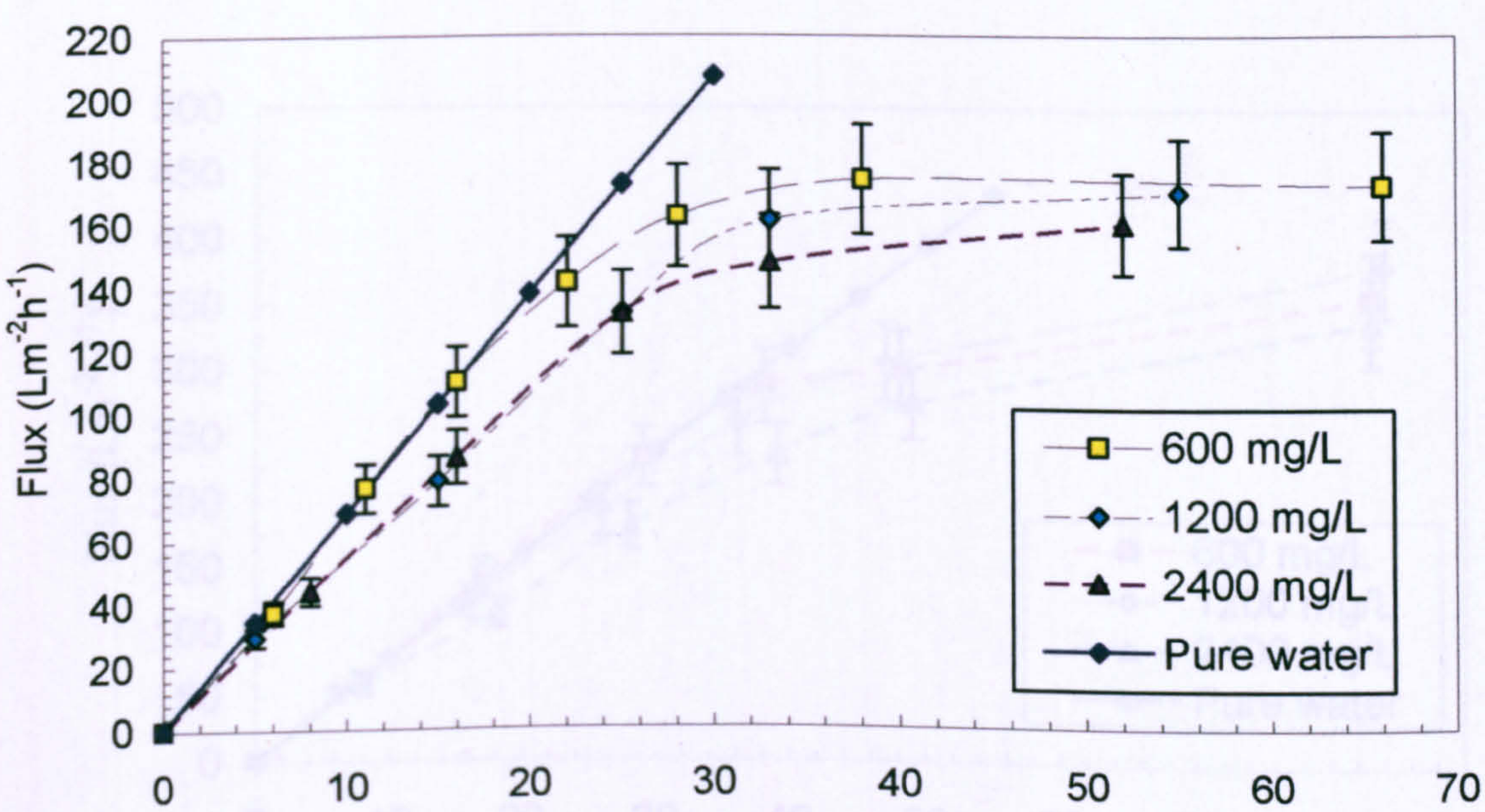

Figure 6.9: Flux performance at different oil feed concentrations for a cross-flow velocity 1.52 m s^{-1}.

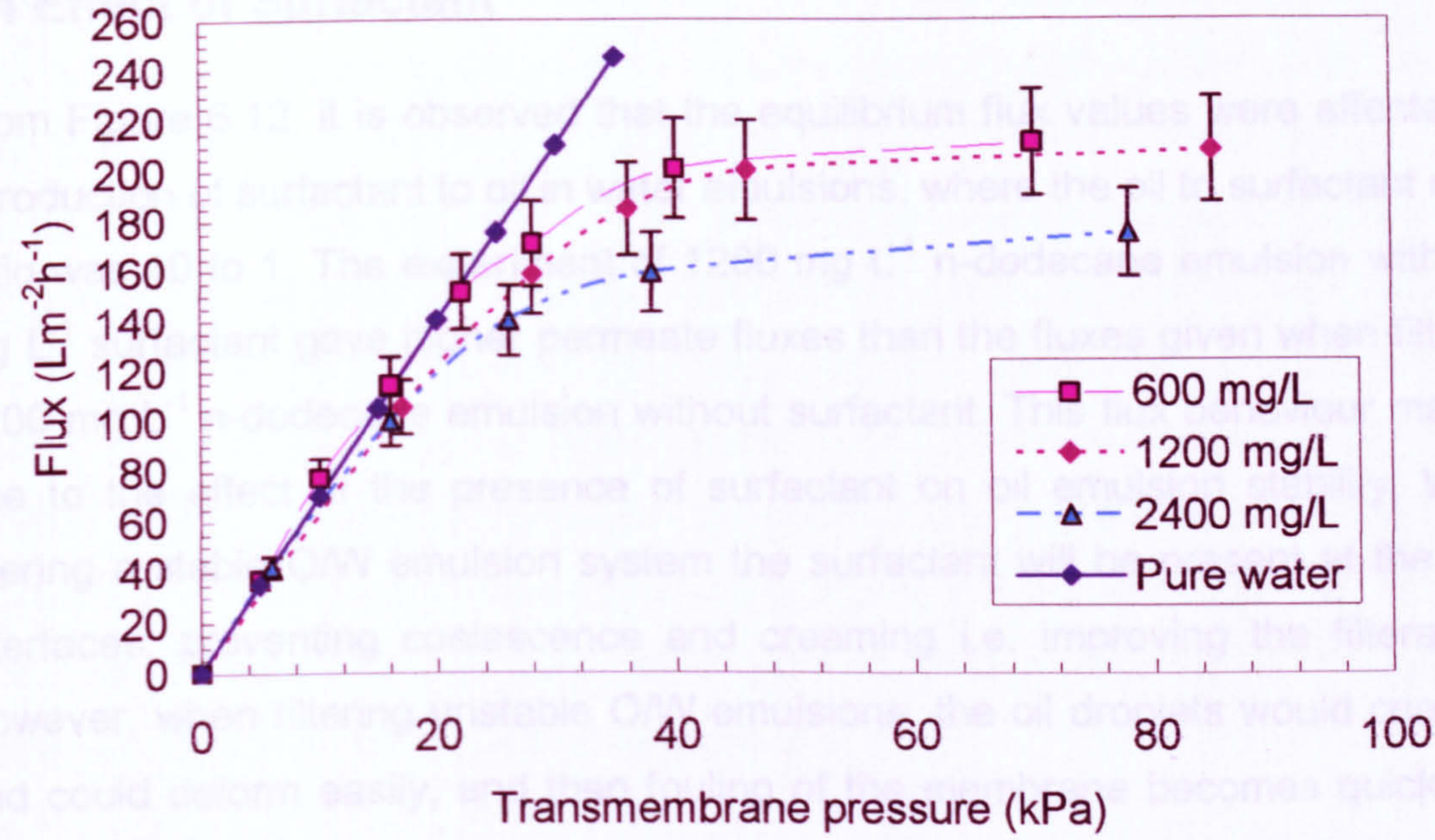

Figure 6.10: Flux performance at different oil feed concentrations for a cross-flow velocity 1.92 m s^{-1}.

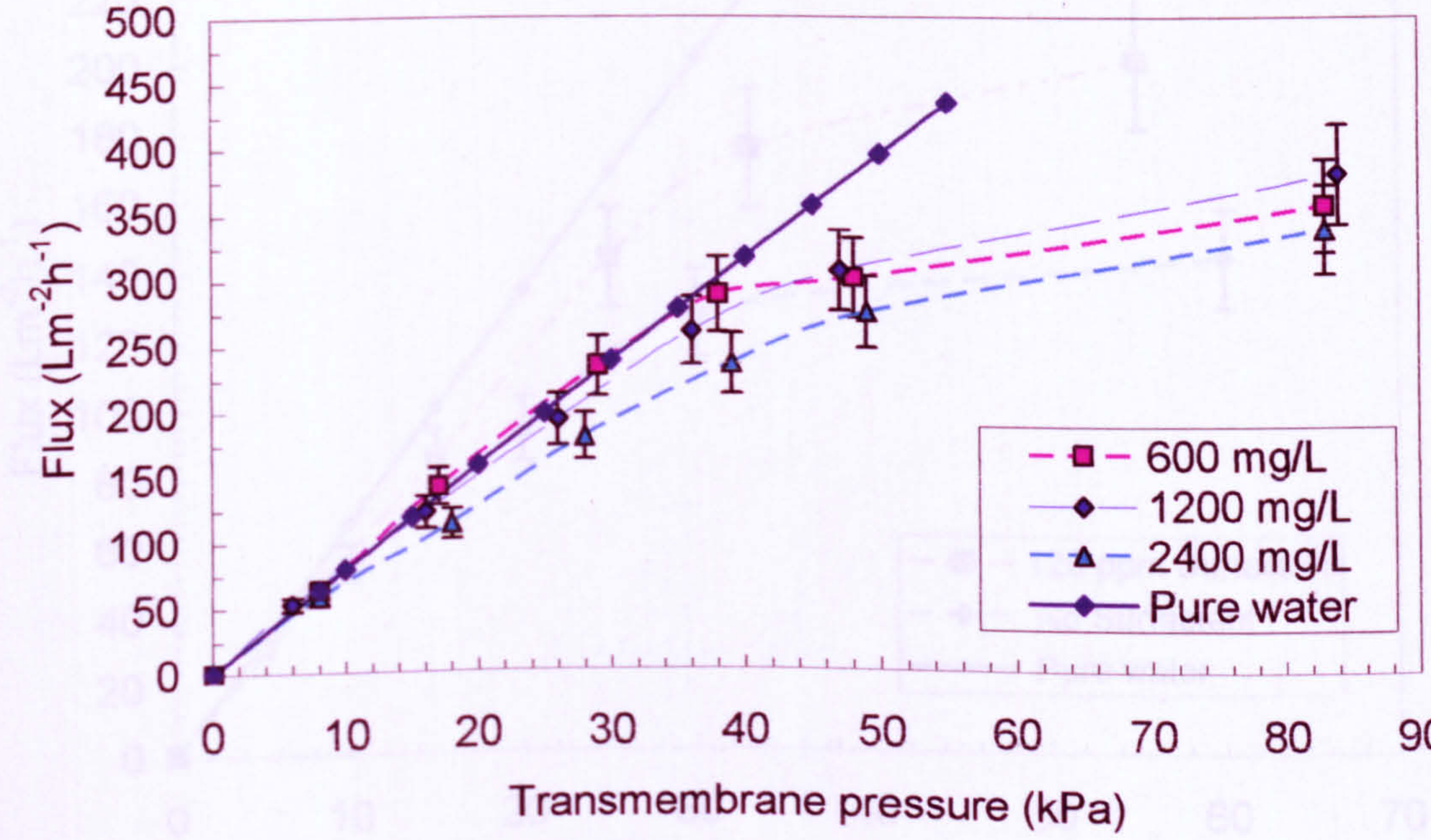

Figure 6.11: Flux performance at different oil feed concentrations for a cross flow velocity 2.28 m s^{-1}.

6.4 Effect of Surfactant

From Figure 6.12, it is observed that the equilibrium flux values were affected by introduction of surfactant to oil in water emulsions, where the oil to surfactant mass ratio was 10 to 1. The experiment of 1200 mg L^{-1} n-dodecane emulsion with 120 mg L^{-1} surfactant gave higher permeate fluxes than the fluxes given when filtering 1200 mg L^{-1} n-dodecane emulsion without surfactant. This flux behaviour may be due to the effect of the presence of surfactant on oil emulsion stability. When filtering a stable O/W emulsion system the surfactant will be present at the O/W interfaces, preventing coalescence and creaming i.e. improving the filterability. However, when filtering unstable O/W emulsions, the oil droplets would coalesce and could deform easily, and then fouling of the membrane becomes quicker as the transmembrane pressure increases, leading to internal fouling of membrane pores.

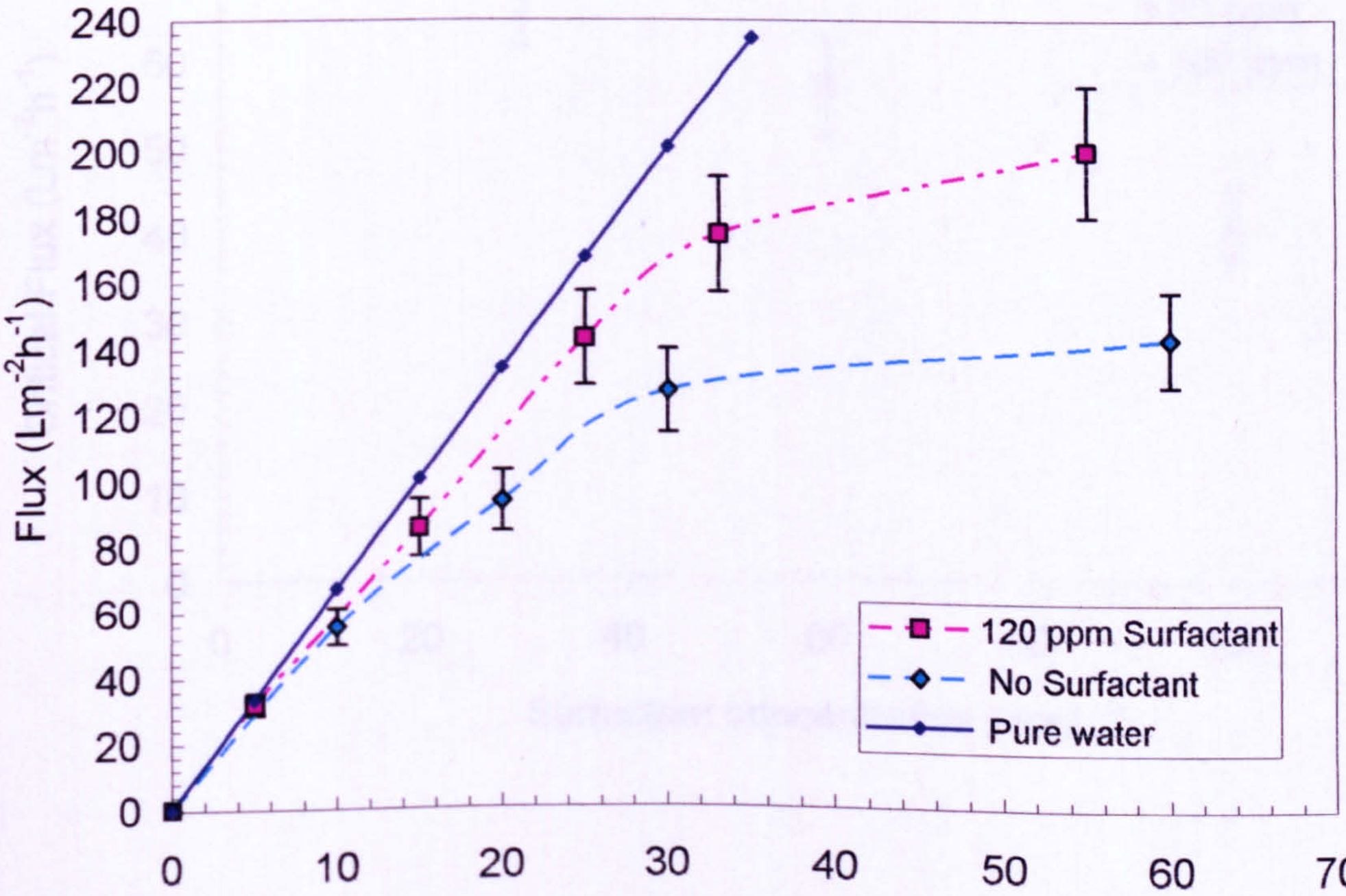

Figure 6.12: Flux performance with different surfactant concentration for 1200 mg L^{-1} n-dodecane emulsions at CF Velocity 1.52 m s^{-1}.

Figure 6.13 demonstrates the variations in the values of critical flux observed after the addition of different amounts of sorbitan monooleate surfactant to the feed. The critical flux falls to very low values, i.e. from 70 L m^{-2} h^{-1} for an emulsion with 30 ppm surfactant to 40 L m^{-2} h^{-1} for an emulsion with 100 ppm surfactants. It is apparent that the addition of surfactant to the oil in water emulsion in an excessive amount results in a decrease in the critical flux. This result is in an agreement with those reported by different other researchers, such as Gésan-Guiziou *et al.* (2001). They reported that for a latex suspension the critical flux decreased as the surfactant content was increased. They ascribed this behaviour to the change in the characteristics of the cake layer with regards to stability, thickness, and irreversibility when the surfactant is present.

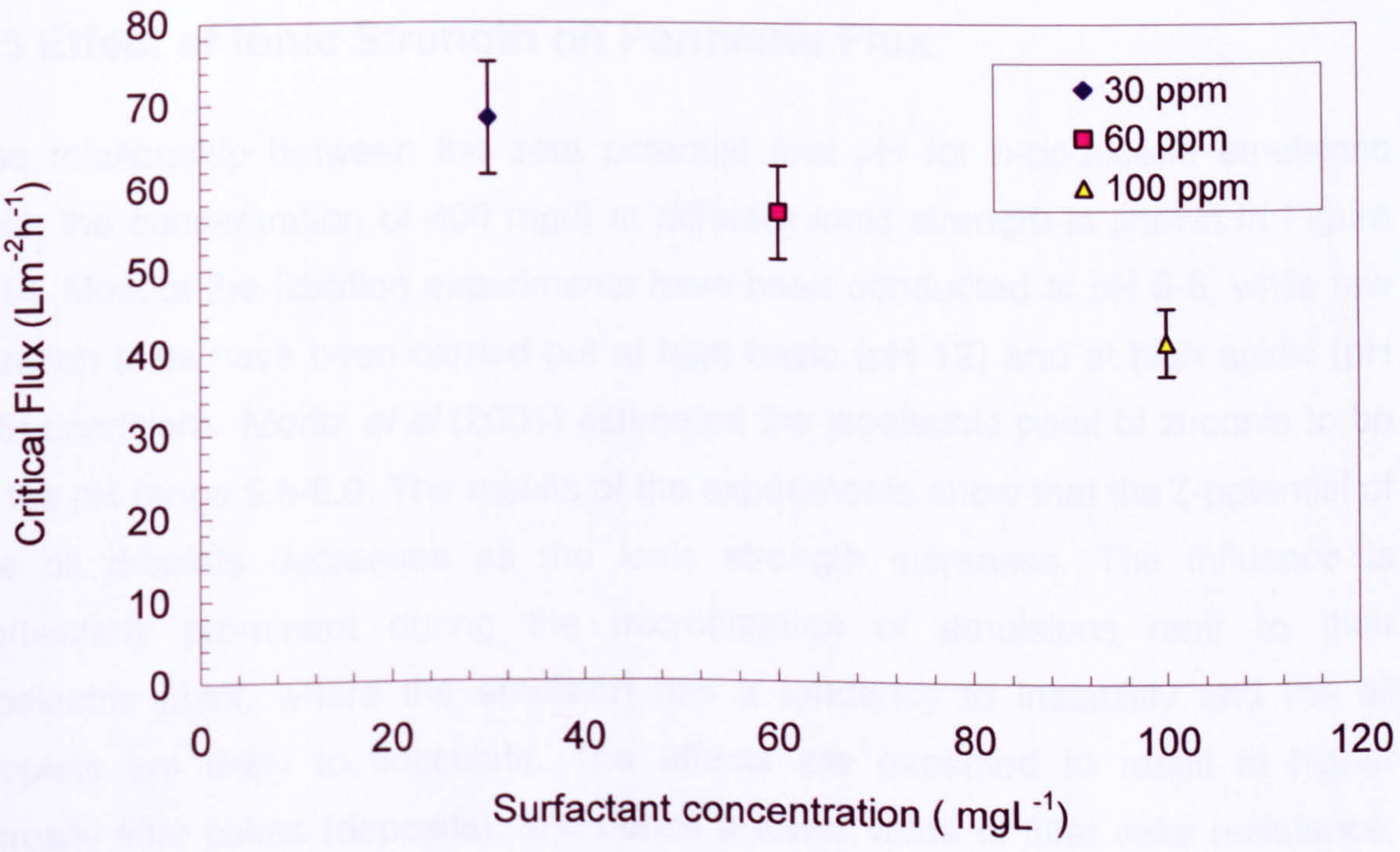

Figure 6.13: Variation of critical flux with different surfactant concentration at crossflow velocity of 1.52 m s^{-1} for 300 ppm n-dodecane emulsion.

Akay and Wakeman (1994) said that adsorption of cationic and anionic surfactants could take place on the membrane surface and inside the pores, so that their extended tails narrow the membrane pore size available for filtration. This leads to increased pore rejection or even pore blockage. In the context of the present study, since sorbitan monooleate (Span 80) is a non-ionic surfactant and when it present in an excess amount, the hydrophilic part could interact with hydrophilic ceramic membrane and the direction of its hydrophobic part towards the bulk. Therefore during crossflow filtration oil-surfactant-water emulsion, the surfactants cover the membrane in the way suggested by Akay and Wakeman (1994). This encourages aggregation and deposition by hydrophobic–hydrophilic interactions. This could provide an explanation of the decrease in the critical flux noticed during the addition of surfactants at higher concentration here.

6.5 Effect of Ionic Strength on Permeate Flux

The relationship between the zeta potential and pH for n-dodecane emulsions (with the concentration of 600 mg/l) at different ionic strength is shown in Figure 6.14. Most of the filtration experiments have been conducted at pH 5-6, while few filtration tests have been carried out at high basic (pH 12) and at high acidic (pH 1.5) conditions. Moritz *et al* (2001) estimated the isoelectric point of zirconia to be in the pH range 5.8-6.0. The results of the experiments show that the ζ-potential of the oil droplets decreases as the ionic strength increases. The influence is particularly prominent during the microfiltration of emulsions near to their isoelectric point, where the emulsion has a tendency to instability and the oil droplets are likely to flocculate. The effects are expected to result in higher porosity filter cakes (deposits), and hence a lower value of filter cake resistance; the permeate flux was found to increase to double the value of a non-treated emulsion.

The contradictory observations about the effect of addition of mono and poly-valent salts at the same ionic strength have raised many questions such as the interaction between oil droplets themselves and with the membrane. When the NaCl salt (monovalent) is added, the emulsion pH was 5.77, and measured zeta

potentials of the oil droplets were approximately -16 mV (0.1 M) and -36 mV (0.05M). In addition, bearing in mind that the isoelectric point of zirconia membrane was reported to be in a pH range 5.8-6.0, a situation is created that favours the particle-membrane attraction or interaction leading the adsorption of emulsified oil droplets i.e. more deposition which would cause flux decline. Alternatively, when the $FeCl_3$ salt (trivalent) was added, the emulsion pH was about 1.6, and measured zeta potentials of the oil droplets were close to the isoelectric point. Consequently, this condition favoured the particle-particle interaction, where large oil droplets form aggregates which sweep away easily by the induced shear, while for large aggregates, that stick on the membrane surface, form cake layer with high porosity structure due to the cross linking by Ca^{+2} and Fe^{+3} ions.

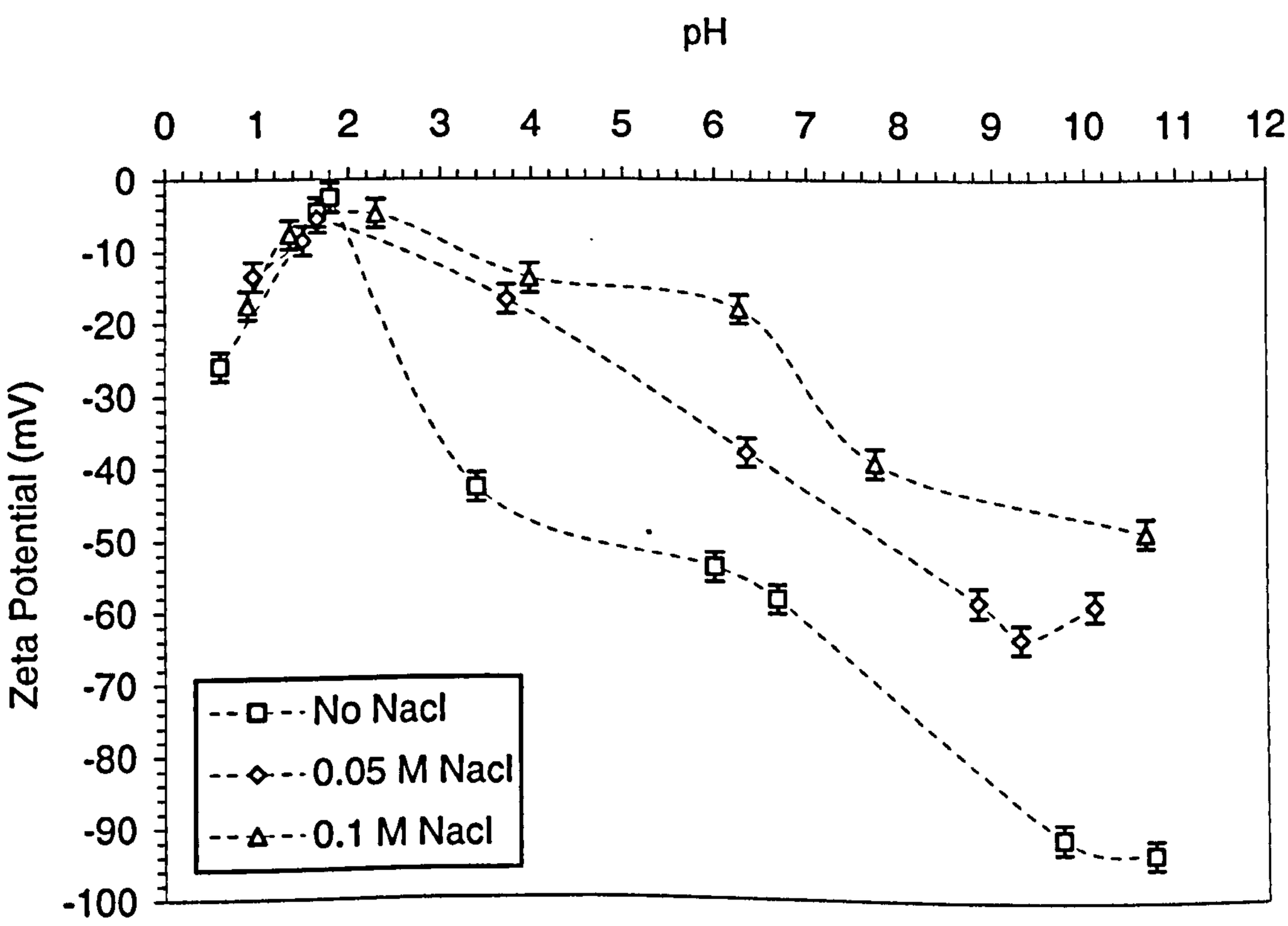

Figure 6.14: Zeta potential measurements for 600 mg L^{-1} n-dodecane emulsions at different ionic strength and pH.

It was found that the permeate flux is dependent on the surface charge of the emulsified oil droplets (Figure 6.15) and also might be dependent on the surface charge of the membrane. High permeate fluxes are obtained at high pH and low salt concentration. Under these conditions the repulsion between the oil droplets is strong. In contrast, low filtration fluxes are measured at high salt concentration, low pH, and with a NaCl electrolyte, i.e. when the surface charges are weak and in the presence of specific cations.

The net energy of interaction between the charged surfaces involved in the filtration tests was calculated using the DLVO theory. Hence, qualitative arguments for the explanation of the observed results, that is, of the highest flux being reached at ionic strength 0.1 M ($FeCl_3$); Figure 6.15 shows that where the lowest minimum energy values were reached at these same conditions, indicating the most stable oil-in-water emulsion.

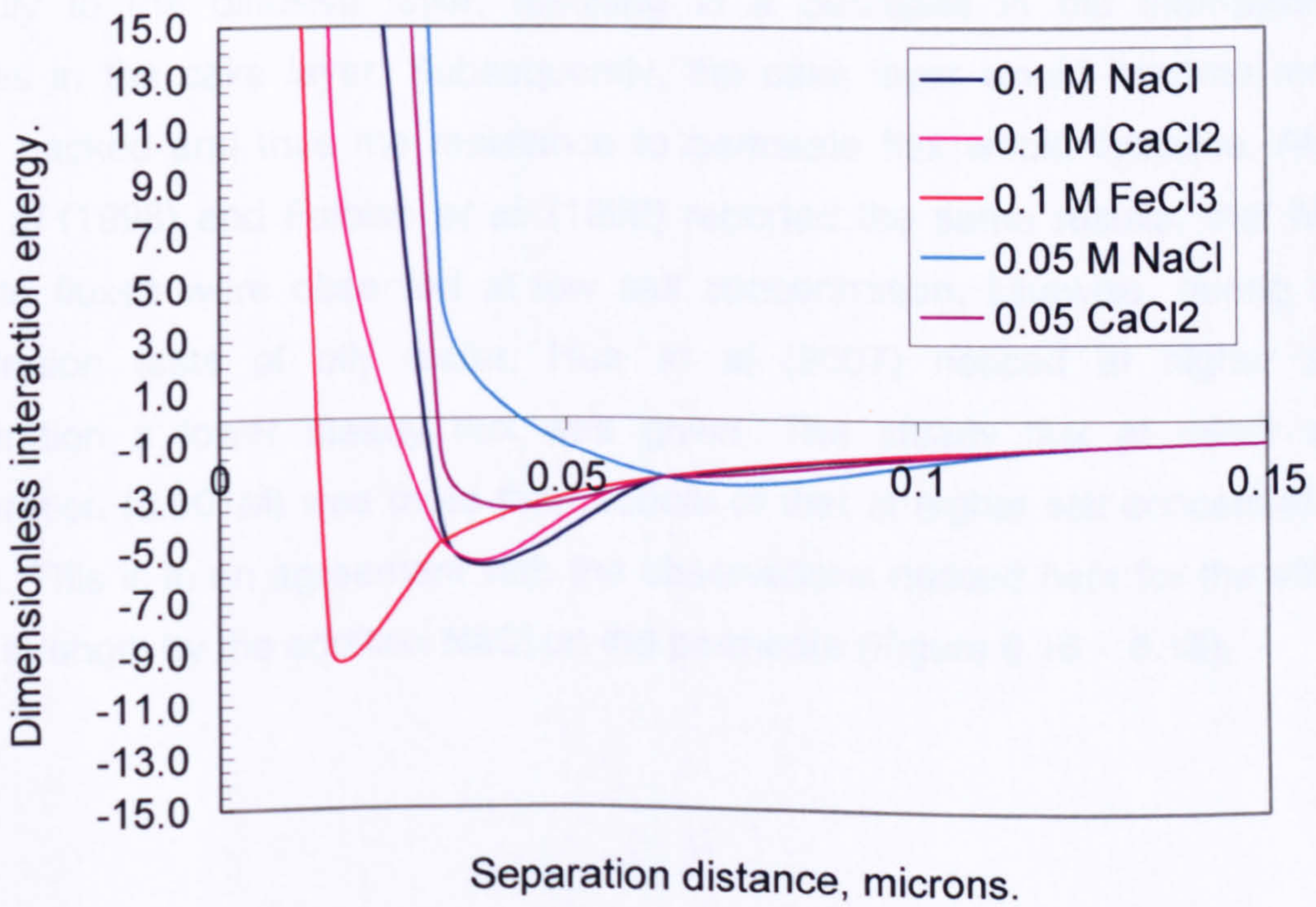

Figure 6.15: Dimensionless interaction energy at a range of ionic strength for NaCl, $CaCl_2$, and $FeCl_3$ salts.

The total potential energy of interaction, by DLVO theory, was estimated using equation 2.1 to 2.3. in chapter two. Then, the dimensionless interaction energy is calculated by dividing the total potential interaction energy by the kinetic energy due to thermal motion as illustrated in the following correlation

$$V_D = \frac{V_T}{k_B T} \tag{6.2}$$

where V_D is the dimensionless interaction energy, V_T is the total interaction energy, k_B is Boltzmann constant, T is the absolute temperature

It was noticed that when the ionic strength (NaCl) increased from 0.05 to 0.1 M, the permeate flux decreased severely, and the steady state flux state was reached faster than at the lower ionic strength. Moreover, at higher ionic strengths, a decline in the range of the electrostatic double layer repulsive forces would occur practically to the diffusive layer, resulting in a decrease in the inter-particle distances in the cake layer. Subsequently, the cake layer would become more densely packed and thus the resistance to permeate flux would increase. Also, Elzo *et al* (1998) and Faibish *et al.* (1998) reported the same results, that high permeate fluxes were observed at low salt concentration. Likewise, during the microfiltration tests of oily water, Hua *et al* (2007) noticed at higher salt concentration a lower steady flux was given. The steady flux at minor salt concentration (0.001M) was more than double of that at higher salt concentration (0.05M). This is in an agreement with the observations noticed here for the effect of ionic strength by the addition NaCl on the permeate (Figure 6.16 - 6.18).

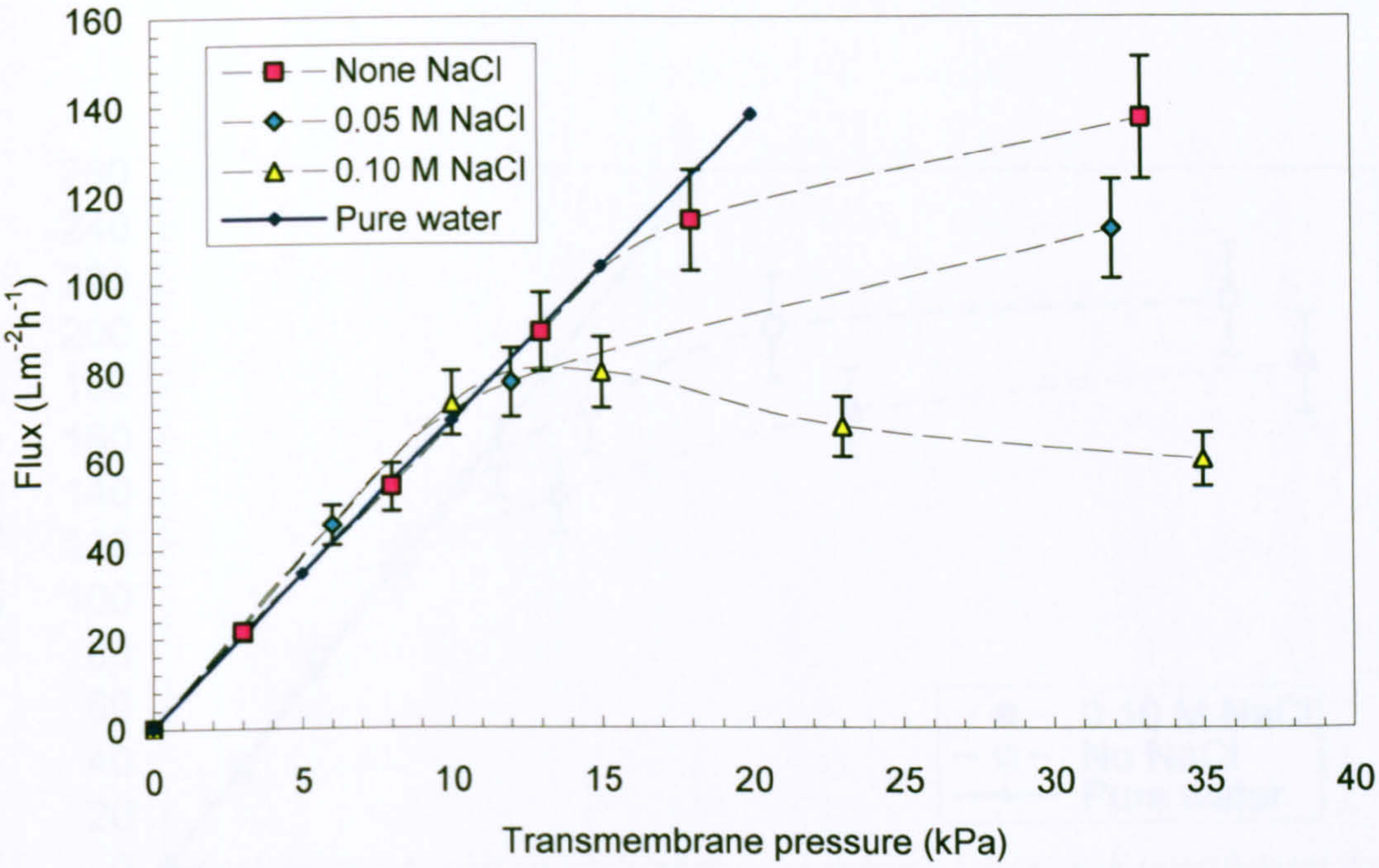

Figure 6.16: Flux performance at different ionic strength (NaCl) for 600 mg L^{-1} n-dodecane emulsions with 60 mg L^{-1} surfactant at crossflow velocity 1.14 m s^{-1}.

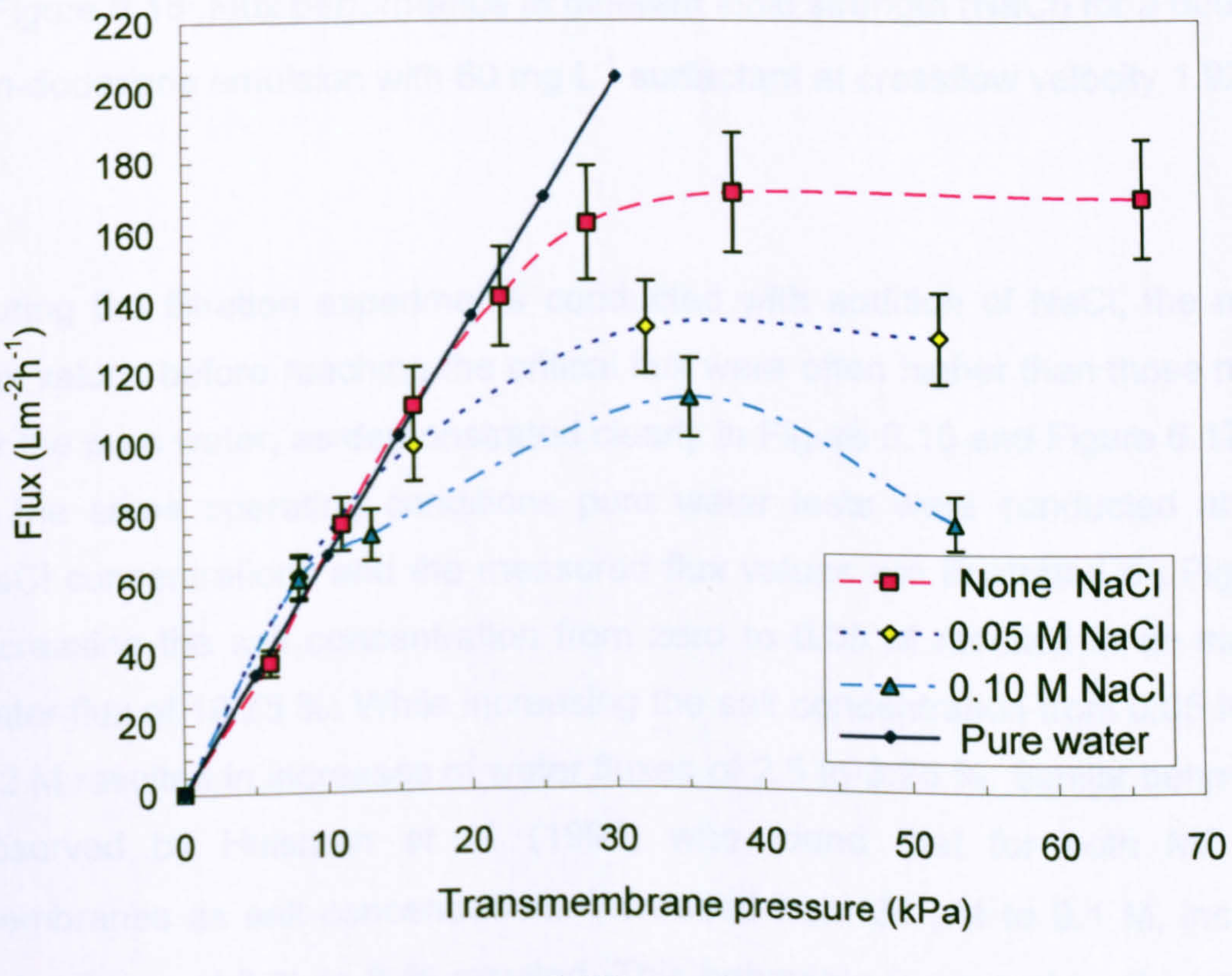

Figure 6.17: Flux performance at different ionic strength (NaCl) for a 600 mg L^{-1} n-dodecane emulsions with 60 mgL^{-1} surfactant at CF velocity 1.52 m s^{-1}.

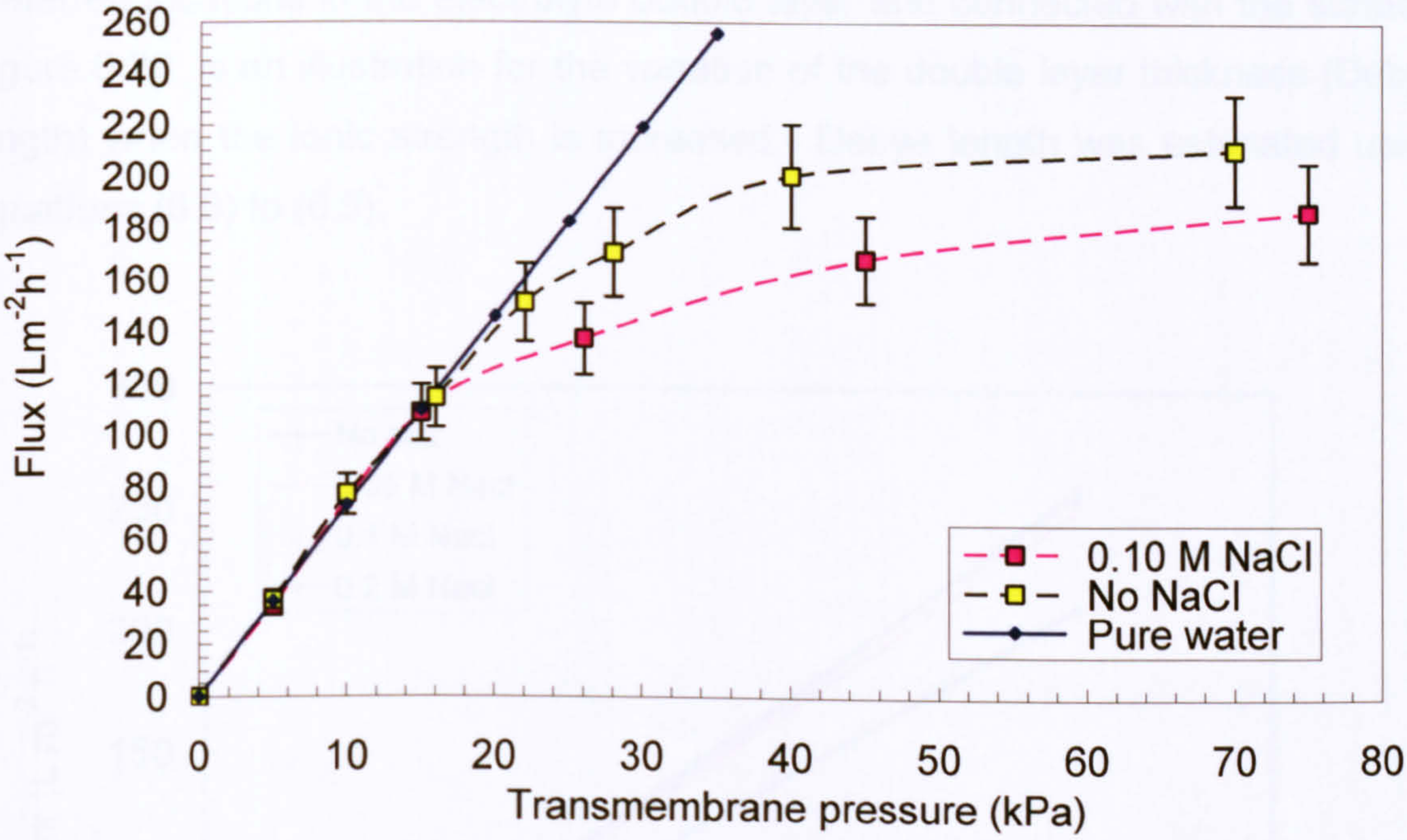

Figure 6.18: Flux performance at different ionic strength (NaCl) for a 600 mg L^{-1} n-dodecane emulsion with 60 mg L^{-1} surfactant at crossflow velocity 1.92 m s^{-1}.

During the filtration experiments conducted with addition of NaCl, the measured flux values before reaching the critical flux were often higher than those measured for the pure water, as demonstrated clearly in Figure 6.16 and Figure 6.17. Hence, at the same operating conditions pure water tests were conducted at different NaCl concentrations and the measured flux values are illustrated on Figure 6.19. Increasing the salt concentration from zero to 0.05 M resulted in an increase in water flux of 18.75 %. While increasing the salt concentration from 0.05 to 0.1 and 0.2 M resulted in increases of water fluxes of 2.5 to 3.75 %. Similar behaviour was observed by Huisman *et al.* (1997) who found that for both MF and UF membranes as salt concentrations increased from 30 μM to 0.1 M, increases in water fluxes of 2 % to 8 % resulted. This behaviour is caused by the use of pure water which might lead to an incredibly thick Gouy-Chapman double layer and electro-viscous resistance in the membrane pores (Bacchin *et al.* , 2006). When

an electrolyte solution is forced by the transmembrane pressure through membrane pores (capillary) with charged surfaces, ions are transported from their preferred locations in the electrolyte double layer and connected with the surface. Figure 6.20 is an illustration for the variation of the double layer thickness (Debye length) when the ionic strength is increased. Debye length was estimated using equations (6.3) to (6.5).

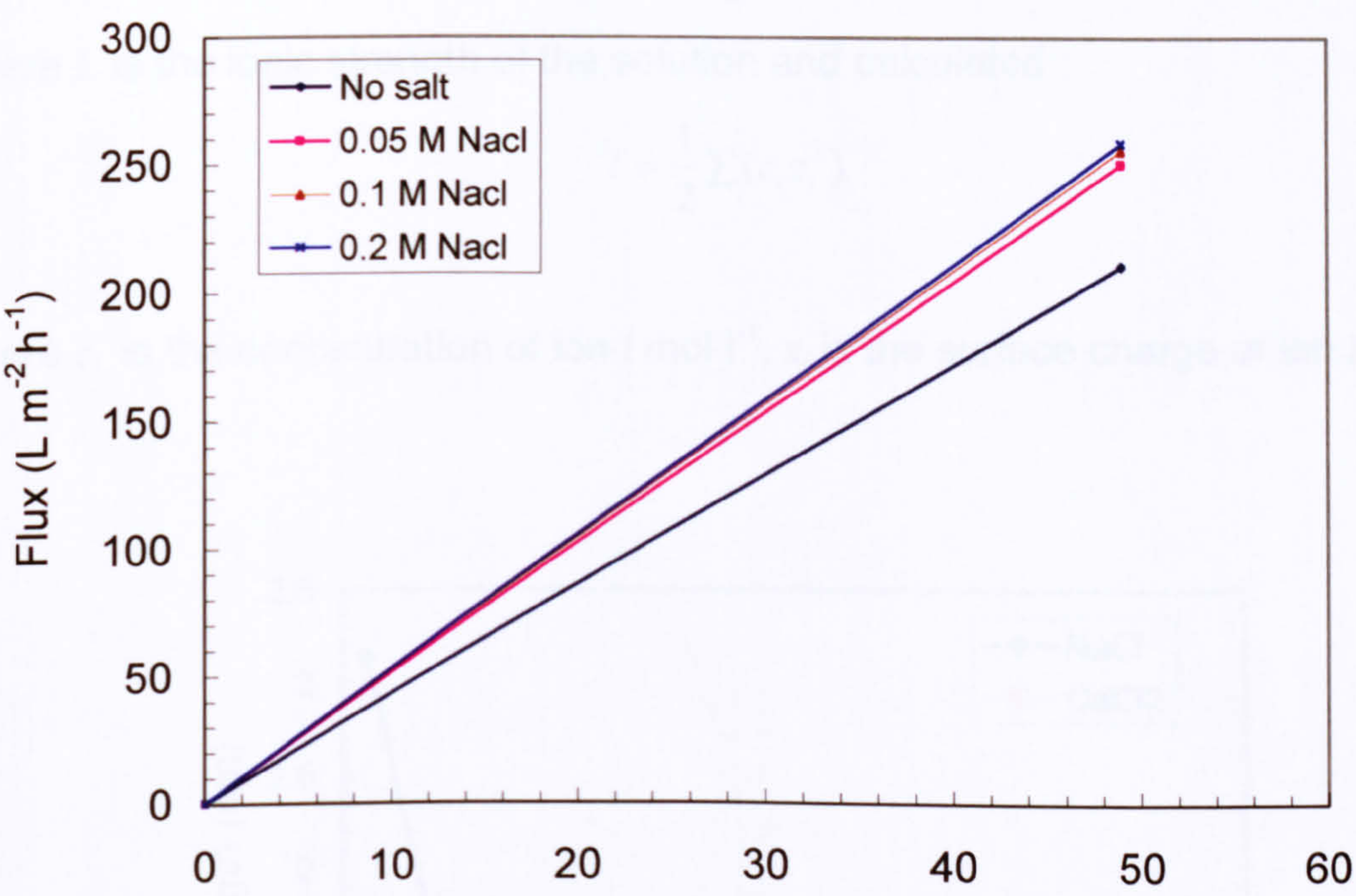

Figure 6.19: Pure water flux values at different NaCl concentration

An electroviscous effect is a physical phenomenon which is closely connected to the viscosity. When an electrolyte solution is sheared, additional energy is needed to overcome the interaction between the ions in the double layers around the particles and the electrical charge on the particle surfaces, hence resulting in an increased apparent viscosity. While the viscosity decreases as the ionic strength increases since the double layer thickness became lesser than at low ionic strength (Shaw, 1992).

The Debye length $(1/\kappa)$ is a measure of the double layer thickness and its magnitude is estimated by using the following correlations (Huisman *et al.*,1997).

for 1:1 electrolytes (e.g., NaCl) $$1/\kappa = \frac{0.3014}{\sqrt{I}} \quad (6.3)$$

for 1:2 electrolytes (e.g., $CaCl_2$) $$1/\kappa = \frac{0.1745}{\sqrt{I}} \quad (6.4)$$

where I is the ionic strength of the solution and calculated :

$$I = \frac{1}{2}\sum(c_i z_i^2) \quad (6.5)$$

where c_i is the concentration of ion i mol l^{-1}, z_i is the surface charge of ion i.

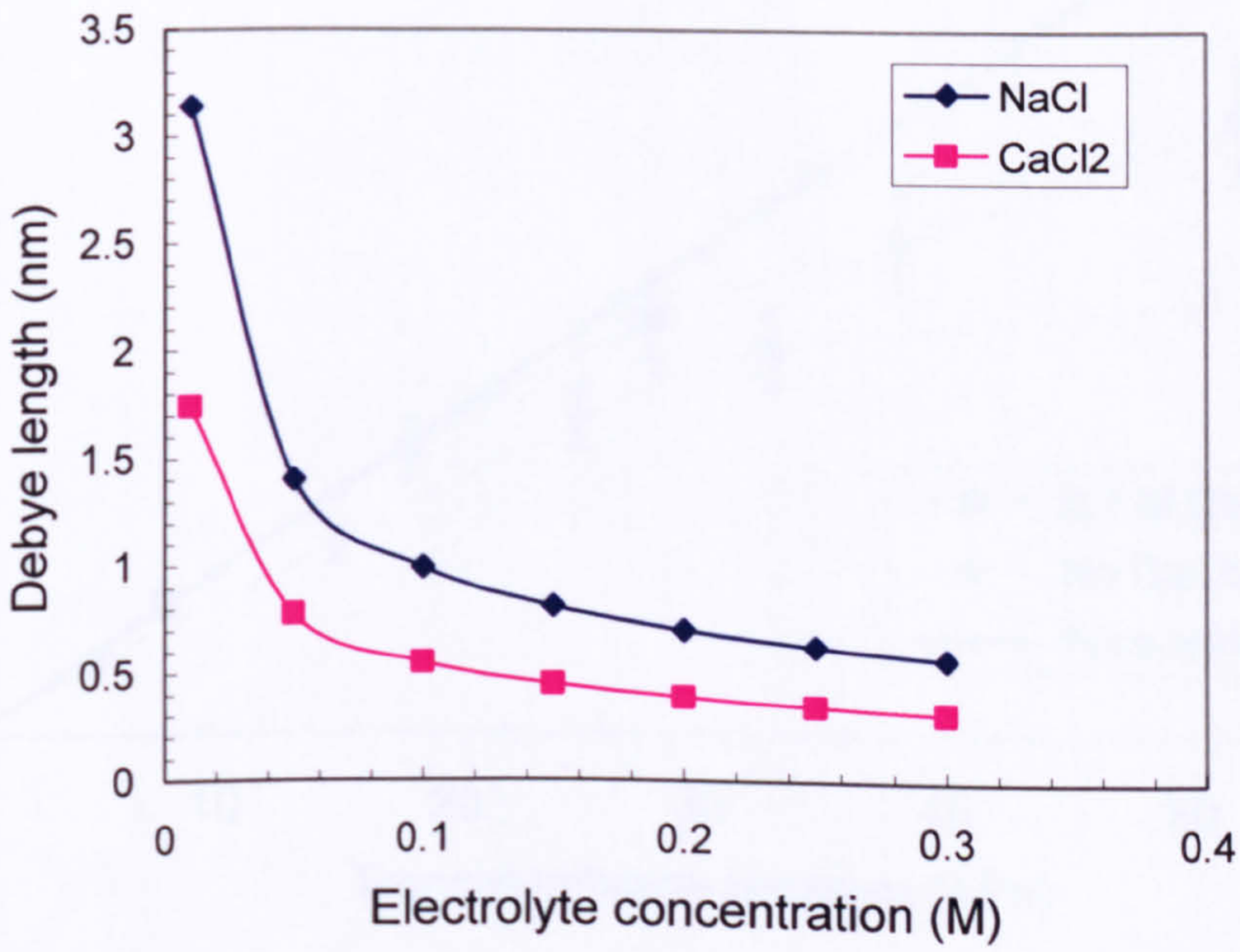

Figure 6.20: Debye length variation at different electrolyte concentrations.

However, the effect of salt concentration on permeate flux is still debated amongst researchers in the field. Tambe and Sharma (1992) suggested high ionic strength seems to reduce the double layer thickness around the oil droplets, thus reducing

the electrostatic repulsion, thereby encouraging coalescence leading to higher permeate flux. In addition, Zhao *et al* (2005) found that when the ionic strength increased, the steady permeate flux became higher.

Such experimental behaviour was encountered in this investigation, as presented in Figures 6.21to 6.23. When divalent electrolytes ($CaCl_2$) and trivalent ($FeCl_3$) were added, the permeate flux increase could be due to ion bridging effects. Moreover, oil droplets tend to flocculate and form aggregates with larger particle size that will lead to formation of a more porous layer on the membrane surface. Hence, an increase in the permeate flux will be reached.

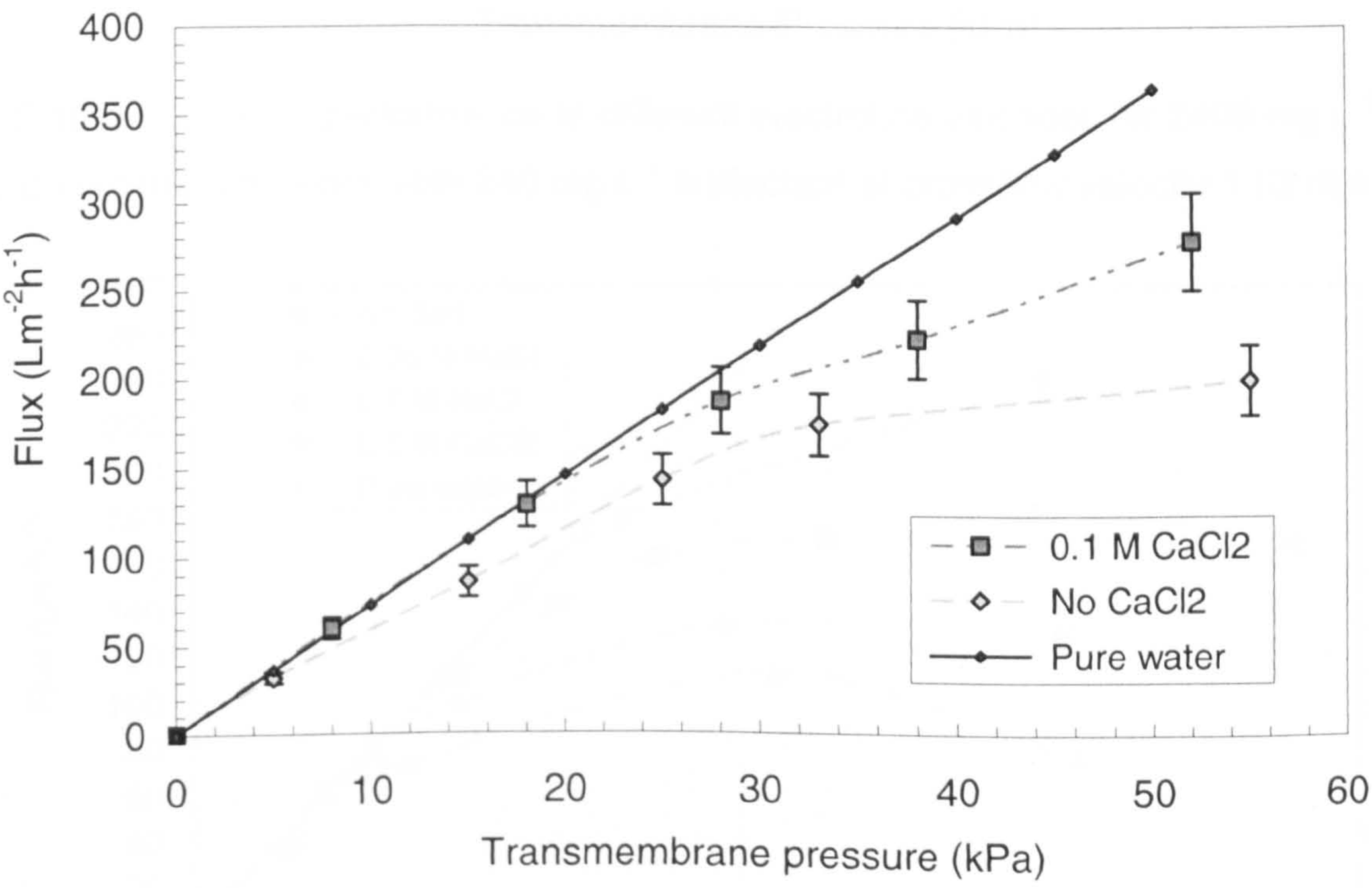

Figure 6.21: Flux performance at different ionic strength ($CaCl_2$) for a 1200 mg L^{-1} n-dodecane emulsions with 120 mg L^{-1} surfactant at crossflow velocity 1.52 m s^{-1}.

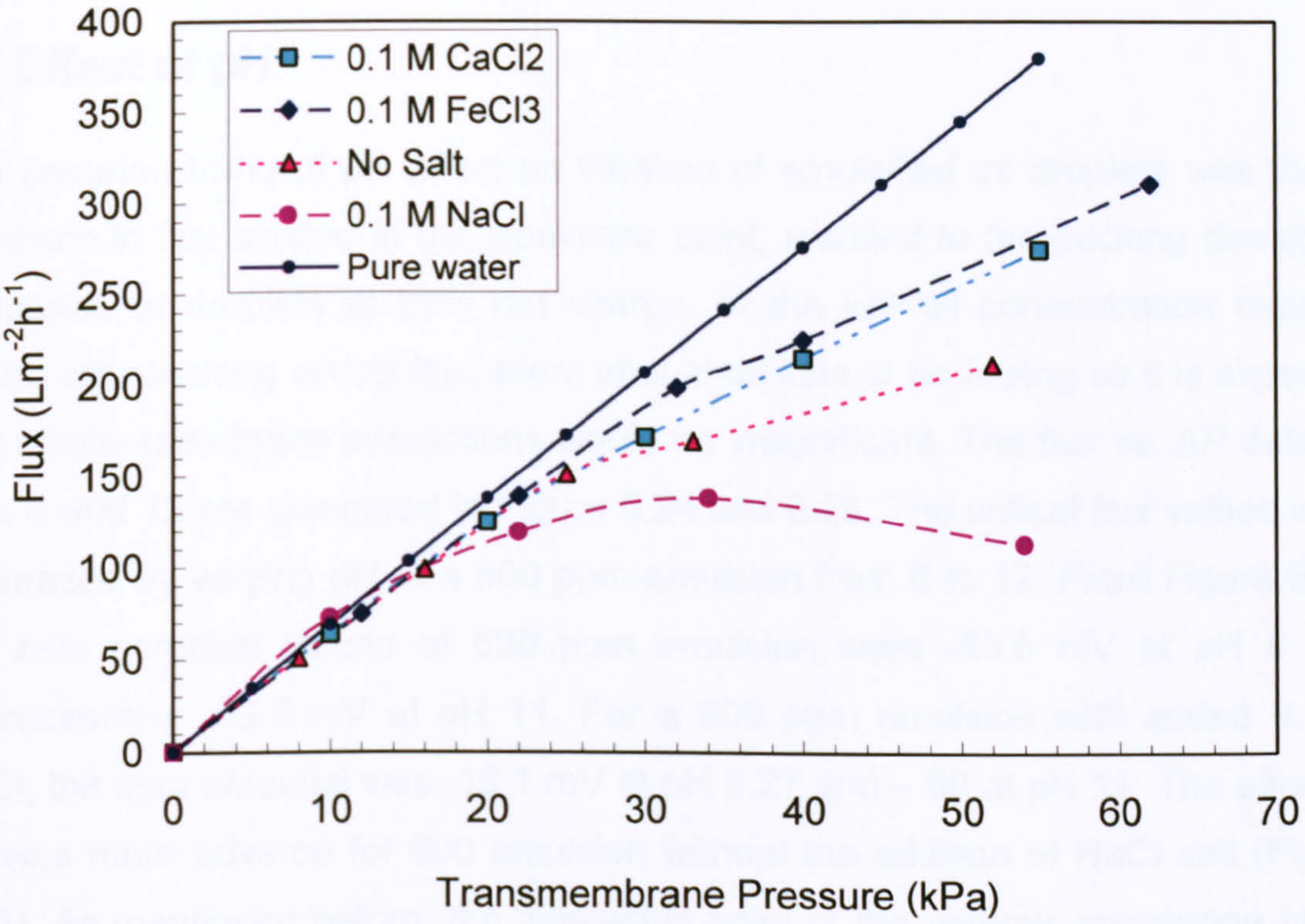

Figure 6.22: Flux performance at different electrolyte valences for 2400 mg L^{-1} n-dodecane emulsions with 240 mg L^{-1} surfactant at crossflow velocity 1.52 m s^{-1}.

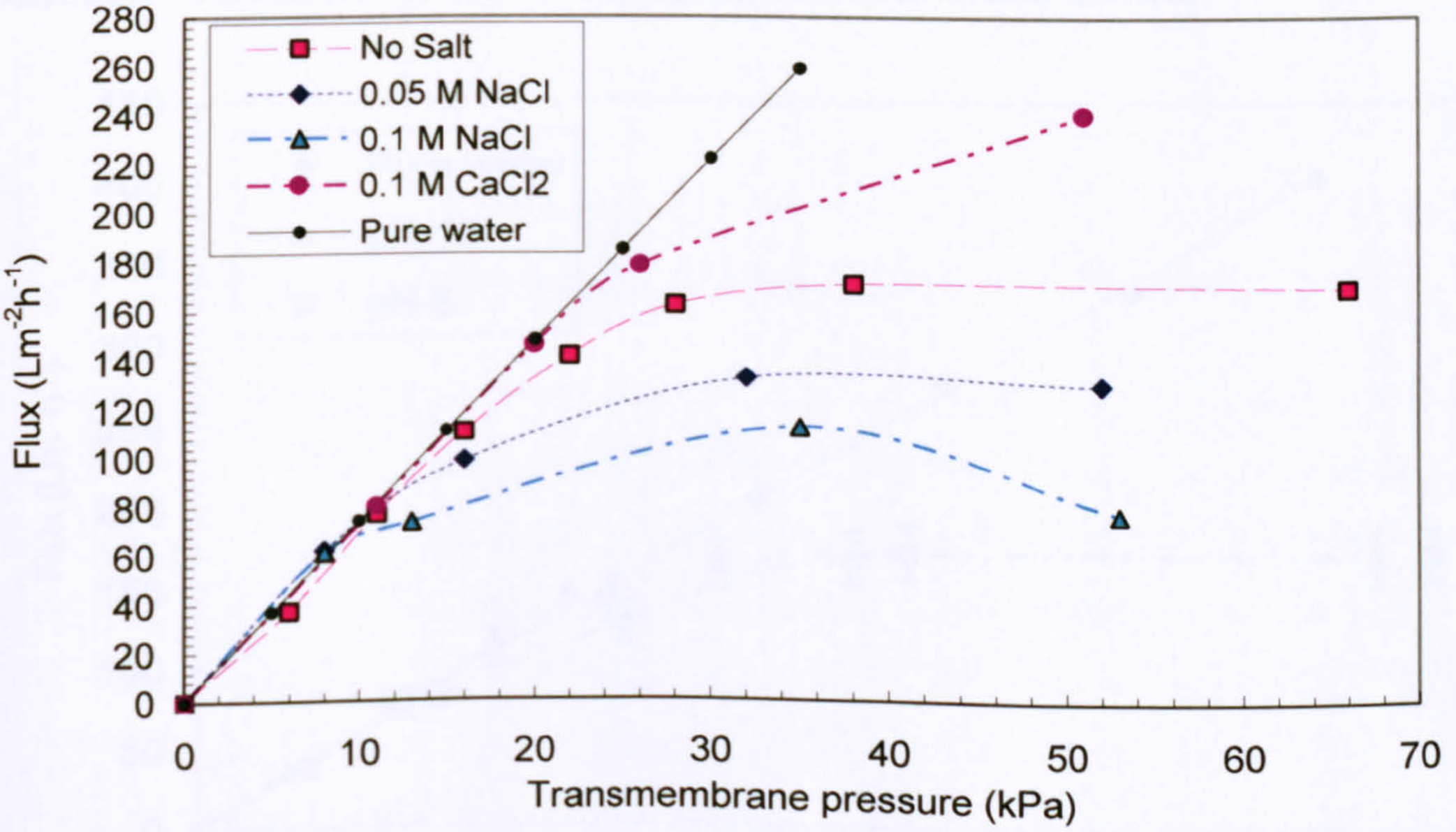

Figure 6.23: Flux performance at different electrolyte valences for 600 mg L^{-1} n-dodecane emulsions with 60 mg L^{-1} surfactant at crossflow velocity 1.52 m s^{-1}.

6.6 Effect of pH

The common trend of pH effect on filtration of emulsified oil droplets was that a minimum in flux existed at the isoelectric point, credited to the packing density of deposited oil droplets at zero net charge. In the low oil concentration regimes before approaching critical flux, there should be little or no fouling so it is expected that solute–membrane interactions would be insignificant. The flux vs. ΔP data for pH's 6 and 12 are compared in Figure 6.24 and 6.25. The critical flux values were decreased by varying pH of a 600 ppm emulsion from 6 to 12. From Figure 6.14, the zeta potential values of 600 ppm emulsion were -53.6 mV at pH 6 and approximately -93.5 mV at pH 11. For a 600 ppm emulsion with added 0.1 M NaCl, the zeta potential was -18.1 mV at pH 6.27 and – 50 at pH 11. The effect of pH was more adverse for 600 emulsion without the addition of NaCl salt (Figure 6.25). As mentioned before, the isoelectric point of the ceramic membrane at pH 5.8 and as the pH increases it seems take on a positive charge. Therefore, increases in the negative zeta potential of emulsified oil droplets will facilitate the electrostatic attraction between the droplets and membrane surface.

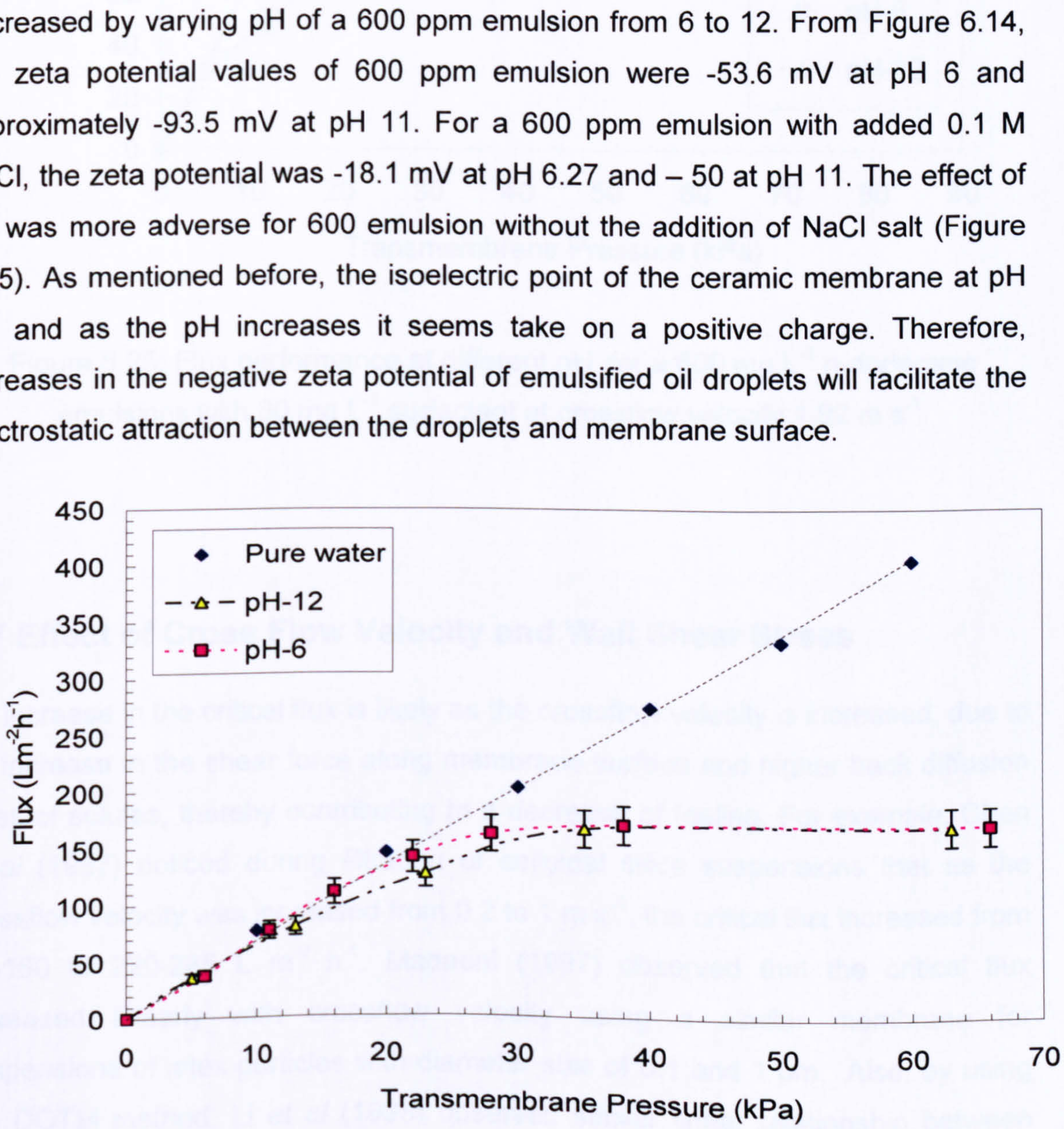

Figure 6.24: Flux performance at different pH with ionic strength (0.1 M NaCl) for a 600 mg L^{-1} n-dodecane emulsions with 60 mg L^{-1} surfactant at crossflow velocity 1.52 m s^{-1}.

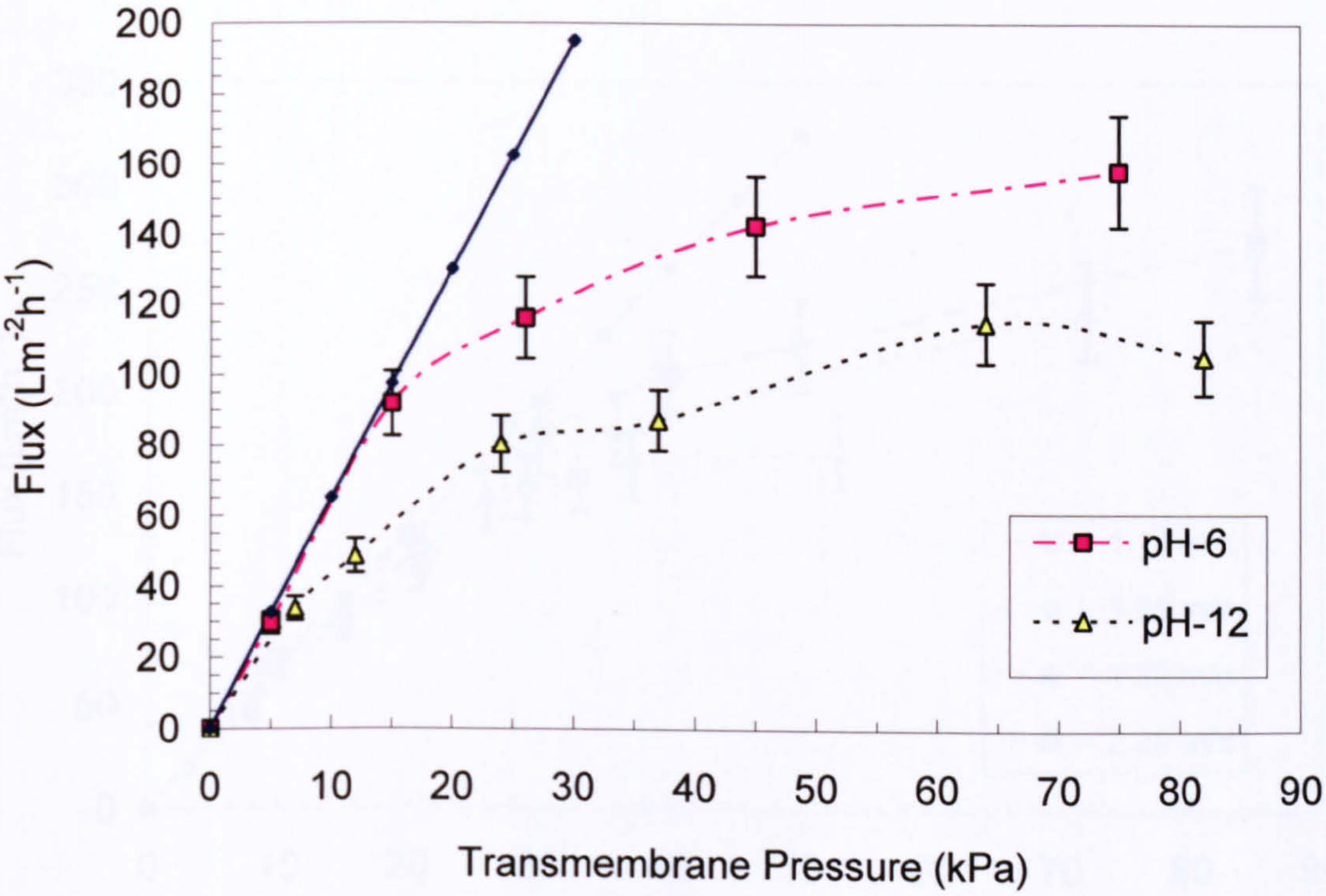

Figure 6.25: Flux performance at different pH for a 600 mg L^{-1} n-dodecane emulsions with 60 mg L^{-1} surfactant at crossflow velocity 1.92 m s^{-1}.

6.7 Effect of Cross Flow Velocity and Wall Shear Stress

An increase in the critical flux is likely as the crossflow velocity is increased, due to an increase in the shear force along membrane surface and higher back diffusion rates of solutes, thereby contributing to a decrease of fouling. For example, Chen *et al* (1997) noticed during filtration of colloidal silica suspensions that as the crossflow velocity was increased from 0.2 to 1 m s^{-1}, the critical flux increased from 30-160 to 220-285 L m^{-2} h^{-1}. Madaeni (1997) observed that the critical flux increased linearly with crossflow velocity using a similar membrane for suspensions of latex particles with diameter size of 0.1 and 1 μm. Also, by using the DOTM method, Li *et al* (1998) observed similar linear relationship between critical flux and crossflow velocity for both latex particles (of sizes 3, 6.4, 11.9 μm) and yeast cells.

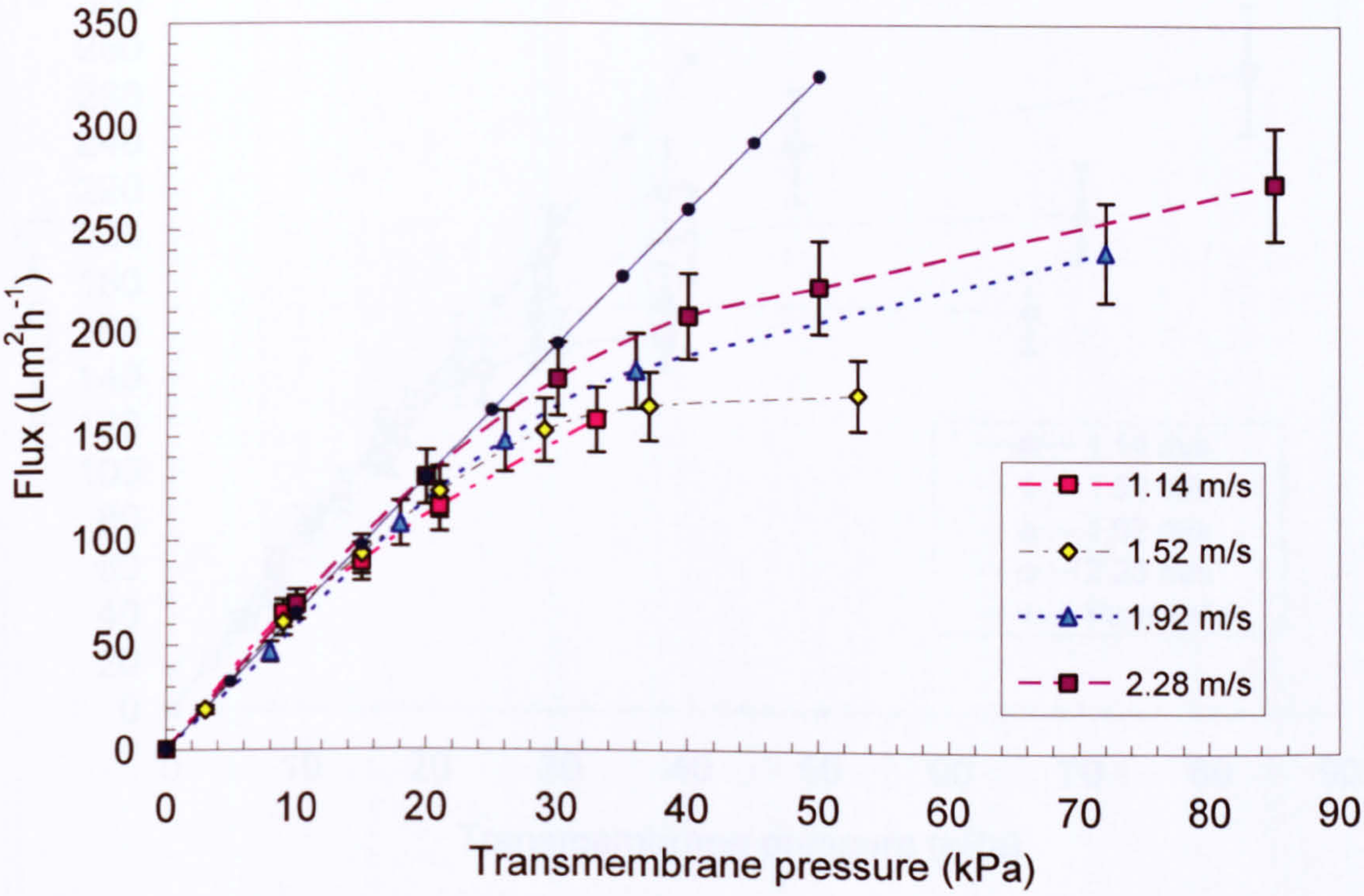

Figure 6.26: Flux performance at different crossflow velocities for a 300 mg L^{-1} n-dodecane emulsions with 30 mg L^{-1} surfactant.

Similar flux behaviour has been observed during filtration tests in the current study as presented in Figures 6.26 to 6.31, the permeate flux increased as the crossflow velocity increased. However, as shown in Figures 6.26 and 6.27, at low oil concentration, the strong form of critical flux was observed where the permeate behaved identically to the pure water until the critical flux was reached. Two distinct regions, before and after critical flux, have been identified where in the first region there is a linear relationship between flux and pressure and in the second region there is non-linear correlation between flux and pressure. Also, it has been observed during filtration of a 600 mg L^{-1} n-dodecane emulsion that when the crossflow velocity was increased from 1.14 to 2.28 m s^{-1}, the critical flux increased from 73 to 217 L m^{-2} h^{-1}. In other words, as the crossflow velocity is doubled, the critical flux value has almost tripled.

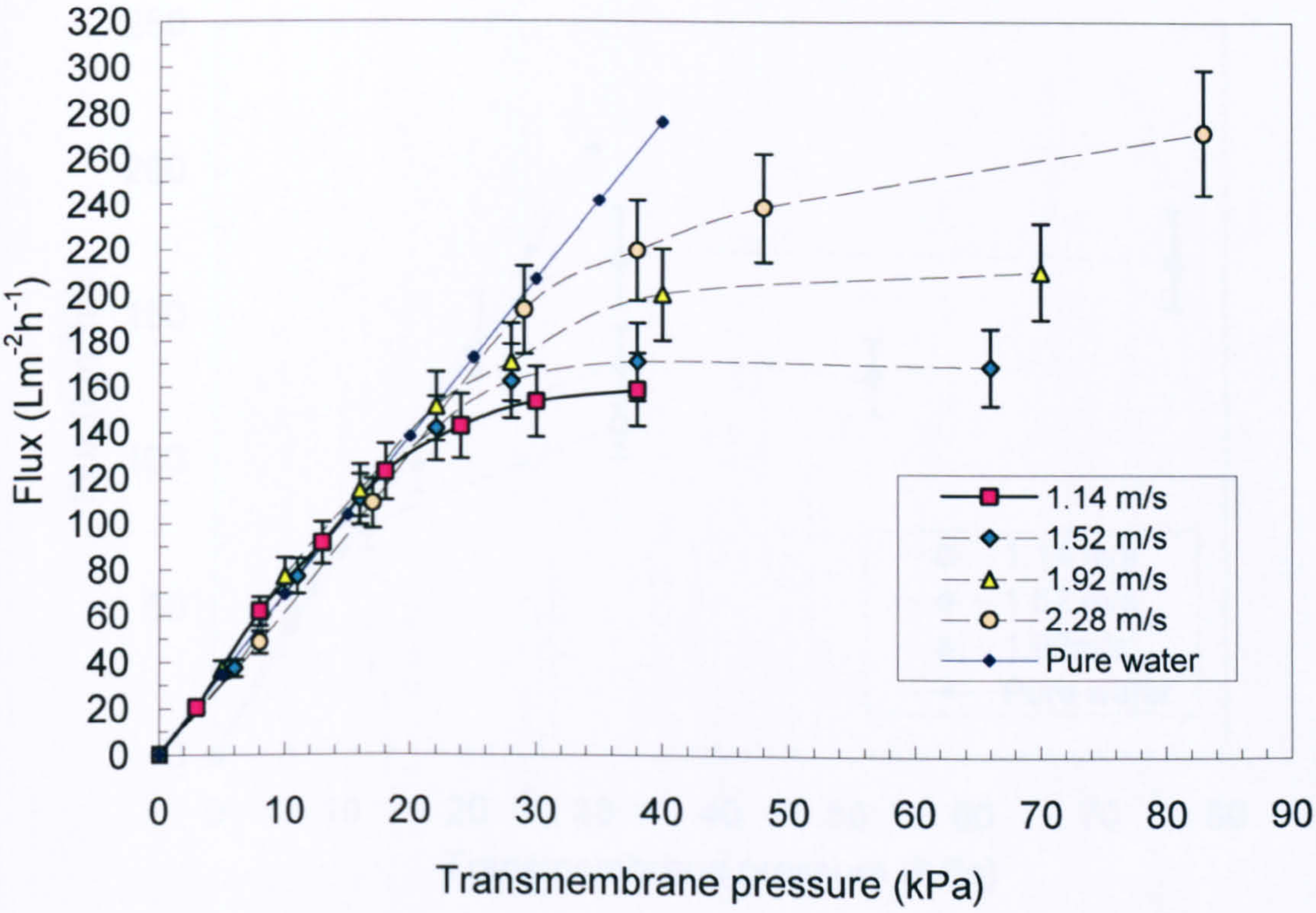

Figure 6.27: Flux performance at different crossflow velocities for a 600 mg L^{-1} n-dodecane emulsions with 60 mg L^{-1} surfactant.

When emulsions with 0.05 and 0.1 M NaCl were filtered, the influence of increasing crossflow velocity on critical flux became more prominent, as presented in Figures 6.28 and 6.29 where as the crossflow velocity increased from 1.14 to 1.92 m s^{-1} the critical flux increased from 45 to 125 L m^{-2} h^{-1}. Furthermore, after the critical flux point is reached, when there is a higher concentration of electrolyte in the solution the apparent divergence between flux–pressure curve behaviours are greater, as shown in Figure 6.29.

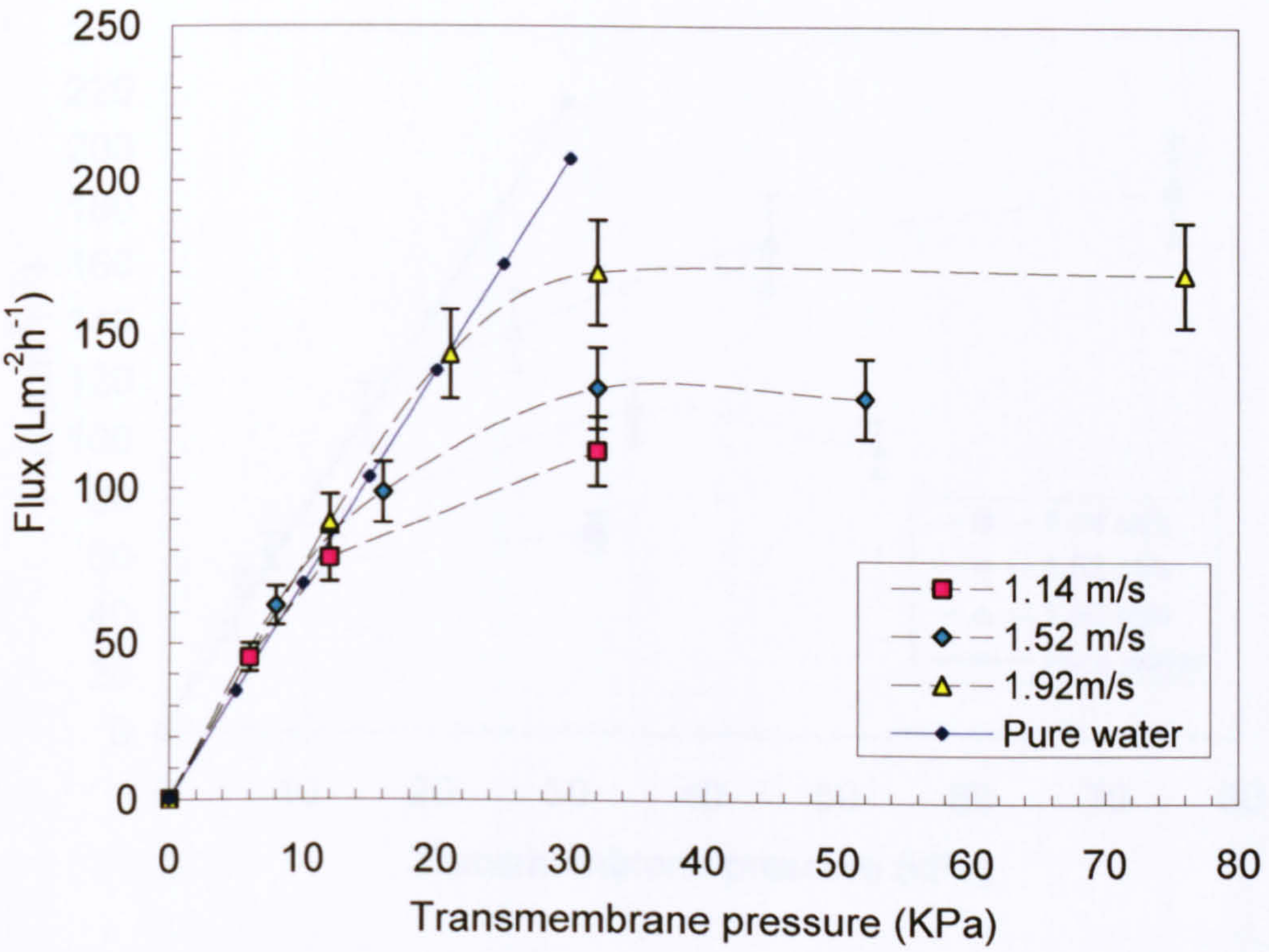

Figure 6.28: Flux performance at different crossflow velocities for a 600 mg L^{-1} n-dodecane emulsions in 0.05 M NaCl with 60 mg L^{-1} surfactant.

These two previous observations could be explained by the coupling effect of flow hydrodynamics and physico-chemical properties of the emulsion on permeate flux behaviour, particularly after the critical flux has been reached or the cake layer has started to build up. Moreover, when the permeate drag force increases due to increased transmembrane pressure, the rate of oil droplet transport to the membrane increases, where it becomes more condensed near membrane surface. Also, the reduction of the electrical double layer around the oil droplets owing to increased ionic strength would facilitate a higher packing density of oil droplets. When the crossflow velocity increased at these operating conditions its effects on flux became profound, but it is likely that the effects of velocity, surface charge and ionic strength interact in a complex way to give the observed behaviours.

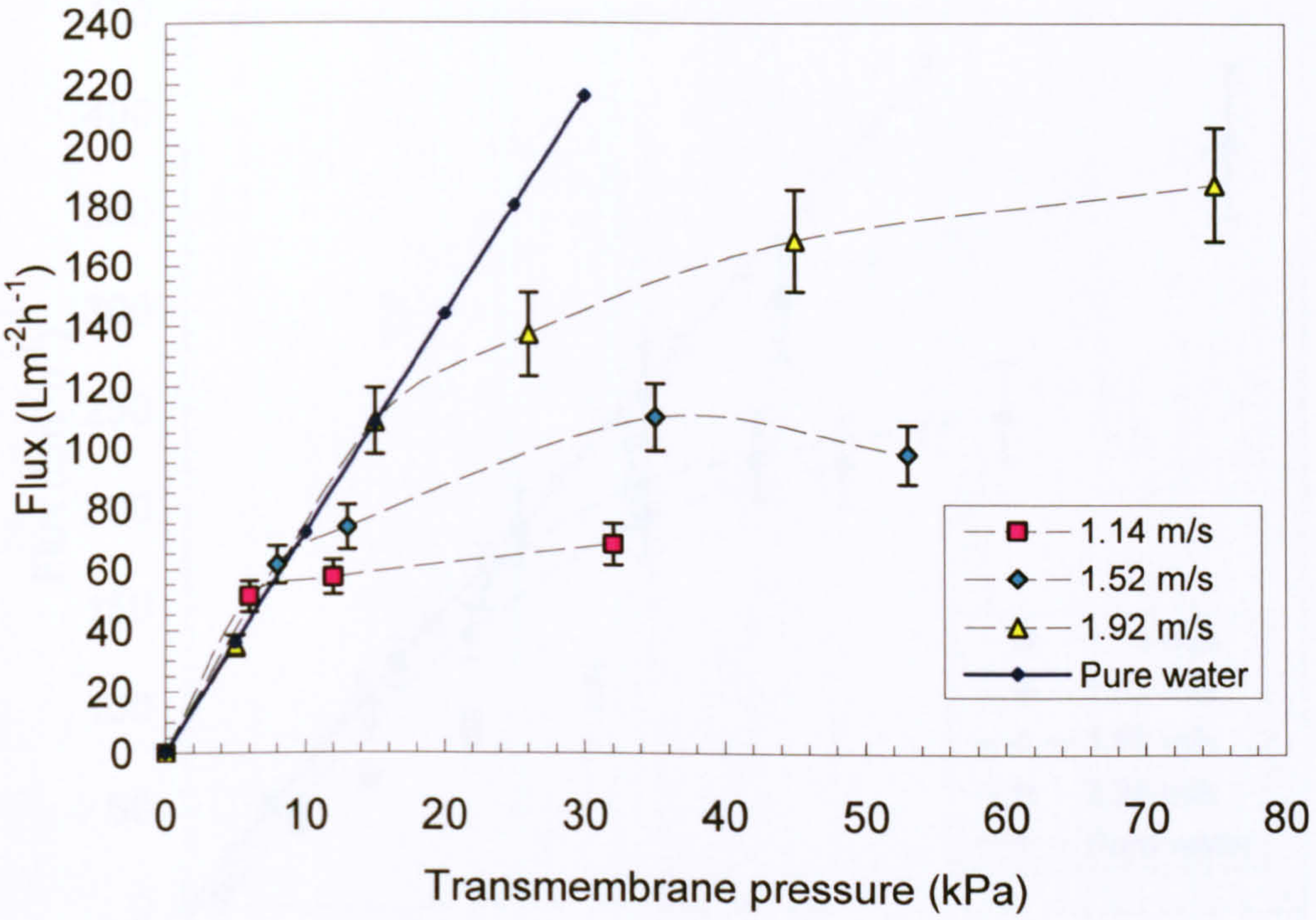

Figure 6.29: Flux performance at different cross-flow velocities for a 600 mg L^{-1} n-dodecane emulsions in 0.1 M NaCl with 60 mg L^{-1} surfactant.

When the emulsions with n-dodecane concentration of 1200 and 2400 mg L^{-1} were filtered, the increase of J_{crit} with crossflow velocity deviated from linearity at lower crossflow velocity (such as the 1.14 and 1.52 m s^{-1} data on Figures 6.30 and 6.31). At higher crossflow velocities 1.92 and 2.28 m s^{-1}, the trend of permeate fluxes were to be linear up to the J_{crit} point. Thus, it appears that the strong form of critical flux occurred at higher crossflow velocity 1.92 and 2.28 m s^{-1}, while the weak form of critical flux has been encountered at relatively lower crossflow velocity such as 1.14 and 1.52 m s^{-1}.

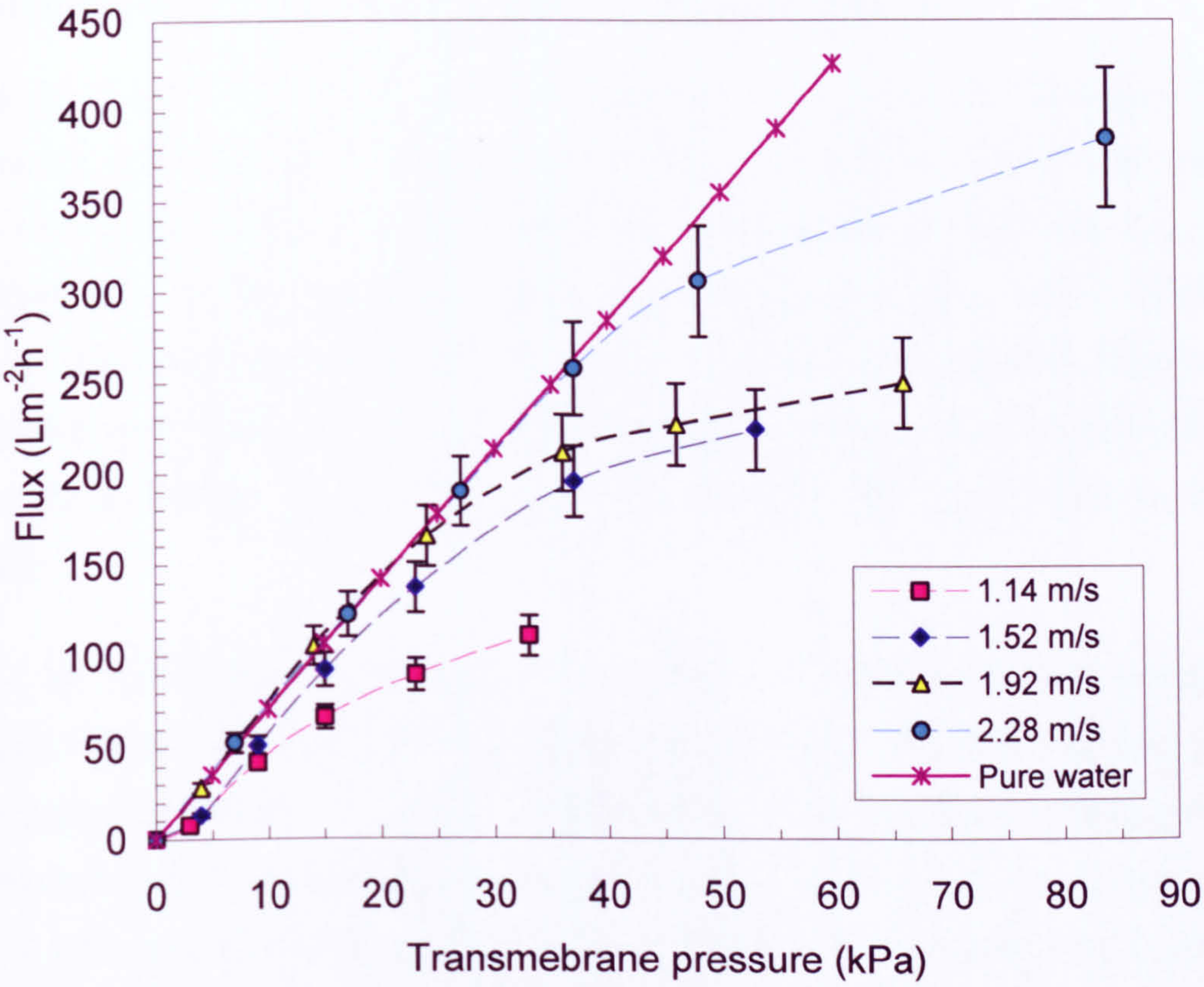

Figure 6.30: Flux performance at different crossflow velocities for a 1200 mg L^{-1} n-dodecane emulsions with 120 mg L^{-1} surfactant.

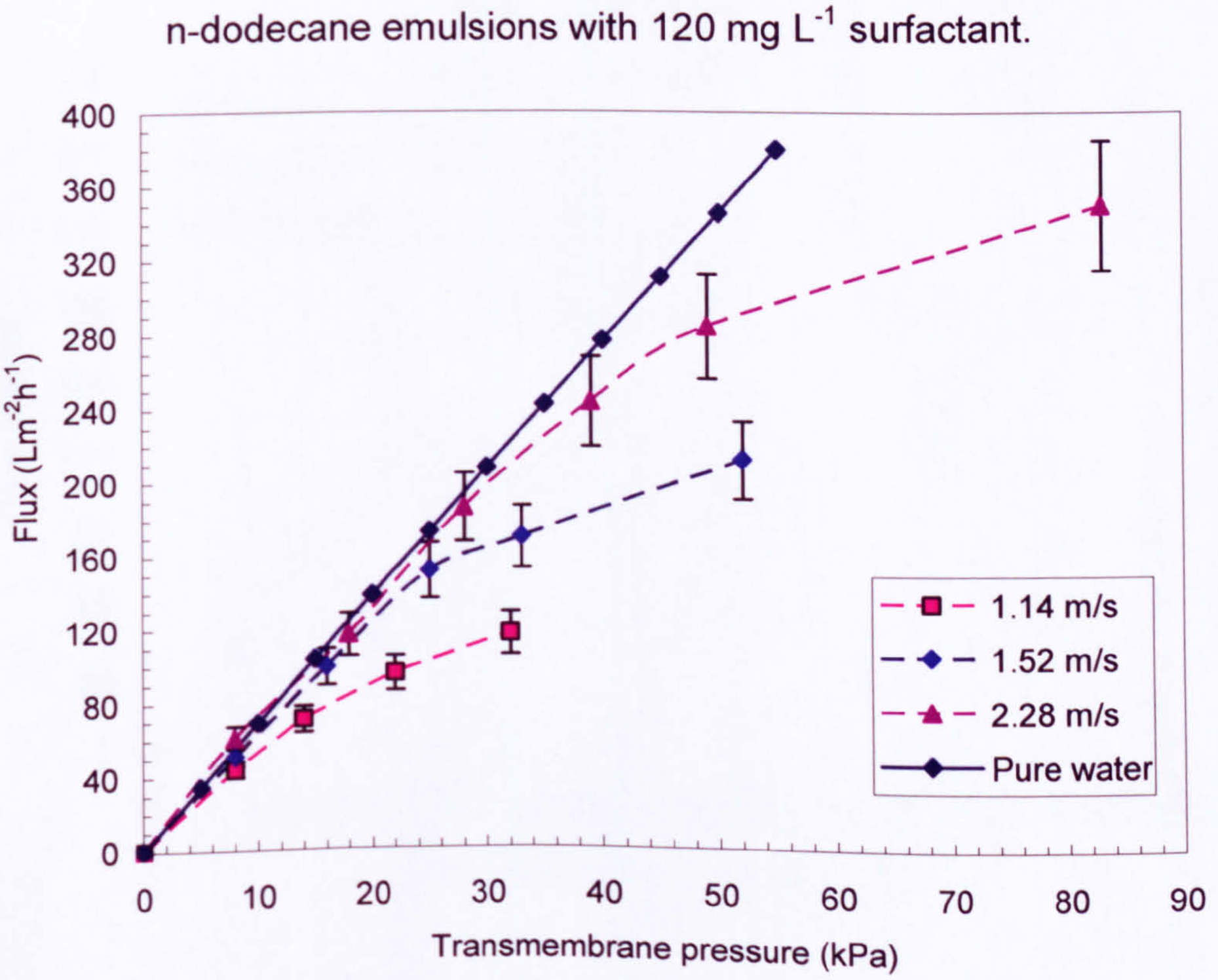

Figure 6.31: Flux performance at different crossflow velocities for a 2400 mg L^{-1} n-dodecane emulsions with 240 mg L^{-1} surfactant.

6.8 Hysteresis During Downwards Pressure Steps

Chen *et al* (1997) carried out an investigation concerning the transition from concentration polarization to cake formation for the membrane filtration of colloidal silica by imposing flux and monitoring the system response. A critical flux (J_{crit}) has been determined, below which the transmembrane pressure drop, ΔP, is stable for increasing and decreasing flux. The flux–pressure profiles for operations below J_{crit} demonstrate small hysteresis in the microfiltration test. Above J_{crit} the pressure has a period of instability for increasing and decreasing flux, and there is major hysteresis.

Similarly, all flux-pressure profiles for oil emulsions filtration tests conducted, above and below critical flux, showed hysteresis during downwards pressure steps such as during filtration of 600 mgL^{-1} emulsions as shown in Figures 6.32 to 6.34. Thus, this could be interpreted that internal fouling has occured. As mentioned in Chapter 4 with respect membrane cleaning, a chemical cleaning method has been effective in cleaning this irreversible oil deposition.

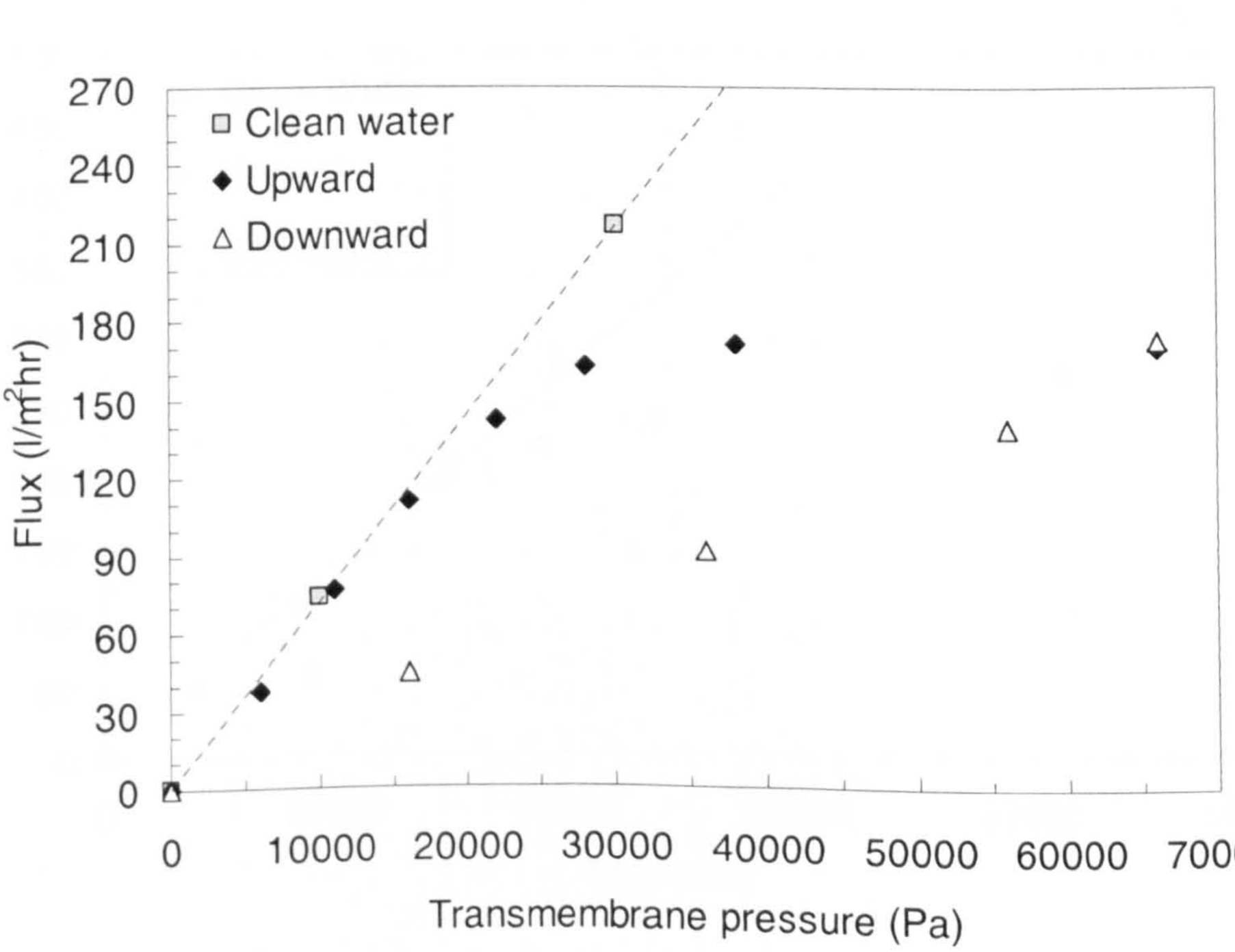

Figure 6.32: Step by step results for the filtration of 600 ppm n-dodecane emulsions, surfactant concentration 60 ppm, crossflow velocity 1.52 m/s.

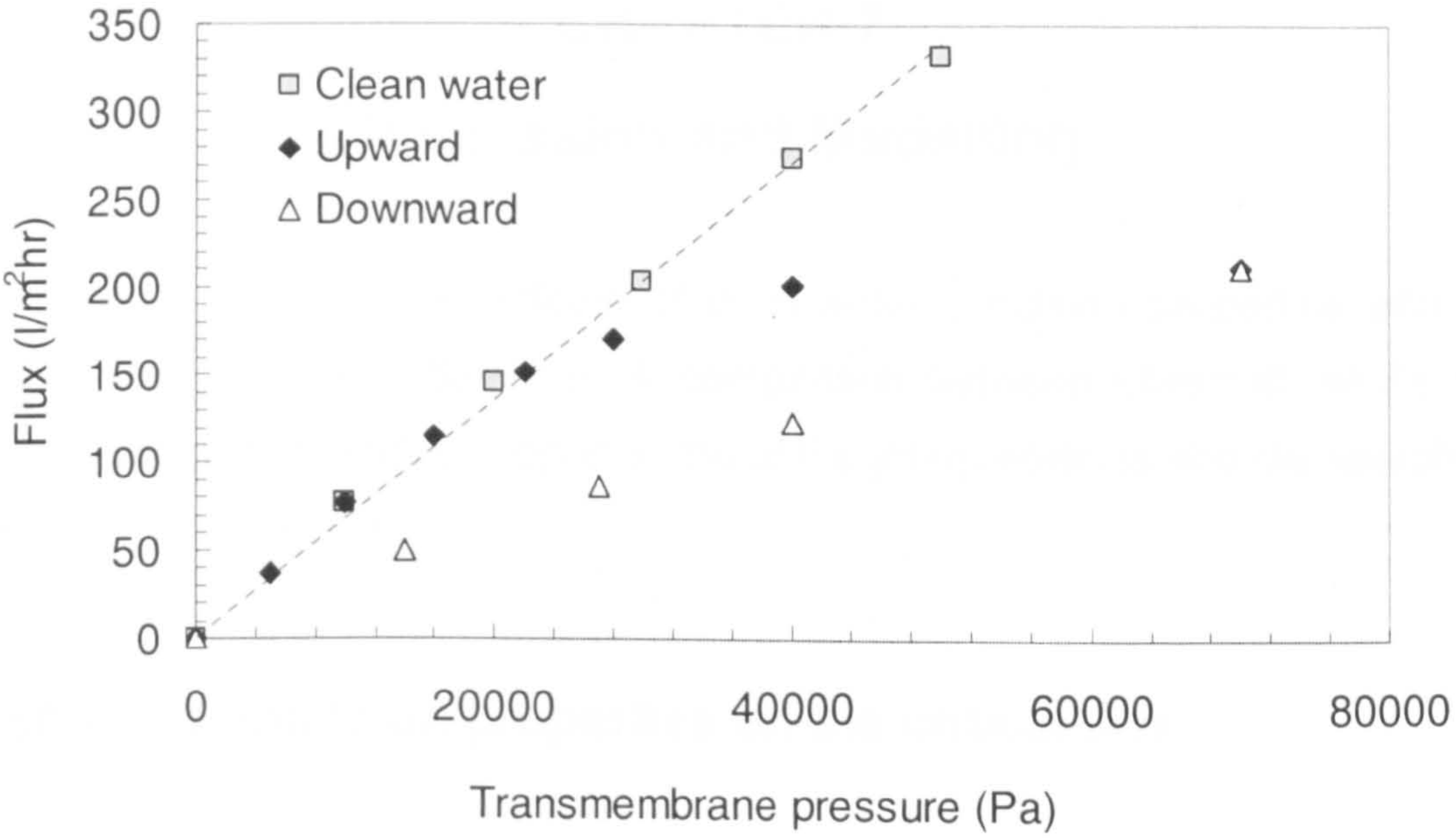

Figure 6.33: Step by step results for the filtration of 600 ppm n-dodecane emulsions, surfactant concentration 60 ppm, crossflow velocity 1.92 m/s.

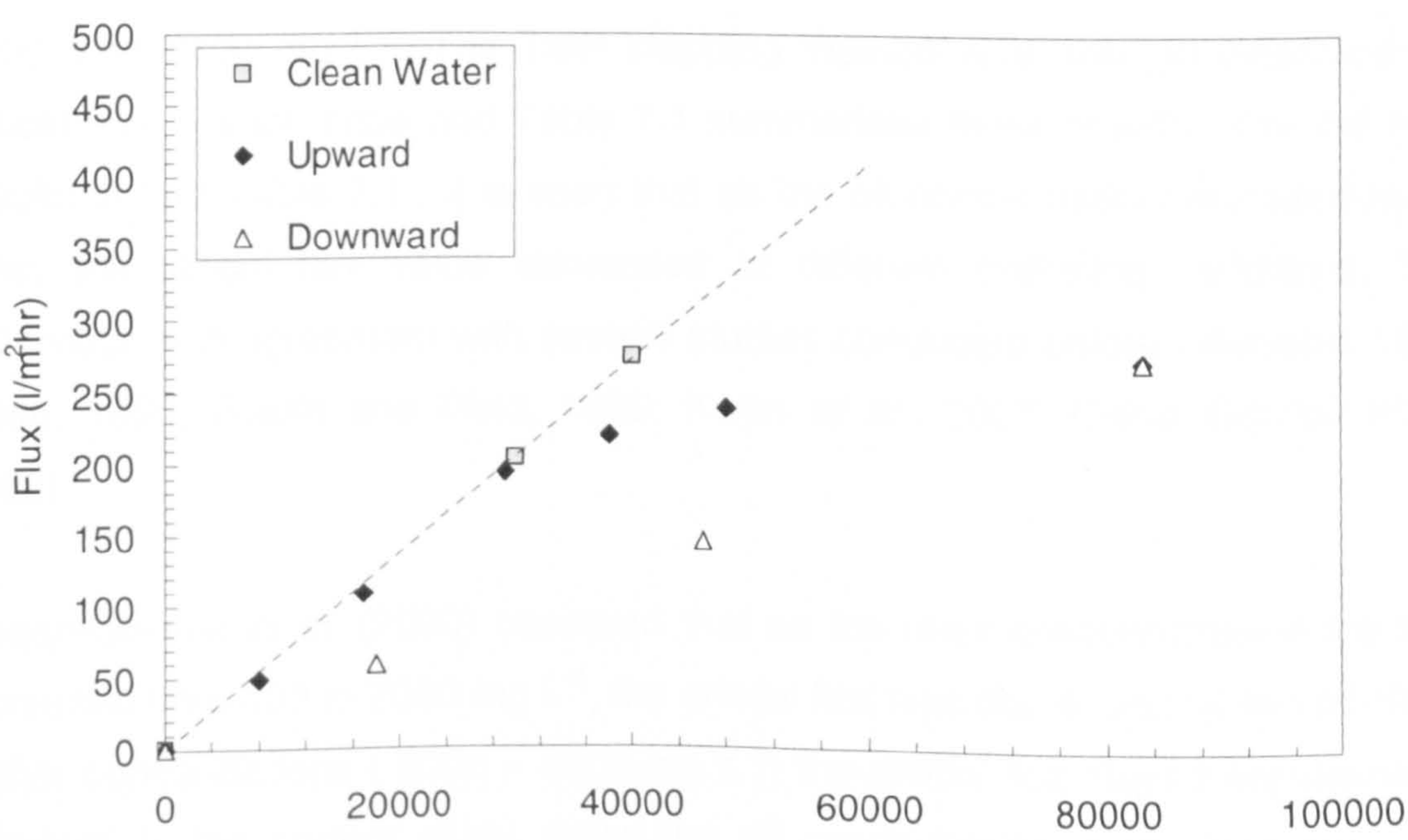

Figure 6.34: Step by step results for the filtration of 600 ppm n-dodecane emulsions, surfactant concentration 60 ppm, crossflow velocity 2.28 m/s.

CHAPTER 7

Discussion and Modelling

This chapter discusses the effects of oil-in-water emulsion properties and the hydrodynamics on the critical flux. A comparison between obtained results and several models is offered to support some of the interpretations and discussions of the experimental results.

7.1 Effect of Emulsion properties on the critical flux

7.1.1 Effect of oil feed concentration

With the 0.2 μm tubular multi-channel ceramic membrane, the critical flux was determined at four different crossflow velocities (1.14, 1.52, 1.92, 2.28 m s^{-1}). At each crossflow velocity, four oil feed concentrations were examined: 300, 600, 1200, and 2400 mg L^{-1}. The TMP stepping method was used to determine the critical flux in each case and Table 7.1 summarises these results. For the most results shown Table 7.1 , it is seen that as the oil concentration increased in the feed, the critical flux value decreased at different operating conditions. This behaviour is in agreement with several studies conducted before (Madaeni, 1997; Chen, 1998; Fradin and Field, 1999; Kwon *et al.*, 2000, Gesan-Guiziou *et al.*, 2002).

Gesan-Guiziou *et al.* (2000) observed that as the latex concentration in the feed increased from 400 to 2000 mg L^{-1}, the critical flux was decreased by two thirds. At higher concentrations (3000 – 8000 mg L^{-1}) the critical flux stayed approximately invariant. In the current study, when the oil concentration in the feed increased from 300 to 2400 mg L^{-1}, the critical flux values were decreased by almost one third while operating at crossflow velocities of 1.14, 1.52, and 1.92 m s^{-1}. For the case of operating at crossflow velocity of 2.28 m s^{-1}, the critical flux values decreased approximately by one quarter as the oil feed increased from 300 to 2400 mg L^{-1} , as shown in the Table 7.1.

As a result of increases in the oil feed concentration, the mass transfer rate of the oil droplets to the membrane surface increased and hence led to more accumulation in the boundary layer near the membrane surface . Consequently, an increase in the membrane resistance is observed due to the expansion of concentration polarization and the formation of thicker cake layer. During filtration of BSA at two different feed concentrations (at 0.1 and 1.0 wt %), the critical flux for the lower concentration was measured to be approximately 66 L m^{-2} h^{-1} while the higher concentration was 200 L m^{-2} h^{-1} (Chen ,1998). He proposed that the most influential parameter that affected the critical flux measurement was local concentration.

Table 7.1 :Summary of estimated critical flux values from TMP stepping experiments at varying oil feed (dodecane) concentrations.

Oil feed Concentration (mg L^{-1})	Crossflow Velocity (m s^{-1})			
	1.14	1.52	1.92	2.28
	Case A	Case B	Case C	Case D
	Apparent Critical Flux (L m^{-2} h^{-1})			
300	65	118	143.36	238
600	73	115.67	137.13	217
1200	47	89	116.42	197.8
2400	44	79.74	99.33	179.9

It can also be seen from Figure 7.1 and Table 7.1 that the critical flux value decreased by 2-4 % as the concentration increased from 300 to 600 mg L^{-1} for the cases B and C, and decreased by 9% for case D. With the exception for the case A, whereby increasing oil feed concentration from 300 to 600 mg L^{-1} resulted in an increase in the critical flux value. Similar behaviour reported by Wakeman and Tarleton (1993) where they noticed that the membrane fouling rate was found higher at lower feed concentration, where a comparatively high rate of TMP increase was noticed. The accumulated particles tend to plug the membrane pores at low feed concentration, because the competition for settling over optimal positions (at the membrane pores) is not too high.

In contrast, the lower rate of TMP increase at higher feed concentration might be caused by the particles bridging over the pores of the membrane to compete for the optimal positions which lead to cake layer formation (Kwon *et al.*, 2000).

Furthermore, by increasing the oil feed concentration from 600 to 1200 mg L^{-1}, the critical flux decreased by 35 % for case A, by 23 % for case B, by 15 % for case C, and by 10 % for case D. As the oil feed concentration increased from 1200 to 2400 mg L^{-1}, for case A the critical flux declined by 2 %; for cases B and D the critical flux declined by 9-10 %; and for case C the critical flux declined by 15 %. Case D showed an inverse relationship between critical flux and feed concentration. As the oil feed concentration increased by 100 % (doubled), the critical flux decreased by approximately 9 -10 % for each increment of oil concentration.

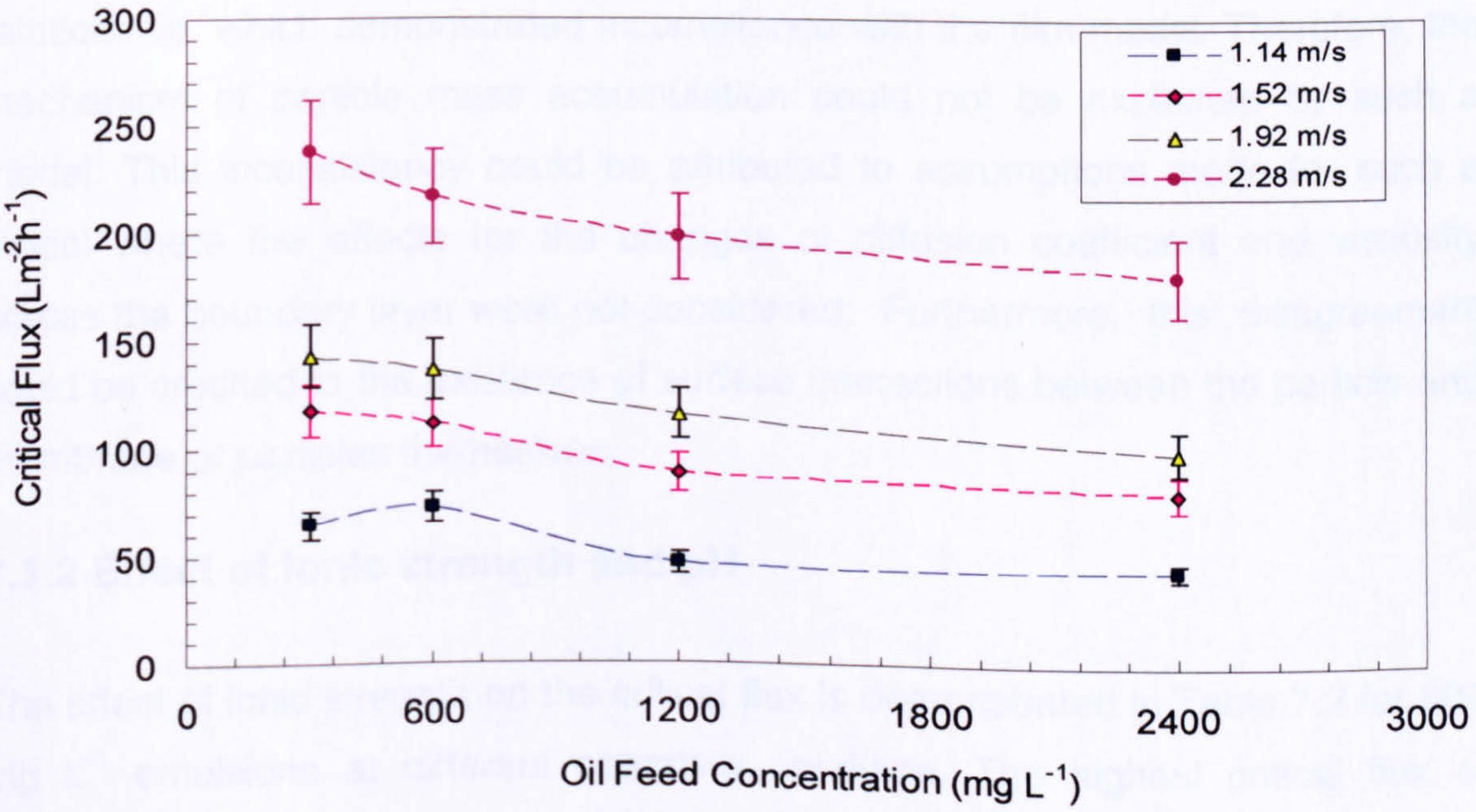

Figure 7.1: Variation of critical flux with oil feed concentration at different crossflow velocities (1.14,1.52, 1.92, 2.28 m s^{-1}).

In general the variation trend of critical flux values was to decline as the oil feed increased up to an oil concentration of 1200 mg L^{-1}, after which the critical flux was almost independent of concentration, as presented in Figure 7.1. The high flux at lower oil concentration (300 - 600 mg L^{-1}) appears to point to the inadequate formation of oil layer onto the membrane surface, which can be removed by the hydrodynamic effect (Ohya *et al.*,1998, Mohammadi *et al.*,2004). While at higher oil concentrations (1200 - 2400 mg L^{-1}), the hydrodynamic effect cannot take away the formed oil layer. Kwon *et al.* (2000) observed similar trend that both critical fluxes (based on mass balance and increase in TMP) decreased as the feed concentration increased. They suggested that this behaviour was due to the higher accumulation of particles onto the membrane surface. Hence, at higher feed concentration more particles tend to accumulate onto the membrane surface for the similar flux step.

On the other hand, Bacchin *et al.* (2006) stated that the plotting the permeate flux as a function of the logarithm of the concentration was not a straight line relationship, which demonstrated incompliance with the film model. Therefore, the mechanism of particle mass accumulation could not be explained by such a model. This inconsistency could be attributed to assumptions made for such a model where the effects for the changes of diffusion coefficient and viscosity across the boundary layer were not considered. Furthermore, this disagreement could be credited to the existence of surface interactions between the particle and membrane or particles themselves.

7.1.2 Effect of Ionic strength and pH

The effect of ionic strength on the critical flux is demonstrated in Table 7.2 for 600 mg L^{-1} emulsions at different operating condition. The highest critical flux of roughly 217 L m^{-2} h^{-1} obtained in the absence of salt at the highest velocity of 2.28 m s^{-1}. Upon the addition of 0.1 M NaCl, a decline of 56 % in the critical flux was observed. Likewise, while operating at a velocity of 1.92 m s^{-1} , the highest critical flux of approximately 137 L m^{-2} h^{-1} was found in the absence of salt. Then when 0.1 M NaCl was added , a drop of 41 % in the critical flux was noticed. Similarly, operating at velocity of 1.52 m s^{-1}, the highest critical flux of 116 L m^{-2} h^{-1} was

when there was no NaCl electrolyte in the feed. However as 0.1 M NaCl was added, a severe decline of 73 % of critical flux was observed. Finally for the case of operating at velocity 1.14 m s^{-1}, the biggest critical flux of 73 L m^{-2} h^{-1} was noticed when there was no salt in the feed emulsion. Nonetheless upon the addition of NaCl, a severe decline of roughly 71 % of critical flux was noticed. In the presence of NaCl ions, the surface charges of the dispersed oil droplets themselves and the membrane are shielded by positive ions. Hence, this reduces replusions between the oil droplets and between the membrane and oil droplets.

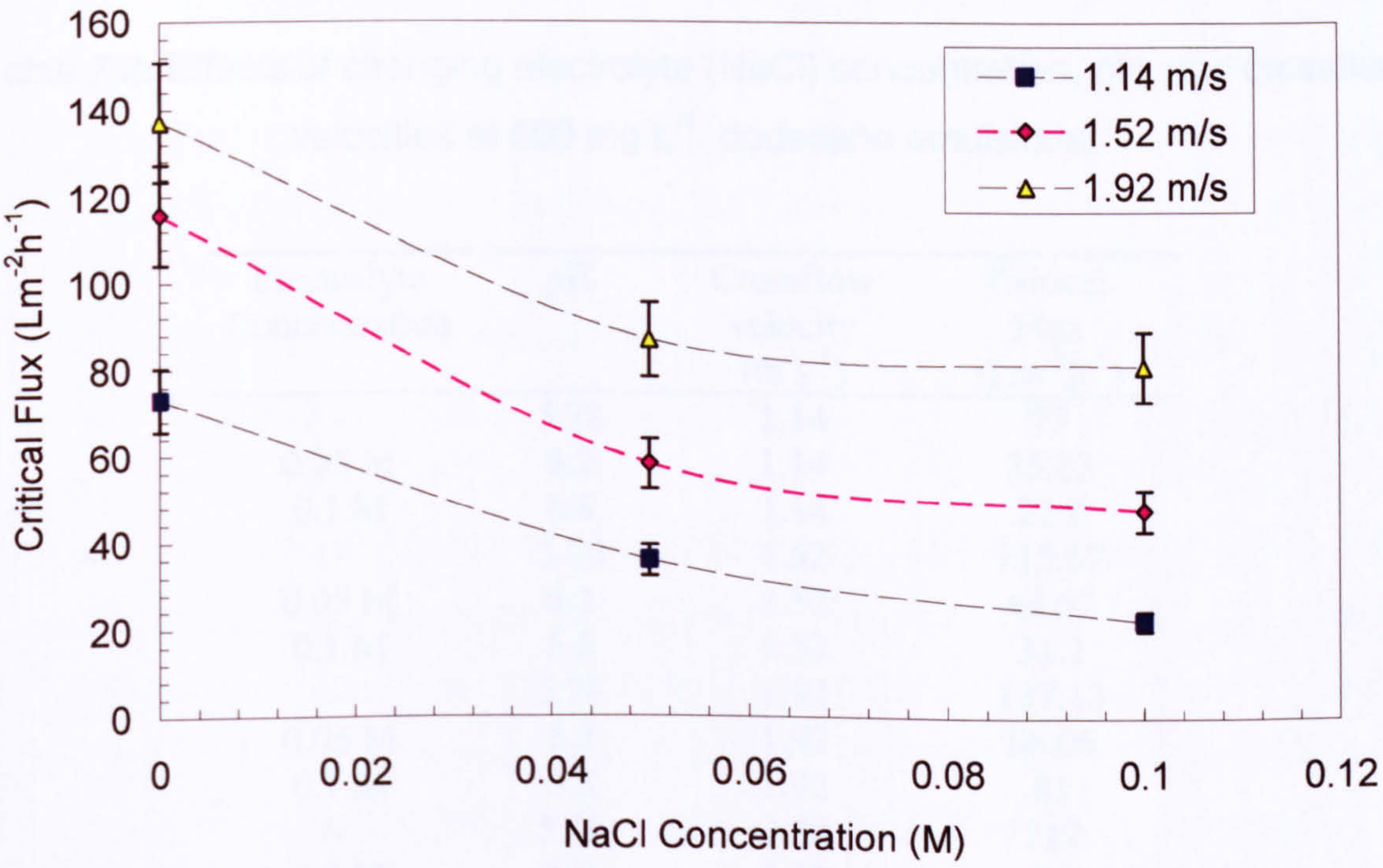

Figure 7.2: Variation of critical flux with NaCl salt concentration at different crossflow velocities (1.14, 1.52, 1.92 m s^{-1}) for 600 mg L^{-1} emulsion.

Similar observations by several researchers (Bacchin *et al.*, 1995, Kwon *et al.*, 2000) noted that a decline of critical flux occurred when the ionic strength was increased. Hua *et al.* (2007) noticed that at higher salt concentration a lower steady flux was given. As the ionic strength increased from 0.001 M to 0.05 M, the measured permeate flux decreased by more than half. For filtration experiments

conducted here with addition of 0.1 M NaCl, it has been observed that the rate of flux decline was greater after the critical flux had been reached and the steady flux was reached faster. Similar behaviour was observed by Faibish *et al.* (1998) that as the ionic strength increased the permeate flux decreased severely, and the period to reach steady state flux condition because much shorter. At higher ionic strengths, a decline in the range of the electrostatic double layer repulsive forces would occur, resulting in a decrease in the interparticle distances in the cake layer. Subsequently, the cake layer would become more densely packed and thus the resistance to permeate flux increased.

Table 7.2: Effects of changing electrolyte (NaCl) concentration, pH, and crossflow velocities at 600 mg L^{-1} dodecane emulsions.

Electrolyte Concentration	pH	Crossflow velocity ($m\ s^{-1}$)	Critical Flux ($Lm^{-2}h^{-1}$)
-	5.78	1.14	73
0.05 M	6.2	1.14	35.82
0.1 M	6.8	1.14	22.2
-	5.78	1.52	115.67
0.05 M	6.2	1.52	49.67
0.1 M	6.8	1.52	31.2
-	5.78	1.92	137.13
0.05 M	6.2	1.92	86.06
0.1 M	6.8	1.92	81
-	5.78	2.28	217
0.1 M	6.8	2.28	96
0.05 M	12	1.52	62.13
0.1 M	12	1.52	47.62

The effect of pH on critical flux is shown in Table 7.2. While operating at a velocity of 1.52 m s^{-1}, upon the increase of pH from 6.2 to 12 for 600 mg L^{-1} (with added 0.05 M NaCl) the critical flux increased from 49.67 to 62.13 L m^{-2} h^{-1}. Hence, an increase of 20 % of critical flux was observed when the pH value was doubled. Similarly at the same velocity, upon the increase of pH from 6.8 to 12 for 600 mg L^{-1} (with added 0.1 M NaCl), the critical flux increased from 31.2 to 47.6 L m^{-2} h^{-1}. Thus, a rise of 34 % of critical flux was noticed as result of increasing the pH. The

zeta potential trends with regards to changing of pH were measured and reported in Chapter 6 for 600 mg L^{-1} n-dodecane emulsions (without and with the addition of 0.05 and 0.1 M NaCl). As shown Figure 6.14, the zeta potential turned out to be more negative with increasing pH. As a result of increases in pH, the electrostatic repulsion between the emulsified oil droplets themselves and between them and membrane surfaced was because of the increase in the negative zeta potential of both membrane and dispersed oil droplet.

Alteration of both the emulsion pH and ionic strength is a practice that enables particle-particle and particle-membrane electrostatic forces to be investigated to highlight their influences on the critical flux. The electrostatic influences of pH can be counterbalanced by the addition of electrolytes to the feed suspension. Electrolyte ions attach to ionised parts of the particles and generate a charge shielding effect, and thus diminishing any electrostatic repulsive or attractive forces and compressing the double layer. Hence, a decrease in the scale of electrostatic repulsive or attractive forces would take place as the ionic strength increases. By the addition of 0.05 M NaCl salt, the zeta potential of for 600 mg L^{-1} emulsion was roughly -38 mV at pH 6.35 and approximately -59 mV at pH 10. Therefore, by increasing pH to 12, an increase in the negative zeta potential of the emulsified oil droplets had led to an increase of the electrostatic repulsion between the oil droplets themselves, where their apparent particle size became larger. Hence they would form a relatively permeable cake layer with lower resistance which resulted in higher critical flux. Similarly, for a 600 mg L^{-1} emulsion with addition 0.1 M NaCl, the measured zeta potential was roughly -18.1 mV at pH 6.27 and -50 at pH 11. The critical flux increased when the pH increased as presented in Table 7.2.

However, by increasing the ionic strength via the addition of 0.1 M $CaCl_2$ as shown in Table 7.3, the critical flux increased by approximately 34 % (174 L m^{-2} h^{-1}) for 600 mg L^{-1} dodecane emulsion. Also for 1200 mg L^{-1} dodecane emulsion, the critical flux increased by roughly 48 % (174 L m^{-2} h^{-1}) as the ionic strength increased by adding 0.1 M $CaCl_2$. Likewise for 2400 mg L^{-1} dodecane emulsion, the critical flux increased by about 43 % (141 L m^{-2} h^{-1}) when the ionic strength increased by the addition of 0.1 M $CaCl_2$. Furthermore, the critical flux almost

doubled (156 L m^{-2} h^{-1}) for 2400 mg L^{-1} dodecane emulsion when the ionic strength increased by the addition of 0.1 M $FeCl_3$ as shown in Table 7.3 and Figure 7.3.

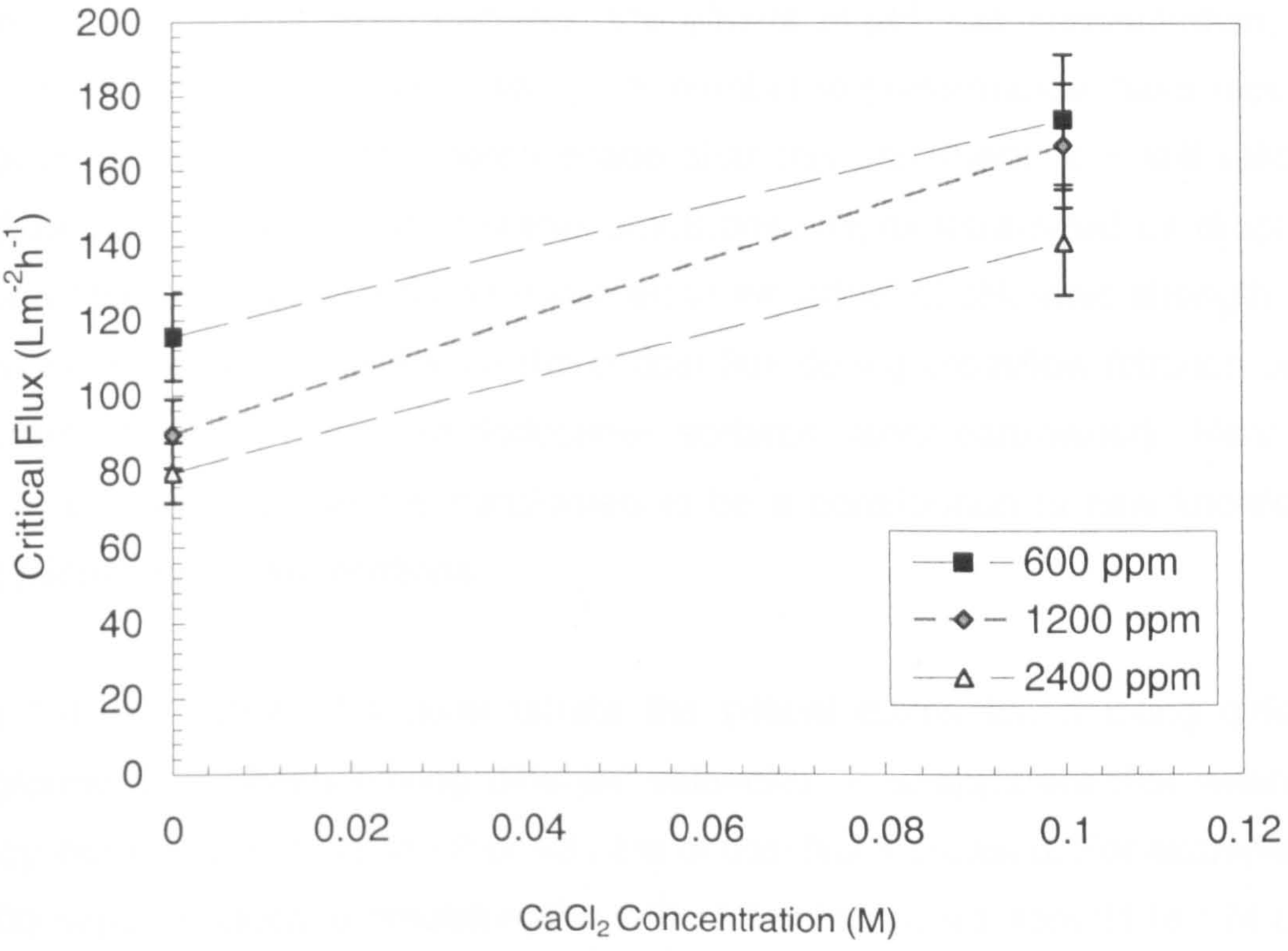

Figure 7.3: Variation of critical flux with $CaCl_2$ salt concentration at different concentrations of dodecane for crossflow velocity of 1.52 m s^{-1}.

In addition, a number of researchers (Tambe and Sharma,1992, Šmídová *et al.*, 2004, Zhao *et al.*, 2005) found that when the ionic strength increased, the steady permeate flux became higher. They suggested that high ionic strength reduces the film thickness around the oil droplets, thus reducing the electrostatic repulsion, and thereby encouraging coalescence to form larger oil droplets. Hence when the larger oil droplets start to deposit and the cake layer was formed, it would have a lower cake resistance and thus higher permeate flux. As reported by several investigations usually as result of increasing the ionic strength by adding mono or poly electrolyte, the critical or permeate flux would increase or decrease. However, at the same ionic strength as shown in Figure 7.4 the critical flux decreased by the addition of mono-electrolyte (NaCl) and the critical flux increased by the addition poly-electrolyte ($CaCl_2$).

7.1.3 Effect of Valency

Elzo *et al.* (1998) stated that "in most of the published work on the cross-flow filtration of micrometre-sized particles, the effects of pH, salt concentration, and especially the influence of salt valency on membrane performance, have received little or no attention". Furthermore decade after this statement, it is still valid for crossflow microfiltration of oil-in-water emulsions (micrometre-sized oil droplets). Certainly little or no attention was allocated to the effect of pH, ionic strength, and particularly electrolyte valency on the critical flux during crossflow filtration of oil-surfactant-water emulsions (n-dodecane- sorbitan monoleate-water). Hence, a study in this research field is considered to be a contribution to new knowledge about microfiltration applications.

Table 7.3 and Figure 7.4 demonstrate the critical fluxes found using different background electrolytes having different valencies. It is apparent that when the valency increases from +1 to +2 or +3 , the critical flux increased. For example, for the 600 mg L^{-1} dodecane emulsion, the critical flux increased from 31 to 174 L m^{-2} h^{-1} (an increase of 82%) when the valency increased from +1 to +2. Also, for the 2400 mg L^{-1} dodecane emulsion, the critical flux increased from 61 to 141 L m^{-2} h^{-1} (an increase of 57%) when the valency increased from +1 to +2.

Table 7.3: Effects of changing electrolyte, electrolyte concentration, ion valency and polyelectrolyte type at crossflow velocity 1.52 m s^{-1}.

Electrolyte	Electrolyte Concentration (M)	Dodecane Concentration (mg L^{-1})	Critical Flux ($Lm^{-2}h^{-1}$)
NaCl	0.1	600	31.2
$CaCl_2$	-	600	115.67
$CaCl_2$	0.1	600	173.96
$CaCl_2$	-	1200	89
$CaCl_2$	0.1	1200	169.9
NaCl	-	2400	79.94
NaCl	0.1	2400	61.21
$CaCl_2$	0.1	2400	141
$FeCl_3$	0.1	2400	156

Furthermore, when the valency increased from +1 to +3 , the critical flux increased from 61 to 156 L m^{-2} h^{-1} (an increase of 61%) (Table 7.3). However, the results obtained here were in disagreement with trends reported by other researchers. Chiu and James found that as the valency increased from +1 (KCl electrolyte) to +2 ($CaCl_2$ electrolyte), the critical flux decreased during crossflow microfiltration of TiO_2 suspensions using a ceramic membrane. Similarly, Elzo *et al.* (1998) studied the influence of valency of the salt on permeate flux, and observed that when the valency increased from +1 (NaCl electrolyte) to +2 ($CaCl_2$ electrolyte), the steady permeate flux decreased by approximately 33%. This flux decline is caused by the decrease of the zeta potential of silica particles from -85 mV (for Nacl electrolyte) to -35 mV (for $CaCl_2$ electrolyte). This decrease in the zeta potential is caused by the shielding effect of adsorbed divalent calcium ions and hence the surface charges on the interacting particles were lowered. Thus, the repulsive forces between particles decreased and the attractive forces became predominant and induced particle deposition.

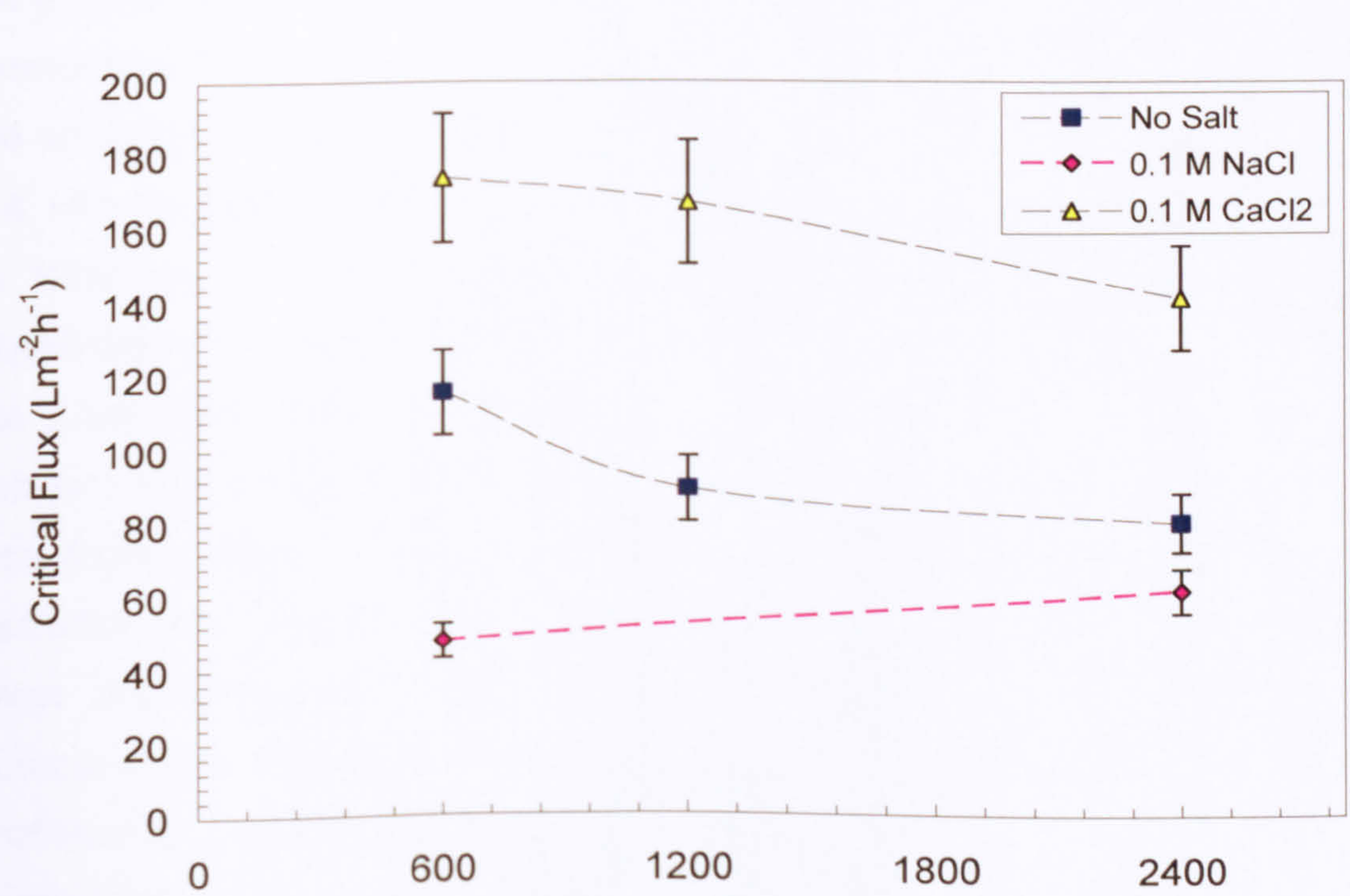

Figure 7.4: Variation of critical flux with different salt concentration at different concentrations of dodecane for crossflow velocity of 1.52 m s^{-1}.

The critical flux behaviour shown in Figure 7.4 when the valency increased could explained by ion bridging. In this mechanism, the calcium ion or ferric ion would adsorb on the surfaces of the oil droplets to build a bridge between them and hence form larger oil droplets which can sweep away from the membrane surface by back transport mechanisms such as shear-induced diffusion and inertial lift velocity. Furthermore, in term poly diversity of particle size of small oil droplets, the finer oil droplets tend to have large negative surface charge density leading to attraction, and hence attachment of positive calcium or ferric ions which link other oil droplets by the ion bridging mechanism and generation of larger oil aggregates. Generally, when these large flocculated oil droplets deposit on the membrane surface the cake layer porosity would increase due to the cross-linking effect which results in a decrease in the cake resistance and an increase in the flux.

Zhao *et al.* (2006) observed the formation of $Mg(OH)_2$ as a dynamic membrane for oily water separation on α-Al_2O_3 porous ceramic tubes using a crossflow filtration process. Similarly, a rationalization of the increase of critical flux behaviour due to the polyelectrolyte addition would be the formation of $Ca(OH)_2$ or $Fe(OH)_3$ dynamic membranes for oily water on zirconia ceramic channels as a result of generation of the solubility product such as $Ca(OH)_2$ and $Fe(OH)_3$. By interpretation of Figure 7.4, with the addition of 0.1 M $CaCl_2$, as the oil concentration increased from 600 to 1200 mg L^{-1}, the decrease rate of critical flux was lower, while as the concentration increased further to 2400 mg L^{-1} the decrease rate was higher. On the other hand, with no salt added a different scenario occurred, as the oil concentration increased from 600 to 1200 mg L^{-1}, the decrease rate of critical flux was higher, while as the concentration increased further to 2400 mg L^{-1} the decrease rate was lower. It could be speculated qualitatively that at relatively lower and moderate oil concentration (respectively 600 and 1200 mg L^{-1}) the number of free Ca^{2+} ions were in excess of the number oil droplets and hence the formation of $Ca(OH)_2$ would be promoted, and thus the effect of doubling the oil concentration was limited. Increasing the oil concentration by four times (2400 mg L^{-1}) at the same added amount of $CaCl_2$ (0.1 M), the number of free Ca^{2+} ions decreased as a result of the increase of the number of oil droplets by the order of four times. Hence, the formation rate of solubility products would much lower and the rate of critical flux decline became higher.

7.2 Effect of hydrodynamics on critical flux

7.2.1 Effect of crossflow velocity and wall shear stress

Figures 7.5 and 7.6 demonstrate the variation of critical flux with increasing crossflow velocity for n-dodecane emulsions. The general observed trend was an increase in critical flux as the crossflow velocity (shear) was increased as shown in Table 7.1 and Figure 7.5. At the higher crossflow velocities, higher shear wall stress was generated and hence less particle deposition at the membrane surfaces due to removal by erosion. For 300 mg L^{-1} emulsions, increasing the crossflow velocity from 1.14 to 2.28 m s^{-1} led to an increase in critical flux by a factor of 3.7. Also, for 600 mg L^{-1} emulsions, increasing the crossflow velocity from 1.14 to 2.28 m s^{-1} led to an increase in critical flux by a factor of 3. While for 1200 mg L^{-1} emulsions, increasing the crossflow velocity from 1.14 to 2.28 m s^{-1} led to an increase in critical flux by a factor of 4.2. Similarly, for 2400 mg L^{-1} emulsions, increasing the crossflow velocity from 1.14 to 2.28 m s^{-1} led to an increase in critical flux by a factor of 4.1.

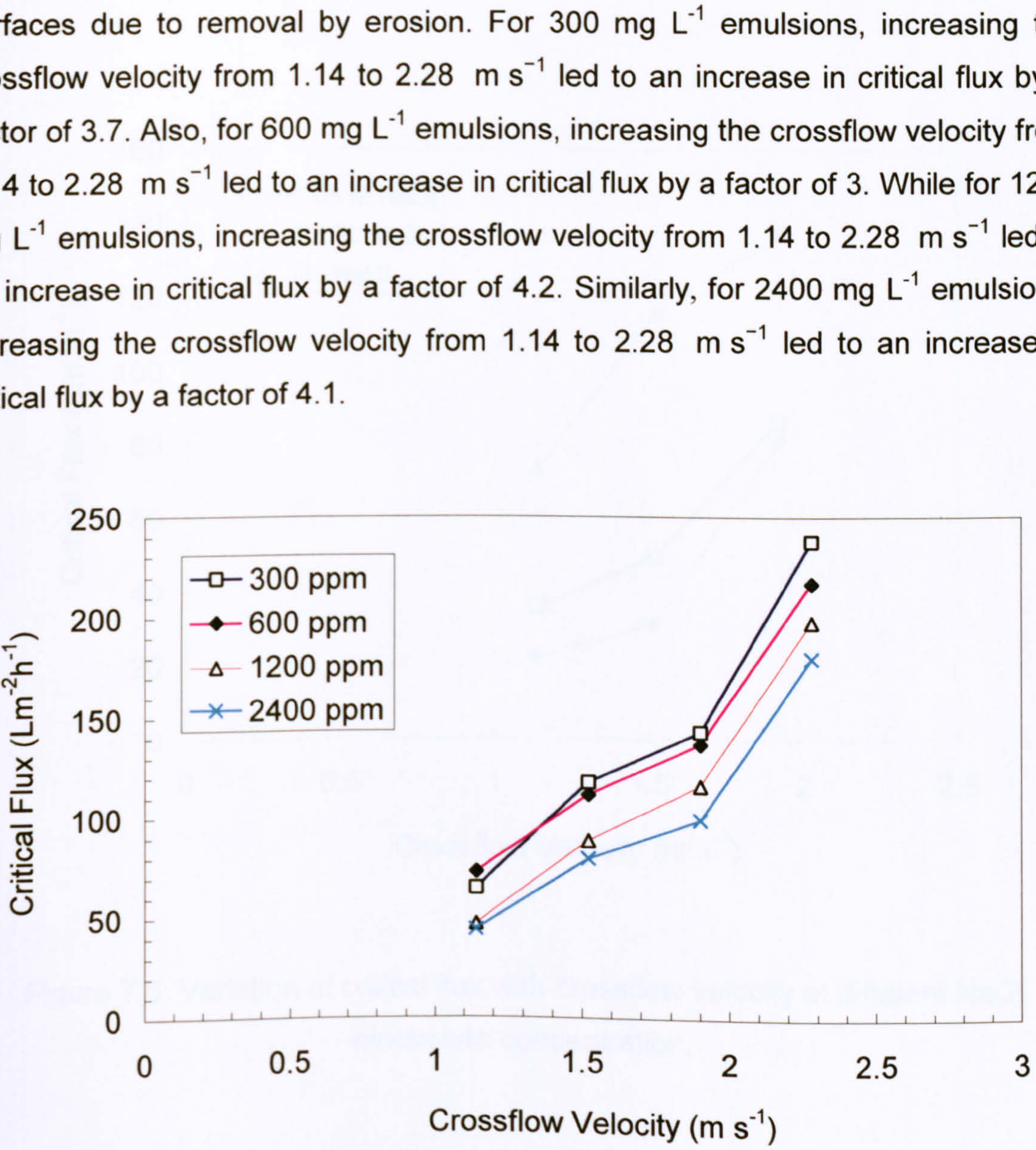

Figure 7.5: Variation of critical flux with crossflow velocity at different oil feed concentration (600, 1200, 2400 mg L^{-1}).

In general, increasing the crossflow velocity from 1.14 to 2.28 m s^{-1} resulted in an increase in critical flux by a factor approximately between 3 and 4. A comparable trend with a similar factor was reported by pervious researchers such as Chen *et al* (1997) and Chiu *et al.* (2005) when the crossflow velocity increased. Chen *et al* (1997) accredited their results to the inception of turbulence at higher crossflow velocities. Similarly in the present study, the Reynolds number at lowest crossflow velocity (1.14 m s^{-1}) was estimated to 5358 and at the highest crossflow velocity (2.28 m s^{-1}) was approximated to 10716. Hence, the flow regime could be described to lay in the turbulent regions.

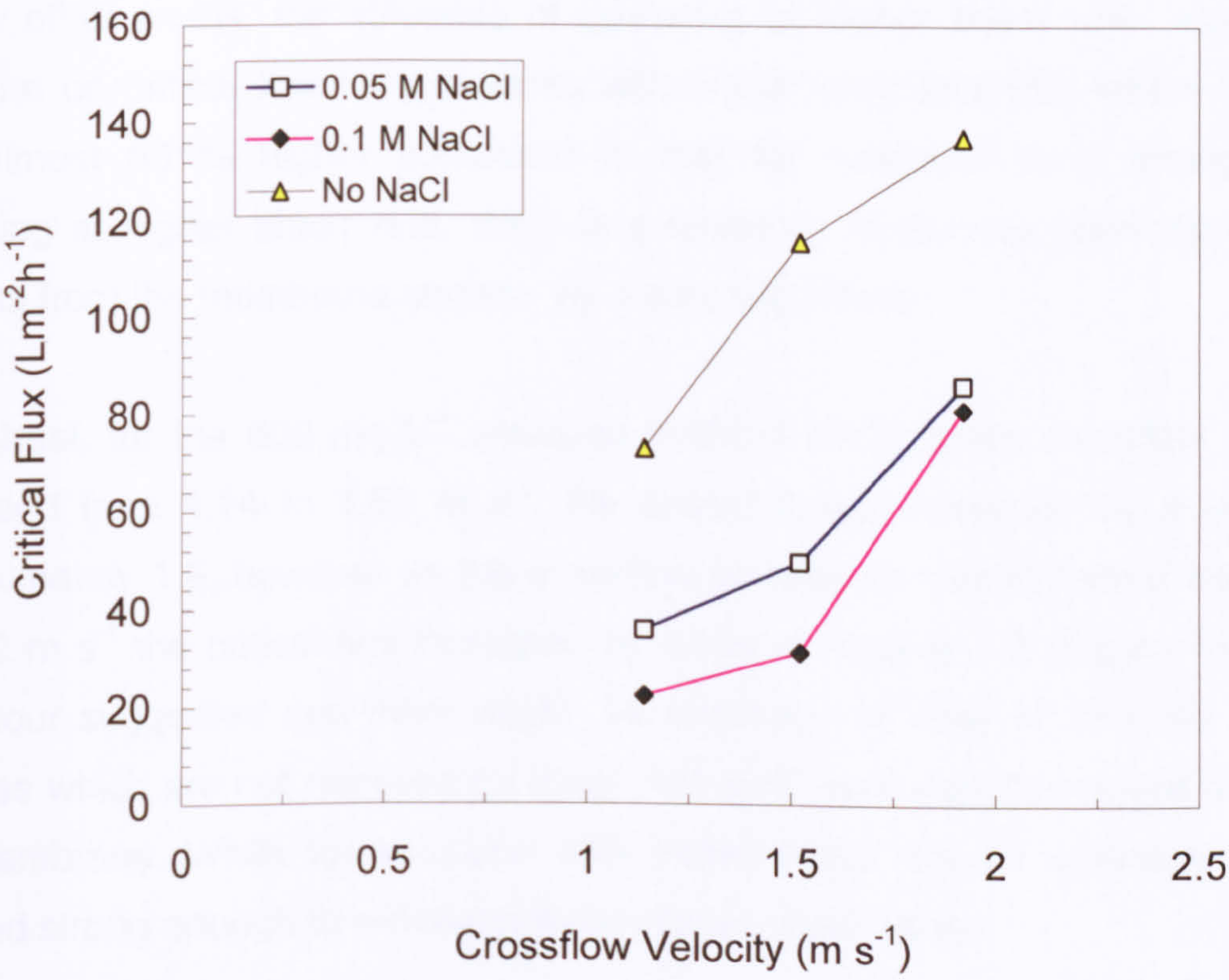

Figure 7.6: Variation of critical flux with crossflow velocity at different NaCl electrolyte concentration.

The critical flux values decreased when the NaCl salt amount increased in a 600 mg L^{-1} emulsion at different crossflow velocities, as shown in Figure 7.6. When no salt was added, increasing the crossflow velocity from 1.14 to 1.92 m s^{-1} led to an

increase in critical flux by a factor of 1.9. Adding 0.05 M NaCl to the 600 mg L^{-1} emulsion and increasing the crossflow velocity from 1.14 to 1.92 m s^{-1} led to an increase in critical flux by a factor of 2.4. By adding 0.1 M NaCl to the 600 mg L^{-1} emulsion and increasing the crossflow velocity from 1.14 to 1.92 m s^{-1}, an increase in critical flux by a factor of 4 resulted. The impact of increasing both ionic strength (0.05 M and 0.1 M NaCl) and crossflow velocity on critical fluxes demonstrated similar curve behaviour, as shown in Figure 7.6. When crossflow velocity increased from 1.14 to 1.52 m s^{-1}, the critical fluxes increased for both ionic strength by factor of almost 1.4, however as the crossflow velocity increased further from 1.52 to 1.92 m s^{-1}, the critical flux for the higher ionic strength (0.1 M) increased by factor 2.6 while for the moderate ionic strength (0.05 M) by factor of 1.7. In other words, the influence of operating at higher shear rate was more profound on critical flux for emulsions with higher ionic strength, where the flux was almost 60 % higher compared to that for moderate ionic strength. By operating at higher shear rate, there is a tendency to remove relatively smaller droplets from the membrane surface by a scouring effect.

In contrast, for the 600 mg L^{-1} emulsion (without NaCl) when crossflow velocity increased from 1.14 to 1.52 m s^{-1}, the critical fluxes increased by a factor of approximately 1.6, however as the crossflow velocity increased further from 1.52 to 1.92 m s^{-1} the critical flux increased by factor of roughly 1.2 (Figure 7.6). This behaviour suggested that there might be breakage of large oil droplets to finer particles which are not removed by shear rate and there may be internal fouled of the membrane. While for emulsion with added NaCl, the oil emulsion stability seemed strong enough to withstand these higher shear rates.

Generally, increasing crossflow velocity led to an increase in the critical flux values as shown in Table 7.2. The best critical flux level was 238 L m^{-2} h^{-1} at experimental conditions where the crossflow velocity was 2.28 m s^{-1}, 300 mg L^{-1} and no NaCl salt was added. Adding 0.1 M NaCl salt at the same experimental conditions, the critical flux value decreased to 88 L m^{-2} h^{-1}. In the other hand, the least critical flux value was 22 L m^{-2} h^{-1}, where experimental conditions were at the lowest crossflow velocity (1.14 m s^{-1}) and the highest NaCl concentration (0.1 M) for 600 mg L^{-1} emulsion.

Assuming cake filtration, the total particle accumulation onto the membrane surface occurs as a result of the convection flow dragging particles toward the membrane becoming higher than the removal rate of particles away to the bulk stream, which is believed to be proportional to shear stress (Fradin and Field, 1999):

$$A(JC_p - a\tau_w) = \frac{dm}{dt} \tag{7.1}$$

where A is the surface area, J is the permeate flux, C_p is the mass concentration of suspension, a is an experimentally determined constant, τ is the shear stress and m is the cake mass. At higher wall shear stresses, fewer particles deposited onto membrane surface and hence higher critical flux values were attained (Figure 7.6). Gèsan-Guiziou *et al.* (2002) suggested a critical parameter (J_{crit}/τ_w), which stayed constant over the range investigated, where J_{crit} increased linearly with τ_w and J_{crit} was found to be independent of initial pore size of the membrane. Their argument was justified based on the work of Fradin and Field (1999) who claimed that at the condition of critical flux there is no particle accumulation (*dm/dt*) and hence *dm/dt* becomes zero in equation (7.1). Therefore, the convective particle deposition (J_{crit}* C_p) is proportional to the shear stress (τ_w), that is $J_{crit}C_p \ \alpha \ a\tau_w$. Gèsan-Guiziou *et al.* (2002) stated that the proof that "a" in equation (7.1) is constant is inadequate; for this to be so implies that the ratio $(J_{crit}C_p)/\tau_w$ has to stay constant, which is not observed experimentally. Similarly, the experimental results obtained in this thesis demonstrate that the critical parameter (J_{crit}/τ_w) did not remain constant as shown in Table 7.4 and Table 7.5. Therefore, Gèsan-Guiziou *et al.* (2002) interpretation of such experimental data is that "a" is not constant, however a function of C_p, which implies that the hypothesis to establish equation (7.1) was not applicable for such cases.

Table 7.4: The critical parameter (J_{crit}/τ_w) values at different crossflow velocity for emulsion A, emulsion B, and emulsion C.

Crossflow Velocity ($m\ s^{-1}$)	Oil feed Concentration ($mg\ L^{-1}$)		
	600	1200	2400
	Emulsion A	Emulsion B	Emulsion C
	J_{crit}/τ_w ($Lm^{-2}h^{-1}Pa^{-1}$)	J_{crit}/τ_w ($Lm^{-2}h^{-1}Pa^{-1}$)	J_{crit}/τ_w ($Lm^{-2}h^{-1}Pa^{-1}$)
1.14	12.15	7.82	7.32
1.52	11.51	8.85	7.93
1.92	9.34	7.93	6.76
2.28	10.74	9.79	8.90
Mean	10.93	8.60	7.73

From Table 7.4 and Figure 7.7, It is apparent that no single linear correlation exists for all the concentrations. In addition, for every concentration there was some non-linearity in the variation of critical flux with shear stress and the proportional correlation between the convective particle deposition and particle back transport erosion (shear stress) exists over a limited range of values. These observations concerning the constancy of (J_{crit}/τ_w) do not entirely agree with the work of Gesan-Guisiou *et al.* (1999, 2002) whose experimental results demonstrated a linear variation of critical flux and wall shear stress. The gradient of the linear relationship (J_{crit}/τ_w) for skimmed milk was 0.95 L m^{-2} h^{-1} Pa^{-1} and for latex particles was 18 L $m^{-2}h^{-1}Pa^{-1}$.

Table 7.5: The critical parameter (J_{crit}/τ_w) values at different NaCl electrolyte for 600 ppm n-dodecane emulsion.

Crossflow Velocity ($m\ s^{-1}$)	Oil feed Concentration ($mg\ L^{-1}$)		
	600	600	600
	No NaCl	0.05 M NaCl	0.1 M NaCl
	J_{crit}/τ_w [$Lm^{-2}h^{-1}Pa^{-1}$]	J_{crit}/τ_w [$Lm^{-2}h^{-1}Pa^{-1}$]	J_{crit}/τ_w [$Lm^{-2}h^{-1}Pa^{-1}$]
1.14	12.15	5.96	3.70
1.52	11.51	4.94	3.10
1.92	9.34	5.86	5.51
Mean	11	5.59	4.10

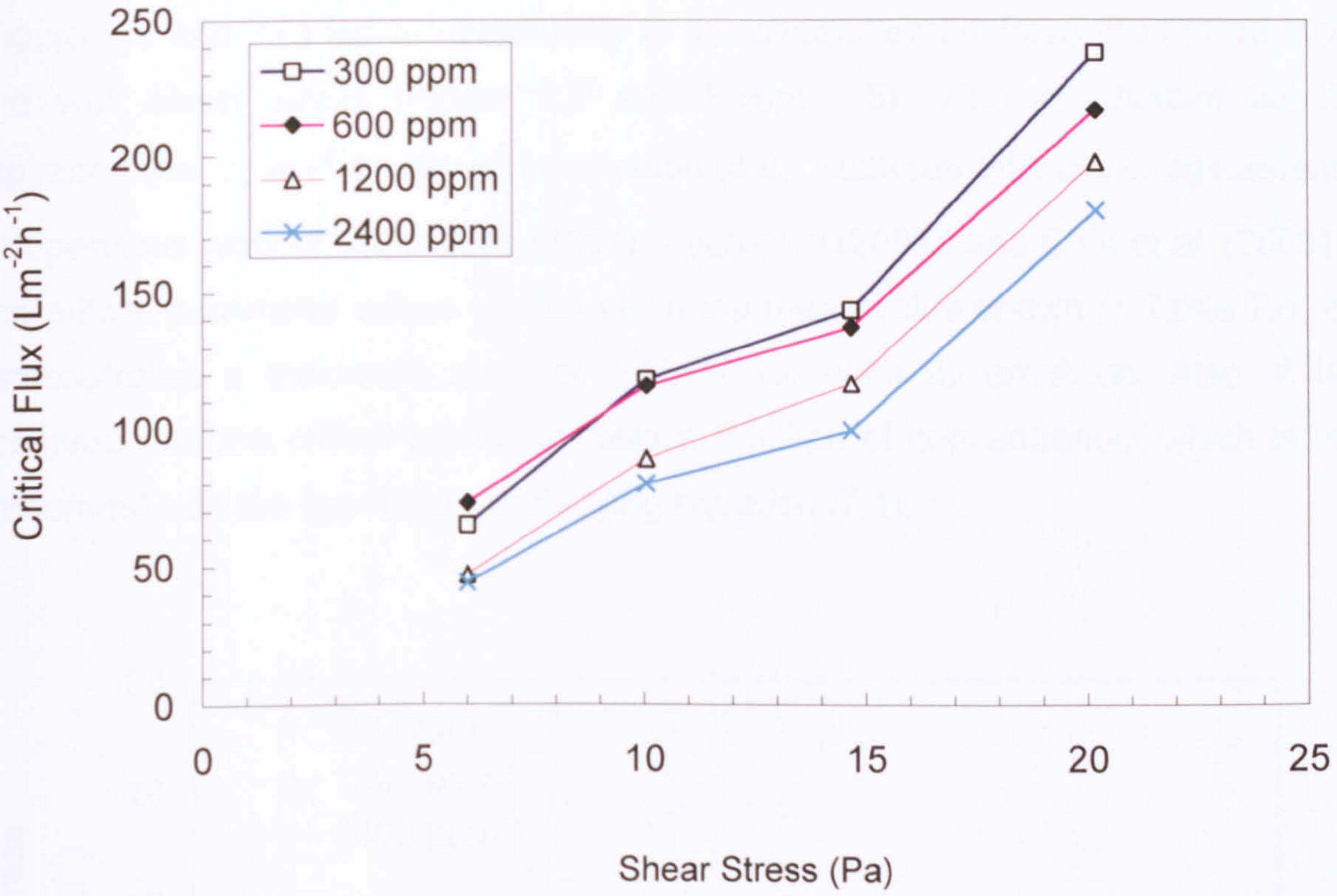

Figure 7.7: Variation of critical flux with wall shear stress at different oil feed concentration (600, 1200, 2400 ppm).

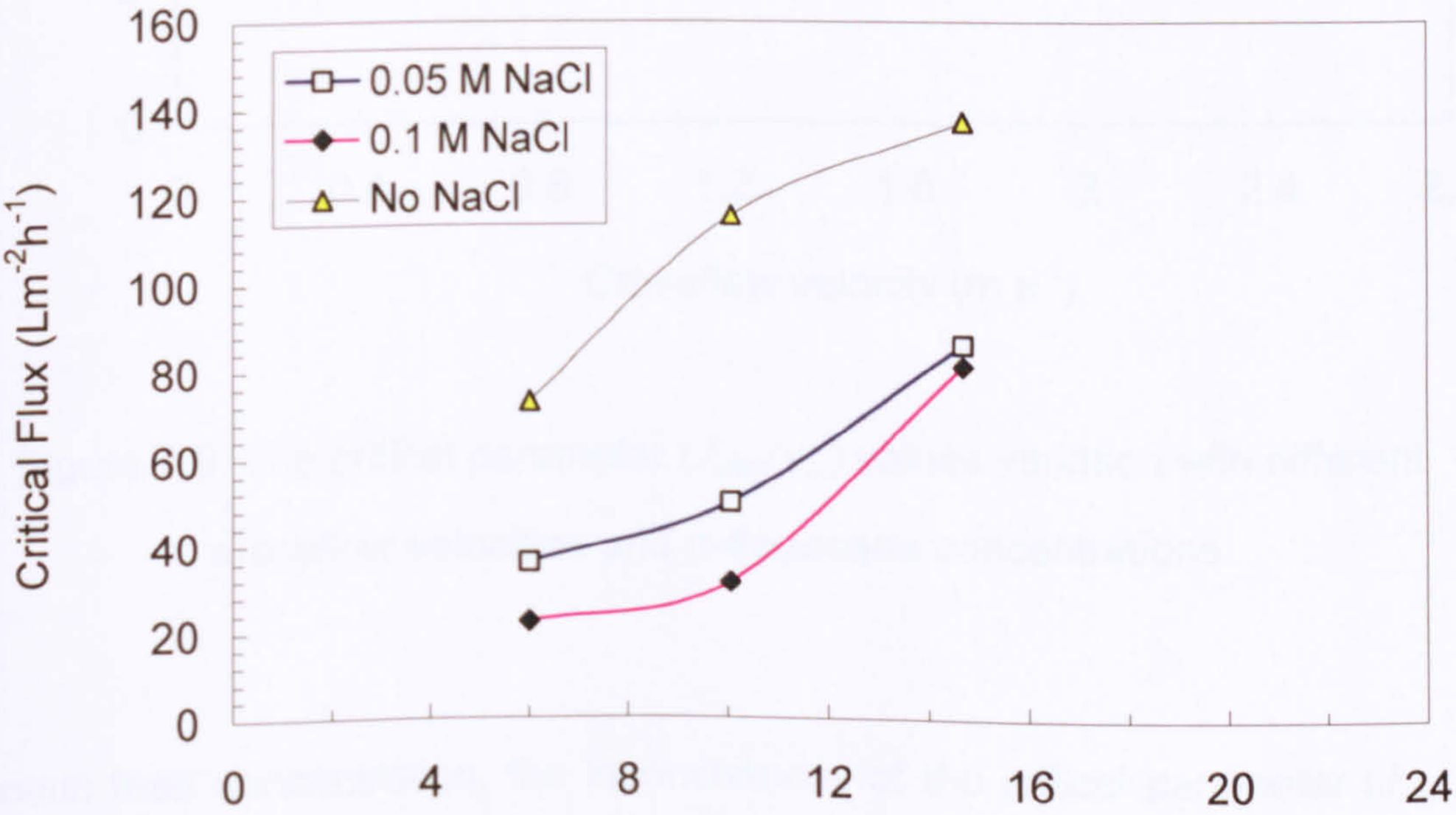

Figure 7.8: Variation of critical flux with wall shear stress at different NaCl electrolyte concentration.

It was observed that the nonlinear relationship of J_{crit} with crossflow velocity (Figure 7.5 and 7.6) led to nonlinearity in the correlation between the critical flux and wall shear stress (Figure 7.7 and Figure 7.8). This observation could explained that $\tau_w \alpha v^2$ as shown in equation (4.4). Such remarks are in agreement with pervious work of Chen *et al.* (1997), Vyas.*et al.*(2002), and Chiu *et al.* (2005). The critical parameter values compared to the mean value shown in Table 7.4, it demonstrated a maximum error of ± 15 % for each oil emulsion. Also, it is observed that the critical parameter was a function of concentration, which is in agreement with the hypothesis underlying equation (7.1).

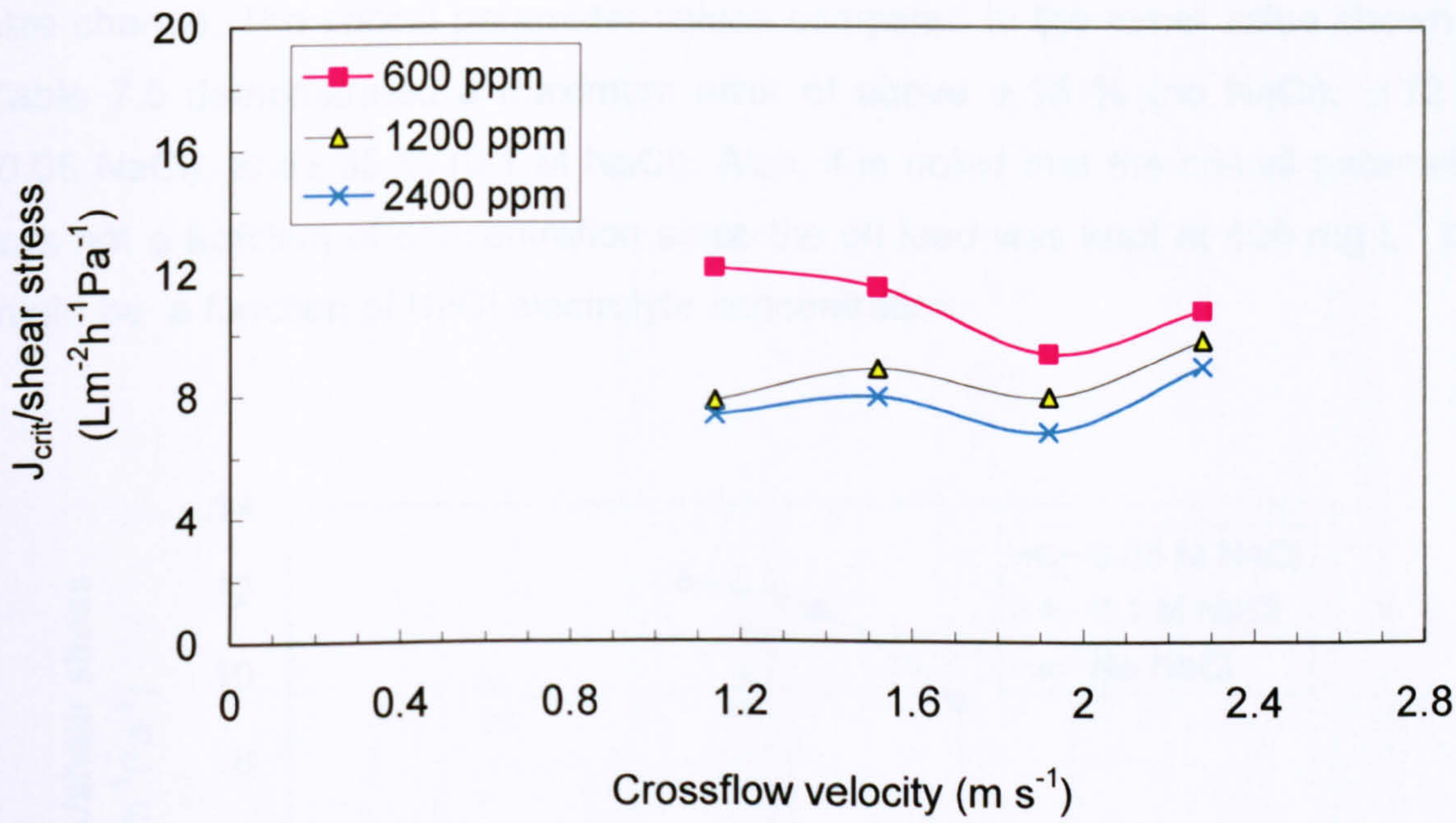

Figure 7.9: The critical parameter (J_{crit}/τ_w) values variation with different crossflow velocities and n-dodecane concentrations.

For each feed concentration, the inconsistency of the critical parameter (J_{crit}/τ_w) values could be linked to the poly dispersed emulsions and the sensitivity of relatively large oil droplets to break at higher shear forces. Certainly these changes could result in a variation of particle sizes and equation (7.1) does not deal with this outcome of particle size variations. The presence of a number of

smaller oil droplets would cause a decrease in critical fluxes. Figure 7.9 illustrates generally that this critical parameter is a function of concentration, and the variation with crossflow velocity at different concentrations was similar. While both 600 ppm emulsions in 0.05 M and 0.1 M in NaCl behaved in a similar manner (Figure 7.10), their critical parameters values seem half or third of those critical parameters measured without the addition of any salt. From Table 7.5, despite keeping the oil feed concentration the same, the critical parameter values showed inconsistency. This suggested that such a critical parameter is not only controlled by the balance between convection and erosion as claimed in equation (7.1). Other variables interrelated to the hydrodynamic condition might need to be considered, particularly for poly dispersed oil-in-water emulsions, such as particle size change. The critical parameter values compared to the mean value shown in Table 7.5 demonstrated a maximum error of above ± 15 % (no NaCl), ± 12 % (0.05 NaCl), and ± 35 % (0.1 M NaCl). Also, it is noted that the critical parameter was not a function of concentration since the oil feed was kept at 600 mg L^{-1} but might be a function of NaCl electrolyte concentration.

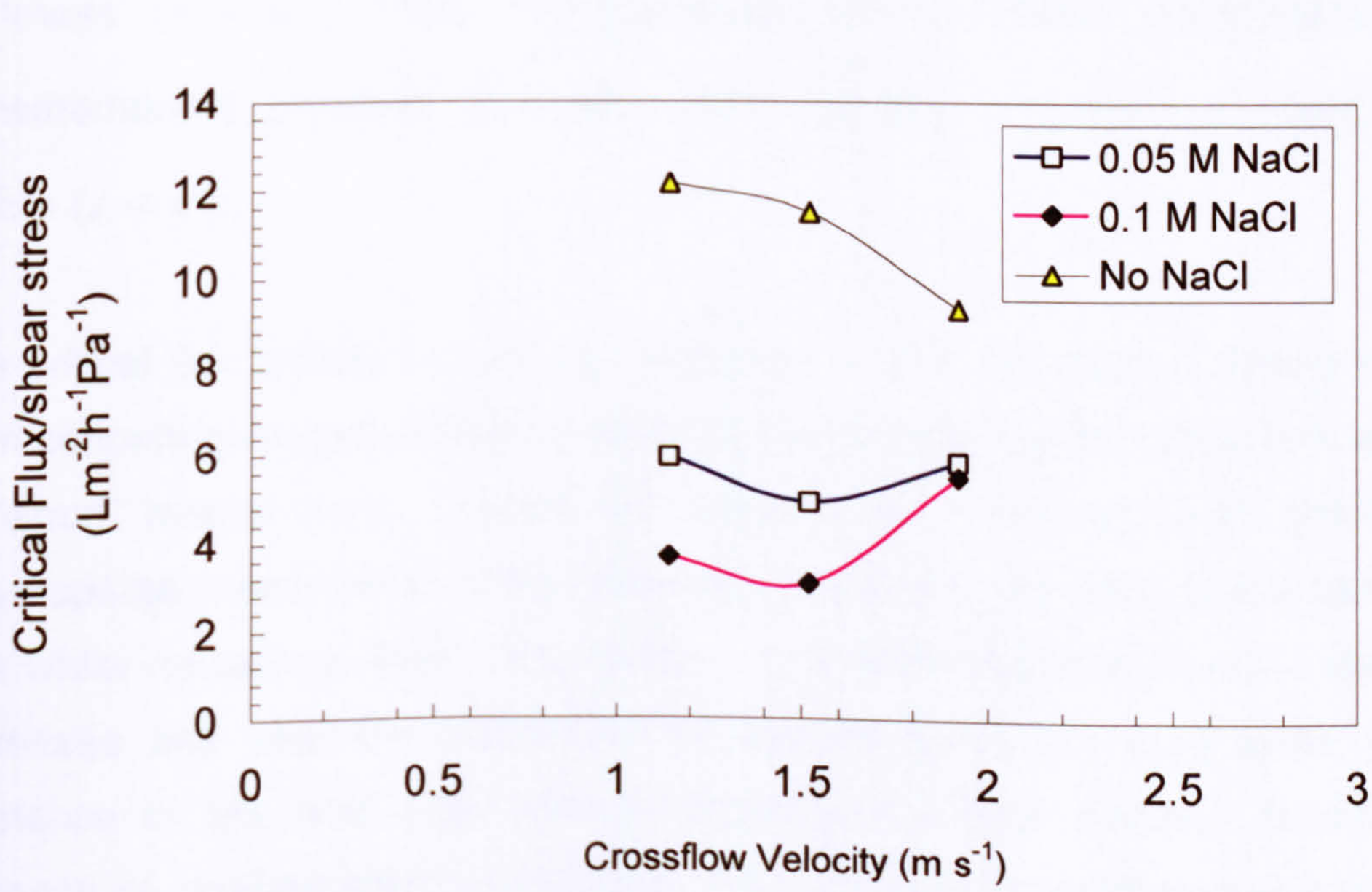

Table 7.10: The critical parameter (J_{crit}/τ_w) values variation with different crossflow velocities and NaCl electrolyte concentrations for 600 mg L^{-1} dodecane emulsion.

7.2.2 Effect of TMP on critical flux

In order to investigate the influence of TMP on critical flux while operating at the same crossflow velocity (shear), the maximum pressures for the high TMP tests were almost doubled for those a low TMP tests at crossflow velocities of 1.14 and 1.52 m s^{-1}. The critical fluxes measured at high TMP operation were found to be approximately twice of those measured at low TMP operation, as demonstrated in Figure 7.11 and Figure 7.12. These observations could be explained by solvent mass transfer using Darcy's law as illustrated in equation (2.13), which was described in Chapter 2. The permeate flux is directly proportional to the transmembrane pressure ($J \propto \Delta P$) and inversely proportional to the filtration resistances ($J \propto 1/(R_m + R_c)$, where resistances arise from the clean membrane(R_m) and cake formation (R_c)). The resistance caused by cake formation is normally estimated by using the Carman-Kozeny equation (2.14), where cake resistance is inversely proportional to both cake porosity ($R_c \propto (1-\varepsilon)^2/\varepsilon_c^3$) and particle radius ($R_c \propto a^{-2}$) and directly proportional to cake thickness ($R_c \propto \delta_c$). Thus, The permeate flux is directly proportional to the transmembrane pressure ($J \propto \Delta P$), cake porosity ($J \propto \varepsilon_c^3/(1-\varepsilon)^2$) and particle radius ($J \propto a^2$).

The critical flux concept could be interpreted to link the point of phase transition from concentration polarization to cake formation due to convective flow and back transport mechanisms caused by velocity and concentration gradient for polydisperse suspensions in the following manner. By operating at the same shear rate while increasing TMP, the number of particles driven toward the membrane increases and also the distribution of particle sizes becomes wider with the existence of fine and large particle resulting in a high porosity despite of the increase of concentration polarisation. Also, the rate of particle depolarization by diffusion from the membrane surface toward the bulk would be induced as a result of a higher concentration gradient where the shear impact of relatively bigger particles is enormous. On the other hand, operating at low TMP, the back transport rate would be lower as a result of concentration gradient and relatively

smaller particles would be present on the concentration polarization region and hence critical fluxes would be lower compared to the cases of operating at TMP.

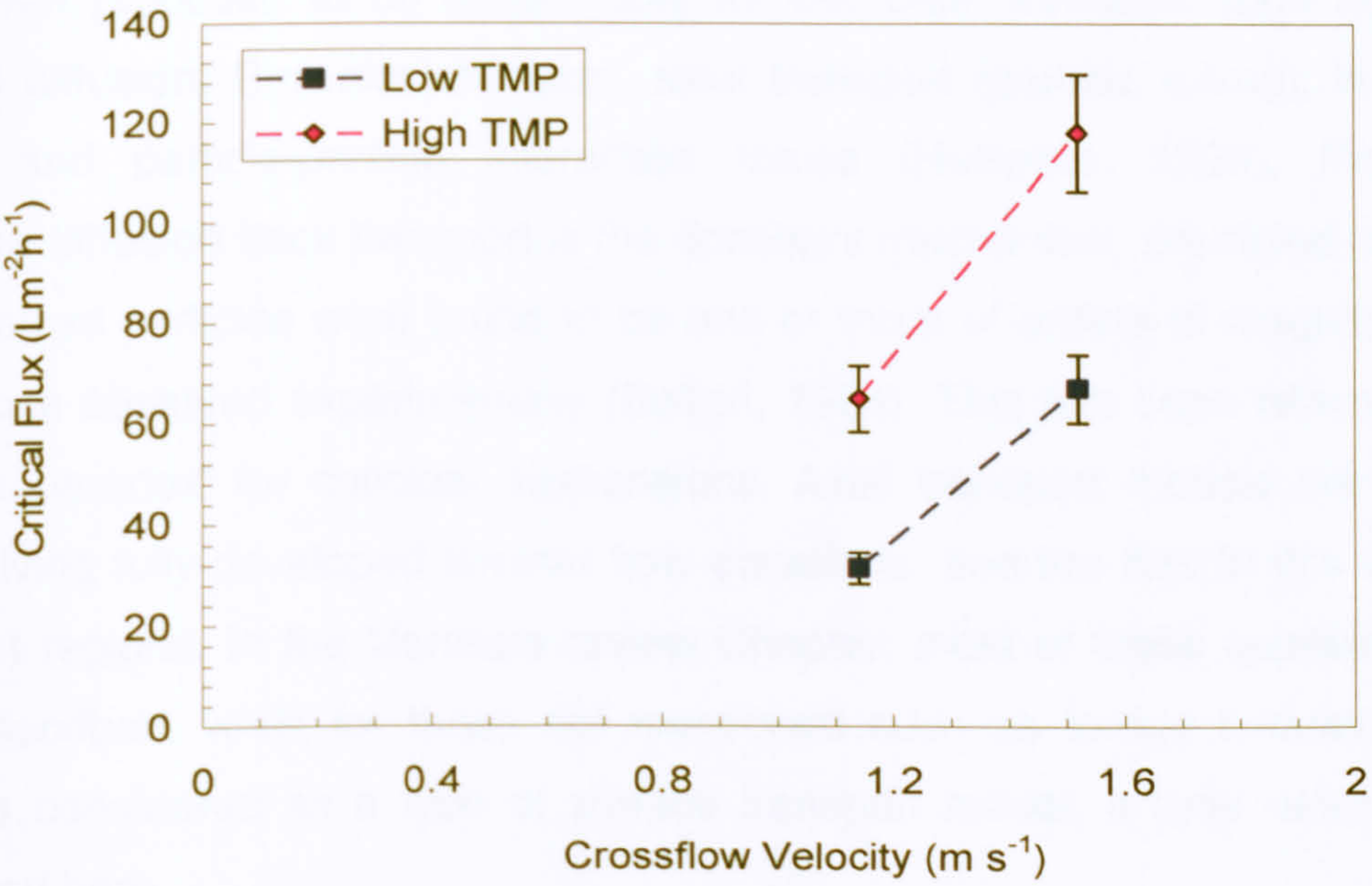

Figure 7.11: Variation of critical flux with crossflow velocity at low and high TMP operation for 300 mg L^{-1} dodecane emulsion.

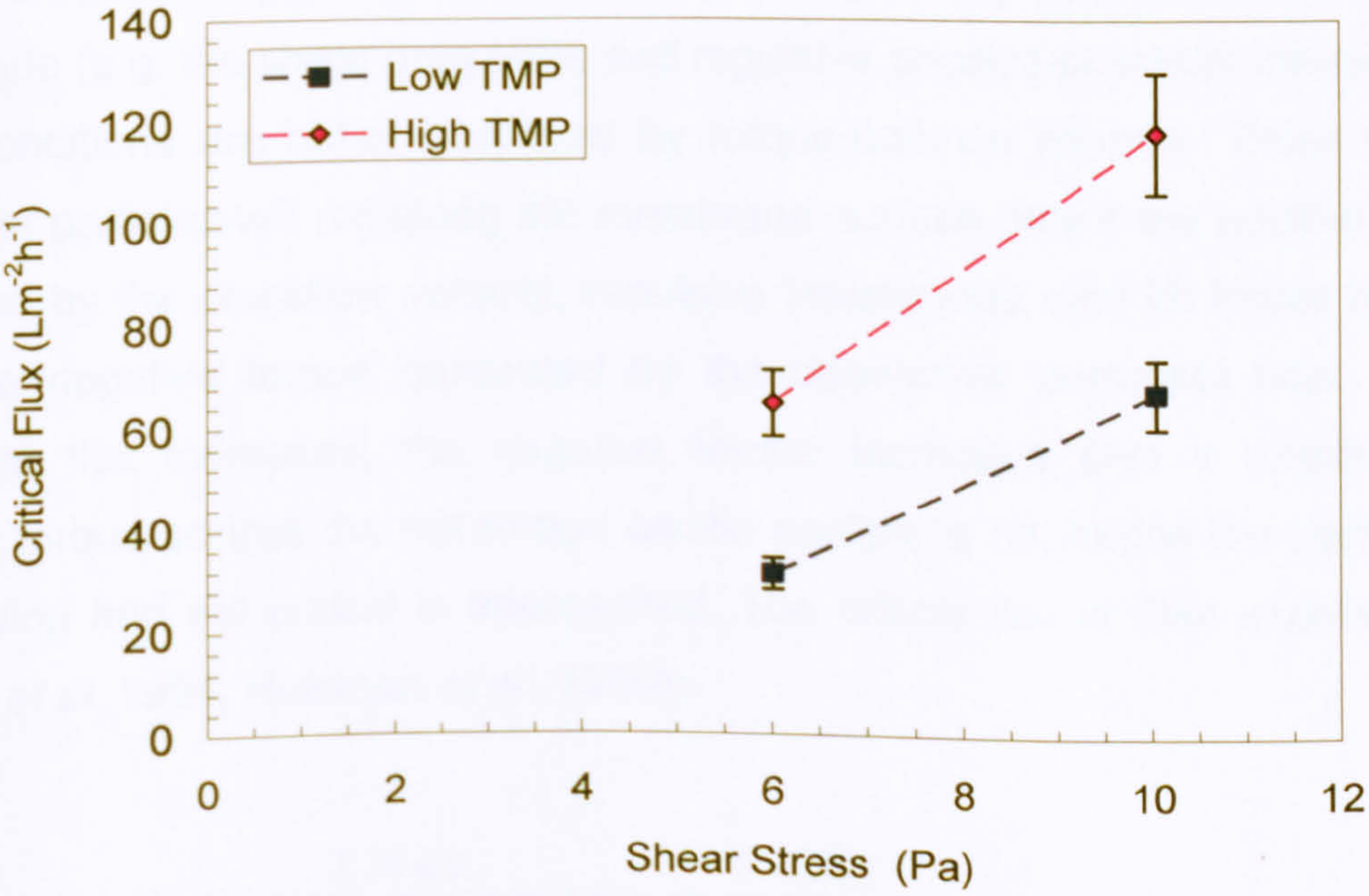

Figure 7.12: Variation of critical flux with wall shear stresd at low and high transmembrane pressure operation for 300 mg L^{-1} dodecane emulsion.

7.3 Comparison between Experimental Results and Models

Generally, it is known that permeate flux drags particles towards the membrane whilst diffusion induces particle back transport into the bulk. Various mechanisms have been proposed to be accountable for this back transport such as shear-induced diffusion, Brownian diffusion, axial transport (particle rolling), inertial lift forces, and particle-particle interaction forces (Huisman, 1999). Presuming Brownian diffusion back transport is the dominant mechanism, predicted fluxes for micron-sized particles were found to be one or more of orders of magnitude less than those observed experimentally (Belfort, 1994). This has been referred to as the 'flux paradox' for colloidal suspensions. Axial transport models are derived from solving fully-developed laminar flow equations, and the flow in this work the turbulent regions. In the literature review Chapter, most of these applied models were described, while for those not mentioned such as torque balance model, which is considered as a type of surface transport model, a brief description is presented here .

A particle deposition could be initiated by the forces pushing it towards the membrane, such that the permeate drag force and attractive physico-chemical interactions, are bigger than the forces taking away the particle from the membrane (e.g. the shear drag force and repulsive physico-chemical interactions). Such conditions are better portrayed by torque-balance models. These models state that particles will roll along the membrane surface only if the positive torque produced by the crossflow velocity, repulsive interactions, and lift forces is larger than the negative torque generated by the convective permeate flow. As the permeate flux increases, the negative torque increases until it balances the positive torque so that the net torque on the particle is nil, hence the particle will stop rolling and the critical is approached. The critical flux is then expressed by (Belfort *et al.*,1994, Huisman *et al.*, 1999):

$$J_{cr} = \frac{2.36\, a\, \tau_w}{\mu_0 \tan\theta (a^2 \hat{R}_m)^{2/5}} + \frac{0.463 F_i}{\pi \mu_0 \sin\theta (a^2 \hat{R}_m)^{2/5}} \qquad (7.2)$$

where a is the particle radius, τ_w is the wall shear stress, μ_0 is the permeate viscosity, θ is the angle of repose (a measure for the surface roughness), $\hat{R}_m$ the specific membrane resistance, and F_i is the membrane-particle interaction force. F_i is positive if the surface charge sign of both the membrane and the particle are the same. F_i is negative if the surface charge sign of both the membrane and the particle are opposite. F_i diminishes if the membrane or the particle are uncharged (or at isoelectric point). Since most of critical flux values were measured at solution pH 5.5 - 6 and, as mentioned in Chapter 6, the reported iso-electric point for ceramic membrane was 5.8 – 6. Thus, the second term of equation (7.2) will be cancelled and the equation is reduced to

$$J_{cr} = \frac{2.36\, a\, \tau_w}{\mu_0 \tan\theta (a^2 \hat{R}_m)^{2/5}} \tag{7.3}$$

Here critical flux is directly proportional to particle radius (a) and wall shear stress (τ_w), since the term ($(a^2\hat{R}_m)^{2/5}$) is treated as a single unit. A torque balance model (TBM), assuming axial transport as the major mechanism gave unrealistically high permeate fluxes. Several researchers, such as Huisman *et al.* (1999) and Belfort *et al* (1994), noticed the same results experimentally and proposed that a promising remedy for the flux paradox will be to take into account the inertial lift consequence. Nonetheless, inertial lift effects were found to be insignificant for micron-sized particles in the current study. Normally, the inertial lift model (ILM) is applicable for particle sizes bigger than 20 μm and consider only single particles (Table 7.6) , whereas the particle size distribution in the present study is between 0.1-10 μm. The results are plotted on Figures 7.13-7.15 to show the TBM and ILM compare with the experimental data.

Particle-particle and particle-membrane interactions are not likely to be the governing mechanism for the majority of experiments conducted in this work as the double layer forces are insignificant. The double layer forces are insignificant since the zeta potential magnitude is relatively low for most of the oil in water emulsions. However, such double layer forces become significant when salt is added to the emulsions since the zeta potential is increased.

Even so, opposite behaviours for permeate flux have been encountered when adding salts of differing valency (NaCl, $CaCl_2$,and $FeCl_3$) at the same ionic strength. For example, as the NaCl amount increased in the feed, the permeate flux decreased. But when $CaCl_2$ and $FeCl_3$ salts were added in different experiments, the permeate flux increased and became higher compared to the filtration experiment at same operating condition without addition of salts. Such flux behaviour has been discussed in Section 7.1 in relation to particle-particle and particle-membrane interactions. Due to this contradictory flux behaviour when salt is added, electrostatic interactions were not considered to be the dominant mechanism for back transport.

The back transport mechanism is more likely to govern the flux behaviour, bearing in mind the range of the measured particle sizes is the shear-induced diffusion. Howell (1995) claimed that the shear-induced diffusion would be the main back transport mechanism for particle within the micron size range. Hence, the shear-induced diffusion model is fitted to the experimental data by using the particle size as the curve fitting parameter, providing physical illustrations of the particle sizes at critical flux value for different crossflow velocities. The shear-induced model (SIDM) makes use of the shear-induced hydrodynamic diffusivity rather than the Brownian diffusivity, determined by using Stokes-Einstein correlation. The model employed here has been obtained from prior researchers (Belfort, 1994, Huisman *et al.*, 1999) where detailed description of the model was provided. Comparisons with other models are shown in Figures 7.13-7.15; the SID model showed a better prediction of experimental results of critical fluxes at different oil feed concentrations and various crossflow velocities than did either the ILM or IBM models.

The distinction between employing Brownian diffusion (D_{BD}) and employing shear-induced diffusion (D_s) in evaluating particle depolarization is important. From equation (2.10), D_{BD} , is a function of particle size and increases as the particle size decreases ($D_{BD}\ \alpha\ a^{-1}$). The implication of Brownian diffusion becoming the predominant mechanism for particle back transport is that the back diffusion turns out to be more significant for finer particles and hence they tend to depolarize from the membrane surface. However, this implication is in disagreement with several experimental observations in which the smaller particles have a preference for deposition on the membrane surface during crossflow filtration. In addition, because D_{BD} is invariable for specified particle size, the degree of back transport founded on D_{BD} would be insensitive to variations of hydrodynamic conditions. This contradicts a number of experimental observations where the rate of particle back transport has increased when the shear rate was increased.

On the contrary, D_s is revealed to be enhanced with increase in particle size and the shear rate ($D_s\ \alpha\ a*\gamma$). Hence, analyzing of particle depolarization in crossflow filtration by using the shear-induced diffusion theory has been more practical for a number of application (Li *et al.*, 2000; Ripperger and Almann, 2002; Tien , 2006). Baruah and Belfort (2003) summarized few prominent models of crossflow microfiltration with their fundamental assumption and applicability as shown in Table 7.6. They suggested that the Brownian diffusion model is more appropriate for particle diameters below ~ 0.1 μm and at low wall shear rates. For the microfiltration case where 0.1 < a < 10 μm, the permeation flux estimated by using equation (7.4) was under-predicted by 1-2 order of magnitudes. As a response to such a flux paradox, Green and Belfort (1980) suggested that the inertial lift mechanism be evaluated using equation (7.4), which showed that the sensitivity of flux was higher for particle size (a^3) and shear (γ^2).

Table 7.6 Summary of prominent back-transport and lift models (Baruah and Belfort, 2003).

Flux model	approaches	Flux equation	Eq. no.	Applicable range
Brownian diffusion	Use Leveque solution for laminar flow in a solid wall tube and Stokes-Einstein diffusion	$J = 0.114\left(\frac{\gamma \kappa^2 T^2}{\mu_0{}^2 a^2 L}\right)^{1/3} \ln\left(\frac{\phi_w}{\phi_b}\right)$	7.4	Applicable for very small diameter particles (< 1μm); under predicts flux by 1-2 orders of magnitude for large particles
Inertial lift	Include the inertial terms in solving the force balance around a single particle	$J = \left(\frac{0.036\rho\, a^3 \gamma^2}{\mu_0}\right)$	7.5	Applicable for large diameter particles (>20μm) and consider only single particles
Shear-induced diffusion	Replace diffusion coefficient with a shear-dependent	$J = 0.078\left(\frac{a^4}{L}\right)^{1/3} \gamma \ln\left(\frac{\phi_w}{\phi_b}\right)$	7.6	Applicable for intermediate diameter particles (1-20μm)

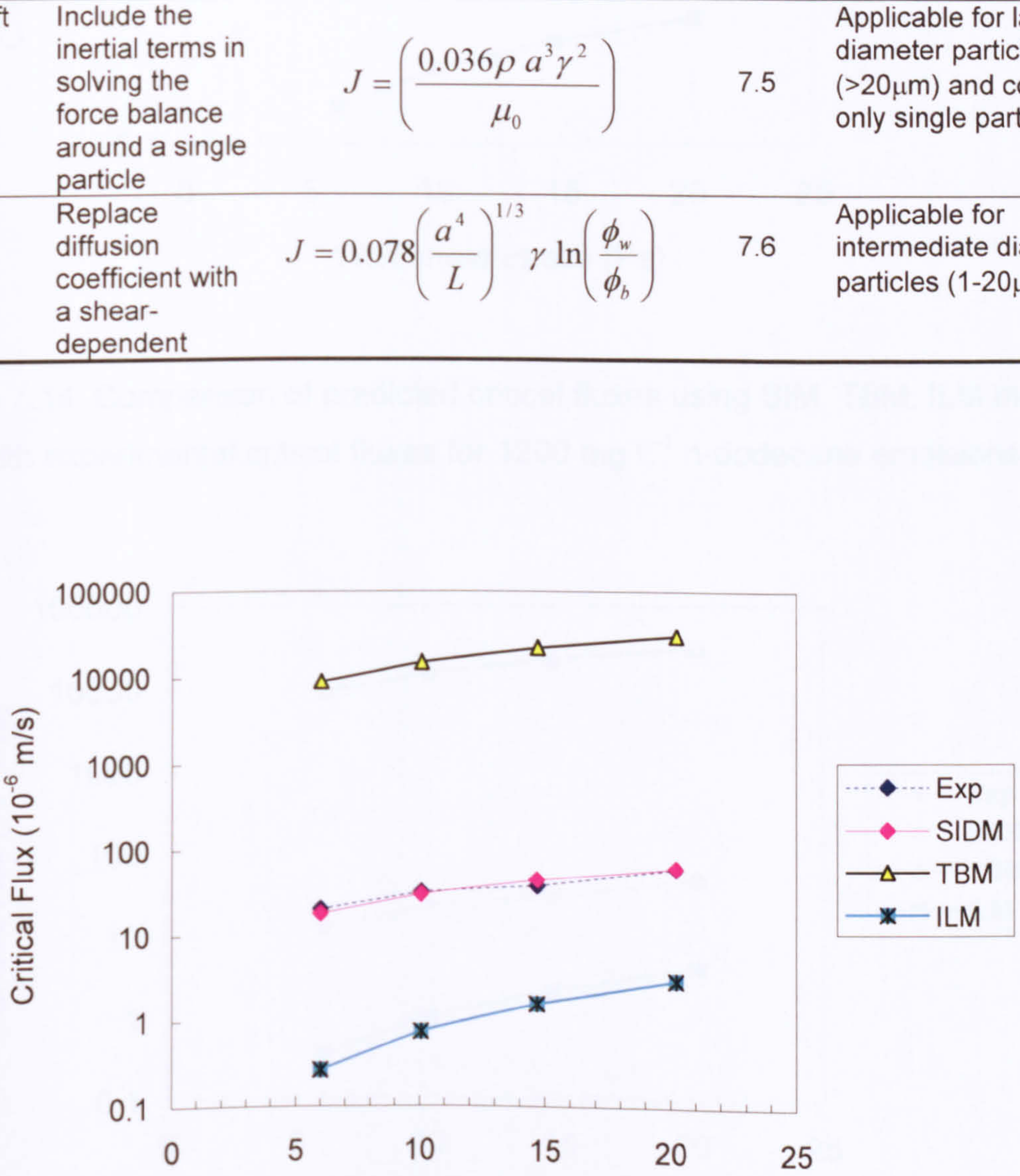

Figure 7.13: Comparison of predicted critical fluxes using SIM, TBM, ILM models with experimental measured critical fluxes for 600 mg L^{-1} n-dodecane emulsion.

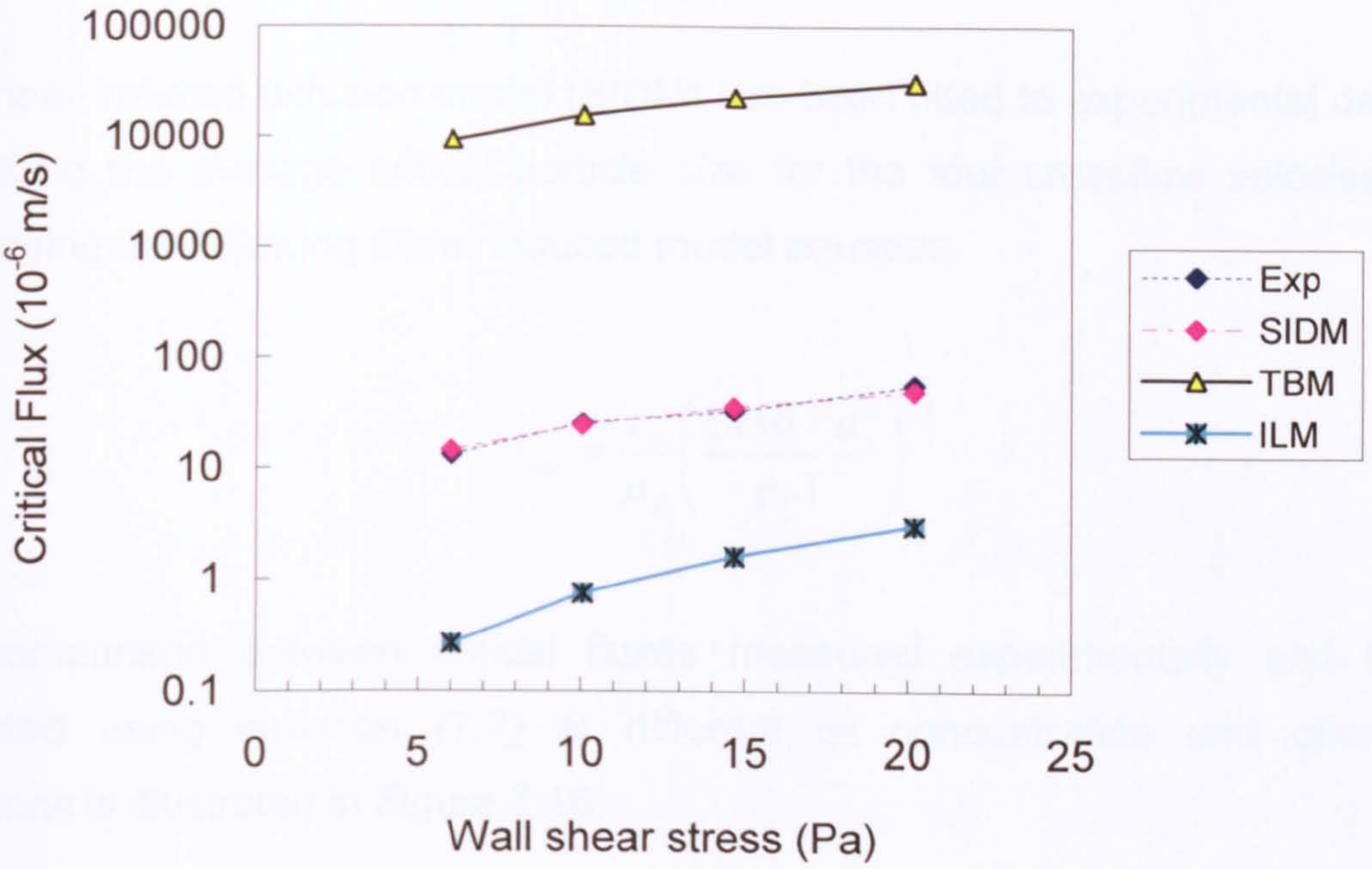

Figure 7.14: Comparison of predicted critical fluxes using SIM, TBM, ILM models with experimental critical fluxes for 1200 mg L^{-1} n-dodecane emulsions.

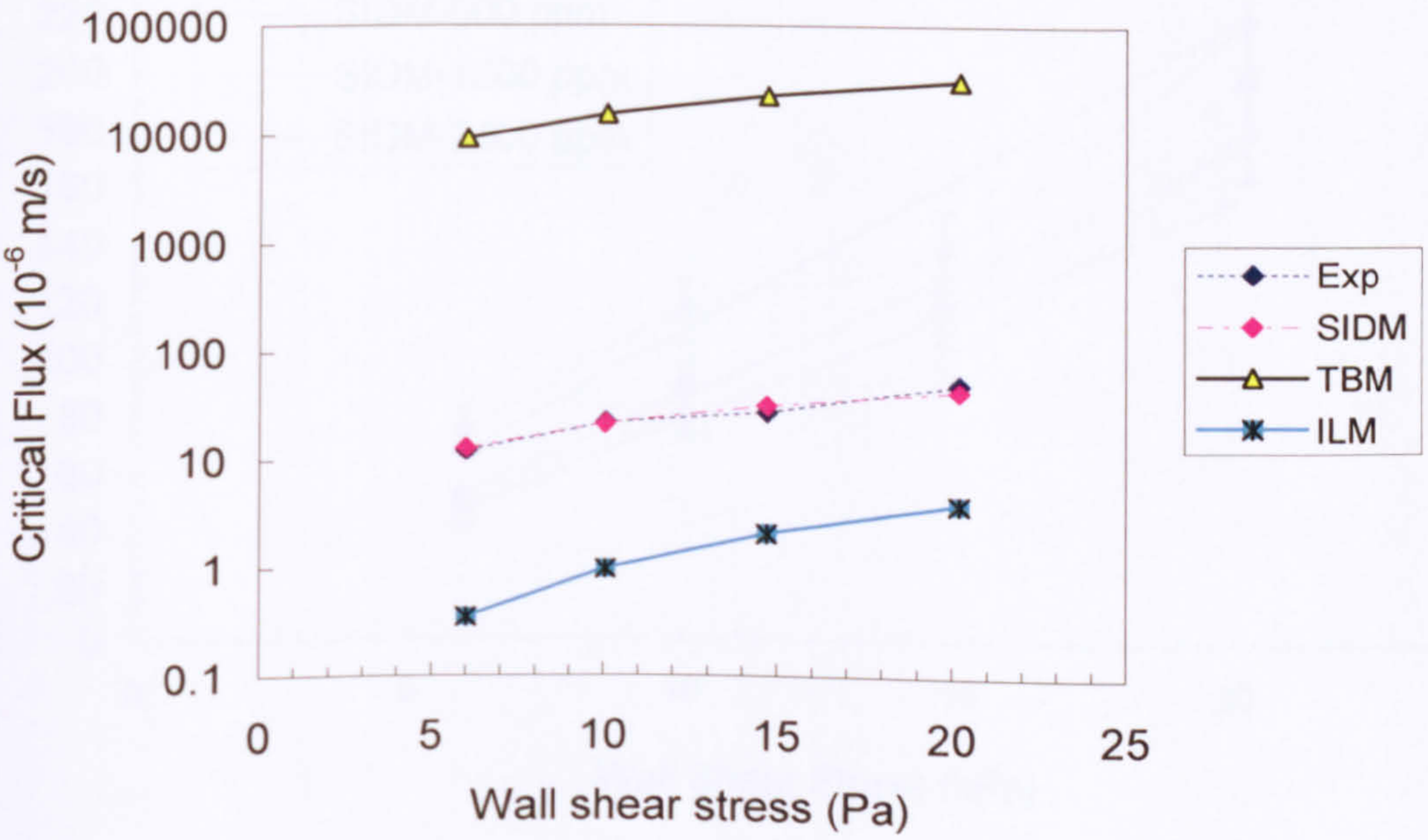

Figure 7.15: Comparison of predicted critical fluxes using SIM, TBM, ILM models with experimental critical fluxes for 2400 mg L^{-1} n-dodecane emulsions.

7. 4 Critical Flux Prediction by Shear-Induced Diffusion Model

The shear induced diffusion model (SIDM) has been fitted to experimental data by calculating the average critical particle size for the four crossflow velocities by rearranging the following shear induced model equation

$$J_{crit} = \frac{\tau_w}{\mu_p}\left(\frac{1\times10^{-4}a^4}{\phi_b X}\right)^{1/3} \quad (7.7)$$

The comparison between critical fluxes measured experimentally and those estimated using equation (7.7) at different oil concentration and operating conditions is illustrated in Figure 7.16.

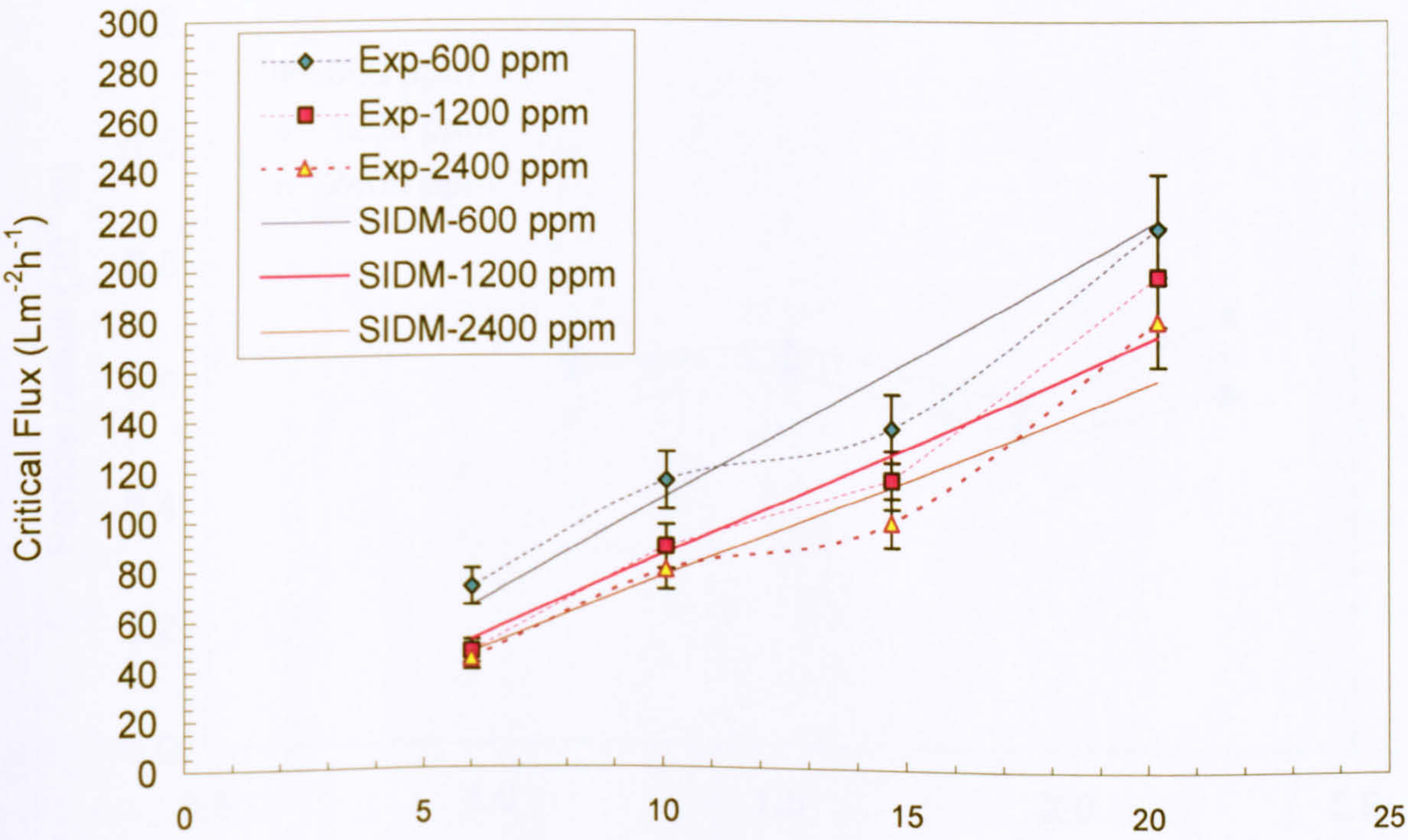

Figure 7.16: Shear-induced diffusion model (SIDM) fitted to experimental data obtained for (600, 1200, 2400 mg L^{-1}) emulsions at various crossflow velocities.

The experimental critical flux values were inserted and the equation (7.7) was rearranged to

$$a_{crit} = \left(\frac{J_{crit} \mu_p}{\tau_w} \right)^{3/4} \left(\frac{\phi_b X}{1 \times 10^{-4}} \right)^{1/4} \tag{7.8}$$

Then a_{crit} was calculated using equation (7.8) and compared with the measured particle size. Hence a_{crit} is considered to be a fitting parameter to give relatively smooth curves that would give 'best' fit the experimental data points. The particle sizes used in the SIDM to fit the model to experimental data at the four crossflow velocities are plotted against crossflow velocity in Figure 7.17.

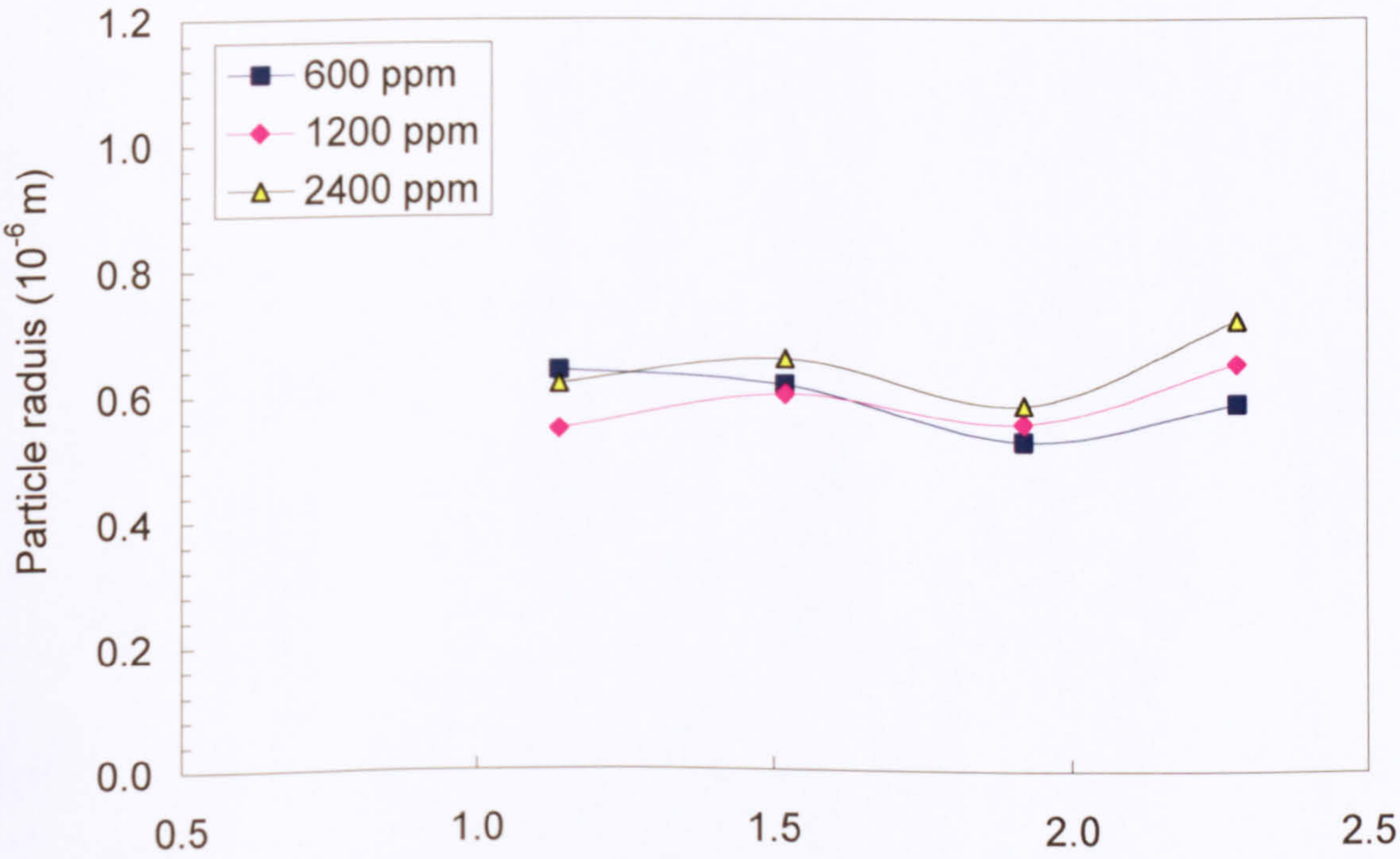

Figure 7.17: Particle radii calculated from the shear-induced model at different crossflow velocities.

The 'fitted' mean particle size for the emulsion with 1200 mg L^{-1} n-dodecane was lower than the others (Figure 7.17), where its mean particle size was about 0.588 µm. While for each individual crossflow velocity the particle radii were approximately 0.548 at the crossflow velocity of 1.14 m s^{-1}, 0.601 µm at the crossflow velocity of 1.52 m s^{-1} , 0.554 µm at the crossflow velocity of 1.92 m s^{-1}, and 0.648 µm at the crossflow velocity of 2.28 m s^{-1}. The other 'fitted' mean particle sizes were 0.592 µm for the emulsion with 600 mg L^{-1} n-dodecane and 0.645 µm at the for the emulsion with 2400 mg L^{-1} n-dodecane. A summary table of particle radii calculated by using the rearranged equation (7.8) presented in Tables 7.7 and 7.8. While for estimated critical particle radii for 600 mg L^{-1} n-dodecane emulsions at various crossflow velocities with different NaCl electrolyte concentrations, it could be observed that the smallest mean particle radius (0.282 µm) was found at the high ionic strength (0.1 M NaCl). For the moderate ionic strength (0.05 M NaCl), the mean particle radius was 0.358 µm, while for emulsion with no salt, the mean particle radius 0.592 µm.

Table 7.7: Estimated critical particle radii for n-dodecane emulsions with different oil feed concentration at various crossflow velocities.

n-Dodecane Concentration	600 (mg L^{-1})	1200 (mg L^{-1})	2400 (mg L^{-1})
Cross flow velocity (m s^{-1})	a_{crit} (µm)	a_{crit} (µm)	a_{crit} (µm)
1.14	0.641	0.548	0.620
1.52	0.616	0.601	0.658
1.92	0.526	0.554	0.584
2.28	0.585	0.648	0.718
Mean a_{crit}	0.592	0.588	0.645

Table 7.8: Estimated critical particle radii for 600 n-dodecane emulsions at various crossflow velocities with different NaCl electrolyte concentrations.

Crossflow Velocity	No NaCl	0.05 M NaCl	0.1 M NaCl
	a_{crit} (µm)	a_{crit} (µm)	a_{crit} (µm)
1.14	0.641	0.376	0.263
1.52	0.616	0.327	0.230
1.92	0.526	0.371	0.355
Mean	0.592	0.358	0.282

7.4.1 Effects of particle size

From the measured particle size distribution, the feed oil emulsions have a wide particle size distribution. As a general rule lower overall flux levels were recorded because a reduced particle size existed in the feed. This can have a major influence on the critical flux, for example the SIDM predicts a critical flux dependence on particle radius to the power of 4/3. Several previous researchers such as Chellam *et al* (1999) and Dharmappa *et al* (1992) have revealed that the existence of smaller particles in the feed often causes lower fluxes during filtration than those anticipated based on the mean particle size. Huisman *et al.* (1999) proposed that the smallest particles in a poly-dispersed feed control the J_{crit} behaviour. Hence, when particle sizes 'smaller' than the mean particle size were incorporated into equation (7.8), a better agreement it was found between the model predicted and the experimental critical fluxes.

Nevertheless, which sizes or percentage size range provided the best fit was not discussed in detailed in most of the previous studies. By comparing the measured particle size distribution for the feed with the particle sizes (at J_{crit}) estimated by the shear-induced diffusion model, it was found that those estimated sizes represent less than 5 % (number) of the number particle size distribution of the feed. These results support the theory that it is the smaller particles in the feed which are dominantly accountable for the formed deposited layer in or on the membrane.

The oil emulsions formed have been shown experimentally to be stable and with adequate strength to resist the shearing to which they are exposed by the two pumps for several hours. It is reasonable to say that if the shear forces are increased further during filtration, there might be a critical pressure above which the shearing can initiate breakage of the oil emulsion for the large oil droplets.

Above this critical flux; particularly at the maximum transmembrane pressure (0.9 bar), the particle size distribution might vary due to compressing the oil cake layer to a high degree, causing a small number of emulsified oil droplets to pass through the membrane pores to be present in the permeate side. According to the size analysis of the permeate this behaviour was never met while operating at or below

the critical flux, but at the higher flux levels trace amounts of oil droplets with size about 1 μm or less existed on the permeate sample measured.

The model that accurately describes critical flux as the point imbalance between the back transport and convective mechanisms where the particles with lower size range have tendency to cause membrane fouling. Consequently, the physical illustrations of particle radii shown in Figure 7.17 can be considered to be logical, and the SIDM may be believed to portray the mechanisms involved during the microfiltration tests performed in this investigation. Nevertheless, it has to be mentioned that this is only a hypothesis that appeared to offer accurate prediction. Wakeman (1994) indicated that a good fit of a model to experimental data does not confirm that the mechanisms underlying the model are essentially a correct understanding of real particle movements near to the membrane surface.

However, previous researchers such as Huisman (1999) and Howell (1995), suggested the SIDM to be the suitable model for particles in this size range. The shear induced model has been drawn to fit experimental data as demonstrated in Figure 7.16. For wall shear stresses in the range of 5 –10 Pa, the predicted critical fluxes using SIDM gave good fit to experimental critical fluxes. However, for higher wall stresses (11- 20 Pa), there was some inconsistency as shown in Figure 7.16. Such discrepancy could attributed be to operating at relatively high turbulent regions where the breakage of larger dispersed oil droplets to finer droplets may occur.

This discrepancy could be linked the critical particle radii which appeared to be smaller at relatively high crossflow velocity (1.92 m s^{-1}) as demonstrated on Figure 7.17. Such a claim is also strengthened by the work of Lu and Ju (1989), where they suggest that the size distribution of particles in the cake layer is crossflow velocity dependent. Hence, at this critical wall shear stress erosion is more dominenat the convection of particle with larger particle sizes. A number of investigators (Baker *et al.*,1985, Riesmeier and Kroner, 1987) stated that in the circumstances of constant permeation flux an increase of crossflow velocity promotes the erosion of larger particles away from the cake layer.

Furthermore, the cake layer would be become densely packed by the finer particles at high wall shear stress, as result of the shear effect on breakage of loosely formed particles. Therefore, increasing the wall shear stress not only reduces the cake layer but also decreases its porosity (Gésan-Geuiziou *et al.*,1995). Figure 7.18 illustrates that the minimum particle radius were at a velocity 1.52 m s^{-1} for both ionic strengths (0.05 and 0.1 M NaCl), while for no salt condition the minimum was at 1.92 m s^{-1}.

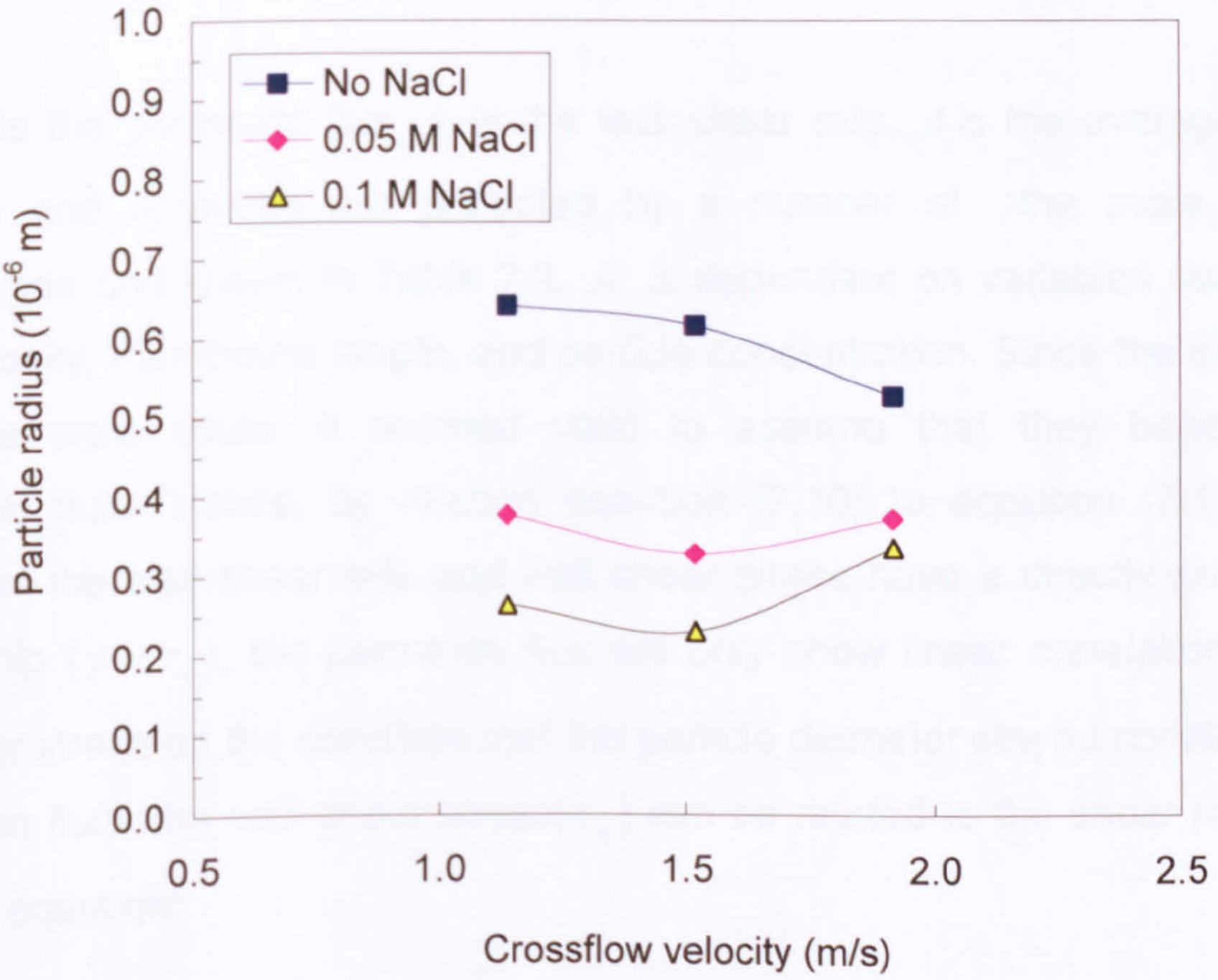

Figure 7.18: Particle radii calculated from the shear-induced model at different crossflow velocities and ionic strengths.

7.5 Relationship of $J_{crit}/(\tau_w a_{crit})$ in common theoretical models

Kim *et al.* (2001) stated that back transport models normally correlate the permeate flux to a number of parameters such as the wall shear rate, average particle diameter, feed viscosity, the particle concentration, and the length of the membrane. However, the focal point of their study was concerned with only two variables; the wall shear stress and particle diameter. For such a case, they suggested the following equation for predicting the permeate flux:

$$J = K(\dot{\gamma})^a (d)^b \tag{7.10}$$

where J is the permeate flux , $\dot{\gamma}$ is the wall shear rate, d is the average particte raduis. a and b values are predicted by a number of the more common hypothesises and shown in Table 7.9. K is dependant on variables such as the feed viscosity, membrane length, and particle concentration. Since the oil-in-water emulsions were dilute, It seemed valid to assume that they behave as a Newtonian fluid. Hence, by relating eqaution (7.10) to eqaution (7.11), which states that the wall shear rate and wall shear stress have a directly proportional relationship ($\dot{\gamma} \propto \tau_w$), the permeate flux will only show linear correlation with the wall shear stress on the condition that the particle diameter stayed constant. For a Newtonian fluid, the wall shear stress(τ_w) can be related to the shear rate by the following eqaution:

$$\dot{\gamma} = \frac{\tau_w}{\mu} \tag{7.11}$$

Since μ is constant for a Newtonian fluid. Thus, by subsituting eqaution (7.11) in eqaution (7.10) resulted in;

$$J = K(\tau_w)^a (d)^b \tag{7.12}$$

The curve of critical parameters (J_{crit}/τ_w) revealed on Figure 7.9 behaved in a similar way as the curve of critical particles sizes shown in Figure 7.17. Hence, this

suggest that this critical parameter is a function of critical particle size. Therefore, the critical parameter term could be modified to include the effect of particle size variation, particularly for polydispersed feeds with deformable structure such as oil-in-water emulsions. Lu and Ju (1989) found that when flux is high and crossflow velocity is low the mechanism of particle deposition is governed by the a friction force balance, which includes the presence of a critical particle diameter for particles present in the formed cake layer at constant crossflow velocity. For prediction of steady state crossflow filtration using a force balance model, Blake *et al.* (1992) found that the model effectively forecasted both linear character of permeate velocity reliance on shear stress and the related slope as being a function of particle diameter. While Gésan *et al.* (1995) concluded that the contest between convection and erosion controls the deposit magnitude and particle size contained in the cake layer formation. Table 7.9 (Kim *et al.*, 2001) displays the values of exponents a and b in equation (7.12) predicted by several commonly applied models, where the share was replaced by the wall shear stress.

Table 7.9: Values of the exponents a and b in eqaution (7.12) predicted by an number of commomaly used theoretical models (Kim *et al.*, 2001).

Model	a	b
Surface transport	1	1
Shear-induced diffusion	1	1.33
Inertial lift	2	3
Brownian diffusion	0.33	-0.67

The critical fluxes are affected by the wall shear stress. Hence, the ratio of J/τ_w has been employed to asses the performance of membrane filtration with regards to fouling and selectivity. The ratio describes the equilibrium of particle fouling rate (linked to J) and particle back transport rate (linked to τ_w) (Gésan-Guiziou *et al.*, 2001). Hence, operating conditions are suggested where the ratio of J/τ_w is lower than the critical value (Grandison *et al.*, 2000). Thus, the significance of such parameter is clear but investigation of its relationship critical particle size estimated by equation (7.8) is a new development.

Firstly, from the surface transport model as summarized in Table 7.9, both value of constant a and b were 1, thus the modified critical parameter ($J_{crit}/\tau_w\ a_{crit}$) values are presented in Table 7.10 and Figure 7.18. The values of critical parameter showed better consistency for each emulsion concentration with less than 4 % error, which imply that it still function of feed concentration.

Table 7.10: The critical parameter ($J_{crit}/\tau_w\ a_{crit}$) value variations with different crossflow velocities and n-dodecane concentration.

Crossflow Velocity ($m\ s^{-1}$)	Oil feed Concentration ($mg\ L^{-1}$)		
	600	1200	2400
	Emulsion A	Emulsion B	Emulsion C
	$J_{crit}/(\tau_w * a_{crit})$ [$Lm^{-2}h^{-1}(\mu m)^{-1}\ Pa^{-1}$]	$J_{crit}/(\tau_w * a_{crit})$ [$Lm^{-2}h^{-1}(\mu m)^{-1}\ Pa^{-1}$]	$J_{crit}/(\tau_w * a_{crit})$ [$Lm^{-2}h^{-1}(\mu m)^{-1}\ Pa^{-1}$]
1.14	18.96	14.28	11.81
1.52	18.68	14.73	12.06
1.92	17.75	14.31	11.58
2.28	18.36	15.11	12.40
Mean	18.44	14.61	11.96

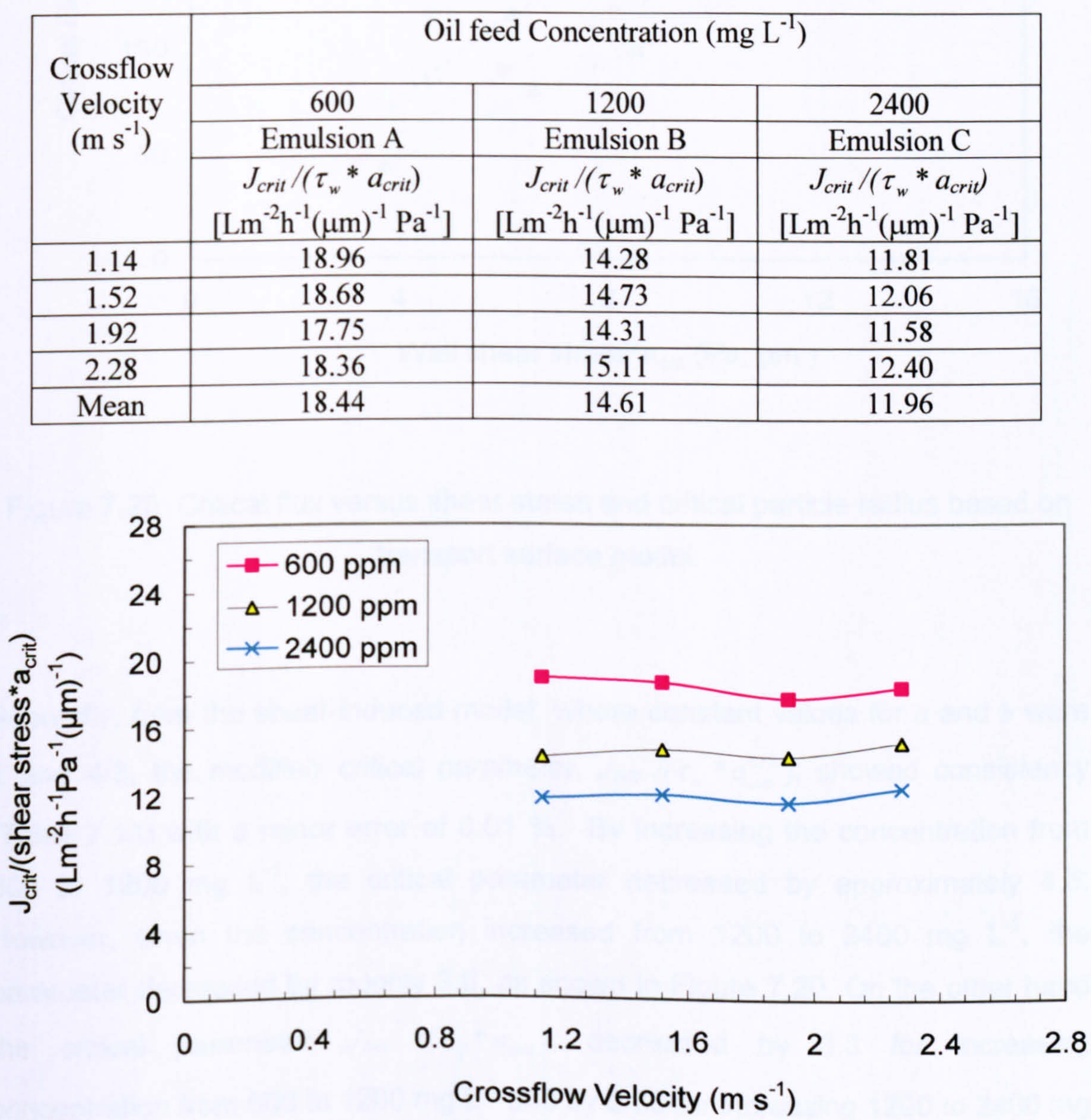

Figure 7.19: The critical parameter ($J_{crit}/\tau_w\ a_{crit}$) value variations with different crossflow velocities at different n-dodecane concentration.

Figure 7.19 demonstrates a linear relationship between the critical flux and wall shear stress multiplied by the critical particle radius for emulsions A, B, and C.

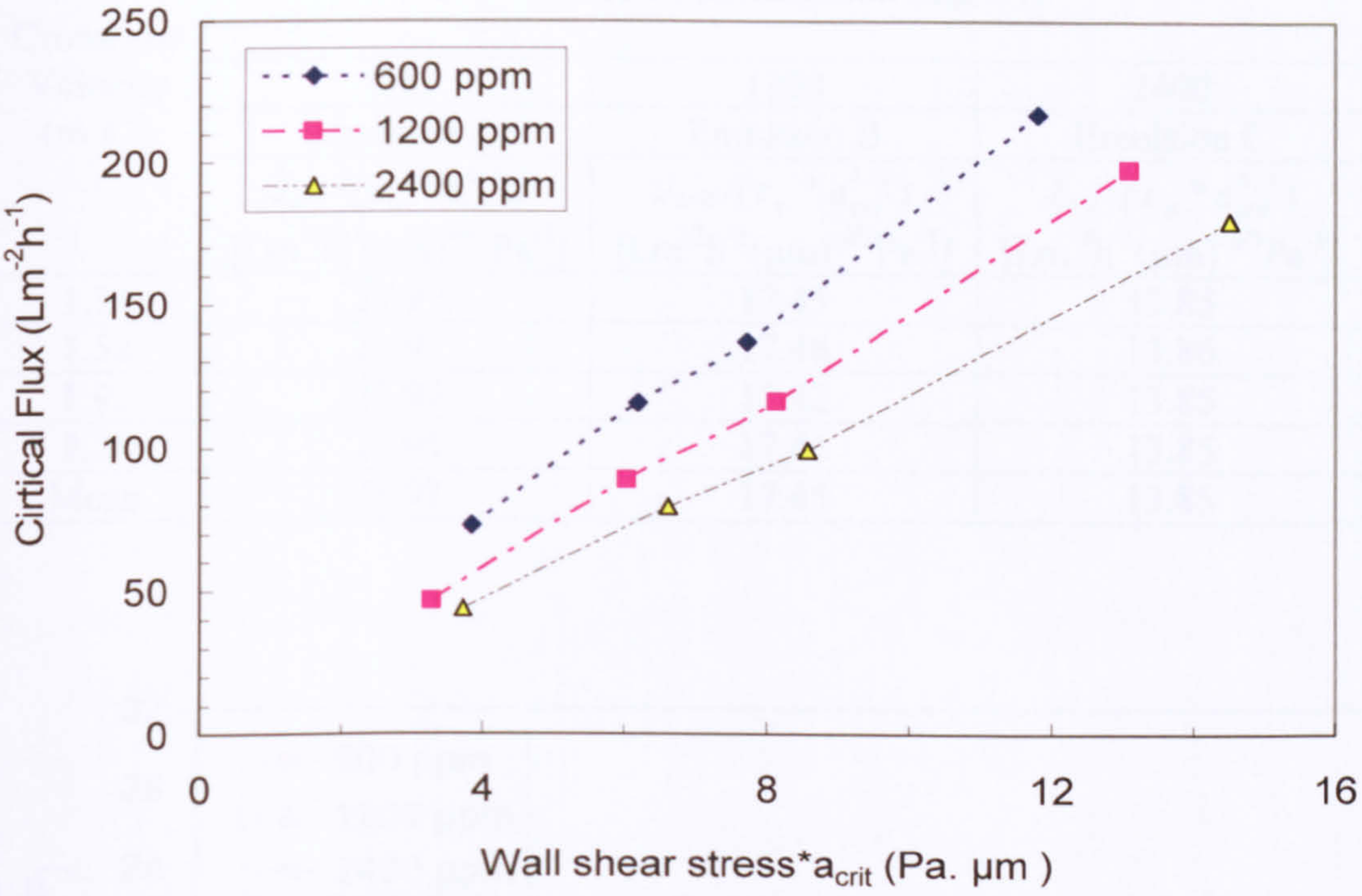

Figure 7.20: Critical flux versus shear stress and critical particle radius based on transport surface model.

Secondly, from the shear-induced model, where constant values for a and b were 1 and 4/3, the modified critical parameter, $J_{crit} /(\tau_w * a_{crit}^{4/3})$, showed consistency (Table 7.11) with a minor error of 0.01 %. By increasing the concentration from 600 to 1200 mg L^{-1}, the critical parameter decreased by approximately 4.5. However, when the concentration increased from 1200 to 2400 mg L^{-1}, the parameter decreased by roughly 3.6, as shown in Figure 7.20. On the other hand the critical parameter ,$J_{crit} /(\tau_w * a_{crit})$, decreased by 3.8 for increasing concentration from 600 to 1200 mg L^{-1} and by 2.65 for increasing 1200 to 2400 mg L^{-1}.

Table 7.11: The critical parameter $J_{crit}/(\tau_w * a_{crit}^{4/3})$ value variations with different crossflow velocities and n-dodecane concentrations.

Crossflow Velocity ($m\ s^{-1}$)	Oil feed Concentration ($mg\ L^{-1}$)		
	600	1200	2400
	Emulsion A	Emulsion B	Emulsion C
	$J_{crit}/(\tau_w * a_{crit}^{4/3})$ $[Lm^{-2}h^{-1}(\mu m)^{-4/3}Pa^{-1}]$	$J_{crit}/(\tau_w * a_{crit}^{4/3})$ $[Lm^{-2}h^{-1}(\mu m)^{-4/3}Pa^{-1}]$	$J_{crit}/(\tau_w * a_{crit}^{4/3})$ $[Lm^{-2}h^{-1}(\mu m)^{-4/3}Pa^{-1}]$
1.14	21.99	17.45	13.85
1.52	21.95	17.46	13.86
1.92	21.99	17.42	13.85
2.28	21.95	17.46	13.85
Mean	21.97	17.45	13.85

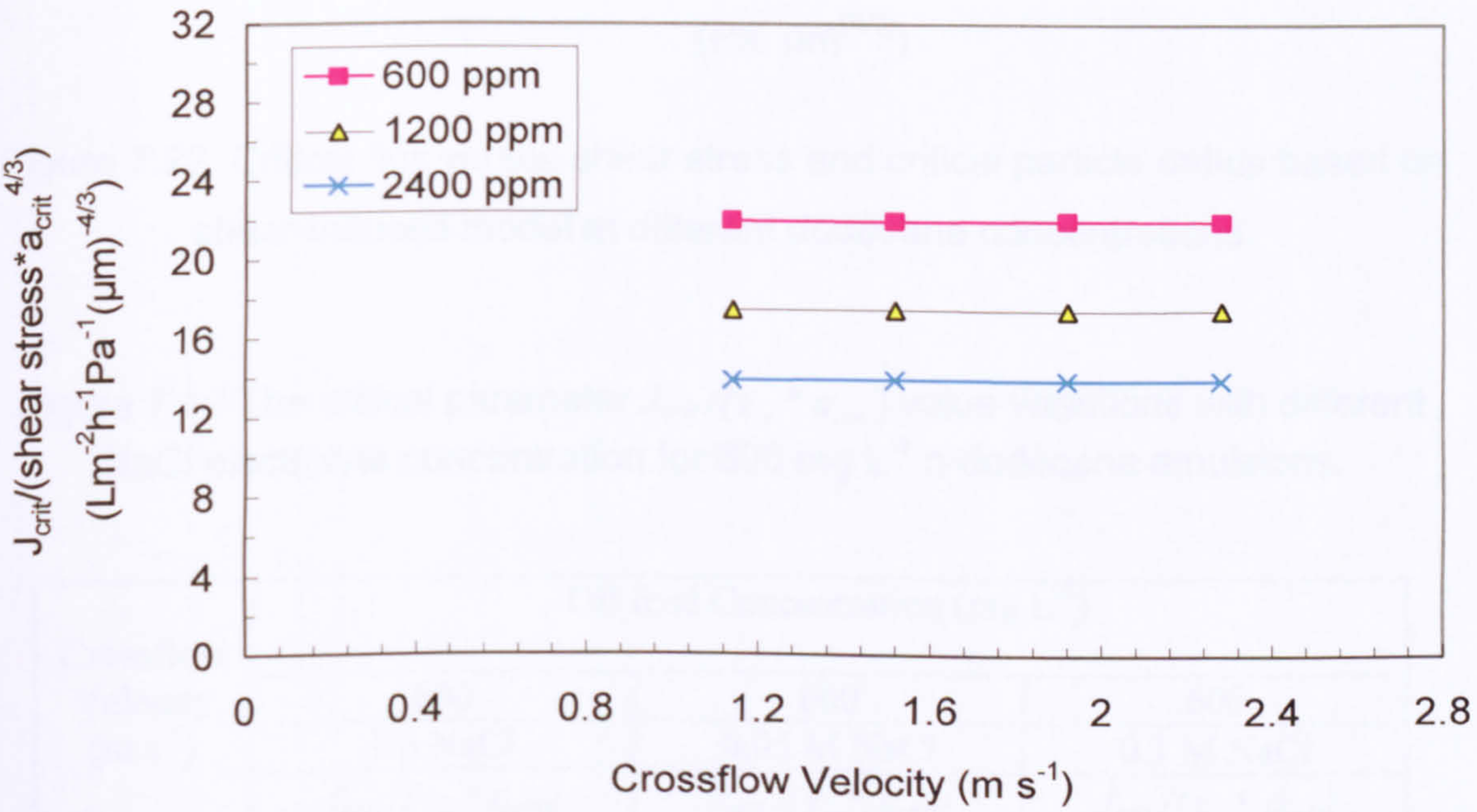

Figure 7.21: The critical parameter $J_{crit}/(\tau_w * a_{crit}^{4/3})$ value variations with different crossflow velocities and n-dodecane concentrations.

Figure 7.21 demonstrated a better constant relationship between critical flux and both wall shear stress and critical particle size compared to Figure 7.19 for different oil feed concentration.

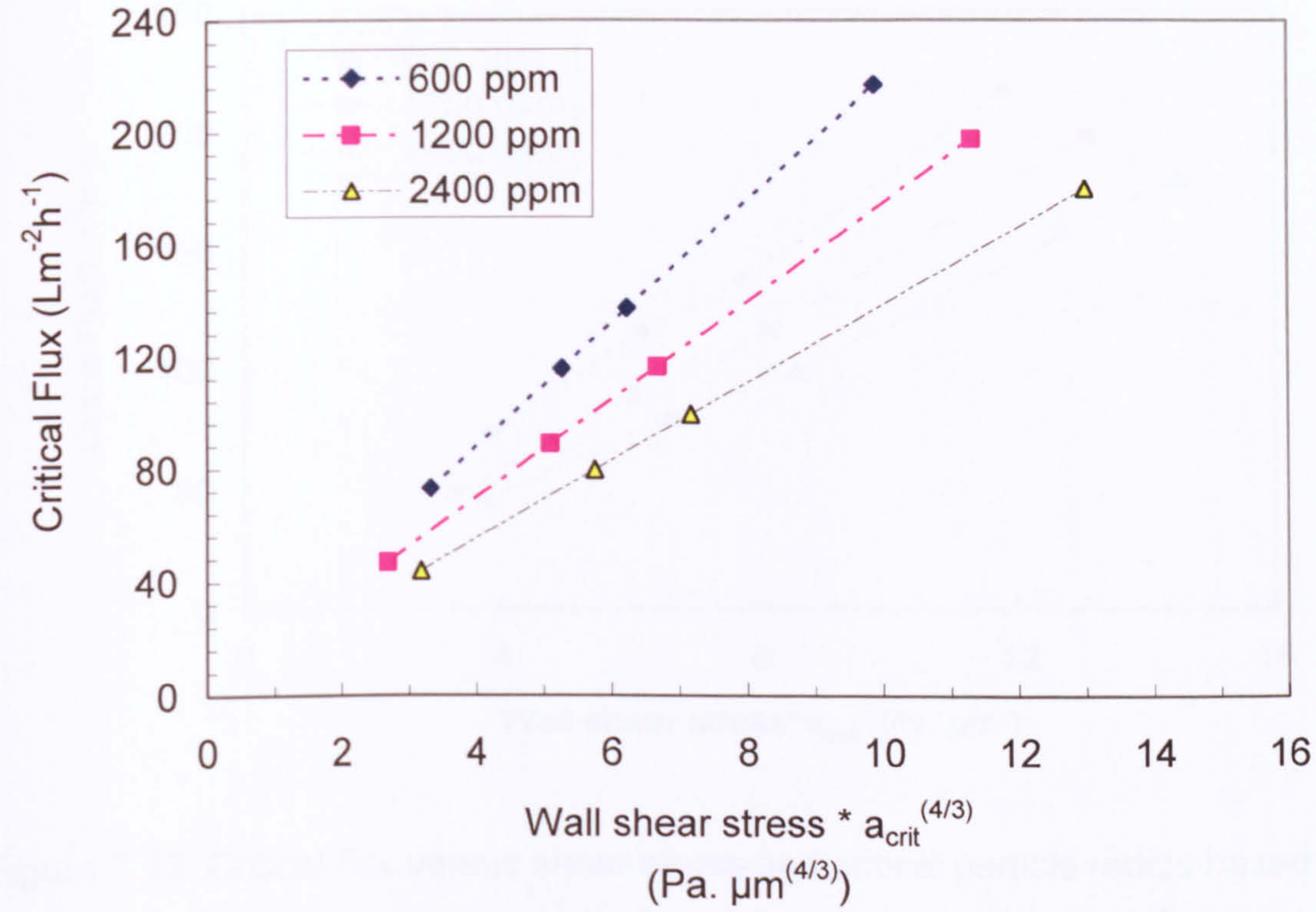

Figure 7.22: Critical flux versus shear stress and critical particle radius based on shear-induced model at different dodecane concentrations.

Figure 7.12 The critical parameter $J_{crit}/(\tau_w * a_{crit})$ value variations with different NaCl electrolyte concentration for 600 mg L^{-1} n-dodecane emulsions.

Crossflow Velocity ($m\ s^{-1}$)	Oil feed Concentration ($mg\ L^{-1}$)		
	600	600	600
	No NaCl	0.05 M NaCl	0.1 M NaCl
	$J_{crit}/(\tau_w * a_{crit})$ $[Lm^{-2}h^{-1}(\mu m)^{-1}Pa^{-1}]$	$J_{crit}/(\tau_w * a_{crit})$ $[Lm^{-2}h^{-1}(\mu m)^{-4/3}Pa^{-1}]$	$J_{crit}/(\tau_w * a_{crit})$ $[Lm^{-2}h^{-1}(\mu m)^{-1}Pa^{-1}]$
1.14	18.96	15.86	14.07
1.52	18.68	15.13	13.47
1.92	17.75	15.79	15.55
Mean	18.46	15.59	14.36

For the same feed concentration at different ionic strength as shown in Table 7.12 and Figure 7.23, a linear relation between J_{crit} and $(\tau_w * a_{crit})$ but with inconsistency with regard to the gradient value.

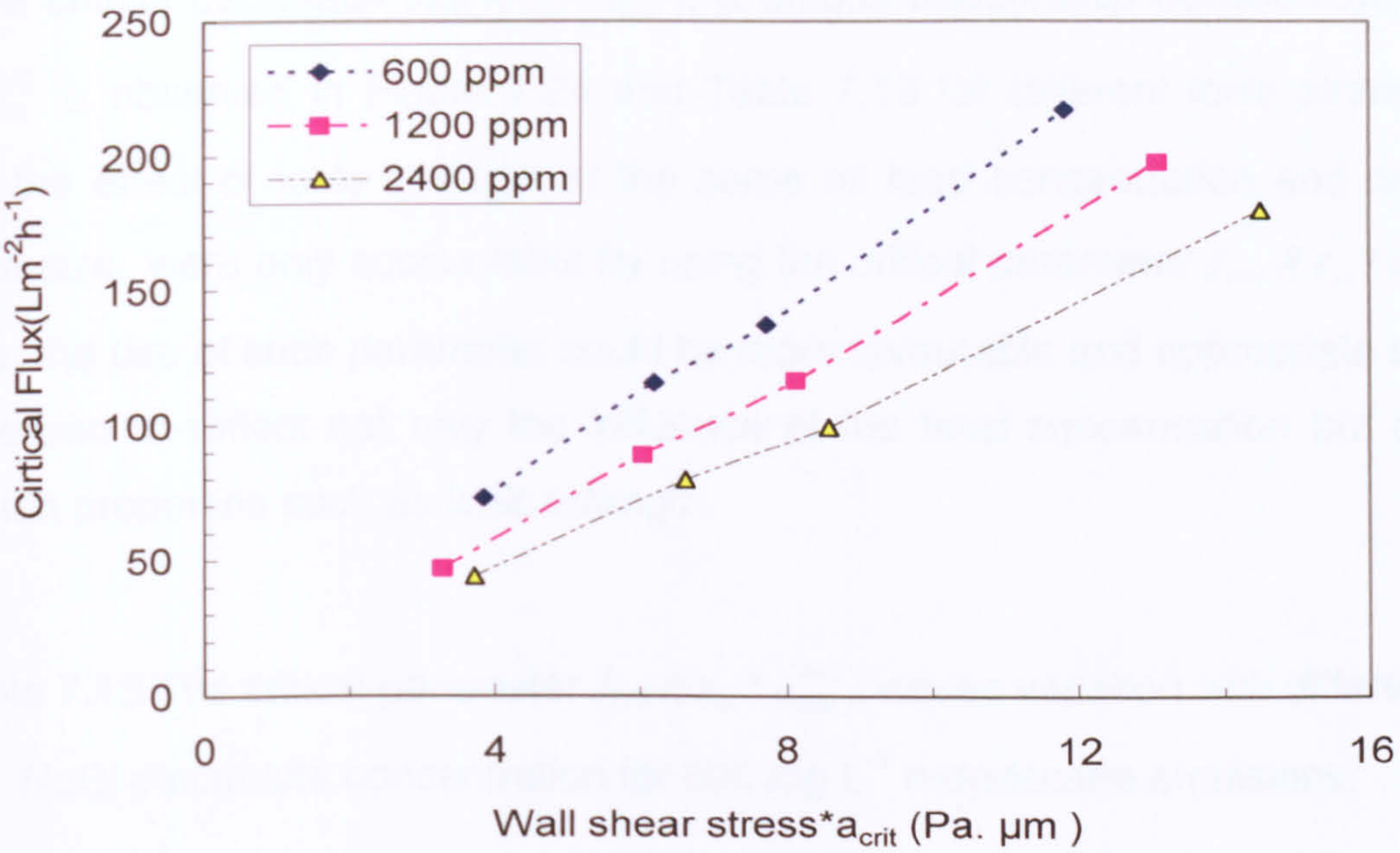

Figure 7.23: Critical flux versus shear stress and critical particle radius based on the surface transport model at different ionic strength for 600 mg L^{-1} emulsion.

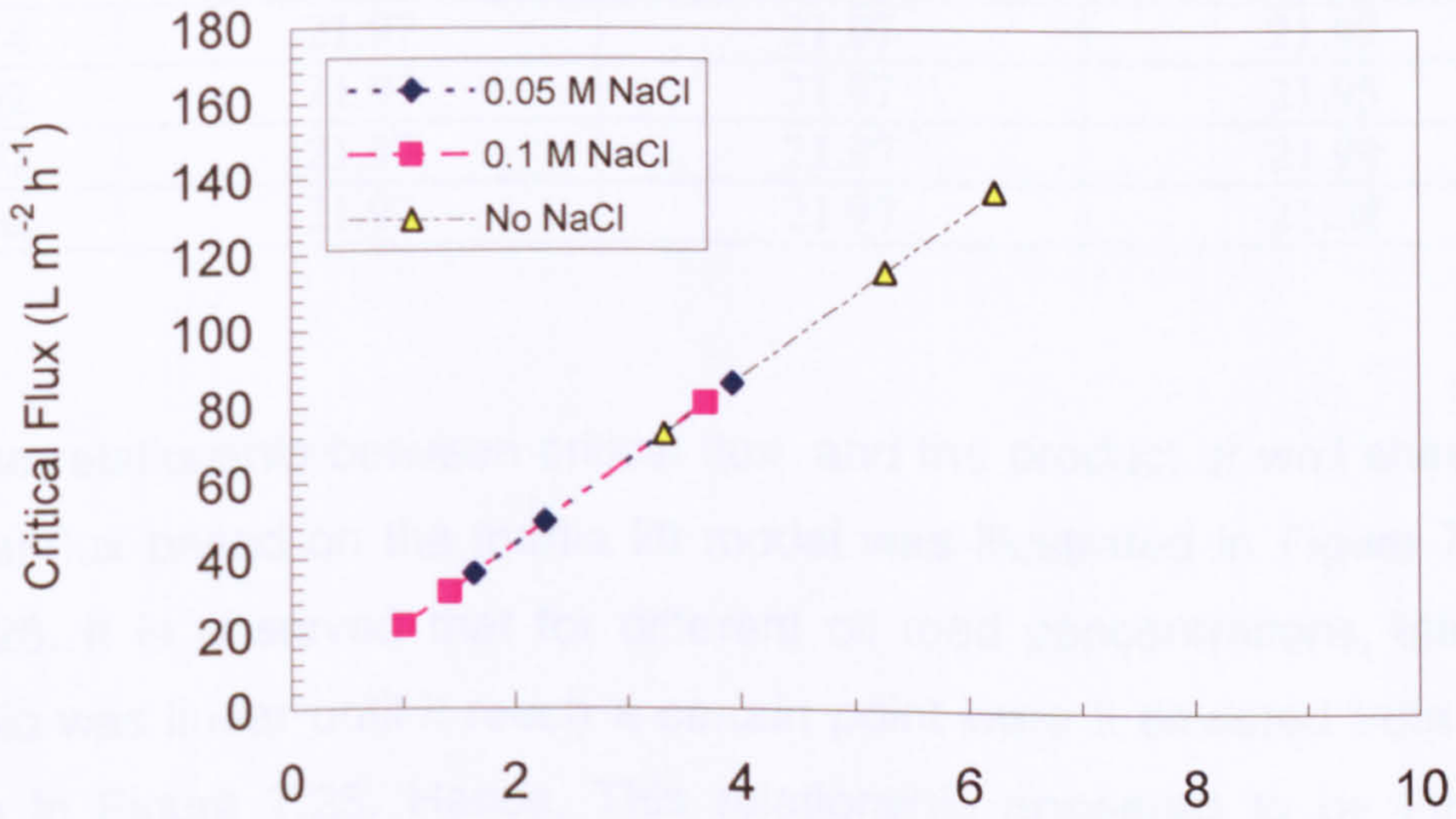

Figure 7.24: Critical flux versus shear stress and critical particle raduis based on the shear-induced model at different ionic strength for 600 mg L^{-1} emulsion.

For the critical parameter $J_{crit}/(\tau_w * a_{crit}^{4/3})$, a unique relationship between J_{crit} and $\tau_w * a_{crit}^{4/3}$ is observed in Figure 7.24 and Table 7.13 for different ionic strengths. Thus, the effect of ionic strength at the same oil feed concentration and critical particle size were only accountable by using the critical parameter $J_{crit}/(\tau_w * a_{crit}^{4/3})$. Hence, the use of such parameter could be more favourable and appropriate since it appeared to reflect not only the influence of the feed concentration but other emulsion properties such as ionic strength.

Table 7.13 The critical parameter $J_{crit}/(\tau_w * a_{crit}^{4/3})$ values variation with different NaCl electrolyte concentration for 600 mg L^{-1} n-dodecane emulsions.

Crossflow Velocity ($m\ s^{-1}$)	Oil feed Concentration (mg L^{-1})		
	600	600	600
	No NaCl	0.05 M NaCl	0.1 M NaCl
	$J_{crit}/(\tau_w * a_{crit}^{4/3})$ [$Lm^{-2}h^{-1}(\mu m)^{-4/3}Pa^{-1}$]	$J_{crit}/(\tau_w * a_{crit}^{4/3})$ [$Lm^{-2}h^{-1}(\mu m)^{-4/3}Pa^{-1}$]	$J_{crit}/(\tau_w * a_{crit}^{4/3})$ [$Lm^{-2}h^{-1}(\mu m)^{-4/3}Pa^{-1}$]
1.14	21.97	21.97	21.99
1.52	21.97	21.97	21.95
1.92	21.97	21.97	21.99
Mean	21.97	21.97	21.98

Thirdly, the relationship between critical flux and the product of wall shear stress and critical flux based on the inertia lift model was illustrated in Figure 7.25 and Figure 7.26. It is observed that for different oil feed concentrations, initially the relationship was linear until it reach a certain point were it deviated from linearity as shown in Figure 7.25. Hence, This relationship appeared to be function of concentration. Figure 7.26 demonstrates the influence of addition of NaCl salt in such correlation for 600 mg L^{-1} emulsions. The critical flux curve trends at ionic strength 0.05 M and 0.1 M NaCl seemed to behave in a similar manner with the initial nonlinearity followed by linearity. While for the case no NaCl salt added, a linear relationship at different crossflow velocity from 1.14 to 1.92 m s^{-1} is shown. Generally the pervious modified critical parameters show better consistency and linearity and hence could be used as a threshold below which it is required to

operate to avoid cake formation and maintain sustainable filtration performance for polydispersed emulsions. Finally, the predicted relationship using Brownian diffusion model illustrated in Figure 7.27 and Figure 2.28 suggests that the critical flux is less sensitive to variations in the critical particle size and the wall shear stress.

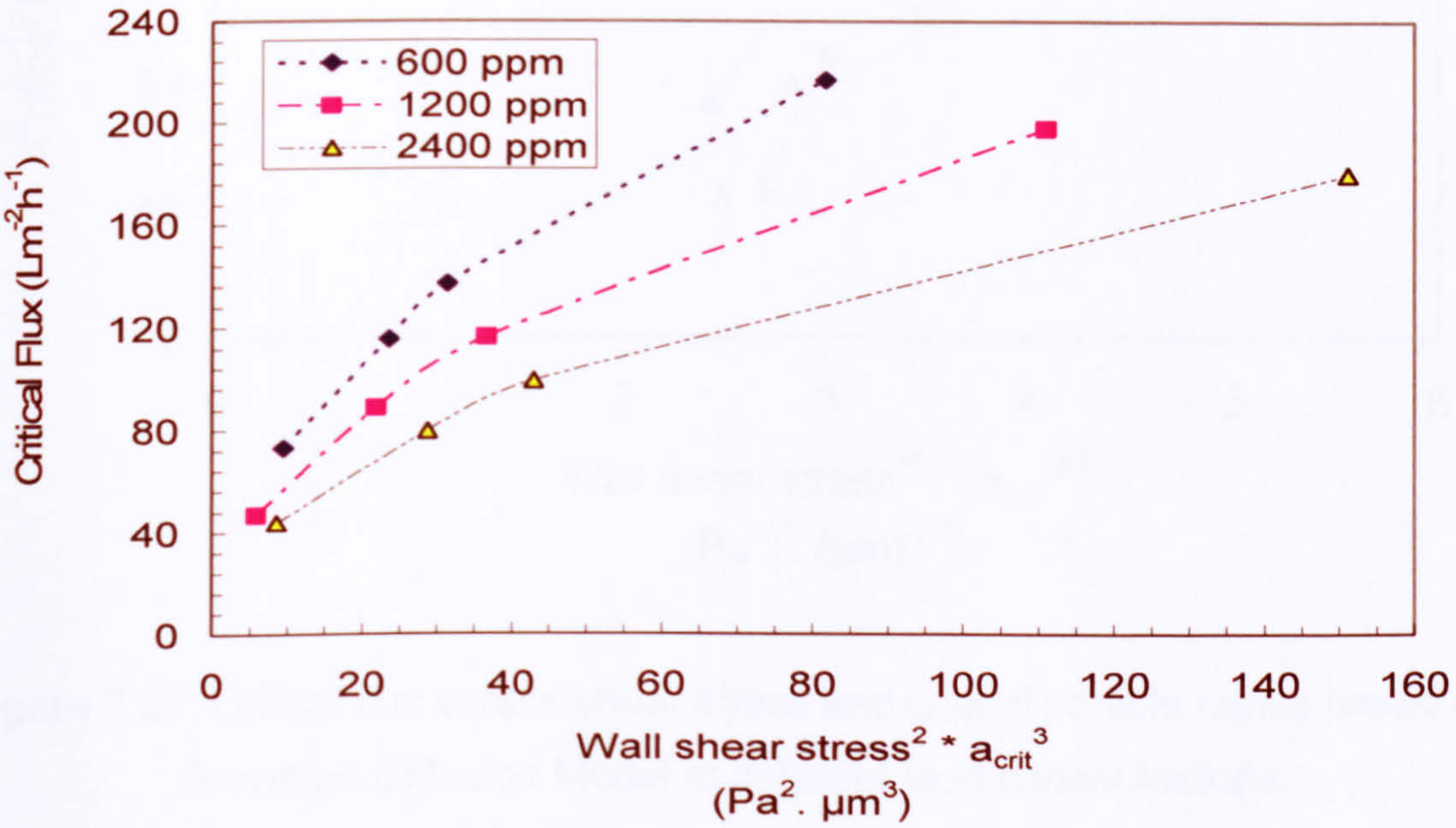

Figure 7.25: Critical flux versus shear stress and critical particle radius based on the inertial lift model at different feed concentrations.

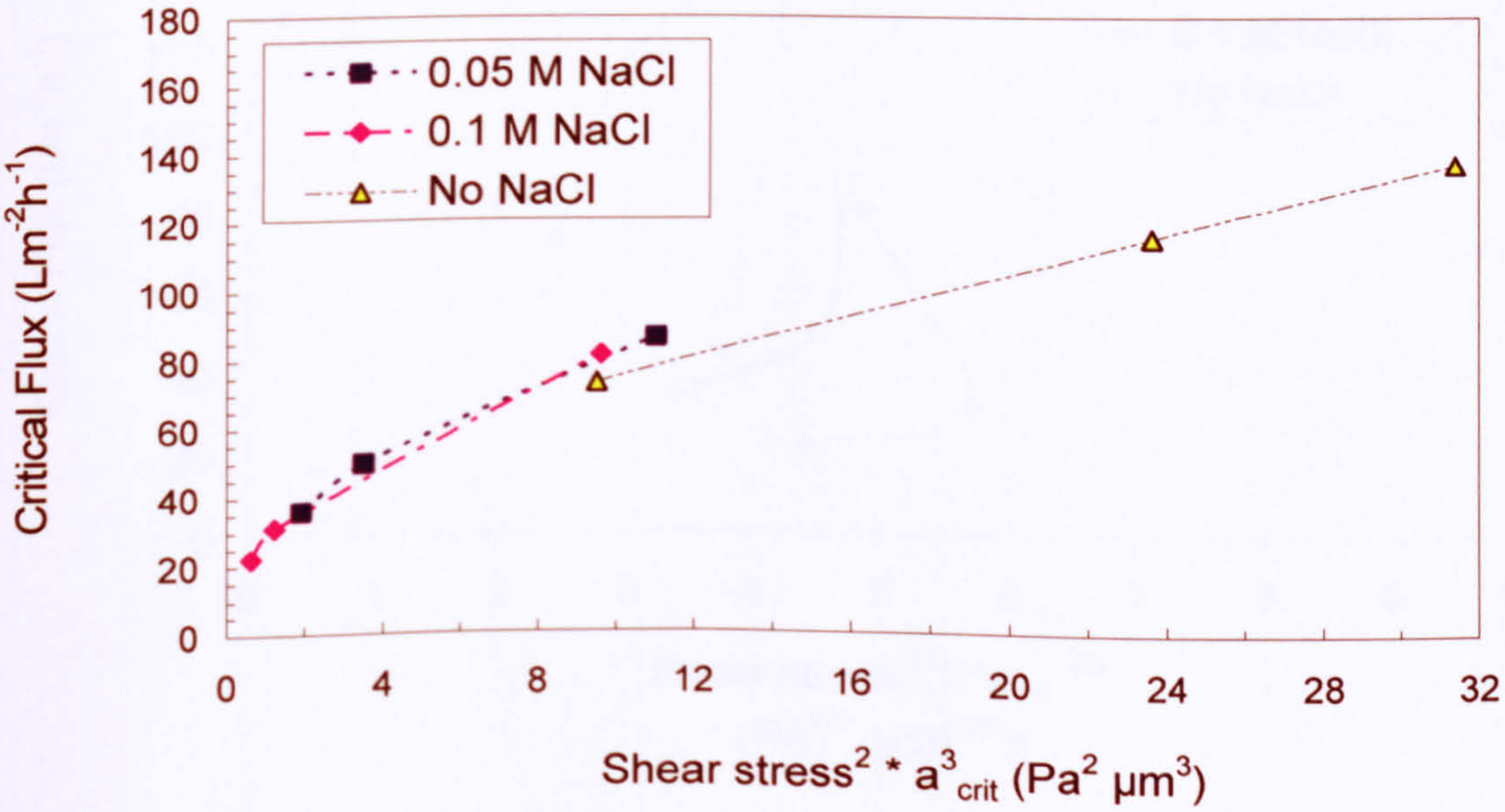

Figure 7.26: Critical flux versus shear stress and critical particle radius based on the inertial lift model at different ionic strength for 600 mg L^{-1} emulsion.

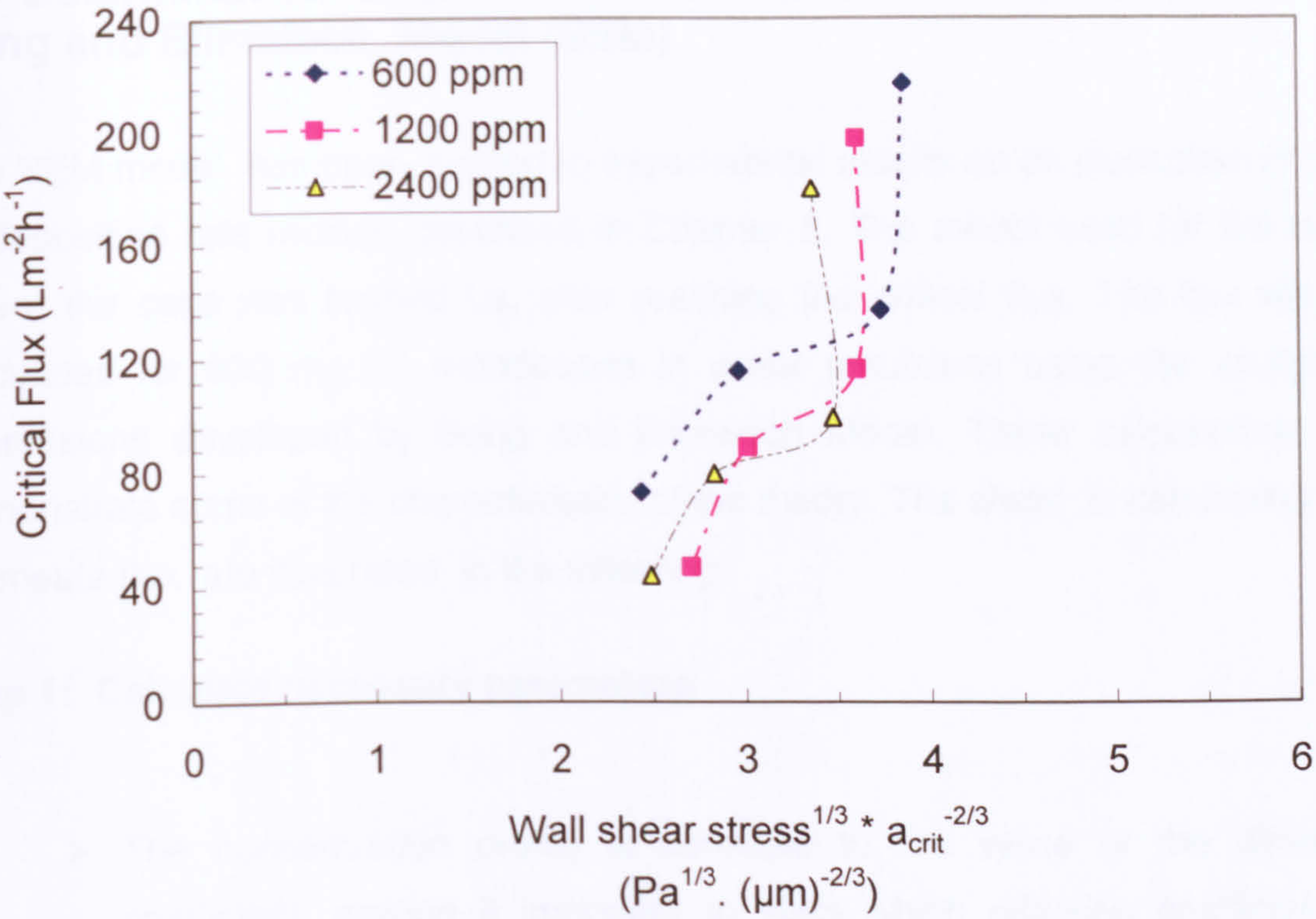

Figure 7.27: Critical flux versus shear stress and critical particle radius based on Brownian Diffusion Model at different feed concentrations.

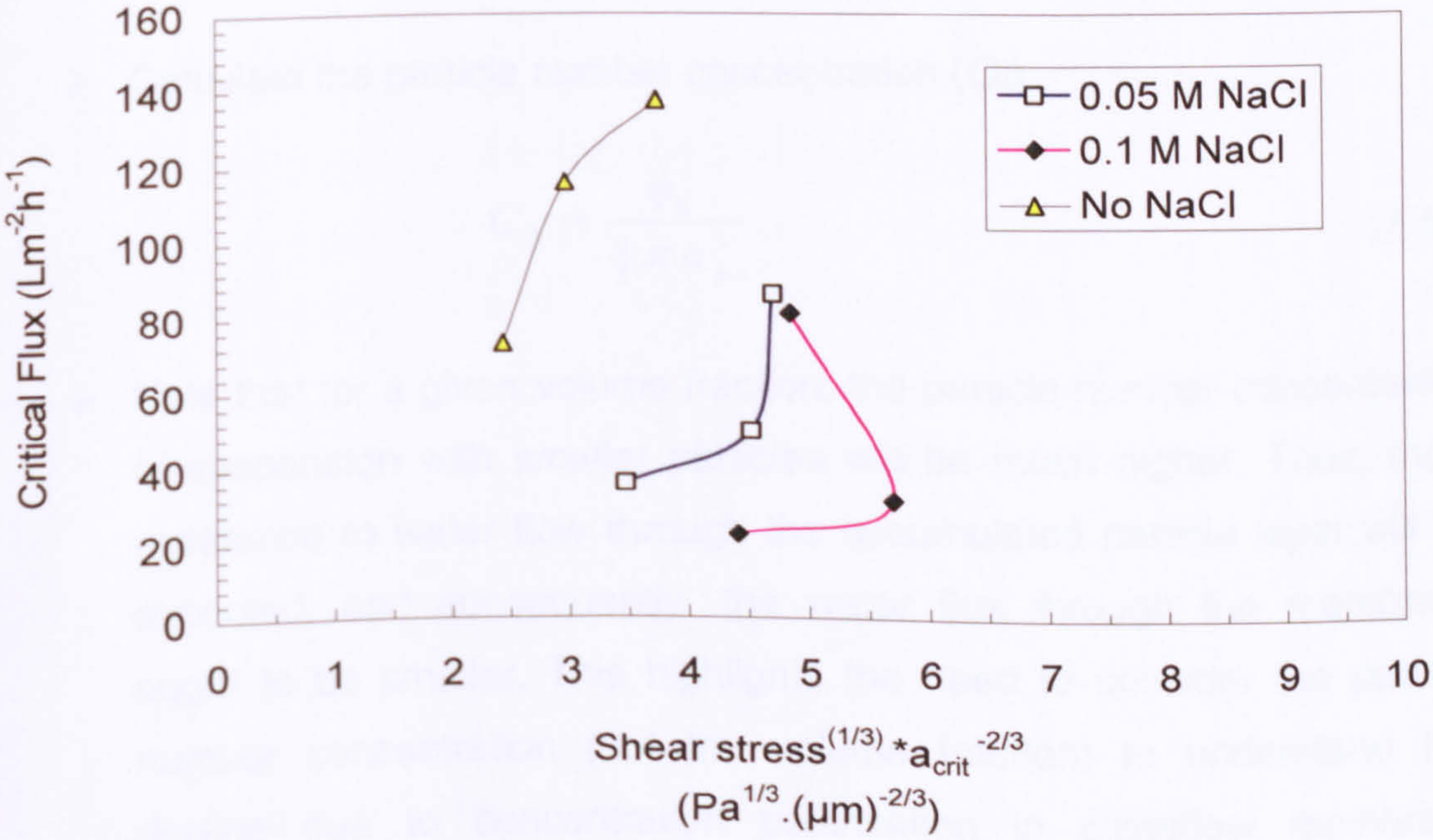

Figure 7.28: Critical flux versus shear stress and critical particle radius based on Brownian Diffusion model at different ionic strength for 600 mg L^{-1} emulsion.

7.6 Determination Steps of the Permeate Flux Values based on Song and Elimelech Model (SEM)

The SEM model has bean applied to experimental results as an illustration of one of deposition rate models described in Chapter 2. The model used for the case where the cake was formed i.e. after reaching the critical flux. The flux will be calculated for 600 mg L^{-1} n-dodecane in water emulsions using the analytical expressions developed by Song and Elimelech Model. These calculations will demonstrate some of the characteristics of the theory. The steps in calculating the permeate flux are illustrated in the following:

Step 1: Calculate necessary parameters

- The concentration profile is sensitive to the value of the diffusion coefficient, making it important to state which diffusion coefficient is used in the calculations. The diffusion coefficient (D) can be calculated from Stokes-Einstein equation, i.e.,

$$D_m = \frac{kT}{6\pi\mu a_p} \tag{7.13}$$

- Calculate the particle number concentration (C_0)

$$C_0 = \frac{\phi_b}{\frac{4}{3}\pi a_p^3} \tag{7.14}$$

- Note that for a given volume fraction, the particle number concentration of suspension with smaller particles will be much higher. Thus, more resistance to water flow through the accumulated particle layer will be expected, and consequently, the water flux through the membrane ought to be smaller. This highlights the need to consider the particle number concentration (not the volume fraction) to understand flux decline due to concentration polarization in crossflow membrane filtration.

Step 2: Calculate the filtration number N_F

- Use the definition of N_F given by the following equation

$$(N_F = \frac{4\pi a_p^3}{3kT}\Delta P_p) \tag{7.15}$$

- N_F is the ratio of the energy needed to bring a particle to the membrane surface from bulk suspension to the thermal (dissipative) energy of the particle.
- A larger value of N_F indicates that more energy is needed to bring a particle from the membrane surface to the bulk suspension.
- For most cases where concentration polarization is appreciably developed, it is safe to neglect membrane resistance because it is usually smaller than that of the retained particle layer. For all cases that have been used in this study, $N_F > N_{Fc}$ (=15.00), where N_{Fc} stands for critical filtration number for cake forming. Hence, we need to consider the equations for Cake Formation.

Step 3: Calculate the cake forming factor N_c

- Because the membrane resistance is usually negligible compared to the resistance provided by accumulated particles (as is the case in MF and most UF operations), the dimensionless number, N_c is termed the cake thickness factor, i.e. we can calculate N_c from equation:

$$\mathrm{N_C} = \frac{\Delta \mathrm{P_c}}{\Delta \mathrm{P_p}} \frac{A_s(\theta^*_{max})}{A_s(\theta^*_{max})} \tag{7.16}$$

- The parameters needed for calculating N_c are obtained as follows:

$\Rightarrow$ Since N_F>15.00, $A_s(\theta^*_{max})$=23.559 (Table 7.14).

Table 7.14: Values of Θ_W and $A_s(\Theta^*)$ for different filtration numbers (Song and Elimelech, 1995).

N_F	θ_W	$A_s(\theta^*)$
0.000	0.000	1.000
1×10^{-8}	0.002	1.002
1×10^{-5}	0.021	1.025
0.010	0.198	1.293
0.100	0.381	1.802
0.500	0.556	2.910
1.000	0.633	3.946
2.000	0.705	5.719
3.000	0.743	7.325
4.000	0.768	8.842
5.000	0.786	10.301
6.000	0.800	11.719
7.000	0.811	13.106
8.000	0.821	14.468
9.000	0.829	15.809
10.000	0.836	17.132
11.000	0.842	18.441
12.000	0.847	19.736
13.000	0.852	21.021
14.000	0.856	22.295
15.000	0.86	23.559

⇒ $A_s(\theta_{max})$ is calculated using the following equation

⇒
$$A_S = \frac{1+\frac{2}{3}\theta^5}{1-\frac{3}{2}\theta+\frac{3}{2}\theta^5-\theta^6} \qquad (7.17)$$

⇒ for $\theta = \theta_{max}$, that is the θ value corresponding to a porosity (ε) of 0.26 (maximum rhomobohedral packing). Note that $\theta=(1-\varepsilon)^{1/3}$.

⇒ Because the membrane resistance is negligible, $\Delta P_c=\Delta P-\Delta P_p$, where ΔP_p is calculated from the equation

⇒
$$\Delta P_p = \frac{N_{Fc} kT}{(4/3)\pi a_p^3} \qquad (7.18)$$

⇒ Thus, with $A_s(\theta^*_{max})$, $A_s(\theta_{max})$, ΔP_c, and ΔP_p, we can use equation (7.16) to calculate N_c.

Step 4: Calculate the average permeate flux

- Use equation (7.19) to calculate the permeate flux, using the values of parameters determined in the previous steps. The result for the permeate velocity are:

$$V = (\frac{3}{2})^{2/3}\left[D^{2/3}\gamma^{2/3}(1+N_C)^{1/3}L^{-1/3}\right]\left(\frac{\Delta P_p}{A_S(\theta^*_{max})kTC_0}\right)^{2/3} \quad (7.19)$$

- Flux comparison between estimated data using the SEM model and the experimental result for 600 mg L^{-1} n-dodecane in water emulsions at various crossflow velocities is presented in Figure 7.29. It is observed clearly that the SEM model underpredicted the permeate fluxes. Therefore, SEM model's modification or improvement would be required in order to give better flux predictions.

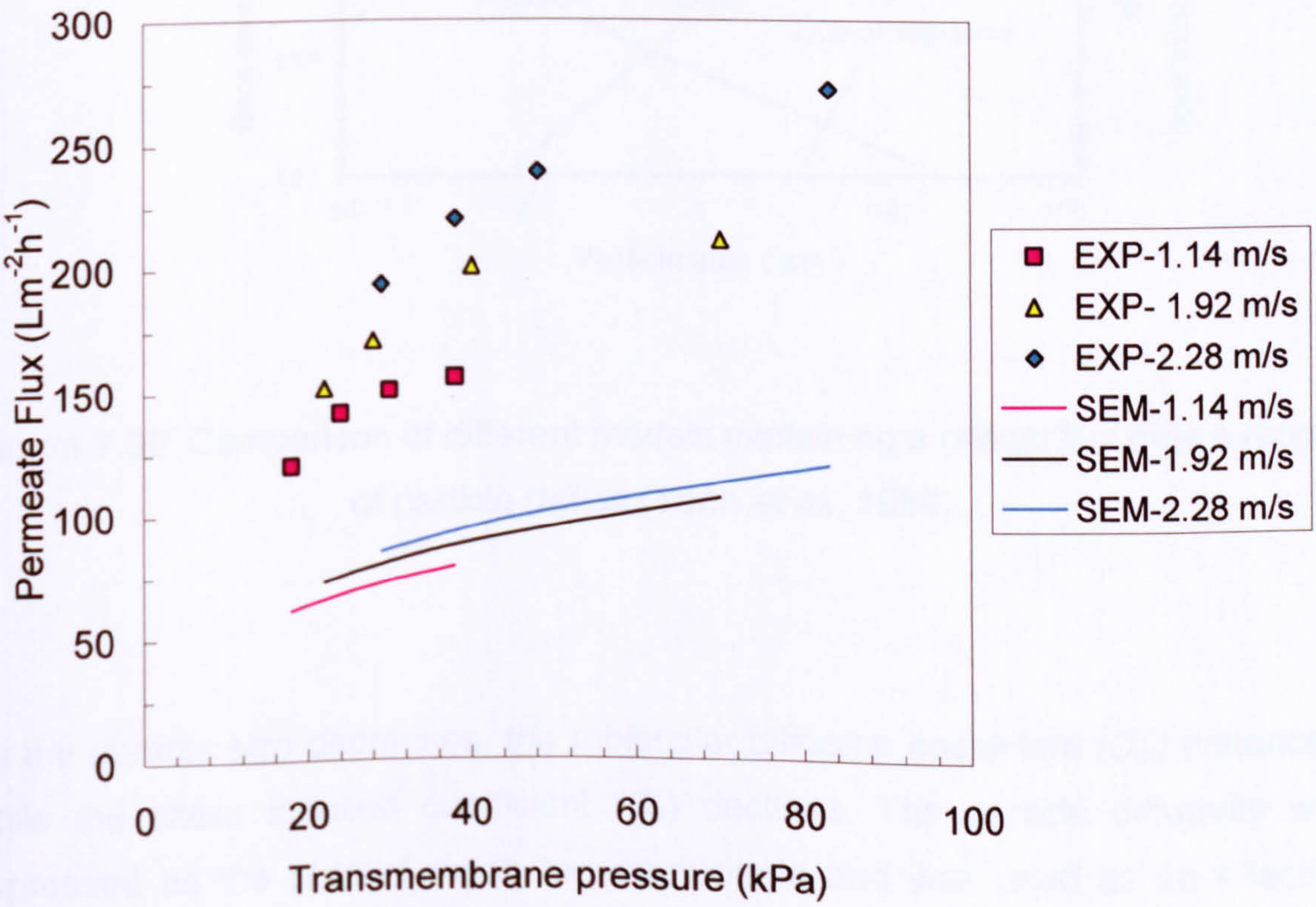

Figure 7.29: Permeate flux comparison between SEM model with experimental data for 600 mg L^{-1} n-dodecane emulsions.

7.6.1 Modified Song and Elimelech Model (SEM)

As shown in Figure 7.30, where a comparison of various common models explaining the critical flux over a range of particle sizes is shown, at a particle radius of about 0.5 μm the influence of Brownian and shear induced diffusion is almost the same. Thus, both of these diffusional mechanisms need to be accounted for in estimating the critical flux.

From experimental data of critical fluxes at various crossflow velocities, the mean critical particle radius has been estimated to be between 0.5-0.67 μm as shown in Table 7.7 (presented in Section 7.3).

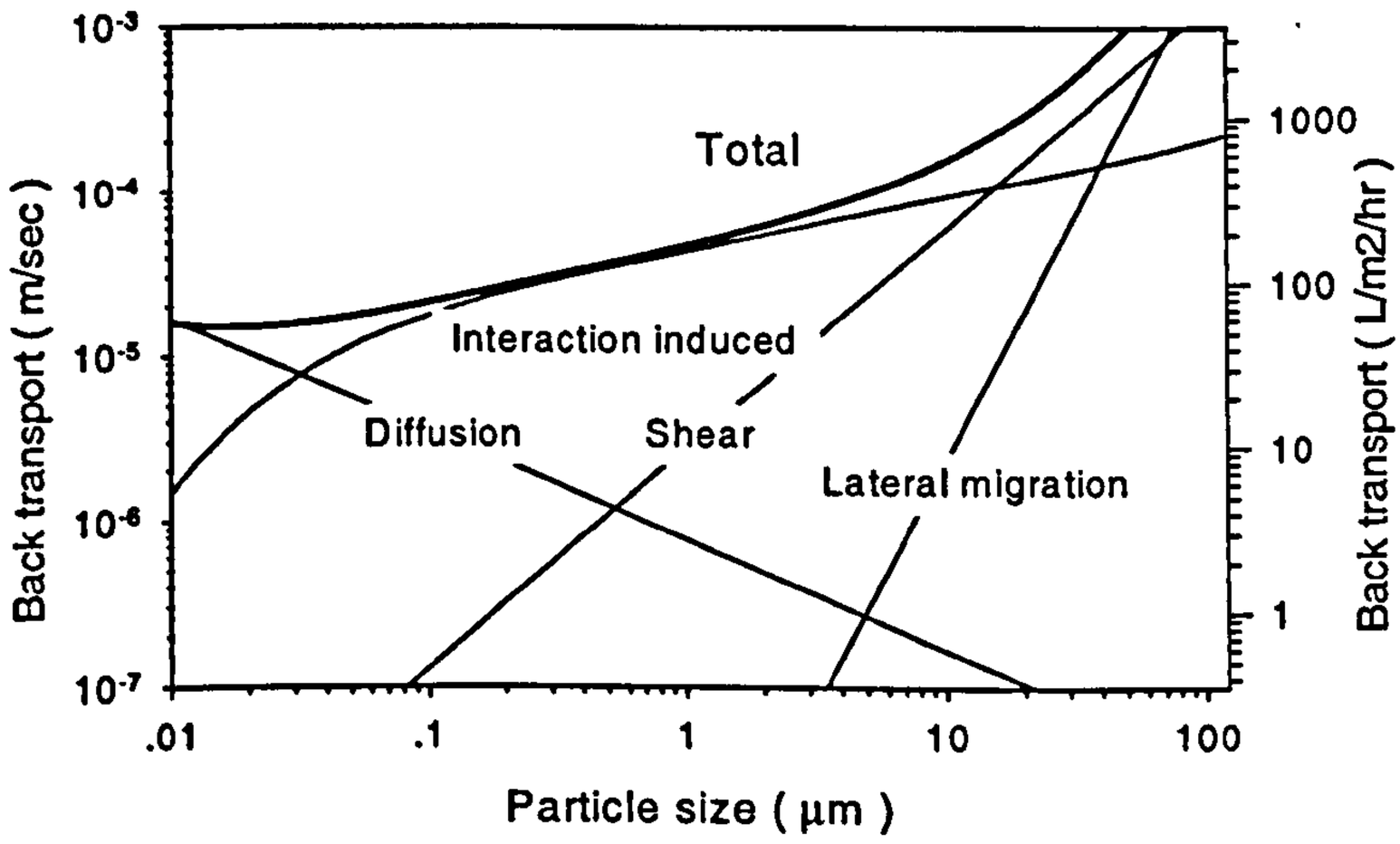

Figure 7.30: Comparison of different models explaining a critical flux over a range of particle radius (Yoon *et al.*, 1999).

As the particle size decreases, the molecular diffusion coefficient *(D_m)* enhances, while the shear induced coefficient (D_s) declines. The particle diffusivity was expressed as the sum of those two coefficients and was used as an effective diffusion coefficient *(D_{eff})* as demonstrated in equation (7.20) (Lee 1997):

$$D_{eff} = D_m + D_s = \frac{kT}{6\pi\mu a_p} + 0.03\gamma a_p^2 \quad (7.20)$$

When the effective diffusion coefficient was implemented on the SEM model, a better prediction of the experimental data was achieved as shown in Figure 7.31.

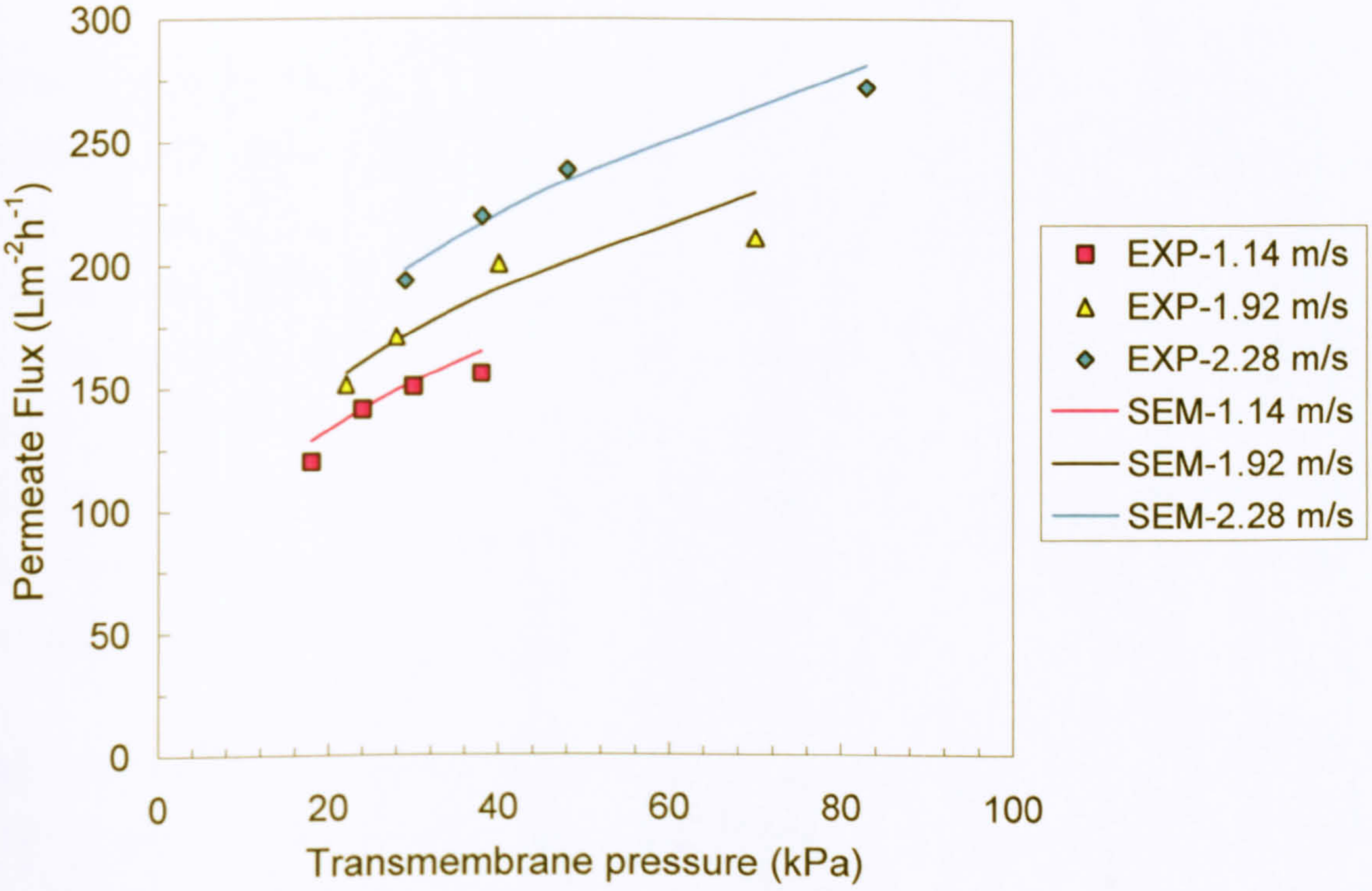

Figure 7.31: Permeate flux comparison between modified SEM model with experimental data for 600 mg L^{-1} n-dodecane in water emulsions.

7.7 Conclusion

Crossflow velocities, oil and surfactant concentrations, ionic strength, pH , and valency effects on equilibrium permeate flux and critical flux were investigated. Increases in crossflow velocity for oil emulsions from 1.14 to 2.28 m s^{-1} caused an increase in the equilibrium permeate flux. In contrast, as feed oil concentrations increased from 600 to 2400 mg L^{-1}, equilibrium permeate fluxes were decreased. For all n-dodecane emulsions filtered, critical flux (J_{crit}) values appeared to

increase proportionally with the crossflow velocity. The J_{crit} enhancement with crossflow velocity was most noticeable at low n-dodecane feed concentration (600 mg L^{-1}) along with the highest crossflow velocity (2.28 m s^{-1}). On the other hand, the lowest critical flux value was reached when oil emulsion with feed concentration (2400 mg L^{-1}) along with the least crossflow velocity (1.14 m s^{-1}). These observations where discussed in term of the hydrodynamics and emulsions properties.

Similarly, when the ionic strength (using NaCl) for the feed emulsions was increased, the permeate flux declined. However, when the ionic strength (using $CaCl_2$ or $FeCl_3$) for the feed emulsions was increased, the permeate flux increased also. These paradoxical observations have been discussed in term of ion valence effect linked to particle-membrane and particle-particle interactions in relation to filtration process. The experimental results encountered in this study appeared to support the concept that equilibrium flux is influenced by both hydrodynamics, i.e. crossflow velocity, and particle interactions (emulsion stability through changes in ionic strength).

The torque balance model, inertial lift model, and shear-induced diffusion model, were compared with the experimental data when particle size was used as a fitting parameter. The 'fitted' particle sizes were in the lower ranges of the measured feed particle size distributions, suggesting that these smaller particles were accountable for the initial permanent particle fouling on the membrane surface at J_{crit}. It is difficult to provide evidence directly by experiment because of the inability to visualise and size particles resting on the membrane in situ in the filter. Several researchers in the field found that the critical parameter (J_{crit} / τ_w) was linear, but this was in disagreement with what was observed in the current investigation.

Therefore as a response to this discrepancy, the relationship between critical flux and the product of the wall shear stress and the critical particle size was studied on the basis of those more commonly used models, presented in Table 7.9. The surface transport model seemed to offer more realistic prediction and showed linear relationship with consistency for a modified critical parameter $J_{crit} /(\tau_w * a_{crit})$.

Also, shear-induced model seemed to provide another interesting critical parameter $J_{crit}/(\tau_w * a_{crit}^{4/3})$, which showed constancy and was a function of oil feed concentration only. For deposition rate modelling, the Song and Elimelech Model (SEM) has been applied to predict equilibrium permeate fluxes which were in disagreement with the experimental results. However, by modifying the SEM Model, a better permeate flux prediction was obtained when the cake layer is formed after the critical flux value was reached. The unique applications of the back transport and deposition rate models in liquid - liquid separations here could be considered a contribution to new knowledge, while for critical parameter $J_{crit}/(\tau_w * a_{crit})$ new development might be claimed.

CHAPTER 8

Practical Implications

8.1 Industrial oily wastewater streams

The practical implications of this current research could be related to a number of oily wastewater streams discharged form different industrial sources, some of which are listed in Table 8.1. Generally, environmental regulations which control the permissible disposal of oil and grease into municipal treatment stations and surface water are becoming more stringent. Oil and grease can be present in effluents in free, dispersed or emulsified forms, these may be classified based on the particle size. Free oil is when the oil droplets are bigger than 150 μm, while dispersed oil refers to oil droplets with sizes in the range 20-150 μm, and emulsified oil composes of droplets with sizes normally below 20 μm.

Table 8.1: Oil and grease concentrations in effluents of selected industries (adapted from Bennet, 1986, and Patterson, 1985).

Industrial Source	Oil and grease concentration (mg/l)
Steel-rolling mills	
Hot rolling	20
Cold rolling	700
Cold rolling coolant	2088 – 48,742
Aluminium rolling	5000-50,000
Metal Rolling	4,000 – 50,0000
Metal rinse water	10 – 1,000
Can production (forming)	200
Metal fabrication	10,000 – 150,000
Food processing	3830
Food processing (Fish)	520-13700
Rendering	14-3551
Wool scouring	1605-12,260
Tanning waste, hide curing	40,200
Metal finishing	4000-6000
Commercial laundry	100 – 2,000
Petroleum refinery	10-3200

Since oil and grease are a general expression, they might comprise of animal and vegetable source oils, petroleum hydrocarbons, surfactants, naphthenic acid, etc (Cheryan and Rajagopalan, 1998). In the literature review (Chapter 2), the complexity of produced water composition was discussed, where the emulsified oil was the most significant contaminant due to its adverse effect on the environment and to plugging of oil wells leading to decline in injectivity. Hence from Chapter 3, the case study provided as with not only effluent analysis data but also the design targets for wastewater treatment plant, which was the reduction of oil from 2000 ppm to 10 ppm with removal of the suspended particles with diameteres in the range of 5-20 μm. However, according to effluent analyses, wastewater treatment using conventional oil/water separation methods failed to remove these suspended coarse particles. In Chapter 4, while operating at different conditions and emulsion properties, from particle size analyses conducted for oil-in-water emulsions that were fed to the filtration rig the oil droplet sizes were found approximately in the range 0.1-10 μm.

Due to the presence of emulsified oil droplets in numerous industrial effluents (Table 8.1), the experimental results for crossflow microfiltration discussed in Chapter 6 and Chapter 7 could be cross linked to some of these oily waste streams. As prerequisite for identification of the implications of this research work, it is necessary to discuss some characteristics of oil wells in terms of location and capacity. Due the relatively small production of oil wells scattered in a broad oilfield, the construction of gathering centres is not feasible economically due the high cost of piping and pumping networks. Therefore, a portable oil/water separation system has been introduced, where incorporation of filtration with other conventional treatment equipment would be cost effective bearing in mind the relatively short life of these small oil wells. For example, oil wells in the southern desert of Oman, where for each barrel of crude oil produced there will be three barrels of produced is mentioned in Chapter 2. These oil wells are in urban areas where the electrical sources needed to run such big production plant are limited or unavailable. To deal with this particular energy resources problem the Shell company has introduced solar membrane distillation where instead of separating the pollutants from produced water, it separated the water as a water vapour by heating by solar energy, however the production rate was relatively low.

8.2 Membrane separation of produced water

The application of membranes for treatment of oil-in-water emulsions is growing in industrial effluents , particularly in cases in which both the environmental and cost effectiveness of the recovered matter are high, such as in the secondary recovery of crude oil from produced water in offshore and onshore platforms. For separation of oil-in-water in downstream treatment, Cheryan and Rajagopalan claimed that membranes are most likely to be used when the feed volume rates are less than 190 m^3/day. Membranes have been widely investigated for elimination of oil and grease from produced water. For example, two industrial applications are demonstrated in Table 8.2. Zaidi *et al.* (1992) stated that the performance of these commercial installations were unsatisfactory due to the failure to meet their primary performance criteria and hence major design alterations were made. According to the annual report from Marathon oil, the downtime was 25 % during 1990. Despite of the reduction of oil and grease levels and the degree of permeate quality reached, the problem of oil well plugging was not eradicated at the Marathon platform, which could be linked to adverse specification of the feed stream.

Table 8.2: Industrial use of membranes for eliminating oil and grease from produced water in petroleum installations (Zaidi *et al.*, 1992).

	Marathon oil	Petro-Canada resources
Date installed	Fall 1989	Fall 1990
Location	EI-349B platform, Gulf of Mexico, USA	Valhalla Field, Alberta, Canada
Design capacity (m^3/day)	1000	1000
Membrane area (m^2)	45	-
Membrane Pore size (µm)	0.8	0.8
Feed	Slipstream from precipitator effluent	5 % from heater treater, 95 % groundwater
Permeate disposal	Reinjection	Reinjection
Pre-treatment	$FeCl_3$	$FeCl_3$

For economic use of membrane equipment in produced water treatment, Zaidi *et al.* (1992) claimed that there is no a clear consensus with respect to a target flux level. Any economical feasibility evaluations should take into account variables

such as equipment cost, weight and space restrictions on offshore platforms, conventional oil removal equipment to be replaced, the enhancement in permeate quality, design capacity, and produced water composition. Table 8.3 provided limited records of the inorganic MF and UF membranes that are potentially appropriate for oil/water separation up to the year 1992. General required features for membranes used for oil/water separation are high porosity, hydrophilic surface, thermal and chemical stability, long lifetime, and low cost.

Table 8.3: Inorganic membrane potentially appropriate for oil/water separation (Zaidi *et al.*, 1992).

Manufacturer	Trade Name	Type	Model	Pore Size	Material
Alcoa/SCT	Membralox	MF	Tubular	0.2-5 µm	$\alpha Al_2O_3/\alpha Al_2O_3$
		UF	Tubular	4-100 nm	ZrO_2/α-Al_2O_3
DuPont/Care		MF	Tubular	0.1 µm	ZrO_2/stainless steel
Carbone		MF	Tubular	0.2, 0.8 µm	Carbon composite
		UF		4-100 nm	
CeraMem		MF	Tubular	0.2, 0.5 µm	$\alpha Al_2O_3/\alpha Al_2O_3$
		UF	Tubular	5000 nm	
Cortane		MF	Tubular	0.2, 0.45, 0.8 µm	$TiO_2/\alpha Al_2O_3$
		UF			
Millipor/Norton	Ceraflo	MF	Tubular	0.2-1 µm	αAl_2O_3
Schelde Delta		MF	Tubular	0.45-8 µm	$S_1C/\alpha Al_2O_3$
TechSep/Rhone-Poulenc	Carbosep	MF	Tubular	0.08-0.45 µm	ZrO_2/C
		UF		15-100 k D	

8.3 Scepter® Membrane

Recently, several new membranes have been developed to give improved flux and separation features even under severe operating conditions or hostile environments; one of the most appealing of these is the Scepter® membrane (Graver Technologies). The mode of operation of the Scepter® Membrane is tangential flow (crossflow) filtration. It contains a sintered titanium dioxide active membrane on a porous, tubular AISI 316L or C-22 support. The Titanium oxide coating is enduringly bonded internally and on to the porous stainless steel surface, with the result being a smooth and foulant resistance membrane, which leads to an improved filtration performance. The configuration of the module is similar to that of shell and tube heat exchangers, where a single module can be supplied with an area of less than $1m^2$ to in excess of 800 m^2.

Figure 8.1 is an illustration of the operation of a microfiltration module. The Scepter® model is exceptionally designed for operating in the most hostile situation in which the temperature is very high up to 400°C; transmembrane pressure is in the range of 40 – 80 bar; pH range 1 -14; and crossflow velocity without any boundary. In North America and the Far East, the Scepter microfiltration technology has been employed successfully for several years. Among its applications has been waste oil recovery and metal finishing for oil elimination. Scepter® microfiltration technology could be used as a polishing stage or a tertiary treatment for the filtration system proposed in Chapter 3 due to its characteristics to cope with severe conditions caused by the produced water nature and composition. From a practical point view it has been already tested, but the cost-effectiveness of such technology is unavailable; data from user is not available, although claims by the manufacturers are that dozens of ceramic or polymeric modules could be replaced by a single Scepter® model with considerable cost and operational savings.

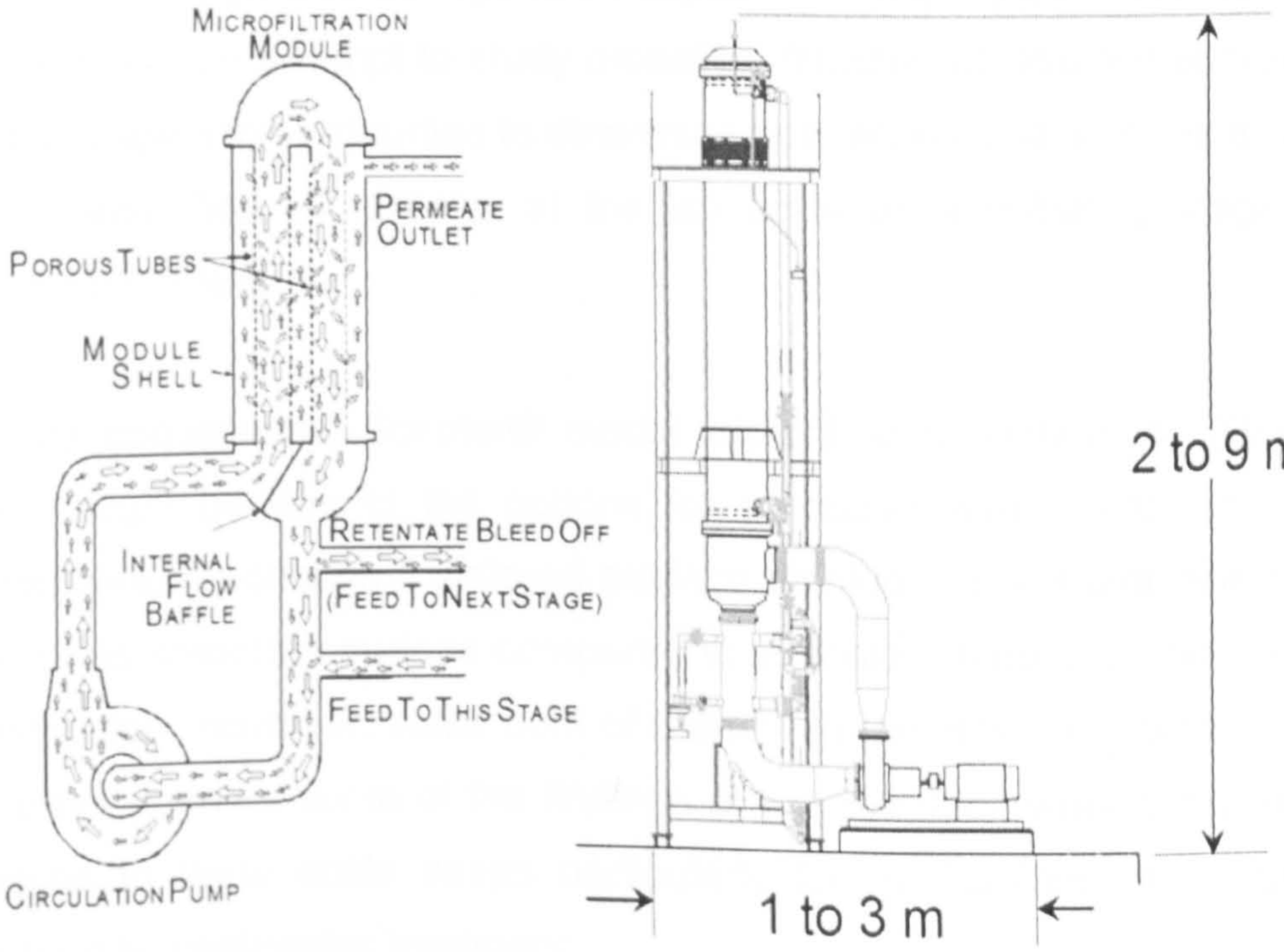

Figure 8.1 : Scepter® model microfiltration technology (Graver Technologies).

8.4 Concluding remarks

Although the motive behind this research project came from a real case study, the economical feasibility of such a system in large scale is beyond the scope of our investigation objectives since the economic aspects depend on several variables and resources. These parameters, including the complexity of feed composition, would require a crossflow filtration pilot plant in the oilfield to treat the produced water for a long term. Also, the water resources, such in Kuwait, are inadequate and using aquifer water mostly for reinjection to maintain the pressure build up in oil wells would be not acceptable in the long run.

In addition, it is already forecasted that the produced water amount would increase as the oil well age increased. Therefore, from a design point of view, a number of future produced water plants will be needed for oil and suspended solid removal. Furthermore, design and consultancy companies have already proposed that filtration technology might be needed at some stage in the future as part of wastewater treatment and injection plant facilities without providing any details with regard to the design and configuration aspects of such system. Hence, this research project was an attempt to study crossflow filtration at different operating conditions and suspension properties to determine at a technical level if it is a valid alternative for emulsified oil removal at the lab scale as a polishing stage for produced water treatment.

For large scale applications, Scepter® model microfiltration technology (Graver Technologies) might be one of the options for produced water treatment in a hostile environment. It contains a sintered titanium dioxide active membrane on a porous, which has smoother surface compared to zirconia membrane used in the current investigation. However, since both of them were ceramic membranes with hydrophilic active surface, some of the findings of this research work at lab scale could be linked to large scale cases particularly for applications of inorganic membranes for oily wastewater treatment .

CHAPTER 9

CONCLUSIONS

9.1 Overall Conclusions

Produced water handling facilities for injection form an essential component of numerous current oilfield plans. Analyses of produced water and formation water characteristics carried out as part of this work aided identification of the most significant parameters that might influence, such as suspended solids and emulsified oil droplets, the injection rate. With respect to formation or pore plugging, the excess quantity of solid particles and oil droplets, oily solid particles, and any other hydrocarbon deposits (Schmoo) could result in fouling and then formation damage. In order to handle such concerns a train of not only pre-treatments such as coagulation, flocculation, and demulsification, is required but also process and equipment such as skim tanks, oily plate separators, gas flotation, and/or hydrocyclones. However, from the case study data, it was found that the injection upper limits for particle size distribution were exceeded for micron sized particles (2-10 μm). To deal with this challenging parameter (size distribution), among the practical treatments that could be used for removal of oil droplets with that size distribution range is crossflow microfiltration.

For produced water reinjection, environmental and operational regulations are stringent, with the maximum allowable disposable concentration for oil (10 mg L^{-1}) and suspended solids (5 mg L^{-1}) for reinjection into the formation. The provision of treated produced water in the desired quality and quantity for both reinjection and disposal purposes is a challenging problem in onshore and offshore oilfields. In the past few decades, as a result of being compact, scalable and durable, membranes have emerge as a possible alternative for produced water treatment, particularly as a polishing stage. An inherent problem of implementation of membranes as separation systems is concentration polarization and the cake formation due to solute rejection by size exclusion. Consequently, a sharp decline in filtration

performance happens and cleaning processes are required, which leads to additional cost for operating such system.

Crossflow Microfiltration has been demonstrated experimentally to be a practical approach for removal of emulsified oil droplets in the size range of 0.1-10 µm from their feed emulsions. However, the use of crossflow microfiltration has been limited as a result of permeation flux decline due to concentration polarization and fouling. Hence, identification of the critical flux, where to operate below it appears that there is no significant fouling, became vital. Therefore, filtration experiments were conducted at different emulsion properties and at different operating conditions to investigate the effect of each parameter on the critical flux. The method used to determine critical flux the was step by step technique (constant TMP). Although the focus of this thesis was toward crossflow microfiltration of emulsified oil droplets from produced water, its findings might be applicable to other oily wastewater streams at comparable conditions.

Despite the introduction of the critical flux concept nearly decade and a half ago, there is still some ambiguity around the relevant meaning of the critical flux. It was identified to be the commencement of fouling or noticeable fouling, and the start of irreversible fouling or the beginning of particle deposition. This imprecision was eradicated by stating that the definition of critical flux is a function of the measurement technique used. Since the method used in this work was flux monitoring (constant TMP stepping) technique depends on detection of hydrodynamic resistance variations and thus the critical flux would be linked to the onset of fouling, where a decline in filtration performance occurs. Hence, the kind of critical flux selected has to be stated clearly, and is determined based on the area under investigation. Since the interest of this research work was associated with the instantaneous decrease in the filtration performance, the TMP step by step method was chosen to detect critical flux as a measure for inception of fouling.

Crossflow velocities, oil and surfactant concentrations, ionic strength and pH effects on equilibrium permeate flux and critical flux were studied. An improvement in the equilibrium permeate fluxes was demonstrated when the crossflow velocity

of the oil in water emulsion was increased. Whereas, when feed oil concentrations increased, equilibrium permeate fluxes declined. For all oil in water emulsions filtered, critical flux (J_{crit}) values increased proportionally with the crossflow velocity. The J_{crit} increase with crossflow velocity was most noticeable at lowest oil feed concentration along with the highest crossflow velocity. Conversely, the least critical flux value was reached when filtering oil emulsion with the highest oil concentration together with the lowest crossflow velocity. These two behaviours have been encountered in the crossflow microfiltration of suspended solids and proteins suspensions. In relation to surfactant present in the feed, when it was not added, a decline in the critical flux value occurred. Whilst when surfactant was added as an emulsifier, an increase in the critical flux value was noticed.

When the ionic strength for the feed emulsions was increased by the addition of NaCl salt, the permeate flux declined. However, when the ionic strength for the feed emulsions was increased by the addition of $CaCl_2$ or $FeCl_3$ salts, the permeate flux also increased. These paradoxical observations are discussed by relating ion valency and ionic strength effects on particle-membrane and particle-particle interactions corresponding to filtration process. The experimental results encountered in this study appeared to support the concept that both hydrodynamics, i.e. crossflow velocity and particle-particle or particle-membrane interactions have impact on equilibrium flux. These observations were examined and discussed at different hydrodynamic conditions and with different oil-in-water emulsion's properties. The effect of ion valency on critical flux for oil-in-water emulsion might be contribution to the new knowledge.

Particle back transport models such as torque balance model, inertial lift model, and shear-induced diffusion model, were compared to experimental data where particle size was used as a fitting parameter at different oil feed concentration and wall shear stresses. The torque balance over predicted by three orders of magnitude of the experimental fluxes, while the inertial lift model under predicted by one order of magnitude. However, the shear-induced model showed a better prediction for the experimental data. The 'fitted' particle sizes were in the lower ranges of the measured feed particle size distributions, suggesting that these smaller particles were responsible for the initial permanent particle fouling on the

membrane surface at J_{crit}. It is difficult to provide proof directly by experiment because of the lack of ability to visualise and size particles resting on the membrane in situ in the filter. In particular for oily wastewater streams, where the measured particle size distribution of feed emulsions was in the range 0.1-10 μm.

In the current investigation, the critical parameter (J_{crit}/τ_w) was not found linear, which in disagreement with the findings of a number of previous research works, where the measured particle sizes were kept invariant and not influenced by the increase in the shear rate. However, there were few researchers who encountered similar behaviour of nonlinearity of the critical parameter (J_{crit}/τ_w) for flocculated feed, where they attributed that to the change of particle size as result on the increase in the shear rate, particularly those of loosely flocculated. Thus, correlation between critical flux the product of the wall shear stress and the critical particle size was investigated on the basis of a number of most commonly used models.

Surface transport model appeared to put forward more reasonable prediction and showed linear relationship with consistency for modified critical parameter $J_{crit}/(\tau_w * a_{crit})$. Furthermore, shear-induced model seemed to provide another interesting critical parameter $J_{crit}/(\tau_w * a_{crit}^{4/3})$, where it showed prefect constancy and was only function of oil feed concentration. This new development of the critical parameter correlation by incorporating the critical particle size seemed to be more appropriate for crossflow microfiltration of polydispersed feed stocks such as oil-in-water emulsions.

On the other hand, for deposition rate modelling, the Song and Elimelech Model (SEM) under predicted permeate fluxes when the cake layer is formed after approaching the critical flux value. This model deficiency was thought to be attributable to estimation of solute mass transport was based only on the Brownian diffusion. Nevertheless, a shear-induced diffusion needed to be incorporated in SEM model since the calculated critical particle size was in sub-micron in radius, where both Brownian and shear-induced diffusions appeared to be influential. Therefore, an effective diffusion coefficient composed of the sum of Brownian and shear-induced diffusions has been introduced. As result of such modification in

SEM model, at the cake layer formation region (after reaching the critical flux condition) a better permeate flux's prediction in comparison with the experimental results has been observed.

The uniqueness of this research project arises mostly from the real case study data, the experimental results based on a programme of work formulated around the data, and the subsequent modelling. The analysis reports of a real produced water were collected from newly commissioned plants (2004) for downstream treatment of the increased produced water and injection. In particular, there is a lack of information availability or accessibility for academic researchers for the produced water characteristics and analysis' reports from the industry due to issues related to the data confidentiality. Certainly, the case study puts on the creates a challenging question about the appropriate method of removal of emulsified oil droplets with average micron size range.

The experimental work tried to answer and address this challenging question by application of crossflow microfiltration of oil-in-water emulsions, using a multi-channel ceramic membrane at different operating conditions and emulsion's properties. According to the published literature. The unique combination of oil-surfactant-water emulsion (n-dodecane-sorbitan monoleate (Span 80)-water) was never used before as a feed stocks for filtration unit or investigated as synthetic representative produced water. However, in order to avoid fouling the membrane, the main drawback for the use of membrane filtration, the system needs to operate below the critical flux value, which was determined experimentally using step by step technique (constant TMP). Although the step by step method for measuring critical flux (wither at constant TMP or at constant flux) has been investigated in many applications, the use of such method described in this work was limited or not existed for oil-in-water emulsion applications.

For the modelling of experimental results in this research work, the unique applications of the back transport models (such as torque balance, inertial lift, and shear-induced models) and deposition rate models such as SEM model in the area of liquid-liquid separations could be considered a contribution to new knowledge. For the experimental critical flux results, the shear-induced model showed a better prediction in comparison with the other back transport models.

While for equilibrium fluxes at cake formation region (after reaching the critical flux), the modified SEM model demonstrated a better forecasting of the experimental data compared to the SEM model. For new improvement of critical parameters $J_{crit}/(\tau_w * a_{crit})$ and $J_{crit}/(\tau_w * a_{crit}^{4/3})$ contribution to new knowledge might be claimed.

CHAPTER 10

Future Work and Recommendations

8.1 Future Work and Recommendations

Regarding the Kuwait West case study, further investigation is still needed to try to find relationships among the eleven operating parameters listed in the effluent data which was collected for a whole year of plant operation with more than 1000 measured samples for monitoring purposes. An appealing thought would be an application of neural networks technique to relate these variables and interpret their correlations. Also, statistical methods such principal component analysis (PCA) could be implemented to the effluent data to identify the relationships between these operating parameters and their effects in the performance of the water re-injection plant that has been commissioned on 2004.

Regarding the experimental part, it would be a motivating idea to perform similar filtration tests with real produced water rather than synthetic produced water by using a tubular multi-channel ceramic (zirconia) membrane model. Also, setting up a membrane pilot plant close to the oil field wells would facilitate further investigation of crossflow filtration of oil from produced water. There are a wide range of ceramic membrane in terms of materials and configurations that could be studied experimentally for produced water filtration. For example, membranes that have a star shape channel and made of γ-alumina material or any other new ceramic membrane element such as the Sceptor membrane (titanium oxide membrane form Graver technologies). Furthermore, there are new modules of ceramic membrane and metal membrane available today in the ultrafiltration market, which could be investigated for oily wastewater treatment applications.

Implementations of the other measuring techniques of critical flux such as constant flux stepping, the DOTM, mass balance, and fouling rate methods in crossflow microfiltration of oil-in-water emulsion would be interesting to examine their

claimed merits and their measurement accuracy. For the TMP stepping method used in this work the step duration was short, it might be an appealing idea to repeat these flirtation tests for long periods to identify whether critical flux point would change drastically. For industrial applications, identification of sustainable flux seemed to be more appropriate than the critical flux concept. Therefore, it is recommended to conduct similar experimental investigations to determine sustainable flux for crossflow microfiltration of oil-in-water emulsions.

Visualization experiments using a high speed video camera to record the behaviour dynamics of emulsified oil droplets near to the membrane surface would give insight into the process. The visual observations of emulsified oil droplet transport mechanisms at different oil concentrations, crossflow velocities, and ionic strengths would assist in validating or invalidating various interpretations presented in this experimental study. Also, the effects of adding various types of surfactants on filterability of oil in water emulsions still need further investigation.

The effects of addition of both mono-valent and poly-valent salts at various concentrations on the filtration performance for oil in water emulsions have not been examined here and might be an interesting topic of future work. Also, on the subject of the prediction models for crossflow microfiltration of oil from water, there is a deficiency in the existing models for permeate fluxes due to them not being able include the ionic strength and pH effect. Most of the developed models for permeate flux prediction in crossflow microfiltration appeared to be macroscopic models, while there were few of them microscopic models. Hence, experimental verifications of these microscopic models would be a good recommendation for future work.

Despite of the complexity of crossflow microfiltration of oil from produced water due to its composition, it will continue to be one of most demanding areas of research for many years to come due to its economical potential. Moreover, oil prices have gone up drastically and the demands for this valuable source of energy have increased recently, and for some wells the production rate has reached its maximum possible value. Also, the quantity of oil reserves are decreasing sharply, and thus each barrel of oil recovered from treated produced

water would be more profitable and precious. Therefore, any scientific breakthrough on the secondary oil recovery separation methods such as filtration could be a point of phase transition in crude oil effluent treatments.

Reference:

AKAY, G. and WAKEMAN, R.J., 1994. Mechanisms of permeate flux decay, solute rejection and concentration polarisation in crossflow filtration of a double chain ionic surfactant dispersion. *Journal of Membrane Science,* **88**(2-3), pp. 177-195.

API, 2000, Overview of Exploration and Production Waste Volumes and Waste Management Practices in the United States, ICF Consulting for the American Petroleum Institute, Washington, DC.

BACCHIN, P., AIMAR, P. and FIELD, R.W., 2006. Critical and sustainable fluxes: Theory, experiments and applications. *Journal of Membrane Science,* **281**(1-2), pp. 42-69.

BACCHIN, P., 2004. A possible link between critical and limiting flux for colloidal systems: consideration of critical deposit formation along a membrane. *Journal of Membrane Science,* **228**(2), pp. 237-241.

BACCHIN, P. and AIMAR, P., 2005. Critical fouling conditions induced by colloidal surface interaction: from causes to consequences. *Desalination,* **175**(1), pp. 21-27.

BACCHIN, P., AIMAR, P. and SANCHEZ, V., 1995. Model for colloidal fouling of membranes. *AIChE J.*, **41**, pp. 368-377.

BACCHIN, P., AIMAR, P. and SANCHEZ, V., 1996. Influence of surface interaction on transfer during colloid ultrafiltration. *Journal of Membrane Science,* **115**(1), pp. 49-63.

BACCHIN, P., MEIRELES, M. and AIMAR, P., 2002. Modelling of filtration: from the polarised layer to deposit formation and compaction. *Desalination,* **145**(1-3), pp. 139-146.

BAKER, R.J., FANE, A.G., FELL, C.J.D. and YOO, B.H., 1985. Factors Affecting Flux in Crossflow Filtration. *Desalination,* **53**, pp. 81-93.

BARUAH, G.L. and BELFORT G., 2003. A Predictive Aggregate Transport Model for Microfiltration of Combined Macromolecular Solutions and Poly-Disperse suspensions: Model Development. *Biotechnol. Prog. 2003,* **19**, pp. 1524-1532.

BENNETT, G.F., 1988. The removal of oil from wastewater by air flotation: a review. *CRC Critical Rev. Environ. Control* **18** (3), pp. 189–253.

BHATTACHARJEE, S., KIM, A.S. and ELIMELECH, M., 1999. Concentration Polarization of Interacting Solute Particles in Cross-Flow Membrane Filtration. *Journal of Colloid and Interface Science,* **212**(1), pp. 81-99.

BELFORT, G., DAVIS, R.H. and ZYDNEY, A.L., 1994/11/28. The behavior of suspensions and macromolecular solutions in crossflow microfiltration. *Journal of Membrane Science,* **96**(1-2), pp. 1-58.

BILSTAD, T., and ESPEDAL, E., 1996. Membrane separation of produced water. *Water Science & Technology,* **34**(9), pp. 239-246.

BLAKE, N.J., CUMMING, I.W. and STREAT, M., 1992. Prediction of steady state crossflow filtration using a force balance model. *Journal of Membrane Science,* **68**(3), pp. 205-215.

BOWEN, W.R. and JENNER, F., 1995. Theoretical descriptions of membrane filtration of colloids and fine particles: An assessment and review. *Advances in Colloid and Interface Science,* **56**, pp. 141-200.

BROMLEY, A.J., HOLDICH, R.G. and CUMMING, I.W., 2002. Particulate fouling of surface microfilters with slotted and circular pore geometry. *Journal of Membrane Science,* **196**(1), pp. 27-37.

CHAN, R. and CHEN, V., 2001. The effects of electrolyte concentration and pH on protein aggregation and deposition: critical flux and constant flux membrane filtration. *Journal of Membrane Science,* **185**(2), pp. 177-192.

CHELLAM, S. and WIESNER, M.R., 1998. Evaluation of crossflow filtration models based on shear-induced diffusion and particle adhesion: Complications induced by feed suspension polydispersivity. *Journal of Membrane Science,* **138**(1), pp. 83-97.

CHEN, V., 1998/9/2. Performance of partially permeable microfiltration membranes under low fouling conditions. *Journal of Membrane Science,* **147**(2), pp. 265-278.

CHEN, V., FANE, A.G., MADAENI, S. and WENTEN, I.G., 1997. Particle deposition during membrane filtration of colloids: transition between concentration polarization and cake formation. *Journal of Membrane Science,* **125**(1), pp. 109-122.

CHEN, V., 1998. Performance of partially permeable microfiltration membranes under low fouling conditions. *Journal of Membrane Science,* **147**(2), pp. 265-278.

CHERYAN, M. and RAJAGOPALAN, N., 1998. Membrane processing of oily streams. Wastewater treatment and waste reduction. *Journal of Membrane Science,* **151**(1), pp. 13-28.

CHIU, T.Y. and JAMES, A.E., 2006/6/1. Microfiltration of amphoteric surfactant using ceramic membranes. *Colloids and Surfaces A: Physicochemical and Engineering Aspects,* **280**(1-3), pp. 58-65.

CIARAPICA, F.E. and GIACCHETTA, G. , 2003. The treatment of produced water in offshore Rig: Comparison between Tradition Installations and Innovative Systems. The Fifth International Membrane Science & Technology Conference, University of New South Wales, Sydney, Australia.

DAVIS, R.H. and LEIGHTON, D.T., 1987. Shear-induced transport of a particle layer along a porous wall. *Chemical Engineering Science,* **42**(2), pp. 275-281.

DAVIS, R.H. and SHERWOOD, J. D., 1990. A similarity solution for steady-state crossflow microfiltration. *Chem. Eng. Sci.* **45**(11), pp. 3203–3209.

DEFRANCE, L. and JAFFRIN M., Y., 1999. Comparison between filtrations at fixed transmembrane pressure and fixed permeate flux : application to a membrane bioreactor used for wastewater treatment *Journal of Membrane Science,* **152** (2), pp. 203-210.

DHARMAPPA, H.B., VERNIK, J., R. BEN AIM, R., YAMAMOTO, K. and VIGNESWARAN, 1992. A comprehensive model for crossflow filtration incorporating polydispersity of the influent. *Journal of Membrane Science* **65**, pp. 173-185

ELZO, D., HUISMAN, I., MIDDELINK, E. and GEKAS, V., 1998. Charge effects on inorganic membrane performance in a cross-flow microfiltration process. *Colloids and Surfaces A: Physicochemical and Engineering Aspects,* **138**(2-3), pp. 145-159.

ESPINASSE, B., BACCHIN, P. and AIMAR, P., 2002. On an experimental method to measure critical flux in ultrafiltration. *Desalination,* **146**(1-3), pp. 91-96.

FAIBISH, R. S., ELIMELECH, M., and COHEN, Y., 1998. Effect of Interparticle Electrostatic Double Layer Interactions on Permeate Flux Decline in Crossflow Membrane Filtration of Colloidal Suspensions: An Experimental Investigation. *J. Colloid Interface Sci.* **204**, pp.77.

FAN, S. and WANG, J., 2000. Treatment of oil-containing wastewater with an inorganic membrane. *Journal of Dalian university of Technology.* pp. 61-63

FIELD, R.W., WU, D., HOWELL, J.A. and GUPTA, B.B., 1995. Critical flux concept for microfiltration fouling. *Journal of Membrane Science,* **100**(3), pp. 259-272.

FRADIN, B. and FIELD, R.W., 1999. Crossflow microfiltration of magnesium hydroxide suspensions: determination of critical fluxes, measurement and modelling of fouling. *Separation and Purification Technology,* **16**(1), pp. 25-45.

GANDER, M., JEFFERSON, B. and JUDD, S., 2000. Aerobic MBRs for domestic wastewater treatment: a review with cost considerations. *Separation and Purification Technology,* **18**(2), pp. 119-130.

GÉSAN-GUIZIOU, G., BOYAVAL, E. and DAUFIN, G., 1999. Critical stability conditions in crossflow microfiltration of skimmed milk: transition to irreversible deposition. *Journal of Membrane Science,* **158**(1-2), pp. 211-222.

GÉSAN-GUIZIOU, G., DAUFIN, G., and MERIN, U., 1995. Performance of whey crossflow microfiltration during transient and stationary operating conditions. *Journal of Membrane Science,* **104**, pp. 271–281.

GÉSAN-GUIZIOU, G., DAUFIN, G., and BOYAVAL, E., 2000. Critical stability conditions in skimmed milk crossflow microfiltration: impact on operating modes. *Lait,* **80**, pp. 129–138.

GÉSAN-GUIZIOU, G., WAKEMAN, R.J. and DAUFIN, G., 2002. Stability of latex crossflow filtration: cake properties and critical conditions of deposition. *Chemical Engineering Journal,* **85**(1), pp. 27-34.

GRANDISON, A., YOURAVONG, W., and LEWIS, M.J., 2000. Hydrodynamic factors affecting flux and fouling during ultrafiltration of skimmed milk. *Lait,* **80**, pp. 165–174.

GREEN, G. and BELFORT, G., 1980. Fouling of ultrafiltration membranes: lateral migration and the particle trajectory model. *Desalination,* **35**, pp. 129-147.

HOWELL, J.A., 1995. Sub-critical flux operation of microfiltration. *Journal of Membrane Science,* **107**(1-2), pp. 165-171.

HUA, F.L., TSANG, Y.F., WANG, Y.J., CHAN, S.Y., CHUA, H. and SIN, S.N., 2007. Performance study of ceramic microfiltration membrane for oily wastewater treatment. *Chemical Engineering Journal,* **128**(2-3), pp. 169-175.

HUISMAN, I.H., DUTRÉ, B., PERSSON, K.M. and TRÄGÅRDH, G., 1997. Water permeability in ultrafiltration and microfiltration: Viscous and electroviscous effects. *Desalination,* **113**(1), pp. 95-103.

HUISMAN, I.H., 1999. Particle transport in crossflow microfiltration – I. Effects of hydrodynamics and diffusion. *Chemical Engineering Science,* **54**(2), pp. 271-280.

HUISMAN, I., TRÄGÅRDH, G. and TRÄGÅRDH, C., 1999. Particle transport in crossflow microfiltration – II. Effects of particle–particle interactions. *Chemical Engineering Science,* **54**(2), pp. 281-289.

HUISMAN, I., VELLENGA, E., TRÄGÅRDH, G. and TRÄGÅRDH, C., 1999. The influence of the membrane zeta potential on the critical flux for crossflow microfiltration of particle suspensions. *Journal of Membrane Science,* **156**(1), pp. 153-158.

JEFFERSON, B., BROOKES, A., Le Clech, P., and JUDD, S.J., 2004. Methods for understanding organic fouling in MBRs, *Water Sci. Technol.* **49**, pp. 237–244.

KIM, J., AKEPRATHUMCHAI, S. and WICKRAMASINGHE, S.R., 2001. Flocculation to enhance microfiltration. *Journal of Membrane Science,* **182**(1-2), pp. 161-172.

KWON, D.Y., VIGNESWARAN, S., FANE, A.G. and AIM, R.B., 2000. Experimental determination of critical flux in cross-flow microfiltration. *Separation and Purification Technology,* **19**(3), pp. 169-181.

KWON, D.Y. and VIGNESWARAN, S., 1998. Influence of particle size and surface charge on critical flux of crossflow microfiltration. *Water Science and Technology,* **38**(4-5), pp. 481-488.

LE CLECH, P., JEFFERSON, B., CHANG, I.S. and JUDD, S.J., 2003. Critical flux determination by the flux-step method in a submerged membrane bioreactor. *Journal of Membrane Science,* **227**(1-2), pp. 81-93.

LEE, S., AURELLE, Y. and ROQUES, H., 1984. Concentration polarization, membrane fouling and cleaning in ultrafiltration of soluble oil. *Journal of Membrane Science,* **19**(1), pp. 23-38.

LEE, Y. and CLARK, M.M., 1998. Modeling of flux decline during crossflow ultrafiltration of colloidal suspensions. *Journal of Membrane Science,* **149**(2), pp. 181-202.

LI, H., FANE, A.G., COSTER, H.G.L. and VIGNESWARAN, S., 2000. An assessment of depolarisation models of crossflow microfiltration by direct observation through the membrane. *Journal of Membrane Science,* **172**(1-2), pp. 135-147.

LI, H., FANE, A.G., COSTER, H.G.L. and VIGNESWARAN, S., 1998. Direct observation of particle deposition on the membrane surface during crossflow microfiltration. *Journal of Membrane Science,* **149**(1), pp. 83-97.

LI, W., XING, W. and XU, N., 2006. Modeling of relationship between water permeability and microstructure parameters of ceramic membranes. *Desalination,* **192**(1-3), pp. 340-345.

LOJKINE, MH., FIELD, RW, and HOWELL, JA., 1992. Crossflow Microfiltration OF CeLL SUSPeNSIONS: A Review OF Models With Emphasis ON Particle Size Effects. *TransICHemE,* **70**(Part C), pp. 149-164.

LOBO, A., CAMBIELLA, Á, BENITO, J.M., PAZOS, C. and COCA, J., 2006. Ultrafiltration of oil-in-water emulsions with ceramic membranes: Influence of pH and crossflow velocity. *Journal of Membrane Science,* **278**(1-2), pp. 328-334.

LU, W. and JU, S., 1989. Selective Particle Deposition in Crossflow Filtration. *Separation Science and Technology,* **24** (7-8), pp. 517-540.

MADAENI, S.S., 1997. The effect of operating conditions on critical flux in membrane filtration of activated sludge. *J. Chem. Techno. Biotechnol.* **74**, pp. 539–543.

MADAENI, S.S., FANE, A.G. and WILEY, D.E., 1999. Factors influencing critical flux in membrane filtration of activated sludge. *Transactions of the IChemE,* **74**(B), pp. 539–543.

MÄNTTÄRI, M. and NYSTRÖM, M., 2000. Critical flux in NF of high molar mass polysaccharides and effluents from the paper industry. *Journal of Membrane Science,* **170**(2), pp. 257-273.

METSÄMUURONEN, S., HOWELL, J. and NYSTRÖM, M., 2002. Critical flux in ultrafiltration of myoglobin and baker's yeast. *Journal of Membrane Science,* **196**(1), pp. 13-25.

MILCENT, S. and CARRÈRE, H., 2001. Clarification of lactic acid fermentation broths. *Separation and Purification Technology,* **22-23**, pp. 393-401.

MOHAMMADI, T., PAK, A. KARBASSIAN, M. and GOLSHAN, M., 2004. Effect of operating conditions on microfiltration of oil-water emulsion by a kaolin membrane. *Desalination*, **168**, PP. 201.

MONDOR, M. and MORESOLI, C., 2002. Shear-induced hydrodynamic diffusion model for cross-flow microfiltration: role of the particle volume fraction. *Desalination,* **145**(1-3), pp. 123-128.

MORITZ, S., BENFER, P., ÁRKI, G. TOMANDI, 2001. Investigation of ceramic membrane materials by streaming potential measurements. *Colloids & Surfaces A: Physicochemical and Engineering Aspects,* **195**, pp. 25.

MUELLER, J., CEN, Y. and DAVIS, R.H., 1997. Crossflow microfiltration of oily water. *Journal of Membrane Science,* **129**(2), pp. 221-235.

NEAL, P.R., LI, H., FANE, A.G. and WILEY, D.E., 2003. The effect of filament orientation on critical flux and particle deposition in spacer-filled channels. *Journal of Membrane Science,* **214**(2), pp. 165-178.

OHYA, H., KIM, J.J., CHINEN, A., AIHARA, M., SEMENOVA, S.I., NEGISHI, Y., MORI, O. and YASUDA, M., 1998. Effects of pore size on separation mechanisms of microfiltration of oily water, using porous glass tubular membrane. *Journal of Membrane Science,* **145**(1), pp. 1-14.

OLIVEIRA, R.C.G., GONZALEZ, G. and OLIVEIRA, J.F., 1999. Interfacial studies on dissolved gas flotation of oil droplets for water purification. *Colloids and Surfaces A: Physicochemical and Engineering Aspects,* **154**(1-2), pp. 127-135.

PALECEK, S.P. and ZYDNEY, A.L., 1994. Hydraulic permeability of protein deposits formed during microfiltration: effect of solution pH and ionic strength. *Journal of Membrane Science,* **95**(1), pp. 71-81.

PATTERSON, J.W., 1985. Industrial Wastewater Treatment Technology. Edition: 2, Butterworths, Stoneham, MA.

PERSSON, A., JONSSON, A.S. and ZACCHI, G. , 2001. Separation of lactic acid-producing bacteria from fermentation broth using a ceramic microfiltration membrane with constant permeate flow. *Biotechnol. Bioeng.* **72**, pp. 269–277.

United Kingdom Department of Trade and Industry, 1997. The Energy Report Oil and Gas Resources of the United Kingdom.

RAUTENBACH, R. and SCHOCK, G., 1988. Ultrafiltration of macromolecular solutions and cross-flow microfiltration of colloidal suspensions. A contribution to permeate flux calculations. *Journal of Membrane Science,* **36**, pp. 231-242.

REAY, D. and Ratcliff, G.A.,1973. Removal of fine particles from water by dispersed air flotation: effects of bubble size and particle size on collection efficiency. *Can. J. Chem. Eng.* **51**, pp. 178–185.

RIEGELMAN, S., and PICHON, G., 1962. A critical re-evaluation of factors affecting emulsion stability. I. The hydrophilic-lipophilic balance postulate. *American Perfumer and Essential Oil Review.* **77**, pp. 31-33.

RIESMEIER, B., KRONER, K.H. and KULA, M.R., 1987. Studies on secondary layer formation and its characterization during cross-flow filtration of microbial cells. *Journal of Membrane Science,* **34**(2), pp. 245-266.

RICHARDSON, J.F. and BACKHURST, J.R., 2002. Coulson and Richardson's Chemical Engineering. Butterworth Heinemann, Oxford.

RIPPERGER, S. and ALTMANN, J., 2002. Crossflow microfiltration – state of the art. *Separation and Purification Technology,* **26**(1), pp. 19-31.

ROMERO, C.A. and DAVIS, R.H., 1988. Global model of crossflow microfiltration based on hydrodynamic particle diffusion. *Journal of Membrane Science,* **39**, pp. 157-185.

ROMERO, C.A. and DAVIS, R.H., 1991. Experimental verification of the shear-induced hydrodynamic diffusion model of crossflow microfiltration. *Journal of Membrane Science,* **62**(3), pp. 249-273.

RUSHTON, A, WARD, S, HOLDICH, R.G., 1995. Solid-Liquid Filtration and Separation Technology. VCH, Germany.

SCHRAMM, L.L., 1992. Emulsions Fundamental and Applications in the Petroleum Industry, The American Chemical Society.

SHAW, D.J., 1992. Introduction to Colloid and Surface Chemistry. Edition: 4, Butterworth-Heinemann.

ŠMÍDOVÁ, D., MIKULÁŠEK, P., WAKEMAN, R. and VELIKOVSKÁ, P., 2004. Influence of ionic strength and pH of dispersed systems on microfiltration. *Desalination,* **163**(1-3), pp. 323-332.

SONG, L. and ELIMELECH, M., 1995. Particle Deposition onto a Permeable Surface in Laminar Flow. *Journal of colloid and interface science,* **173**(1), pp. 165-180.

SONG, L. and ELIMELECH, M., 1995. Theory of Concentration Polarization in Crossflow Filtration. *J. CHEM. SOC. FARADAY TRANS.,* **91**(19), pp. 3389-3398.

SRIJAROONRAT, P., JULIEN, E. and AURELLE, Y., 1999. Unstable secondary oil/water emulsion treatment using ultrafiltration: fouling control by backflushing. *Journal of Membrane Science,* **159**(1-2), pp. 11-20.

SUKI, A., FANE, A.G. and FELL, C.J.D., 1984. Flux decline in protein ultrafiltration. *Journal of Membrane Science,* **21**(3), pp. 269-283.

TAMBE, D. and SHARMA, M., 1993. Factors Controlling the Stability of Colloid-Stabilized Emulsions: I. An Experimental Investigation. *Journal of Colloid and Interface Science,* **157**(1), pp. 244-253.

TARLETON, E.S. and WAKEMAN, R.J., 1993. Understanding flux decline in crossflow microfiltration- Part 3:Effects of membrane morphology. *Trans. I Chem. E,* **71**(Part A), pp. 521.

TCHOBANOGLOUS, G., BURTON, F.L., 1991. Wastewater Engineering; Treatment Disposal; Reuse. Metcalf & Eddy, Inc., McGraw-Hill, New York.

TIEN, C., 2006. Introduction to Cake Filtration: Analyses, Experiments and Applications. Edition:1, Elsevier.

VEIL, J.A., PUDER, M.G., ELCOCK, D., and REDWEIK, R.J., 2004. A White Paper Describing Produced Water from Production of Crude Oil, Natural Gas, and Coal Bed Methane. ANL Report under DOE (NETL) Contract W-31-109-Eng-38.

VYAS, H.K., BENNETT, R.J. and MARSHALL, A.D., 2002. Performance of crossflow microfiltration during constant transmembrane pressure and constant flux operations. *International Dairy Journal,* **12**(5), pp. 473-479.

WAKEMAN, R.J., 1994. Visualization of cake formation in crossflow microfiltration. *Transactions of the IChemE,* **72**(A), pp. 530-540.

WAKEMAN, R.J. and TARLETON, E.S., 1999. Filtration: Equipment Selection, Modelling and Process Simulation, Elsevier Advanced Technology.

WAKEMAN, R.J. and TARLETON, E.S., 2005. Solid/Liquid separation: Principle of Industrial Filtration, Modelling and Process Simulation, Elsevier Advanced Technology.

WU, D., HOWELL, J.A. and FIELD, R.W., 1999. Critical flux measurement for model colloids. *Journal of Membrane Science,* **152**(1), pp. 89-98.

YOON, S., LEE, C., KIM, K. and FANE, A., 1999. Three-dimensional simulation of the deposition of multi-dispersed charged particles and prediction of resulting flux during cross-flow microfiltration. *Journal of Membrane Science,* **161**(1-2), pp. 7-20.

ZAIDI, K. and SIMMS, K., 1992, The use of micro/ultrafiltration for removal of oil and suspended solids from oilfields brines. *Water Science Technology.*

ZHANG, Y.P., FANE, A.G. and LAW, A.W.K., 2006. Critical flux and particle deposition of bidisperse suspensions during crossflow microfiltration. *Journal of Membrane Science,* **282**(1-2), pp. 189-197.

ZHAO, Y., TAN, Y., WONG, F., FANE, A.G. and XU, N., 2006. Formation of Mg(OH)2 dynamic membranes for oily water separation: effects of operating conditions. *Desalination,* **191**(1-3), pp. 344-350.

ZHAO, Y., TAN, Y., WONG, F., FANE, A.G. and XU, N., 2005. Formation of dynamic membranes for oily water separation by crossflow filtration. *Separation and Purification Technology,* **44**(3), pp. 212-220.

ZHAO, Y., ZHANG, Y., XING, W. and XU, N., 2005. Influences of pH and ionic strength on ceramic microfiltration of TiO2 suspensions. *Desalination,* **177**(1-3), pp. 59-68.

ZHAO, Y., XING, W., XU, N. and WONG, F., 2005. Effects of inorganic salt on ceramic membrane microfiltration of titanium dioxide suspension. *Journal of Membrane Science,* **254**(1-2), pp. 81-88.

ZOUBOULIS, A.I. and AVRANAS, A., 2000. Treatment of oil-in-water emulsions by coagulation and dissolved-air flotation. *Colloids and Surfaces A: Physicochemical and Engineering Aspects,* **172**(1-3), pp. 153-161.

ZHU, W., XIA, C., LIN, S., MENG, G., 2000. Cross-flow of an oily emulsion using alumina membranes. *Journal of Porous Media*, **3**(3).

ZYDNEY, A.L. and COLTON, C.K., 1986. A concentration polarization model for the filtrate flux in cross-flow microfiltration of particulate suspensions. *Chemical Engineering Communications,* **47,** pp. 3219-3224.

APPENDICES

Appendix A: Tabulated Step by Step Experimental Data

Appendix B: Experimental Plots for Critical Flux Determination

Appendix C: Case Study Data Reports

Appendix D: Matlab code for critical flux estimation

Appendix E: Publication Arising from the Research

Appendix A

Tabulated Step by Step Experimental Data

A summary of Filtration Experiments Conducted at different Operating Conditions and Emulsion Properties

Experiment	n-dodecane (oil model) Concentration (mg/L)	Sorbiton Monooleate Concentration (mg/L)	Crossflow Velocity (m/s)	NaCl (M)	$CaCl_2$ (M)	$FeCl_3$ (M)	pH
1	600	60	1.14	-	-	-	6
2	600	60	1.52	-	-	-	6
3	600	60	1.92	-	-	-	6
4	600	60	2.28	-	-	-	6
5	600	60	1.14	0.1	-	-	6
6	600	60	1.14	0.05	-	-	6
7	600	60	1.52	0.1	-	-	6
8	600	60	1.52	0.05	-	-	6
9	600	60	1.92	0.1	-	-	5.8
10	600	60	1.92	0.05	-	-	5.8
11	600	60	1.52	-	-	-	12
12	600	60	1.92	0.1	-	-	12
13	1200	120	1.14	-	-	-	5
14	1200	120	1.52	-	-	-	5
15	1200	120	1.92	-	-	-	5
16	1200	120	1.52	-	0.1	-	4.8
17	1200	120	192	-	0.05	-	4.8
18	2400	240	1.14	-	-	-	5
19	2400	240	1.52	-	-	-	5
20	2400	240	1.92	-	-	-	5
21	2400	240	2.28	-	-	-	5
22	2400	240	1.52	0.1	-	-	5
23	2400	240	1.52	-	0.1	-	6
24	2400	240	1.52	-	-	0.1	1.5
25	300	30	1.14	-	-	-	6
26	300	30	1.52	-	-	-	6
27	300	30	1.92	-	-	-	6
28	300	30	2.28	-	-	-	6

Tabulated Step by Step Test Data for 600 ppm Emulsion at Crossflow Velocity 1.14 m/s

Time(min)	P_f	*Pr*	*Pp*	*TMP(bar)*	*TMP(Pa)*	*Vol.(ml)*	*A (m2)*	*Flux(L/m²h)*
0	0.41	0.35	0.38	0	0	0	0.056854	0.00
4	0.41	0.35	0.35	0.03	3000	78	0.056854	20.58
8	0.41	0.35	0.35	0.03	3000	76	0.056854	20.05
12	0.41	0.35	0.35	0.03	3000	76	0.056854	20.05
16	0.41	0.35	0.35	0.03	3000	76	0.056854	20.05
20	0.41	0.35	0.35	0.03	3000	76	0.056854	20.05
24	0.41	0.35	0.3	0.08	8000	234	0.056854	61.74
28	0.41	0.35	0.3	0.08	8000	232	0.056854	61.21
32	0.41	0.35	0.3	0.08	8000	230	0.056854	60.68
36	0.41	0.35	0.3	0.08	8000	230	0.056854	60.68
40	0.41	0.35	0.3	0.08	8000	230	0.056854	60.68
44	0.41	0.35	0.25	0.13	13000	344	0.056854	90.76
48	0.41	0.35	0.25	0.13	13000	344	0.056854	90.76
52	0.41	0.35	0.25	0.13	13000	340	0.056854	89.70
56	0.41	0.35	0.25	0.13	13000	340	0.056854	89.70
60	0.41	0.35	0.25	0.13	13000	340	0.056854	89.70
64	0.41	0.35	0.2	0.18	18000	460	0.056854	121.36
68	0.41	0.35	0.2	0.18	18000	460	0.056854	121.36
72	0.41	0.35	0.2	0.18	18000	455	0.056854	120.04
76	0.41	0.35	0.2	0.18	18000	455	0.056854	120.04
80	0.41	0.35	0.2	0.18	18000	455	0.056854	120.04
84	0.41	0.35	0.14	0.24	24000	540	0.056854	142.47
88	0.41	0.35	0.14	0.24	24000	555	0.056854	146.43
92	0.41	0.35	0.14	0.24	24000	540	0.056854	142.47
96	0.41	0.35	0.14	0.24	24000	535	0.056854	141.15
100	0.41	0.35	0.14	0.24	24000	535	0.056854	141.15
104	0.41	0.35	0.14	0.24	24000	530	0.056854	139.83
108	0.41	0.35	0.14	0.24	24000	530	0.056854	139.83
112	0.41	0.35	0.08	0.3	30000	600	0.056854	158.30
116	0.41	0.35	0.08	0.3	30000	728	0.056854	153.66
120	0.41	0.35	0.08	0.3	30000	570	0.056854	150.39
124	0.41	0.35	0.08	0.3	30000	570	0.056854	150.39
128	0.41	0.35	0	0.38	38000	675	0.056854	178.09
132	0.41	0.35	0	0.38	38000	613	0.056854	161.73
136	0.41	0.35	0	0.38	38000	600	0.056854	158.30
140	0.41	0.35	0	0.38	38000	590	0.056854	155.66
144	0.41	0.35	0	0.38	38000	590	0.056854	155.66
148	0.41	0.35	0.1	0.28	28000	400	0.056854	105.53
152	0.41	0.35	0.1	0.28	28000	400	0.056854	105.53
156	0.41	0.35	0.1	0.28	28000	400	0.056854	105.53
160	0.41	0.35	0.2	0.18	18000	335	0.056854	70.71
164	0.41	0.35	0.2	0.18	18000	270	0.056854	71.24
168	0.41	0.35	0.2	0.18	18000	270	0.056854	71.24
172	0.41	0.35	0.33	0.05	5000	65	0.056854	17.15
176	0.41	0.35	0.33	0.05	5000	65	0.056854	17.15
180	0.41	0.35	0.33	0.05	5000	65	0.056854	17.15
184	0.41	0.35	0.38	0	0	0	0.056854	0.00

Tabulated Step by Step Test Data for 600 ppm Emulsion at Crossflow Velocity 1.52 m/s

Time(min)	P_f	Pr	Pp	TMP(bar)	TMP(Pa)	Vol.(ml)	A (m2)	Flux(L/m^2h)
0	0.71	0.61	0.66	0	0	0	0.056854	0
4	0.71	0.61	0.6	0.06	6000	142	0.056854	36.93672
8	0.71	0.61	0.6	0.06	6000	295	0.056854	36.93672
12	0.71	0.61	0.6	0.06	6000	440	0.056854	36.93672
16	0.71	0.61	0.6	0.06	6000	580	0.056854	36.93672
20	0.71	0.61	0.6	0.06	6000	721	0.056854	36.93672
23	0.71	0.61	0.55	0.11	11000	225	0.056854	78.79833
26	0.71	0.61	0.55	0.11	11000	225	0.056854	78.09477
29	0.71	0.61	0.55	0.11	11000	223	0.056854	77.39121
32	0.71	0.61	0.55	0.11	11000	223	0.056854	77.39121
35	0.71	0.61	0.55	0.11	11000	223	0.056854	77.39121
38	0.71	0.61	0.5	0.16	16000	325	0.056854	114.3279
41	0.71	0.61	0.5	0.16	16000	320	0.056854	114.3279
44	0.71	0.61	0.5	0.16	16000	320	0.056854	114.3279
47	0.71	0.61	0.5	0.16	16000	320	0.056854	114.3279
50	0.71	0.61	0.5	0.16	16000	320	0.056854	114.3279
53	0.71	0.61	0.44	0.22	22000	416	0.056854	151.2646
56	0.71	0.61	0.44	0.22	22000	410	0.056854	151.2646
59	0.71	0.61	0.44	0.22	22000	410	0.056854	151.2646
62	0.71	0.61	0.44	0.22	22000	410	0.056854	151.2646
65	0.71	0.61	0.44	0.22	22000	410	0.056854	151.2646
68	0.71	0.61	0.38	0.28	28000	485	0.056854	181.1658
71	0.71	0.61	0.38	0.28	28000	478	0.056854	179.4069
74	0.71	0.61	0.38	0.28	28000	478	0.056854	174.1302
77	0.71	0.61	0.38	0.28	28000	475	0.056854	174.1302
80	0.71	0.61	0.38	0.28	28000	470	0.056854	170.6124
83	0.71	0.61	0.38	0.28	28000	470	0.056854	170.6124
86	0.71	0.61	0.28	0.38	38000	555	0.056854	170.6124
89	0.71	0.61	0.28	0.38	38000	540	0.056854	214.5847
92	0.71	0.61	0.28	0.38	38000	518	0.056854	211.0669
95	0.71	0.61	0.28	0.38	38000	505	0.056854	209.3081
98	0.71	0.61	0.28	0.38	38000	500	0.056854	205.7903
101	0.71	0.61	0.28	0.38	38000	495	0.056854	204.0314
104	0.71	0.61	0.28	0.38	38000	495	0.056854	211.0669
107	0.71	0.61	0	0.66	66000	640	0.056854	200.5136
110	0.71	0.61	0	0.66	66000	575	0.056854	200.5136
113	0.71	0.61	0	0.66	66000	550	0.056854	258.557
116	0.71	0.61	0	0.66	66000	540	0.056854	239.2092
119	0.71	0.61	0	0.66	66000	515	0.056854	223.3792
122	0.71	0.61	0	0.66	66000	676	0.056854	219.8614
125	0.71	0.61	0	0.66	66000	490	0.056854	214.5847
128	0.71	0.61	0	0.66	66000	490	0.056854	211.0669
131	0.71	0.61	0.1	0.56	56000	398	0.056854	123.1224
134	0.71	0.61	0.1	0.56	56000	396	0.056854	123.1224
137	0.71	0.61	0.1	0.56	56000	526	0.056854	123.1224
140	0.71	0.61	0.1	0.56	56000	396	0.056854	86.18567
143	0.71	0.61	0.3	0.36	36000	344	0.056854	86.18567
146	0.71	0.61	0.3	0.36	36000	265	0.056854	86.18567
149	0.71	0.61	0.3	0.36	36000	260	0.056854	49.24895
152	0.71	0.61	0.3	0.36	36000	260	0.056854	49.24895
155	0.71	0.61	0.3	0.36	36000	260	0.056854	49.24895

Tabulated Step by Step Test Data for 600 ppm Emulsion at Crossflow Velocity 1.92 m/s

Time(min)	P_f	Pr	Pp	TMP(bar)	TMP(Pa)	Vol.(ml)	A (m2)	Flux(L/m^{2}h)
0	0.76	0.66	0.7	0	0	0	0.056854	0
3	0.76	0.66	0.65	0.05	5000	105	0.056854	36.93672
6	0.76	0.66	0.65	0.05	5000	105	0.056854	36.93672
9	0.76	0.66	0.65	0.05	5000	105	0.056854	36.93672
12	0.76	0.66	0.65	0.05	5000	105	0.056854	36.93672
15	0.76	0.66	0.65	0.05	5000	105	0.056854	36.93672
18	0.76	0.66	0.6	0.1	10000	224	0.056854	78.79833
21	0.76	0.66	0.6	0.1	10000	222	0.056854	78.09477
24	0.76	0.66	0.6	0.1	10000	220	0.056854	77.39121
27	0.76	0.66	0.6	0.1	10000	220	0.056854	77.39121
30	0.76	0.66	0.6	0.1	10000	220	0.056854	77.39121
33	0.76	0.66	0.54	0.16	16000	325	0.056854	114.3279
36	0.76	0.66	0.54	0.16	16000	325	0.056854	114.3279
39	0.76	0.66	0.54	0.16	16000	325	0.056854	114.3279
42	0.76	0.66	0.54	0.16	16000	325	0.056854	114.3279
45	0.76	0.66	0.54	0.16	16000	325	0.056854	114.3279
48	0.76	0.66	0.48	0.22	22000	430	0.056854	151.2646
51	0.76	0.66	0.48	0.22	22000	430	0.056854	151.2646
54	0.76	0.66	0.48	0.22	22000	430	0.056854	151.2646
57	0.76	0.66	0.48	0.22	22000	430	0.056854	151.2646
60	0.76	0.66	0.48	0.22	22000	430	0.056854	151.2646
63	0.76	0.66	0.42	0.28	28000	515	0.056854	181.1658
66	0.76	0.66	0.42	0.28	28000	510	0.056854	179.4069
69	0.76	0.66	0.42	0.28	28000	495	0.056854	174.1302
72	0.76	0.66	0.42	0.28	28000	495	0.056854	174.1302
75	0.76	0.66	0.42	0.28	28000	485	0.056854	170.6124
78	0.76	0.66	0.42	0.28	28000	485	0.056854	170.6124
81	0.76	0.66	0.42	0.28	28000	485	0.056854	170.6124
84	0.76	0.66	0.3	0.4	40000	610	0.056854	214.5847
87	0.76	0.66	0.3	0.4	40000	600	0.056854	211.0669
90	0.76	0.66	0.3	0.4	40000	595	0.056854	209.3081
93	0.76	0.66	0.3	0.4	40000	585	0.056854	205.7903
96	0.76	0.66	0.3	0.4	40000	580	0.056854	204.0314
99	0.76	0.66	0.3	0.4	40000	660	0.056854	211.0669
102	0.76	0.66	0.3	0.4	40000	570	0.056854	200.5136
105	0.76	0.66	0.3	0.4	40000	570	0.056854	200.5136
108	0.76	0.66	0	0.7	70000	735	0.056854	258.557
111	0.76	0.66	0	0.7	70000	680	0.056854	239.2092
114	0.76	0.66	0	0.7	70000	635	0.056854	223.3792
117	0.76	0.66	0	0.7	70000	625	0.056854	219.8614
120	0.76	0.66	0	0.7	70000	610	0.056854	214.5847
123	0.76	0.66	0	0.7	70000	600	0.056854	211.0669
126	0.76	0.66	0.3	0.4	40000	350	0.056854	123.1224
129	0.76	0.66	0.3	0.4	40000	350	0.056854	123.1224
132	0.76	0.66	0.3	0.4	40000	350	0.056854	123.1224
135	0.76	0.66	0.43	0.27	27000	245	0.056854	86.18567
138	0.76	0.66	0.43	0.27	27000	245	0.056854	86.18567
141	0.76	0.66	0.43	0.27	27000	245	0.056854	86.18567
144	0.76	0.66	0.56	0.14	14000	140	0.056854	49.24895
147	0.76	0.66	0.56	0.14	14000	140	0.056854	49.24895
150	0.76	0.66	0.56	0.14	14000	140	0.056854	49.24895

Tabulated Step by Step Test Data for 600 ppm Emulsion at Crossflow Velocity 2.28 m/s

Time(min)	P_f	*Pr*	*Pp*	*TMP(bar)*	*TMP(Pa)*	*Vol.(ml)*	*A (m2)*	*Flux(L/m^{2}h)*
0	0.94	0.71	0.88	0	0	0	0.056854	0
2	0.94	0.71	0.8	0.08	8000	120	0.056854	63.32008
4	0.94	0.71	0.8	0.08	8000	120	0.056854	63.32008
6	0.94	0.71	0.8	0.08	8000	120	0.056854	63.32008
8	0.94	0.71	0.8	0.08	8000	120	0.056854	63.32008
10	0.94	0.71	0.71	0.17	17000	270	0.056854	142.4702
12	0.94	0.71	0.71	0.17	17000	270	0.056854	142.4702
14	0.94	0.71	0.71	0.17	17000	270	0.056854	142.4702
16	0.94	0.71	0.71	0.17	17000	270	0.056854	142.4702
18	0.94	0.71	0.59	0.29	29000	480	0.056854	253.2803
20	0.94	0.71	0.59	0.29	29000	480	0.056854	253.2803
22	0.94	0.71	0.59	0.29	29000	480	0.056854	253.2803
24	0.94	0.71	0.59	0.29	29000	480	0.056854	253.2803
26	0.94	0.71	0.59	0.29	29000	480	0.056854	253.2803
28	0.94	0.71	0.5	0.38	38000	545	0.056854	287.5787
30	0.94	0.71	0.5	0.38	38000	545	0.056854	287.5787
32	0.94	0.71	0.5	0.38	38000	545	0.056854	287.5787
34	0.94	0.71	0.5	0.38	38000	545	0.056854	287.5787
36	0.94	0.71	0.4	0.48	48000	630	0.056854	332.4304
38	0.94	0.71	0.4	0.48	48000	620	0.056854	327.1538
40	0.94	0.71	0.4	0.48	48000	610	0.056854	321.8771
42	0.94	0.71	0.4	0.48	48000	608	0.056854	320.8218
44	0.94	0.71	0.4	0.48	48000	605	0.056854	319.2388
46	0.94	0.71	0.4	0.48	48000	600	0.056854	316.6004
48	0.94	0.71	0.4	0.48	48000	595	0.056854	313.9621
50	0.94	0.71	0.4	0.48	48000	592	0.056854	312.3791
52	0.94	0.71	0.4	0.48	48000	592	0.056854	312.3791
54	0.94	0.71	0.4	0.48	48000	592	0.056854	312.3791
56	0.94	0.71	0.05	0.83	83000	845	0.056854	445.8789
58	0.94	0.71	0.05	0.83	83000	820	0.056854	432.6872
60	0.94	0.71	0.05	0.83	83000	1160	0.056854	408.0628
62	0.94	0.71	0.05	0.83	83000	730	0.056854	385.1972
64	0.94	0.71	0.05	0.83	83000	720	0.056854	379.9205
66	0.94	0.71	0.05	0.83	83000	710	0.056854	374.6438
68	0.94	0.71	0.05	0.83	83000	700	0.056854	369.3672
70	0.94	0.71	0.05	0.83	83000	690	0.056854	364.0905
72	0.94	0.71	0.05	0.83	83000	675	0.056854	356.1755
74	0.94	0.71	0.05	0.83	83000	675	0.056854	356.1755
76	0.94	0.71	0.05	0.83	83000	675	0.056854	356.1755
78	0.94	0.71	0.42	0.46	46000	360	0.056854	189.9602
80	0.94	0.71	0.42	0.46	46000	360	0.056854	189.9602
82	0.94	0.71	0.42	0.46	46000	360	0.056854	189.9602
84	0.94	0.71	0.42	0.46	46000	360	0.056854	189.9602
86	0.94	0.71	0.7	0.18	18000	146	0.056854	77.03943
88	0.94	0.71	0.7	0.18	18000	146	0.056854	77.03943
90	0.94	0.71	0.7	0.18	18000	146	0.056854	77.03943
92	0.94	0.71	0.88	0	0	0	0.056854	0

Tabulated Step by Step Test Data for 600 ppm Emulsion in 0.1 M NaCl at Crossflow Velocity 1.14 m/s

Time(min)	P_f	Pr	Pp	TMP(bar)	TMP(Pa)	Vol.(ml)	A (m2)	Flux(L/m^{2}h)
0	0.38	0.3	0.35	0	0	0	0.056854	0
2	0.38	0.3	0.25	0.1	10000	139	0.056854	73.34576
4	0.38	0.3	0.25	0.1	10000	138	0.056854	72.8181
6	0.38	0.3	0.25	0.1	10000	138	0.056854	72.8181
8	0.38	0.3	0.25	0.1	10000	138	0.056854	72.8181
10	0.38	0.3	0.2	0.15	15000	168	0.056854	88.64812
12	0.38	0.3	0.2	0.15	15000	165	0.056854	87.06511
14	0.38	0.3	0.2	0.15	15000	165	0.056854	86.18567
16	0.38	0.3	0.2	0.15	15000	154	0.056854	81.26077
18	0.38	0.3	0.2	0.15	15000	151	0.056854	79.67777
20	0.38	0.3	0.2	0.15	15000	151	0.056854	79.67777
22	0.38	0.3	0.12	0.23	23000	200	0.056854	105.5335
24	0.38	0.3	0.12	0.23	23000	182	0.056854	96.03546
26	0.38	0.3	0.12	0.23	23000	154	0.056854	81.26077
28	0.38	0.3	0.12	0.23	23000	148	0.056854	78.09477
30	0.38	0.3	0.12	0.23	23000	148	0.056854	78.09477
32	0.38	0.3	0.12	0.23	23000	138	0.056854	72.8181
34	0.38	0.3	0.12	0.23	23000	128	0.056854	67.54142
36	0.38	0.3	0.12	0.23	23000	128	0.056854	67.54142
38	0.38	0.3	0	0.35	35000	190	0.056854	100.2568
40	0.38	0.3	0	0.35	35000	175	0.056854	92.34179
42	0.38	0.3	0	0.35	35000	158	0.056854	83.37144
44	0.38	0.3	0	0.35	35000	156	0.056854	82.31611
46	0.38	0.3	0	0.35	35000	140	0.056854	73.87343
48	0.38	0.3	0	0.35	35000	114	0.056854	60.15408
50	0.38	0.3	0	0.35	35000	114	0.056854	60.15408
52	0.38	0.3	0	0.35	35000	114	0.056854	60.15408
54	0.38	0.3	0.1	0.25	25000	85	0.056854	44.85173
56	0.38	0.3	0.1	0.25	25000	85	0.056854	44.85173
58	0.38	0.3	0.1	0.25	25000	85	0.056854	44.85173
60	0.38	0.3	0.2	0.15	15000	70	0.056854	36.93672
62	0.38	0.3	0.2	0.15	15000	70	0.056854	36.93672
64	0.38	0.3	0.2	0.15	15000	70	0.056854	36.93672
66	0.38	0.3	0	0.35	0	0	0.056854	0

Tabulated Step by Step Test Data for 600 ppm Emulsion in 0.05 M NaCl at Crossflow Velocity 1.14 m/s

Time(min)	P_f	Pr	Pp	TMP(bar)	TMP(Pa)	Vol.(ml)	A (m2)	Flux(L/m^2h)
0	0.4	0.32	0.32	0	0	0	0.056854	0
2	0.4	0.35	0.26	0.06	6000	68	0.056854	35.88138
4	0.4	0.35	0.26	0.06	6000	68	0.056854	35.88138
6	0.4	0.35	0.26	0.06	6000	68	0.056854	35.88138
8	0.4	0.35	0.2	0.12	12000	154	0.056854	81.26077
10	0.4	0.35	0.2	0.12	12000	166	0.056854	76.16764
12	0.4	0.35	0.2	0.12	12000	130	0.056854	68.59676
14	0.4	0.35	0.2	0.12	12000	130	0.056854	68.59676
16	0.4	0.35	0.2	0.12	12000	125	0.056854	65.95842
18	0.4	0.35	0.2	0.12	12000	120	0.056854	63.32008
20	0.4	0.35	0.2	0.12	12000	116	0.056854	61.20941
22	0.4	0.35	0.2	0.12	12000	116	0.056854	61.20941
24	0.4	0.35	0.2	0.12	12000	116	0.056854	61.20941
26	0.4	0.35	0	0.32	32000	285	0.056854	150.3852
28	0.4	0.35	0	0.32	32000	245	0.056854	129.2785
30	0.4	0.35	0	0.32	32000	230	0.056854	121.3635
32	0.4	0.35	0	0.32	32000	215	0.056854	113.4485
34	0.4	0.35	0	0.32	32000	200	0.056854	105.5335
36	0.4	0.35	0	0.32	32000	190	0.056854	100.2568
38	0.4	0.35	0	0.32	32000	180	0.056854	94.98012
40	0.4	0.35	0	0.32	32000	174	0.056854	91.81412
42	0.4	0.35	0	0.32	32000	173	0.056854	91.28645
44	0.4	0.35	0	0.32	32000	170	0.056854	89.70345
46	0.4	0.35	0	0.32	32000	170	0.056854	89.70345
48	0.4	0.35	0	0.32	32000	168	0.056854	88.64812
50	0.4	0.35	0	0.32	32000	168	0.056854	88.64812
52	0.4	0.35	0	0.32	32000	168	0.056854	88.64812
54	0.4	0.35	0.2	0.12	12000	78	0.056854	41.15805
56	0.4	0.35	0.2	0.12	12000	78	0.056854	41.15805
58	0.4	0.35	0.2	0.12	12000	78	0.056854	41.15805
60	0.4	0.35	0.26	0.06	6000	50	0.056854	26.38337
62	0.4	0.35	0.26	0.06	6000	50	0.056854	26.38337
64	0.4	0.35	0.26	0.06	6000	50	0.056854	26.38337
66	0.4	0.35	0	0.32	0	0	0.056854	0

Tabulated Step by Step Test Data for 600 ppm Emulsion in 0.1 M NaCl at Crossflow Velocity 1.52 m/s

Time(min)	P_f	*Pr*	*Pp*	*TMP(bar)*	*TMP(Pa)*	*Vol.(ml)*	*A (m2)*	*Flux(L/m²h)*
0	0.78	0.62	0.53	0	0	0	0.056854	0
2	0.4	0.35	0.45	0.08	8000	120	0.056854	63.32008
4	0.4	0.35	0.45	0.08	8000	120	0.056854	63.32008
6	0.4	0.35	0.45	0.08	8000	120	0.056854	63.32008
8	0.4	0.35	0.4	0.13	13000	192	0.056854	98.02819
10	0.4	0.35	0.4	0.13	13000	166	0.056854	87.59278
12	0.4	0.35	0.4	0.13	13000	148	0.056854	78.09477
14	0.4	0.35	0.4	0.13	13000	144	0.056854	75.9841
16	0.4	0.35	0.4	0.13	13000	144	0.056854	75.9841
18	0.4	0.35	0.4	0.13	13000	144	0.056854	75.9841
20	0.4	0.35	0.4	0.13	13000	144	0.056854	75.9841
22	0.4	0.35	0.4	0.13	13000	144	0.056854	75.9841
24	0.4	0.35	0.18	0.35	35000	280	0.056854	147.7469
26	0.4	0.35	0.18	0.35	35000	710	0.056854	124.8813
28	0.4	0.35	0.18	0.35	35000	220	0.056854	92.86946
30	0.4	0.35	0.18	0.35	35000	220	0.056854	92.86946
32	0.4	0.35	0	0.53	53000	555	0.056854	146.4277
34	0.4	0.35	0	0.53	53000	170	0.056854	89.70345
36	0.4	0.35	0	0.53	53000	220	0.056854	116.0868
38	0.4	0.35	0	0.53	53000	210	0.056854	110.8101
40	0.4	0.35	0	0.53	53000	200	0.056854	105.5335
42	0.4	0.35	0	0.53	53000	190	0.056854	100.2568
44	0.4	0.35	0	0.53	53000	180	0.056854	94.98012
46	0.4	0.35	0	0.53	53000	170	0.056854	89.70345
48	0.4	0.35	0	0.53	53000	150	0.056854	79.1501
50	0.4	0.35	0	0.53	53000	150	0.056854	79.1501
52	0.4	0.35	0	0.53	53000	150	0.056854	79.1501
54	0.4	0.35	0	0.53	53000	150	0.056854	79.1501
56	0.4	0.35	0.18	0.35	35000	135	0.056854	71.23509
58	0.4	0.35	0.18	0.35	35000	135	0.056854	71.23509
60	0.4	0.35	0.18	0.35	35000	135	0.056854	71.23509
62	0.4	0.35	0.4	0.13	13000	84	0.056854	44.32406
64	0.4	0.35	0.4	0.13	13000	84	0.056854	44.32406
66	0.4	0.35	0.4	0.13	13000	84	0.056854	44.32406
68	0.4	0.35	0.53	0	0	0	0.056854	0

Tabulated Step by Step Test Data for 600 ppm Emulsion in 0.05 M NaCl at Crossflow Velocity 1.52 m/s

Time(min)	P_f	Pr	Pp	TMP(bar)	TMP(Pa)	Vol.(ml)	A (m2)	Flux(L/m^2h)
0	0.55	0.43	0.52	0	0	0	0.056854	0
2	0.55	0.43	0.44	0.08	8000	110	0.056854	58.04341
4	0.55	0.43	0.44	0.08	8000	110	0.056854	58.04341
6	0.55	0.43	0.44	0.08	8000	110	0.056854	58.04341
8	0.55	0.43	0.36	0.16	16000	200	0.056854	105.5335
10	0.55	0.43	0.36	0.16	16000	198	0.056854	104.4781
12	0.55	0.43	0.36	0.16	16000	195	0.056854	102.8951
14	0.55	0.43	0.36	0.16	16000	182	0.056854	96.03546
16	0.55	0.43	0.36	0.16	16000	185	0.056854	97.61846
18	0.55	0.43	0.36	0.16	16000	528	0.056854	92.86946
20	0.55	0.43	0.36	0.16	16000	175	0.056854	92.34179
22	0.55	0.43	0.36	0.16	16000	175	0.056854	92.34179
24	0.55	0.43	0.36	0.16	16000	175	0.056854	92.34179
26	0.55	0.43	0.2	0.32	32000	295	0.056854	155.6619
28	0.55	0.43	0.2	0.32	32000	260	0.056854	137.1935
30	0.55	0.43	0.2	0.32	32000	240	0.056854	126.6402
32	0.55	0.43	0.2	0.32	32000	235	0.056854	124.0018
34	0.55	0.43	0.2	0.32	32000	235	0.056854	124.0018
36	0.55	0.43	0.2	0.32	32000	235	0.056854	124.0018
38	0.55	0.43	0	0.52	52000	385	0.056854	203.1519
40	0.55	0.43	0	0.52	52000	350	0.056854	184.6836
42	0.55	0.43	0	0.52	52000	510	0.056854	179.4069
44	0.55	0.43	0	0.52	52000	330	0.056854	174.1302
46	0.55	0.43	0	0.52	52000	330	0.056854	174.1302
48	0.55	0.43	0	0.52	52000	300	0.056854	158.3002
50	0.55	0.43	0	0.52	52000	300	0.056854	158.3002
52	0.55	0.43	0	0.52	52000	290	0.056854	153.0235
54	0.55	0.43	0	0.52	52000	280	0.056854	147.7469
56	0.55	0.43	0	0.52	52000	270	0.056854	142.4702
58	0.55	0.43	0	0.52	52000	230	0.056854	121.3635
60	0.55	0.43	0	0.52	52000	230	0.056854	121.3635
62	0.55	0.43	0	0.52	52000	230	0.056854	121.3635
64	0.55	0.43	0.36	0.16	16000	100	0.056854	52.76674
66	0.55	0.43	0.36	0.16	16000	100	0.056854	52.76674
68	0.55	0.43	0.36	0.16	16000	100	0.056854	52.76674
70	0.55	0.43	0.52	0	0	0		0

Tabulated Step by Step Test Data for 600 ppm Emulsion in 0.1 M NaCl at Crossflow Velocity 1.92 m/s

Time(min)	P_f	Pr	Pp	TMP(bar)	TMP(Pa)	Vol.(ml)	A (m2)	Flux(L/m^{2}h)
0	0.78	0.62	0.75	0	0	0	0.056854	0
2	0.4	0.35	0.7	0.05	5000	56	0.056854	29.54937
4	0.4	0.35	0.7	0.05	5000	56	0.056854	29.54937
6	0.4	0.35	0.7	0.05	5000	56	0.056854	29.54937
8	0.4	0.35	0.6	0.15	15000	174	0.056854	91.81412
10	0.4	0.35	0.6	0.15	15000	174	0.056854	91.81412
12	0.4	0.35	0.6	0.15	15000	174	0.056854	91.81412
14	0.4	0.35	0.49	0.26	26000	270	0.056854	142.4702
16	0.4	0.35	0.49	0.26	26000	260	0.056854	137.1935
18	0.4	0.35	0.49	0.26	26000	880	0.056854	132.6707
20	0.4	0.35	0.49	0.26	26000	230	0.056854	121.3635
22	0.4	0.35	0.49	0.26	26000	230	0.056854	121.3635
24	0.4	0.35	0.49	0.26	26000	440	0.056854	116.0868
26	0.4	0.35	0.49	0.26	26000	220	0.056854	116.0868
28	0.4	0.35	0.49	0.26	26000	220	0.056854	116.0868
30	0.4	0.35	0.49	0.26	26000	220	0.056854	116.0868
32	0.4	0.35	0.3	0.45	45000	345	0.056854	182.0452
34	0.4	0.35	0.3	0.45	45000	315	0.056854	166.2152
36	0.4	0.35	0.3	0.45	45000	310	0.056854	163.5769
38	0.4	0.35	0.3	0.45	45000	310	0.056854	163.5769
40	0.4	0.35	0.3	0.45	45000	290	0.056854	153.0235
42	0.4	0.35	0.3	0.45	45000	275	0.056854	145.1085
44	0.4	0.35	0.3	0.45	45000	270	0.056854	142.4702
46	0.4	0.35	0.3	0.45	45000	270	0.056854	142.4702
48	0.4	0.35	0.3	0.45	45000	270	0.056854	142.4702
50	0.4	0.35	0	0.75	75000	425	0.056854	224.2586
52	0.4	0.35	0	0.75	75000	410	0.056854	216.3436
54	0.4	0.35	0	0.75	75000	380	0.056854	200.5136
56	0.4	0.35	0	0.75	75000	360	0.056854	189.9602
58	0.4	0.35	0	0.75	75000	340	0.056854	179.4069
60	0.4	0.35	0	0.75	75000	320	0.056854	168.8536
62	0.4	0.35	0	0.75	75000	310	0.056854	163.5769
64	0.4	0.35	0	0.75	75000	300	0.056854	158.3002
66	0.4	0.35	0	0.75	75000	300	0.056854	158.3002
68	0.4	0.35	0	0.75	75000	300	0.056854	158.3002
70	0.4	0.35	0.3	0.45	45000	190	0.056854	100.2568
72	0.4	0.35	0.3	0.45	45000	190	0.056854	100.2568
74	0.4	0.35	0.3	0.45	45000	190	0.056854	100.2568
76	0.4	0.35	0.5	0.25	25000	110	0.056854	58.04341
78	0.4	0.35	0.5	0.25	25000	110	0.056854	58.04341
80	0.4	0.35	0.5	0.25	25000	110	0.056854	58.04341
82	0.4	0.35	0.75	0	0	0	0.056854	0

Tabulated Step by Step Test Data for 600 ppm Emulsion at 1.92 m/s (0.05 M NaCl)

Time(min)	P_f	Pr	Pp	TMP(bar)	TMP(Pa)	Vol.(ml)	A (m2)	Flux(L/m^{2}h)
0	0.85	0.66	0.82	0	0	0	0.056854	0
2	0.85	0.66	0.77	0.05	5000	60	0.056854	31.66004
4	0.85	0.66	0.77	0.05	5000	60	0.056854	31.66004
6	0.85	0.66	0.77	0.05	5000	60	0.056854	31.66004
8	0.85	0.66	0.7	0.12	12000	147	0.056854	77.5671
10	0.85	0.66	0.7	0.12	12000	146	0.056854	77.03943
12	0.85	0.66	0.7	0.12	12000	146	0.056854	77.03943
14	0.85	0.66	0.7	0.12	12000	146	0.056854	77.03943
16	0.85	0.66	0.58	0.24	24000	248	0.056854	130.8615
18	0.85	0.66	0.58	0.24	24000	246	0.056854	129.8062
20	0.85	0.66	0.58	0.24	24000	246	0.056854	129.8062
22	0.85	0.66	0.58	0.24	24000	246	0.056854	129.8062
24	0.85	0.66	0.5	0.32	32000	290	0.056854	153.0235
26	0.85	0.66	0.5	0.32	32000	270	0.056854	142.4702
28	0.85	0.66	0.5	0.32	32000	270	0.056854	142.4702
30	0.85	0.66	0.5	0.32	32000	270	0.056854	142.4702
32	0.85	0.66	0.5	0.32	32000	270	0.056854	142.4702
34	0.85	0.66	0.3	0.52	52000	400	0.056854	211.0669
36	0.85	0.66	0.3	0.52	52000	375	0.056854	197.8753
38	0.85	0.66	0.3	0.52	52000	355	0.056854	187.3219
40	0.85	0.66	0.3	0.52	52000	350	0.056854	184.6836
42	0.85	0.66	0.3	0.52	52000	350	0.056854	184.6836
44	0.85	0.66	0.3	0.52	52000	350	0.056854	184.6836
46	0.85	0.66	0	0.82	82000	500	0.056854	263.8337
48	0.85	0.66	0	0.82	82000	485	0.056854	255.9187
50	0.85	0.66	0	0.82	82000	470	0.056854	248.0037
52	0.85	0.66	0	0.82	82000	460	0.056854	242.727
54	0.85	0.66	0	0.82	82000	450	0.056854	237.4503
56	0.85	0.66	0	0.82	82000	450	0.056854	237.4503
58	0.85	0.66	0	0.82	82000	430	0.056854	226.897
60	0.85	0.66	0	0.82	82000	430	0.056854	226.897
62	0.85	0.66	0	0.82	82000	420	0.056854	221.6203
64	0.85	0.66	0	0.82	82000	410	0.056854	216.3436
66	0.85	0.66	0	0.82	82000	800	0.056854	211.0669
68	0.85	0.66	0	0.82	82000	390	0.056854	205.7903
70	0.85	0.66	0	0.82	82000	770	0.056854	203.1519
72	0.85	0.66	0	0.82	82000	380	0.056854	200.5136
74	0.85	0.66	0	0.82	82000	740	0.056854	195.2369
76	0.85	0.66	0	0.82	82000	365	0.056854	192.5986
78	0.85	0.66	0	0.82	82000	365	0.056854	192.5986
80	0.85	0.66	0	0.82	82000	365	0.056854	192.5986
82	0.85	0.66	0.3	0.52	52000	225	0.056854	118.7252
84	0.85	0.66	0.3	0.52	52000	225	0.056854	118.7252
86	0.85	0.66	0.3	0.52	52000	225	0.056854	118.7252
88	0.85	0.66	0.5	0.32	32000	160	0.056854	84.42678
90	0.85	0.66	0.5	0.32	32000	160	0.056854	84.42678
92	0.85	0.66	0.5	0.32	32000	160	0.056854	84.42678
94	0.85	0.66	0.7	0.12	12000	70	0.056854	36.93672
96	0.85	0.66	0.7	0.12	12000	70	0.056854	36.93672
98	0.85	0.66	0.7	0.12	12000	70	0.056854	36.93672
100	0.85	0.66	0.82	0	0	0	0.056854	0

Tabulated Step by Step Test Data for 600 ppm Emulsion at Velocity 1.52 m/s (pH 12)

Time(min)	P_f	Pr	Pp	TMP(bar)	TMP(Pa)	Vol.(ml)	A (m2)	Flux(L/m^{2}h)
0	0.66	0.56	0.63	0	0	0	0.056854	0
2	0.66	0.56	0.58	0.05	5000	53.2	0.056854	28.0719
4	0.66	0.56	0.58	0.05	5000	53.2	0.056854	28.0719
6	0.66	0.56	0.58	0.05	5000	53.2	0.056854	28.0719
8	0.66	0.56	0.58	0.05	5000	53.2	0.056854	28.0719
10	0.66	0.56	0.58	0.05	5000	53.2	0.056854	28.0719
12	0.66	0.56	0.5	0.13	13000	120	0.056854	63.32008
14	0.66	0.56	0.5	0.13	13000	120	0.056854	63.32008
16	0.66	0.56	0.5	0.13	13000	120	0.056854	63.32008
18	0.66	0.56	0.5	0.13	13000	120	0.056854	63.32008
20	0.66	0.56	0.5	0.13	13000	120	0.056854	63.32008
22	0.66	0.56	0.5	0.13	13000	120	0.056854	63.32008
24	0.66	0.56	0.4	0.23	23000	208	0.056854	109.7548
26	0.66	0.56	0.4	0.23	23000	205	0.056854	108.1718
28	0.66	0.56	0.4	0.23	23000	204	0.056854	107.6441
30	0.66	0.56	0.4	0.23	23000	200	0.056854	105.5335
32	0.66	0.56	0.4	0.23	23000	196	0.056854	103.4228
34	0.66	0.56	0.4	0.23	23000	194	0.056854	102.3675
36	0.66	0.56	0.4	0.23	23000	192	0.056854	101.3121
38	0.66	0.56	0.4	0.23	23000	190	0.056854	100.2568
40	0.66	0.56	0.4	0.23	23000	190	0.056854	100.2568
42	0.66	0.56	0.4	0.23	23000	190	0.056854	100.2568
44	0.66	0.56	0.4	0.23	23000	190	0.056854	100.2568
46	0.66	0.56	0.28	0.35	35000	272	0.056854	143.5255
48	0.66	0.56	0.28	0.35	35000	260	0.056854	137.1935
50	0.66	0.56	0.28	0.35	35000	260	0.056854	137.1935
52	0.66	0.56	0.28	0.35	35000	250	0.056854	131.9168
54	0.66	0.56	0.28	0.35	35000	250	0.056854	131.9168
56	0.66	0.56	0.28	0.35	35000	250	0.056854	131.9168
58	0.66	0.56	0.28	0.35	35000	250	0.056854	131.9168
60	0.66	0.56	0	0.63	63000	400	0.056854	211.0669
62	0.66	0.56	0	0.63	63000	370	0.056854	195.2369
64	0.66	0.56	0	0.63	63000	360	0.056854	189.9602
66	0.66	0.56	0	0.63	63000	430	0.056854	181.5176
68	0.66	0.56	0	0.63	63000	340	0.056854	179.4069
70	0.66	0.56	0	0.63	63000	330	0.056854	174.1302
72	0.66	0.56	0	0.63	63000	330	0.056854	174.1302
74	0.66	0.56	0	0.63	63000	325	0.056854	171.4919
76	0.66	0.56	0	0.63	63000	325	0.056854	171.4919
78	0.66	0.56	0	0.63	63000	320	0.056854	168.8536
80	0.66	0.56	0	0.63	63000	320	0.056854	168.8536
82	0.66	0.56	0	0.63	63000	320	0.056854	168.8536
84	0.66	0.56	0.28	0.35	35000	200	0.056854	105.5335
86	0.66	0.56	0.28	0.35	35000	200	0.056854	105.5335
88	0.66	0.56	0.28	0.35	35000	200	0.056854	105.5335
90	0.66	0.56	0.28	0.35	35000	200	0.056854	105.5335
92	0.66	0.56	0.4	0.23	23000	150	0.056854	79.1501
94	0.66	0.56	0.4	0.23	23000	150	0.056854	79.1501
96	0.66	0.56	0.4	0.23	23000	150	0.056854	79.1501
98	0.66	0.56	0.4	0.23	23000	150	0.056854	79.1501
100	0.66	0.56	0.63	0.00	0	0	0.056854	0

Tabulated Step by Step Test Data for 600 ppm Emulsion at 1.92 m/s (0.1 M NaCl, pH 12)

Time(min)	P_f	Pr	Pp	TMP(bar)	TMP(Pa)	Vol.(ml)	A (m2)	Flux(L/m^{2}h)
0	0.85	0.66	0.82	0	0	0	0.056854	0
2	0.85	0.66	0.75	0.07	7000	64	0.056854	33.77071
4	0.85	0.66	0.75	0.07	7000	64	0.056854	33.77071
6	0.85	0.66	0.75	0.07	7000	64	0.056854	33.77071
8	0.85	0.66	0.7	0.12	12000	92	0.056854	48.5454
10	0.85	0.66	0.7	0.12	12000	92	0.056854	48.5454
12	0.85	0.66	0.7	0.12	12000	92	0.056854	48.5454
14	0.85	0.66	0.7	0.12	12000	92	0.056854	48.5454
16	0.85	0.66	0.58	0.24	24000	160	0.056854	84.42678
18	0.85	0.66	0.58	0.24	24000	152	0.056854	80.20544
20	0.85	0.66	0.58	0.24	24000	152	0.056854	80.20544
22	0.85	0.66	0.58	0.24	24000	152	0.056854	80.20544
24	0.85	0.66	0.45	0.37	37000	190	0.056854	100.2568
26	0.85	0.66	0.45	0.37	37000	185	0.056854	97.61846
28	0.85	0.66	0.45	0.37	37000	183	0.056854	96.56313
30	0.85	0.66	0.45	0.37	37000	182	0.056854	96.03546
32	0.85	0.66	0.45	0.37	37000	165	0.056854	87.06511
34	0.85	0.66	0.45	0.37	37000	165	0.056854	87.06511
36	0.85	0.66	0.45	0.37	37000	165	0.056854	87.06511
38	0.85	0.66	0.18	0.64	64000	246	0.056854	129.8062
40	0.85	0.66	0.18	0.64	64000	234	0.056854	123.4742
42	0.85	0.66	0.18	0.64	64000	228	0.056854	120.3082
44	0.85	0.66	0.18	0.64	64000	218	0.056854	115.0315
46	0.85	0.66	0.18	0.64	64000	218	0.056854	115.0315
48	0.85	0.66	0.18	0.64	64000	218	0.056854	115.0315
50	0.85	0.66	0	0.82	82000	880	0.056854	132.6707
52	0.85	0.66	0	0.82	82000	815	0.056854	122.8711
54	0.85	0.66	0	0.82	82000	220	0.056854	116.0868
56	0.85	0.66	0	0.82	82000	220	0.056854	116.0868
58	0.85	0.66	0	0.82	82000	320	0.056854	112.569
60	0.85	0.66	0	0.82	82000	210	0.056854	110.8101
62	0.85	0.66	0	0.82	82000	210	0.056854	110.8101
64	0.85	0.66	0	0.82	82000	205	0.056854	108.1718
66	0.85	0.66	0	0.82	82000	205	0.056854	108.1718
68	0.85	0.66	0	0.82	82000	200	0.056854	105.5335
70	0.85	0.66	0	0.82	82000	200	0.056854	105.5335
72	0.85	0.66	0	0.82	82000	200	0.056854	105.5335
74	0.85	0.66	0.2	0.62	62000	130	0.056854	68.59676
76	0.85	0.66	0.2	0.62	62000	126	0.056854	66.48609
78	0.85	0.66	0.2	0.62	62000	126	0.056854	66.48609
80	0.85	0.66	0.2	0.62	62000	126	0.056854	66.48609
82	0.85	0.66	0.5	0.32	32000	80	0.056854	42.21339
84	0.85	0.66	0.5	0.32	32000	80	0.056854	42.21339
86	0.85	0.66	0.5	0.32	32000	80	0.056854	42.21339
88	0.85	0.66	0.5	0.32	32000	80	0.056854	42.21339
90	0.85	0.66	0.82	0	0	0	0.056854	0

Tabulated Step by Step Test Data for 1200 ppm Emulsion at Velocity 1.14 m/s)

Time(min)	P_f	Pr	Pp	TMP(bar)	TMP(Pa)	Vol.(ml)	A (m2)	Flux(L/m^{2}h)
0	0.82	0.62	0.33	0	0	0	0.056854	0
3	0.76	0.62	0.3	0.03	3000	22	0.056854	7.739121
6	0.76	0.62	0.3	0.03	3000	22	0.056854	7.739121
9	0.76	0.62	0.3	0.03	3000	22	0.056854	7.739121
12	0.76	0.62	0.24	0.09	9000	120	0.056854	42.21339
15	0.76	0.62	0.24	0.09	9000	120	0.056854	42.21339
18	0.76	0.62	0.24	0.09	9000	120	0.056854	42.21339
21	0.76	0.62	0.18	0.15	15000	196	0.056854	68.94853
24	0.76	0.62	0.18	0.15	15000	189	0.056854	66.48609
27	0.76	0.62	0.18	0.15	15000	194	0.056854	68.24498
30	0.76	0.62	0.18	0.15	15000	189	0.056854	66.48609
33	0.76	0.62	0.18	0.15	15000	189	0.056854	66.48609
36	0.76	0.62	0.18	0.15	15000	189	0.056854	66.48609
39	0.76	0.62	0.18	0.15	15000	315	0.056854	107.5827
42	0.76	0.62	0.1	0.23	23000	295	0.056854	103.7746
45	0.76	0.62	0.1	0.23	23000	289	0.056854	101.6639
48	0.76	0.62	0.1	0.23	23000	278	0.056854	97.79435
51	0.76	0.62	0.1	0.23	23000	275	0.056854	96.73902
54	0.76	0.62	0.1	0.23	23000	260	0.056854	91.46234
57	0.76	0.62	0.1	0.23	23000	255	0.056854	89.70345
60	0.76	0.62	0.1	0.23	23000	255	0.056854	89.70345
63	0.76	0.62	0	0.33	33000	390	0.056854	137.1935
66	0.76	0.62	0	0.33	33000	368	0.056854	129.4544
69	0.76	0.62	0	0.33	33000	345	0.056854	121.3635
72	0.76	0.62	0	0.33	33000	325	0.056854	114.3279
75	0.76	0.62	0	0.33	33000	315	0.056854	110.8101
78	0.76	0.62	0.1	0.23	23000	125	0.056854	65.95842
80	0.76	0.62	0.1	0.23	23000	125	0.056854	65.95842
82	0.76	0.62	0.1	0.23	23000	125	0.056854	65.95842
84	0.76	0.62	0.22	0.11	11000	56	0.056854	29.54937
86	0.76	0.62	0.22	0.11	11000	56	0.056854	29.54937
88	0.76	0.62	0.22	0.11	11000	56	0.056854	29.54937
90	0.76	0.62	0.33	0	0	0	0.056854	0

Tabulated Step by Step Test Data for 1200 ppm Emulsion at Velocity 1.52 m/s

Time(min)	P_f	Pr	Pp	TMP(bar)	TMP(Pa)	Vol.(ml)	A (m2)	Flux(L/m^{2}h)
0	0.6	0.5	0.55	0	0	0	0.056854	0
2	0.6	0.5	0.5	0.05	5000	56	0.056854	29.54937
4	0.6	0.5	0.5	0.05	5000	56	0.056854	29.54937
6	0.6	0.5	0.5	0.05	5000	56	0.056854	29.54937
8	0.6	0.5	0.4	0.15	15000	150	0.056854	79.1501
10	0.6	0.5	0.4	0.15	15000	150	0.056854	79.1501
12	0.6	0.5	0.4	0.15	15000	150	0.056854	79.1501
14	0.6	0.5	0.4	0.15	15000	150	0.056854	79.1501
16	0.6	0.5	0.3	0.25	25000	255	0.056854	134.5552
18	0.6	0.5	0.3	0.25	25000	250	0.056854	131.9168
20	0.6	0.5	0.3	0.25	25000	250	0.056854	131.9168
22	0.6	0.5	0.3	0.25	25000	250	0.056854	131.9168
24	0.6	0.5	0.22	0.33	33000	320	0.056854	168.8536
26	0.6	0.5	0.22	0.33	33000	308	0.056854	162.5215
28	0.6	0.5	0.22	0.33	33000	308	0.056854	162.5215
30	0.6	0.5	0.22	0.33	33000	305	0.056854	160.9385
32	0.6	0.5	0.22	0.33	33000	305	0.056854	160.9385
34	0.6	0.5	0.22	0.33	33000	305	0.056854	160.9385
37	0.6	0.5	0	0.55	55000	750	0.056854	263.8337
40	0.6	0.5	0	0.55	55000	710	0.056854	249.7625
43	0.6	0.5	0	0.55	55000	695	0.056854	244.4859
46	0.6	0.5	0	0.55	55000	680	0.056854	239.2092
49	0.6	0.5	0	0.55	55000	1980	0.056854	232.1736
52	0.6	0.5	0	0.55	55000	650	0.056854	228.6559
55	0.6	0.5	0	0.55	55000	630	0.056854	221.6203
58	0.6	0.5	0	0.55	55000	620	0.056854	218.1025
61	0.6	0.5	0	0.55	55000	620	0.056854	218.1025
64	0.6	0.5	0	0.55	55000	620	0.056854	218.1025
67	0.6	0.5	0.2	0.35	35000	250	0.056854	131.9168
70	0.6	0.5	0.2	0.35	35000	250	0.056854	131.9168
73	0.6	0.5	0.2	0.35	35000	250	0.056854	131.9168
76	0.6	0.5	0.4	0.15	15000	100	0.056854	52.76674
79	0.6	0.5	0.4	0.15	15000	100	0.056854	52.76674
82	0.6	0.5	0.4	0.15	15000	100	0.056854	52.76674
85	0.6	0.5	0	0.55	0	0	0.056854	0

Tabulated Step by Step Test Data for 1200 ppm Emulsion at 1.92 m/s

Time(min)	P_f	Pr	Pp	TMP(bar)	TMP(Pa)	Vol.(ml)	A (m2)	Flux(L/m^{2}h)
0	0.94	0.82	0.88	0	0	0	0.056854	0
2	0.94	0.82	0.7	0.18	18000	200	0.056854	105.5335
4	0.94	0.82	0.7	0.18	18000	200	0.056854	105.5335
6	0.94	0.82	0.7	0.18	18000	200	0.056854	105.5335
8	0.94	0.82	0.6	0.28	28000	300	0.056854	158.3002
10	0.94	0.82	0.6	0.28	28000	300	0.056854	158.3002
12	0.94	0.82	0.6	0.28	28000	300	0.056854	158.3002
14	0.94	0.82	0.54	0.34	34000	360	0.056854	189.9602
16	0.94	0.82	0.54	0.34	34000	355	0.056854	187.3219
18	0.94	0.82	0.54	0.34	34000	350	0.056854	184.6836
20	0.94	0.82	0.54	0.34	34000	350	0.056854	184.6836
22	0.94	0.82	0.54	0.34	34000	350	0.056854	184.6836
24	0.94	0.82	0.44	0.44	44000	455	0.056854	240.0886
26	0.94	0.82	0.44	0.44	44000	450	0.056854	237.4503
28	0.94	0.82	0.44	0.44	44000	430	0.056854	226.897
30	0.94	0.82	0.44	0.44	44000	425	0.056854	224.2586
32	0.94	0.82	0.44	0.44	44000	425	0.056854	224.2586
34	0.94	0.82	0.44	0.44	44000	415	0.056854	218.982
36	0.94	0.82	0.44	0.44	44000	415	0.056854	218.982
38	0.94	0.82	0.44	0.44	44000	415	0.056854	218.982
40	0.94	0.82	0.05	0.83	83000	760	0.056854	401.0272
42	0.94	0.82	0.05	0.83	83000	730	0.056854	385.1972
44	0.94	0.82	0.05	0.83	83000	695	0.056854	366.7288
46	0.94	0.82	0.05	0.83	83000	685	0.056854	361.4521
48	0.94	0.82	0.05	0.83	83000	670	0.056854	353.5371
50	0.94	0.82	0.05	0.83	83000	660	0.056854	348.2605
52	0.94	0.82	0.05	0.83	83000	640	0.056854	337.7071
54	0.94	0.82	0.05	0.83	83000	640	0.056854	337.7071
56	0.94	0.82	0.05	0.83	83000	640	0.056854	337.7071
58	0.94	0.82	0.3	0.58	58000	425	0.056854	224.2586
60	0.94	0.82	0.3	0.58	58000	425	0.056854	224.2586
62	0.94	0.82	0.3	0.58	58000	420	0.056854	221.6203
64	0.94	0.82	0.3	0.58	58000	420	0.056854	221.6203
66	0.94	0.82	0.54	0.34	34000	250	0.056854	131.9168
68	0.94	0.82	0.54	0.34	34000	250	0.056854	131.9168
70	0.94	0.82	0.54	0.34	34000	250	0.056854	131.9168
72	0.94	0.82	0.88	0	0	0	0.056854	0

Tabulated Step by Step Test Data for 1200 ppm Emulsion in 0.1 M $CaCl_2$ at Velocity 1.52 m/s

Time(min)	P_f	Pr	Pp	TMP(bar)	TMP(Pa)	Vol.(ml)	A (m2)	Flux(L/m^{2}h)
0	0.78	0.62	0.58	0	0	0	0.056854	0
2	0.78	0.62	0.5	0.08	8000	243	0.056854	85.48211
4	0.78	0.62	0.5	0.08	8000	162	0.056854	85.48211
6	0.78	0.62	0.5	0.08	8000	162	0.056854	85.48211
8	0.78	0.62	0.5	0.08	8000	162	0.056854	85.48211
10	0.78	0.62	0.5	0.08	8000	162	0.056854	85.48211
12	0.78	0.62	0.4	0.18	18000	310	0.056854	163.5769
14	0.78	0.62	0.4	0.18	18000	310	0.056854	163.5769
16	0.78	0.62	0.4	0.18	18000	310	0.056854	163.5769
18	0.78	0.62	0.4	0.18	18000	310	0.056854	163.5769
20	0.78	0.62	0.4	0.18	18000	310	0.056854	163.5769
22	0.78	0.62	0.3	0.28	28000	450	0.056854	237.4503
24	0.78	0.62	0.3	0.28	28000	450	0.056854	237.4503
26	0.78	0.62	0.3	0.28	28000	450	0.056854	237.4503
28	0.78	0.62	0.3	0.28	28000	450	0.056854	237.4503
30	0.78	0.62	0.3	0.28	28000	450	0.056854	237.4503
32	0.78	0.62	0.2	0.38	38000	560	0.056854	295.4937
34	0.78	0.62	0.2	0.38	38000	550	0.056854	290.217
36	0.78	0.62	0.2	0.38	38000	540	0.056854	284.9404
38	0.78	0.62	0.2	0.38	38000	584	0.056854	284.4095
40	0.78	0.62	0.2	0.38	38000	538	0.056854	283.885
42	0.78	0.62	0.2	0.38	38000	535	0.056854	282.302
44	0.78	0.62	0.2	0.38	38000	535	0.056854	282.302
46	0.78	0.62	0.2	0.38	38000	535	0.056854	282.302
48	0.78	0.62	0.06	0.52	52000	725	0.056854	382.5588
50	0.78	0.62	0.06	0.52	52000	720	0.056854	379.9205
52	0.78	0.62	0.06	0.52	52000	710	0.056854	374.6438
54	0.78	0.62	0.06	0.52	52000	705	0.056854	372.0055
56	0.78	0.62	0.06	0.52	52000	700	0.056854	369.3672
58	0.78	0.62	0.06	0.52	52000	695	0.056854	366.7288
60	0.78	0.62	0.06	0.52	52000	1000	0.056854	361.829
62	0.78	0.62	0.06	0.52	52000	670	0.056854	353.5371
64	0.78	0.62	0.06	0.52	52000	670	0.056854	353.5371
66	0.78	0.62	0.06	0.52	52000	670	0.056854	353.5371
68	0.78	0.62	0.2	0.38	38000	480	0.056854	253.2803
70	0.78	0.62	0.2	0.38	38000	480	0.056854	253.2803
72	0.78	0.62	0.2	0.38	38000	480	0.056854	253.2803
74	0.78	0.62	0.4	0.18	18000	220	0.056854	116.0868
76	0.78	0.62	0.4	0.18	18000	220	0.056854	116.0868
78	0.78	0.62	0.4	0.18	18000	220	0.056854	116.0868
80	0.78	0.62	0.5	0.08	8000	100	0.056854	52.76674
82	0.78	0.62	0.5	0.08	8000	100	0.056854	52.76674
84	0.78	0.62	0.5	0.08	8000	100	0.056854	52.76674
86	0.78	0.62	0	0.58	0	0	0.056854	0

Tabulated Step by Step Test Data for 1200 ppm Emulsion(1.92 m/s, 0.05 M NaCl)

Time(min)	P_f	Pr	Pp	TMP(bar)	TMP(Pa)	Vol.(ml)	A (m2)	Flux(L/m^2h)
0	0.86	0.72	0.8	0	0	0	0.056854	0
2	0.86	0.72	0.72	0.08	8000	56	0.056854	29.54937208
4	0.86	0.72	0.72	0.08	8000	56	0.056854	29.54937208
6	0.86	0.72	0.72	0.08	8000	56	0.056854	29.54937208
8	0.86	0.72	0.66	0.14	14000	114	0.056854	60.15407887
10	0.86	0.72	0.66	0.14	14000	112	0.056854	59.09874415
12	0.86	0.72	0.66	0.14	14000	112	0.056854	59.09874415
14	0.86	0.72	0.66	0.14	14000	112	0.056854	59.09874415
16	0.86	0.72	0.54	0.26	26000	197	0.056854	103.9504696
18	0.86	0.72	0.54	0.26	26000	197	0.056854	103.9504696
20	0.86	0.72	0.54	0.26	26000	197	0.056854	103.9504696
22	0.86	0.72	0.54	0.26	26000	197	0.056854	103.9504696
24	0.86	0.72	0.54	0.26	26000	197	0.056854	103.9504696
26	0.86	0.72	0.44	0.36	36000	270	0.056854	142.4701868
28	0.86	0.72	0.44	0.36	36000	270	0.056854	142.4701868
30	0.86	0.72	0.44	0.36	36000	270	0.056854	142.4701868
32	0.86	0.72	0.44	0.36	36000	270	0.056854	142.4701868
34	0.86	0.72	0.34	0.46	46000	338	0.056854	178.3515672
36	0.86	0.72	0.34	0.46	46000	329	0.056854	173.6025609
38	0.86	0.72	0.34	0.46	46000	330	0.056854	174.1302283
40	0.86	0.72	0.34	0.46	46000	323	0.056854	170.4365568
42	0.86	0.72	0.34	0.46	46000	329	0.056854	173.6025609
44	0.86	0.72	0.34	0.46	46000	325	0.056854	171.4918915
46	0.86	0.72	0.34	0.46	46000	325	0.056854	171.4918915
48	0.86	0.72	0.34	0.46	46000	325	0.056854	171.4918915
50	0.86	0.72	0.2	0.6	60000	415	0.056854	218.9819538
52	0.86	0.72	0.2	0.6	60000	411	0.056854	216.8712843
54	0.86	0.72	0.2	0.6	60000	400	0.056854	211.0669434
56	0.86	0.72	0.2	0.6	60000	400	0.056854	211.0669434
58	0.86	0.72	0.2	0.6	60000	380	0.056854	200.5135962
60	0.86	0.72	0.2	0.6	60000	365	0.056854	192.5985859
62	0.86	0.72	0.2	0.6	60000	365	0.056854	192.5985859
64	0.86	0.72	0.2	0.6	60000	365	0.056854	192.5985859
66	0.86	0.72	0	0.8	80000	720	0.056854	253.2803321
68	0.86	0.72	0	0.8	80000	465	0.056854	245.3653217
70	0.86	0.72	0	0.8	80000	465	0.056854	245.3653217
72	0.86	0.72	0	0.8	80000	440	0.056854	232.1736377
74	0.86	0.72	0	0.8	80000	430	0.056854	226.8969642
76	0.86	0.72	0	0.8	80000	950	0.056854	200.5135962
78	0.86	0.72	0	0.8	80000	900	0.056854	189.9602491
80	0.86	0.72	0	0.8	80000	360	0.056854	189.9602491
82	0.86	0.72	0	0.8	80000	360	0.056854	189.9602491
84	0.86	0.72	0	0.8	80000	360	0.056854	189.9602491
86	0.86	0.72	0.34	0.46	46000	192	0.056854	101.3121328
88	0.86	0.72	0.34	0.46	46000	192	0.056854	101.3121328
90	0.86	0.72	0.34	0.46	46000	192	0.056854	101.3121328
92	0.86	0.72	0.66	0.14	14000	70	0.056854	36.93671509
94	0.86	0.72	0.66	0.14	14000	70	0.056854	36.93671509
96	0.86	0.72	0.66	0.14	14000	70	0.056854	36.93671509
98	0.86	0.72	0.8	0	0	0	0.056854	0

Tabulated Step by Step Test Data for 2400 ppm Emulsion at Crossflow Velocity 1.14 m/s

Time(min)	P_f	Pr	Pp	TMP(bar)	TMP(Pa)	Vol.(ml)	A (m2)	Flux(L/m^{2}h)
0	0.32	0.28	0.3	0	0	0	0.056854	0
2	0.32	0.28	0.23	0.07	7000	84	0.056854	44.32406
4	0.32	0.28	0.24	0.06	6000	84	0.056854	44.32406
6	0.32	0.28	0.24	0.06	6000	84	0.056854	44.32406
8	0.32	0.28	0.16	0.14	14000	178	0.056854	93.92479
10	0.32	0.28	0.16	0.14	14000	168	0.056854	88.64812
12	0.32	0.28	0.16	0.14	14000	168	0.056854	88.64812
14	0.32	0.28	0.1	0.2	20000	205	0.056854	108.1718
16	0.32	0.28	0.1	0.2	20000	198	0.056854	104.4781
18	0.32	0.28	0.1	0.2	20000	200	0.056854	105.5335
20	0.32	0.28	0.1	0.2	20000	190	0.056854	100.2568
22	0.32	0.28	0.1	0.2	20000	195	0.056854	102.8951
24	0.32	0.28	0.1	0.2	20000	495	0.056854	104.4781
26	0.32	0.28	0.1	0.2	20000	195	0.056854	102.8951
28	0.32	0.28	0.1	0.2	20000	195	0.056854	102.8951
30	0.32	0.28	0.1	0.2	20000	195	0.056854	102.8951
32	0.32	0.28	0.1	0.2	20000	195	0.056854	102.8951
34	0.32	0.28	0.1	0.2	20000	195	0.056854	102.8951
36	0.32	0.28	0.05	0.25	25000	250	0.056854	131.9168
38	0.32	0.28	0.05	0.25	25000	245	0.056854	129.2785
40	0.32	0.28	0.05	0.25	25000	240	0.056854	126.6402
42	0.32	0.28	0.05	0.25	25000	242	0.056854	127.6955
44	0.32	0.28	0.05	0.25	25000	240	0.056854	126.6402
46	0.32	0.28	0.05	0.25	25000	240	0.056854	126.6402
48	0.32	0.28	0	0.3	30000	300	0.056854	158.3002
50	0.32	0.28	0	0.3	30000	300	0.056854	158.3002
52	0.32	0.28	0	0.3	30000	280	0.056854	147.7469
54	0.32	0.28	0	0.3	30000	275	0.056854	145.1085
56	0.32	0.28	0	0.3	30000	260	0.056854	137.1935
58	0.32	0.28	0	0.3	30000	260	0.056854	137.1935
60	0.32	0.28	0	0.3	30000	260	0.056854	137.1935
62	0.32	0.28	0.1	0.2	20000	160	0.056854	84.42678
64	0.32	0.28	0.1	0.2	20000	160	0.056854	84.42678
66	0.32	0.28	0.1	0.2	20000	160	0.056854	84.42678
68	0.32	0.28	0.2	0.1	10000	72	0.056854	37.99205
70	0.32	0.28	0.2	0.1	10000	72	0.056854	37.99205
72	0.32	0.28	0.2	0.1	10000	72	0.056854	37.99205
74	0.32	0.28	0.3	0	0	0	0.056854	0

Tabulated Step by Step Test Data for 2400 ppm Emulsion at Crossflow Velocity 1.52 m/s

Time(min)	P_f	Pr	Pp	TMP(bar)	TMP(Pa)	Vol.(ml)	A (m2)	Flux(L/m^{2}h)
0	0.58	0.48	0.52	0	0	0	0.056854	0
2	0.58	0.48	0.44	0.08	8000	84	0.056854	44.32406
4	0.58	0.48	0.44	0.08	8000	84	0.056854	44.32406
6	0.58	0.48	0.44	0.08	8000	84	0.056854	44.32406
8	0.58	0.48	0.44	0.08	8000	84	0.056854	44.32406
10	0.58	0.48	0.36	0.16	16000	164	0.056854	86.53745
12	0.58	0.48	0.36	0.16	16000	164	0.056854	86.53745
14	0.58	0.48	0.36	0.16	16000	164	0.056854	86.53745
16	0.58	0.48	0.36	0.16	16000	164	0.056854	86.53745
18	0.58	0.48	0.36	0.16	16000	164	0.056854	86.53745
20	0.58	0.48	0.27	0.25	25000	256	0.056854	135.0828
22	0.58	0.48	0.27	0.25	25000	250	0.056854	131.9168
24	0.58	0.48	0.27	0.25	25000	250	0.056854	131.9168
26	0.58	0.48	0.27	0.25	25000	250	0.056854	131.9168
28	0.58	0.48	0.19	0.33	33000	320	0.056854	168.8536
30	0.58	0.48	0.19	0.33	33000	304	0.056854	160.4109
32	0.58	0.48	0.19	0.33	33000	290	0.056854	153.0235
34	0.58	0.48	0.19	0.33	33000	282	0.056854	148.8022
36	0.58	0.48	0.19	0.33	33000	280	0.056854	147.7469
38	0.58	0.48	0.19	0.33	33000	280	0.056854	147.7469
40	0.58	0.48	0.19	0.33	33000	280	0.056854	147.7469
42	0.58	0.48	0	0.52	52000	410	0.056854	216.3436
44	0.58	0.48	0	0.52	52000	380	0.056854	200.5136
46	0.58	0.48	0	0.52	52000	370	0.056854	195.2369
48	0.58	0.48	0	0.52	52000	365	0.056854	192.5986
50	0.58	0.48	0	0.52	52000	350	0.056854	184.6836
52	0.58	0.48	0	0.52	52000	350	0.056854	184.6836
54	0.58	0.48	0.18	0.34	34000	220	0.056854	116.0868
56	0.58	0.48	0.18	0.34	34000	220	0.056854	116.0868
58	0.58	0.48	0.18	0.34	34000	220	0.056854	116.0868
60	0.58	0.48	0.34	0.18	18000	122	0.056854	64.37542
62	0.58	0.48	0.34	0.18	18000	122	0.056854	64.37542
64	0.58	0.48	0.34	0.18	18000	122	0.056854	64.37542
66	0.58	0.48	0.34	0.18	18000	122	0.056854	64.37542
68	0.58	0.48	0.52	0	0	0	0.056854	0

Tabulated Step by Step Test Data for 2400 ppm Emulsion at Crossflow Velocity 1.92 m/s

Time(min)	P_f	Pr	Pp	TMP(bar)	TMP(Pa)	Vol.(ml)	A (m2)	Flux(L/m^{2}h)
0	0.82	0.68	0.78	0	0	0	0.056854	0
2	0.82	0.68	0.72	0.06	6000	84	0.056854	44.32406
4	0.82	0.68	0.72	0.06	6000	84	0.056854	44.32406
6	0.82	0.68	0.72	0.06	6000	84	0.056854	44.32406
8	0.82	0.68	0.62	0.16	16000	200	0.056854	105.5335
10	0.82	0.68	0.62	0.16	16000	200	0.056854	105.5335
12	0.82	0.68	0.62	0.16	16000	200	0.056854	105.5335
14	0.82	0.68	0.62	0.16	16000	200	0.056854	105.5335
16	0.82	0.68	0.52	0.26	26000	290	0.056854	153.0235
18	0.82	0.68	0.52	0.26	26000	285	0.056854	150.3852
20	0.82	0.68	0.52	0.26	26000	280	0.056854	147.7469
22	0.82	0.68	0.52	0.26	26000	280	0.056854	147.7469
24	0.82	0.68	0.52	0.26	26000	280	0.056854	147.7469
26	0.82	0.68	0.52	0.26	26000	280	0.056854	147.7469
28	0.82	0.68	0.4	0.38	38000	365	0.056854	192.5986
30	0.82	0.68	0.4	0.38	38000	355	0.056854	187.3219
32	0.82	0.68	0.4	0.38	38000	355	0.056854	187.3219
34	0.82	0.68	0.4	0.38	38000	333	0.056854	175.7132
36	0.82	0.68	0.4	0.38	38000	325	0.056854	171.4919
38	0.82	0.68	0.4	0.38	38000	318	0.056854	167.7982
40	0.82	0.68	0.4	0.38	38000	318	0.056854	167.7982
42	0.82	0.68	0.4	0.38	38000	475	0.056854	167.0947
44	0.82	0.68	0.4	0.38	38000	318	0.056854	167.7982
46	0.82	0.68	0	0.78	78000	542	0.056854	285.9957
48	0.82	0.68	0	0.78	78000	490	0.056854	258.557
50	0.82	0.68	0	0.78	78000	478	0.056854	252.225
52	0.82	0.68	0	0.78	78000	440	0.056854	232.1736
54	0.82	0.68	0	0.78	78000	435	0.056854	229.5353
56	0.82	0.68	0	0.78	78000	420	0.056854	221.6203
58	0.82	0.68	0	0.78	78000	415	0.056854	218.982
60	0.82	0.68	0	0.78	78000	405	0.056854	213.7053
62	0.82	0.68	0	0.78	78000	400	0.056854	211.0669
64	0.82	0.68	0	0.78	78000	390	0.056854	205.7903
66	0.82	0.68	0	0.78	78000	390	0.056854	205.7903
68	0.82	0.68	0	0.78	78000	380	0.056854	200.5136
70	0.82	0.68	0	0.78	78000	380	0.056854	200.5136
72	0.82	0.68	0	0.78	78000	372	0.056854	196.2923
74	0.82	0.68	0	0.78	78000	375	0.056854	197.8753
76	0.82	0.68	0	0.78	78000	368	0.056854	194.1816
78	0.82	0.68	0	0.78	78000	370	0.056854	195.2369
80	0.82	0.68	0	0.78	78000	355	0.056854	187.3219
82	0.82	0.68	0	0.78	78000	355	0.056854	187.3219
84	0.82	0.68	0	0.78	78000	350	0.056854	184.6836
86	0.82	0.68	0	0.78	78000	350	0.056854	184.6836
88	0.82	0.68	0.4	0.38	38000	175	0.056854	92.34179
90	0.82	0.68	0.4	0.38	38000	175	0.056854	92.34179
92	0.82	0.68	0.4	0.38	38000	175	0.056854	92.34179
94	0.82	0.68	0.52	0.26	26000	80	0.056854	42.21339
96	0.82	0.68	0.52	0.26	26000	80	0.056854	42.21339
98	0.82	0.68	0.52	0.26	26000	80	0.056854	42.21339
100	0.82	0.68	0.78	0	0	0	0.056854	0

Tabulated Step by Step Test Data for 2400 ppm Emulsion at Velocity 2.28 m/s

Time(min)	P_f	Pr	Pp	TMP(bar)	TMP(Pa)	Vol.(ml)	A (m2)	Flux(L/m^{2}h)
0	0.93	0.72	0.88	0	0	0	0.056854	0
2	0.93	0.72	0.8	0.08	8000	112	0.056854	59.09874
4	0.93	0.72	0.8	0.08	8000	112	0.056854	59.09874
6	0.93	0.72	0.8	0.08	8000	112	0.056854	59.09874
8	0.93	0.72	0.7	0.18	18000	214	0.056854	112.9208
10	0.93	0.72	0.7	0.18	18000	214	0.056854	112.9208
12	0.93	0.72	0.7	0.18	18000	214	0.056854	112.9208
14	0.93	0.72	0.6	0.28	28000	348	0.056854	183.6282
16	0.93	0.72	0.6	0.28	28000	345	0.056854	182.0452
18	0.93	0.72	0.6	0.28	28000	340	0.056854	179.4069
20	0.93	0.72	0.6	0.28	28000	340	0.056854	179.4069
22	0.93	0.72	0.6	0.28	28000	340	0.056854	179.4069
24	0.93	0.72	0.49	0.39	39000	455	0.056854	240.0886
26	0.93	0.72	0.49	0.39	39000	455	0.056854	240.0886
28	0.93	0.72	0.49	0.39	39000	450	0.056854	237.4503
30	0.93	0.72	0.49	0.39	39000	450	0.056854	237.4503
32	0.93	0.72	0.49	0.39	39000	445	0.056854	234.812
34	0.93	0.72	0.49	0.39	39000	445	0.056854	234.812
36	0.93	0.72	0.49	0.39	39000	445	0.056854	234.812
38	0.93	0.72	0.39	0.49	49000	530	0.056854	279.6637
40	0.93	0.72	0.39	0.49	49000	520	0.056854	274.387
42	0.93	0.72	0.39	0.49	49000	520	0.056854	274.387
44	0.93	0.72	0.39	0.49	49000	520	0.056854	274.387
46	0.93	0.72	0.39	0.49	49000	520	0.056854	274.387
48	0.93	0.72	0.05	0.83	83000	715	0.056854	377.2822
50	0.93	0.72	0.05	0.83	83000	700	0.056854	369.3672
52	0.93	0.72	0.05	0.83	83000	675	0.056854	356.1755
54	0.93	0.72	0.05	0.83	83000	670	0.056854	353.5371
56	0.93	0.72	0.05	0.83	83000	660	0.056854	348.2605
58	0.93	0.72	0.05	0.83	83000	645	0.056854	340.3454
60	0.93	0.72	0.05	0.83	83000	640	0.056854	337.7071
62	0.93	0.72	0.05	0.83	83000	640	0.056854	337.7071
64	0.93	0.72	0.05	0.83	83000	640	0.056854	337.7071
66	0.93	0.72	0.28	0.6	60000	350	0.056854	184.6836
68	0.93	0.72	0.28	0.6	60000	350	0.056854	184.6836
70	0.93	0.72	0.28	0.6	60000	350	0.056854	184.6836
72	0.93	0.72	0.6	0.28	28000	160	0.056854	84.42678
74	0.93	0.72	0.6	0.28	28000	160	0.056854	84.42678
76	0.93	0.72	0.6	0.28	28000	160	0.056854	84.42678
78	0.93	0.72	0.88	0	0	0	0.056854	0

Tabulated Step by Step Test Data for 2400 ppm Emulsion in 0.1 M NaCl at Crossflow Velocity 1.52 m/s

Time(min)	P_f	Pr	Pp	TMP(bar)	TMP(Pa)	Vol.(ml)	A (m2)	Flux(L/m^{2}h)
0	0.58	0.5	0.54	0	0	0	0.056854	0
2	0.58	0.5	0.44	0.1	10000	116	0.056854	61.20941
4	0.58	0.5	0.44	0.1	10000	116	0.056854	61.20941
6	0.58	0.5	0.44	0.1	10000	116	0.056854	61.20941
8	0.58	0.5	0.44	0.1	10000	116	0.056854	61.20941
10	0.58	0.5	0.44	0.1	10000	116	0.056854	61.20941
12	0.58	0.5	0.32	0.22	22000	232	0.056854	122.4188
14	0.58	0.5	0.32	0.22	22000	228	0.056854	120.3082
16	0.58	0.5	0.32	0.22	22000	226	0.056854	119.2528
18	0.58	0.5	0.32	0.22	22000	226	0.056854	119.2528
20	0.58	0.5	0.32	0.22	22000	205	0.056854	108.1718
22	0.58	0.5	0.32	0.22	22000	195	0.056854	102.8951
24	0.58	0.5	0.32	0.22	22000	190	0.056854	100.2568
26	0.58	0.5	0.32	0.22	22000	190	0.056854	100.2568
28	0.58	0.5	0.32	0.22	22000	190	0.056854	100.2568
30	0.58	0.5	0.2	0.34	34000	265	0.056854	139.8319
32	0.58	0.5	0.2	0.34	34000	255	0.056854	134.5552
34	0.58	0.5	0.2	0.34	34000	245	0.056854	129.2785
36	0.58	0.5	0.2	0.34	34000	230	0.056854	121.3635
38	0.58	0.5	0.2	0.34	34000	220	0.056854	116.0868
40	0.58	0.5	0.2	0.34	34000	220	0.056854	116.0868
42	0.58	0.5	0.2	0.34	34000	220	0.056854	116.0868
44	0.58	0.5	0.2	0.34	34000	220	0.056854	116.0868
46	0.58	0.5	0	0.54	54000	355	0.056854	187.3219
48	0.58	0.5	0	0.54	54000	345	0.056854	182.0452
50	0.58	0.5	0	0.54	54000	335	0.056854	176.7686
52	0.58	0.5	0	0.54	54000	300	0.056854	158.3002
54	0.58	0.5	0	0.54	54000	280	0.056854	147.7469
56	0.58	0.5	0	0.54	54000	217	0.056854	114.5038
58	0.58	0.5	0	0.54	54000	206	0.056854	108.6995
60	0.58	0.5	0	0.54	54000	200	0.056854	105.5335
62	0.58	0.5	0	0.54	54000	195	0.056854	102.8951
64	0.58	0.5	0	0.54	54000	190	0.056854	100.2568
66	0.58	0.5	0	0.54	54000	190	0.056854	100.2568
68	0.58	0.5	0	0.54	54000	180	0.056854	94.98012
70	0.58	0.5	0	0.54	54000	180	0.056854	94.98012
72	0.58	0.5	0	0.54	54000	180	0.056854	94.98012
74	0.58	0.5	0.2	0.34	34000	100	0.056854	52.76674
76	0.58	0.5	0.2	0.34	34000	100	0.056854	52.76674
78	0.58	0.5	0.2	0.34	34000	100	0.056854	52.76674
80	0.58	0.5	0.4	0.14	14000	48	0.056854	25.32803
82	0.58	0.5	0.4	0.14	14000	48	0.056854	25.32803
84	0.58	0.5	0.4	0.14	14000	48	0.056854	25.32803
86	0.58	0.5	0.54	0	0	0	0.056854	0

Tabulated Step by Step Test Data for 2400 ppm Emulsion in 0.1M $CaCl_2$ at Crossflow Velocity 1.52 m/s

Time(min)	P_f	Pr	Pp	TMP(bar)	TMP(Pa)	Vol.(ml)	A (m2)	Flux(L/m^2h)
0	0.62	0.52	0.6	0	0	0	0.056854	0
2	0.62	0.52	0.5	0.1	10000	158	0.056854	83.37144
4	0.62	0.52	0.5	0.1	10000	158	0.056854	83.37144
6	0.62	0.52	0.5	0.1	10000	158	0.056854	83.37144
8	0.62	0.52	0.5	0.1	10000	158	0.056854	83.37144
10	0.62	0.52	0.5	0.1	10000	158	0.056854	83.37144
12	0.62	0.52	0.4	0.2	20000	310	0.056854	163.5769
14	0.62	0.52	0.4	0.2	20000	310	0.056854	163.5769
16	0.62	0.52	0.4	0.2	20000	310	0.056854	163.5769
18	0.62	0.52	0.4	0.2	20000	310	0.056854	163.5769
20	0.62	0.52	0.4	0.2	20000	310	0.056854	163.5769
22	0.62	0.52	0.3	0.3	30000	455	0.056854	240.0886
24	0.62	0.52	0.3	0.3	30000	450	0.056854	237.4503
26	0.62	0.52	0.3	0.3	30000	450	0.056854	237.4503
28	0.62	0.52	0.3	0.3	30000	450	0.056854	237.4503
30	0.62	0.52	0.3	0.3	30000	425	0.056854	224.2586
32	0.62	0.52	0.3	0.3	30000	425	0.056854	224.2586
34	0.62	0.52	0.3	0.3	30000	425	0.056854	224.2586
36	0.62	0.52	0.3	0.3	30000	425	0.056854	224.2586
38	0.62	0.52	0.3	0.3	30000	425	0.056854	224.2586
40	0.62	0.52	0.2	0.4	40000	558	0.056854	294.4384
42	0.62	0.52	0.2	0.4	40000	555	0.056854	292.8554
44	0.62	0.52	0.2	0.4	40000	540	0.056854	284.9404
46	0.62	0.52	0.2	0.4	40000	532	0.056854	280.719
48	0.62	0.52	0.2	0.4	40000	530	0.056854	279.6637
50	0.62	0.52	0.2	0.4	40000	530	0.056854	279.6637
52	0.62	0.52	0.2	0.4	40000	520	0.056854	274.387
54	0.62	0.52	0.2	0.4	40000	520	0.056854	274.387
56	0.62	0.52	0.2	0.4	40000	480	0.056854	253.2803
58	0.62	0.52	0.2	0.4	40000	480	0.056854	253.2803
60	0.62	0.52	0.2	0.4	40000	480	0.056854	253.2803
62	0.62	0.52	0.05	0.55	55000	695	0.056854	366.7288
64	0.62	0.52	0.05	0.55	55000	680	0.056854	358.8138
66	0.62	0.52	0.05	0.55	55000	680	0.056854	358.8138
68	0.62	0.52	0.05	0.55	55000	680	0.056854	358.8138
70	0.62	0.52	0.05	0.55	55000	680	0.056854	358.8138
72	0.62	0.52	0.2	0.4	40000	470	0.056854	248.0037
74	0.62	0.52	0.2	0.4	40000	470	0.056854	248.0037
76	0.62	0.52	0.2	0.4	40000	470	0.056854	248.0037
78	0.62	0.52	0.4	0.2	20000	240	0.056854	126.6402
80	0.62	0.52	0.4	0.2	20000	240	0.056854	126.6402
82	0.62	0.52	0.4	0.2	20000	240	0.056854	126.6402
84	0.62	0.52	0.6	0	0	0	0.056854	0

Tabulated Step by Step Test Data for 2400 ppm Emulsion in 0.1M $FeCl_3$ at Crossflow Velocity 1.52 m/

Time(min)	P_f	Pr	Pp	TMP(bar)	TMP(Pa)	Vol.(ml)	A (m2)	Flux(L/m^{2}h)
0	0.65	0.52	0.62	0	0	0	0.056854	0
2	0.65	0.52	0.5	0.12	12000	114	0.056854	60.15408
4	0.65	0.52	0.5	0.12	12000	114	0.056854	60.15408
6	0.65	0.52	0.5	0.12	12000	114	0.056854	60.15408
8	0.65	0.52	0.5	0.12	12000	114	0.056854	60.15408
10	0.65	0.52	0.5	0.12	12000	114	0.056854	60.15408
12	0.65	0.52	0.4	0.22	22000	210	0.056854	110.8101
14	0.65	0.52	0.4	0.22	22000	210	0.056854	110.8101
16	0.65	0.52	0.4	0.22	22000	210	0.056854	110.8101
18	0.65	0.52	0.4	0.22	22000	210	0.056854	110.8101
20	0.65	0.52	0.4	0.22	22000	210	0.056854	110.8101
22	0.65	0.52	0.3	0.32	32000	320	0.056854	168.8536
24	0.65	0.52	0.3	0.32	32000	310	0.056854	163.5769
26	0.65	0.52	0.3	0.32	32000	305	0.056854	160.9385
28	0.65	0.52	0.3	0.32	32000	300	0.056854	158.3002
30	0.65	0.52	0.3	0.32	32000	300	0.056854	158.3002
32	0.65	0.52	0.3	0.32	32000	300	0.056854	158.3002
34	0.65	0.52	0.22	0.4	40000	350	0.056854	184.6836
36	0.65	0.52	0.22	0.4	40000	345	0.056854	182.0452
38	0.65	0.52	0.22	0.4	40000	350	0.056854	184.6836
40	0.65	0.52	0.22	0.4	40000	345	0.056854	182.0452
42	0.65	0.52	0.22	0.4	40000	340	0.056854	179.4069
44	0.65	0.52	0.22	0.4	40000	340	0.056854	179.4069
46	0.65	0.52	0.22	0.4	40000	340	0.056854	179.4069
48	0.65	0.52	0	0.62	62000	510	0.056854	269.1104
50	0.65	0.52	0	0.62	62000	500	0.056854	263.8337
52	0.65	0.52	0	0.62	62000	490	0.056854	258.557
54	0.65	0.52	0	0.62	62000	474	0.056854	250.1143
56	0.65	0.52	0	0.62	62000	470	0.056854	248.0037
58	0.65	0.52	0	0.62	62000	470	0.056854	248.0037
60	0.65	0.52	0	0.62	62000	470	0.056854	248.0037
62	0.65	0.52	0.2	0.42	42000	310	0.056854	163.5769
64	0.65	0.52	0.2	0.42	42000	310	0.056854	163.5769
66	0.65	0.52	0.2	0.42	42000	310	0.056854	163.5769
68	0.65	0.52	0.4	0.22	22000	170	0.056854	89.70345
70	0.65	0.52	0.4	0.22	22000	170	0.056854	89.70345
72	0.65	0.52	0.4	0.22	22000	170	0.056854	89.70345
74	0.65	0.52	0.62	0	0	0	0.056854	0

Tabulated Step by Step Test Data for 300 ppm Emulsion at 1.14 m/s

Time(min)	P_f	Pr	Pp	TMP(bar)	TMP(Pa)	Vol.(ml)	A (m2)	Flux(L/m^{2}h)
0	0.36	0.32	0.33	0	0	0	0.056854	0
3	0.36	0.32	0.3	0.03	3000	200	0.056854	13.36757
6	0.36	0.32	0.3	0.03	3000	200	0.056854	13.36757
9	0.36	0.32	0.3	0.03	3000	200	0.056854	13.36757
12	0.36	0.32	0.24	0.09	9000	300	0.056854	65.07897
15	0.36	0.32	0.24	0.09	9000	300	0.056854	65.07897
18	0.36	0.32	0.24	0.09	9000	300	0.056854	65.07897
21	0.36	0.32	0.18	0.15	15000	360	0.056854	105.5335
24	0.36	0.32	0.18	0.15	15000	355	0.056854	103.7746
27	0.36	0.32	0.18	0.15	15000	350	0.056854	102.0157
30	0.36	0.32	0.18	0.15	15000	350	0.056854	101.3121
33	0.36	0.32	0.18	0.15	15000	350	0.056854	98.84969
36	0.36	0.32	0.18	0.15	15000	455	0.056854	91.46234
39	0.36	0.32	0.18	0.15	15000	450	0.056854	89.70345
42	0.36	0.32	0.18	0.15	15000	430	0.056854	89.70345
45	0.36	0.32	0.12	0.21	21000	425	0.056854	128.3991
48	0.36	0.32	0.12	0.21	21000	425	0.056854	128.3991
51	0.36	0.32	0.12	0.21	21000	415	0.056854	124.8813
54	0.36	0.32	0.12	0.21	21000	415	0.056854	117.8457
57	0.36	0.32	0.12	0.21	21000	415	0.056854	117.8457
60	0.36	0.32	0.12	0.21	21000	760	0.056854	116.0868
63	0.36	0.32	0.12	0.21	21000	730	0.056854	116.0868
66	0.36	0.32	0.12	0.21	21000	695	0.056854	116.0868
69	0.36	0.32	0	0.33	33000	685	0.056854	189.9602
72	0.36	0.32	0	0.33	33000	670	0.056854	181.1658
75	0.36	0.32	0	0.33	33000	660	0.056854	172.3713
78	0.36	0.32	0	0.33	33000	640	0.056854	161.818
81	0.36	0.32	0	0.33	33000	640	0.056854	160.0591
84	0.36	0.32	0	0.33	33000	640	0.056854	158.3002
87	0.36	0.32	0	0.33	33000	425	0.056854	158.3002
90	0.36	0.32	0.16	0.17	17000	425	0.056854	80.90899
93	0.36	0.32	0.16	0.17	17000	420	0.056854	80.90899
96	0.36	0.32	0.16	0.17	17000	420	0.056854	80.90899
99	0.36	0.32	0.25	0.08	8000	250	0.056854	42.91695
102	0.36	0.32	0.25	0.08	8000	250	0.056854	42.91695
105	0.36	0.32	0.25	0.08	8000	250	0.056854	42.91695
108	0.36	0.32	0.33	0	0	0	0.056854	0

Tabulated Step by Step Test Data for 300 ppm Emulsion at 1.52 m/s

Time(min)	P_f	Pr	Pp	TMP(bar)	TMP(Pa)	Vol.(ml)	A (m2)	Flux(L/m^{2}h)
0	0.76	0.66	0.53	0	0	0	0.056854	0
3	0.76	0.66	0.5	0.03	3000	55	0.056854	19.3478
6	0.76	0.66	0.5	0.03	3000	55	0.056854	19.3478
9	0.76	0.66	0.5	0.03	3000	55	0.056854	19.3478
12	0.76	0.66	0.44	0.09	9000	173	0.056854	60.85764
15	0.76	0.66	0.44	0.09	9000	173	0.056854	60.85764
18	0.76	0.66	0.44	0.09	9000	173	0.056854	60.85764
21	0.76	0.66	0.44	0.09	9000	170	0.056854	59.8023
24	0.76	0.66	0.44	0.09	9000	170	0.056854	59.8023
27	0.76	0.66	0.44	0.09	9000	170	0.056854	59.8023
30	0.76	0.66	0.38	0.15	15000	265	0.056854	93.22123
33	0.76	0.66	0.38	0.15	15000	265	0.056854	93.22123
36	0.76	0.66	0.38	0.15	15000	265	0.056854	93.22123
39	0.76	0.66	0.38	0.15	15000	265	0.056854	93.22123
42	0.76	0.66	0.32	0.21	21000	355	0.056854	124.8813
45	0.76	0.66	0.32	0.21	21000	350	0.056854	123.1224
48	0.76	0.66	0.32	0.21	21000	350	0.056854	123.1224
51	0.76	0.66	0.32	0.21	21000	350	0.056854	123.1224
54	0.76	0.66	0.24	0.29	29000	435	0.056854	153.0235
57	0.76	0.66	0.24	0.29	29000	430	0.056854	151.2646
60	0.76	0.66	0.24	0.29	29000	435	0.056854	153.0235
63	0.76	0.66	0.24	0.29	29000	435	0.056854	153.0235
66	0.76	0.66	0.24	0.29	29000	435	0.056854	153.0235
69	0.76	0.66	0.16	0.37	37000	490	0.056854	172.3713
72	0.76	0.66	0.16	0.37	37000	485	0.056854	170.6124
75	0.76	0.66	0.16	0.37	37000	468	0.056854	164.6322
78	0.76	0.66	0.16	0.37	37000	470	0.056854	165.3358
81	0.76	0.66	0.16	0.37	37000	468	0.056854	164.6322
84	0.76	0.66	0.16	0.37	37000	468	0.056854	164.6322
87	0.76	0.66	0	0.53	53000	570	0.056854	200.5136
90	0.76	0.66	0	0.53	53000	535	0.056854	188.2014
93	0.76	0.66	0	0.53	53000	515	0.056854	181.1658
96	0.76	0.66	0	0.53	53000	500	0.056854	175.8891
99	0.76	0.66	0	0.53	53000	500	0.056854	175.8891
102	0.76	0.66	0	0.53	53000	485	0.056854	170.6124
105	0.76	0.66	0	0.53	53000	485	0.056854	170.6124
108	0.76	0.66	0.19	0.34	34000	315	0.056854	110.8101
111	0.76	0.66	0.19	0.34	34000	315	0.056854	110.8101
114	0.76	0.66	0.19	0.34	34000	315	0.056854	110.8101
117	0.76	0.66	0.38	0.15	15000	165	0.056854	58.04341
120	0.76	0.66	0.38	0.15	15000	165	0.056854	58.04341
123	0.76	0.66	0.38	0.15	15000	165	0.056854	58.04341
126	0.76	0.66	0.44	0.09	9000	100	0.056854	35.17782
129	0.76	0.66	0.44	0.09	9000	100	0.056854	35.17782
132	0.76	0.66	0.44	0.09	9000	100	0.056854	35.17782
135	0.76	0.66	0.44	0.09	9000	100	0.056854	35.17782
138	0.76	0.66	0.53	0	0	0	0.056854	0

Tabulated Step by Step Test Data for 300 ppm Emulsion at 1.92 m/s

Time(min)	P_f	Pr	Pp	TMP(bar)	TMP(Pa)	Vol.(ml)	A (m2)	Flux(L/m^{2}h)
0	0.76	0.62	0.74	0.76	0	0	0.056854	0
3	0.76	0.62	0.66	0.76	0.08	165	0.056854	58.04341
6	0.76	0.62	0.66	0.76	0.08	165	0.056854	58.04341
9	0.76	0.62	0.66	0.76	0.08	165	0.056854	58.04341
12	0.76	0.62	0.56	0.76	0.18	380	0.056854	133.6757
15	0.76	0.62	0.56	0.76	0.18	380	0.056854	133.6757
18	0.76	0.62	0.56	0.76	0.18	380	0.056854	133.6757
21	0.76	0.62	0.48	0.76	0.26	525	0.056854	184.6836
24	0.76	0.62	0.48	0.76	0.26	525	0.056854	184.6836
27	0.76	0.62	0.48	0.76	0.26	520	0.056854	182.9247
30	0.76	0.62	0.48	0.76	0.26	520	0.056854	182.9247
33	0.76	0.62	0.48	0.76	0.26	520	0.056854	182.9247
36	0.76	0.62	0.38	0.76	0.36	685	0.056854	240.9681
39	0.76	0.62	0.38	0.76	0.36	680	0.056854	239.2092
42	0.76	0.62	0.38	0.76	0.36	675	0.056854	237.4503
45	0.76	0.62	0.38	0.76	0.36	660	0.056854	232.1736
48	0.76	0.62	0.38	0.76	0.36	640	0.056854	225.1381
51	0.76	0.62	0.38	0.76	0.36	640	0.056854	225.1381
54	0.76	0.62	0.38	0.76	0.36	640	0.056854	225.1381
57	0.76	0.62	0.02	0.76	0.72	1120	0.056854	393.9916
60	0.76	0.62	0.02	0.76	0.72	1060	0.056854	372.8849
63	0.76	0.62	0.02	0.76	0.72	1045	0.056854	367.6083
66	0.76	0.62	0.02	0.76	0.72	1020	0.056854	358.8138
69	0.76	0.62	0.02	0.76	0.72	1015	0.056854	357.0549
72	0.76	0.62	0.02	0.76	0.72	990	0.056854	348.2605
75	0.76	0.62	0.02	0.76	0.72	955	0.056854	335.9482
78	0.76	0.62	0.02	0.76	0.72	950	0.056854	334.1893
81	0.76	0.62	0.02	0.76	0.72	940	0.056854	330.6715
84	0.76	0.62	0.02	0.76	0.72	940	0.056854	330.6715
87	0.76	0.62	0.31	0.76	0.43	590	0.056854	207.5492
90	0.76	0.62	0.31	0.76	0.43	590	0.056854	207.5492
93	0.76	0.62	0.31	0.76	0.43	580	0.056854	204.0314
96	0.76	0.62	0.31	0.76	0.43	580	0.056854	204.0314
99	0.76	0.62	0.5	0.76	0.24	335	0.056854	117.8457
102	0.76	0.62	0.5	0.76	0.24	335	0.056854	117.8457
105	0.76	0.62	0.5	0.76	0.24	335	0.056854	117.8457
108	0.76	0.62	0.68	0.76	0.06	85	0.056854	29.90115
111	0.76	0.62	0.68	0.76	0.06	80	0.056854	28.14226
114	0.76	0.62	0.68	0.76	0.06	80	0.056854	28.14226
117	0.76	0.62	0.68	0.76	0.06	80	0.056854	28.14226
120	0.76	0.62	0.68	0.76	0.06	80	0.056854	28.14226
123	0.76	0.62	0.74	0.76	0	0	0.056854	0

Tabulated Step by Step Test Data for 300 ppm Emulsion at 2. 28 m/s

Time(min)	P_f	Pr	Pp	TMP(bar)	TMP(Pa)	Vol.(ml)	A (m2)	Flux(L/m^{2}h)
0	0.94	0.71	0.9	0	0	0	0.056854	0
2	0.94	0.71	0.8	0.1	10000	160	0.056854	84.42678
4	0.94	0.71	0.8	0.1	10000	160	0.056854	84.42678
6	0.94	0.71	0.8	0.1	10000	160	0.056854	84.42678
8	0.94	0.71	0.8	0.1	10000	160	0.056854	84.42678
10	0.94	0.71	0.7	0.2	20000	300	0.056854	158.3002
12	0.94	0.71	0.7	0.2	20000	300	0.056854	158.3002
14	0.94	0.71	0.7	0.2	20000	300	0.056854	158.3002
16	0.94	0.71	0.7	0.2	20000	300	0.056854	158.3002
18	0.94	0.71	0.6	0.3	30000	410	0.056854	216.3436
20	0.94	0.71	0.6	0.3	30000	410	0.056854	216.3436
22	0.94	0.71	0.6	0.3	30000	410	0.056854	216.3436
24	0.94	0.71	0.6	0.3	30000	410	0.056854	216.3436
26	0.94	0.71	0.5	0.4	40000	480	0.056854	253.2803
28	0.94	0.71	0.5	0.4	40000	480	0.056854	253.2803
30	0.94	0.71	0.5	0.4	40000	480	0.056854	253.2803
32	0.94	0.71	0.4	0.5	50000	567	0.056854	299.0115
34	0.94	0.71	0.4	0.5	50000	560	0.056854	295.4937
36	0.94	0.71	0.4	0.5	50000	553	0.056854	291.9759
38	0.94	0.71	0.4	0.5	50000	513	0.056854	270.8692
40	0.94	0.71	0.4	0.5	50000	513	0.056854	270.8692
42	0.94	0.71	0.4	0.5	50000	513	0.056854	270.8692
44	0.94	0.71	0.3	0.6	60000	587	0.056854	309.5649
46	0.94	0.71	0.3	0.6	60000	580	0.056854	306.0471
48	0.94	0.71	0.3	0.6	60000	573	0.056854	304.2882
50	0.94	0.71	0.3	0.6	60000	573	0.056854	302.5293
52	0.94	0.71	0.3	0.6	60000	573	0.056854	302.5293
54	0.94	0.71	0.05	0.85	85000	750	0.056854	395.7505
56	0.94	0.71	0.05	0.85	85000	725	0.056854	382.5588
58	0.94	0.71	0.05	0.85	85000	700	0.056854	369.3672
60	0.94	0.71	0.05	0.85	85000	680	0.056854	360.1825
62	0.94	0.71	0.05	0.85	85000	680	0.056854	358.8138
64	0.94	0.71	0.05	0.85	85000	680	0.056854	358.8138
66	0.94	0.71	0.05	0.85	85000	670	0.056854	353.5371
68	0.94	0.71	0.05	0.85	85000	655	0.056854	345.6221
70	0.94	0.71	0.05	0.85	85000	650	0.056854	342.9838
72	0.94	0.71	0.05	0.85	85000	650	0.056854	342.9838
74	0.94	0.71	0.05	0.85	85000	630	0.056854	332.4304
76	0.94	0.71	0.05	0.85	85000	630	0.056854	332.4304
78	0.94	0.71	0.05	0.85	85000	630	0.056854	332.4304
80	0.94	0.71	0.3	0.6	60000	418	0.056854	220.565
82	0.94	0.71	0.3	0.6	60000	418	0.056854	220.565
84	0.94	0.71	0.3	0.6	60000	418	0.056854	220.565
86	0.94	0.71	0.5	0.4	40000	280	0.056854	147.7469
88	0.94	0.71	0.5	0.4	40000	280	0.056854	147.7469
90	0.94	0.71	0.5	0.4	40000	280	0.056854	147.7469
92	0.94	0.71	0.7	0.2	20000	154	0.056854	81.26077
94	0.94	0.71	0.7	0.2	20000	154	0.056854	81.26077
96	0.94	0.71	0.7	0.2	20000	154	0.056854	81.26077
98	0.94	0.71	0.7	0.2	20000	154	0.056854	81.26077
100	0.94	0.71	0.9	0	0	0	0.056854	0

Appendix B

Experimental Plots for Critical Flux Determination

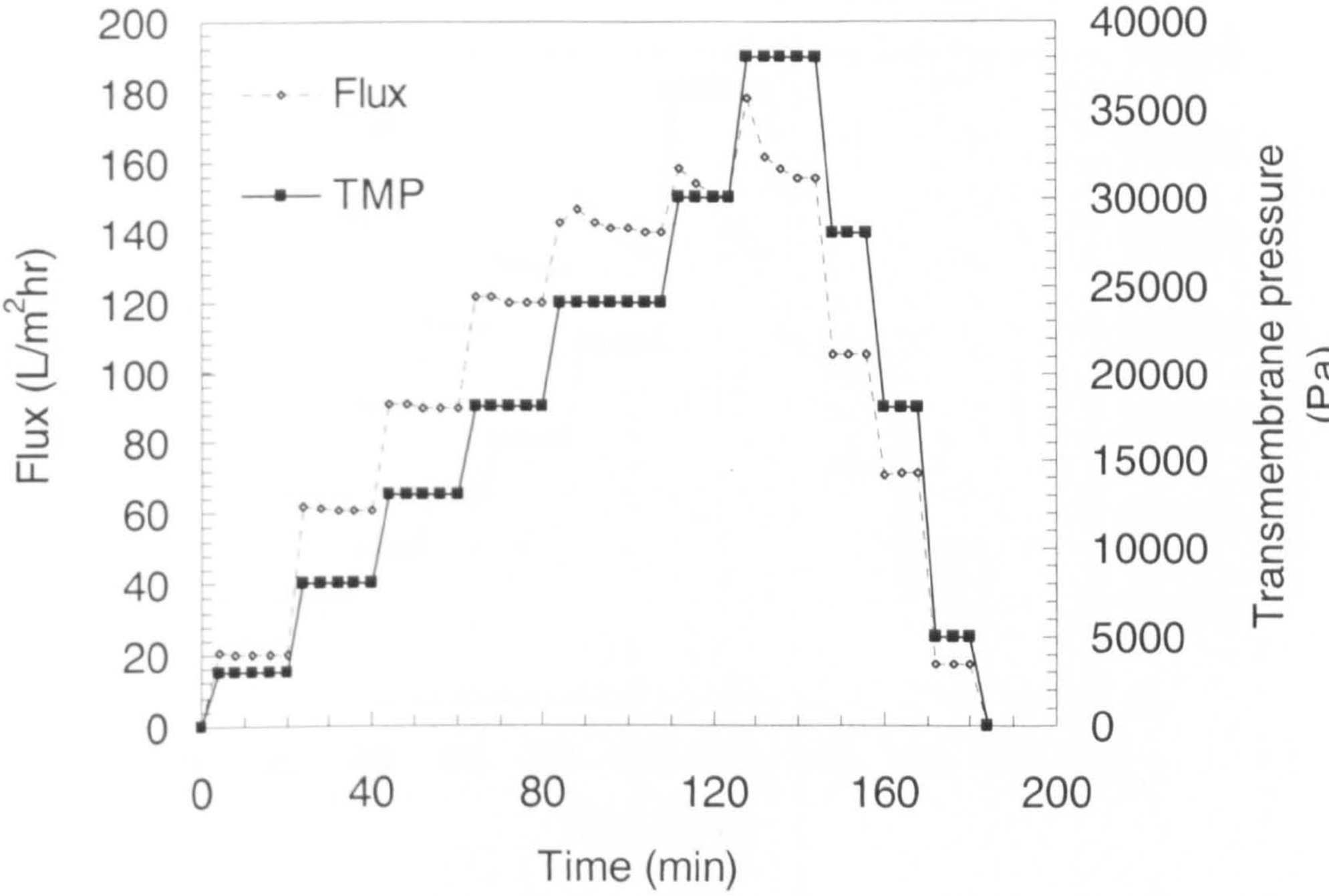

(a)

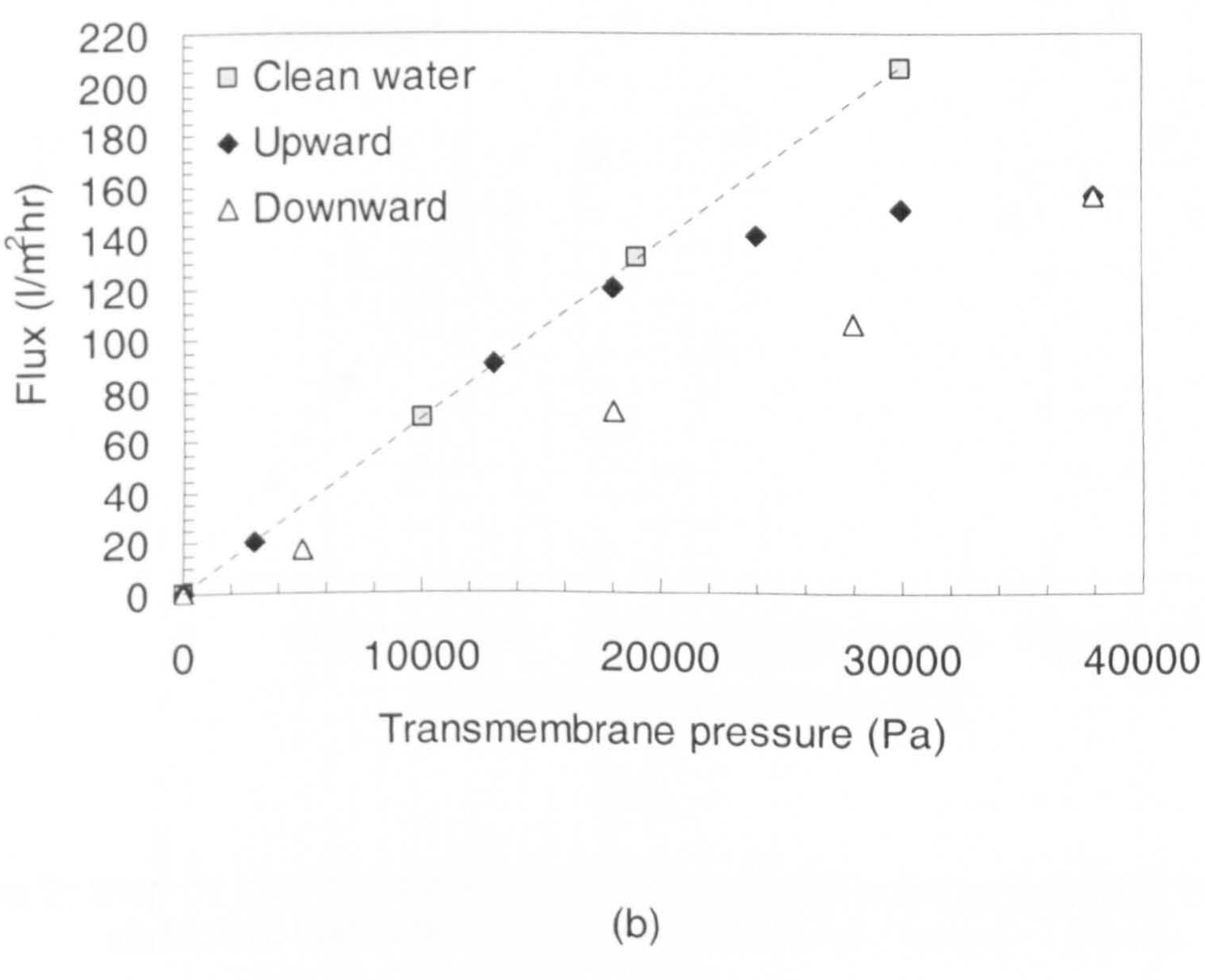

(b)

Figure 1: Step by step results for the filtration of 600 ppm n-dodecane emulsions, Surfactant Concentration 60 ppm, crossflow velocity 1.14 m/s

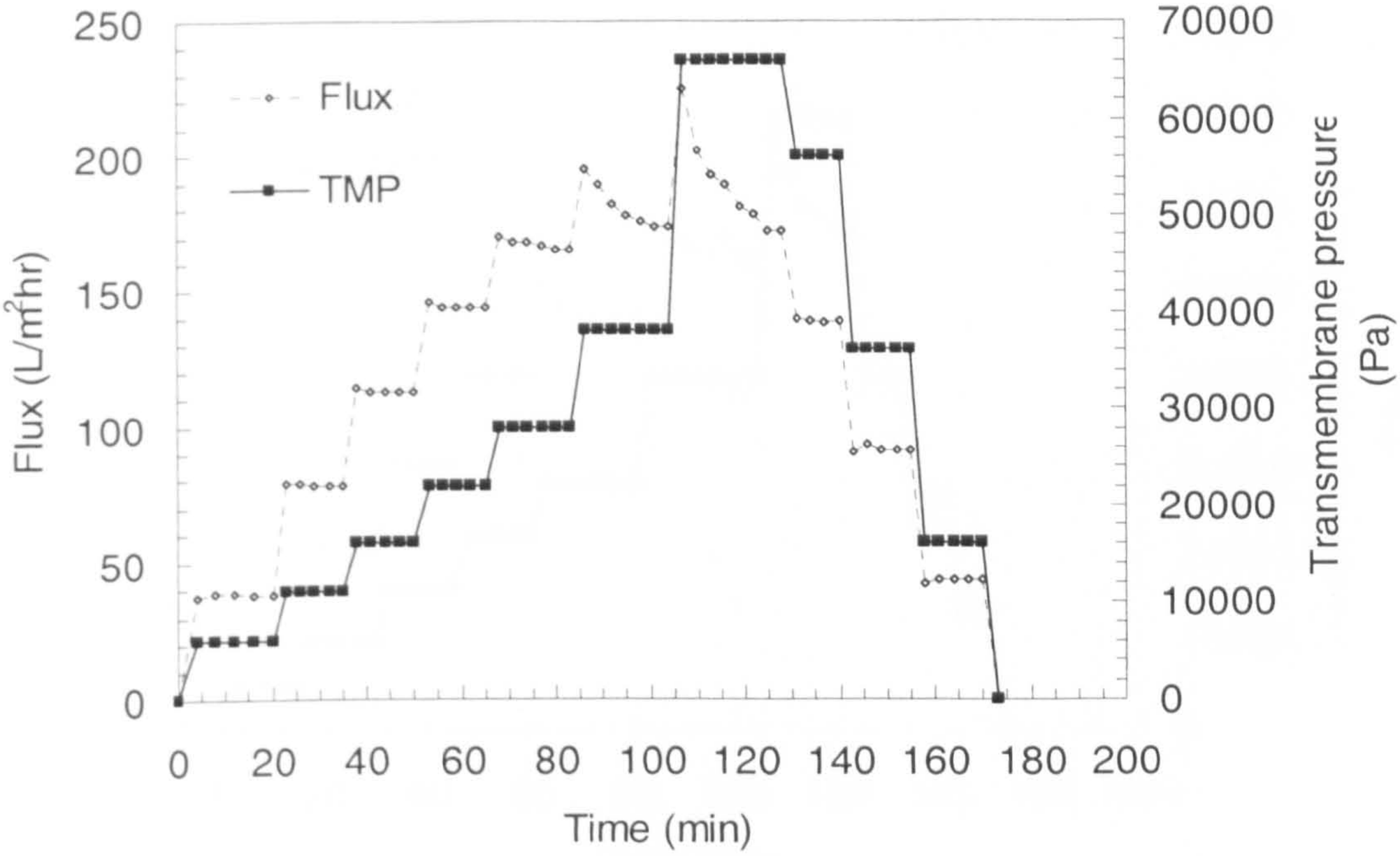

(a)

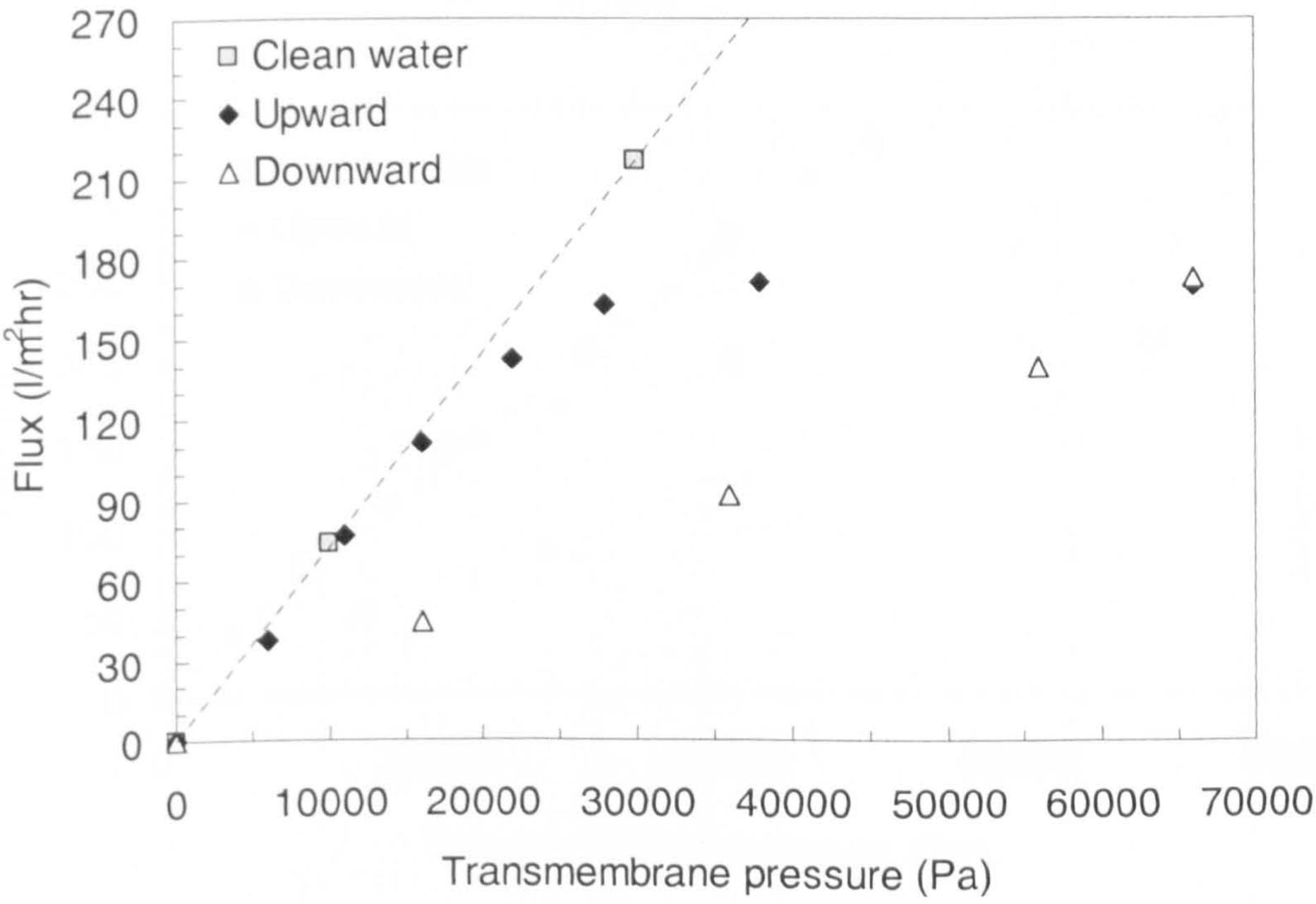

(b)

Figure 2: Step by step results for the filtration of 600 ppm n-dodecane emulsions, surfactant concentration 60 ppm, crossflow velocity 1.52m/s

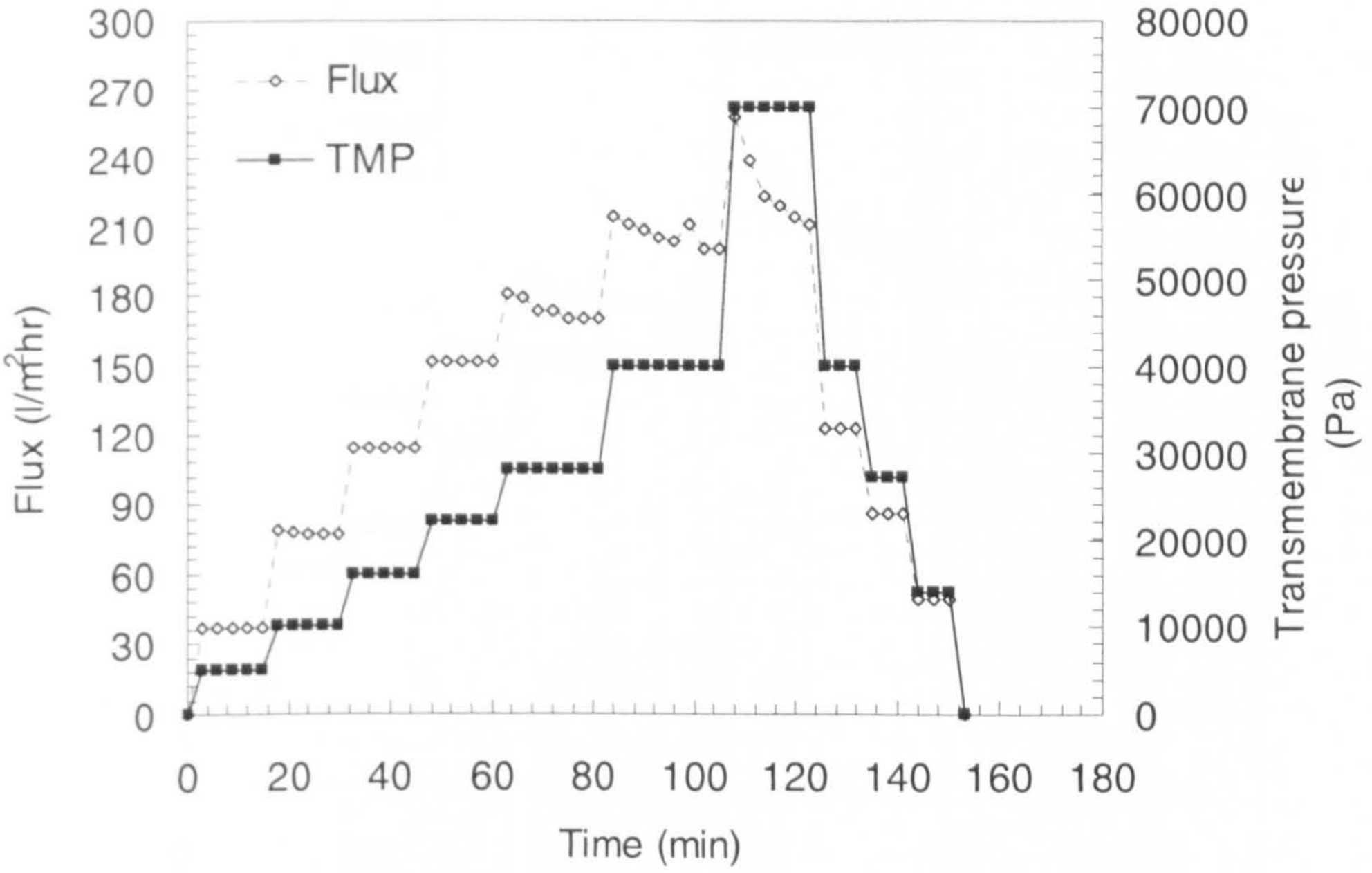

(a)

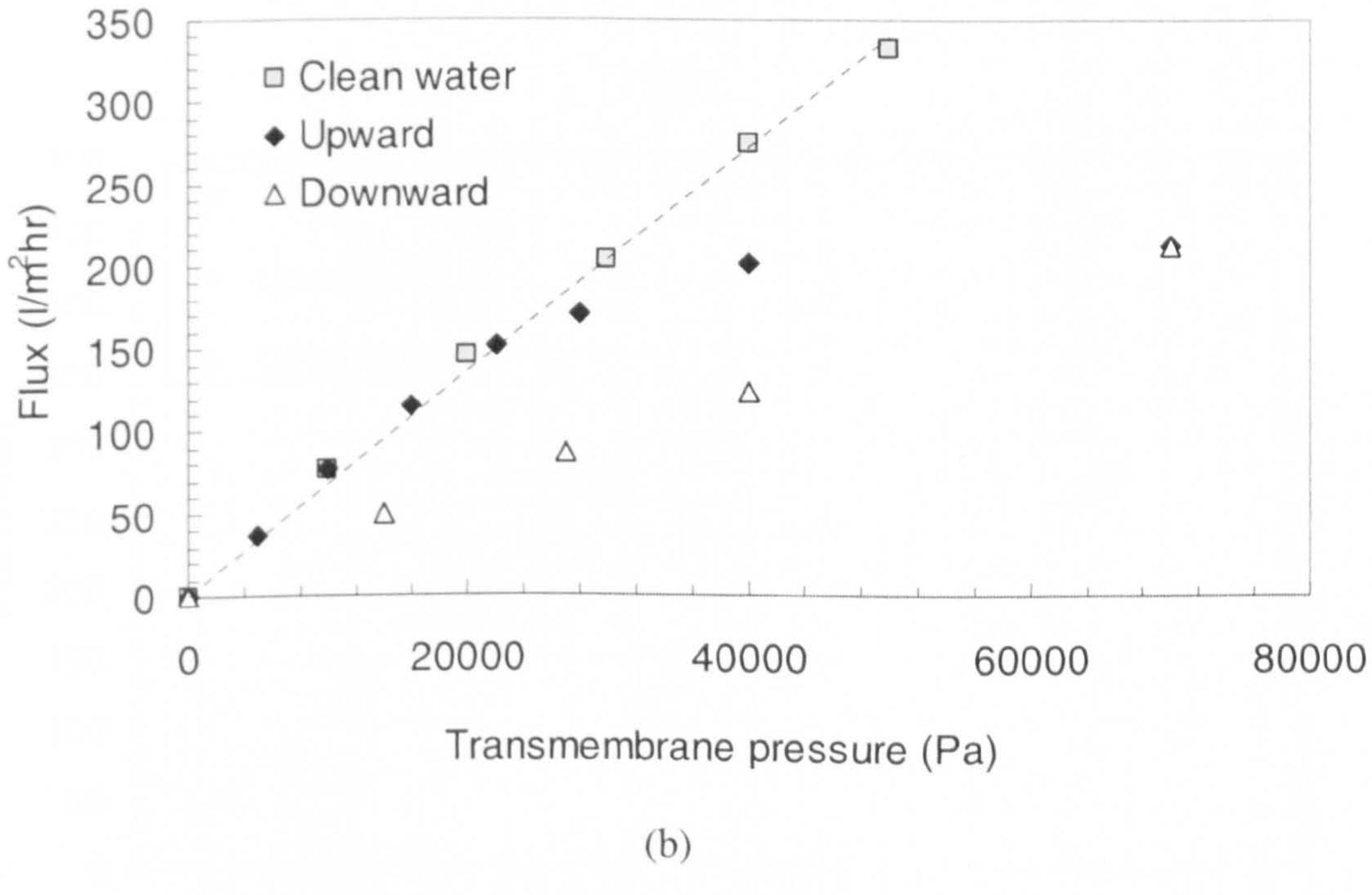

(b)

Figure 3: Step by step results for the filtration of 600 ppm n-dodecane emulsions, surfactant concentration 60 ppm, crossflow velocity 1.92m/s

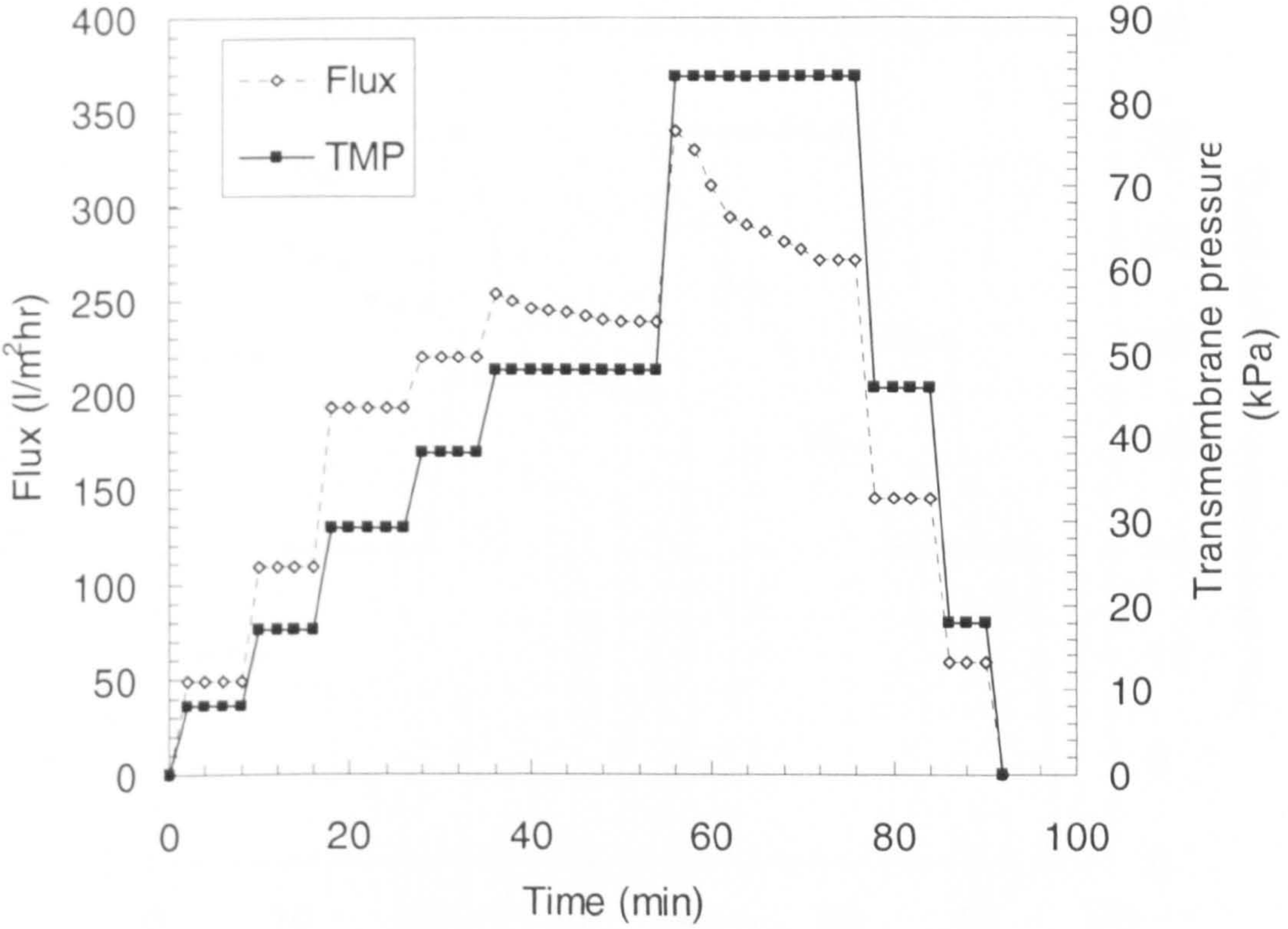

(a)

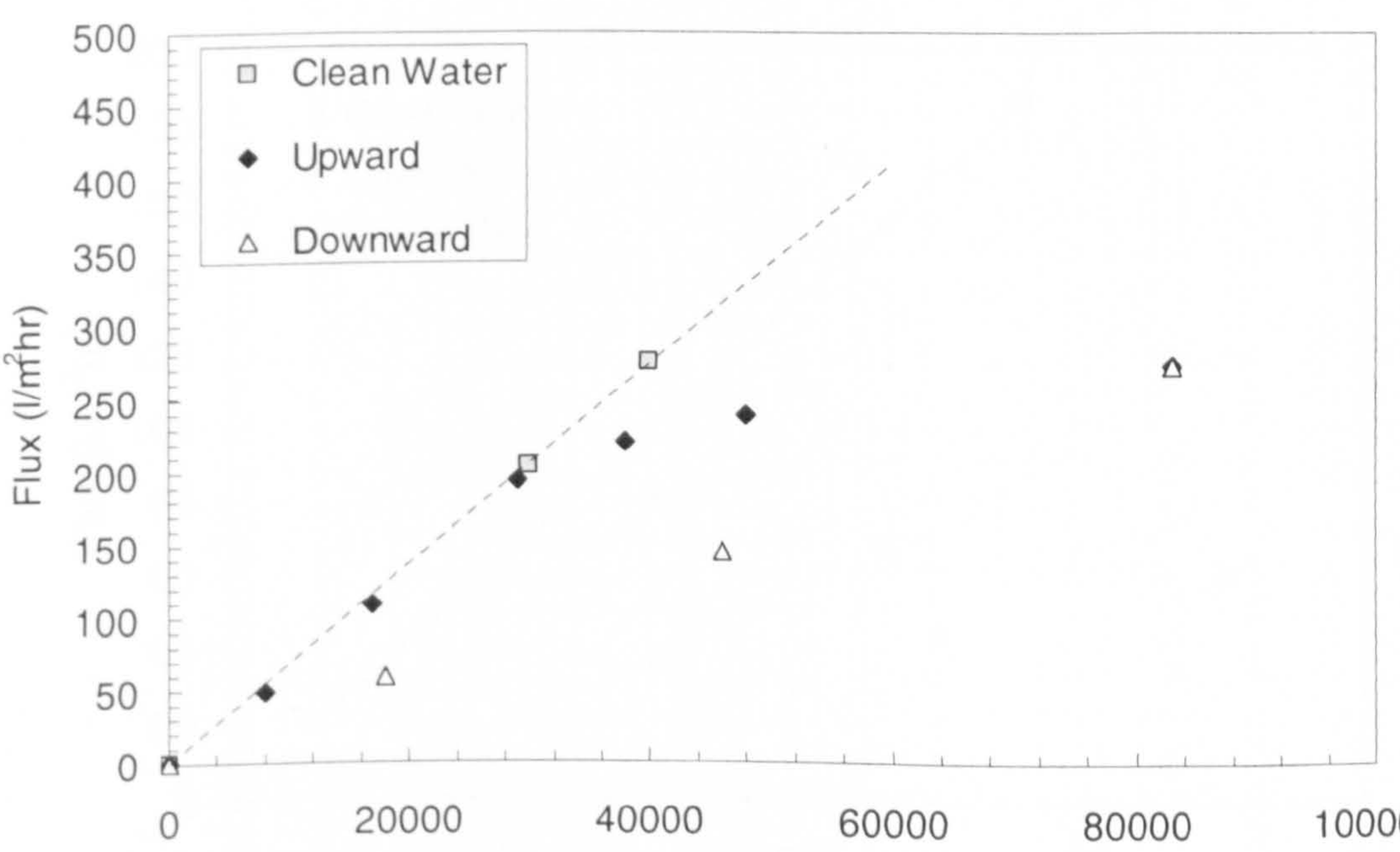

(b)

Figure 4: Step by step results for the filtration of 600 ppm n-dodecane emulsions, surfactant Concentration 60 ppm, crossflow velocity 2.28 m/s

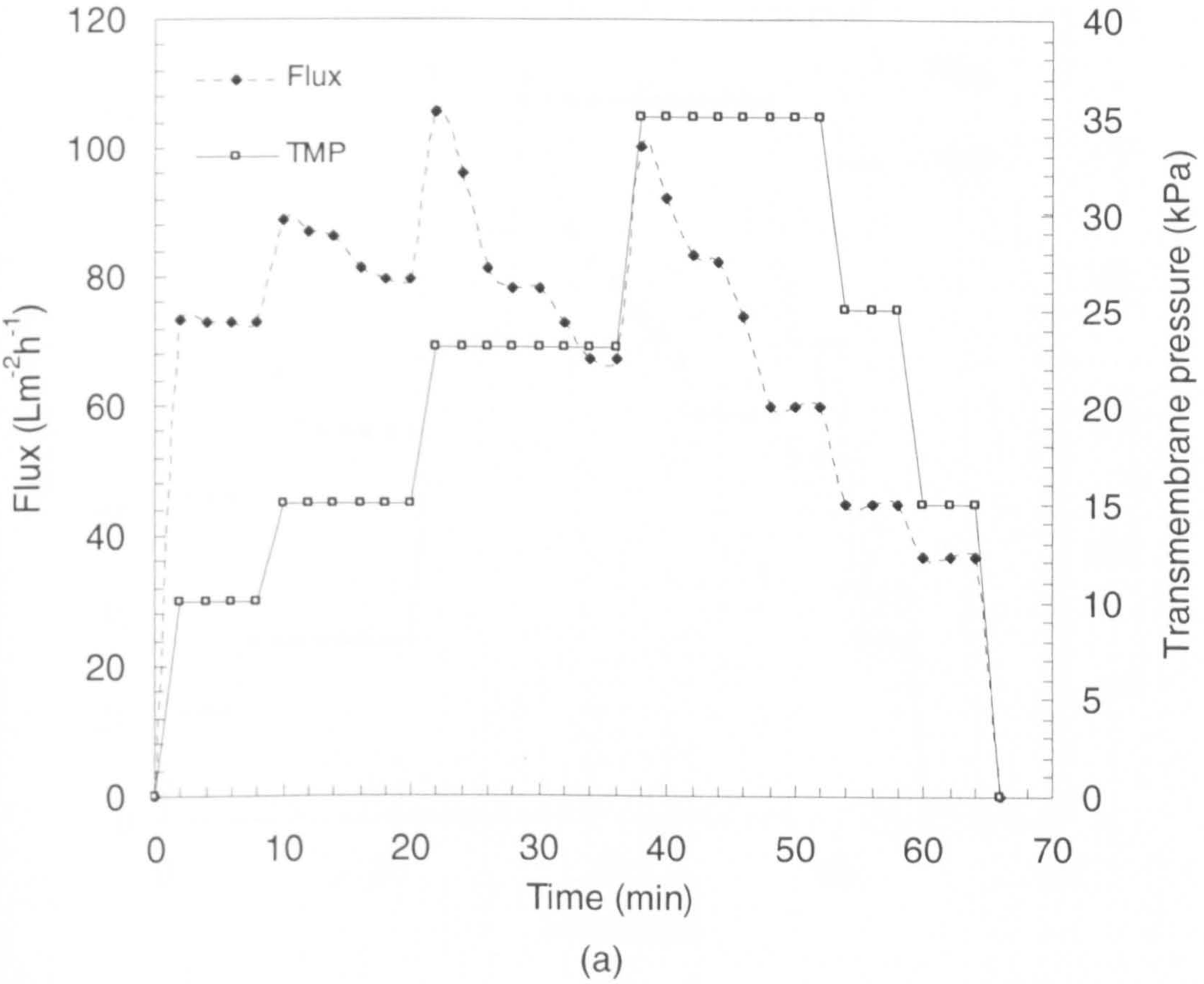

(a)

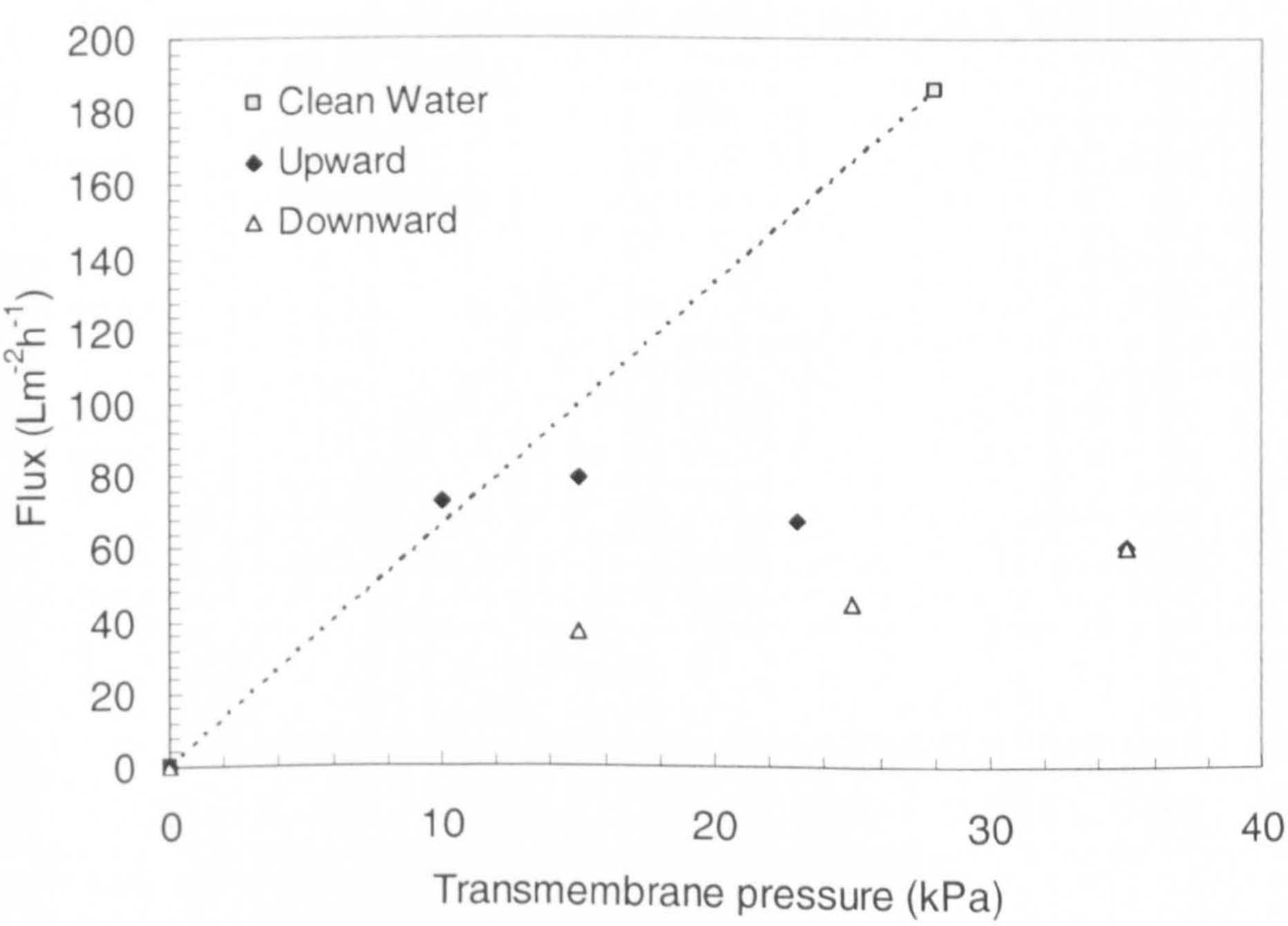

(b)

Figure 5: Step by step results for the filtration of 600 ppm n-dodecane emulsions, surfactant concentration 60 ppm, crossflow velocity 1.14 m/s, NaCl 0.1 M

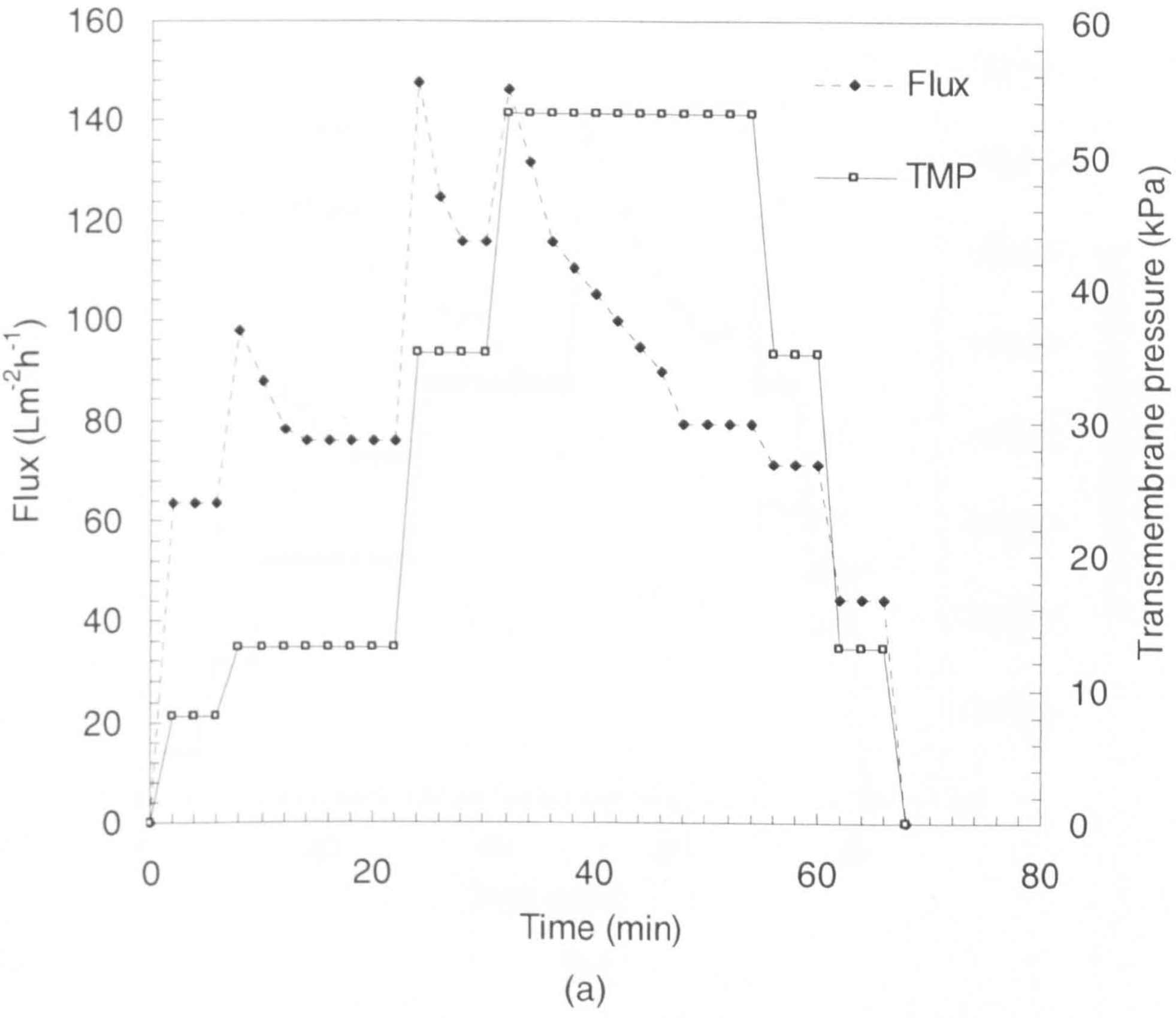

(a)

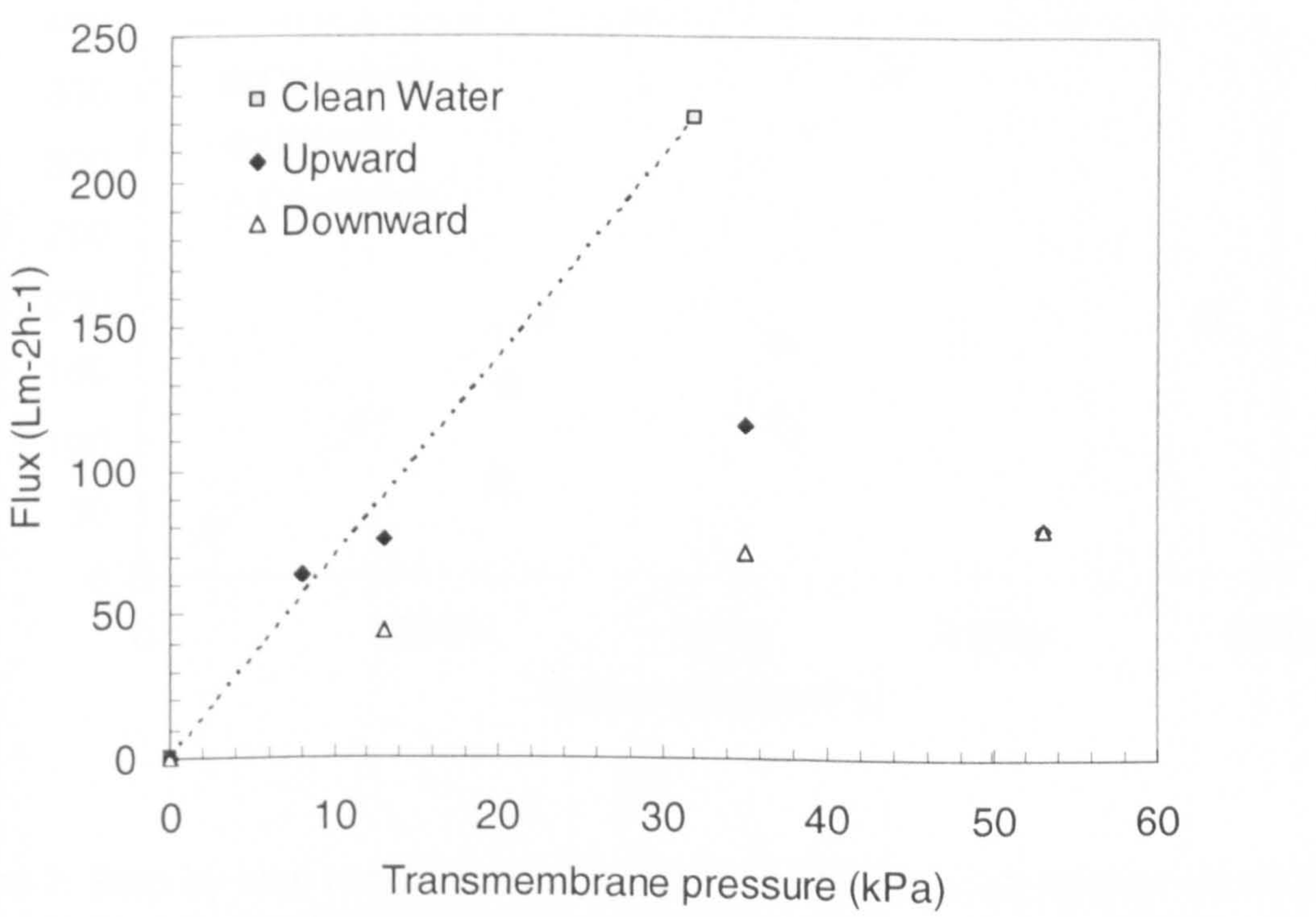

(b)

Figure 6: Step by step results for the filtration of 600 ppm n-dodecane emulsions, surfactant concentration 60 ppm, crossflow velocity 1.52 m/s, NaCl 0.1 M

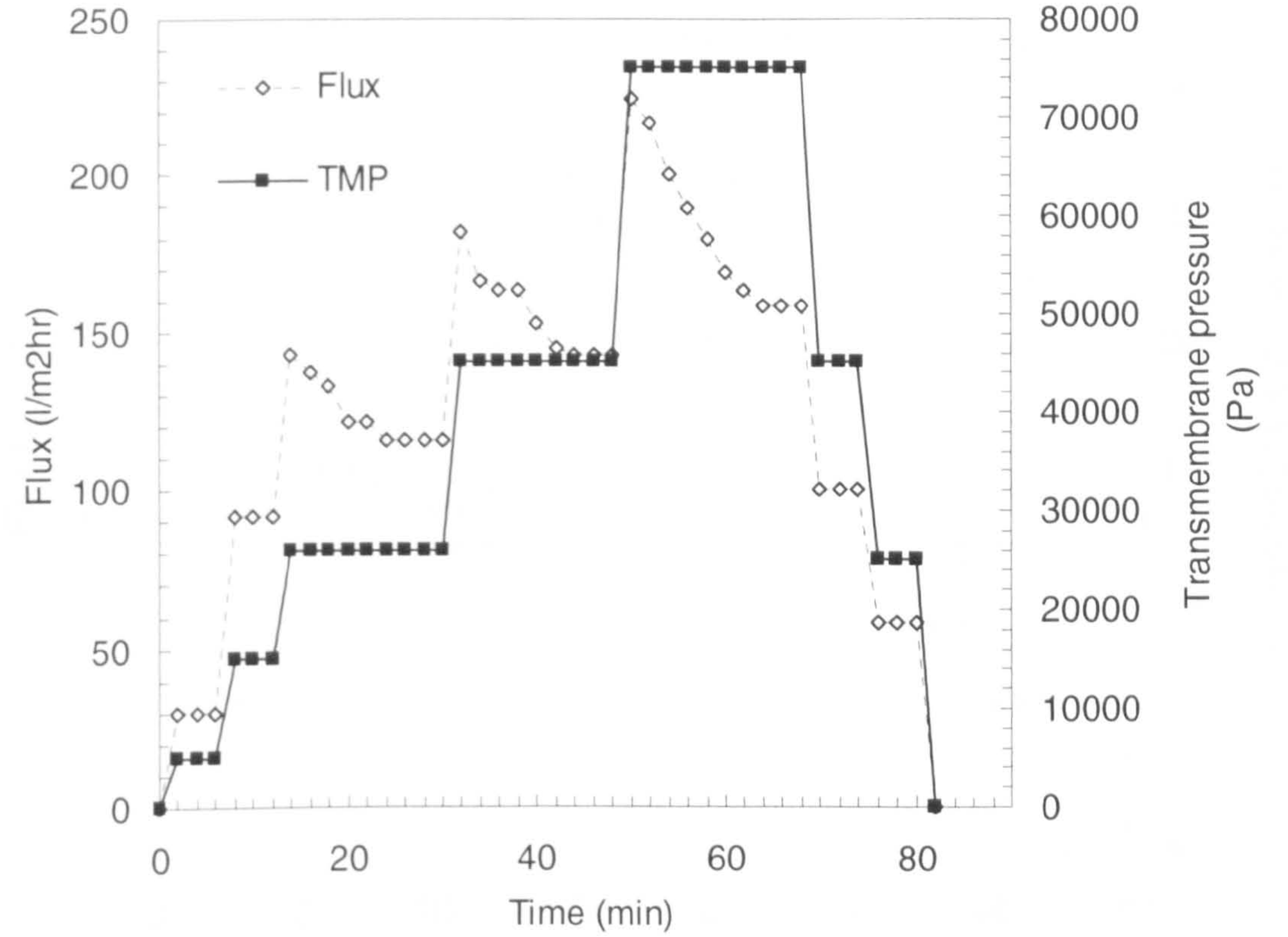

(a)

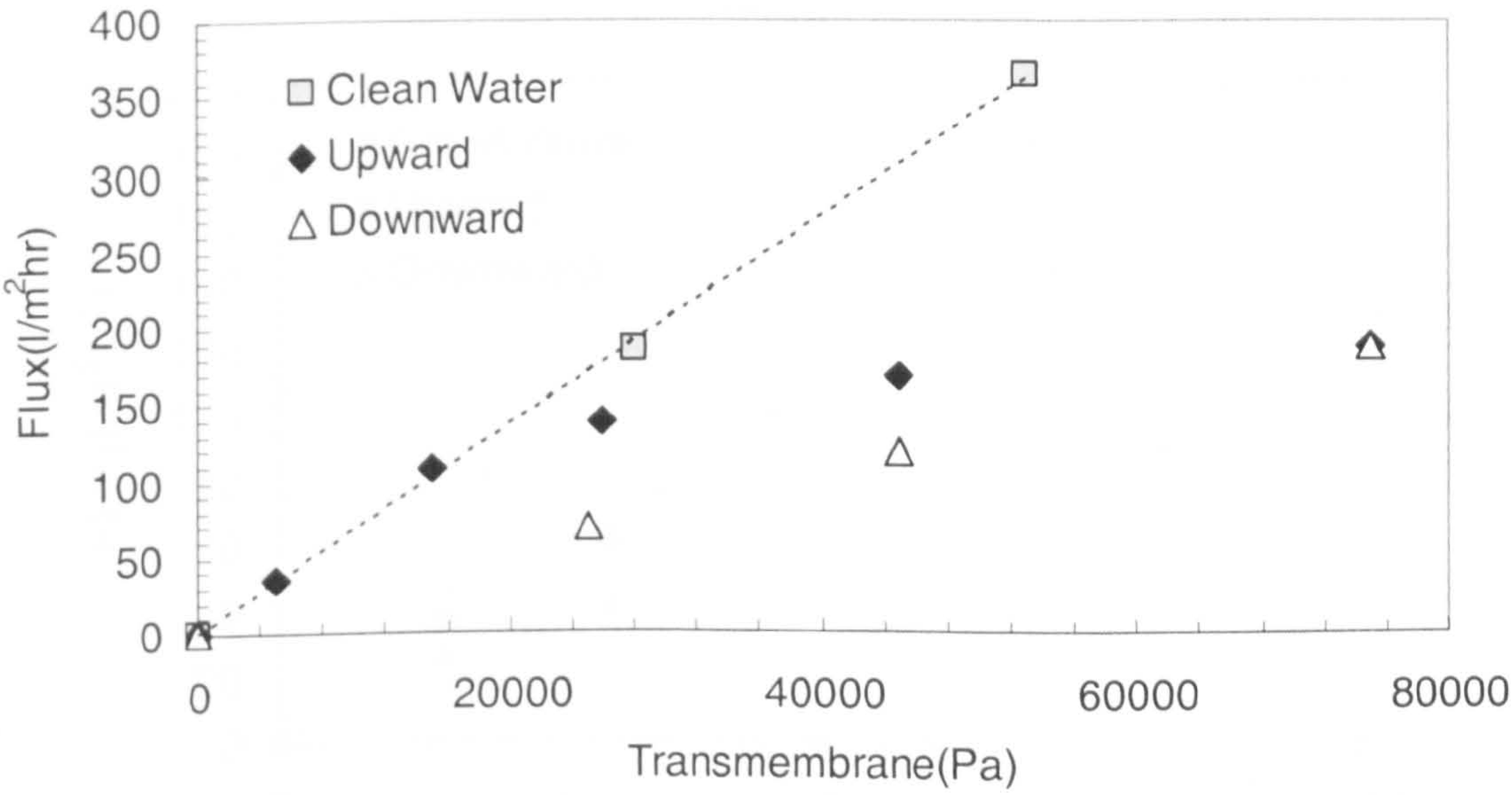

(b)

Figure 7: Step by step results for the filtration of 600 ppm n-dodecane emulsions, surfactant concentration 60 ppm, crossflow velocity 1.92 m/s, NaCl 0.1 M

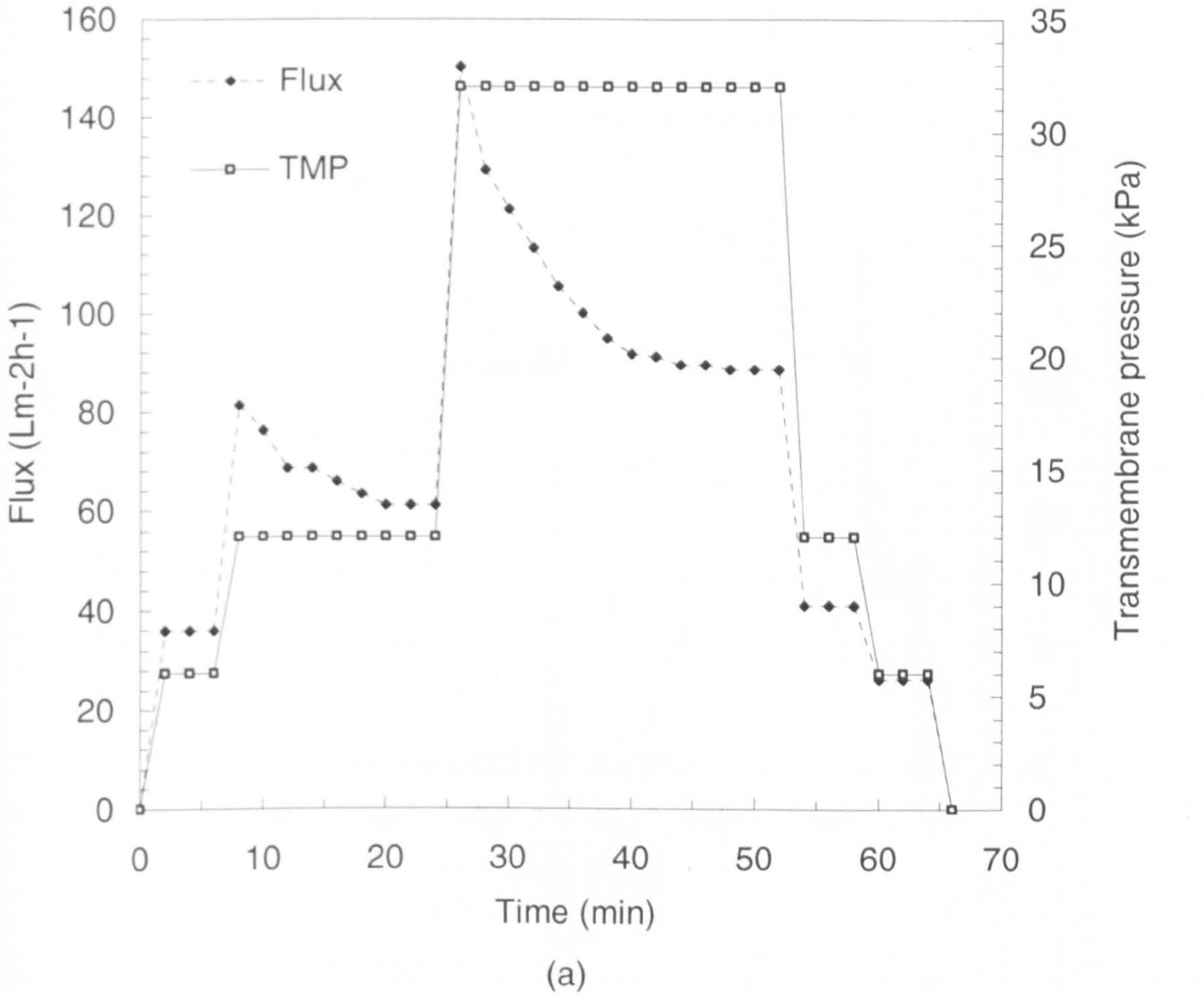

(a)

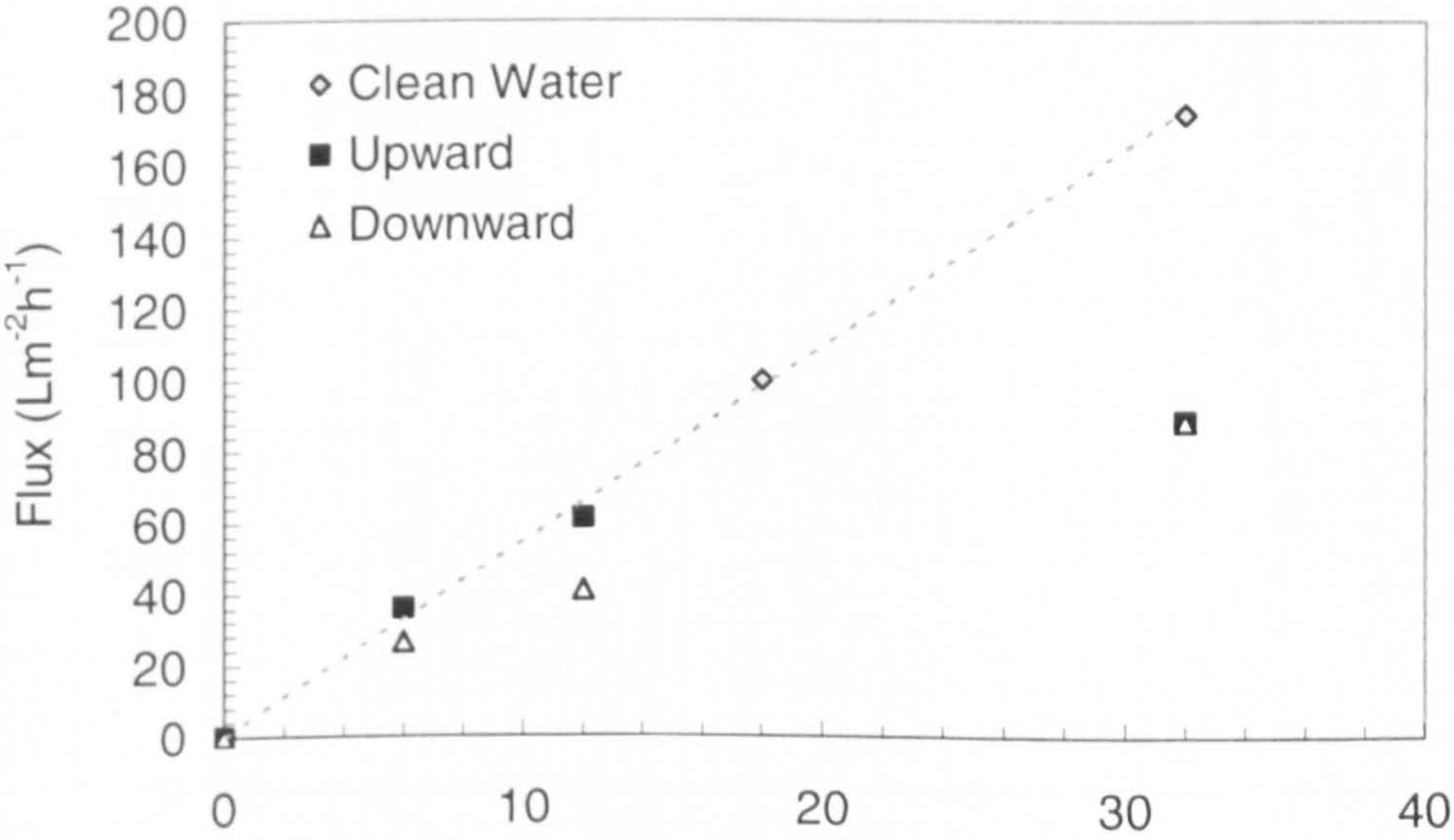

(b)

Figure 8: Step by step results for the filtration of 600 ppm n-dodecane emulsions, surfactant concentration 60 ppm, crossflow velocity 1.14 m/s, NaCl 0.05 M

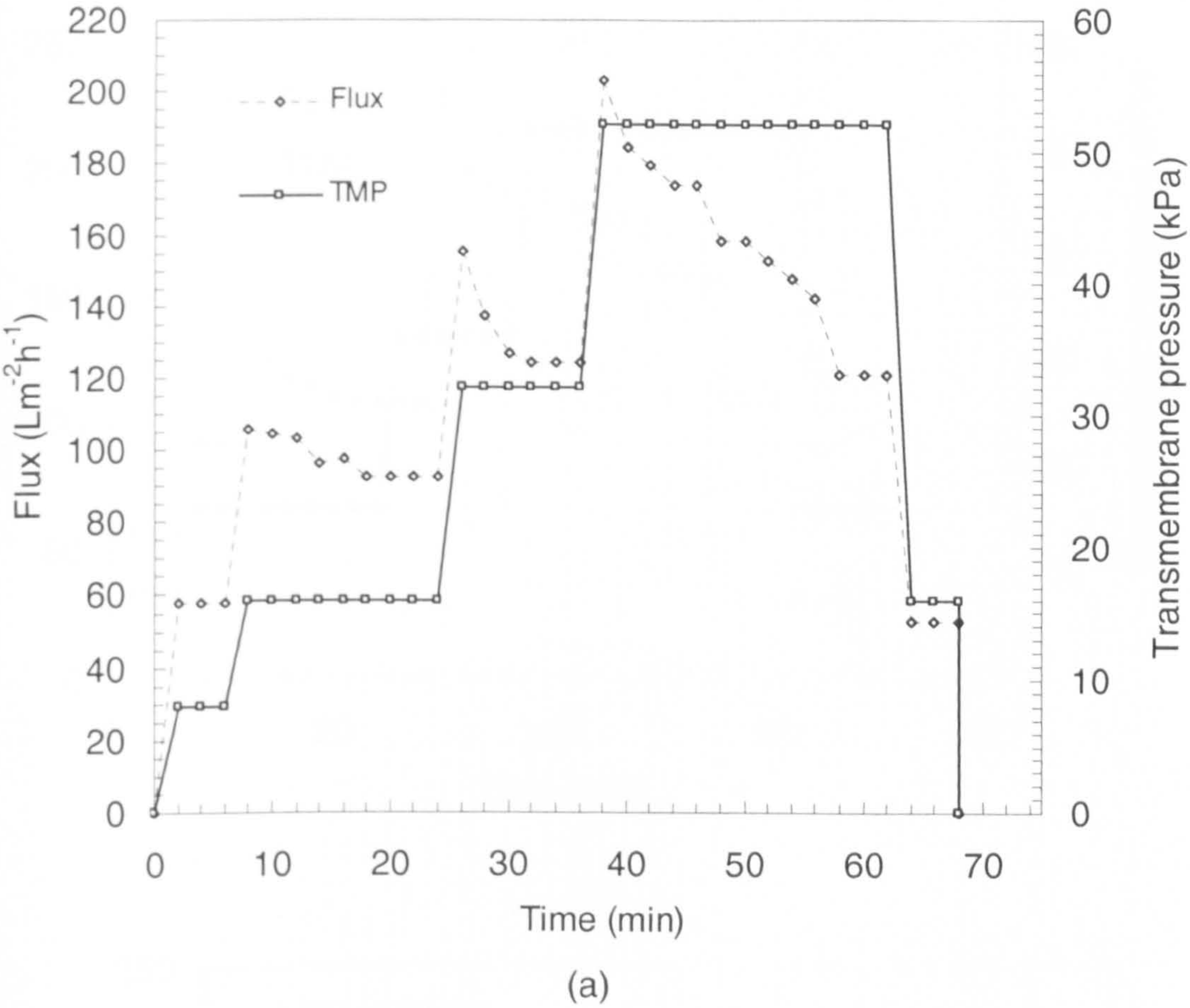

(a)

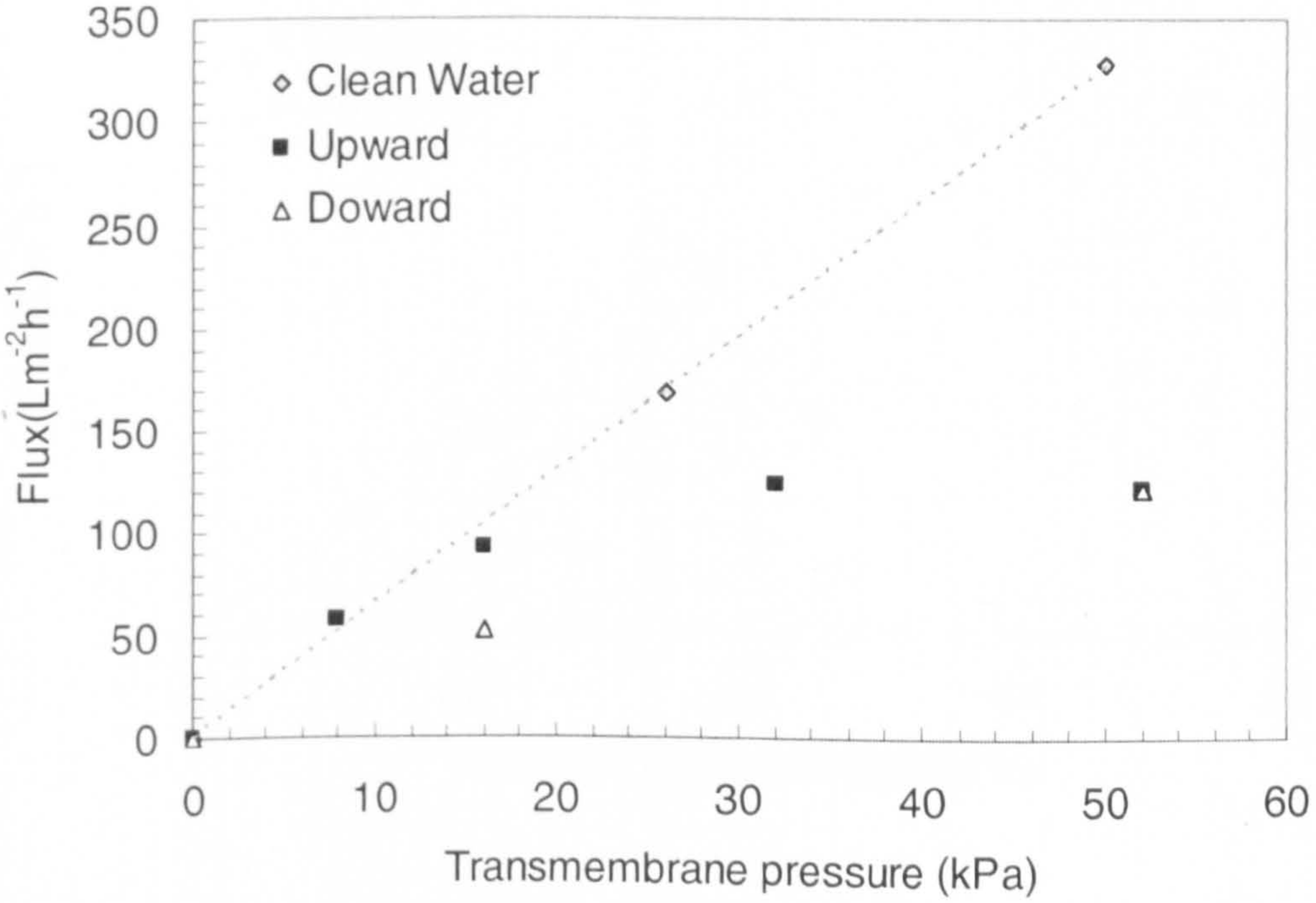

(b)

Figure 9: Step by Step Results for the filtration of 600 ppm n-dodecane emulsions, surfactant concentration 60 ppm, crossflow velocity 1.52 m/s, NaCl 0.05 M

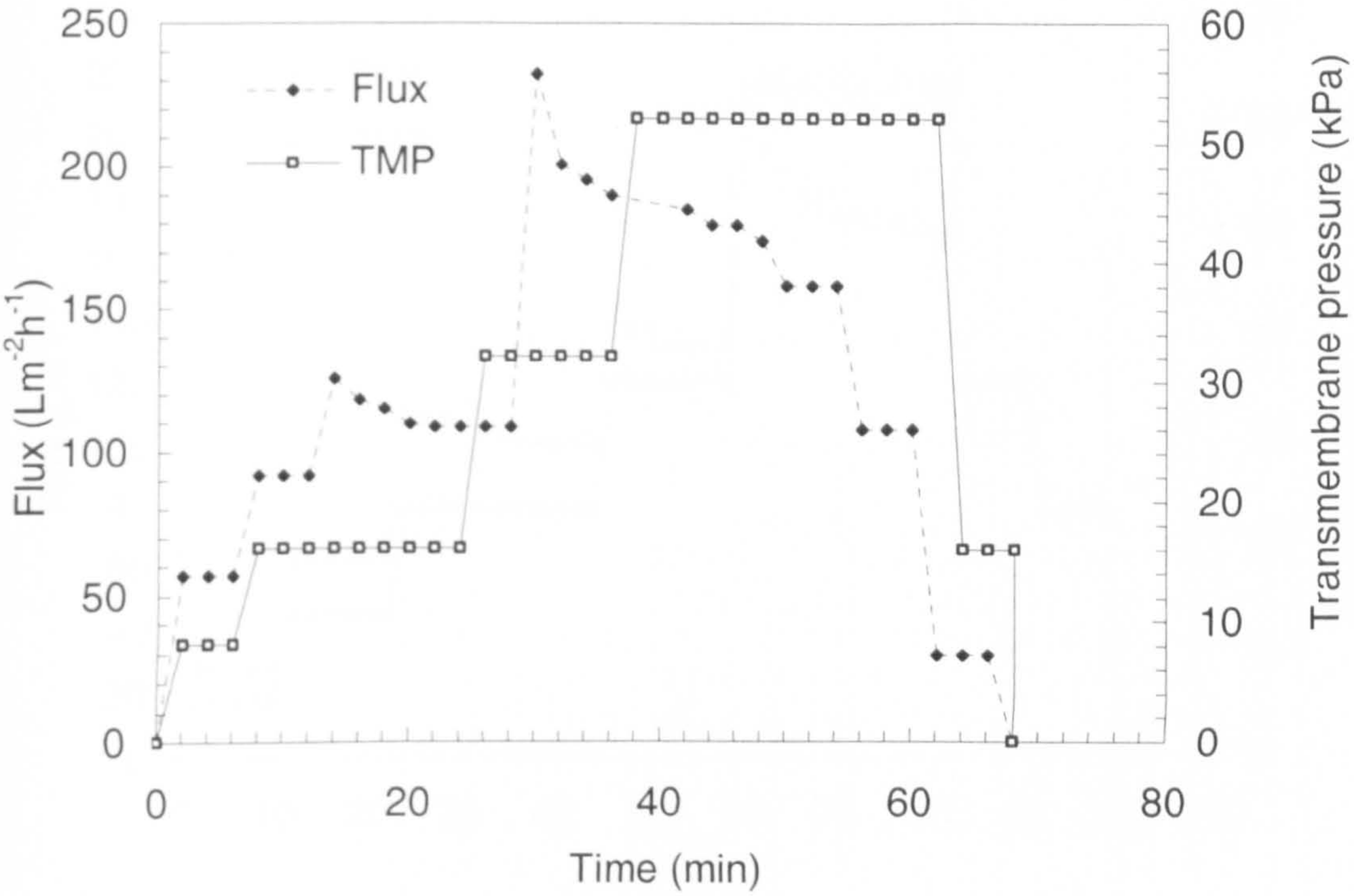

(a)

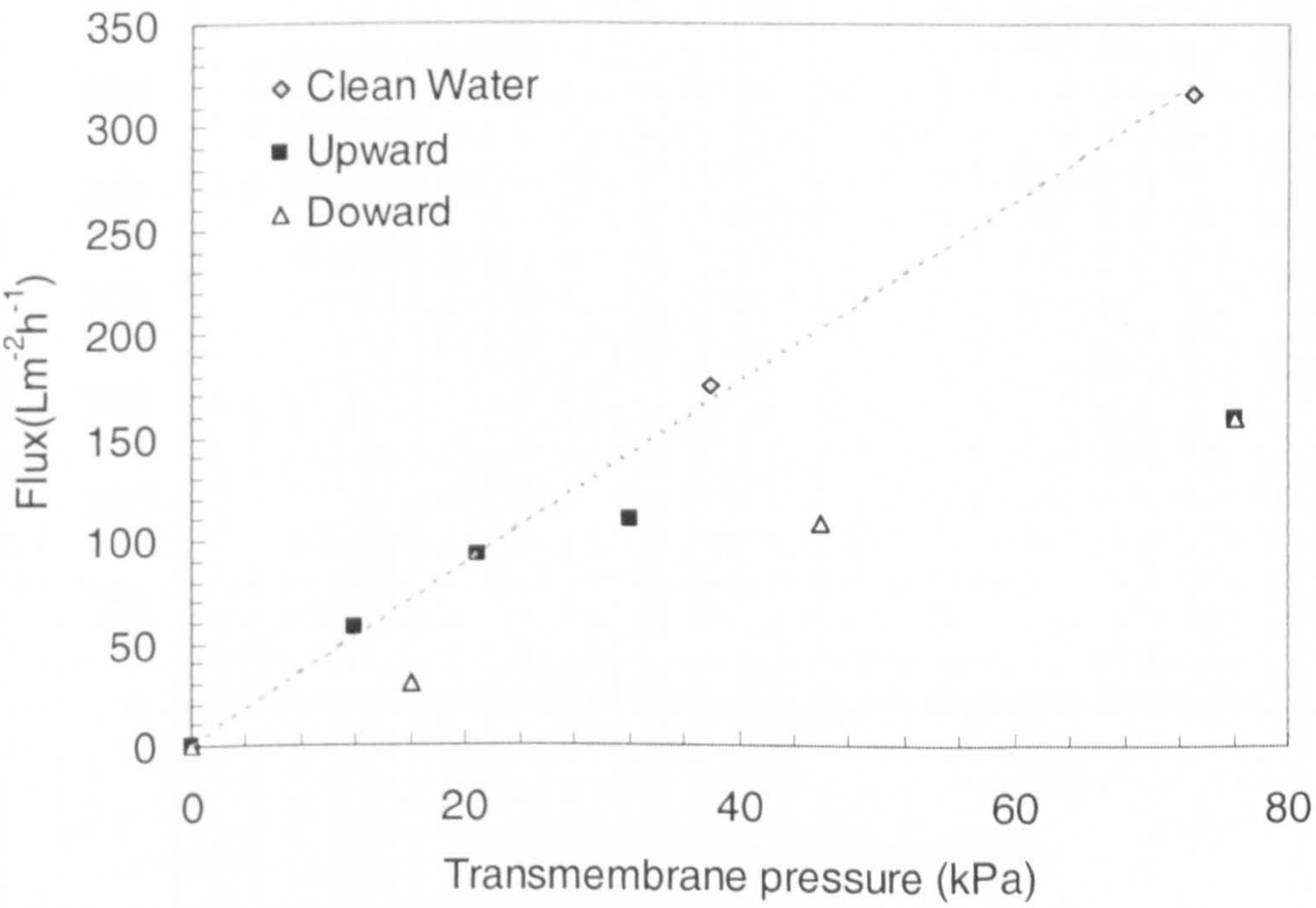

(b)

Figure 10: Step by step results for the filtration of 600 ppm n-dodecane emulsions, surfactant concentration 60 ppm, crossflow velocity 1.92 m/s, NaCl 0.05 M

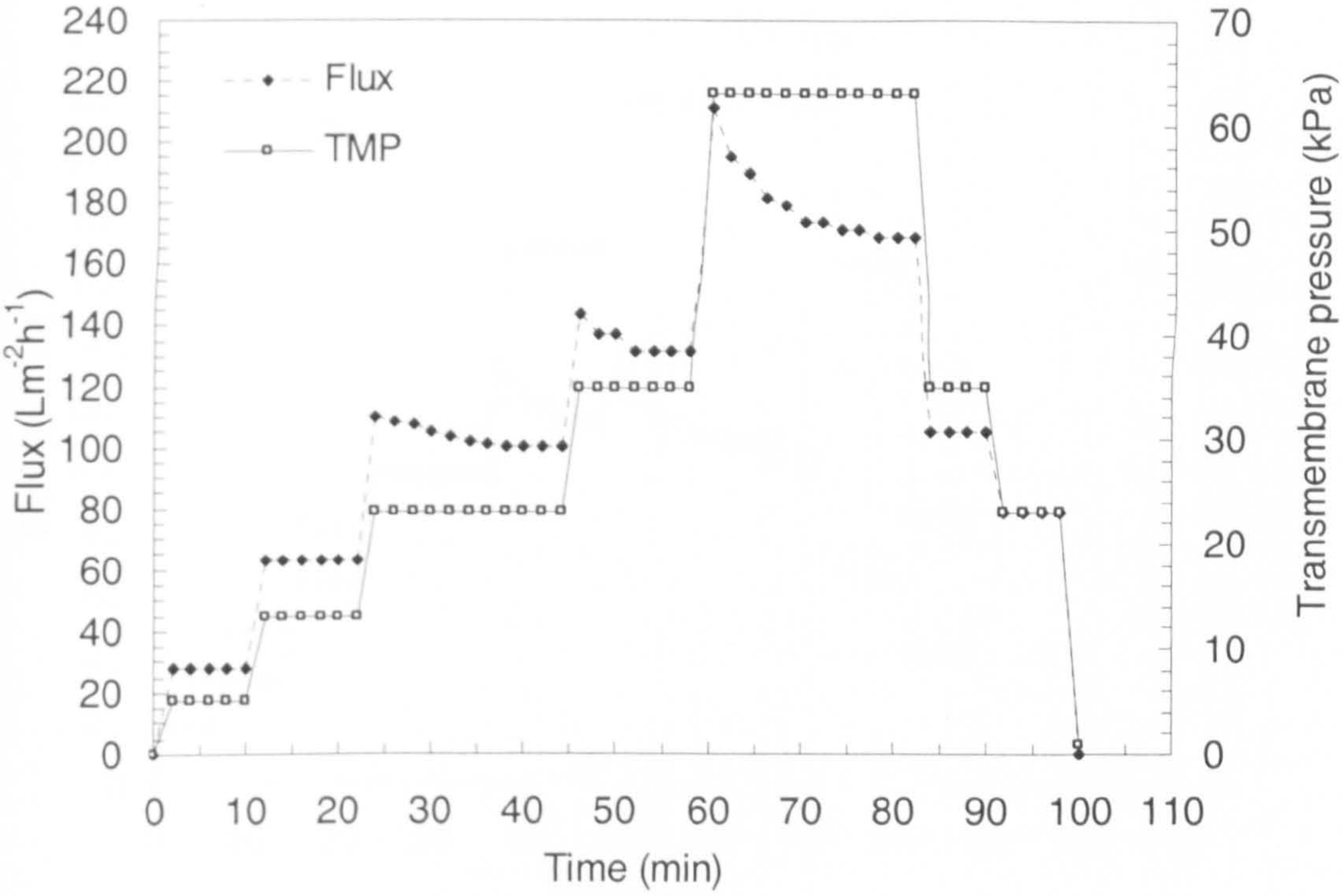

(a)

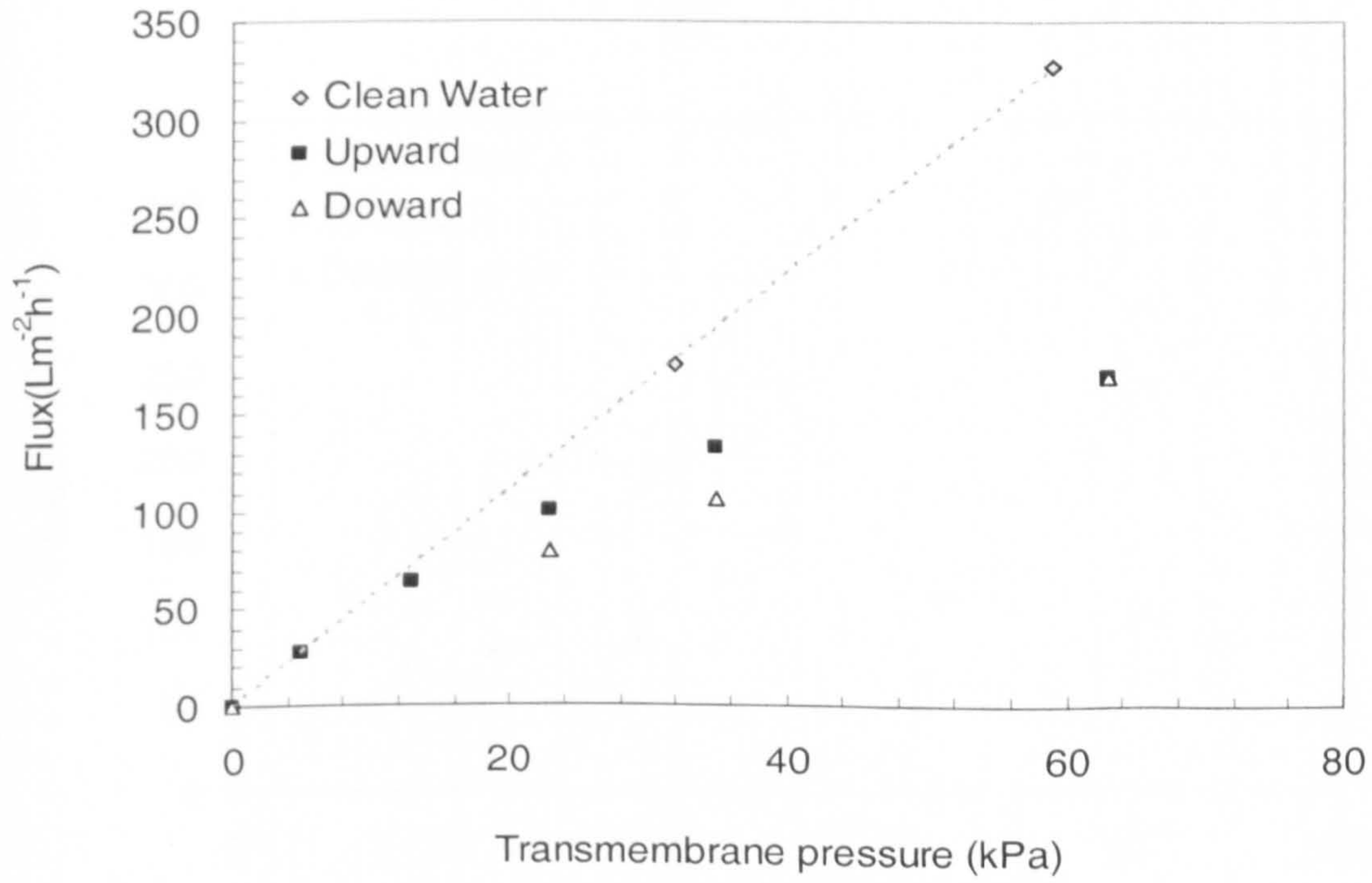

(b)

Figure 11: Step by step results for the filtration of 600 ppm n-dodecane emulsions, surfactant concentration 60 ppm, crossflow velocity 1.52 m/s, pH= 12

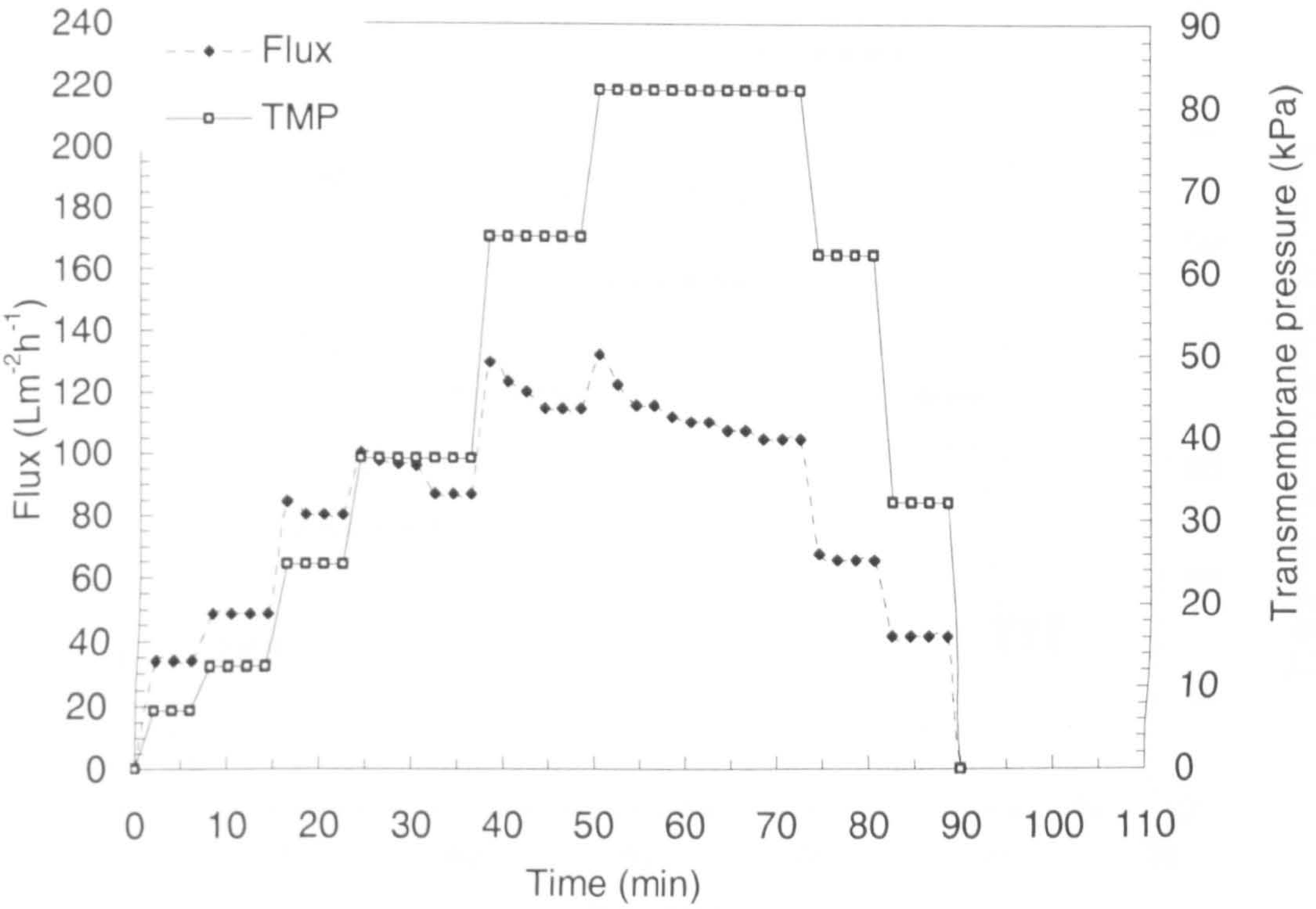

(a)

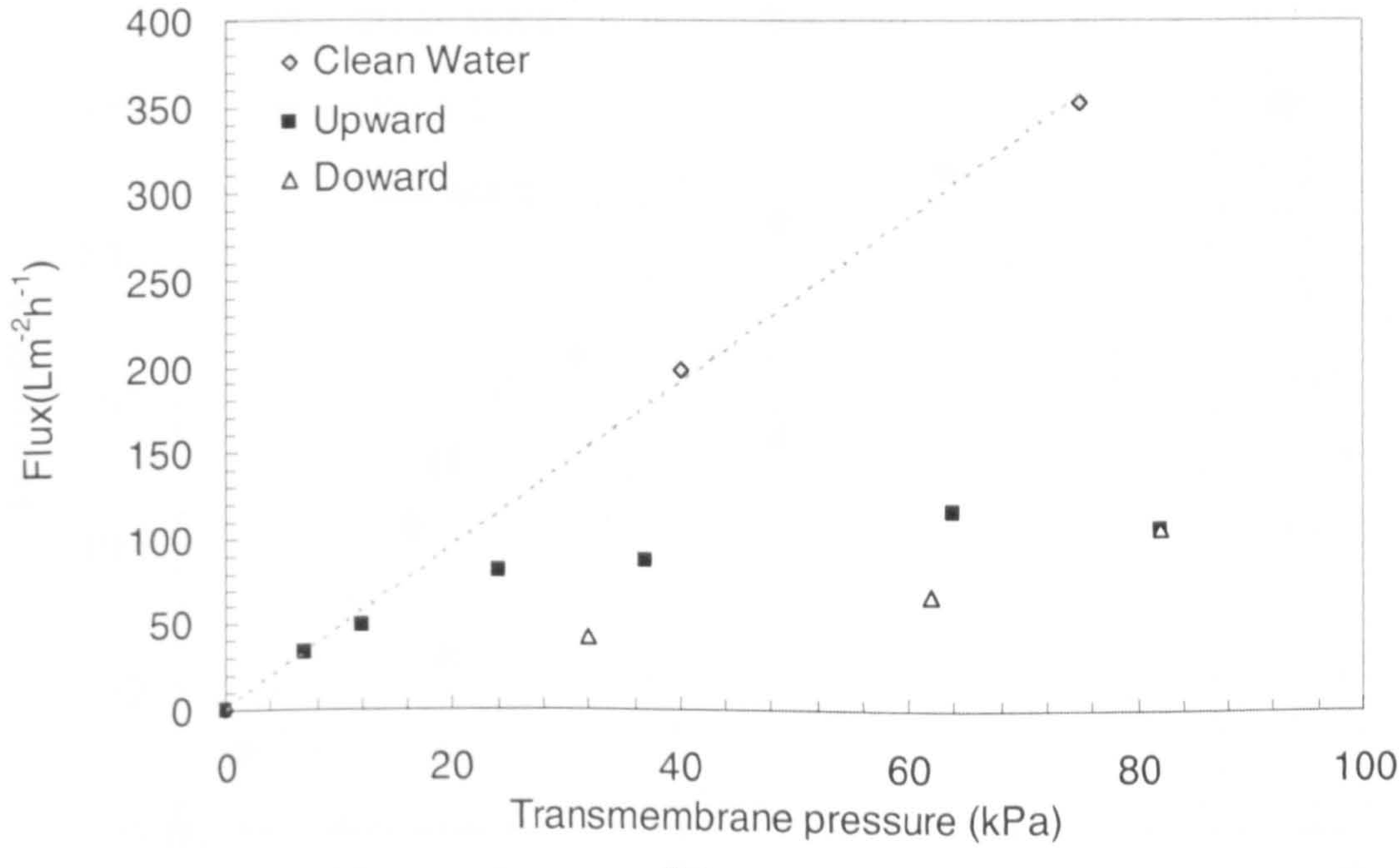

(b)

Figure 12: Step by step results for the filtration of 600 ppm n-dodecane emulsion, surfactant concentration 60 ppm, crossflow velocity 1.92 m/s, NaCl 0.05 M, pH 12

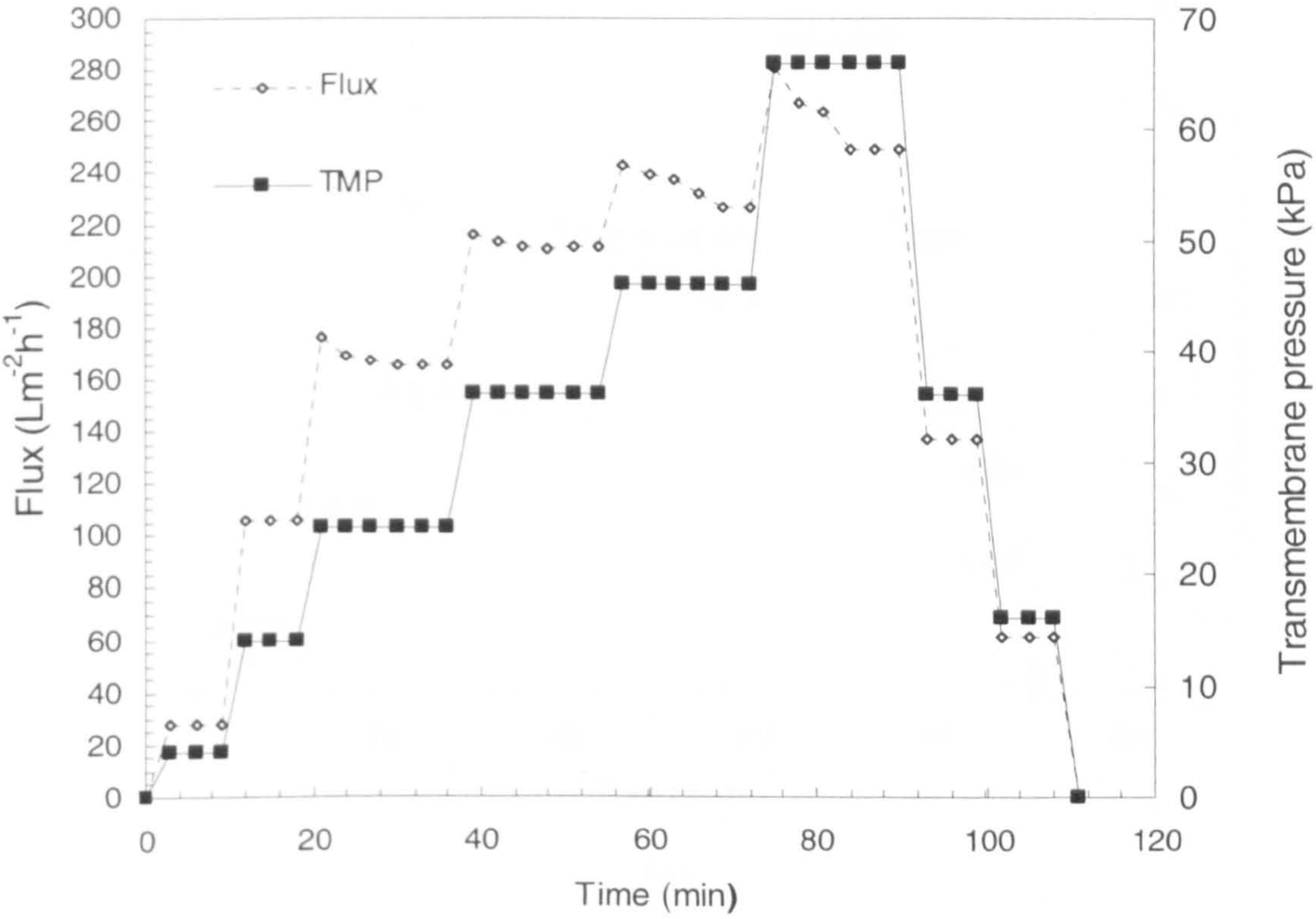

(a)

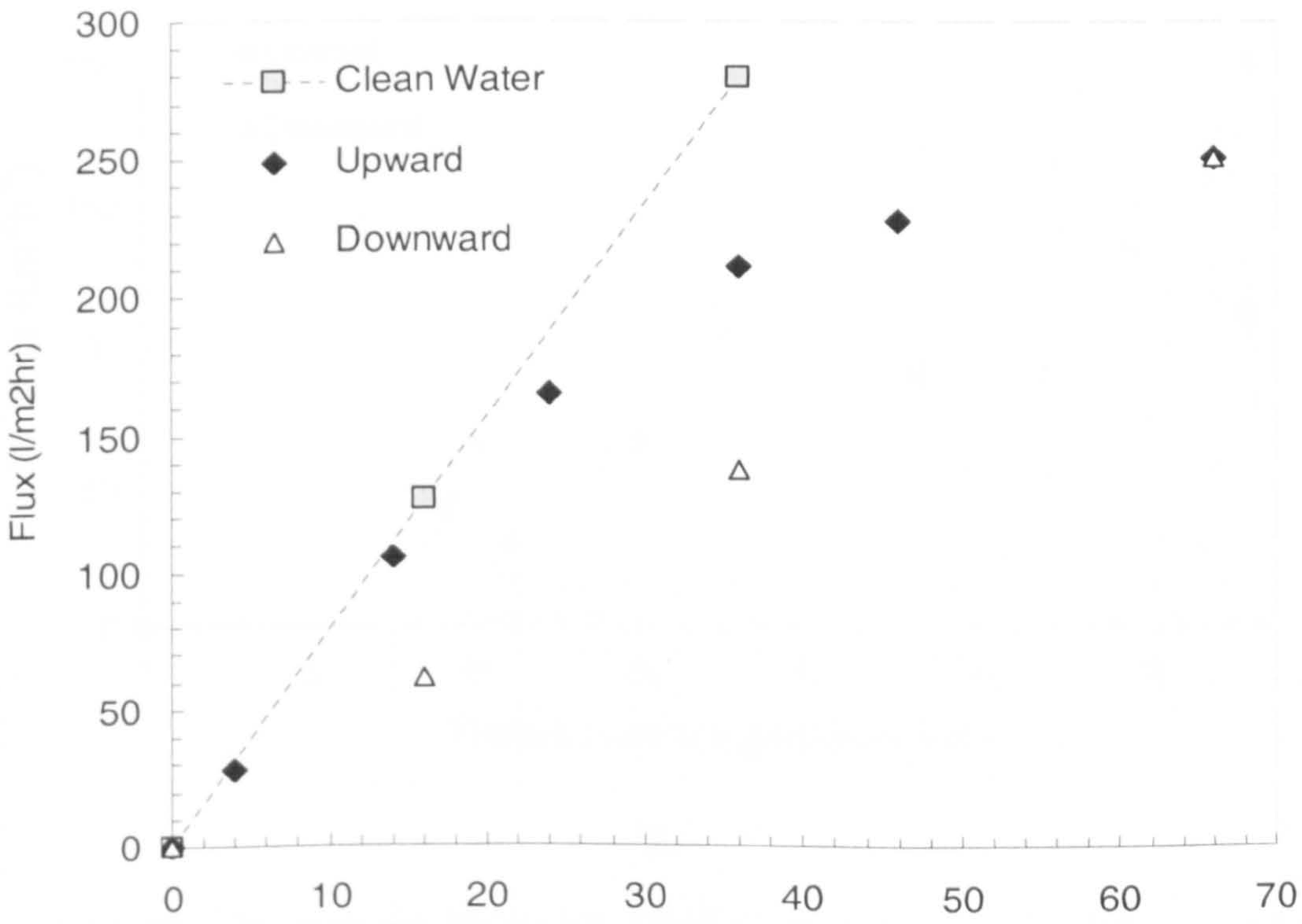

(b)

Figure 13: Step by step results for the filtration of 1200 ppm emulsion, surfactant concentration 120 ppm, crossflow velocity 1.92 m/s

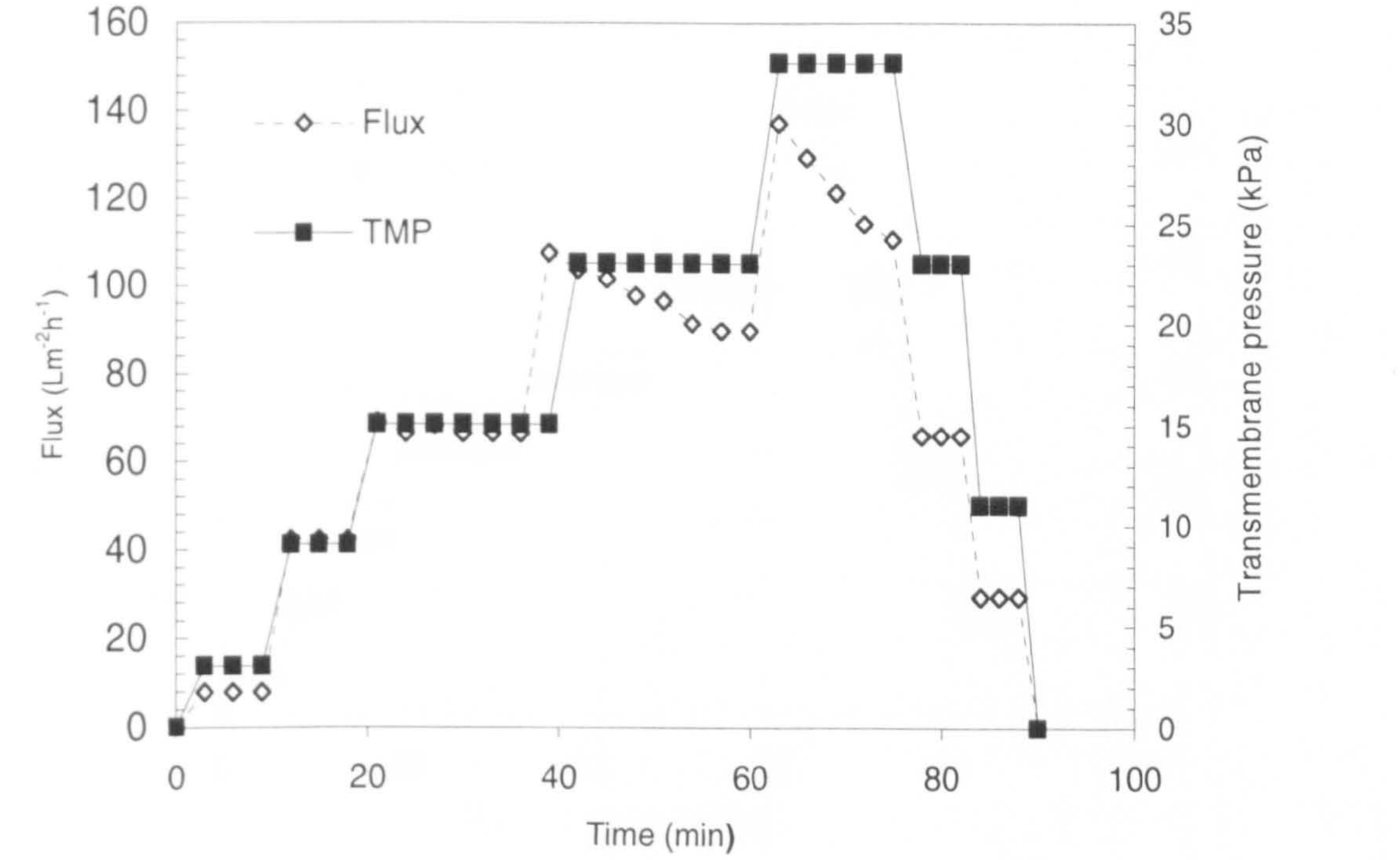

(a)

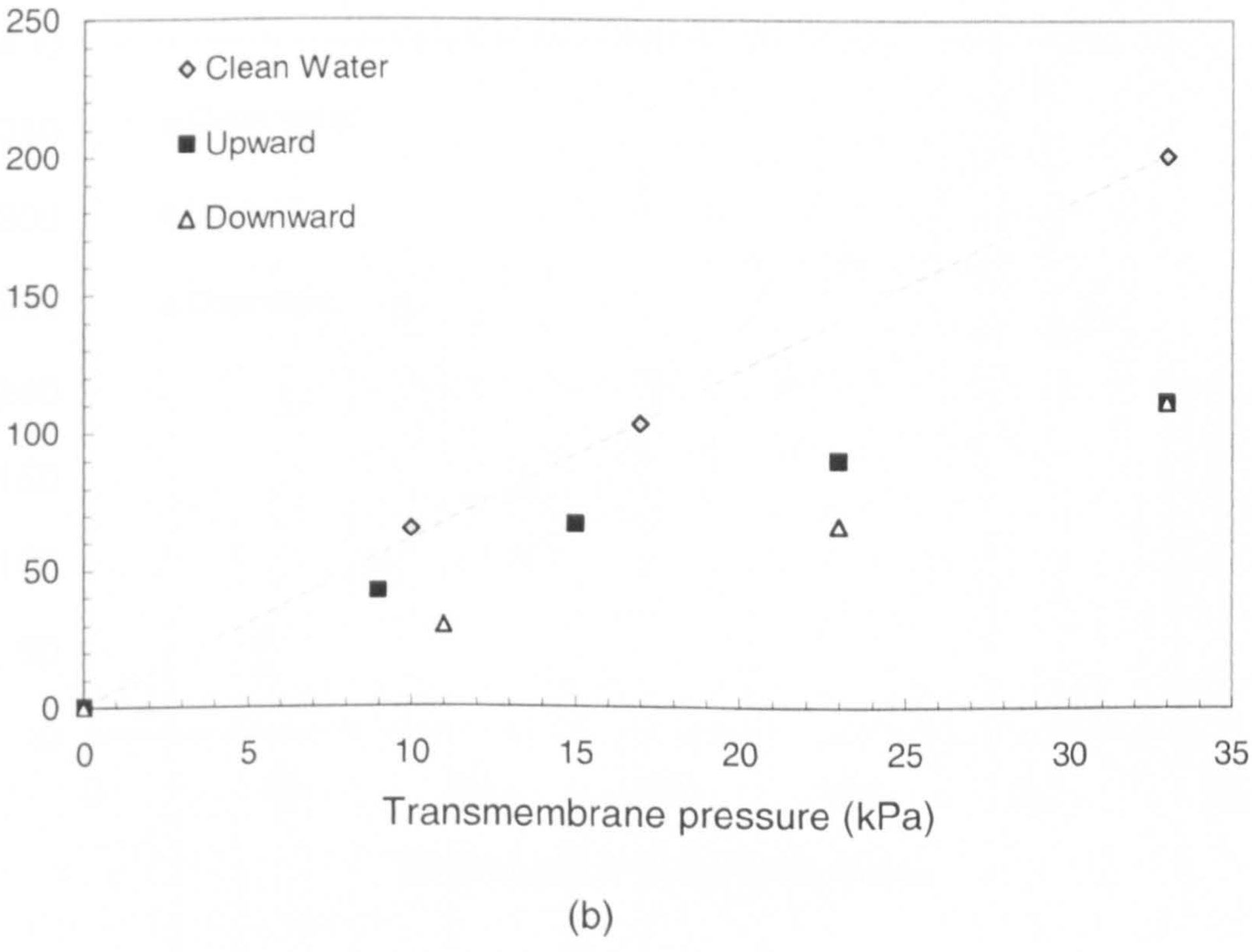

(b)

Figure 14 Step by step results for the filtration of 1200 ppm emulsion, surfactant concentration 120 ppm, crossflow velocity 1.14 m/s

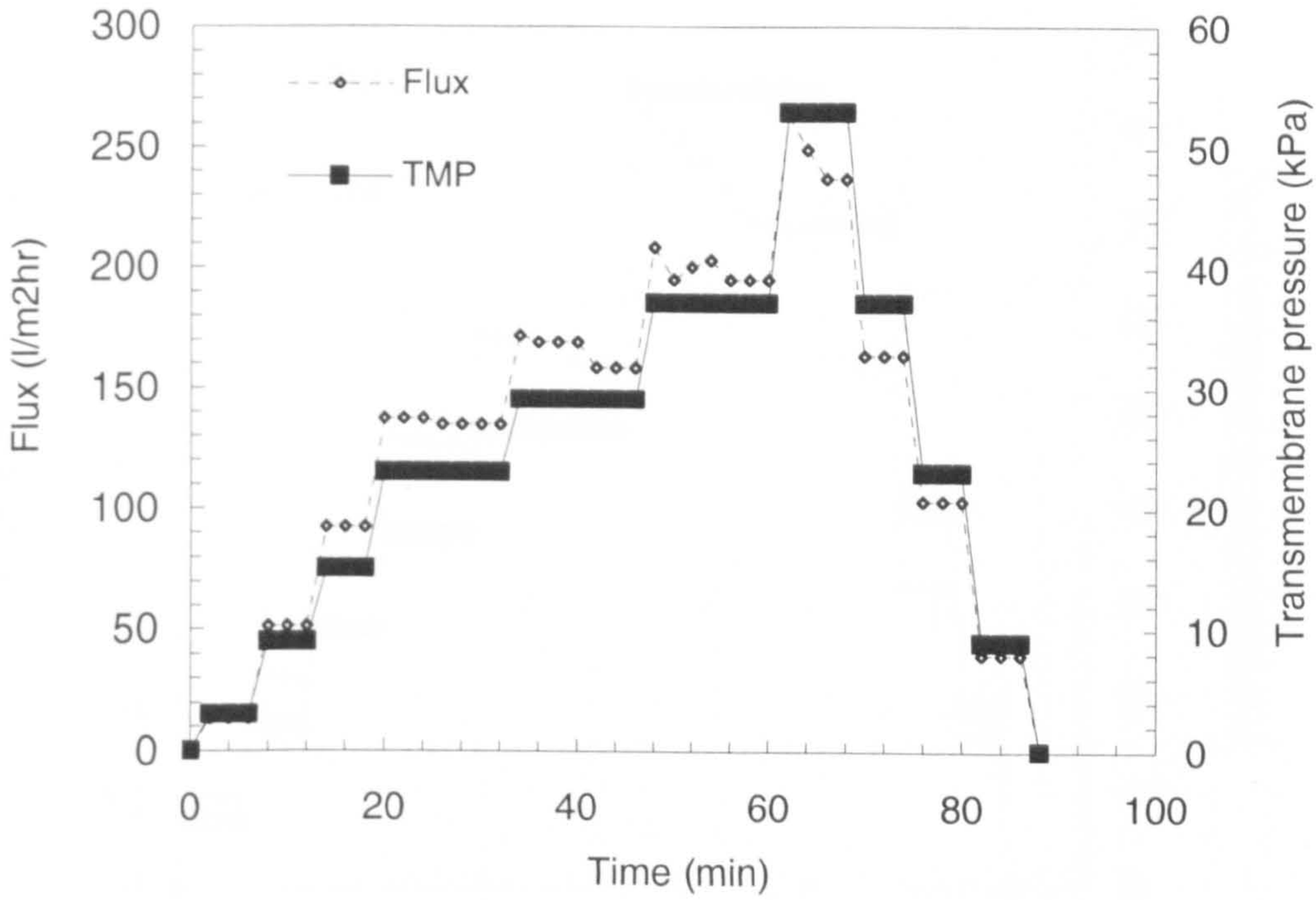

(a)

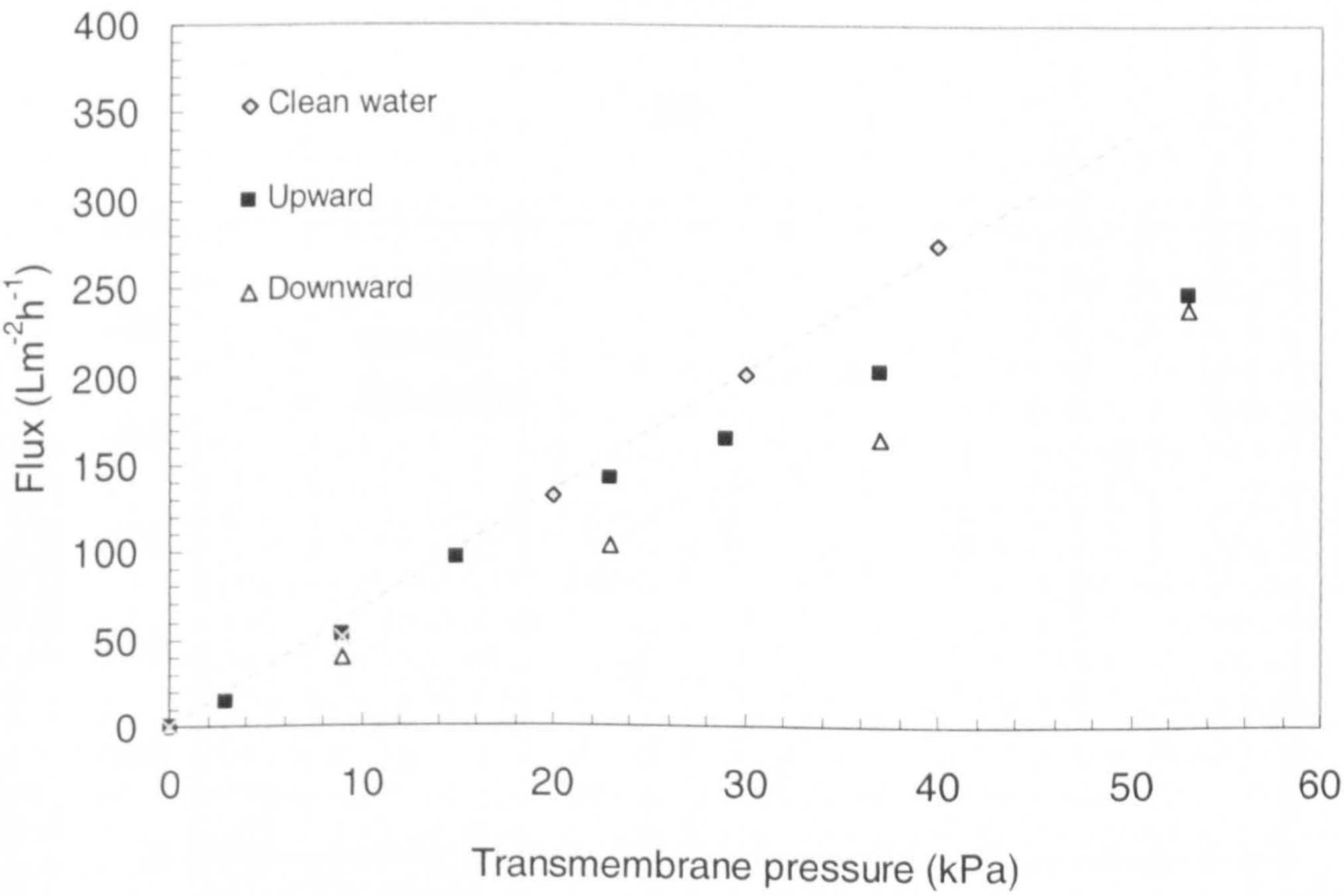

(b)

Figure 15: Step by step results for the filtration of 1200 ppm emulsion, surfactant concentration 120 ppm, crossflow velocity 1.52 m/s

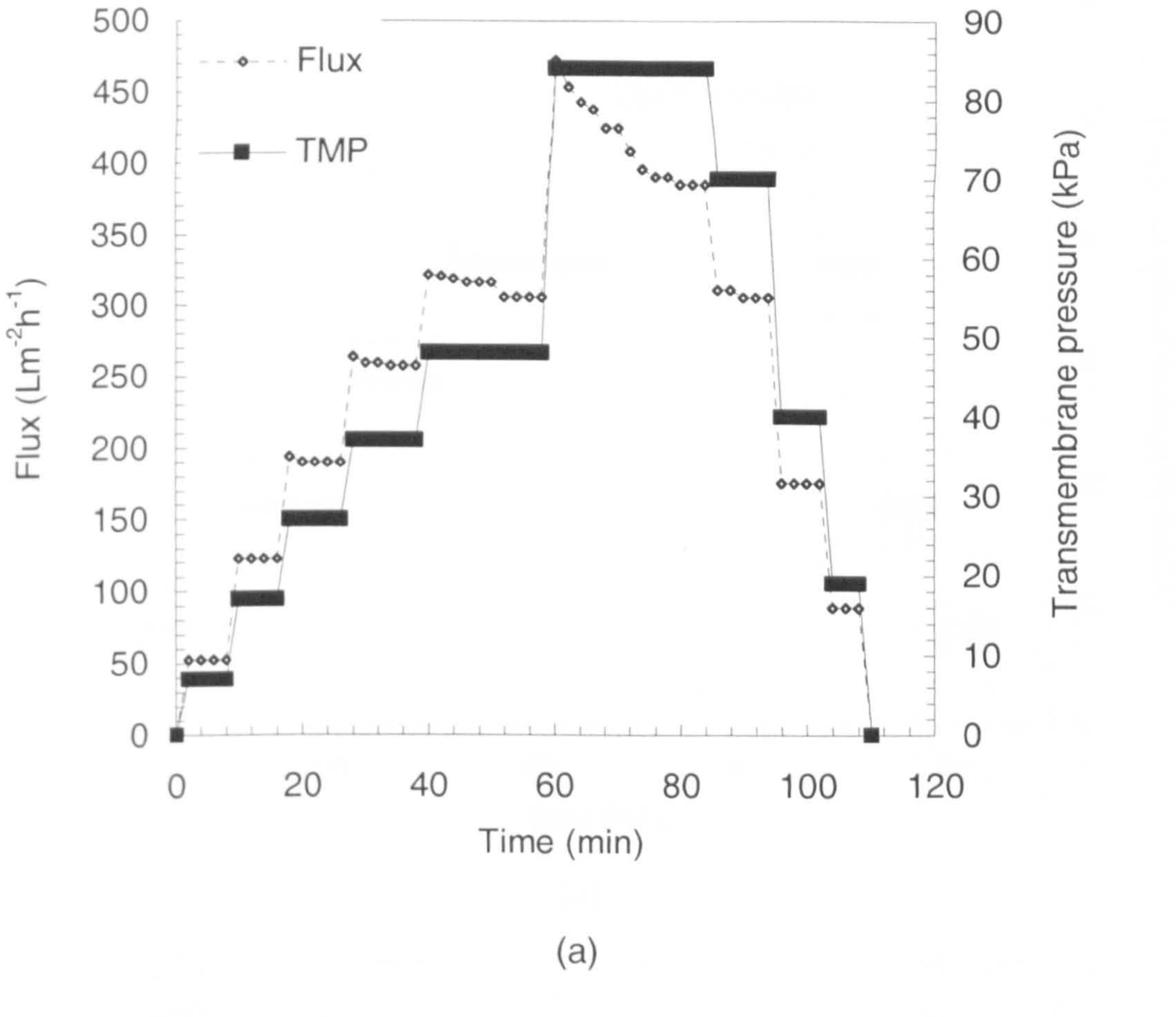

(a)

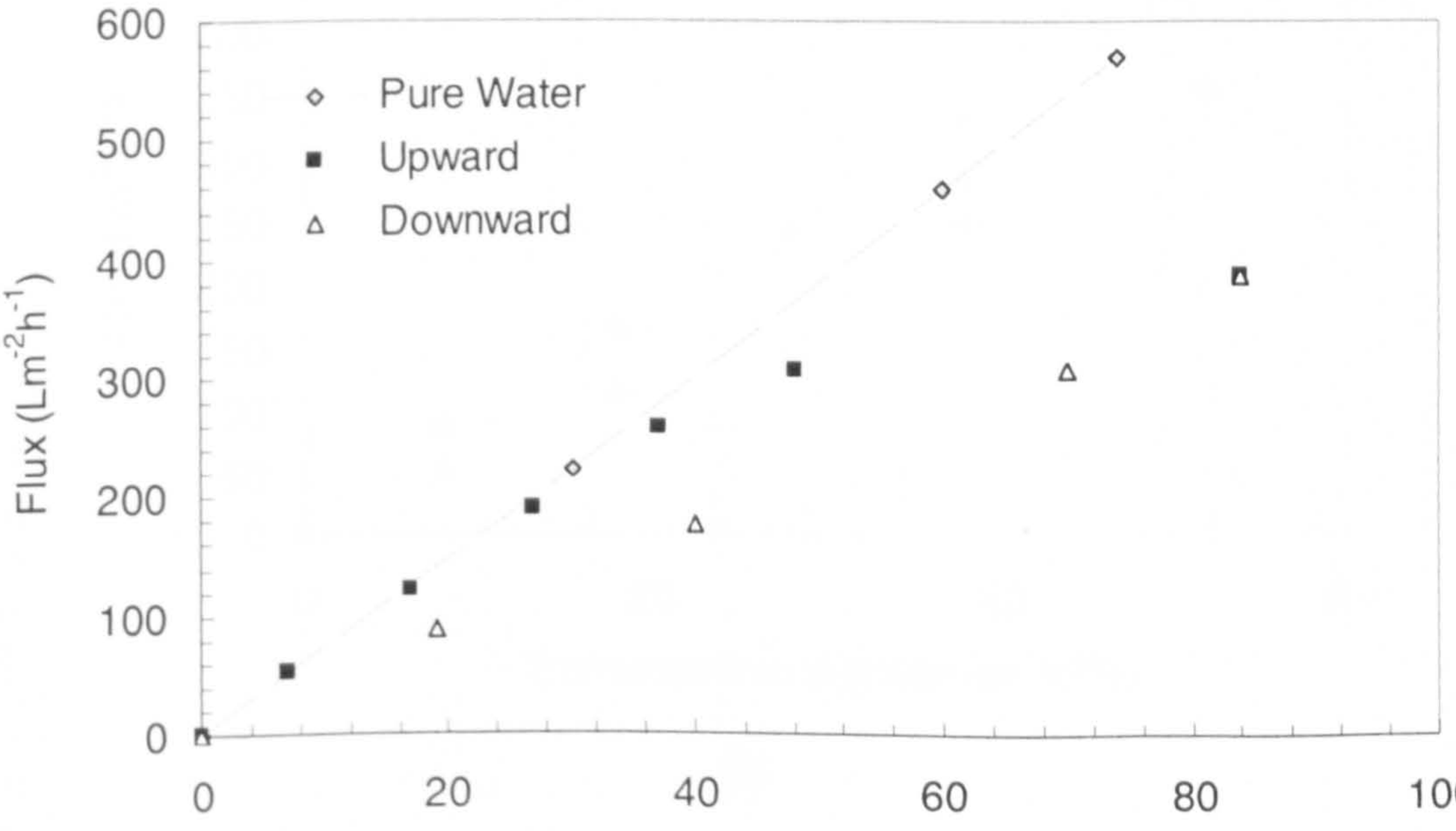

(b)

Figure 16: Step by step results for the filtration of 1200 ppm emulsion, surfactant concentration 120 ppm, crossflow velocity 2.28 m/s

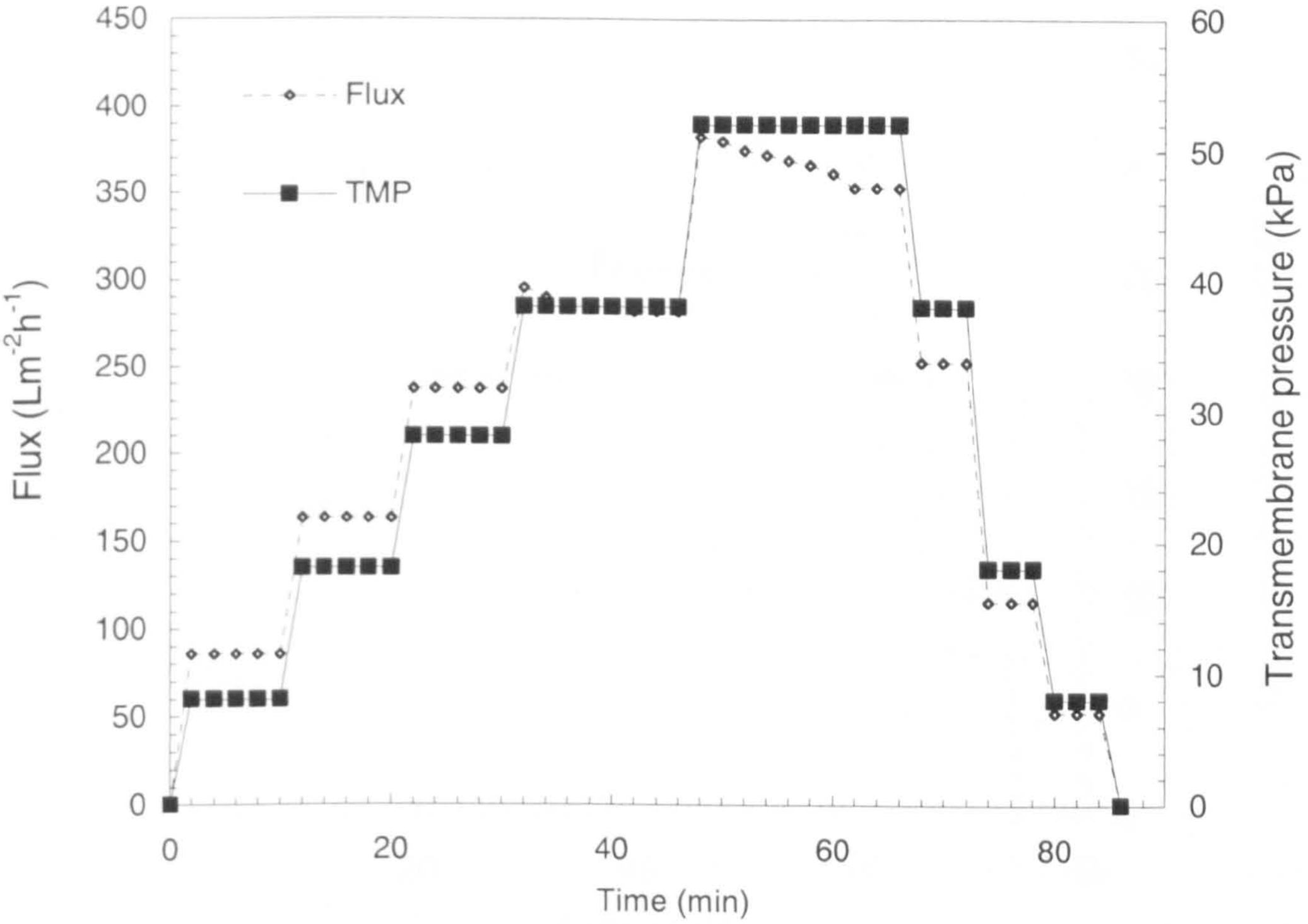

(a)

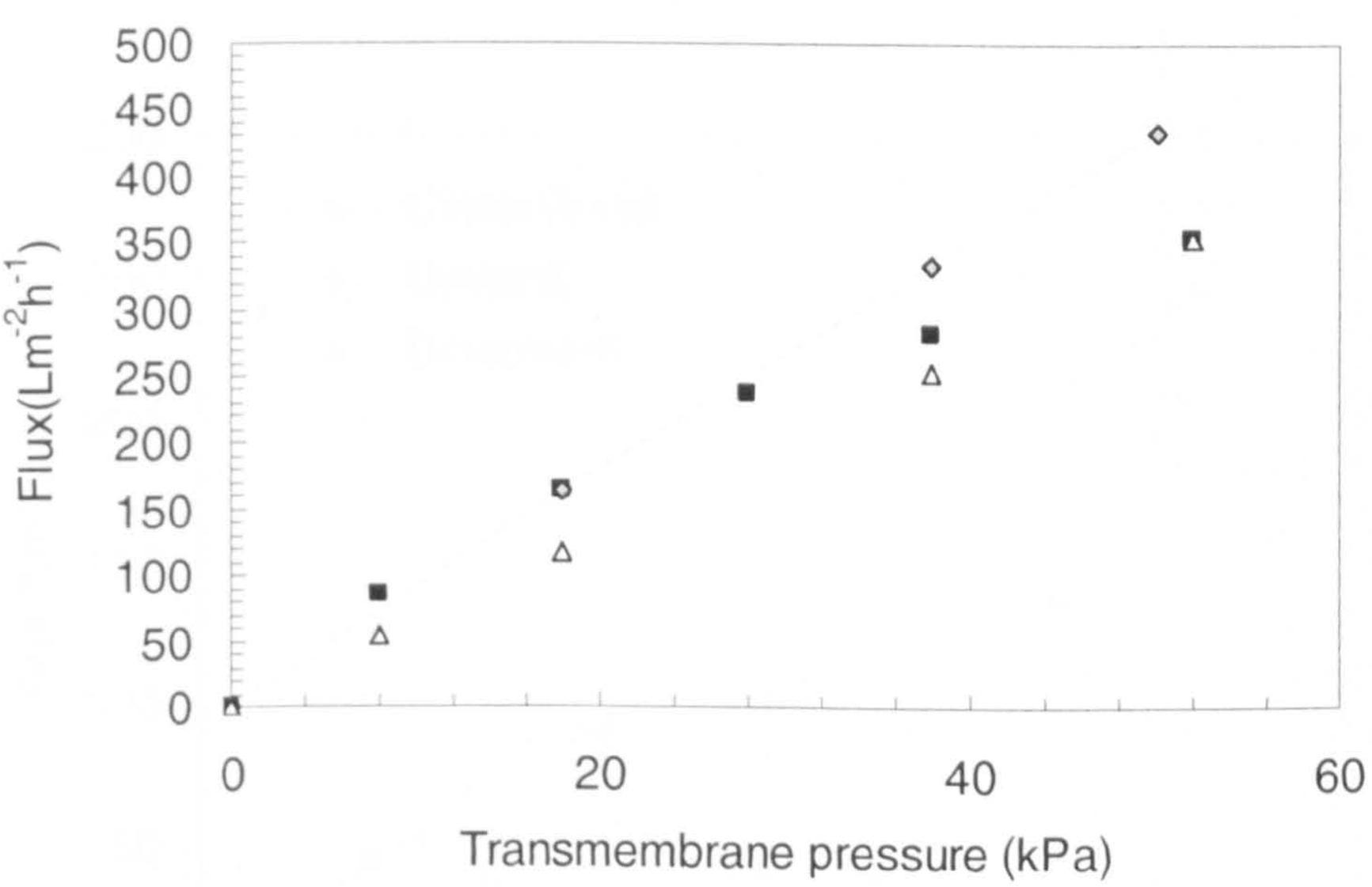

(b)

Figure 17: Step by step results for the filtration of 1200 ppm emulsion, ionic strength 0.1 M $CaCl_2$, surfactant Concentration 120 ppm, velocity 2.28 m/s

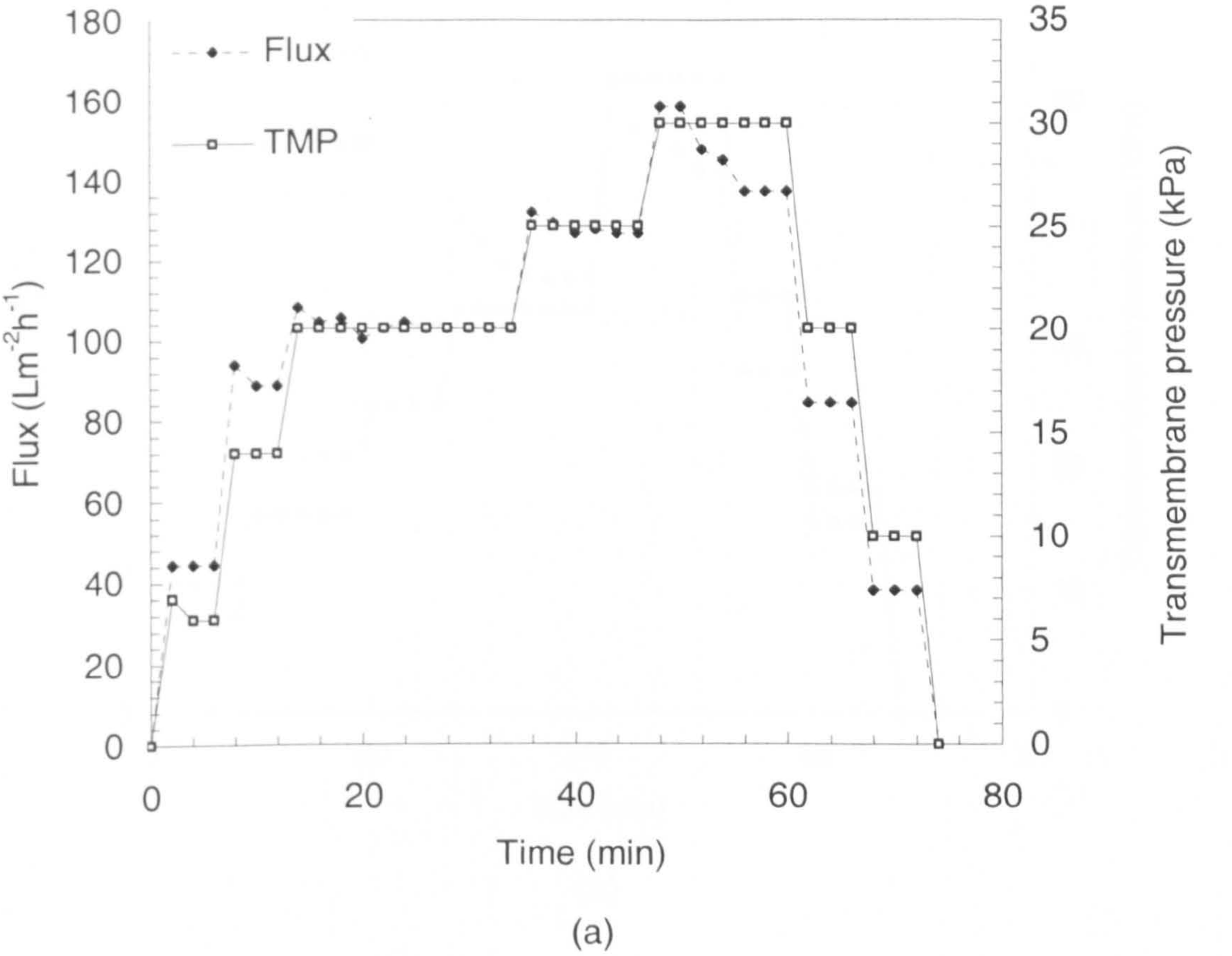

(a)

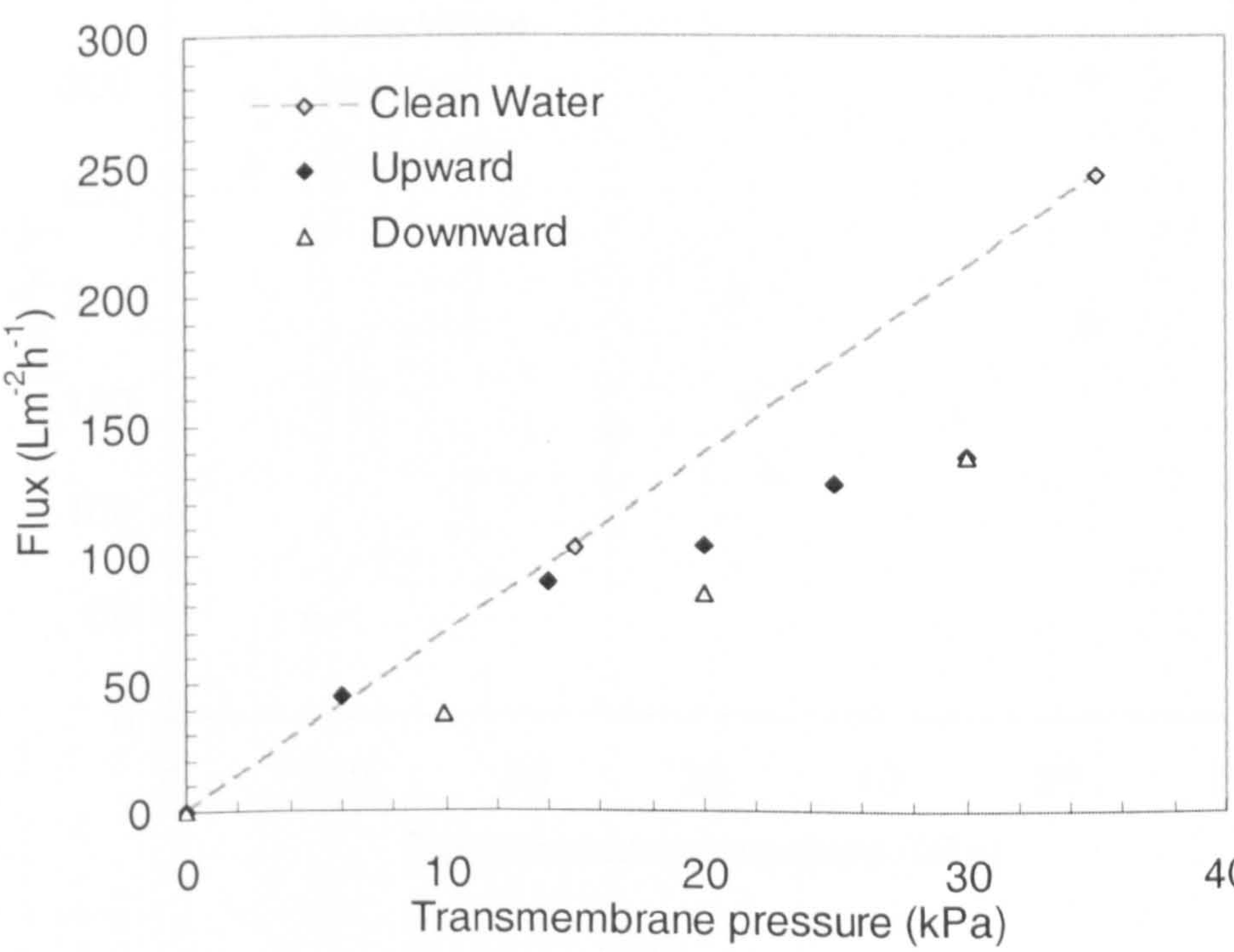

(b)

Figure 18: Step by step results for the filtration of 2400 ppm emulsion, surfactant Concentration 240 ppm, Crossflow velocity 1.14 m/s

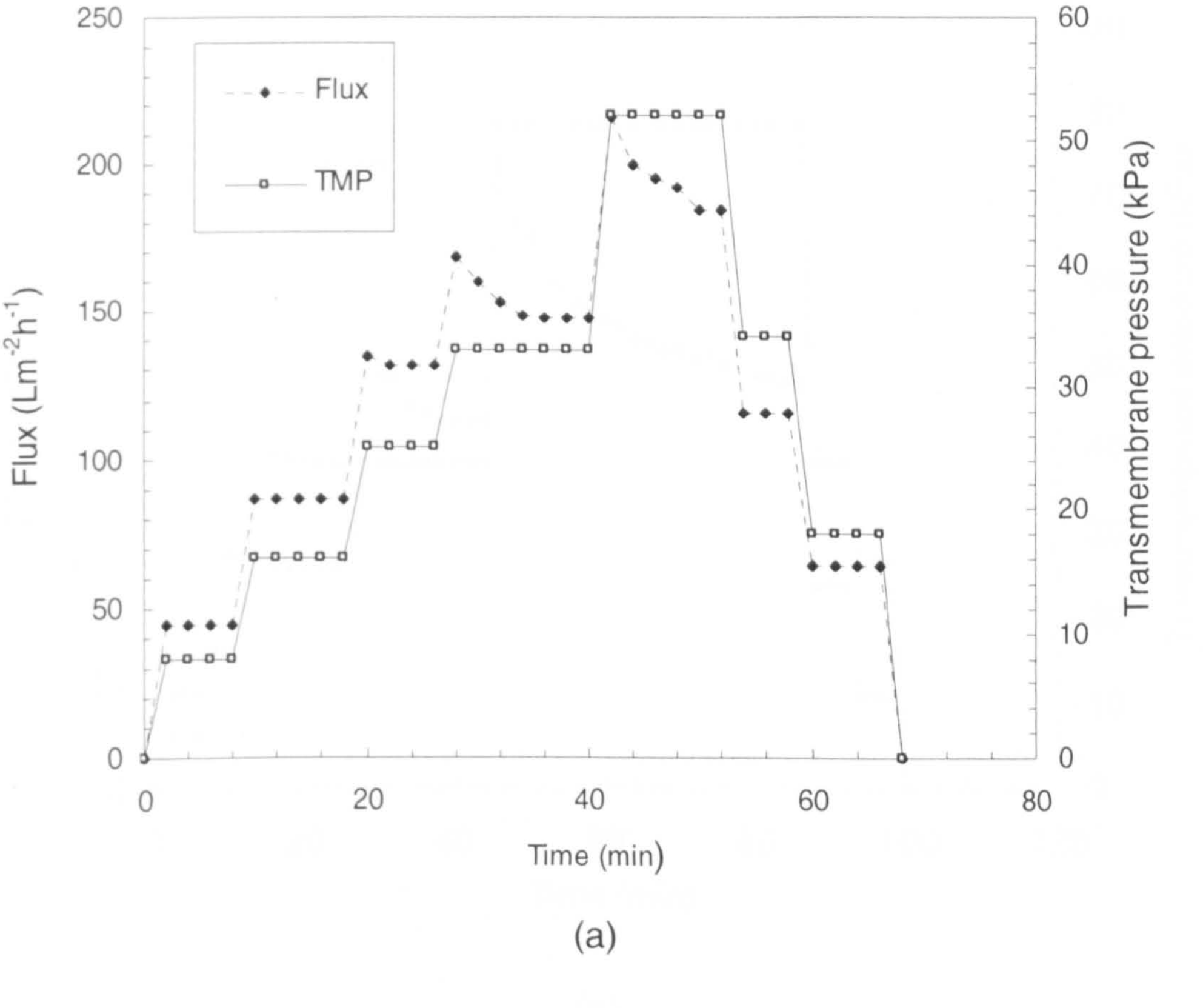

(a)

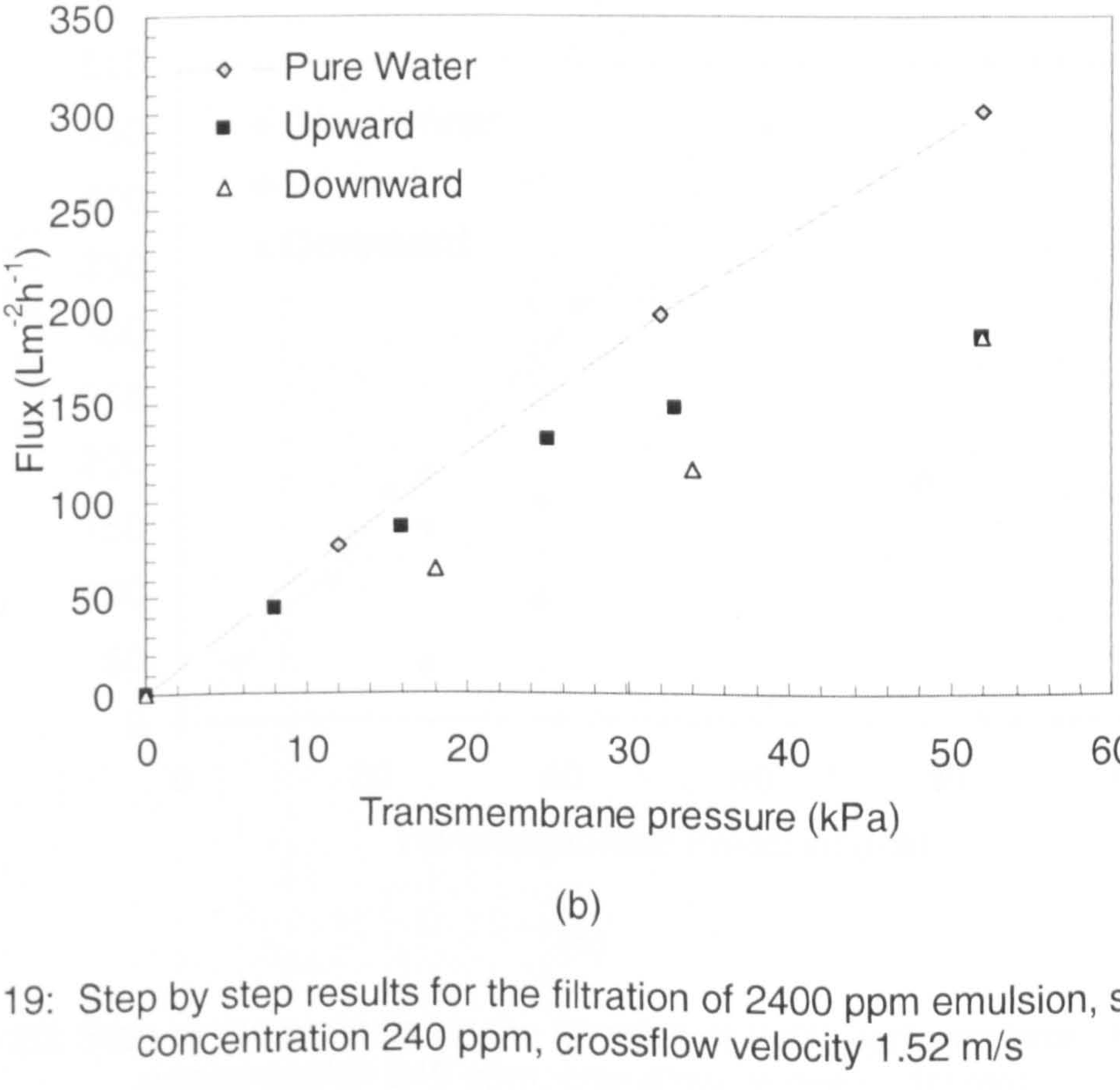

(b)

Figure 19: Step by step results for the filtration of 2400 ppm emulsion, surfactant concentration 240 ppm, crossflow velocity 1.52 m/s

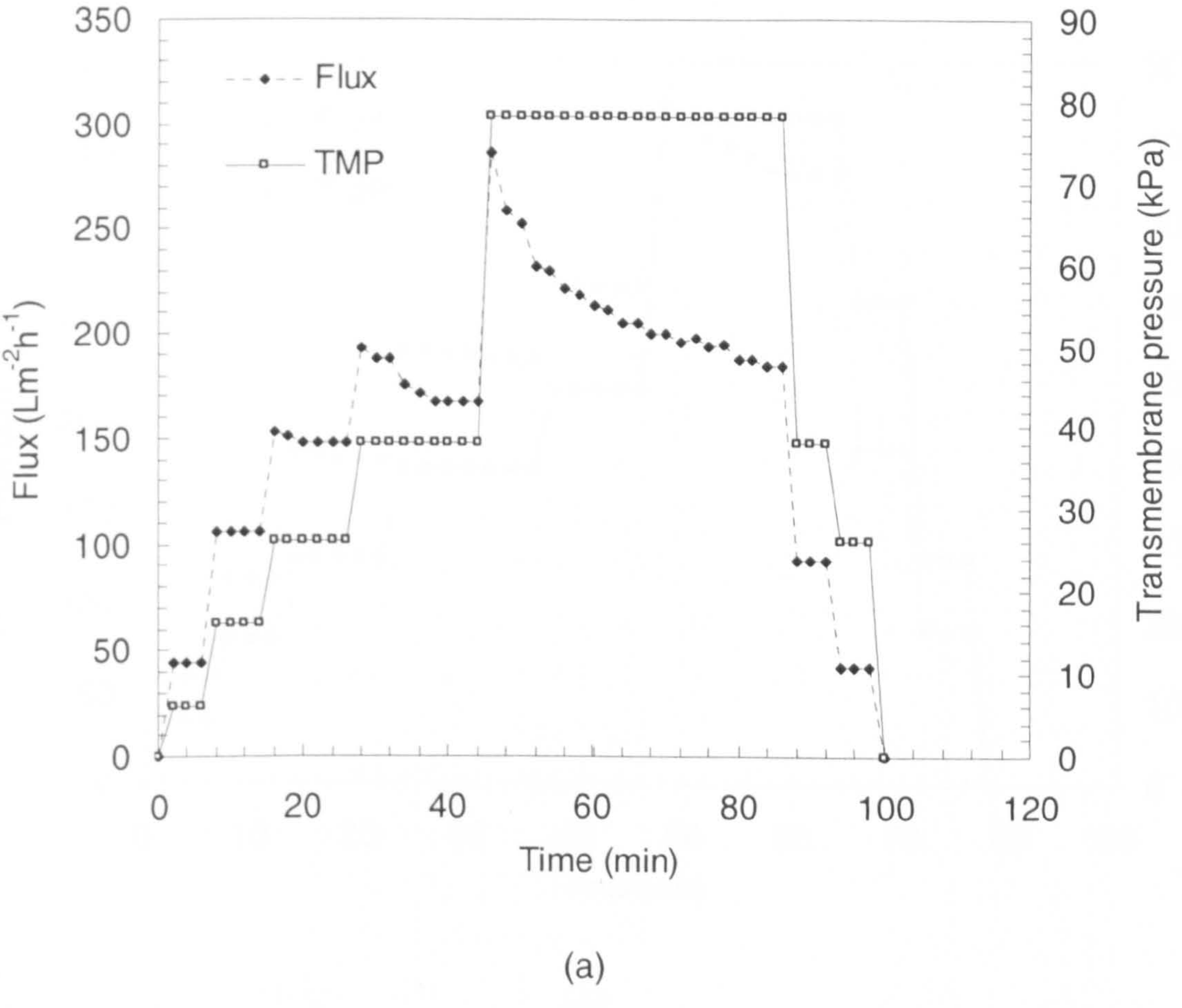

(a)

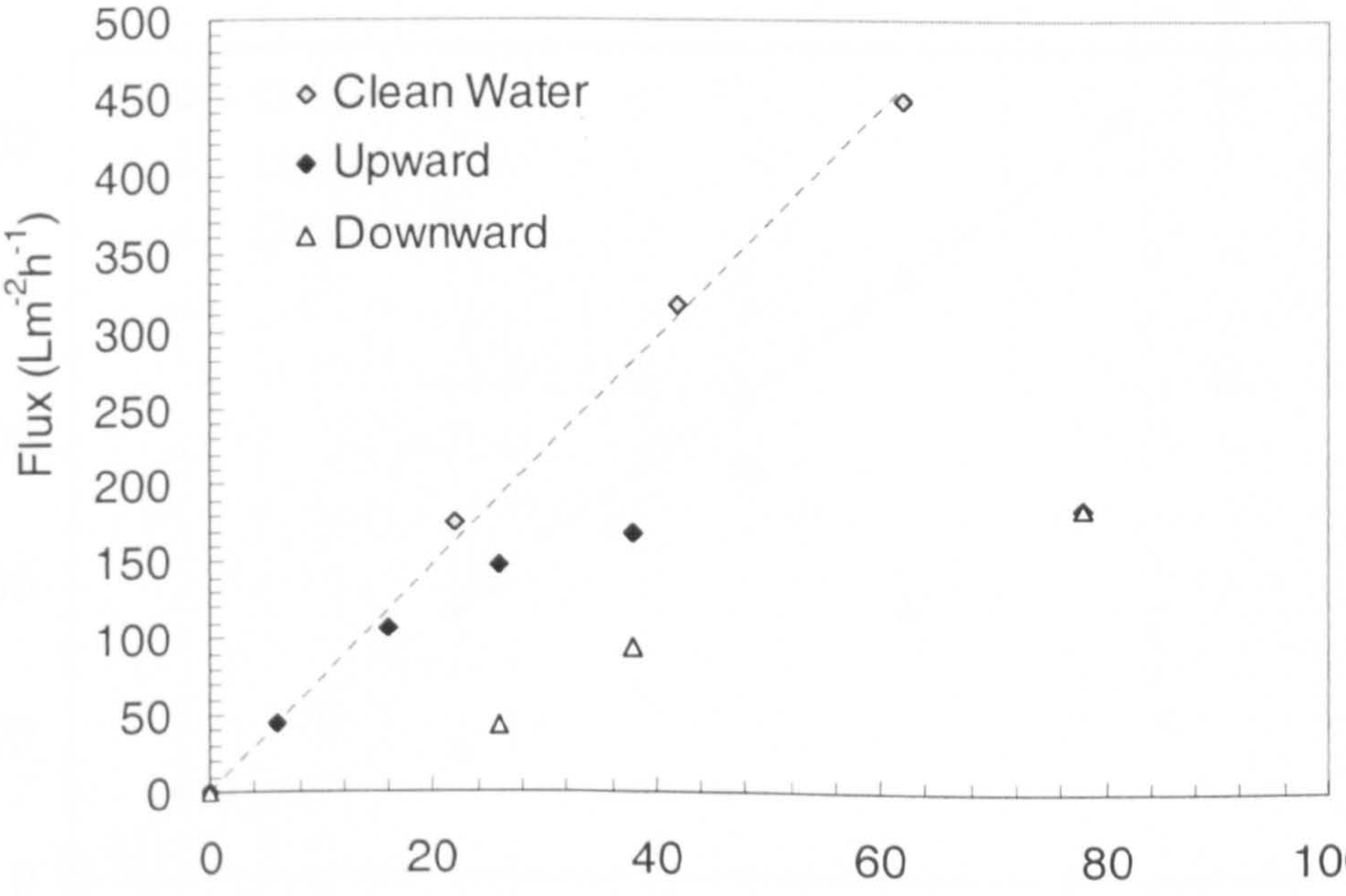

(b)

Figure 20: Step by step results for the filtration of 2400 ppm emulsion, surfactant concentration 240 ppm, crossflow velocity 1.92 m/s

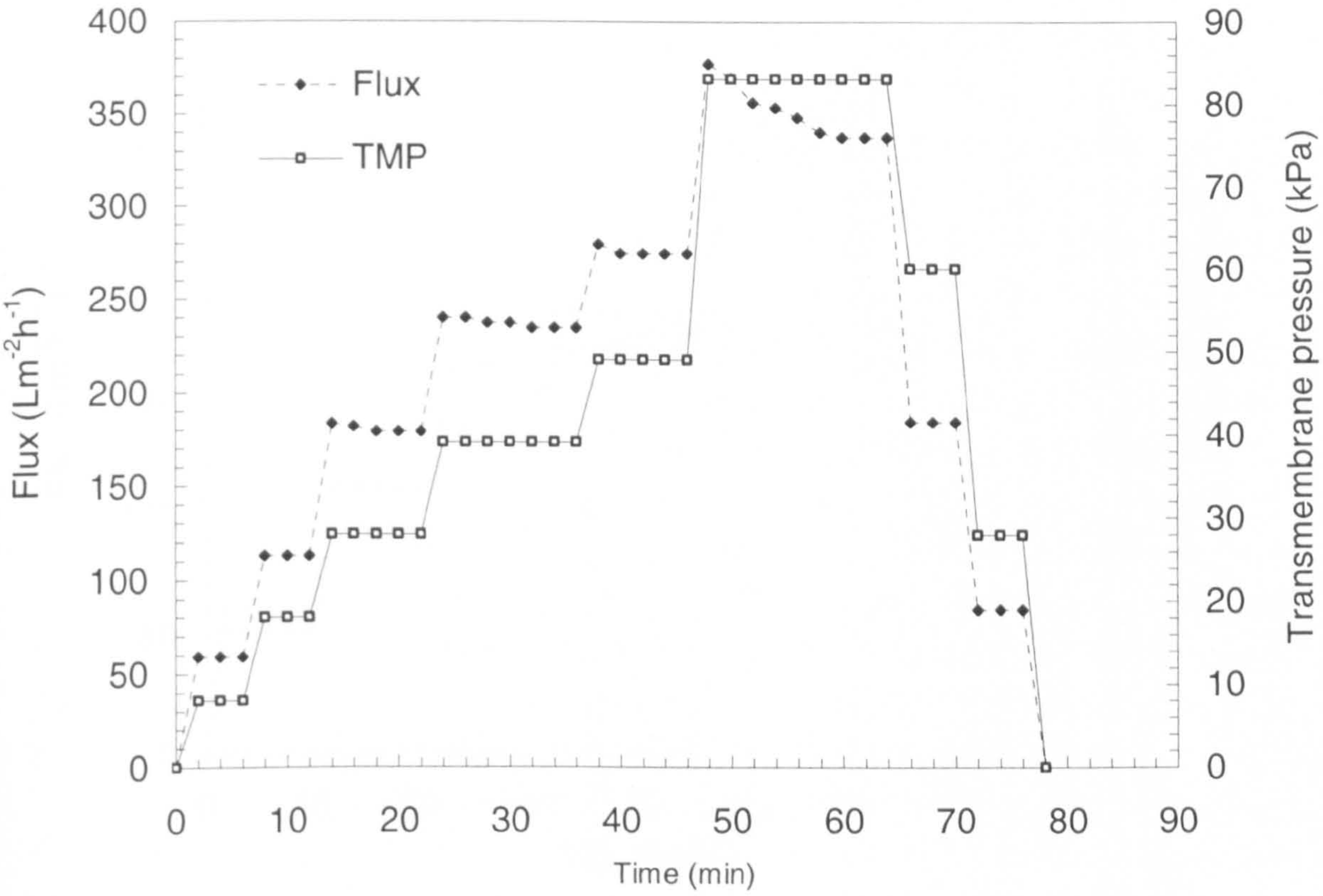

(a)

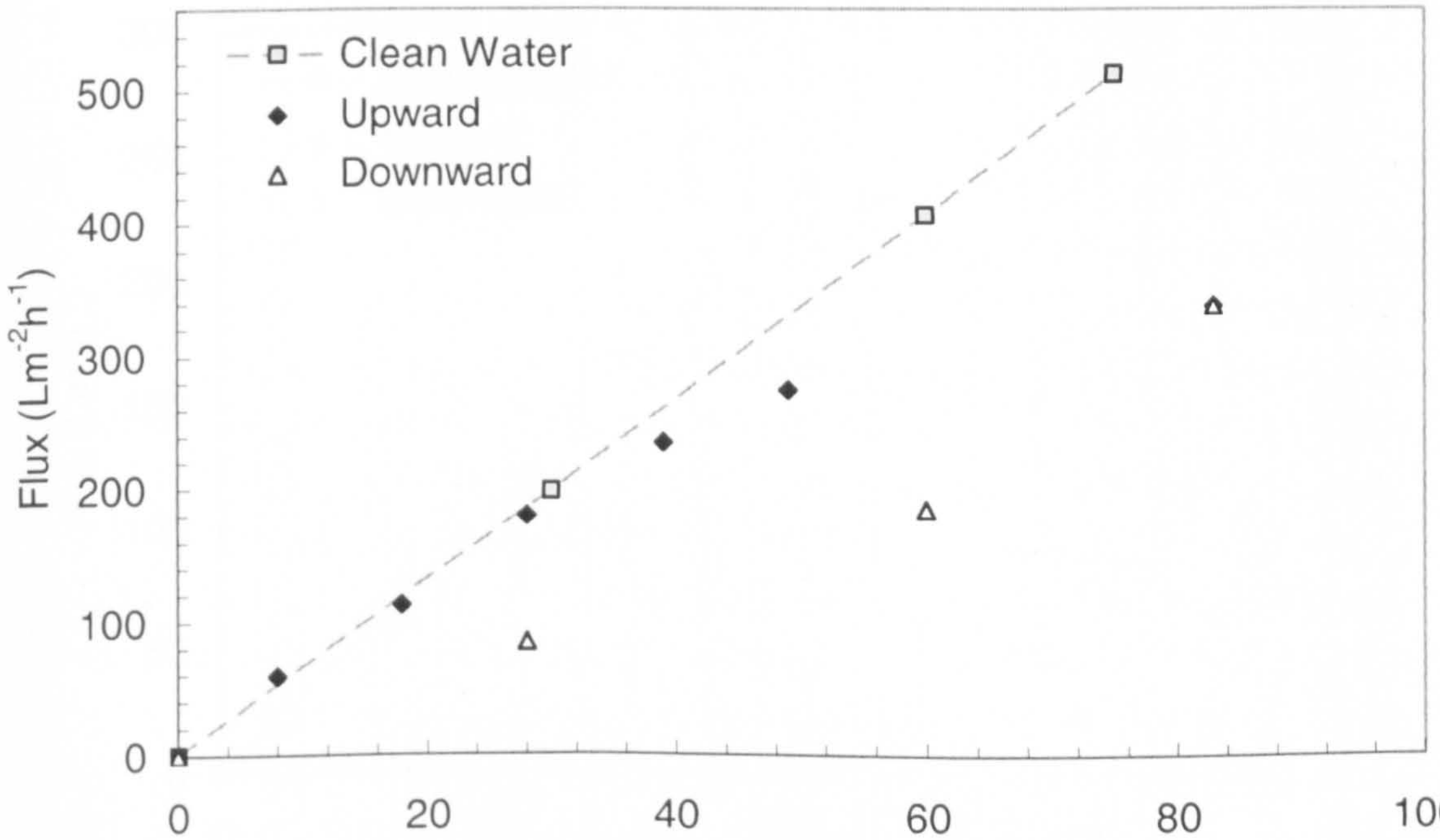

(b)

Figure 21: Step by step results for the filtration of 2400 ppm emulsion, surfactant Concentration 240 ppm, crossflow velocity 2.28 m/s

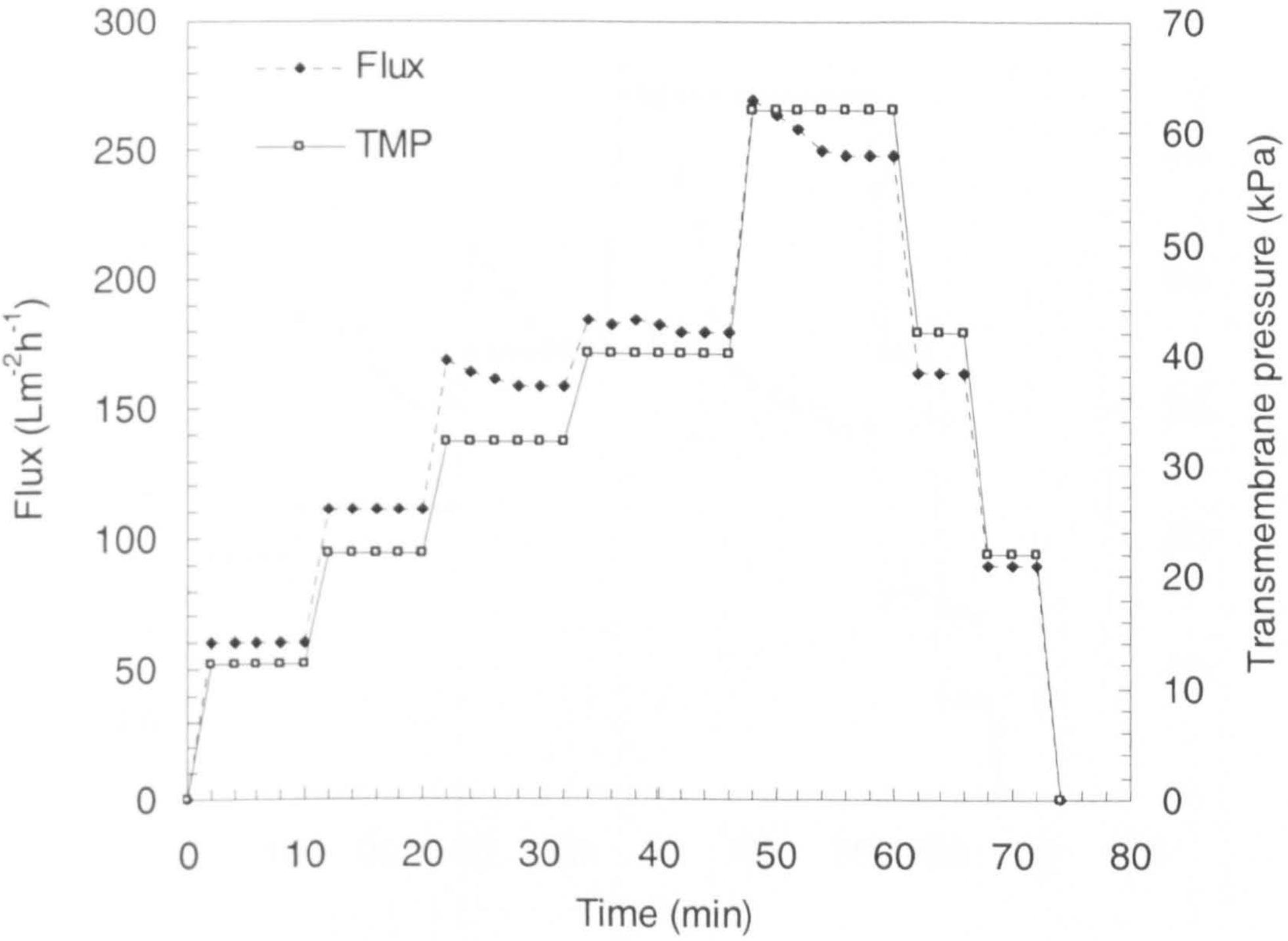

(a)

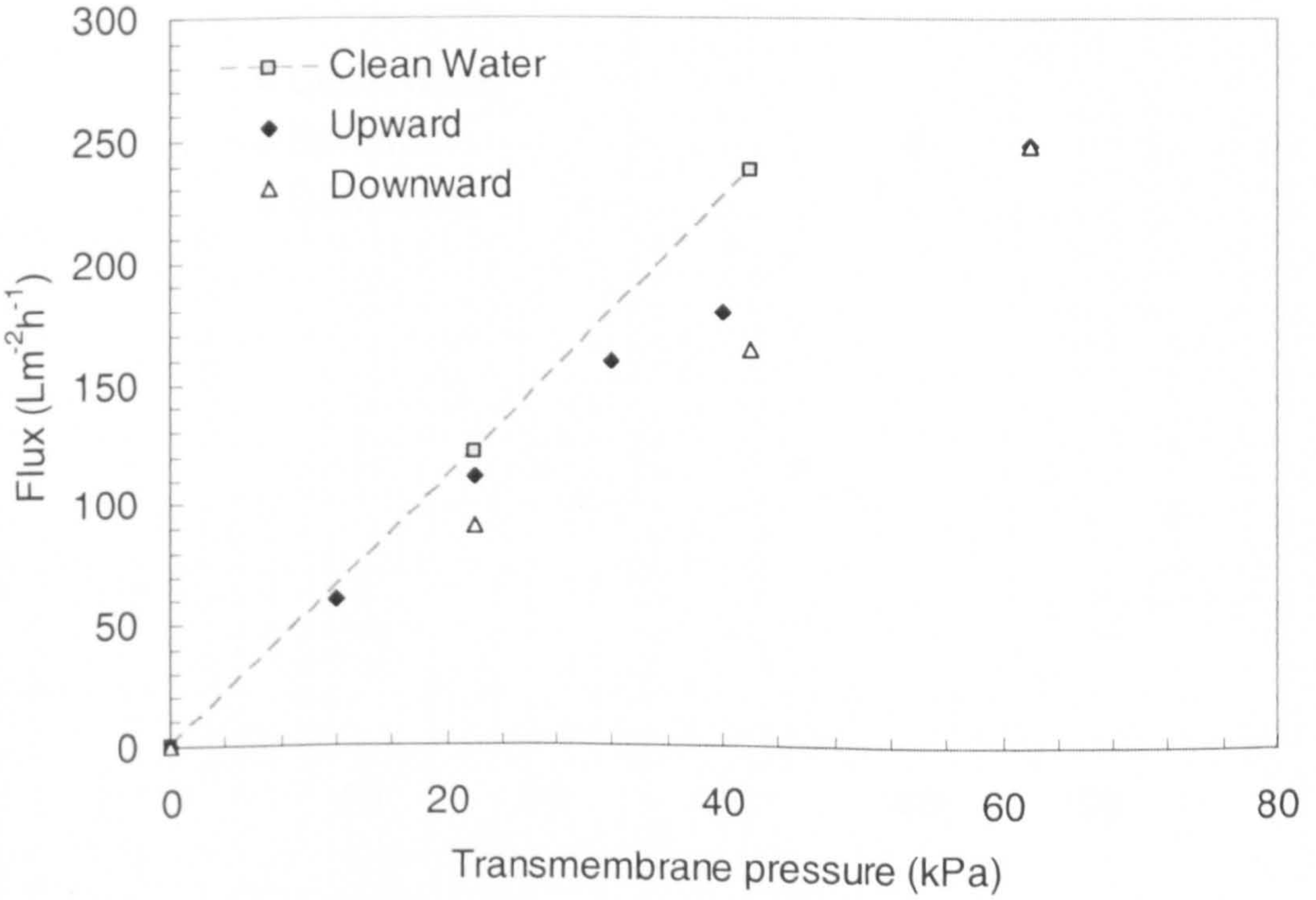

(b)

Figure 22: Step by step results for the filtration of 2400 ppm emulsion, surfactant concentration 240 ppm, crossflow velocity 1.52 m/s, ionic strength 0.1 M $FeCl_3$

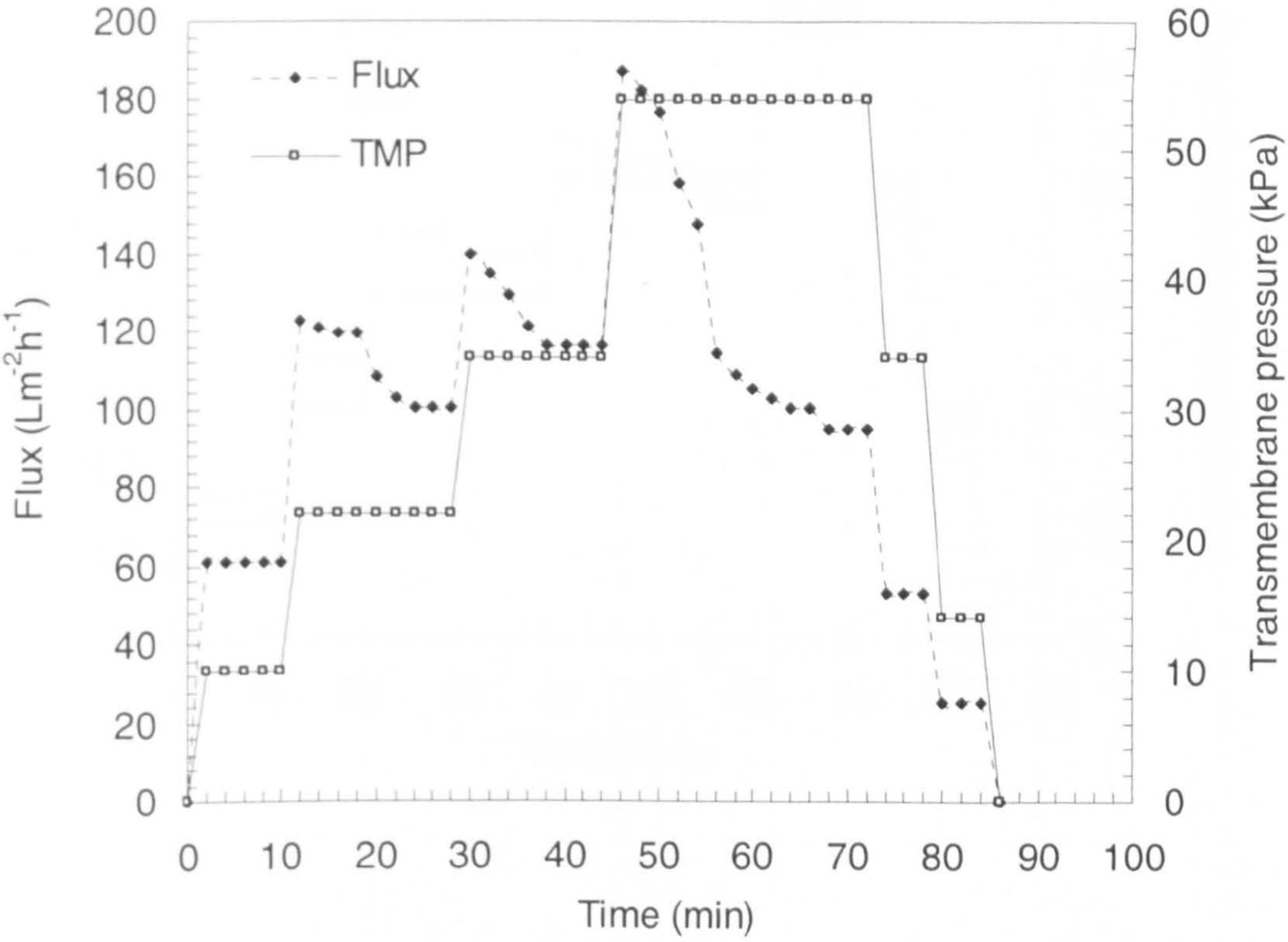

(a)

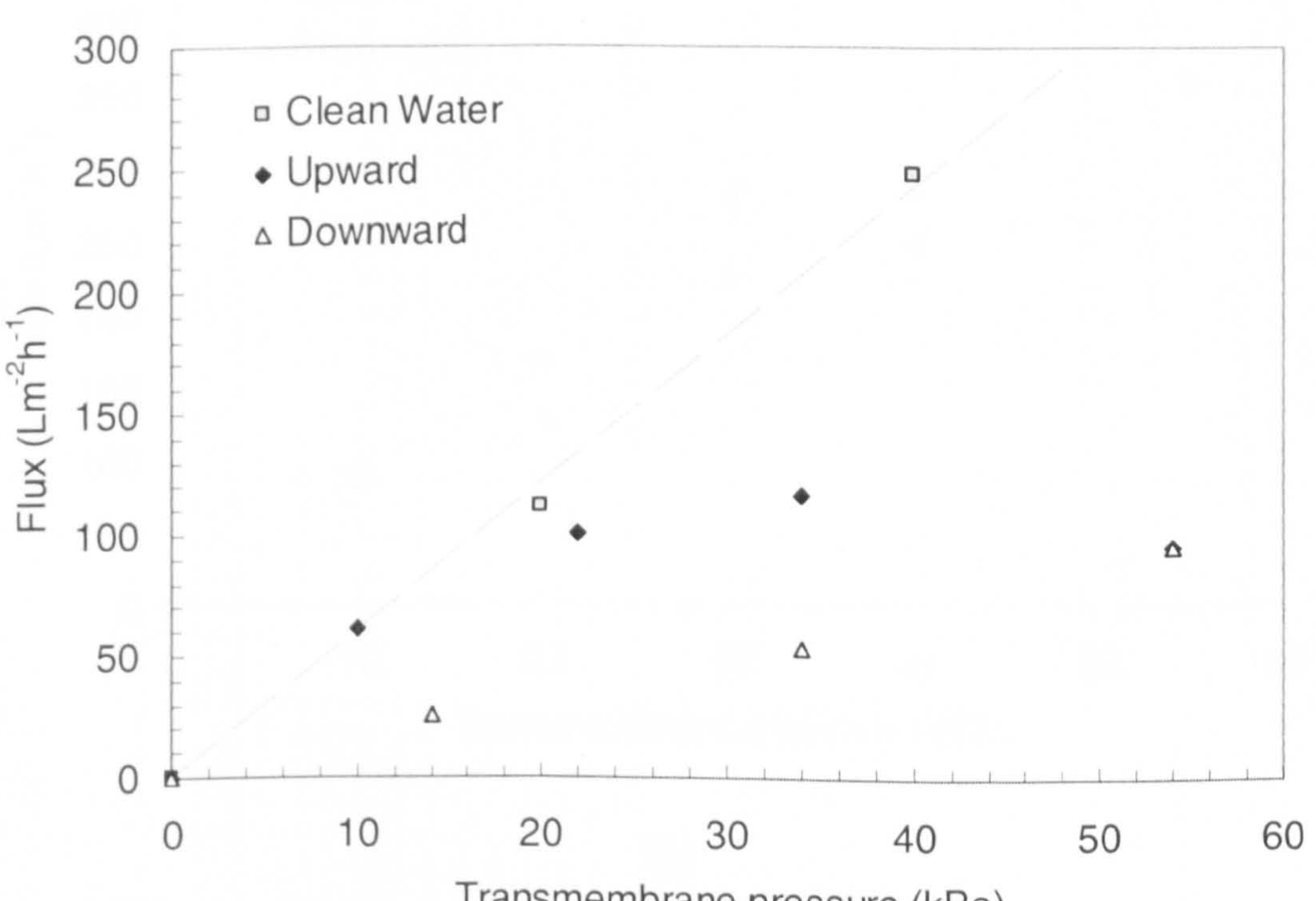

(b)

Figure 23: Step by step results for the filtration of 2400 ppm emulsion, surfactant concentration 240 ppm, crossflow velocity 1.52 m/s, ionic strength 0.1 M NaCl

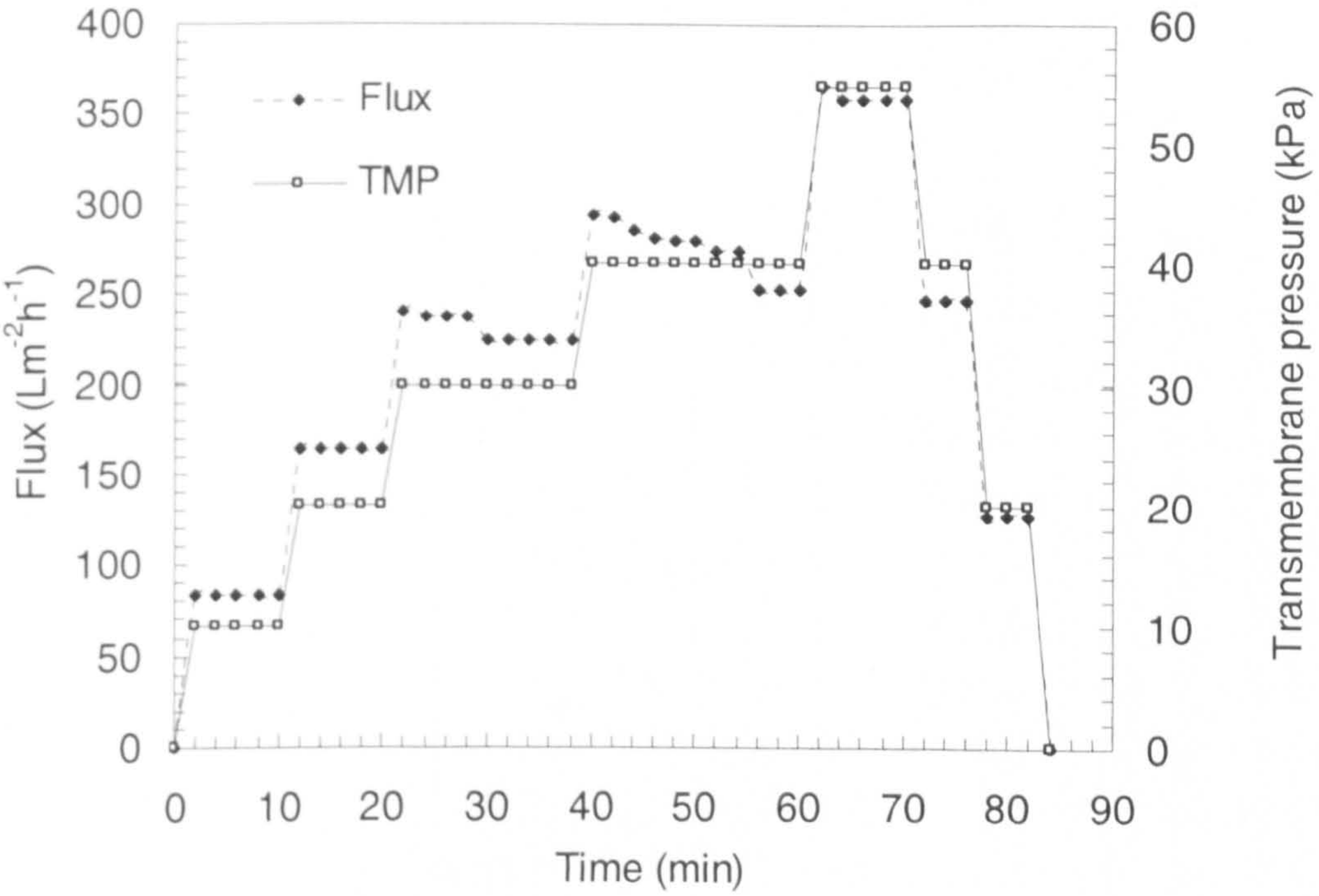

(a)

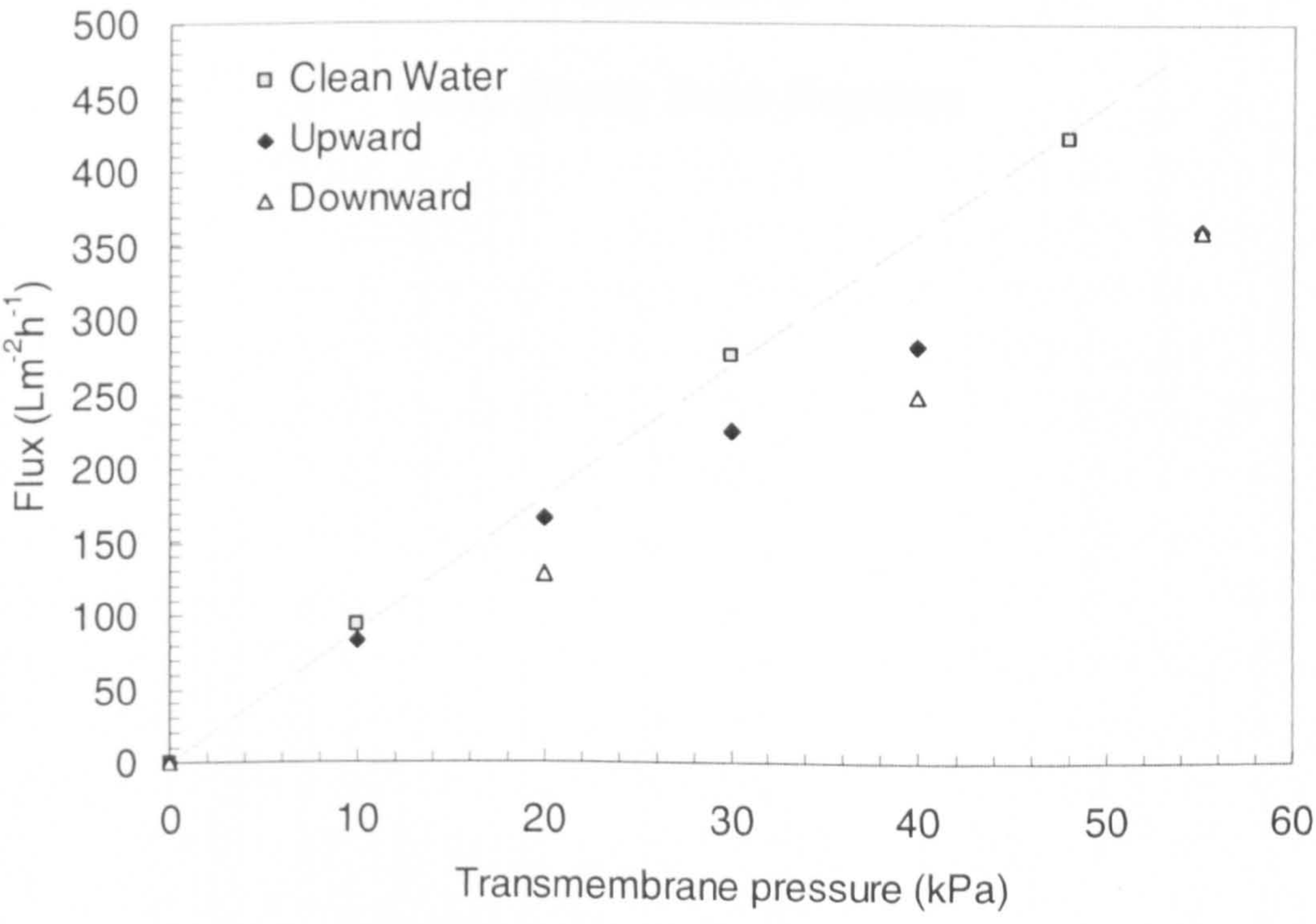

(b)

Figure 24: Step by step results for the filtration of 2400 ppm emulsion, surfactant concentration 240 ppm, Cross-flow Velocity 1.52 m/s, ionic strength 0.1 M $CaCl_2$

Appendix C

Case Study Data Reports

Table 1: Effluent Water Analysis (01/01/2004)

DATE	01/01/2004		AREA	Location	D1 TANK INLET	DI TANK OUTLET	D1 TANK INLET	DI TANK OUTLET
S.NO.	Parameter	Units	Upper limit for injection	TIME	07.50RS	08.00HRS	14.45HRS	14.55HRS
1	pH	at 25 C	NOT SPECIFIED		6.34	6.40	6.36	6.4
2	Temperature	Deg C	NOT SPECIFIED		43.29	43	43	43.8
3	Conductivity	Micro Siemens/Cm	NOT SPECIFIED		302600	301800	294600	301000
4	Turbidity	NTU	NOT SPECIFIED		10.31	11.55	9.81	11.65
5	Total Suspended Solids	ppm	5		9.59	10.07	10.45	9.61
6	Total Dissolved Solids	ppm	250000		211820	211260	206220	217000
7	Oil in Water	ppm	10		20.8	44.5	NAn	NAn
8	Total iron	ppm	30		0.1	0.1	NAn	NAn
9	H2S	ppm	NOT SPECIFIED		NAn	NAn	NAn	NAn
10	Chloride	ppm	NOT SPECIFIED		NAn	NAn	NAn	NAn
11	Dissolved Oxygen	ppb	5		0	0	NAn	NAn
12	Particle Size Distribution in 0.1 ml							
	Above 2 Microns	Nos.,	NOT SPECIFIED		HIGH	HIGH	HIGH	HIGH
	Above 3 Microns	Nos.,	NOT SPECIFIED		HIGH	HIGH	HIGH	HIGH
	Above 5 Microns	Nos.,	200		6846	7005	6008	6891
	Above 8 Microns	Nos.,	75		1536	1615	1635	1579
	Above 10 Microns	Nos.,	25		507	521	550	571
	Above 12 Microns	Nos.,	20		159	150	139	141
	Above 15 Microns	Nos.,	10		24	20	20	18
	Above 20 Microns	Nos.,	0		2	1	2	1

Table 2: Effluent Water Analysis (12/4/2004)

DATE	12.04.2004		AREA	LOCATION	D1 IN	D1 OUT	D1 IN	D1 OUT
S.NO.	Parameter	Units	Upper limit for injection	TIME	08:10	08:30	15:00	15:15
1	pH	at 25 C	NOT SPECIFIED		6.05	6.12	6.08	6.22
2	Temperature	Deg C	NOT SPECIFIED		41	38.5	40.0	37.0
3	Conductivity	Micro Siemens/Cm	NOT SPECIFIED		192300	214000	215000	202000
4	Turbidity	NTU	NOT SPECIFIED		9.5	3.54	3.49	5.95
5	Total Suspended Solids	ppm	5		3.3	4.55	4.35	5.95
6	Total Dissolved Solids	ppm	250000		134610	149800	150500	141400
7	Oil in Water	ppm	10		12.5	10.4	NAN	NAN
8	Total iron	ppm	30		NAN	NAN	NAN	NAN
9	H2S	ppm	NOT SPECIFIED		NAN	NAN	NAN	NAN
10	Dissolved Oxygen	ppb	5		0	0	0	0
11	Particle Size Distribution in 0.1 ml							
	Above 2 Microns	Nos.,	NOT SPECIFIED		43435	29385	32969	27501
	Above 3 Microns	Nos.,	NOT SPECIFIED		8593	4150	5669	4523
	Above 5 Microns	Nos.,	200		1612	635	881	715
	Above 8 Microns	Nos.,	75		300	85	97	100
	Above 10 Microns	Nos.,	25		119	29	24	35
	Above 12 Microns	Nos.,	20		49	12	10	13
	Above 15 Microns	Nos.,	10		17	5	4	5
	Above 20 Microns	Nos.,	0		3	2	1	1

Table 3: Effluent Water Analysis (30/5/2004)

DATE	30/5/2004		AREA	D1 IN	D1 OUT	D1 IN	D1 OUT
S.NO.	Parameter	Units	Upper limit for injection	08:30	08:45	14:00	14:15
1	pH	at 25 C	NOT SPECIFIED	6.34	6.26	6.36	6.29
2	Temperature	Deg C	NOT SPECIFIED	46	44	47	45
3	Conductivity	Micro Siemens/Cm	NOT SPECIFIED	200000	209000	202000	204000
4	Turbidity	NTU	NOT SPECIFIED	12.4	1.95	13.8	0.48
5	Total Suspended Solids	ppm	5	9.3	4.95	9.7	5.45
6	Total Dissolved Solids	ppm	250000	140000	146300	141400	142800
7	Oil in Water	ppm	10	8.9	7.2	NAN	NAN
8	Total iron	ppm	30	NAN	NAN	NAN	NAN
9	H2S	ppm	NOT SPECIFIED	0	0	0	0
10	Dissolved Oxygen	ppb	5	NAN	NAN	NAN	NAN
11	Particle Size Distribution in 0.1 ml						
	Above 2 Microns	Nos.,	NOT SPECIFIED	25602	29558	26321	31891
	Above 3 Microns	Nos.,	NOT SPECIFIED	8588	8884	7436	11762
	Above 5 Microns	Nos.,	200	1695	1426	1372	2303
	Above 8 Microns	Nos.,	75	225	182	241	239
	Above 10 Microns	Nos.,	25	74	63	63	52
	Above 12 Microns	Nos.,	20	30	32	21	15
	Above 15 Microns	Nos.,	10	5	11	4	5
	Above 20 Microns	Nos.,	0	0	3	0	1

Table 4: Effluent Water Analysis (24/6/2004)

DATE	24/06/2004		AREA	LOCATION	D1INLET	D1OUTLET	D1 INLET	D1 OUTLET
S.NO.	Parameter	Units	Upper limit for injection	TIME	07:45	08:00	14:30	14:50
1	pH	at 25 C	NOT SPECIFIED		6.36	6.38	6.37	6.20
2	Temperature	Deg C	NOT SPECIFIED		46	44	48.0	45.0
3	Conductivity	Micro Siemens/Cm	NOT SPECIFIED		216000	215000	213000	214000
4	Turbidity	NTU	NOT SPECIFIED		8.34	7.81	7.6	6.9
5	Total Suspended Solids	ppm	5		8.1	6.7	8.5	5.3
6	Total Dissolved Solids	ppm	250000		151200	150500	149100	149800
7	Oil in Water	ppm	10		5.0	4.7	NAN	NAN
8	Total iron	ppm	30		NAN	NAN	NAN	NAN
9	H2S	ppm	NOT SPECIFIED		NAN	10	NAN	NABN
10	Dissolved Oxygen	ppb	5		0	0	0	0
11	Particle Size Distribution in 0.1 ml							
	Above 2 Microns	Nos.,	NOT SPECIFIED		33168	27641	33758	23953
	Above 3 Microns	Nos.,	NOT SPECIFIED		6907	4312	5812	5007
	Above 5 Microns	Nos.,	200		1011	1171	1133	1211
	Above 8 Microns	Nos.,	75		260	126	300	115
	Above 10 Microns	Nos.,	25		89	64	67	55
	Above 12 Microns	Nos.,	20		30	18	26	14
	Above 15 Microns	Nos.,	10		9	6	6	5
	Above 20 Microns	Nos.,	0		1	1	1	1

Table 5: Effluent Water Analysis (20/7/2004)

DATE	20/07/02004		AREA	LOCATION	F/P	D1 IN	D1 OUT
S.NO.	Parameter	Units	Upper limit for injection	TIME	19:30	20:15	20:35
1	pH	at 25 C	NOT SPECIFIED		6.26	6.31	6.38
2	Temperature	Deg C	NOT SPECIFIED		49	49.5	48
3	Conductivity	Micro Siemens/Cm	NOT SPECIFIED		208000	213000	209000
4	Turbidity	NTU	NOT SPECIFIED		9.37	6.09	8.99
5	Total Suspended Solids	ppm	5		8.75	7.2	6.52
6	Total Dissolved Solids	ppm	250000		145600	149100	146300
7	Oil in Water	ppm	10		10.4	6.7	5.1
8	Total iron	ppm	30		NAN	NAN	NAN
9	H2S	ppm	NOT SPECIFIED		0	0	0
10	Dissolved Oxygen	ppb	5		0	0	0
11	Particle Size Distribution in 0.1 ml						
	Above 2 Microns	Nos.,	NOT SPECIFIED		46045	19209	22930
	Above 3 Microns	Nos.,	NOT SPECIFIED		22633	6981	8653
	Above 5 Microns	Nos.,	200		4357	2069	1976
	Above 8 Microns	Nos.,	75		375	541	335
	Above 10 Microns	Nos.,	25		88	219	106
	Above 12 Microns	Nos.,	20		24	49	36
	Above 15 Microns	Nos.,	10		6	21	12
	Above 20 Microns	Nos.,	0		1	6	2

Table 6: Effluent Water Analysis (12/8/2004)

DATE	12/08/2004		AREA	LOCATION	D1 IN	D1 OUT	D1 IN	D1 OUT
S.NO.	Parameter	Units	Upper limit for injection	TIME	08:30	08:45	14:30	14:45
1	pH	at 25 C	NOT SPECIFIED		6.3	6.26	6.18	6.21
2	Temperature	Deg C	NOT SPECIFIED		50	45	52	48
3	Conductivity	Micro Siemens/Cm	NOT SPECIFIED		214000	210000	211000	207000
4	Turbidity	NTU	NOT SPECIFIED		5.9	13.7	4.9	11.9
5	Total Suspended Solids	ppm	5		6.3	10.9	5.6	8.76
6	Total Dissolved Solids	ppm	250000		149800	147000	147700	144900
7	Oil in Water	ppm	10		2.5	4.4	NAN	NAN
8	Total iron	ppm	30		NAN	NAN	NAN	NAN
9	H2S	ppm	NOT SPECIFIED		0	0	0.1	NAN
10	Dissolved Oxygen	ppb	5		0	0	0	NAN
11	Particle Size Distribution in 0.1 ml							
	Above 2 Microns	Nos.,	NOT SPECIFIED		3542	13933	3135	11253
	Above 3 Microns	Nos.,	NOT SPECIFIED		1293	4087	1094	3769
	Above 5 Microns	Nos.,	200		247	889	221	628
	Above 8 Microns	Nos.,	75		31	127	26	107
	Above 10 Microns	Nos.,	25		10	40	8	31
	Above 12 Microns	Nos.,	20		4	18	3	14
	Above 15 Microns	Nos.,	10		0	4	0	6
	Above 20 Microns	Nos.,	0		0	1	0	1

Table 7: Effluent Water Analysis (1/9/2004)

DATE	1-09-2004		AREA	D1 IN	D1 OUT	F/P	D1 IN	D1 OUT
S.NO.	Parameter	Units	Upper limit for injection	08:15	08:30	15:00	15:20	15:35
1	pH	at 25 C	NOT SPECIFIED	6.41	6.28	6.29	6.46	6.35
2	Temperature	Deg C	NOT SPECIFIED	45	43	45	46.5	44
3	Conductivity	Micro Siemens/Cm	NOT SPECIFIED	212000	212000	209000	211000	212000
4	Turbidity	NTU	NOT SPECIFIED	7.1	6.3	3.35	7.95	8.3
5	Total Suspended Solids	ppm	5	6.18	7.08	3.82	5.41	6.7
6	Total Dissolved Solids	ppm	250000	148400	148400	146300	147700	148400
7	Oil in Water	ppm	10	8.3	6.1	NAN	NAN	NAN
8	Total Iron	ppm	30	NAN	NAN	NAN	NAN	NAN
9	H2S	ppm	NOT SPECIFIED	15	10	10	5	10
10	Dissolved Oxygen	ppb	5	0	0	0	0	0
11	Particle Size Distribution in 0.1 ml							
	Above 2 Microns	Nos.,	NOT SPECIFIED	19826	23261	2521	17945	21472
	Above 3 Microns	Nos.,	NOT SPECIFIED	10128	9894	992	7982	8716
	Above 5 Microns	Nos.,	200	1294	1526	103	1131	1319
	Above 8 Microns	Nos.,	75	281	301	29	269	271
	Above 10 Microns	Nos.,	25	91	106	15	78	92
	Above 12 Microns	Nos.,	20	48	55	9	38	43
	Above 15 Microns	Nos.,	10	11	14	3	9	11
	Above 20 Microns	Nos.,	0	2	2	1	2	2

Table 8: Effluent Water Analysis (1/10/2004)

DATE	1-10-2004		AREA	LOCATION	D1 IN	D1 OUT	D1 IN	D1 OUT
S.NO.	Parameter	Units	Upper limit for injection	TIME	08:15	08:25	14:15	14:25
1	pH	at 25 C	NOT SPECIFIED		6.06	6.2	6.09	6.15
2	Temperature	Deg C	NOT SPECIFIED		45	43	44	42
3	Conductivity	Micro Siemens/Cm	NOT SPECIFIED		209000	210000	210000	209000
4	Turbidity	NTU	NOT SPECIFIED		9.44	5.15	8.4	6
5	Total Suspended Solids	ppm	5		10.1	11.2	9.3	10.1
6	Total Dissolved Solids	ppm	250000		146300	147000	147000	146300
7	Oil in Water	ppm	10		8.2	11.3	7.7	10.2
8	Total iron	ppm	30		NAN	NAN	NAN	NAN
9	H2S	ppm	NOT SPECIFIED		15	15	15	10
10	Dissolved Oxygen	ppb	5		0	0	0	0
11	Particle Size Distribution in 0.1 ml							
	Above 2 Microns	Nos.,	NOT SPECIFIED		77204	59094	83099	70011
	Above 3 Microns	Nos.,	NOT SPECIFIED		38697	13853	42710	16310
	Above 5 Microns	Nos.,	200		4169	899	4780	1405
	Above 8 Microns	Nos.,	75		409	100	4190	210
	Above 10 Microns	Nos.,	25		89	35	97	48
	Above 12 Microns	Nos.,	20		29	19	37	19
	Above 15 Microns	Nos.,	10		6	3	7	3
	Above 20 Microns	Nos.,	0		1	1	1	2

Table 9: Effluent Water Analysis (28/11/2004)

DATE	28-11-2004		AREA	LOCATION	D1 IN LET	D1 OUT LET	D1 IN LET	D1 OUT LET
S.NO.	Parameter	Units	Upper limit for injection	TIME	07:30	07:45	13:15	13:35
1	pH	at 25 C	NOT SPECIFIED		6.22	6.21	6.2	6.19
2	Temperature	Deg C	NOT SPECIFIED		38	40	38	40
3	Conductivity	Micro Siemens/Cm	NOT SPECIFIED		208000	209000	209000	207000
4	Turbidity	NTU	NOT SPECIFIED		21.2	6.95	18.1	6.83
5	Total Suspended Solids	ppm	5		6.9	7.7	6.6	7.2
6	Total Dissolved Solids	ppm	250000		145600	146300	146300	144900
7	Oil in Water	ppm	10		16.3	12.8	14.1	10.5
8	Total iron	ppm	30		NAN	NAN	NAN	NAN
9	H2S	ppm	NOT SPECIFIED		25	25	25	25
10	Dissolved Oxygen	ppb	5		0	0	0	0
11	Particle Size Distribution in 0.1 ml							
	Above 2 Microns	Nos.,	NOT SPECIFIED		55726	78420	63817	69373
	Above 3 Microns	Nos.,	NOT SPECIFIED		16275	23313	19383	20351
	Above 5 Microns	Nos.,	200		1883	2299	1599	2380
	Above 8 Microns	Nos.,	75		110	129	113	117
	Above 10 Microns	Nos.,	25		21	30	19	28
	Above 12 Microns	Nos.,	20		7	15	6	13
	Above 15 Microns	Nos.,	10		1	2	1	2
	Above 20 Microns	Nos.,	0		0	1	0	1

Table 10: Effluent Water Analysis (2/12/2004)

DATE	2-12-2004		AREA	LOCATION	D1 IN LET	D1 OUT LET	D1IN LET	D1 OUT LET
S.NO.	Parameter	Units	Upper limit for injection	TIME	08:15	08:30	13:15	13:35
1	pH	at 25 C	NOT SPECIFIED		5.86	5.97	5.91	5.95
2	Temperature	Deg C	NOT SPECIFIED		35	32	35.0	33.0
3	Conductivity	Micro Siemens/Cm	NOT SPECIFIED		215000	211000	213000	212000
4	Turbidity	NTU	NOT SPECIFIED		20	9.0	18.0	9.5
5	Total Suspended Solids	ppm	5		5.7	4.3	5.5	4.7
6	Total Dissolved Solids	ppm	250000		150500	147700	149100	148400
7	Oil in Water	ppm	10		9.6	8.4	10.2	8.1
8	Total Iron	ppm	30		NAN	NAN	NAN	NAN
9	H2S	ppm	NOT SPECIFIED		20	25	20	25
10	Dissolved Oxygen	ppb	5		0	0	0	0
11	Particle Size Distribution in 0.1 ml							
	Above 2 Microns	Nos.,	NOT SPECIFIED		84680	87097	76791	91077
	Above 3 Microns	Nos.,	NOT SPECIFIED		40731	42212	40993	39215
	Above 5 Microns	Nos.,	200		4007	2675	4105	2588
	Above 8 Microns	Nos.,	75		866	329	858	411
	Above 10 Microns	Nos.,	25		345	126	332	137
	Above 12 Microns	Nos.,	20		145	46	151	42
	Above 15 Microns	Nos.,	10		31	10	30	9
	Above 20 Microns	Nos.,	0		3	1	2	1

Appendix D

Matlab code for critical flux estimation

```
%loading oil experiment data
    load exper20.dat;
    tmpo=exper20(:,1);
    jo=exper20(:,2);

    %loading pure water data
    load water20.dat;
    tmpw=water20(:,1);
    jw=water20(:,2);

%Curve fitting for oil data
po=polyfit(tmpo,jo,2);

%Curve fitting for water data
pw=polyfit(tmpw,jw,1);

%plotting the data

TMP=0:10:30000;
jwnew=polyval(pw,TMP);
jonew=polyval(po,TMP);

plot(TMP,jwnew,TMP,jonew);

% Iteration loop for caculation the difference between water line
point and oil curve point. When the difference is less than or
eqaul 0.01 stop the loop and print the solution for the flux and
TMP

tmp=5000;
while tmp <50000
    tmp=tmp+1;
    jwnew=polyval(pw,tmp);
    jonew=polyval(po,tmp);
    Diff=jonew-jwnew;
    if Diff <= 0.01
        fprintf('\nSolution found at TMP %f\n',tmp);
        fprintf('\nSolution found at Flux %f\n',jonew);
        break
    end
end
```

Solution found at TMP 23873.000000

Solution found at Flux 96.819157

Critical flux value estimation for experiment 20 using Matlab code.

Appendix E

Publication Arising from the Research

CROSSFLOW MICROFILTRATION OF OIL FROM SYNTHETIC PRODUCED WATER

Y.H.D. Alanezi, R.J. Wakeman , R.G. Holdich ,
Department of Chemical Engineering, Loughborough University, Loughborough, Leicestershire LE11 3TU, England.

ABSTRACT

Crossflow microfiltration of oil from water was studied experimentally under various operating conditions using a multi-channel ceramic membrane. Crossflow velocities, oil concentrations, and ionic strength effects on equilibrium permeate flux were investigated. An increase in crossflow velocity for oil emulsions from 1.14 to 1.94 m/s caused an increase in the equilibrium permeate flux. In contrast, as feed oil concentrations increased from 300 to 2400 ppm, equilibrium permeate fluxes were decreased. Likewise, when the ionic strength for the feed emulsions was increased, the permeate flux declined. These different observations are discussed in term of the hydrodynamics and particle interactions in relation to the filtration process.

KEYWORDS

Ceramic Membrane, Crossflow Microfiltration, Oil Filtration, Effluent, Emulsion

1 Introduction

Produced water is water formed in underground formations and is brought up to the surface along with crude oil during production. It comprises mainly of dispersed oil, organic compounds, and suspended solids. The most popular preference to deal with produced water is to re-inject it back into the formation. Produced water re-injection (PWRI) needs a modified treatment such as separation units to eliminate oil and suspended solids before re-injection for pressure build up. De-oiling treatment normally consists of an API gravity or corrugated plate separator and a gas flotation unit. However, gravity separation is not successful with emulsified oil droplets smaller than 20 µm. The reason is that as the oil droplets size reduces, the essential retention time to obtain an acceptable separator efficiency increases considerably.

A promising membrane technology is crossflow microfiltration (MF) for removal of suspended particles and emulsified oil droplets in the size range of 0.1-20 µm from their feed suspensions. For the technique to be industrially acceptable it must provide an increase of the filtrate volume with an oil concentration of less than 5 mg/l and also eliminate any solids in suspension. In contrast, the main drawback associated with MF relates to fouling ,i.e. the membrane surfaces or pores become dogged.

2 Case Study

Due to the increasing amounts of produced water during oil production in Kuwait, the establishment of wastewater treatment unit for produced water re-injection purposes had become essential. It is estimated there that oil wells generate in quantity of 15 to 40% of produced water. The unit consists of surge tank, oily water treatment, and oil drum. The oily water treatment comprises of parallel/corrugated plate separator and induced gas flotation. The main objective of this treatment train is reduce the oil in

Table 1: Produced Water Characteristics.

Chemical Component	Concentration (mg/l)
Cl^-	145,900
HCO_3^-	196
Ca	23,250
Na	42,191
SO_4	256
Oil	2000
H_2S	150

water concentration from 2000 to 10 ppm, the maximum allowable concentration for reinjection and disposal. The produced water characteristics are presented in Table 1.

3 Experimental

3.1 Materials

Dodecane and sorbitan monooleate (Aldrich Chemical) were used to form oil in water emulsions. Emulsion particle size distributions were measured using a Malvern Zetasizer 3000HS; the average particle size of the distributions was 3-5 μm.

The membrane used was a tubular ceramic (zirconia) microfiltration module obtained from Fairey Industrial Ceramics Ltd. The membrane average pore diameter was 0.2 μm and its effective length was 0.55 m. The membrane consists of 7 channels, each being circular with an inner diameter of 4.7 mm. The membrane was mounted horizontally in a stainless steel module.

3.2 Crossflow microfiltration rig

The schematic diagram of the microfiltration rig used in the study is shown in Fig. 1. The oil in water emulsions were pumped into the membrane module via a variable speed lobe pump. The transmembrane pressure was monitored using three pressure gauges, one at each of the feed and retentate ends of the membrane and one in the permeate stream. The temperature of the feed stream was regulated using a secondary circuit in which a plate type heat exchanger kept the feed temperature at 25±2°C. This secondary circuit also provided most of the mixing effects, to keep particles in the suspension well dispersed. The ΔP for a given crossflow velocity was therefore controlled by manipulating the permeate pressure, P_p, using the valve in the permeate stream.

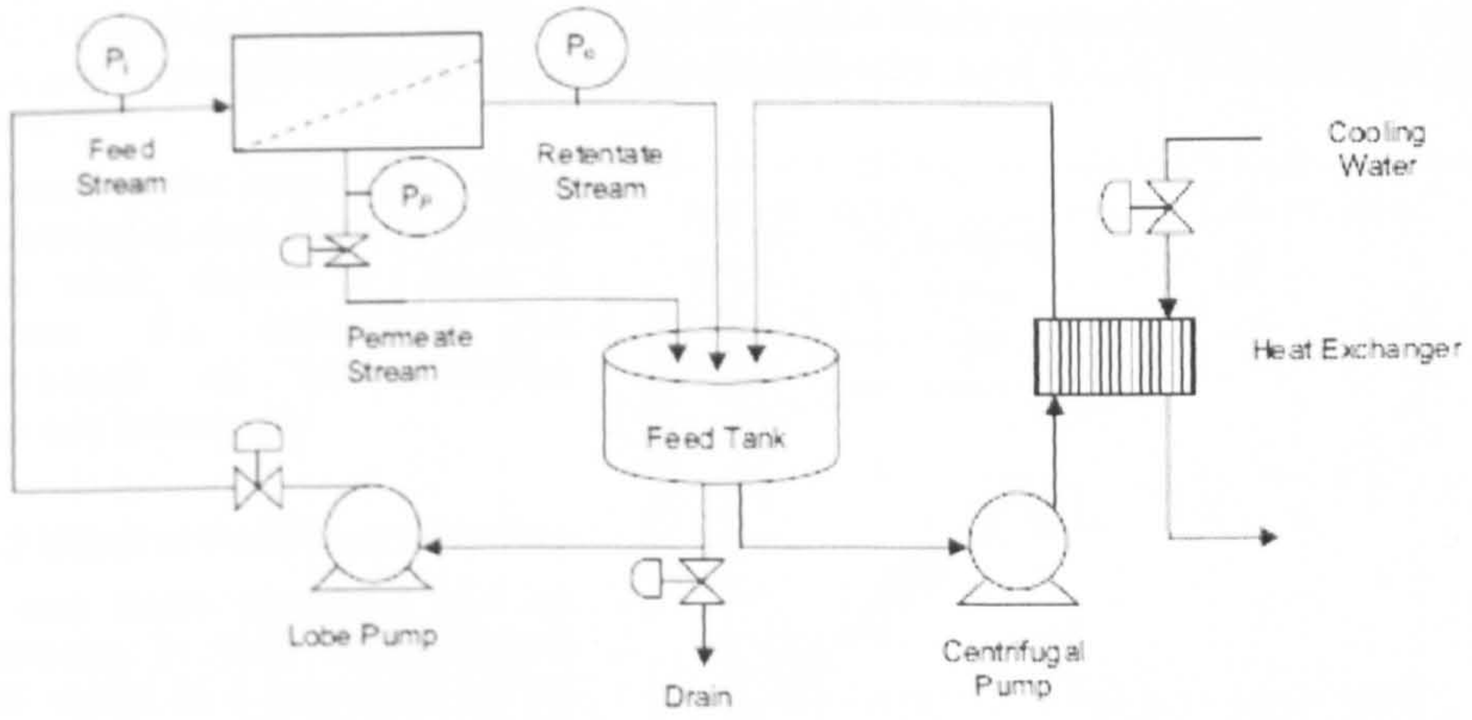

Fig. 1. Schematic diagram of the experimental setup.

3.3 Experimental Procedure

Prior to the start of a filtration experiment, the oil-in-water emulsions were prepared by mixing n-dodecane (model oil) and sorbiton monooleate (surfactant) with deionised water for half an hour by using a high shear laboratory mixer at a speed of

4000 rpm. The emulsions were then flowed through the rig with the permeate valve closed for 10 mins before the start of an experiment to stabilize the crossflow velocity and to allow equilibrium to be achieved between the suspension and the surfaces in the rig (including the heat exchanger circuit). The clean water flux and total membrane resistance were be determined before and after each experiment to ensure that the permeability of the membrane was approximately the same at the start of each experiment. This was necessary to enable analysis of the extent of irreversible fouling and the efficiency of the cleaning method.

J_{crit} is the critical flux; this was measured experimentally by successive increments/decrements of transmembrane pressure using a step by step technique. The technique consisted of systematic increases of ΔP, each step had a minimum 15 min duration or until the equilibrium permeate flux had been reached. The first unstable permeation flux was determined when the flux declined over the course of time at a given ΔP step. After incrementing the pressure to a point beyond the critical ΔP, the pressure is then decremented. The flux points corresponding to the upwards and downwards steps are plotted against ΔP and the deviation point from the clean water flux or first step extrapolation line was obtained.

4 Results and discussion

4.1 Effect of Crossflow Velocity

An increase in the critical flux is likely as the crossflow velocity is increased, which resulted in an increase in the shear forces along membrane surface and causes higher back diffusion rates of solutes, thereby contributing to a decrease of fouling. For example, Chen *et al* (1997) noticed during filtration of colloidal silica suspensions that as the crossflow velocity was increased from 0.2 to 1m/s, the critical flux increased from 30-160 to 220-285 l/m^{2}h. Madaeni (1997) observed that the critical flux increased linearly with crossflow velocity using a similar membrane for suspensions of latex particles with diameter size of 0.1 and 1 µm. Also, by using the DOTM method, Li *et al* (1998) observed similar linear relationship between critical flux and crossflow velocity for both latex particles (of sizes 3, 6.4, 11.9 µm) and yeast cells.

Similar behaviour has been observed during filtration tests in this work, shown in Figure 2, where the permeate flux increased as the crossflow velocity increased.

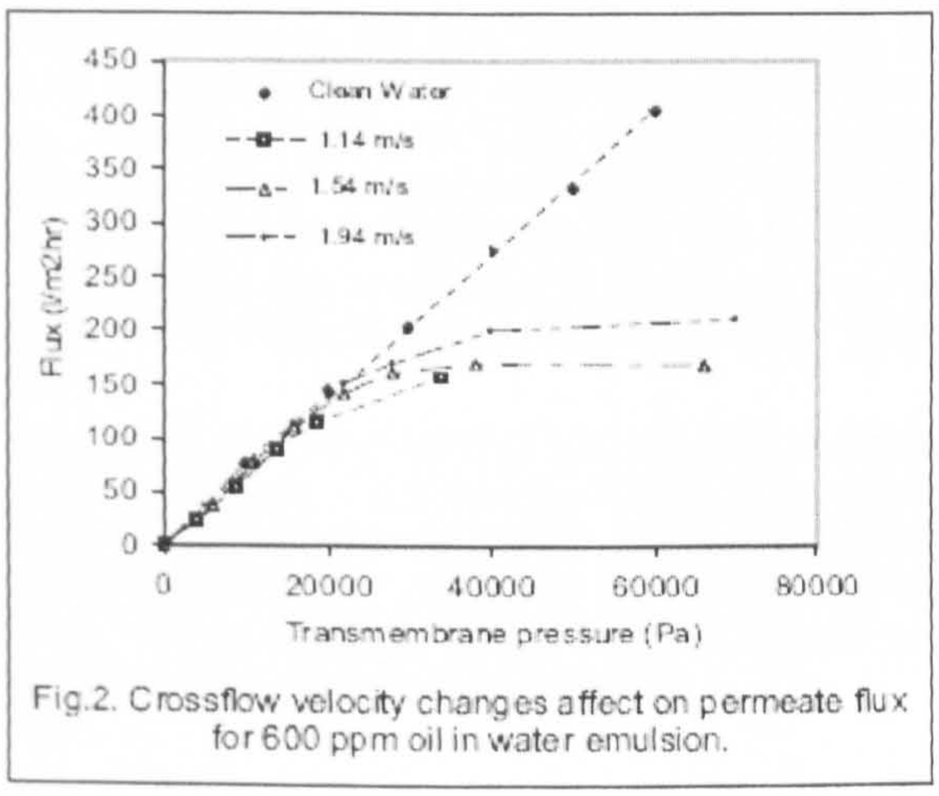

Fig.2. Crossflow velocity changes affect on permeate flux for 600 ppm oil in water emulsion.

4.2 Effect of Feed Concentration

It has been observed that an increase in feed concentration will result in a decrease in the critical flux (Madaeni, 1997; Chen, 1998; Fradin and Field, 1999; Kwon *et al*, 2000). As consequence of a feed concentration increase, a rise in

the solute mass transfer rate and then accumulation in the boundary film near the membrane surface is expected. Accordingly, a rise in hydraulic resistance is observed due to the enhancement of concentration polarization and probability of fouling. The effect of this is shown in Figure 3 in which it is observed that as the oil concentration increased from 300 to 2400 ppm the equilibrium flux declined.

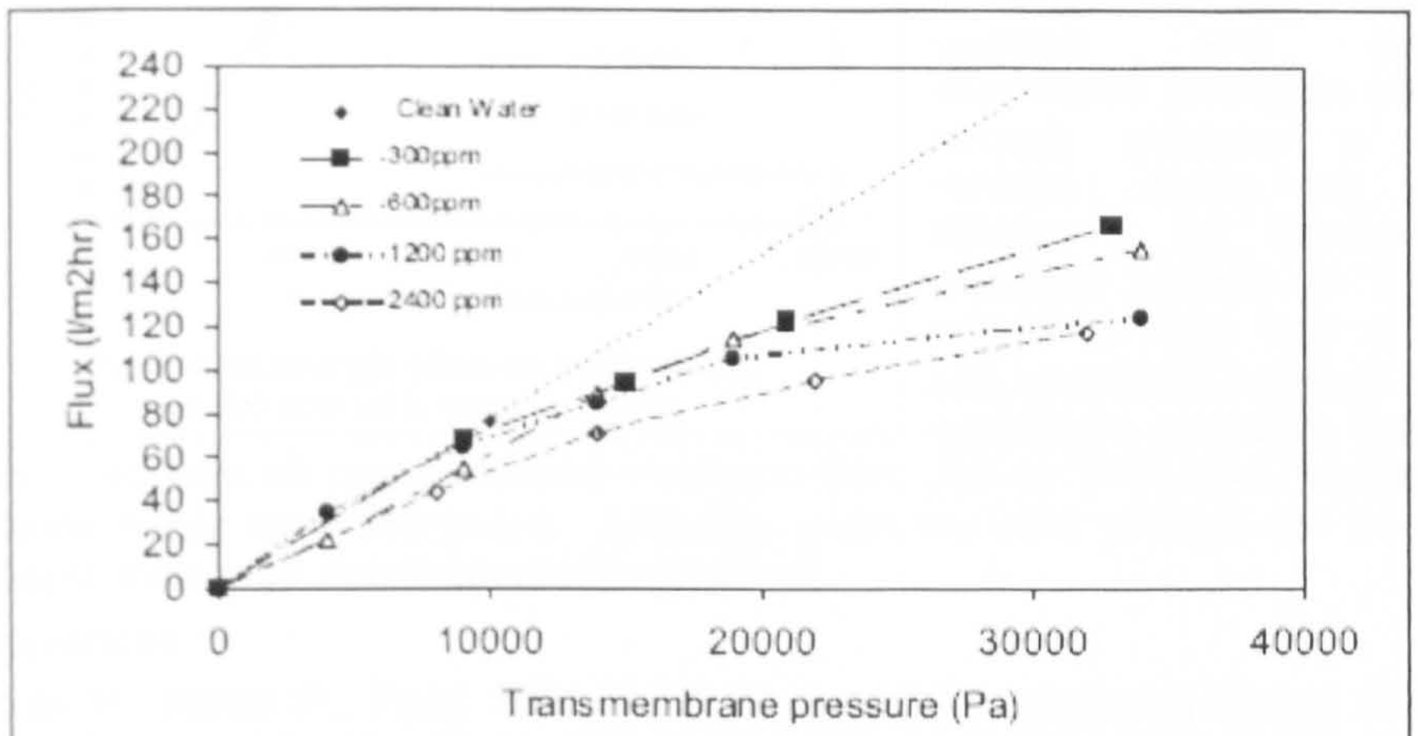

Fig.3. Oil in water concentration changes affect on permeate flux.

4.3 Effect of Ionic Strength

Permeate flux decline is caused by concentration polarization and fouling processes, which are governed by the hydrodynamic effects and physicochemical operational conditions, such as ionic strength. Therefore, any change in these conditions would result in apparent changes in behaviour of the flux decline. For instance, in stable colloidal suspensions, as a consequence of the increase in ionic strength, the diffuse double layer around the charged particles would be compressed. Therefore, particles would be densely packed in the cake film, leading to a decrease in the permeate flux. Faibish *et al* (1998) observed that as the ionic strength increased, the permeate flux decreased severely, and the steady-state flux state was reached faster than in the lower ionic strength case. Moreover, at higher ionic strengths, a decline in the range of the electrostatic double layer repulsive forces would occur, resulting in a decrease in the interparticle distance in cake layer. Subsequently, the cake layer would become more densely packed and thus the resistance to permeate flux has increased. Elzo *et al* (1998) reported similar effects, that is, high permeate fluxes were observed at low salt concentration.

During the microfiltration tests of oily water, Hua *et al* (2007) noticed that at higher salt concentration a lower steady flux was given. The steady flux at a lower salt concentration (10^{-3}M) was more than double of that at higher salt concentration (0.05M). Similar behaviour has been observed in this work; an investigation of the effects of ionic strength on the oily water filtration found that at higher salt concentrations the steady permeate flux declined as shown in Figure 5.

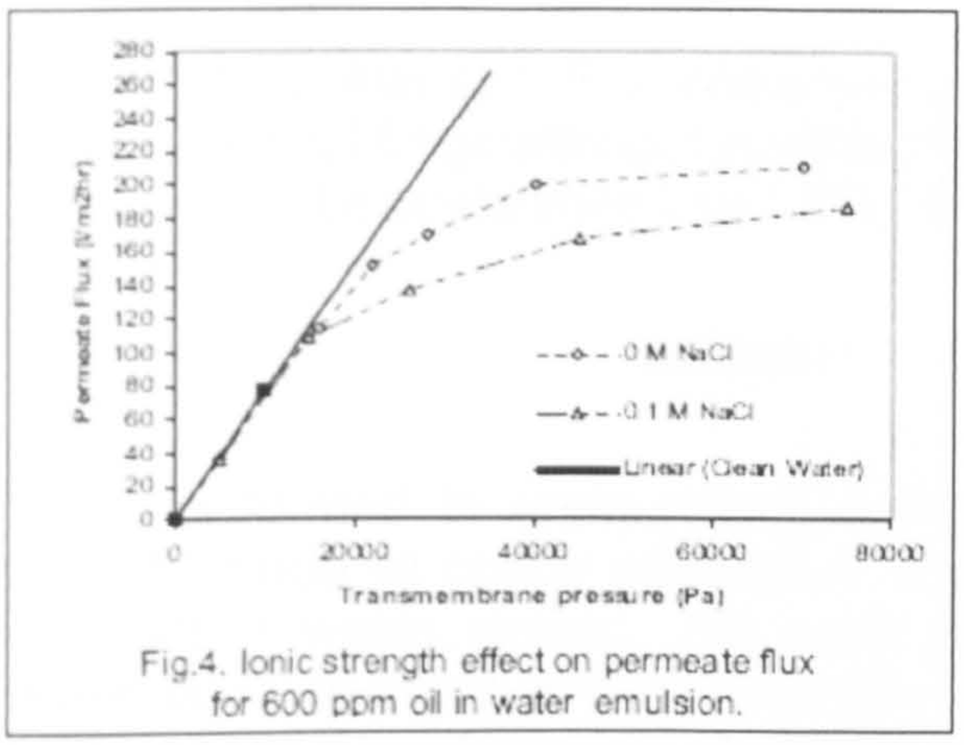

Fig.4. Ionic strength effect on permeate flux for 600 ppm oil in water emulsion.

5 Conclusion

The experimental results from this is study have supported the concept that equilibrium flux is influenced by both hydrodynamics (i.e. crossflow velocity) and particle interactions (emulsion stability through changes in ionic strength) during oily water filtration. An increase in crossflow velocity for the oil emulsions from 1.14 to 1.94 m/s caused an increase in the equilibrium permeate flux. In contrast, as feed oil concentrations increased from 300 to 2400 ppm, equilibrium permeate fluxes were decreased. Likewise, when the ionic strength for the feed emulsions increased, the permeate flux declined.

6 References

Bacchin P., Aimar P., Field R.W., 2006. Critical and sustainable fluxes: Theory, experiments and applications. *Journal of Membrane Science*, **281**, 42-69.

Chen V., 1998. Performance of partially permeable microfiltration membranes under low fouling conditions. *Journal of Membrane Science*, **147**(2), 265-278.

Chiu T.Y. and James A.E., 2005. Critical flux determination of non-circular multi-channel ceramic membranes using TiO_2 suspensions. *Journal of Membrane Science*, **254**, 295-301.

Elzo D., Huisman I., Middelink E. and Gekas V., 1998. Charge effects on inorganic membrane performance in a cross-flow microfiltration process. *Colloids and Surfaces A: Physicochemical and Engineering Aspects*, **138**(2-3), 145-159.

Field R.W., Wu D., Howell J.A. and Gupta B.B., 1995. Critical flux concept for microfiltration fouling. Journal *Membrane Science*, **100**, 259-272.

Fradin B. and Field R.W., 1999. Crossflow microfiltration of magnesium hydroxide suspensions: determination of critical fluxes, measurement and modelling of fouling. *Separation and Purification Technology*, **16**(1), 25-45.

Gésan-Guiziou G., Boyaval E. and Daufin G., 1999. Critical stability conditions in crossflow microfiltration of skimmed milk: transition to irreversible deposition. *Journal of Membrane Science*, **158**, 211-222.

Gésan-Guiziou G., Wakeman R.J. and Daufin G., 2002. Stability of latex crossflow filtration: cake properties and critical conditions of deposition. *Chemical Engineering Journal*, **85**(1), 27-34.

Hua F.L., Tsang Y.F., Wang Y.J., Chan S.Y., Chua H. and Sin S.N., 2007. "Performance study of ceramic microfiltration membrane for oily wastewater treatment", *Chemical Engineering Journal*, **128**(2-3), 169-175.

Kwon D.Y., Vigneswaran S., Fane A.G. and Ben Aim R., 2000. Experimental determination of critical flux in cross-flow microfiltration. *Separation and Purification Technology*, **19**(3), 169-181.

Li H., Fane A.G., Coster H.G.L. and Vigneswaran S., 2000. An assessment of depolarisation models of crossflow microfiltration by direct observation through the membrane. *Journal of Membrane Science*, **172**(1-2), 135-147.

CROSSFLOW MICROFILTRATION OF OIL FROM SYNTHETIC EFFLUENT WATER

Y.H.D. Alanezi*, R.J. Wakeman , R.G. Holdich ,
Department of Chemical Engineering, Loughborough University, Loughborough, Leicestershire LE11 3TU, England.

Abstract

Produced water is formed in underground formations and brought up to the surface along with crude oil during production. It is considered by far the largest volume by-product or waste stream. The most popular preference to deal with produced water is to re-inject it back into the formation. Produced water re-injection (PWRI) needs a treatment before injection to prevent formation blockage. Due to the increase of produced water during oil production in the west of Kuwait, an effluent treatment and water injection plants were established and commissioned in 2004 so that produced water could be used for re-injection purposes. Usually it is estimated that oil wells in the west of Kuwait produce 15 to 40 % of produced water. The main aim of this treatment train is to reduce not only the oil-in-water amount to less than 10 ppm, but also total suspended solids to 5 ppm which is the maximum allowable concentration for re-injection and disposal. Furthermore, with respect to the upper limit for injection, the maximum number of particles between 5 to 8 microns is 200 in 0.1 ml. In practice the number is found to exceed this limit by 10 times. Hence, crossflow microfiltration of oil from synthetic produced water was studied experimentally under various operating conditions using a tubular multi-channel ceramic membrane. Crossflow velocities, oil concentrations, and ionic strength variation effects on equilibrium permeate flux were investigated. An increase in crossflow velocity for oil emulsions from 1.14 to 2.28 m/s caused an increase in the equilibrium permeates flux. In contrast, as feed oil concentrations increased from 300 to 2400 ppm, equilibrium permeate fluxes were decreased. Likewise, when the ionic strength for the feed emulsions was increased by addition NaCl salt, the permeate flux declined. While, as the ionic strength increased by addition of $CaCl_2$ and $FeCl_3$, the permeate flux increased. These different observations are discussed in term of the hydrodynamics and particle interactions in relation to the filtration process. Particle size was used as a parameter to fit the shear-induced hydrodynamic diffusion model, to the experimental filtration data (Figure 1). However, inertial left model and torque balance models were compared and showed to be inappropriate for the particles sizes of the emulsified oil droplets measured. Song and Elimelech Model (SEM) was compared to the experimental results and by modifying the diffusion coefficient to include the shear diffusion coefficient showed better agreement. (Figure 2).

KEYWORDS
Ceramic Membrane, Crossflow Microfiltration, Critical Flux, Effluent, Emulsion

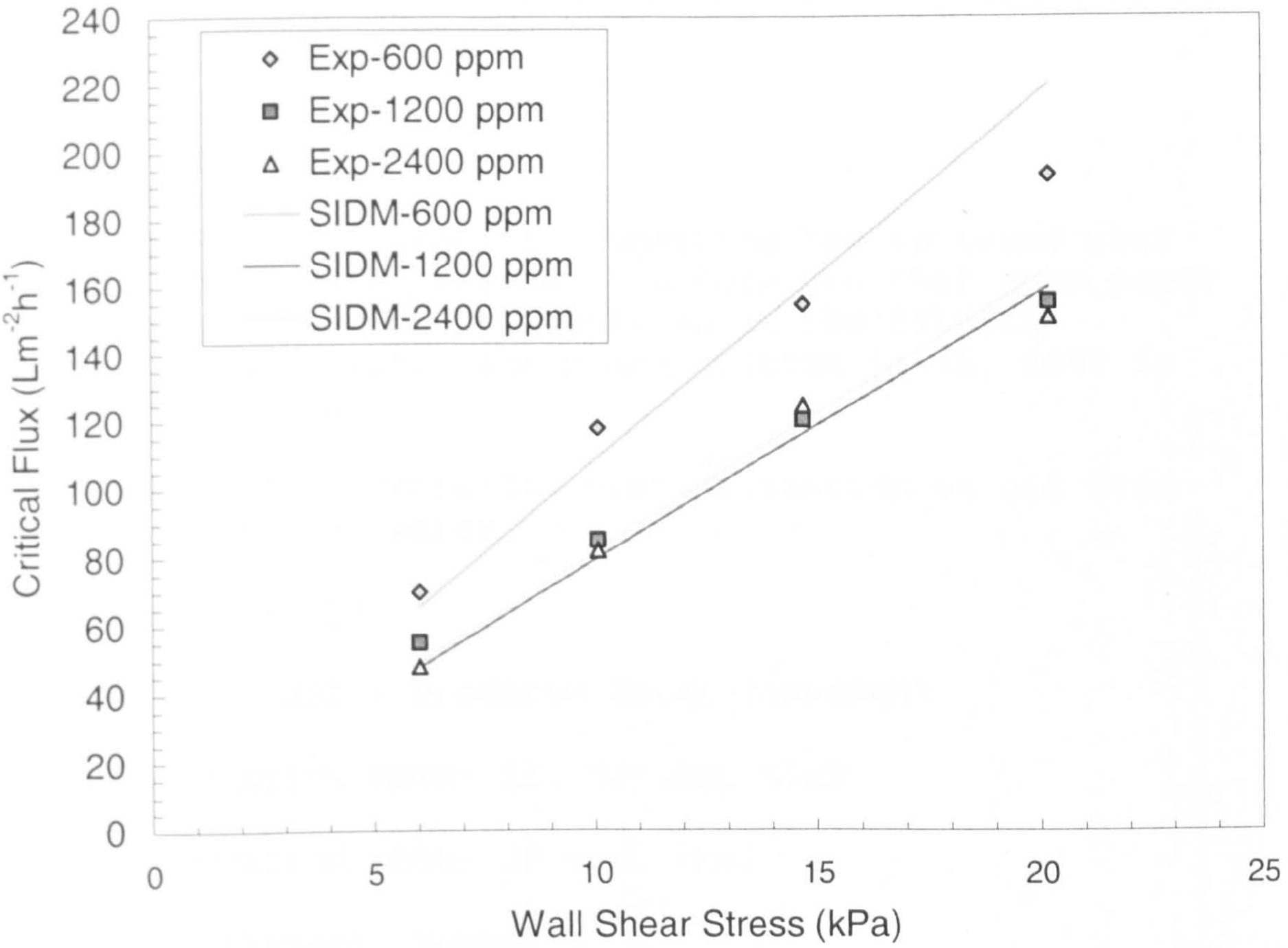

Figure 1: Shear-induced diffusion model (SIDM) fitted to experimental data obtained for (600,1200,2400 mg L^{-1}) emulsions at various crossflow velocities.

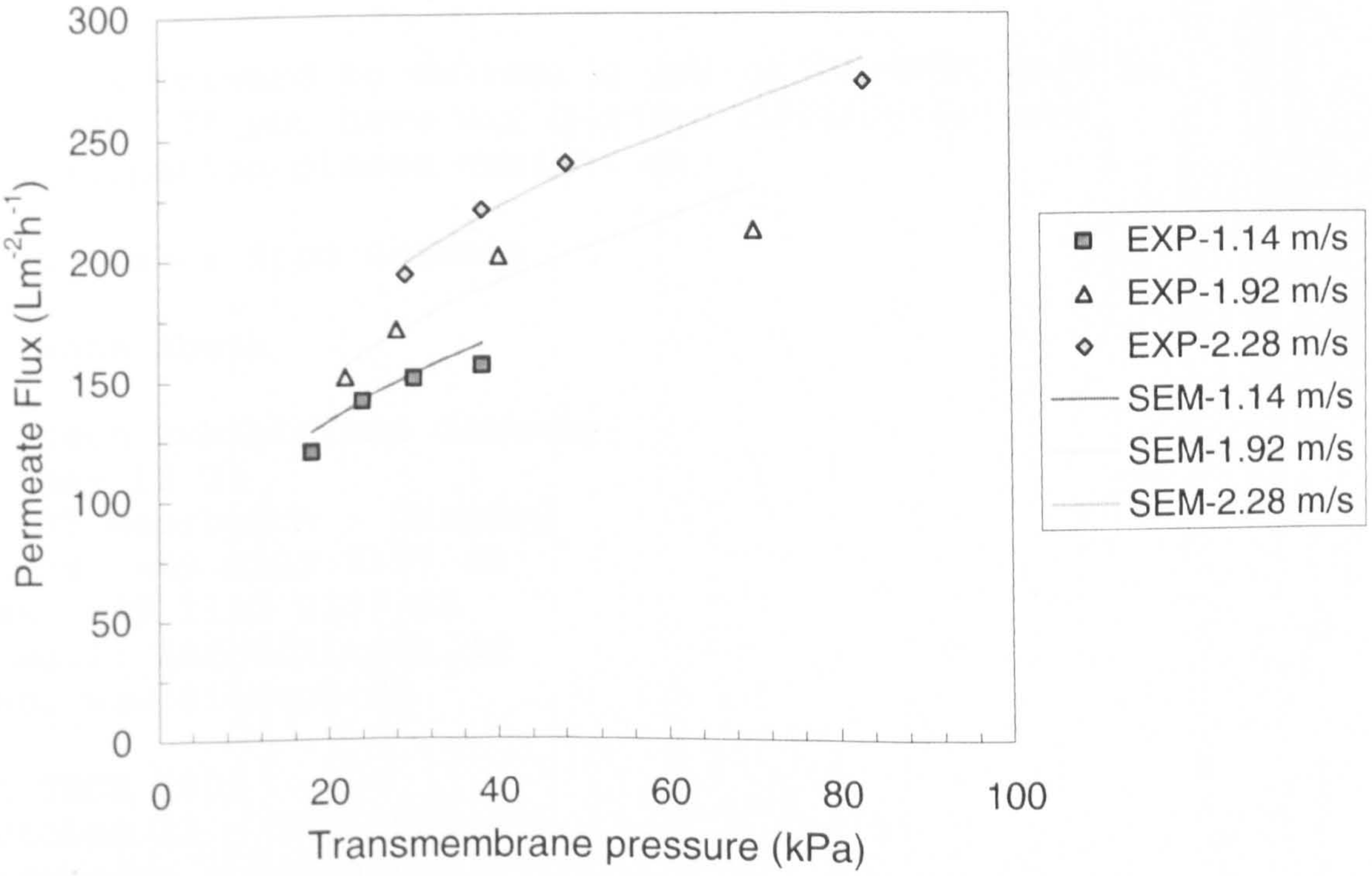

Figure 2: Permeate flux comparison between modified SEM model with experimental data for 600 mg L^{-1} n-dodecane in water emulsions.

On Tue, 17 Feb 2009 19:56:58 FILTECH 2009 - Suzanne Abetz <info@filtech.de> wrote:

Dear Mr. Alanezi,

The FILTECH 2009 Scientific Committee has reviewed your abstract and we are pleased to inform you that your paper has been accepted for presentation at the FILTECH Conference which will take place OCTOBER 13-15, 2009 in WIESBADEN, GERMANY.

YOUR PAPER TITLE: Crossflow microfiltration of oil from synthetic effluent water

YOUR PAPER NO: 109

YOUR SESSION: M02 - Produced Water Treatment

YOUR PRESENTATION DATE: 13. October 2009

YOUR PRESENTATION MODE: 20 min. oral

PRESENTER: Alanezi, Yousef H. D.

FILTECH 2009 VENUE: Rhein-Main-Halls - Wiesbaden - Germany

We look forward to welcoming you to FILTECH 2009 in Germany. If you have any queries concerning your participation please contact me.

Best wishes from Germany

Suzanne Abetz

Filtech Exhibitions Germany
PO Box 12 25
40637 Meerbusch - Germany
Phone: +49 2132 9357 60
Fax: +49 2132 9357 62
e-mail: info@filtech.de
web: www.filtech.de

FILTECH 2009
October 13 - 15, 2009
Wiesbaden - Germany

Managing Directors: Mike Taylor/Suzanne Abetz
VAT Reg. No. DE812928313